



National Aeronautics and  
Space Administration

NASA CP-2113

---

**George C. Marshall Space Flight Center**  
Marshall Space Flight Center, Alabama 35812

NASA-CP-2113 19800006718

## HEAO SCIENCE SYMPOSIUM

HELD AT MSFC MAY 8-9, 1979

Edited by Carroll Dailey and Wendell Johnson  
HEAO Office

November 1979

**FOR REFERENCE**

**NOT TO BE TAKEN FROM THIS ROOM**

LIBRARY COPY

FEB 2 1980

LANGLEY RESEARCH CENTER  
LIBRARY, NASA  
HAMPTON, VIRGINIA

# TABLE OF CONTENTS (Concluded)

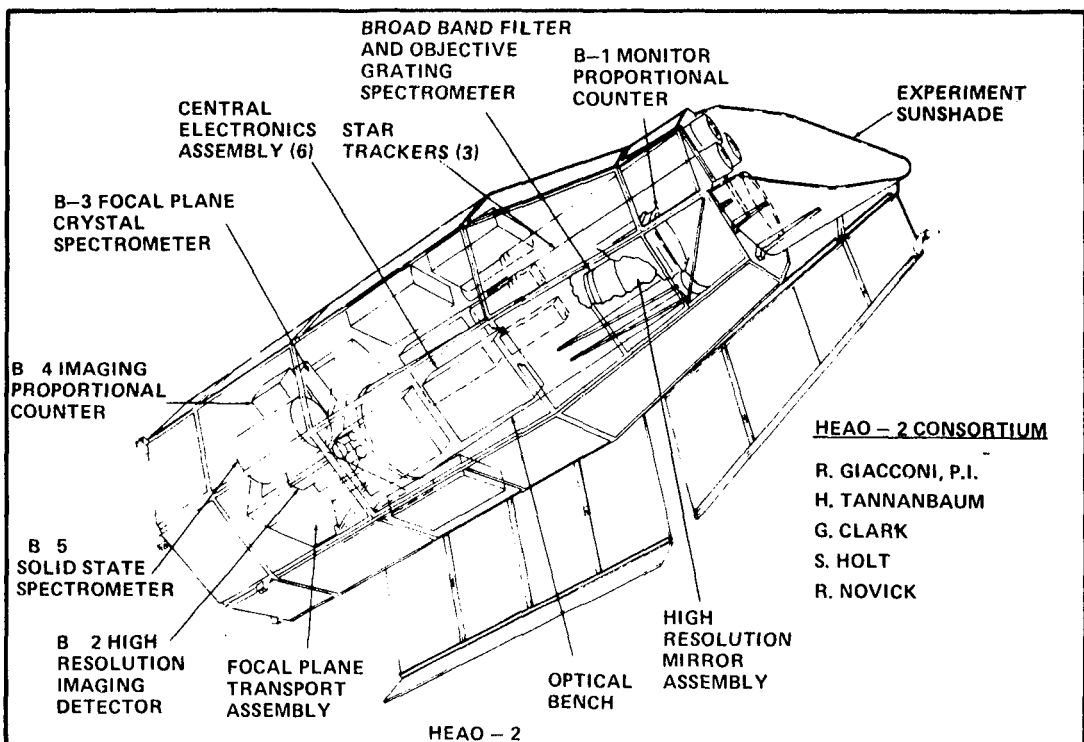
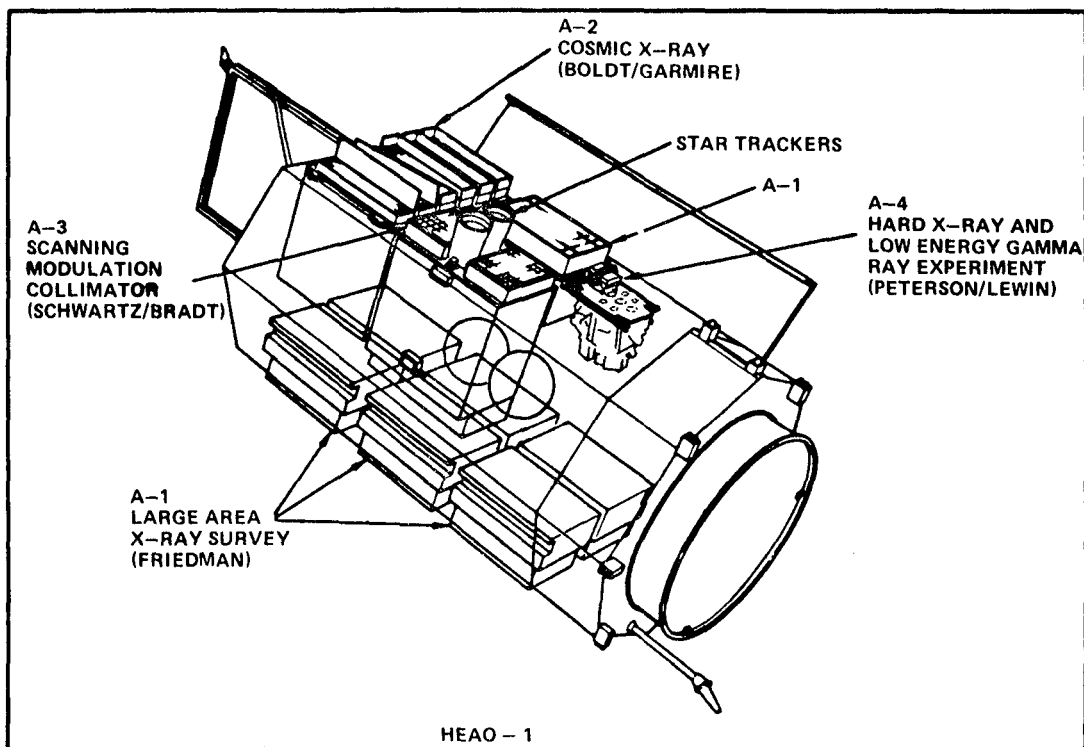
	Page
SESSION III — RESULTS FROM HEAO-2 NON-IMAGING INSTRUMENTS .....	261
A HIGH ENERGY ASTRONOMY OVERVIEW .....	262
NONDISPERSIVE SPECTROSCOPY OF CELESTIAL X-RAY SOURCES .....	292
HIGH RESOLUTION X-RAY SPECTROSCOPY ON THE EINSTEIN OBSERVATORY .....	329
MONITOR PROPORTIONAL COUNTER .....	347
SESSION IV — RESULTS FROM HEAO-2 IMAGING INSTRUMENTS .....	367
EINSTEIN OBSERVATIONS OF EXTENDED GALACTIC X-RAY SOURCES .....	368
EINSTEIN OBSERVATIONS OF ACTIVE GALAXIES AND QUASARS .....	390
THE STRUCTURE AND EVOLUTION OF X-RAY CLUSTERS OF GALAXIES .....	409
COLUMBIA/EINSTEIN OBSERVATIONS OF GALACTIC X-RAY SOURCES .....	422
COLUMBIA/EINSTEIN OBSERVATIONS OF EXTRAGALACTIC X-RAY SOURCES.....	439





# TABLE OF CONTENTS

	Page
INTRODUCTION .....	1
WELCOMING ADDRESS .....	2
SESSION I — RESULTS FROM HEAO-1 PRINCIPAL INVESTIGATOR PROGRAMS.....	5
HEAO-1 OVERVIEW .....	6
X-RAY VARIABILITY OBSERVED WITH HEAO A-1 .....	10
PROGRESS OF THE HEAO A-1 CATALOG .....	30
THE SCIENTIFIC RESULTS OF THE LOW ENERGY PORTION OF A-2 .....	49
HEAO A-2 EXTRAGALACTIC RESULTS.....	82
A-3 SCIENTIFIC RESULTS .....	101
A-3 SCIENTIFIC RESULTS — EXTRAGALACTIC.....	114
HIGH ENERGY X-RAY RESULTS FROM HEAO-1: X-RAY PULSARS, AND THE ALL SKY SURVEY .....	140
A-4 SCIENTIFIC RESULTS .....	166
SESSION II — RESULTS FROM HEAO-1 GUEST OBSERVER PROGRAM .....	195
HEAO-1 GUEST INVESTIGATOR PROGRAM.....	196
X-RAY EMISSION FROM THE REGION OF $\gamma$ 195+5.....	201
DIFFUSE X-RAY EMISSION FROM ABELL CLUSTERS .....	209
CORRELATED GROUND BASED OBSERVATIONS IN SUPPORT OF THE HEAO-1 X-RAY OBSERVATORY.....	214
THE HEAO-1 NEUTRON STAR TIMING EXPERIMENT.....	223
X-RAY IRON-LINE EMISSION FROM THE SN 185 REMNANT .....	244
OPTICAL IDENTIFICATION AND SPECTROSCOPY OF X-RAY SOURCES PRECISELY POSITIONED WITH A-3 .....	251





## INTRODUCTION

This document contains the presentations made at the HEAO Science Symposium held at MSFC on May 8 and 9. The scientific results are from the early analysis of data from the entire HEAO-1 mission, which terminated January 9, 1979, and the first half year of HEAO-2 operation.

The material is based on transcribed recordings of the oral presentations. In several instances however, speakers have elected to submit new or substantially revised papers for inclusion in the document. Some have supplied bibliographies or references. To preserve the scientific integrity of the presentations, editing has been limited primarily to that required to make them compatible with a document format.

The speakers and their organizations are listed below. The HEAO Project Office wishes to thank these and other members of the HEAO scientific team for their contributions to the symposium.

Dr. Frank McDonald	Goddard Space Flight Center
Dr. Herbert Friedman	Naval Research Laboratory
Dr. Kent Wood	Naval Research Laboratory
Dr. Gordon Garmire	California Institute of Technology
Dr. Elihu Boldt	Goddard Space Flight Center
Dr. Roger Doxsey	Massachusetts Institute of Technology
Dr. Daniel Schwartz	Harvard/Smithsonian Astrophysical Observatory
Dr. Alan Levine	Massachusetts Institute of Technology
Dr. James Matteson	University of California, San Diego
Dr. Gerald Fishman	Marshall Space Flight Center
Dr. Richard Lamb	Iowa State University
Dr. Melvin Ulmer	Northwestern University
Dr. Stuart Mufson	Indiana University
Dr. Fred Lamb	University of Illinois
Dr. Frank Winkler	Middlebury College
Dr. Richard Griffiths	Harvard/Smithsonian Astrophysical Observatory
Dr. Riccardo Giacconi	Harvard/Smithsonian Astrophysical Observatory
Dr. Stephen Holt	Goddard Space Flight Center
Dr. George Clark	Massachusetts Institute of Technology
Dr. Martin Weisskopf	Marshall Space Flight Center
Dr. Fred Seward	Harvard/Smithsonian Astrophysical Observatory
Dr. Ethan Schreier	Harvard/Smithsonian Astrophysical Observatory
Dr. Christine Jones	Harvard/Smithsonian Astrophysical Observatory
Dr. Knox Long	Columbia Astrophysical Laboratory
Dr. William Ku	Columbia Astrophysical Laboratory

In addition, the Project Office wishes to thank the following session chairmen:

Session I — Dr. Martin Weisskopf	MSFC
Session II — Dr. Gerald Fishman	MSFC
Session III — Dr. Thomas Parnell	MSFC
Session IV — Dr. Charles O'Dell	MSFC

## WELCOMING ADDRESS

Dr. W. R. Lucas  
Director, Marshall Space Flight Center

It is my pleasure to welcome this group to one of the proud events in the 20-year history of the Marshall Space Flight Center. This is the bottom line of space science, the determination and spreading of new knowledge. When the HEAO program began, we could hardly imagine the startling results that have been found and that will be discussed in this symposium.

How fascinating the universe is today. Yesterday's picture of a slowly expanding universe, filled with unchanging galaxies and gracefully aging stars, has given way to a new picture. This new picture has carried our understanding back to the first impulse of the big bang and has shown that even the most quiescent galaxies have the property of activity. We now know that stars do not simply go out with a whimper. Instead, they go out with a bang; and, even then, that is when the action really begins in at least a few of them.

It is appropriate that this gathering is being held on the centennial of the birth of Albert Einstein, that scientific revolutionary and scholar. A superb intellect, who was also born at the right time, he left an indelible mark on science and the world through his achievements and imagination. But today's picture of the universe goes beyond even those horizons foreseen by Einstein. Discovery has always been part of the truly scientific enterprise, and the last two decades have seen quantum jumps in our knowledge; with the tools now at hand in space, we are only at the beginning.

We are gathered here to learn about the new results from the first true observatories in the brief history of high energy astronomy. It is hardly surprising that fascinating and violent astronomical objects are now being found, because it takes conditions difficult and even impossible to produce here on the Earth to generate sufficient amounts of X and gamma radiation to be detected at large distances.

Of course, the detections must first be made and therein lies the challenge. It took strong scientific foundations and intuition, engineering skill and imagination, and leadership and cooperation to bring the High Energy Astronomy Observatories into reality. It took the commitment of scientists who were willing to devote a major part of their professional lives to becoming part of an enormous team. It took program leaders who could recognize the appropriate path for development of this new discipline and who had the tenacity to stay with that goal. It also took engineers and managers both within NASA and industry who could

enthusiastically take up the challenge of not only building something unique, but doing it simpler and cheaper than had ever been done. The fact that we are gathered here this morning is evidence that these challenges were met.

Permit me a moment of pride on behalf of those people that are the Marshall Space Flight Center, many of whom are in the audience. Our involvement with the HEAO program goes back more than a decade to when the astronomy missions board first identified and supported the concept that became HEAO. Although this was a body of largely non-NASA scientists and we were a center most noted for the development of large rockets, our imagination was fired by the challenge and we made it clear that our experience could also be brought to bear on this kind of development. Though several difficulties were met on the way, the challenge of developing a low-cost, multiple-use observatory was accepted and met. The design life of six months for HEAO-1 was extended to 17 months, and there is the reasonable expectation after the first 6 months of its operation that the HEAO-2 will exceed its original mission life of 12 months. All this with almost 100 percent scientific success and at a lower cost per pound than any other NASA automated spacecraft.

One member of the Marshall team is not here to share this success. James A. Power, who managed the HEAO-2 telescope effort during some of its most crucial periods of development, was killed in an aircraft crash traveling to an HEAO meeting. Many others gathered here have shared Jim's dedication to the success of the HEAO program and respectfully attribute to his efforts a substantial contribution to that success which we now recognize.

It would be presumptuous of me to try to speak for the scientists here today or to evaluate their work, but I believe that all of us will be surprised and pleased with the scientific productivity of HEAO 1 and 2.

I opened my greetings by remarking on how interesting the universe is today. I believe that the magnificence of the universe is now becoming much more apparent through the results from the High Energy Astronomy Observatories which you will be discussing today and tomorrow and in the months ahead. I wish for you very rewarding hours of discussion and deliberation.

Now, I would like to present the first session chairman, Dr. Martin Weisskopf, MSFC.





## SESSION I

### RESULTS FROM HEAO-1 PRINCIPAL INVESTIGATOR PROGRAMS

## HEAO-1 OVERVIEW

Frank McDonald  
Goddard Space Flight Center

I am going to leave the scientific overview for the experimenters themselves; I thought I would make a very few brief remarks. It has been almost 21 months since the launch of HEAO-1. It has been a little over 10 years since we began the serious work here with Marshall planning the HEAO program. From our standpoint, it was in many respects a dramatic one. We started with two large super observatories, 25,000 lb range or 12,000 kg. For a variety of reasons, these were restructured into two much smaller observatories and there was the addition of the grazing incidence telescope for a third mission. What emerged first was the HEAO-1, which as Dr. Lucas pointed out, was the largest unmanned scientific observatory that the U.S. has launched. The restructured program contains four highly integrated complementary experiments for the HEAO-1 mission. Their objective was to make an all sky survey to look with maximum sensitivity over as wide an energy range as possible to locate sources. There were budgetary constraints applied both by Marshall and NASA Headquarters, as well as volume and weight constraints by the Atlas Centaur.

Figure 1 presents the experiments to orient you to what you will be hearing today. It shows a view of modules of the A-1 experiment with 1 module on one side and 6 modules on the other side. This was the experiment to do an all sky survey with great sensitivity. The A-2 experiment was primarily to look at the diffuse x-ray background and to provide very precise spectral measurements over a range extending from roughly 150 eV to 60 keV. The A-3 experiment was to provide very accurate source locations, because if one is going to tie into the rest of astrophysics, then it is extremely important that the sources be identified with the associated astronomical object. Finally, the A-4 experiment provided the crucial extension up into the high energy range from roughly around 20 keV up to 10 MeV. As one will see, this extended energy range really complements very nicely what we will hear from the discussions of the very exciting pictures from HEAO-B.

In Figure 2, one sees how this translates into an actual spacecraft. Keep in mind that the solar panels point at the Sun, the observatory spins about that axis with the solar panels themselves always pointed to the Sun. I think one of the remarkable features of HEAO-1 is that once it was launched, the spacecraft worked extremely well. The redundant systems that were there were essentially not needed. The gyros which had hiccuped several times prior to launch worked perfectly, and I think the spacecraft itself really in all respects lived up to or exceeded the expectations we had for it. It was designed for six months. If the gas supply and orbit considerations had allowed, it would be alive and working over the coming years.

The experiments, as you will see, have more than met their objectives. When one writes a proposal, one has to make a list of what one is going to do and that is more or less like taking a PhD exam, or some other hurdle. But the true importance is the flexibility to do the unexpected things with these experiments. You will see ample evidence of that capability on HEAO-1 as well as HEAO-2. A very important part of what happened with HEAO-1 was that after completion of the first all-sky survey in 6 months, the observatory fortunately worked so well that the mission was extended to allow almost 3 all sky surveys.

More importantly though, with the cooperation of the project, experimenters and TRW, HEAO-1 was turned into a true observatory. Ways were found to stop the scan, point at objects; to take these very large experiments with their extended energy ranges and look at a single source. This was done literally hundreds of times and with the establishment of a timeline committee under Jim Matteson (who devoted a very large part of his time) targets were selected by the experimenters. Essentially, control of the observatory and responsibility for assuring the maximum utilization was fully carried out by the timeline committee. Jim set it up, the operations were then taken over by Dan Schwartz and later by Kent Woods who incorporated the guest observer program. I think it is really one way of illustrating how the experimenters and spacecraft contractors, the Project Office, and Headquarters worked together in a remarkably successful way to secure maximum scientific return from the mission.

## HEAO-A EXPERIMENTS

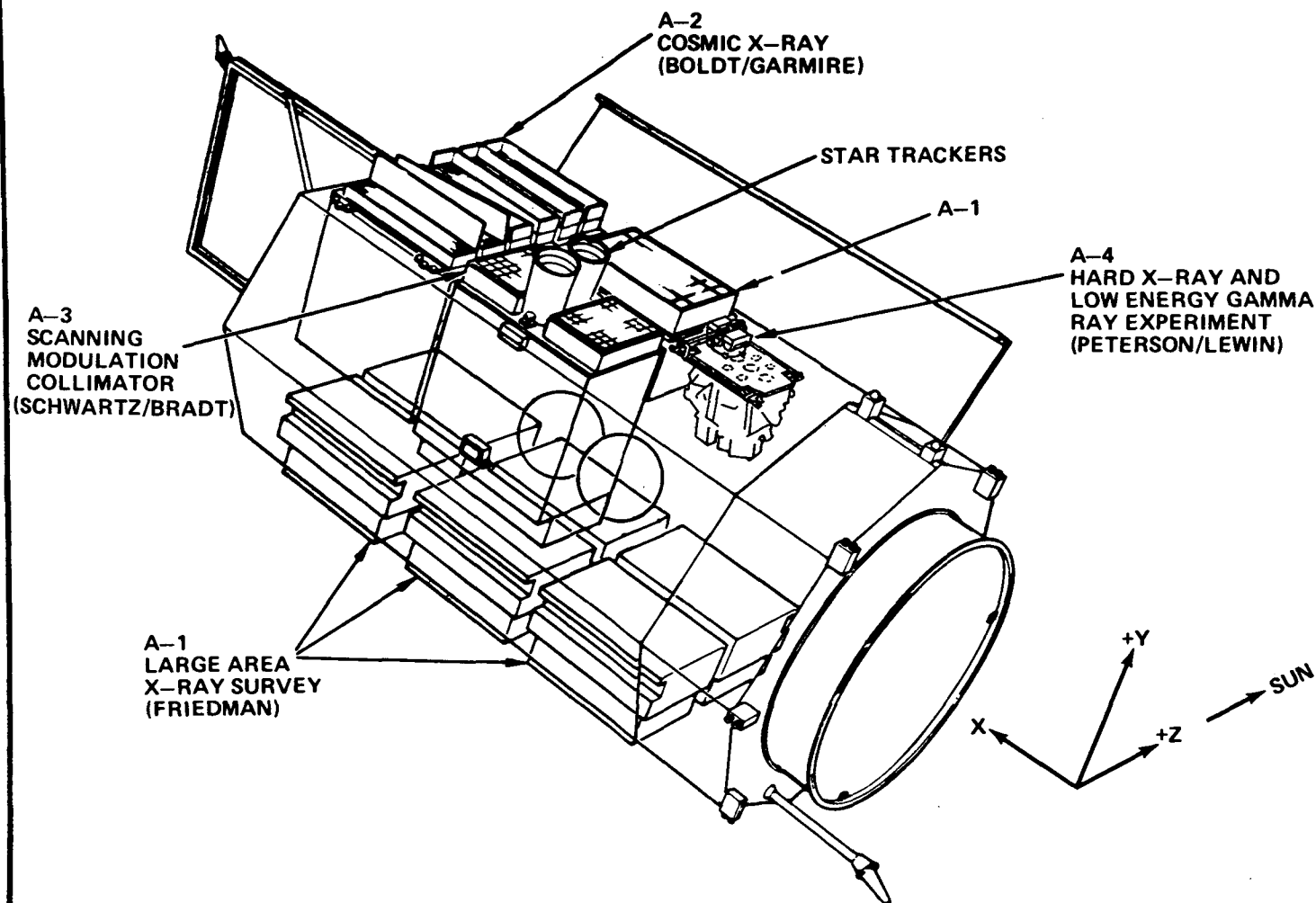


Figure 1. HEAO-A experiments.

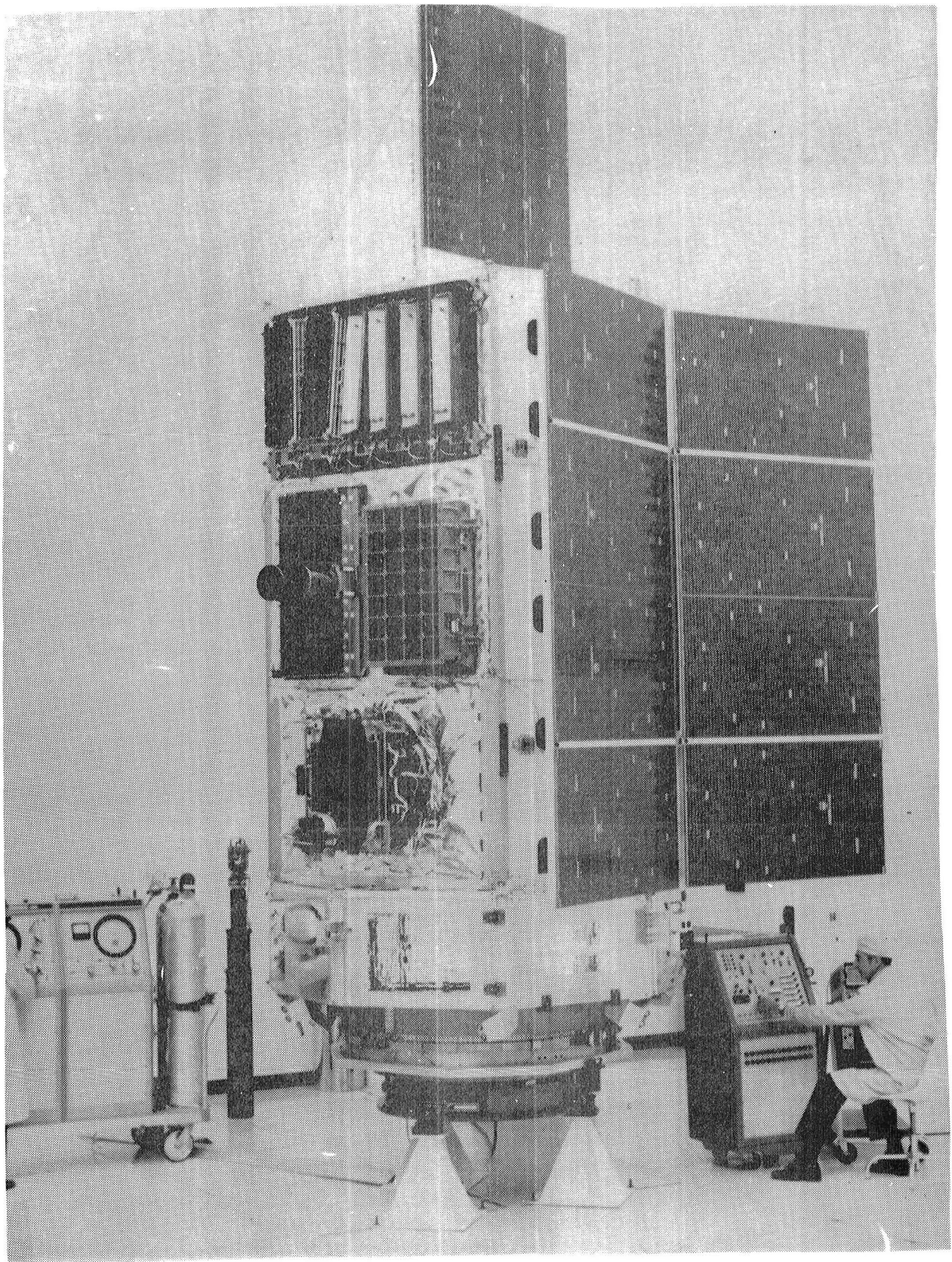


Figure 2. HEAO observatory.

## X-RAY VARIABILITY OBSERVED WITH HEAO A-1

Herbert Friedman  
Naval Research Laboratory

The A-1 instrument was designed to extend the range of temporal variability that was observed in previous missions. In Figure 1, we indicate the variety of time scales that are covered, 10 msec to 40 sec in scanning data on single scans. We could go to microsecond time scales and high bit rate data, but only when the spacecraft was over a ground station capable of receiving telemetry in real time. High ecliptic latitude objects could be scanned for many days. Repeat sequences of scan were observed at 6-month intervals, over the 17 months of the mission. We have in hand data with which to complete an all-sky survey for X-ray pulsars in the high frequency range, and we can look for the detailed features of the temporal variations of the black hole candidates. The burst sources are especially interesting because, with the large areas of the A-1 instrument, we can get better profiles than previous missions have obtained and we can search them for evidence of pulsation or other variability intrinsic to the burst itself.

I shall start with an example of evidence for longer term variation in extragalactic objects. Figure 2 shows positional data on Pks 2155-304, a radio source, believed to be a BL Lac object, and illustrates how the various experiments in the mission combined to refine the error boxes. The A-3 experiment produces the diamond-shaped arrays of potential error boxes. A-1 and A-2 can then bracket these error boxes and A-1 particularly can select the one diamond which is the true position of the source. Figure 3 is a sample of flux measurements over a period of 6 days, which shows the degree of variability on this time scale. In the region around day 316, oscillations in the flux are observed on a time scale of the order of 6 hr, implying that the size of the source is less than 6 light hr. Such dimensions are comparable to the size of the solar system. Figure 4 fits a source identified with BL Lac object 3C 371. It shows the A-2 and A-1 error boxes; the suspected source lies on the edge of the A-1 error box, which is about  $1/10$  of a square degree. Figure 5 is a sample of the flux variations, which could be followed for about 60 days, because the source is very close to the ecliptic pole. Around day 238 we see what looks like a flare lasting on the order of a day, superimposed on a rather steady decline in the flux, and then a rise again around days 273 to 280. Optically, the source is observed to vary by about 1.2 visual magnitudes; the evidence here is for similar variations in the X-ray range of the spectrum. Such observations add significantly to the information that is gained optically for these sources. By comparisons of optical information and high energy information we can develop a more detailed model of the mechanisms that are operating in these very powerful sources.

So much for samples of what can be done with extragalactic sources. If we turn to the sources within the galaxy, perhaps the most interest attaches to candidate black holes. The leading candidate for a black hole is still Cygnus X-1. Interestingly, it was one of the earliest sources picked up in rocket surveys; we observed it in 1964 and again in 1965, and found that it had changed its intensity by about a factor of four. Uhuru quickly detected the very short term variability character of the source; it produces its emission in erratic, bursting fashion. Our chairman for this session, Marty Weisskopf, has been modelling the variability characteristics of this source, and has made a very good case for describing the emission as shot noise, random bursts of emission which have a typical time characteristic on the order of a fraction of a second (0.3 to 0.5 sec).

The top profile of Figure 6 shows a transit of Cygnus X-1 through the A-1 collimator; the passage takes approximately 10 sec from one corner of the collimator triangle to the other. Below it is a similar transit of GX 339-4, which Uhuru observed as a long term variable, but which HEAO shows is almost a duplicate of Cygnus X-1 in its short term variability. And there is a third source, Circinus X-1, which also shows this type of variability. The persuasive evidence for the black hole character of Cygnus X-1 comes out of the dynamics of the binary system in which it occurs. The evidence is that the mass of the compact object, Cygnus X-1, exceeds six solar masses. In theory, if the mass exceeds three solar masses, it cannot be a neutron star; it must be a black hole. We do not have similar evidence for GX 339-4 and Circinus X-1. They are candidate black holes only because their temporal variations so closely resemble Cygnus X-1.

Figure 7 shows integral chi-squared distributions for Cyg X-1; in the 30 to 300 msec range there is a very large deviation from a Poisson distribution. The discrepancy exists all the way down to the 1 to 10 msec range. Only in the 0.3 to 3 msec range do the data fit a Poisson distribution. In Figure 8 we show the autocorrelation; the upper curve is stretched out by a large factor (the bottom scale is 1 sec, while the scale at the top is 100 msec). Toward the origin there is a strong component at around 3 to 4 msec. It appears that, in addition to the approximately 0.5 sec shot noise pattern which has been confirmed by many observers, there is an additional component around 3 to 4 msec. One can speculate about the significance of this pattern in terms of black hole models. If Cygnus X-1 is a six solar mass black hole, the material at the edge of the accretion disc at the innermost stable orbit, would be circulating the black hole with a period of 3 or 4 msec. The approximately 0.5 sec shots may be associated with turbulence over a large portion of the accretion disc. Perhaps the 3 msec component is indicative of material which is tearing off the edge of the accretion disc and falling into the black hole, surviving less than one Keplerian orbit. That is just pure speculation, but the 3 msec effect is worthy of serious theoretical interpretation.

Figure 9 is a tabular summary of the rapid fluctuations in the 3 to 4 msec range. While the total count rate is approximately 1,000 counts per second, the time average of these bursts is approximately 50 counts per second; they represent a twentieth of all the luminosity. Individually each one of these fast bursts is about as luminous as one of the longer 300 msec bursts.

Figure 10 shows samples of data from GX 339-4, three transits through the scan collimators with 40 msec bins. Wide fluctuations are evident. Over a fraction of a second there are intensity excursions of factors of three or four above average. Figure 11 shows the integral chi-squared distribution against chi-squared; the solid line represents a Poisson distribution. In the ranges from 5 to 50, 40 to 400, 80 to 800, 160 to 1600 msec, there are very wide deviations revealing the shot noise character. We do not have data at the very short time scale end of the distribution because these were taken in our 5 msec timing mode and not the high bit rate data mode. Figure 12 is an attempt to summarize what we know about the three candidate sources, Cygnus X-1, Circinus X-1, and GX 339-4. In the case of Cygnus X-1 and Circinus X-1, we have clear evidence for binary orbital periods. A bimodal characteristic of the X-ray spectrum appears in all three sources. Extended off-periods exist for Circinus X-1 and GX 339-4. The strong resemblances in these three sources suggest a common model and they will be the object of much more detailed analysis with data that are in hand from the HEAO-1 mission.

We have had a few opportunities in the mission to look at bursters with the A-1 instrument. Figure 13 shows a burst from 1728-34. The rise time of the burst reveals a great deal of fluctuation. We have tried to search the data on this source at high frequencies to see if there is any evidence for rapid periodicity or quasi-periodicity in the source. The generally accepted model for a black hole and its accretion disc is that hot spots will form in the accretion disc as differential rotation winds up magnetic fields and eventually leads to a tearing mode instability resembling a solar flare. The flare becomes a hot spot which is carried around with the spin of the disc and because of gravitational focussing and doppler effects, the signal is likely to be strongly modulated. If the hot spot can survive several rotations, we should see the periodicity of the Keplerian motion; if it can not survive a few rotations, no periodicity will be observed. If it survives long enough, we might even observe the drift of the material as it spirals inward toward the black hole with decreasing Keplerian period. The evidence for 1728-34 has been very tantalizing. Although the statistical evidence is marginal, there appears to be a periodicity around 12 msec, in one strong burst. Off the burst, this source has a steady component of emission with no evidence of periodicity. Three other bursts have been observed with less statistical significance. In one of them there is a hint of pulsation closer to 10 msec, enough to make one wonder whether a black hole



model for the burster ought to be considered seriously in competition with all the evidence for bursters being neutron stars. Of course, a fast spinning accretion disk model for a neutron star burster is not excluded.

These are some samples of the kind of information that we have from the mission and what we are trying to do with the data. I would like to end with some historical comments about the program. Dr. Lucas has already mentioned how far back the effort at Marshall goes, but it goes back considerably further than that. In 1965, at a meeting of the Space Science Board at Woods Hole, Riccardo Giacconi and I were the senior scientists (I wonder what we are now), and I pushed hard for large area detectors while Riccardo pressed for a mirror. Now we have seen both these approaches accomplished in the HEAO program. Here at Huntsville, Ernst Stuhlinger was my principal contact in the late sixties, and serious plans were made to carry very large arrays of detectors on left-over Apollo hardware. With Saturn V hardware it would have been possible to put a big fence of detectors on the moon (Fig. 14) looking over a lunar horizon to observe occultations of X-ray sources at the horizon. These drawings were made here at Huntsville. Figure 15 is a sketch of how one might put 100 ft<sup>2</sup> of detector modules on the LEM, or put a large folded array that could be deployed like solar panels on the service module (Fig. 16). You all know the history of what happened to the Apollo hardware, and how the HEAO concept was taken away from the manned missions and run as an unmanned program, how it went through one drastic reduction around 1973, and how it finally came to the successful launches of HEAO-1 and HEAO-2 in the last couple of years.

## A-1 SURVEY OF X-RAY SOURCE VARIABILITY

- UTILIZE LARGE COLLECTING AREA AND WIDE RANGE OF ACCESSIBLE TIMESCALES
- 10 msec - 40 sec IN SCANNING DATA, SINGLE SCANS. LONGER TIMESCALES (UP TO 1 yr) BY COMPARING SCANS
- MICROSECOND TIMESCALES IN HIGH BIT RATE DATA
- QUASARS, BL LACERTAE, ACTIVE GALACTIC NUCLEI: 1 hr TO 1 yr
- HIGH-SENSITIVITY SEARCH FOR X-RAY PULSARS
- DETAILED STUDY OF KNOWN BLACK HOLE CANDIDATES
  - PERIODICITY SEARCH AT SHORT TIMESCALES
  - SHOT NOISE MODELING
  - SEARCH FOR SHORT DURATION SPIKES
- PERIOD FLUCTUATION STUDY IN BINARY PULSARS
- X-RAY AND GAMMA-RAY BURSTS

Figure 1

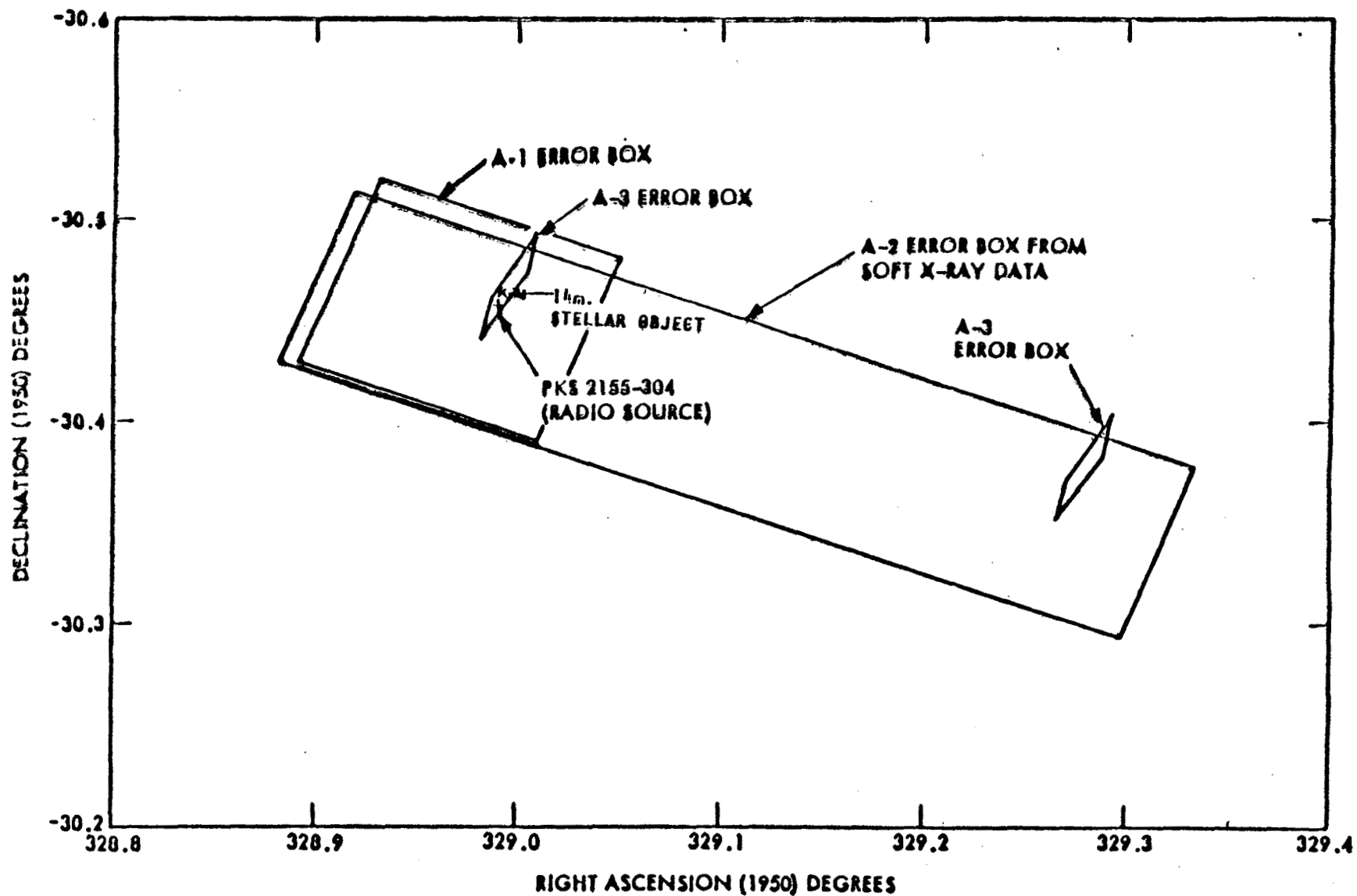


Figure 2

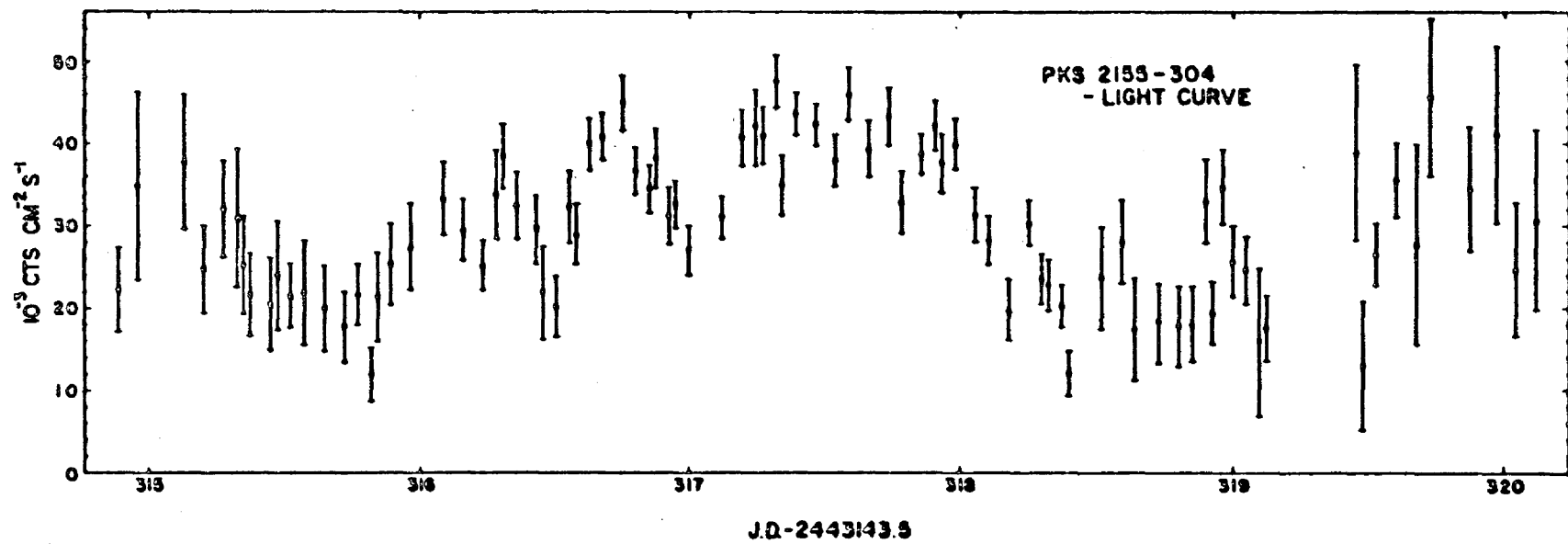


Figure 3

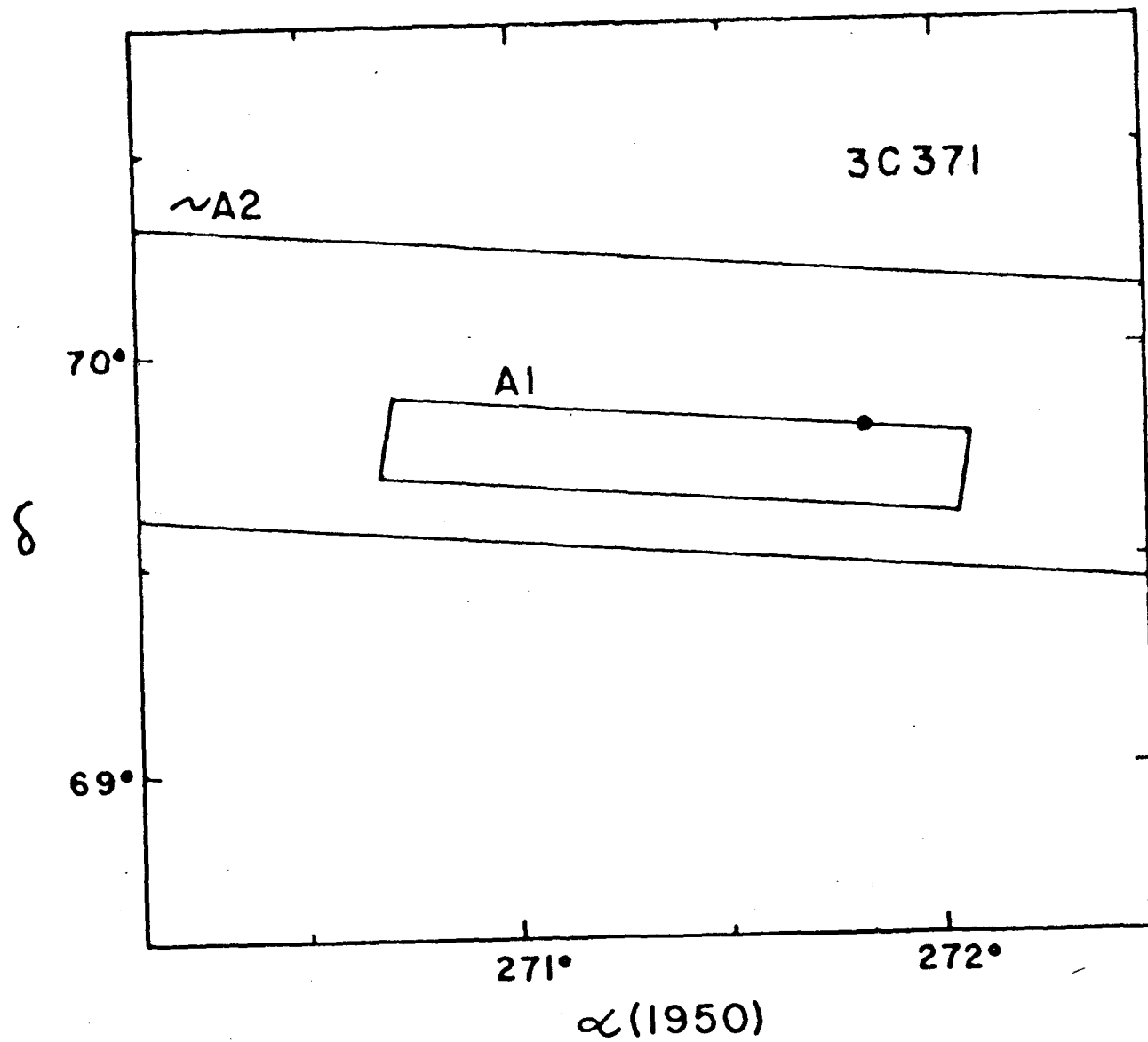


Figure 4

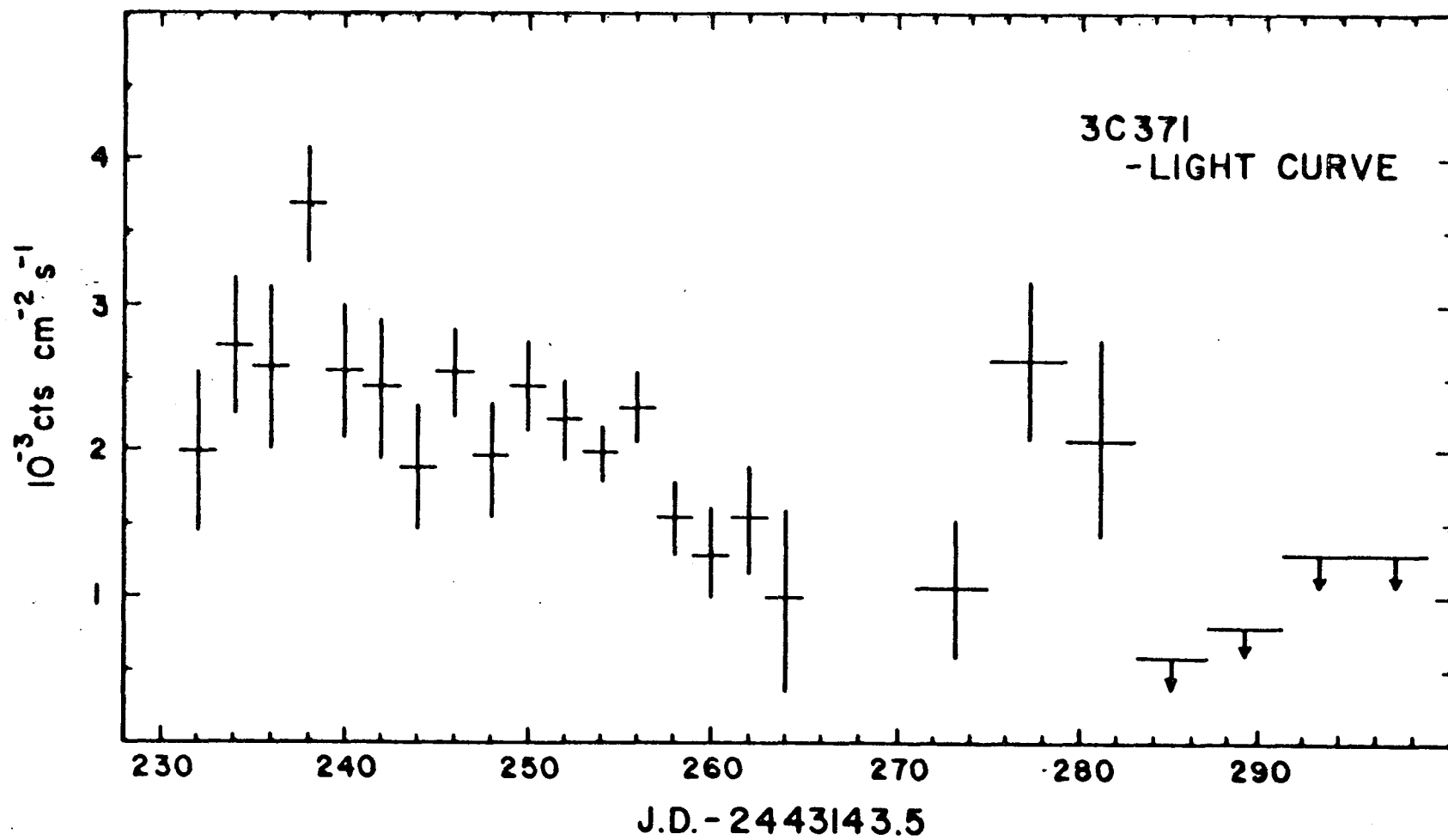


Figure 5

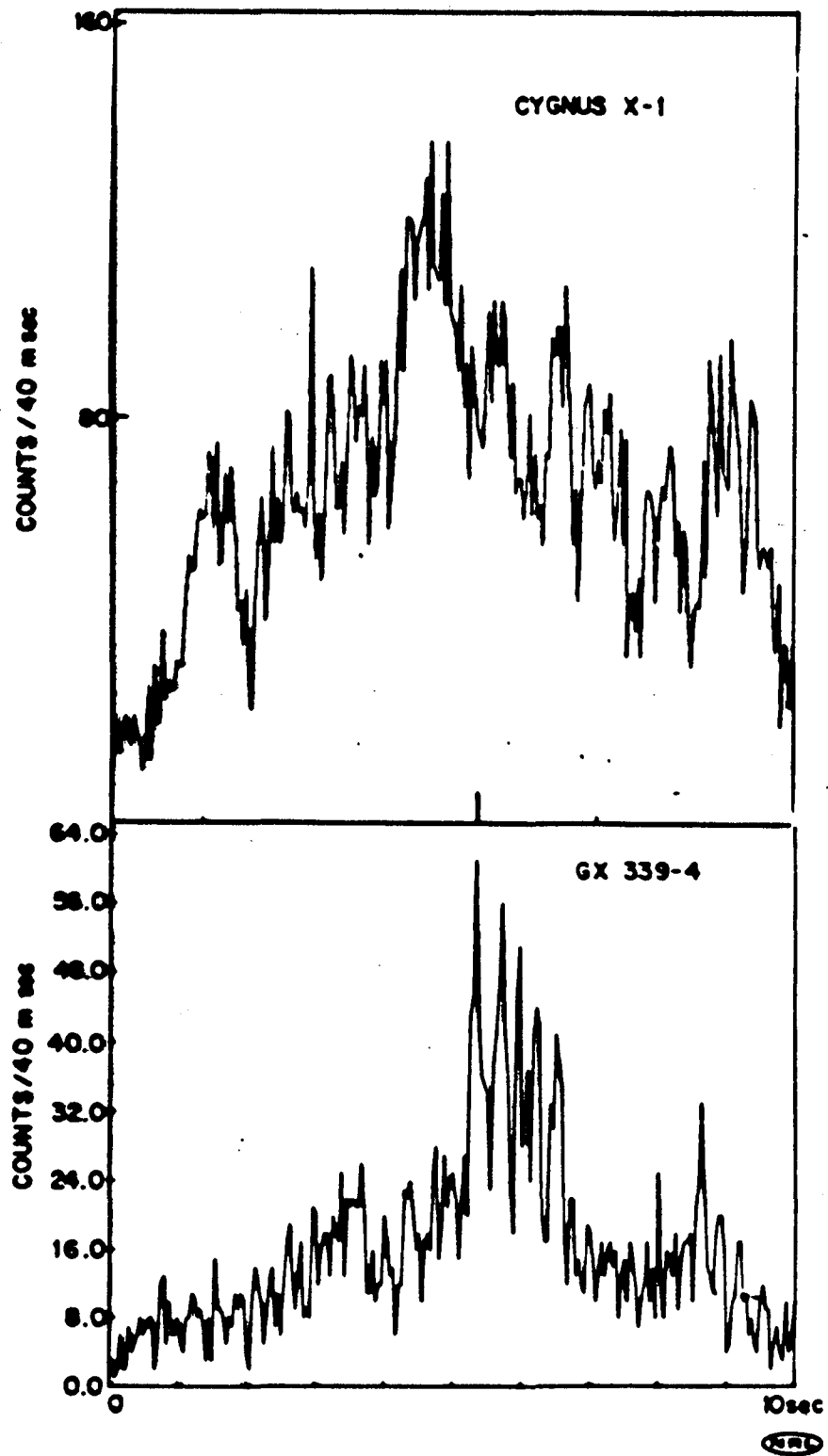


Figure 6

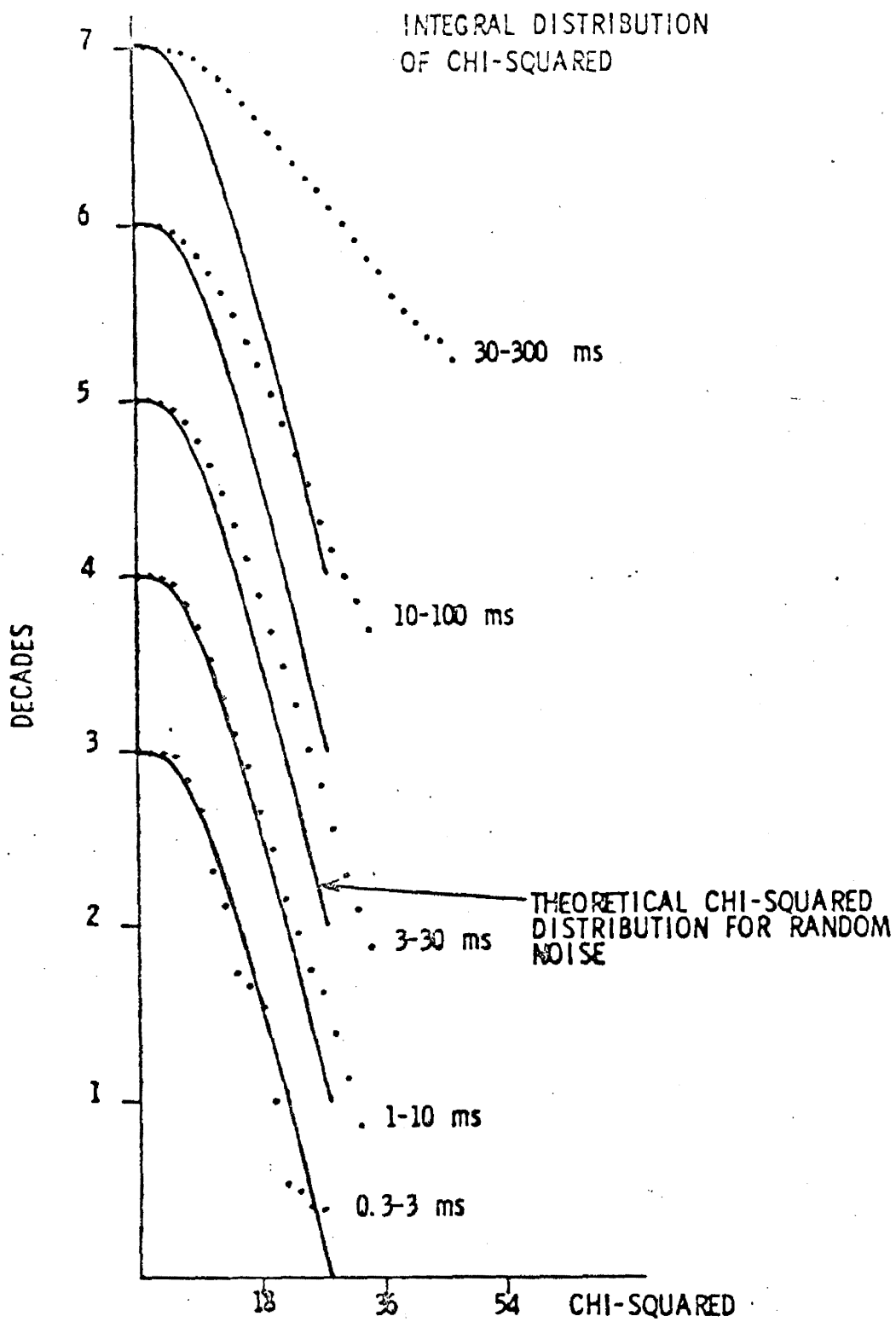


Figure 7



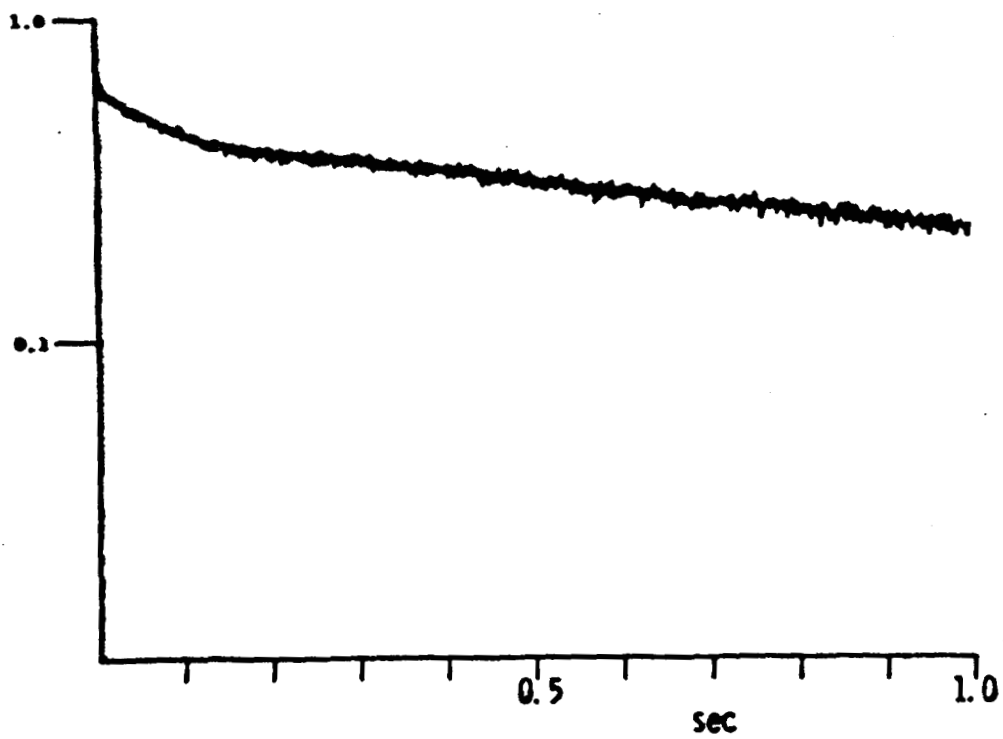
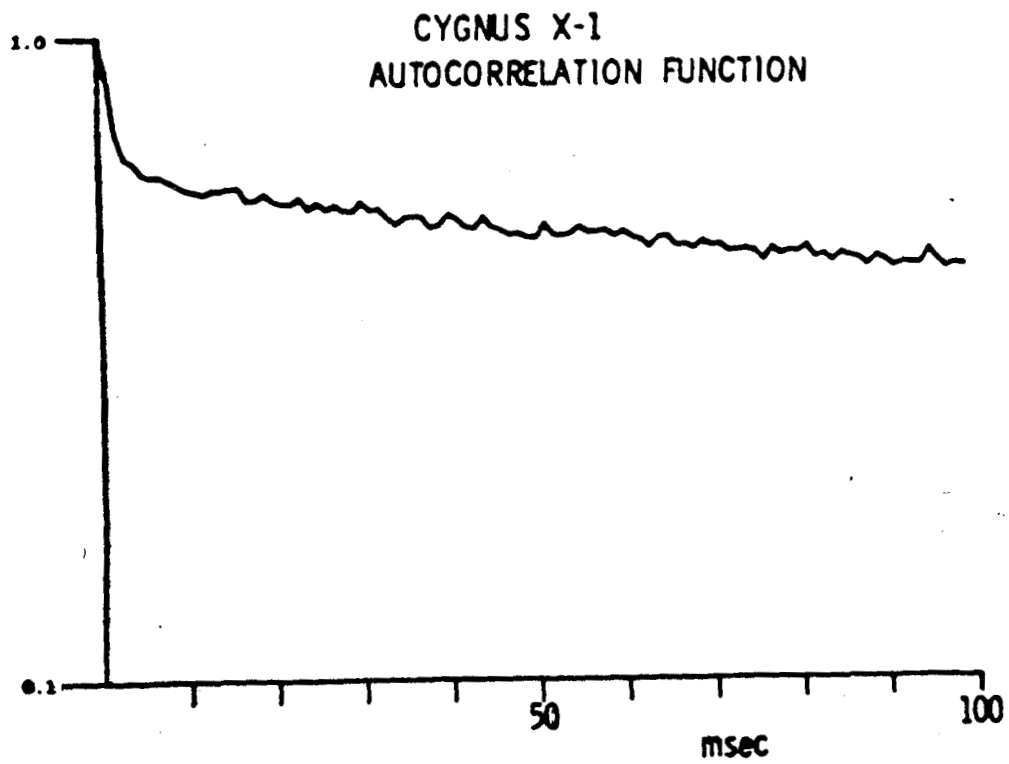


Figure 8

## CYGNUS X-1 RAPID FLUCTUATIONS

- STATISTICALLY SIGNIFICANT EXCESS OF EVENTS ON TIMESCALES 1 - 10 msec
- FREQUENT SMALL-AMPLITUDE EVENTS RATHER THAN A SMALL NUMBER OF LARGE EVENTS
- AUTOCORRELATION FUNCTION GIVES MINIMUM CHARACTERISTIC TIMESCALE: 3-4 ms

RATE OF OCCURRENCE:  $\geq 10$  EVENTS/s

	<u>EVENT</u>	<u>TIME-AVERAGE</u>
FLUX	1 ct/cm <sup>2</sup> s	$3 \times 10^{-2}$ ct/cm <sup>2</sup> s
LUMINOSITY	$10^{37}$ ergs/s	$3 \times 10^{35}$ ergs/s
COUNT RATE	1500 cts/s	50 cts/s

(TOTAL SOURCE COUNT RATE IS 1000 cts/s)

Figure 9

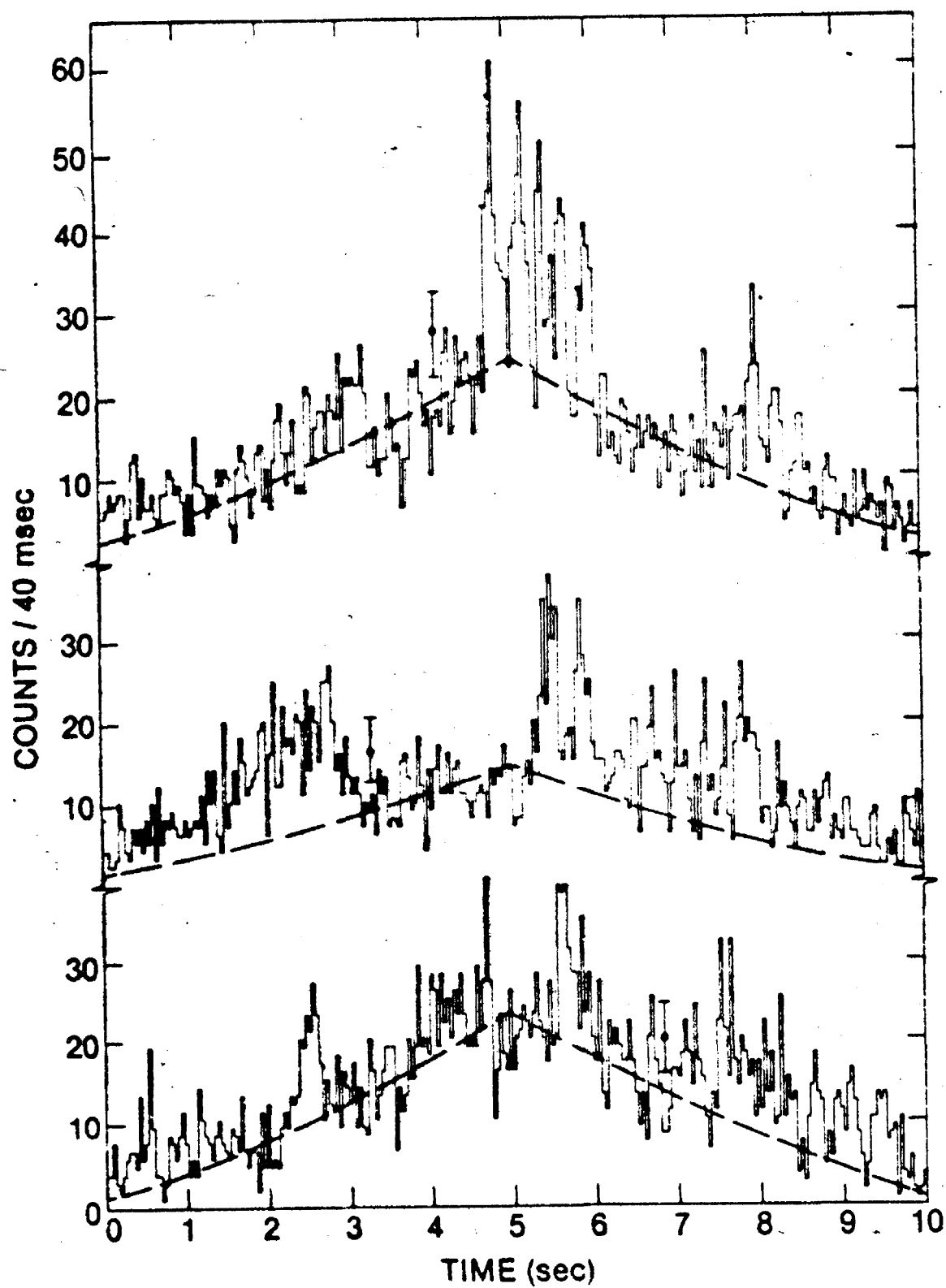


Figure 10

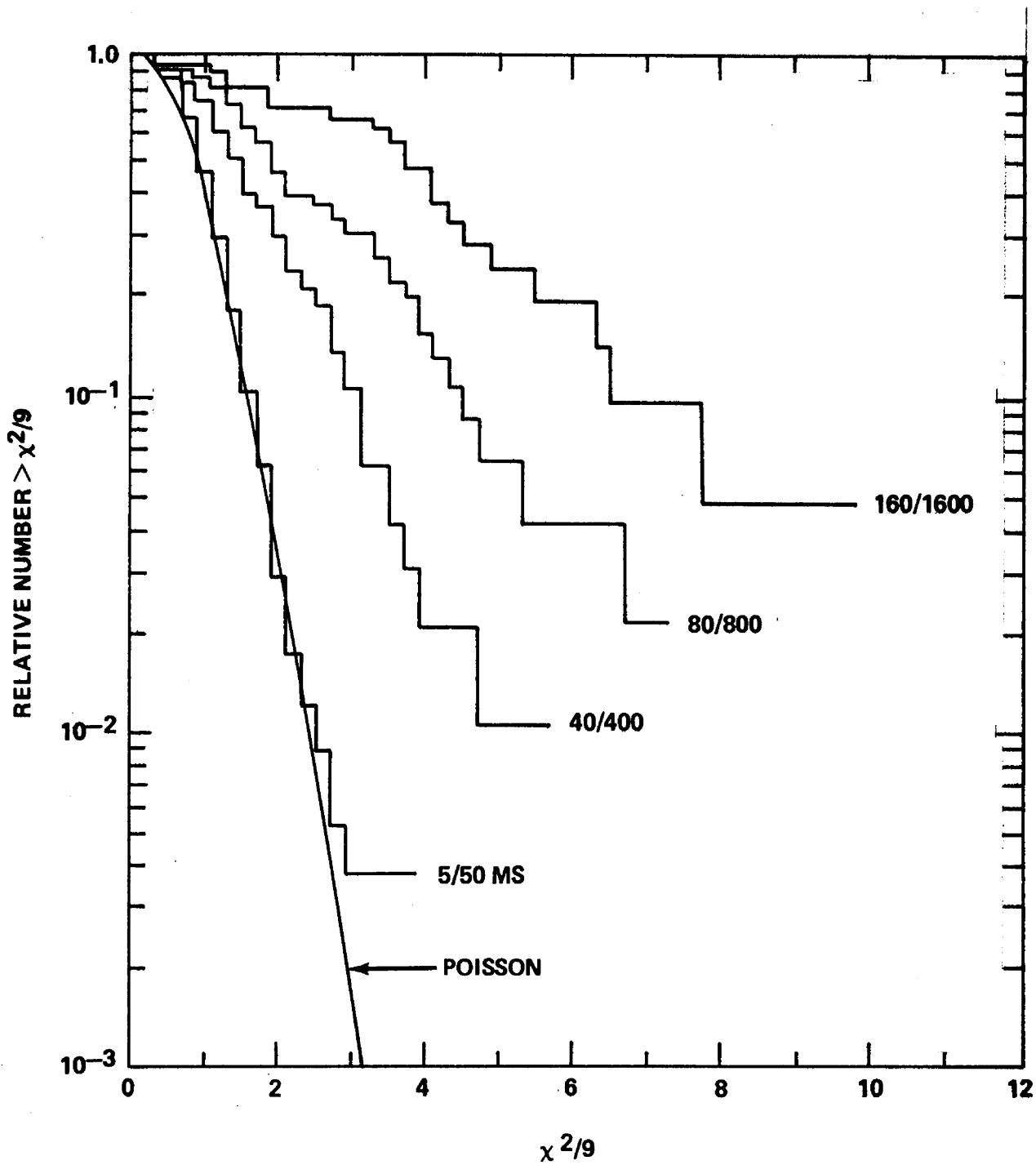


Figure 11

# CHARACTERISTICS OF BLACK HOLE CANDIDATES

	CYG X-1	CIR X-1	GX 339-4
1. VARIABILITY			
ORBITAL PERIOD	5.60 d	16.6 d	—
BIMODAL X-RAY SPECTRUM	YES	YES	YES
EXTENDED "OFF" STATES	NO	YES	YES
CORRELATION TIME	0.5 s	VARIABLE	0.3 - 0.6 s
SHORTEST TIME SCALE	$\geq 1$ ms	$\geq 1$ ms	$\geq 10$ ms
2. OPTICAL COMPANION/ EMISSION LINES	HD 226868 09.7 lab $M_V = 8.9$	FAINT HIGHLY REDDENED $m_R = 16$ STRONG He AND $H_{E1}$	$m_V = 16.6$
3. MASS FUNCTION $M_x$	0.22 $M_\odot$ $\geq 10 M_\odot$	— —	— —
4. DISTANCE	$\sim 2.5$ kpc	$\geq 8$ kpc <sup>14</sup>	$\geq 4$ kpc
5. MAXIMUM LUMINOSITY ergs/s	$\sim 2 \times 10^{37}$	$\geq 10^{38}$	$\geq 2 \times 10^{37}$
6. OTHER EMISSION	RADIO, IR	RADIO	—

Figure 12

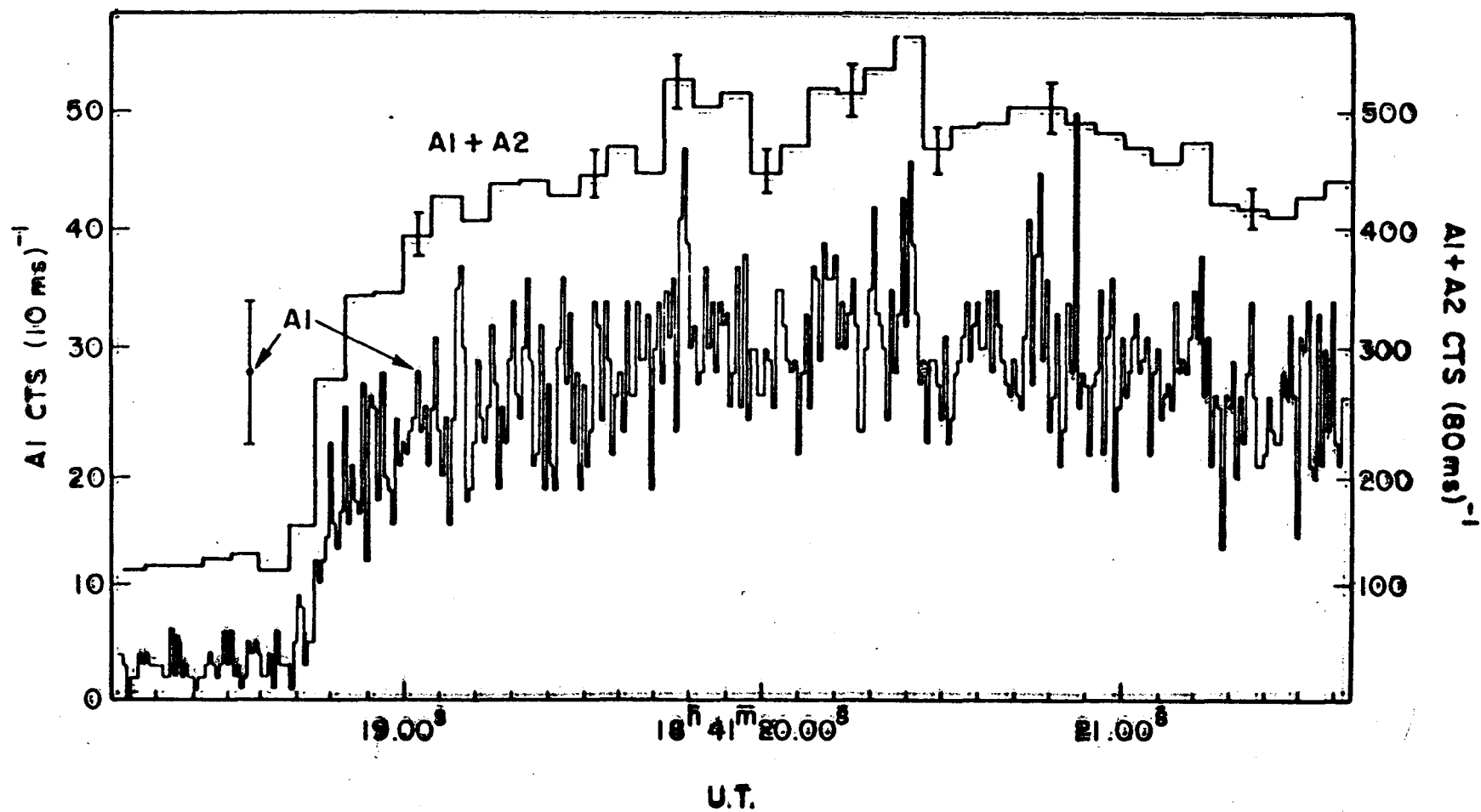


Figure 13

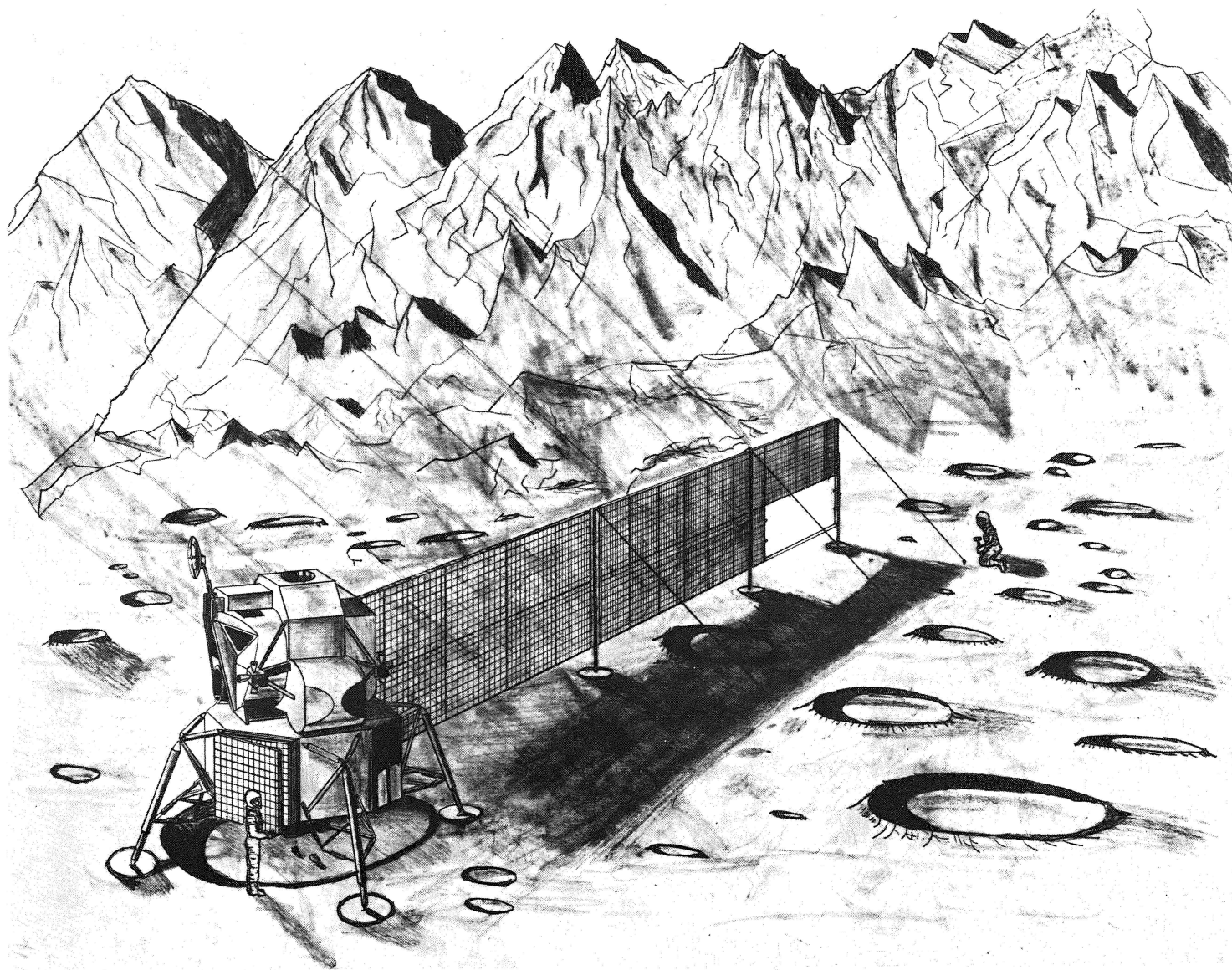


Figure 14

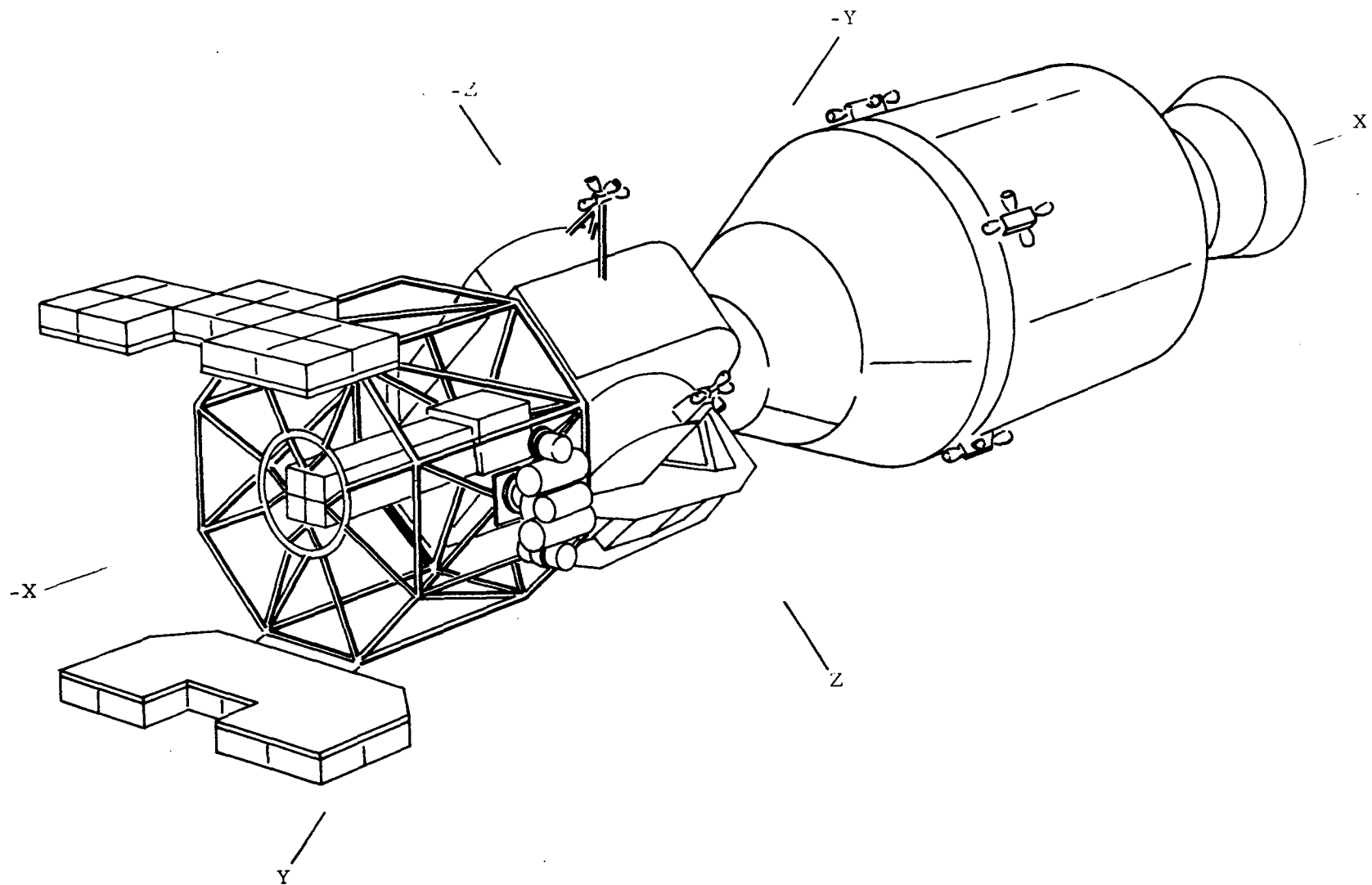


Figure 15



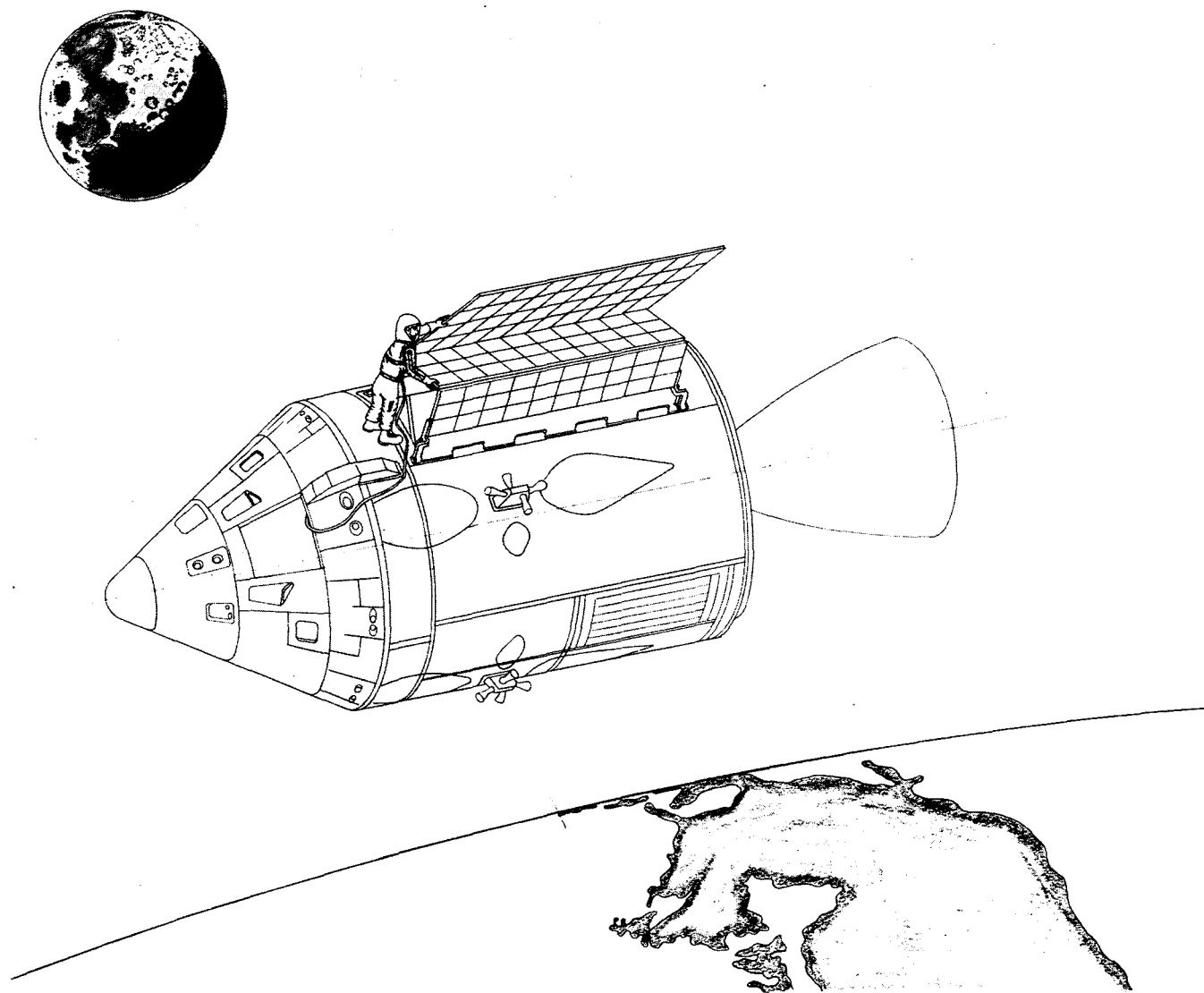


Figure 16

## PROGRESS OF THE HEAO A-1 CATALOG

Kent Wood  
Naval Research Laboratory

It is very nice to be here today at MSFC to remember HEAO-1 and celebrate the successful launch of the Einstein Observatory. I would like to extend my own personal thanks to all the Marshall people who helped make both of these missions successful. I am going to be talking about the results of HEAO A-1, the NRL Large Area Sky Survey.

As you can see from Figure 1, this was the largest of the HEAO-1 experiments and had a total effective collecting area of approximately  $1 \text{ m}^2$ . Most of it is in the six modules shown in Figure 1.

I am going to describe the A-1 catalog of X-ray sources, that is, the overall picture of the sky as it appears in X-rays. Sky mapping was (as Dr. McDonald said) one of the primary purposes of HEAO-1 and the main feature of the design. Dr. Friedman will discuss a complementary aspect of this experiment, the study of rapid variability in compact objects. Later, talks by Drs. Ulmer, Mufson, and Lamb will elaborate still further on the detailed studies of the particular classes of X-ray sources.

The A-1 all-sky survey is a second generation survey in the part of X-ray spectrum from  $1/2$  to 20 keV. The earlier surveys in this range included sounding rockets, the Uhuru satellite, Ariel 5, ANS, OSO 7, and others. By surveying systematically with large instruments such as A-1, we gain many kinds of new information. Most obviously, the larger collecting area permits us to detect many more sources resulting in about a factor of 3 increase in the total number over what is now known. The observatory scanning pattern, which is a regular progression across the sky, results in a complete coverage and a uniform overall picture. Sources which were detected at marginal significance by earlier surveys have both their positions and their intensities more precisely determined, leading to identifications with objects in other channels. It is important that this entire survey is carried out at a significantly different epoch in time from the earlier ones, so we learn something about the long term variability of the x-ray sources. Finally, there are some changes in the picture of the classes of objects observed. This happens several ways. First, some of the classes which were previously represented by only one or two members become enlarged as we find fainter sources. Finding more members of a group, clarifies characteristics of the population. Second, by surveying to lower flux levels, it turns out, because of geometrical effects, that the balance between sources at low and higher galactic latitudes shifts in favor of the latter. We tend to find more sources away from our own galactic plane, and many of these are extragalactic.

Figure 2 summarizes the history of HEAO A-1. Also listed are a few of the basic parameters of the instrument. There were seven modules with three different fields of view. The goal for the A-1 catalog was to survey the sky to about one-tenth of a Uhuru flux unit, leading to detection of about 1000 sources. The total accumulated exposure during the mission; that is, area times time on each region of the sky, equaled or exceeded our original goal over more than 95 percent of the sky. Figure 3 shows several large adjacent strips of the sky as they appear after summation of scans. We sum up many scans over the same region of the sky. This is a rather remarkable display in that one can see on the single figure about 125 different sources from one-ninth of the sky just as they appear in the data. About half of these are sources which were not previously known. The ones identified previously provide a representative mix of the x-ray emitting classes: pulsars, supernova remnants, possible black holes, transient sources, quasars, clusters of galaxies, and BL Lacertae objects. In each case, we must determine why this particular kind of object should be producing high energy photons.

Except for the bright transients, the newly-detected sources are primarily the fainter ones. The first task for all the new objects and for many of the old ones as well is to position them well enough to permit identification with known optical or radio objects. Past experience shows that to obtain an identification for an object which is a star in our galaxy, one needs very precise position such as is obtained by the A-3 instrument or the Einstein Observatory. For extragalactic objects, an error box of one square degree has usually been sufficient. One makes identification in this instance on the statistical basis that it is unlikely to find an intrinsically rare object in the error box by chance. The majority of the identifications made in this manner have withstood the test of time, which means that the statistical method is sound. The first cataloging task is thus to derive the error boxes for unidentified sources seen in the A-1 data. This is done by fitting the instrument's collimator response to the data. For a steady point source, the expected response will be triangular in two directions, along the scan and perpendicular to it. If the source is precisely constant over time, we apply this strategy to derive its coordinates in both directions in a two-stage fitting process. If the source is to some extent variable, the variability can influence the fit. That is, by making the invalid assumption that the source is constant, one derives a slightly erroneous position for it. In practice, this does not constitute any serious problem for fitting in the direction of the scan; most sources do not vary measurably during the 10 sec they take to pass through the field of view. (Dr. Friedman will be talking about some exceptions.) Even those which do vary on short time scales will almost always give a satisfactory approximation to the collimator response when many scans are averaged together.

The second stage of the fitting process makes use of the fact that the observatory spin axis advances by one degree per day, always remaining in the ecliptic plane. This causes the source to move slowly through the field of view (typically over a period of 8-10 days), with the apparent daily intensity rising and falling according to the collimator response. Figure 4 represents the geometry of this process. The figure is drawn in galactic coordinates and shows the ecliptic plane and three representative scan paths. The scans are perpendicular to the ecliptic plane where they intersect it. The dark arrows show the direction of the daily advance of the scan plane. In the direction of the advancing scan plane (ecliptic longitude) source variability on a timescale of a few days can affect the fit adversely. This situation is common enough to be of some cause for concern. There is a simple procedure for meeting the difficulty. We carry out the second stage of our fitting under two distinct sets of assumptions. First, we assume that the source is possibly variable. Secondly, we assume that it is constant. The first type of fit treats each day's sighting as yielding a truncated line of possible positions on the sky where the source might be, and these lines of position taken together can then be used to derive an error box and mean source intensity. The second type of fit explicitly assumes source constancy and uses the additional information provided by daily apparent intensities to refine the error box. The box derived in this way will be smaller.

Figure 5 shows the daily variations of source intensity as the sources pass through the field of view. At scan azimuth  $15^\circ$ , we have an instance of a rather faint new source (identified with the distant cluster Abell 2163) which enters and leaves the field of view in a pattern consistent with a constant source. As an extreme alternative, Hercules X-1 is at scan azimuth  $57^\circ$ . It had moved halfway through the field of view when it precipitously turned on.

Figure 6 shows sky coverage for the portion of the sky that we have mapped to date. Figure 7 displays (on the same galactic coordinate grid as Fig. 6) the available source fits thus far performed. We have arbitrarily cut this off at a minimum intensity of four-tenths of an Uhuru flux unit. It represents the first 70 days of the HEAO-1 mission, or about one-third of the sky. The large blank regions common to Figures 6 and 7 represent the two-thirds of the sky where fitting has yet to be performed. In Figure 7, the size of the octagon representing a source is proportional to the logarithm of its measured flux. The brightest source in the sky, Sco X-1, appears slightly above the center. The faintest ones are more than  $10^4$  fainter. Figure 7 shows 300 sources, and the full sky map should contain about 1000. Certain nonuniformities in the data and the fitting affect the display in Figure 7; for example there is a greater sensitivity near the ecliptic poles, where all scans converge. Nevertheless, trends representing global characteristics of the new catalog can be seen.

Figure 8 shows the number of sources as a function of their measured flux. One-half are fainter than 1 Uhuru flux unit ( $2.4 \cdot 10^{-11}$  erg cm<sup>-2</sup> s<sup>-1</sup>). 85% of the error boxes are smaller than 1 square degree.

Figures 9 and 10 show what happens when the sources in Figure 7 are subdivided into two groups according to whether they have been previously detected. (There is some arbitrariness in judging this, particularly when error boxes lie close to one another but do not actually overlap; such cases have been treated as previous detections. Figure 9, the previously-detected sample, closely resembles maps of the same regions in the Uhuru and Ariel V surveys. Most of the sources are seen again but some transients are missing. Figure 10, the new sources, shows them to be primarily at higher galactic latitudes and very faint. The lack of new sources near the plane is to some extent an artifact resulting from disposition of doubtful cases in favor of previous detection and partly from the difficulty of fitting faint sources in the highly confused regions of the plane, where our finest field of view has not yet been utilized. Thus, we expect some of this blank space to eventually fill in, but the greater density of new objects at high galactic latitudes should remain.

We are still very much in the process of making fits and identifications to the whole sky. Identifications are done primarily by computer searches at catalogs of unusual objects (quasars, seyfert galaxies, clusters, supernova remnants) which might possibly turn out to be X-ray emitters. (We do not attempt to work with catalogs of normal stars.) Dr. Ulmer will describe in detail the work done on clusters of galaxies using A-1, but I will mention here that cluster detections are plentiful. We have already found 16 new clusters (Fig. 11), including some in Abell distance class 6, which corresponds to a red shift of about 0.2. The energy range of the A-1 experiment is favorable for finding new clusters.

The BL Lacertae objects (Fig. 12) are another source class that occurs with some frequency among new identifications. The BL Lac objects are, along with some of the more active quasars, the most rapidly varying high luminosity extra galactic sources. They are almost certainly closely related to both the quasars and the various kinds of excited galaxies. They are distinguished by being notably free of evidence for matter surrounding the central nucleus, and provide the most unobstructed view of the most violent energy release encountered in nature. The rapid variability suggests a small size, which is favorable to their being X-ray emitters. Markarian 501 had been proposed as the identification for an Uhuru source positioned early in the HEAO-1 mission using a combination of A1 and A3 error boxes. The region so obtained coincided with the BL Lac object and the identification became firm. Since that time, there have been subsequent detections of BL Lacertae objects by A1, A2 and A3. Figure 12 summarizes the BL Lacertae objects seen in the large area sky survey to date.

Figure 13 compares X-ray and optical properties of the detected objects. The ratio of the flux in the two bands is not distributed over a very large range. We have also searched for, but not detected, X-ray emission from another 16 objects shown in Figure 14. For all of these, we placed 2 sigma upper limits of about 0.15 Uhuru flux units. The undetected group is fainter optically, and the explanation may very well be that we are not seeing these because their X-ray fluxes are slightly below our threshold. This concludes my survey of the progress of the HEAO A-1 catalog. I would again like to express my gratitude to the organizers of this symposium for providing the opportunity for me to be here today, and to extend my most sincere thanks to all of those who worked with the HEAO project for their contributions toward making the Large Area Sky Survey a possibility.

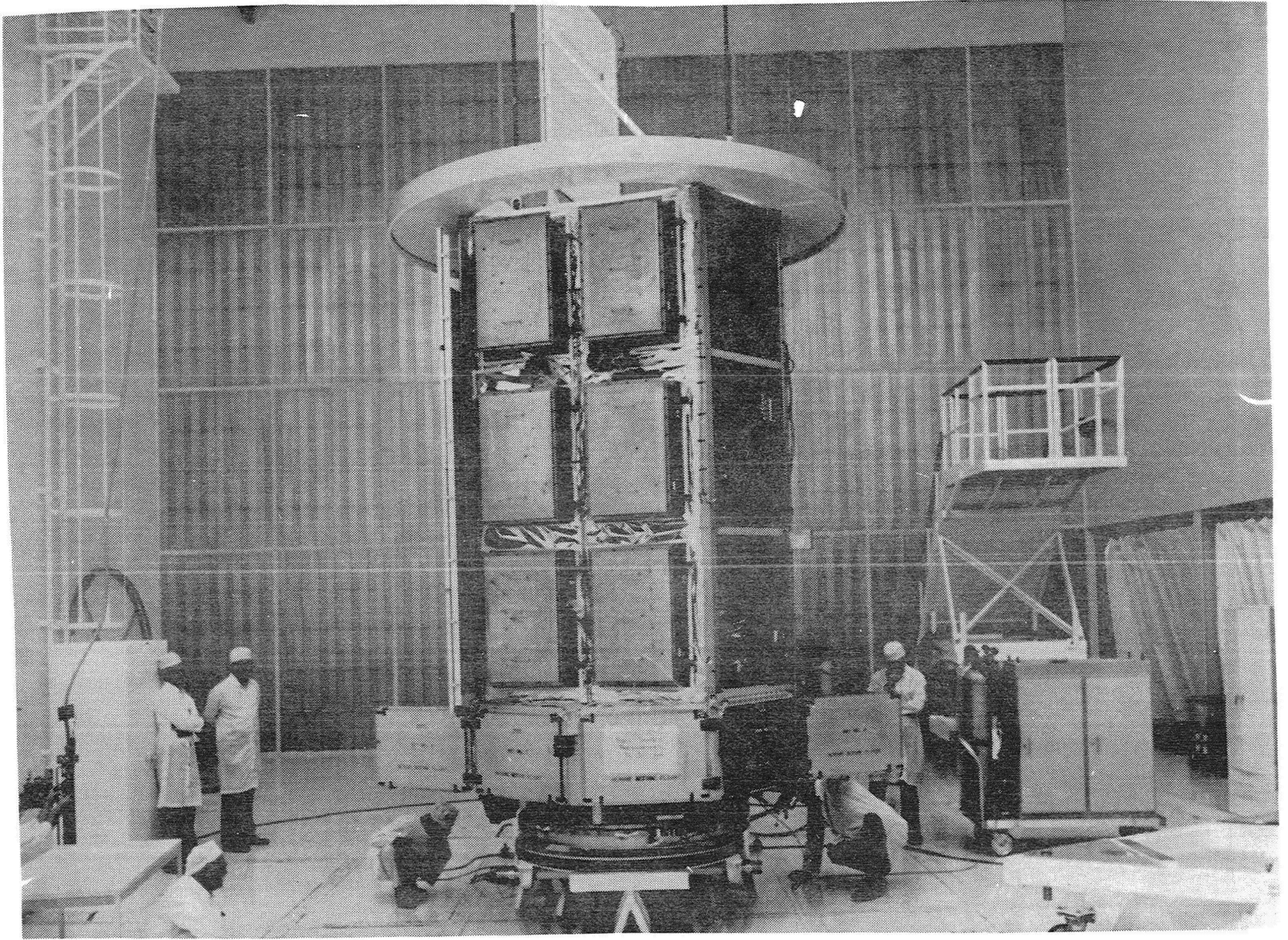


Figure 1

HEAO A-1  
LARGE AREA SKY SURVEY  
(NRL)

H. FRIEDMAN, P.I.

T.A. CHUBB, CO. P.I.

E. T. BYRAM, R. CRUDDACE, W. EVANS, R. HEDLER, W. N. JOHNSON,  
R. KINZER, D. P. McNUTT, J. MEEKINS, R. MORIN, J. SAMIMI, G.  
SHARE, S. SHULMAN, H. SMATHERS, W. SNYDER, K. WOOD, D. YENTIS

INSTRUMENTATION:

PROPORTIONAL COUNTER ARRAY (7 MODULES)

AREA (TOTAL)	:	$1.1 \text{ m}^2$
ENERGY RANGE	:	.5-20 keV
FIELDS OF VIEW	:	$1^\circ \times 4^\circ$ , $\frac{1}{2}^\circ \times 1^\circ$ , $8^\circ \times 2^\circ$

GOAL FOR CATALOG:

MAP SKY TO ABOUT 0.1 U.F.U., OR  $10^3$  SOURCES

MISSION HISTORY:

TOTAL ACCUMULATED EXPOSURE (AREA X TIME) EQUALED OR  
EXCEEDED THE ORIGINAL GOAL OVER MORE THAN 95% OF THE SKY.

Figure 2



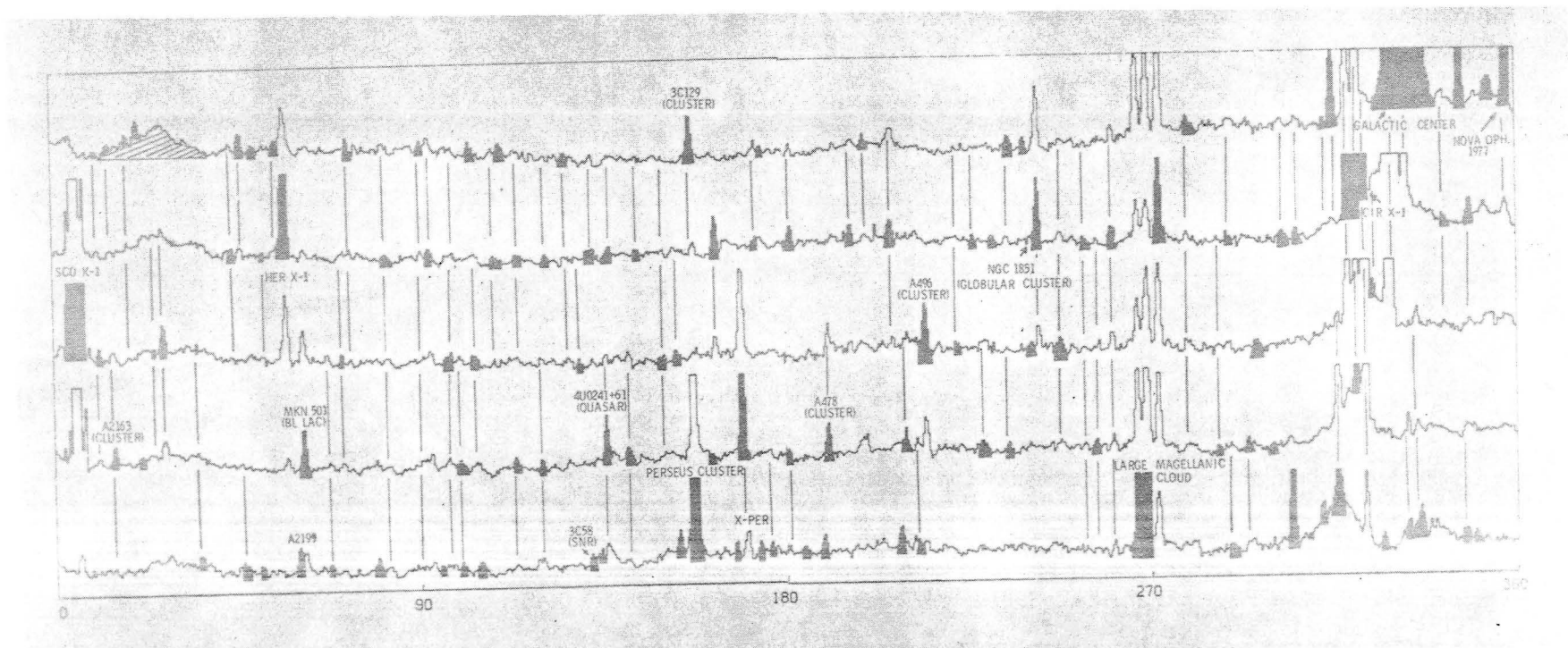


Figure 3

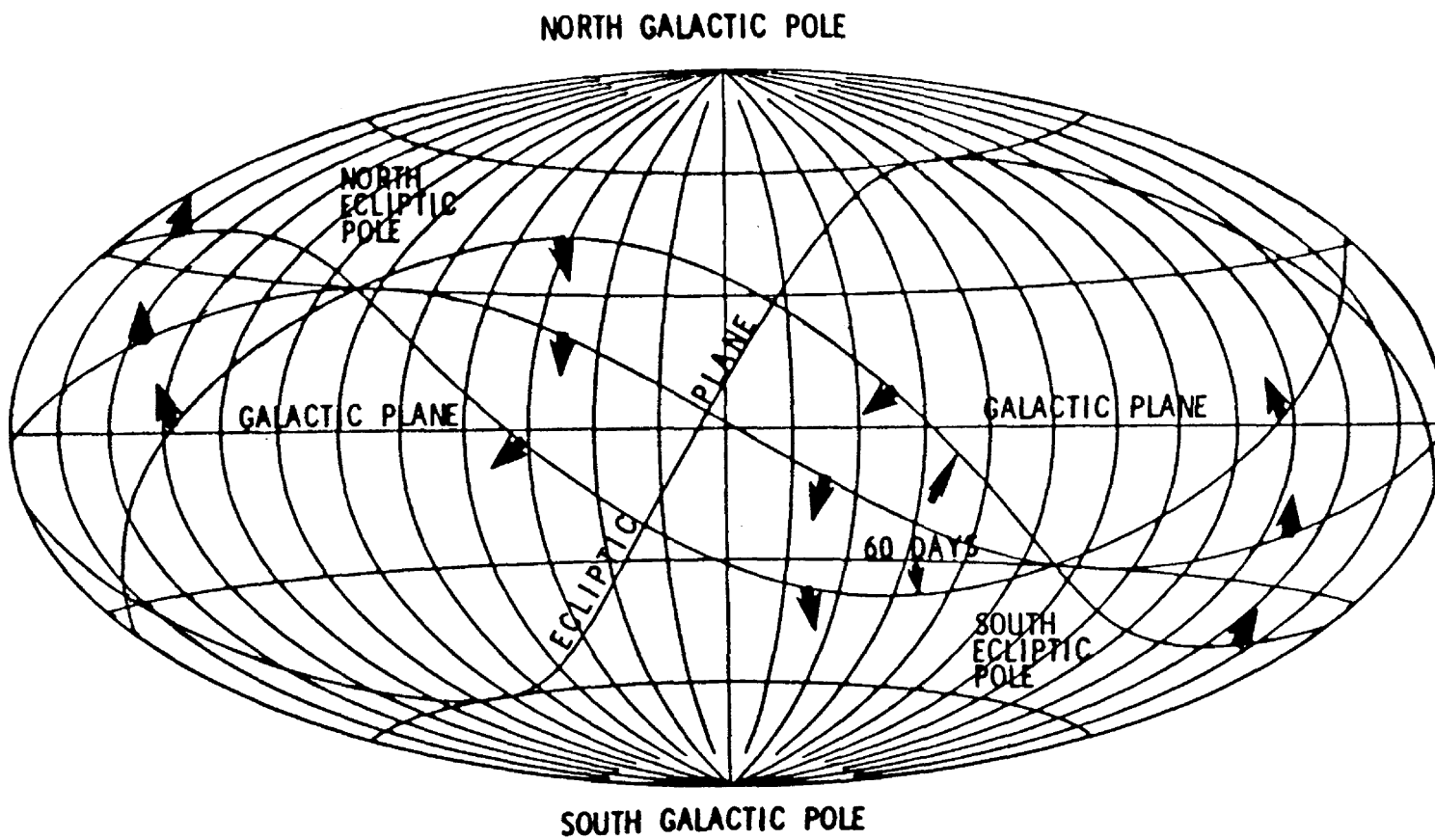


Figure 4. Scan geometry.

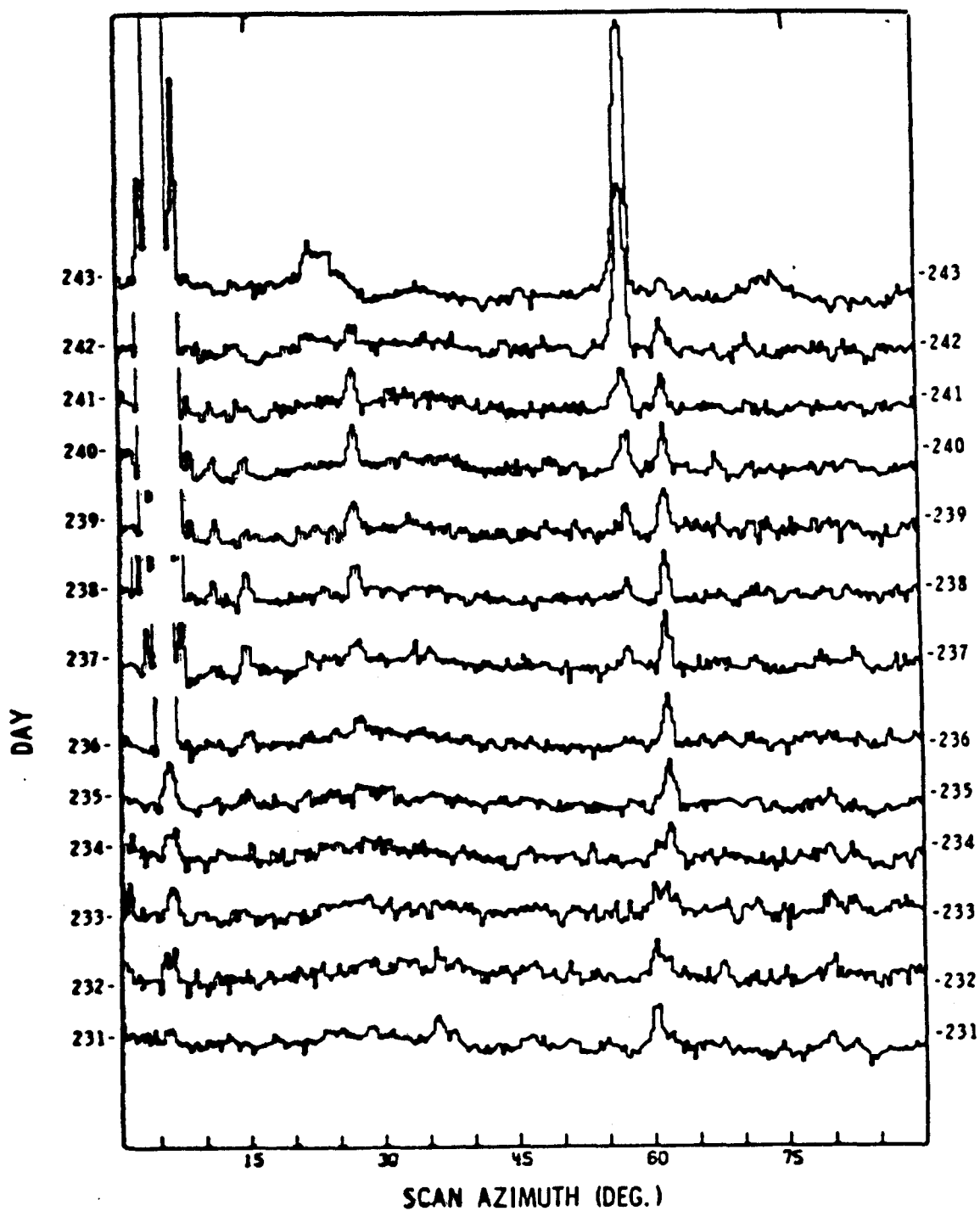


Figure 5. Daily variation of source intensity.

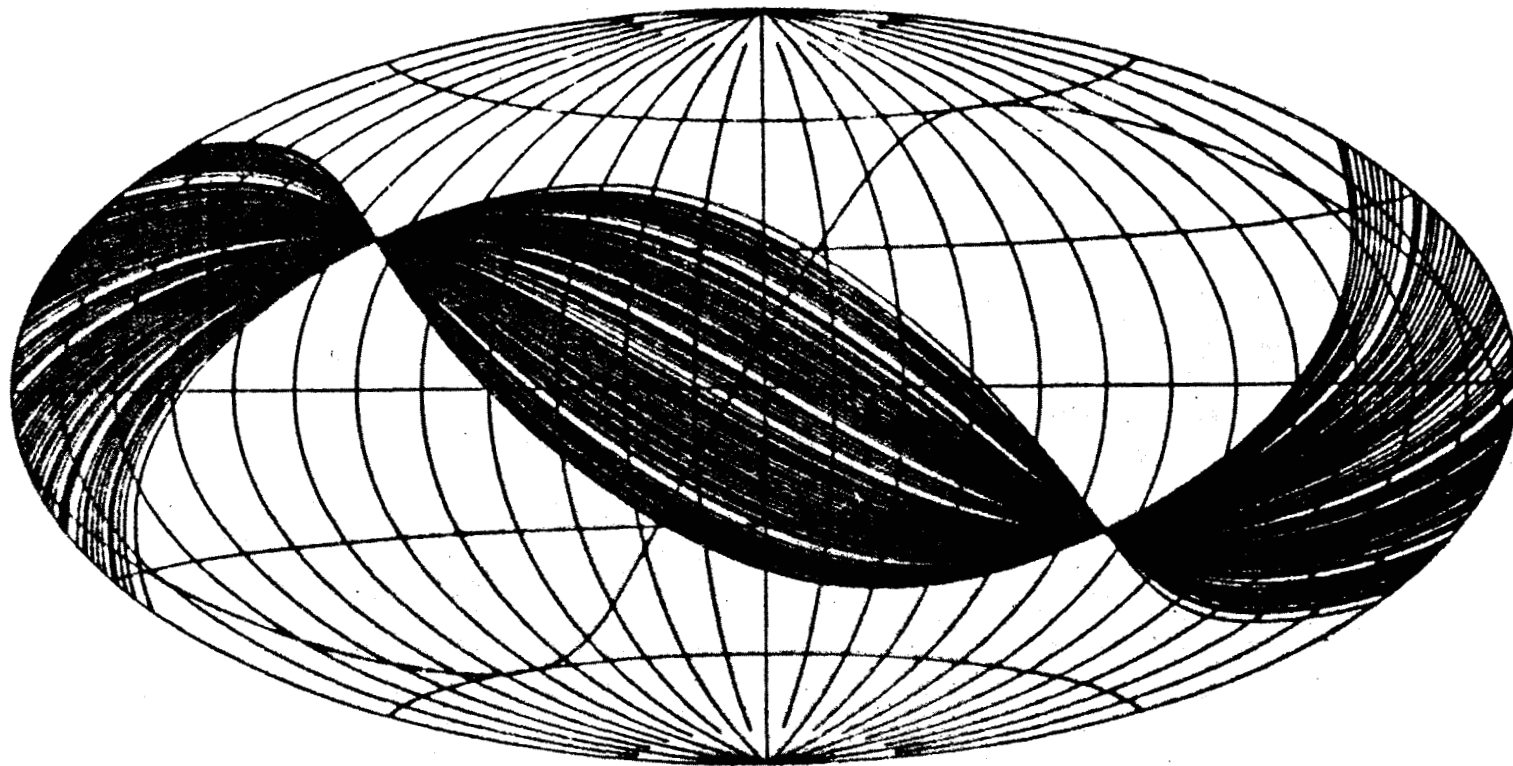


Figure 6. X-ray sky coverage.

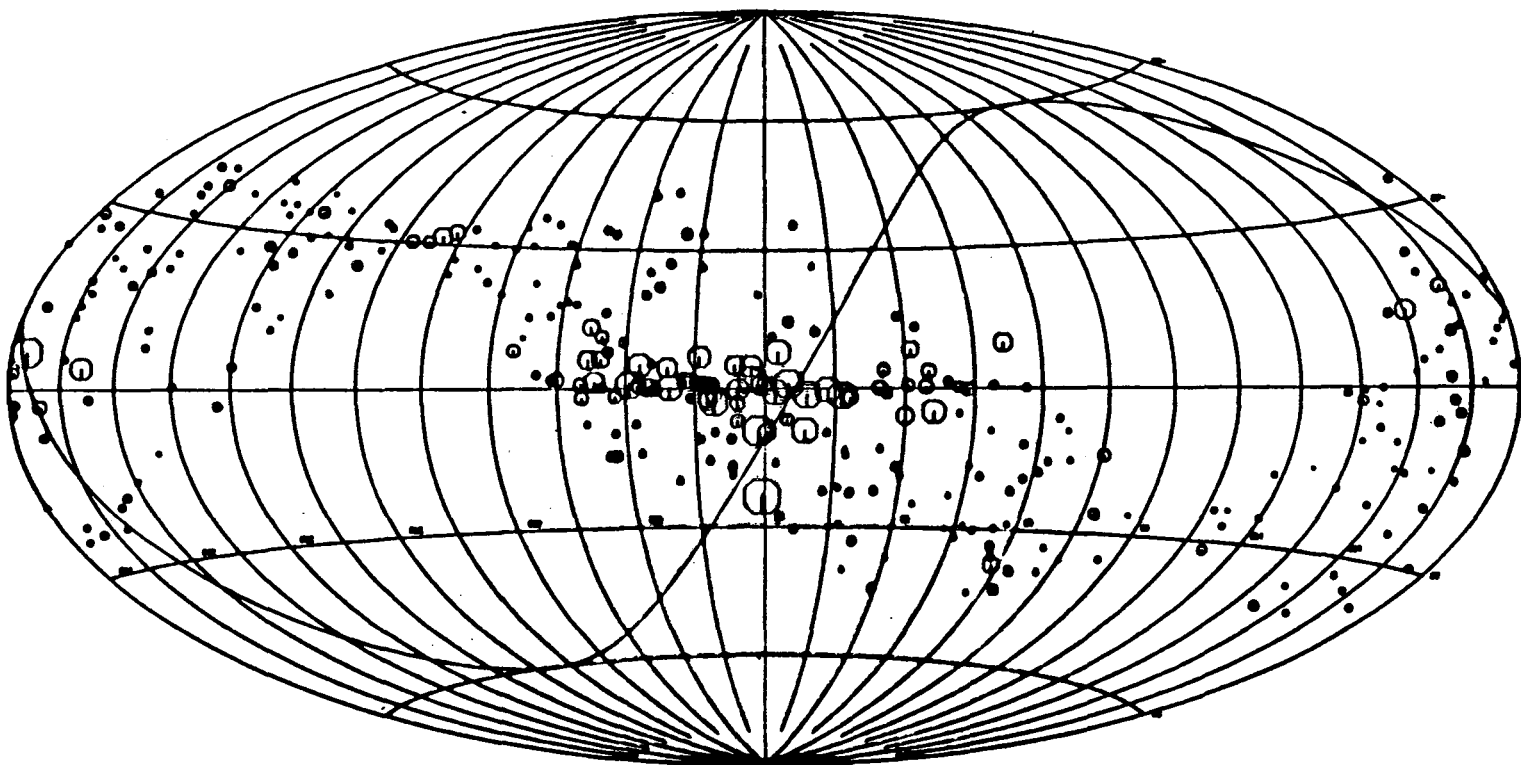


Figure 7. Source fits (first 70 days).

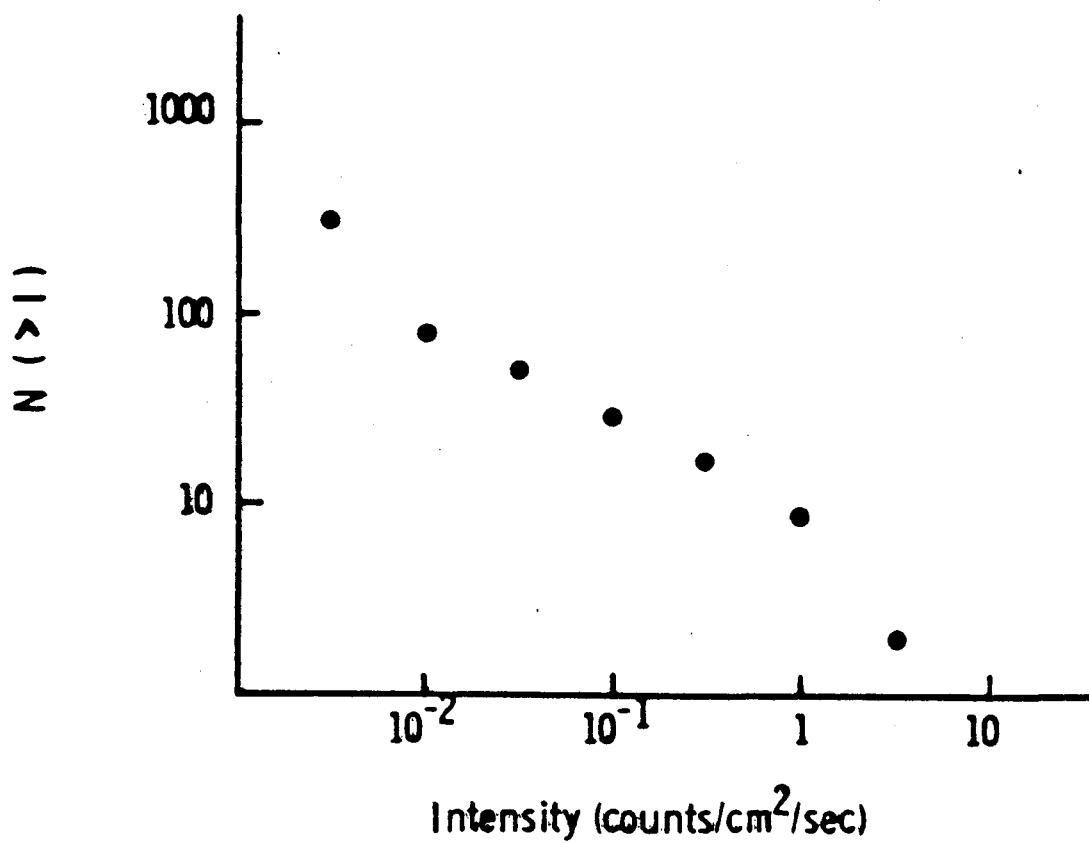


Figure 8. Sources as a function of flux.

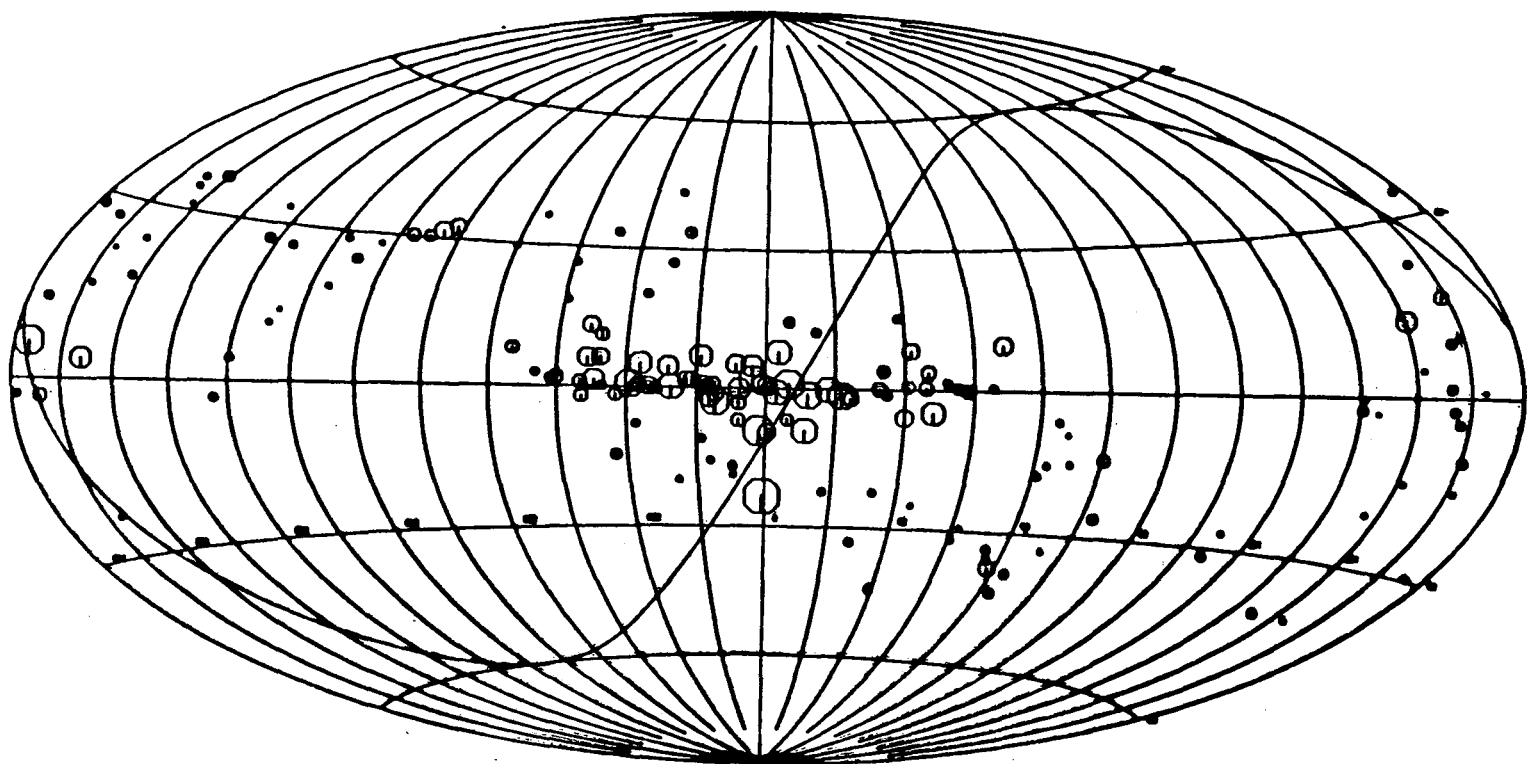


Figure 9. Previously detected sources.

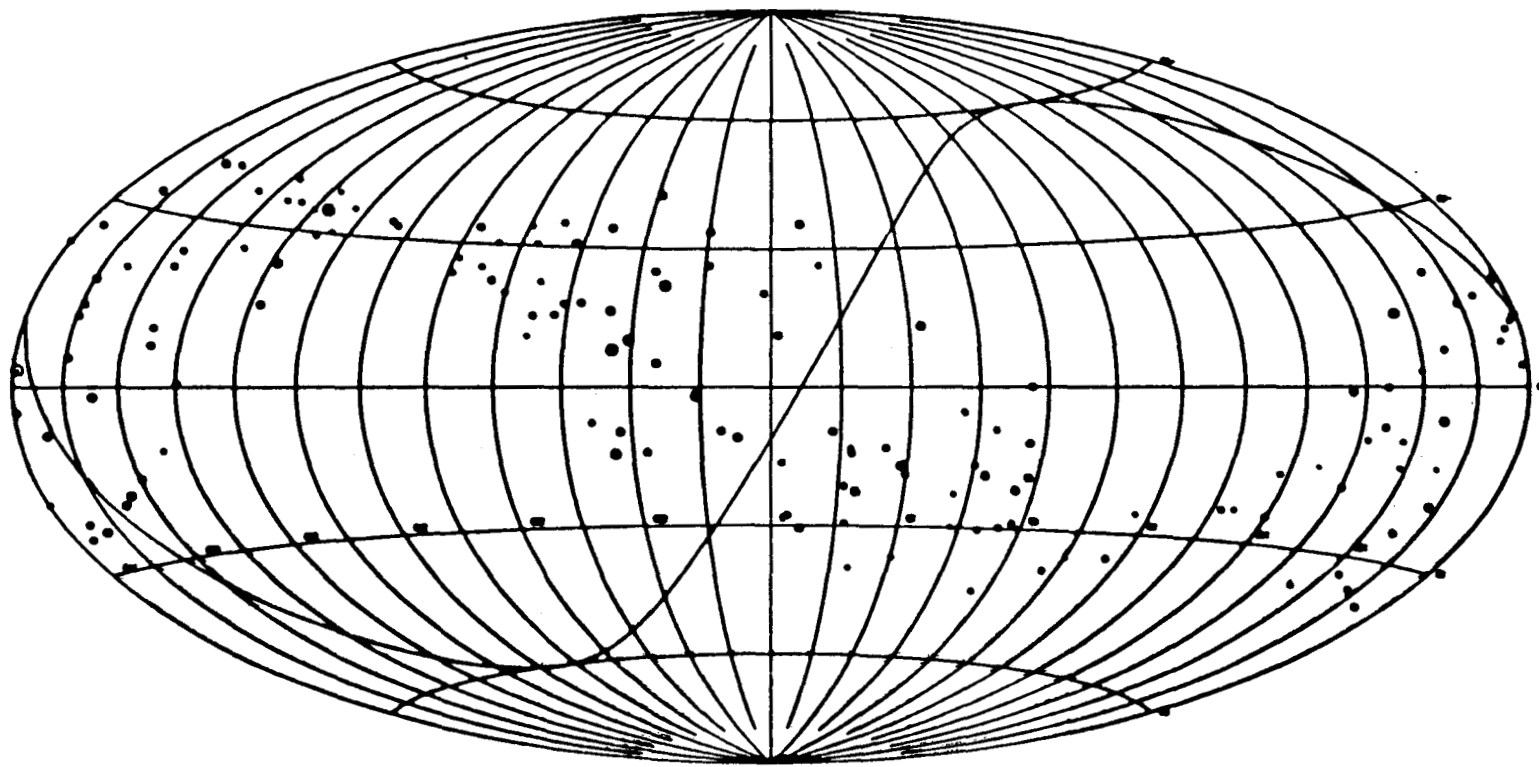


Figure 10. New sources.



Cluster	Intensity (cts/cm <sup>2</sup> sec × 10 <sup>3</sup> )	Error Box (sq deg)	Dist Class	Rich Class	U-H	Z	Luminosity (log 10-ergs/sec)	Conclusions
A475**	2.3 ± 0.6	0.86	6	1	III	0.271	45.31	
A480*	5.7 ± 0.7	0.52	6	0		0.189	45.43	
A488 (1)	1.9 ± 0.5	1.04	6	1	III	0.220	45.08	
A520 (2)	2.5 ± 0.4	0.43	6	3		0.180	45.06	0.23° outside 95% error box
A521*(3)	3.8 ± 0.6	0.43	6	1	III	0.200	45.30	0.19° outside 95% error box
A2159*	2.3 ± 0.2	0.22	4	0		0.094	44.42	0.23° outside 95% error box
A2163***	5.6 ± 0.1	0.37	6	2		0.189	45.42	
A2177**	2.4 ± 0.6	0.73	6	0		0.189	45.05	
A2178***	1.5 ± 0.3	0.50	5	1	II	0.157	41.68	
A2204**	6.5 ± 0.4	0.28	5	3		0.142	45.23	0.03° outside 90% error box
A2224***	4.0 ± 1.0	0.50	6	3	III	0.201	45.33	
A2228*	2.4 ± 0.3	0.50	5	1	I-II	0.128	44.71	0.25° outside 95% error box
A2234(4)	4.0 ± 0.2	0.46	5	1	III	0.175	45.21	
A2244*	2.3 ± 0.7	0.16	5	2	I-II?	0.104	44.51	0.13° outside 95% error box
A2252***	2.6 ± 0.3	0.21	6	1	II-III	0.188	45.08	
A2301***	2.4 ± 0.7	0.11	4	0	II?	0.080	44.30	A2304 is 0.26° outside 95% error box

(1) Confused with A486, A491 both distance class 6, richness class 1

(2) A508, A509 within 3°, both distance class 6, richness class 1

(3) Member of supercluster candidate 4U0443-09

(4) Centered between A2235, A2250 but both outside error box.

Figure 11. Cluster detections.

OBJECT	I ( $10^{-3}$ cts cm $^{-2}$ s $^{-1}$ )	I (UHURU)	ERROR BOX (SQ DEG)
MKN421	9.248 $\pm$ 0.428	1.752 $\pm$ 0.081	---
MKN501	8.434 $\pm$ 0.164	1.587 $\pm$ 0.031	0.04
0548-322	8.918 $\pm$ 0.111	1.689 $\pm$ 0.021	0.02
2155-304	22.664 $\pm$ 0.421	4.293 $\pm$ 0.080	0.02*
3C371	2.103 $\pm$ 0.094	0.398 $\pm$ 0.018	0.10*
IZW186	1.059 $\pm$ 0.294	0.201 $\pm$ 0.056	0.42
0521-365	1.961 $\pm$ 0.140	0.371 $\pm$ 0.027	0.60*
0537-441	1.412 $\pm$ 0.209	0.267 $\pm$ 0.040	0.81*
1831+731	1.110 $\pm$ 0.165	0.210 $\pm$ 0.031	0.49

\* LINE OF POSITION

Figure 12. X-ray emitting BL Lacs.

<u>OBJECT</u>	<u>V</u> <u>(mag.)</u>	<u>F(v)</u> <u>(10<sup>-11</sup> erg cm<sup>-2</sup> s<sup>-1</sup>)</u>	<u>F(x)</u> <u>(10<sup>-11</sup> erg cm<sup>-2</sup> s<sup>-1</sup>)</u>	<u>L(v)</u> <u>(10<sup>44</sup> erg s<sup>-1</sup>)</u>	<u>L(x)</u> <u>(10<sup>44</sup> erg s<sup>-1</sup>)</u>	<u>L(x)/L(v)</u>
PKS0548-322	15.5	1.32	4.05	2.70	8.31	3.07
MKN 501	13.8	6.31	3.83	3.14	1.90	0.61
MKN 421	13.5	8.32	4.20	3.22	1.62	0.50
3C 371	14.9	2.29	0.96	2.47	1.03	0.42
IZW 186	16	0.83	0.48	1.08	0.62	0.58
PKS0521-365	16	0.83	0.89	1.08	1.16	1.07
PKS0537-441	15.5	1.32	0.64			0.48
PKS2155-304	14.5 <sub>B</sub>	4.25 <sub>B</sub>	10.30			2.42

Figure 13. X-ray and optical properties of X-ray sources.

<u>OBJECT</u>	<u>V</u>	<u>F(x) EXPECTED<sup>+</sup></u>	<u>F(x) OBSERVED<sup>+</sup></u>
0300 + 470	18.0	0.03	$0.03 \pm 0.07$
0422 + 004	17.0	0.08	$0.06 \pm 0.05$
0735 + 178	16	0.21	$0.001 \pm 0.08$
* 0743 + 744	15.0	0.52	$\leq 0.19 \pm 0.06$
* 0754 + 100	16.5	0.13	$0.11 \pm 0.06$
* 0818 + 129	16.0	0.21	$0.001 \pm 0.04$
0829 + 046	16.5	0.13	$0.03 \pm 0.07$
* 0851 + 202	15.5	0.33	$0.06 \pm 0.07$
0906 + 430	19	0.01	$0.09 \pm 0.07$
* 0912 + 297	16	0.21	$0.10 \pm 0.06$
0954 + 556			$0.02 \pm 0.07$
0957 + 226	18	0.03	$0.03 \pm 0.07$
1523 + 298			$0.00 \pm 0.07$
1749 + 096	17.5	0.05	$0.03 \pm 0.08$
1749 + 701	17	0.08	$\leq 1.374 \pm 0.355$
2117 + 025	18	0.03	$0.02 \pm 0.14$
+UHURU COUNTS			

Figure 14. Upper limits for undetected X-ray sources.

## THE SCIENTIFIC RESULTS OF THE LOW ENERGY PORTION OF A-2

Gordon Garmire  
California Institute of Technology

The A-2 experiment is a collaboration between the Goddard Space Flight Center and Cal Tech with co-investigators at JPL and UCB. I would like to thank the Marshall people who have been involved these many years in the HEAO program for providing us with such a rich data base of X-ray information that we are going to be analyzing for many years. Dr. Boldt will present the extragalactic observations in the following talk and I will concentrate on some of the galactic results obtained from the experiment in this presentation. I am going to give you a little bit of the flood of data that we have already analyzed. I can assure you that there is a considerable amount of work remaining to pull out the results from all the different levels that we have within the data, so what I am giving you now is perhaps not the first look anymore, but it is sort of an intermediate stage of the analysis.

The primary goal of the A-2 experiment has been to study the diffuse background, and our particular portion of this experiment is to study the low energy diffuse background. We have collimators on our detectors which are  $3^\circ \times 3^\circ$  and  $1\frac{1}{2}^\circ \times 3^\circ$ , and what I would first like to show is that these detectors in fact are responding primarily to the diffuse background and not internal detector effects of different kinds which are also present. The upper squares and circles in Figure 1 are two different regions in the sky. In particular let's examine the lowest energies. At the lowest energies the sky has quite a bit of structure, and here the squares are at the polar regions (the galactic poles) and you see that at the poles, the low energy flux is considerably higher than say the flux coming from the plane of the Galaxy (circles). As you go to higher energies these two merge until up above a kilovolt, they become essentially the same. The structure that we see is predominantly in the energy range below 1 keV. This is due, we believe, to a very hot component to the interstellar medium, perhaps filling more than half the space between the stars in our Galaxy.

In Figure 2, I just want to point out a little bit of physics of this part of the spectrum because it is a bit different from what you have been hearing and will hear the rest of the day. This is the cross-section of the composite gas of the interstellar medium. Typically toward high galactic latitudes, if you invert this number, you can see out to about a kiloparsec in this spectral band. At high galactic latitudes where the disc of the Galaxy is only a hundred parsecs thick, we can actually look out of the Galaxy and see extragalactic objects. Dr. Boldt will mention a few of

those at the lower energy. At higher energies, the gas becomes completely transparent and we see everything in the Galaxy through the penetration of the X-rays.

Now our primary goal has been to map the Galaxy in different colors. Figure 3 shows the lowest energy data. This is quarter keV data and there is a tremendous amount of structure here. In fact, there is more structure than is real. That is part of the job we are currently working on, but I thought I would give you a brief progress report to show you the kind of problems we have and also a flavor of what we are seeing. The top and bottom of the map are the galactic poles which have been known for sometime, starting in 1968, I guess, with Bowyer's rocket flight which detected the bright region in the North Galactic polar area. At a longitude of about  $30^\circ$  toward the north is the North Polar Spur; there is a bright region in Hercules north of a longitude of  $90^\circ$  and there are a number of different sources. We have a  $3^\circ \times 3^\circ$  collimator, so these are  $3^\circ \times 3^\circ$  cells, which essentially do not respond very well, individually, to point sources. The cygnus Loop is at  $90^\circ$  longitude, the Vela diffuse region is over at  $270^\circ$  longitude and the Lupus region is north of the plane at  $330^\circ$ . The South Galactic Pole is also quite bright. There are a couple of fingers, or wisps of low energy X-ray photons coming from regions in the South in Eridanus south of  $210\text{--}240^\circ$  longitude and over here is the Gemini-Monoceros region north of the plane at about  $200^\circ$  longitude. It is quite an extended region. The stripes you see on the map are occasional electrons coming past our contamination flag, for example, that come in during solar activity. We have not eliminated those completely from this data. These data primarily summed data which have been used to search for discrete sources, so we have not taken great pains to separate out the stripes.

Now I should point out that the enhancement here in Figure 3 has been increased; the contrast has been turned up to a high level. The difference between the plane and the pole is at most about a factor of 4 in this energy band, and so these really dark regions are at most only a factor of 4 above the bulk of the region along the galactic plane. At higher energy (above 400 eV), Figure 4 shows that the sky changes completely. It is much more uniform. Again, the contrast is enhanced a bit too much. In fact I am afraid that the photographic process overdid what the computer already had done. As you can see, there is a bright region toward the galactic center. The North Polar Spur comes down near  $30^\circ$  again, and the rest of these dark bands are just streaks having to do with some electron effects or a little bit of bad data that came through the data filtering process. Bright objects like the Cygnus Loop and Cygnus X-2 are prominent, and just north of the plane at a longitude of  $70^\circ$  is a supernova remnant and some features around Cygnus X-6, as well as SS Cygni. At  $275^\circ$  longitude and  $-32^\circ$  are the Large Magellanic Cloud sources, again the Vela region shows up at  $265^\circ$ , and the Crab is at about  $185^\circ$  just below the plane.

Figure 5 shows a very preliminary source map of the soft X-ray sky. The lower map is a coverage map; we had some trouble with our detector at different times and so the coverage by no means is uniform. The strongest coverage is in this very dark band corresponding to the beginning of the mission, and later on in the mission after we discovered how to play our detector without problems, we got quite a bit more coverage. Then we ran out of gas in the latter part of May 1978, so we were not able to completely fill in everything. There are still a few small gaps in our map of the sky. One thing I want to point out; at low energy the sources that we see are not at all concentrated in the plane of the Galaxy. However, you have to take out the effects of nonuniform scanning, which is a little hard to do by your eye.

If you consider the number of sources brighter than some flux level,  $S$ , then this number,  $S$ , typically follows a power law. For a disc population of sources you might find the number falls as the first power of  $S$ , and for a volume distribution the number falls as  $S$  to the  $3/2$  power. We find the  $1/4$  keV sources follow a  $3/2$  law pretty well down to a level of  $S$  equal to 2 HEAO-1 low energy counts. This is an energy flux of about  $10^{-12}$  ergs/cm<sup>2</sup> sec for which there are about 50 sources observed. The map is still being filled in, but this is the first look at the  $1/4$  keV X-ray sky available from HEAO-1.

One of our first interesting surprises while we were scanning the sky was that we suddenly came upon U Geminorum when it was in outburst (Fig. 6). The optical outburst occurred actually during the upper scan in Figure 6. There was no soft X-ray flux at that time; however, the next day the soft X-ray flux became very bright and this turned out to be one of the brightest sources in the sky for us for a few days. U Geminorum is a cataclysmic variable, thought to be a white dwarf with a companion star that occasionally pours (almost periodically, in fact, on about a one hundred day period), a large amount of its outer envelope onto a white dwarf companion and thereby produces X-rays as this matter falls into the white dwarf gravitation potential. Some of the history of that object is shown in Figure 7. The optical brightening occurred at this time and here you see the soft X-rays. They became very bright and then they appeared to die away even while the optical light was still at a high level. The optical flux increased by some factor of 100 and perhaps by more than that even in soft X-rays. In the hard X-ray band it also became visible for a short time; this is in some contradistinction to other sources like EX Hydrae and SS Cygni which seem to have a hard flux during optically quiescent periods.

Another object which we saw in the very early data which I include (Fig. 8) for historical interest is the supernovae remnant MSH 14-63. At low energy we separated out a component that is centered at a slightly different celestial position. This position corresponds to the star Alpha Centauri, which is one of the closest, in fact, with Proxima Centauri, is the closest of systems of stars to us. The flux of soft X-rays we see is comparable to the that from the Sun.

Figure 10 is a light curve of Alpha Centauri and over a period of about 4 or 5 days. It was rather constant within statistics, so that we did not just observe it in a flaring state but it was something that was there rather continuously.

Figure 11 illustrates another class of object which we've detected in the low energy X-ray range. These are the RS CVn stars, named after RS Canum Venaticorum, the prototypical star in the constellation Canes Venatici. Capella, a long period member of the class, was one of the stars we saw earlier in the mission. It showed a very interesting feature in its spectrum corresponding to an iron emission of a plasma at a temperature of 10 million degrees. However, to show that these stars are not homogenous in their composition, we also have an equivalent spectrum of UX Arietis. Here we do not see any strong feature in the same part of the spectrum at all and can put a limit on the iron abundance as less than 3 percent of solar abundance at this temperature. It appears that there are quite large compositional variations in this class of object. The X-ray emitting list has grown in the class of objects as shown in Table 1. You can see that their luminosities are typically in the range of about  $10^{31}$  ergs per second.

The neutron star systems and blackhole candidates that have been talked about by Dr. Friedman are much more luminous than the RS CVn stars, more in the range of  $10^{35}$  -  $10^{37}$  ergs per second, so that we are talking about a class of objects here which have a much lower X-ray luminosity; however, I should point out that they are still considerably stronger than the Sun in soft X-rays, which emits typically in the neighborhood of  $10^{27}$  ergs per second. Therefore, this is an intermediate class; these stars are rather larger in surface area than the Sun so that the surface activity is only 100 times that of the Sun rather than the  $10^4$  or more that you see exhibited in their luminosity difference.

An object that we detected early in the mission was U Geminorum, a dwarf nova (Fig. 12). Later on in the mission we had a pointing at this object, and here you can see a very interesting feature; first of all the optical light curve of the object is given here in the inset, the Julian Day number is along the abscissa indicating that the outburst lasts for some 5 days. This is another tribute to the flexibility in the HEAO program which allowed us to point the spacecraft within a couple of days of the start of the outburst so that we were able to see what was happening while the outburst was in progress even though this was not in the normal pointing schedule. As you can see there is very chaotic behavior although it does appear to have a rather periodic intensity variation of around 25 sec. More about this next where we have a better example.

SS Cygni, another dwarf nova, was also observed as shown in Figure 13. This is an object which was seen in December 1977 during a quiescent period and then we had a pointing at it in June 1978 in outburst. This



pointing was done after our liquid propane gas was essentially gone. We did this pointing by using just the remaining gas phase propane in the tank. The liquid gas that we used, propane, had all vaporized and turned into gas and we were working on the residual gas left in the tank. Here you see the pulsations of the objects; this is about an 8.8 sec period and I want to emphasize that this is a new class of behavior that we've seen in the X-ray sky.

These are low energy X-rays (Fig. 14), X-rays at a quarter keV, and there are a couple of things I would like to point out. This is the pulsed fraction which goes up to about 1.0 and as you can see it goes along and it jitters a lot. That is, most of the time it is down around 0.2, but goes up to about 0.75 to 1.0. If you assume the pulses have a constant pulsation period, and then you look at the phase with respect to that period it tends to wander around and have jumps in it. Now one of the things that we discovered earlier about this source, was that in contradistinction to pulsars which have period noise, it appears from our analysis that rather these kinds of objects, which are white dwarfs, have a rather constant period but the phase jitters. You can do an analysis on the jitter by assuming a random walk behavior of the pulses with respect to time (Fig. 15). Period noise in pulsars tends to grow with an uncertainty like time to the third power. It does not get better as you add more data when you have real period noise. However, the period here does get better but what happens is that the phase changes in an unpredictable way. We have been studying this in terms on random phase analysis. We have superimposed a long stretch of data bringing each pulse successively on top of the next pulse at zero in the figure, so that each pulse is zeroed here at zero and then this oscillating curve represents some 25 oscillations of the source before and after zero. The phase noise produces an exponential decay in the amplitude of the signal as you superimpose the data at a given reference point, which is the peak of each pulse. This is because the pulses go out of phase after a characteristic number of pulses and add incoherently. One other feature of these pulses which I should emphasize, is that rather than being highly structured like neutron star pulses, these are beautiful sinusoids with less than a few percent in higher harmonics; they look very, very sinusoidal. We think what this represents is the Keplerian orbit of matter just above the surface of the white dwarf star where there is a strong interaction boundary or shock between the orbiting material and the white dwarf surface. There is a shock boundary layer that forms just above the surface and so we are seeing a period which is like the period of the inner Keplerian orbit right at the shock front. What may be happening is that the shock is being pulsed by the material coming in from the accretion disc and we see an oscillation characteristic of that time. This hypothesis plus an equation of state for the white dwarf permits us to obtain the white dwarf mass. For example, for SS Cygni this gives about one solar mass, and for U Geminorum around 0.4 or 0.5 solar masses.

In Figure 16 we have analyzed four different aspects of the SS Cygni pulsations. The intensity during that observation was rather constant with a slight dropoff toward the end. The amplitude of the oscillation for SS Cygni changed quite a bit. These are individual orbits, five orbits of data plus a partial orbit. You see that the amplitude variation is rather smooth going over almost a factor of 3. The period slowly decreases during the time we are watching the source but it is not decreasing very much; it decreases something like  $10^{-5}$  of the period per period. The strength of the phase noise changed during the interval of the observation by a factor of about 2. Figure 17 shows a similar analysis on U Geminorum. In Figure 18 the spectrum of U Geminorum is shown demonstrating how very cool the spectra of these white dwarf accreting objects are. Figure 19 is a plot of SS Cygni as a function of time just showing how the phase walks around. Here are the individual pulses; this is a superposition of about 15 pulses or so and you can see that the period just wanders around randomly. The amplitude changes and it goes through a minimum and then jumps. It could jump that way or could jump this way; I am not quite sure how it jumps, since it goes almost  $180^\circ$  at this point. It does that over and over again during the observations.

Figure 20 shows pulses from 4U 1626-67, a neutron star. At the higher energies, it appears that during the pulsations, which repeat every 7 sec, we see quite marked changes. Up around 19 keV you can see a strong feature which, as you go through the pulses, tends to die out and then comes back again. This is one complete cycle of pulsation for a period of 7 sec, folded over and over on itself to build up its statistics. We call this pulse phase spectroscopy. The interesting part about this source is that if you add the data from low energy all the way to high energy, it does not look pulsed. That is, the behavior of the pulsation is a very energy dependent thing. I do not have different energy bins out here to show that, but if you add all the data together the pulse seems to go away, indicating that the changes represent a scattering effect in an atmosphere of some kind where you are not losing photons but you are changing their energy distribution as the neutron star rotates around.

Figure 21 shows Hercules X-1, which is an old favorite in the X-ray business. This is a low-state spectrum when the X-ray emission is off in terms of the early analysis from Uhuru. The source is detectable in its low-state by the more sensitive HEAO-1 detectors. During the low-state, the 1.24 sec pulsations associated with the rotation of the neutron star disappear. Both the PHA and unfolded spectral fitted data show a strong iron feature at 6.4 keV. The spectrum in Figure 22 is extremely flat at the middle of the binary period but during the early part of the 1.7 day orbital period tends to steepen. There is strong iron line emission which has also been analyzed in terms of fluorescence from the atmosphere of the other star and the accretion disc. The low-state iron

line energy is 6.4 keV while during the high state it is 6.8 keV. The equivalent width changes from about 550 eV in the low-state to 300 eV in the high state, and broadens to an energy width of 1.3 keV. The narrow low-state line and shift of energy to lower X-ray energies agree with a fluorescence hypothesis.

Figure 23 shows a transient source 4U 0115+63, pulsating at a period of about 3.6 sec, which exhibits strong energy dependence during the phasing of the source as it rotates around. The two bins shown, 2 and 3, are out of ten bins for a complete rotation of the neutron star. It is clear that there is quite a bit of anisotropy in these sources as they rotate, tied in probably to a strong magnetic field. This spectrum obtained for HED III is very hard with a power law number index of 0.1.

Figure 24 shows an interesting object that has just come into prominence during the last few weeks in the press, SS433. It is an Uhuru source from sometime ago (4U 1908+05) but just began to be studied optically, and you probably have all read the press bulletins on it. In the X-ray band it shows an iron-line feature, very similar to most binary X-ray sources, so it does not seem to reveal anything special in the X-ray band.

In conclusion, I've shown a number of the interesting galactic phenomena at high energy which have been studied using the HEAO-1 detectors. I've omitted a discussion of supernova remnants for a lack of time, but I should just mention that we have discovered about nine or ten new remnants, almost doubling the pre-HEAO-1 number. Dr. Boldt will now continue with a presentation of the extragalactic results.

## BIBLIOGRAPHY

- Cash, W., Bowyer, S., Charles, P., Lampton, M., Garmire, G., and Riegler, G.: *Astrophys. J. Lett.*, 223, L21, 1978.
- Cordova, F.: Ph.D. thesis, California Institute of Technology, 1979.
- Cordova, F. A., Chester, T. J., Tuohy, I. R., and Garmire, G. P.: to be published in *Astrophys J.*, 1979.
- Cruddace, R., Paresce, F., Bowyer, C. S., and Lampton, M.: *Astrophys. J.*, 187, 497, 1974.
- Hall, D. S.: In *Multiple Periodic Variable Stars*, ed. W. S. Fitch (Reidel: Dordrecht), 1976.
- Marshall, F. E., Swank, J. H., Boldt, E. A., Holt, S. S., and Serlemitsos, P. J.: *Astrophys. J. Lett.*, 230, L145, 1979.
- Mason, K. O., Cordova, F. A., and Swank, J. R.: *Proc. of the COSPAR Symp.*, Innsbruck, Austria, June 1978.
- Nugent, J., and Garmire, G.: *Astrophys. J. Lett.*, 226, L83, 1978.
- Pravdo, S. H., Boldt, E. A., Holt, S. S., Rothschild, R. E., and Serlemitsos, P. J.: *Astrophys. J. Lett.*, 225, L53, 1978.
- Pravdo, S. H., White, N. E., Boldt, E. A., Holt, S. S., Serlemitsos, P. J., Swank, J. H., Szymkowiak, A. E., Tuohy, I. R., and Garmire, G.: submitted to *Astrophys. J.*, 1979.
- Rose, L. A., Pravdo, S. H., Kaluzienski, L. J., Marshall, F. E., Holt, S. S., Boldt, E. A., Rothschild, R. E., and Serlemitsos, P. J.: *Astrophys. J.*, 231, 919, 1979.
- Rothschild, R., Boldt, E., Holt, S., Serlemitsos, P., Garmire, G., Agrawal, P., Riegler, G., Bowyer, S., and Lampton, M.: *Space Sci. Instr.*, 4, 279, 1979.
- Walter, F., Charles, P., and Bowyer, C. S.: *Astrophys. J. Lett.*, 225, L119, 1978.
- Walter, F., Charles, F., and Bowyer, C. S.: *Astron. J.*, 83, 1539, 1978.

TABLE I

Name	Date (UT)	$L_x$ (erg s <sup>-1</sup> ) (.2-2.8 keV)	D <sup>(1)</sup> (pc)
UX Ari	1977 17-22 August	$2.1 \pm .04 \times 10^{31}$	50
HR 1099	1977 17 August 1978 9-10 February	$1.1 \pm .1 \times 10^{31}$	33
RS CVn	1977 20 December	$1.1 \pm 2 \times 10^{32}$	145
RS CVn	1977 19,21 December	$< 4.4 \times 10^{32} \quad (3\sigma)$	145
AR Lac	1977 19-22 December	$1.5 \pm 1 \times 10^{31}$	50
LX Per	1977 21-23 August	$2.2 \pm .2 \times 10^{31}$	145
RW UMa	1977 24 November	$9.6 \pm .7 \times 10^{32}$	150
RW UMa	1977 22,23 November	$< 5.7 \times 10^{32} \quad (3\sigma)$	150
$\alpha$ Aur <sup>(2)</sup>	1977 14-16 August	$4 \times 10^{30}$	14
HK Lac	1977 19-22 December	$1.3 \pm 1 \times 10^{32}$	150
$\sigma$ Gem	1977 14-16 October	$1.3 \pm .1 \times 10^{32}$	150
Z Her	1977 21-23 September 1978 19-20 March	$< 9.8 \times 10^{30} \quad (3\sigma)$	85
SZ Psc	1977 11-12 December	$< 1.4 \times 10^{32} \quad (3\sigma)$	100
TY Pyx	1977 22-23 November	$< 8.8 \times 10^{30} \quad (3\sigma)$	85
HR 5110	1977 24-26 December	$< 4.4 \times 10^{30} \quad (3\sigma)$	50

(1) Hall (1976)

(2) Cash et al. (1978)

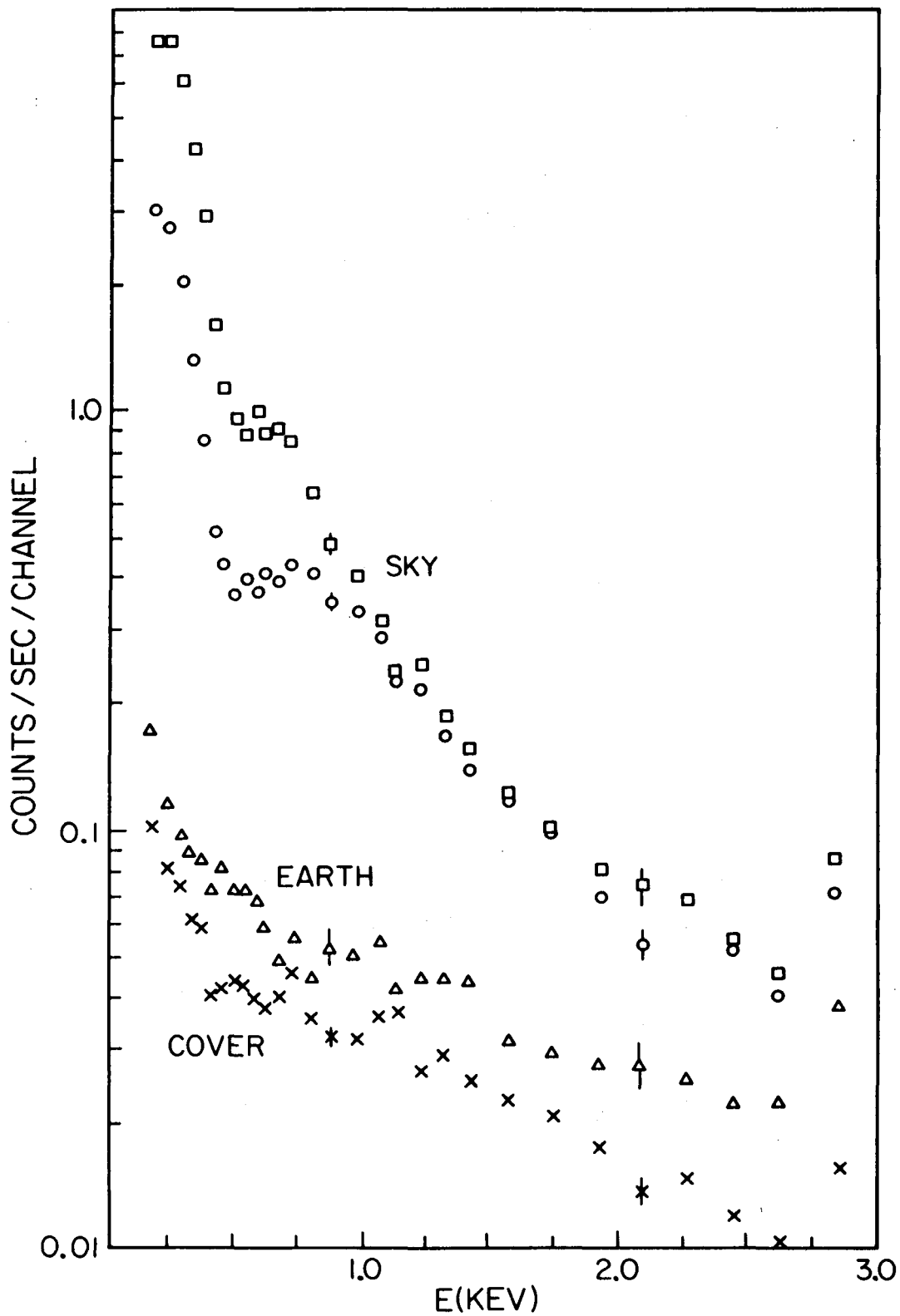


Figure 1. The pulse height spectrum of events recorded from the galactic pole ( $\square$ ), the galactic plane ( $\circ$ ), the Earth and the detector with the acoustic door closed. The excess Earth events over the cover-closed events are probably electron background.

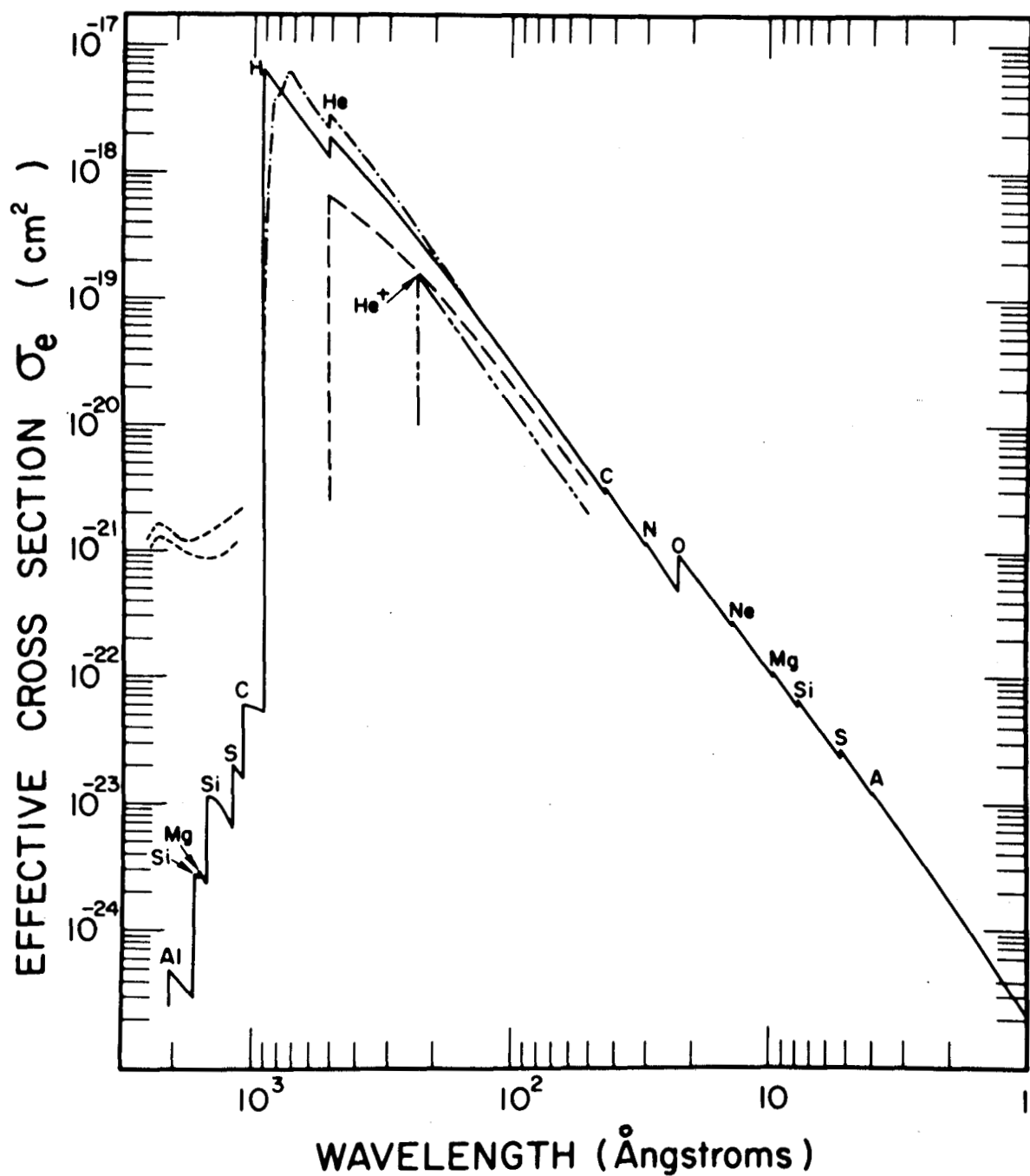


Figure 2. This is a figure from Cruddace et al. (1975), which shows the absorption properties of the interstellar medium. The density of gas in the galaxy is about  $0.5 \text{ atoms/cm}^3$ , so at  $10 \text{ \AA}$  we can "see" out to a distance of about 7 kps, and at  $50 \text{ \AA}$  out to a distance of about 80 pc.

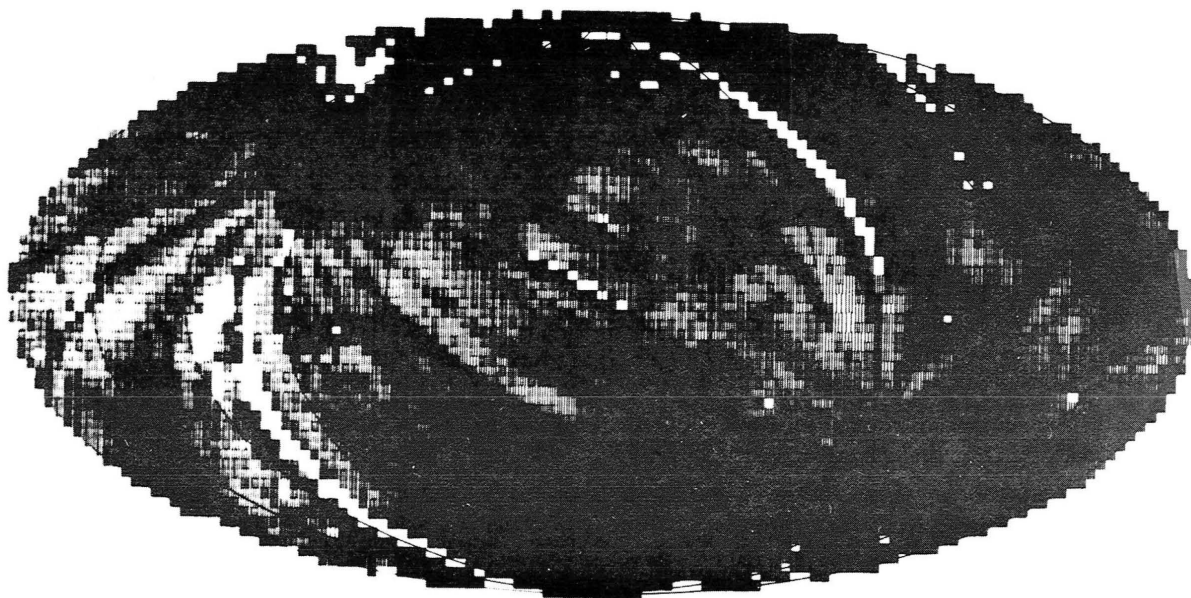


Figure 3. The 1/4 keV sky. Dark areas are brighter. The North Galactic Pole is at the top and  $0^\circ$ , the Galactic Center, is at the center. Light streaks are missing data. Dark streaks are electron contamination.



North

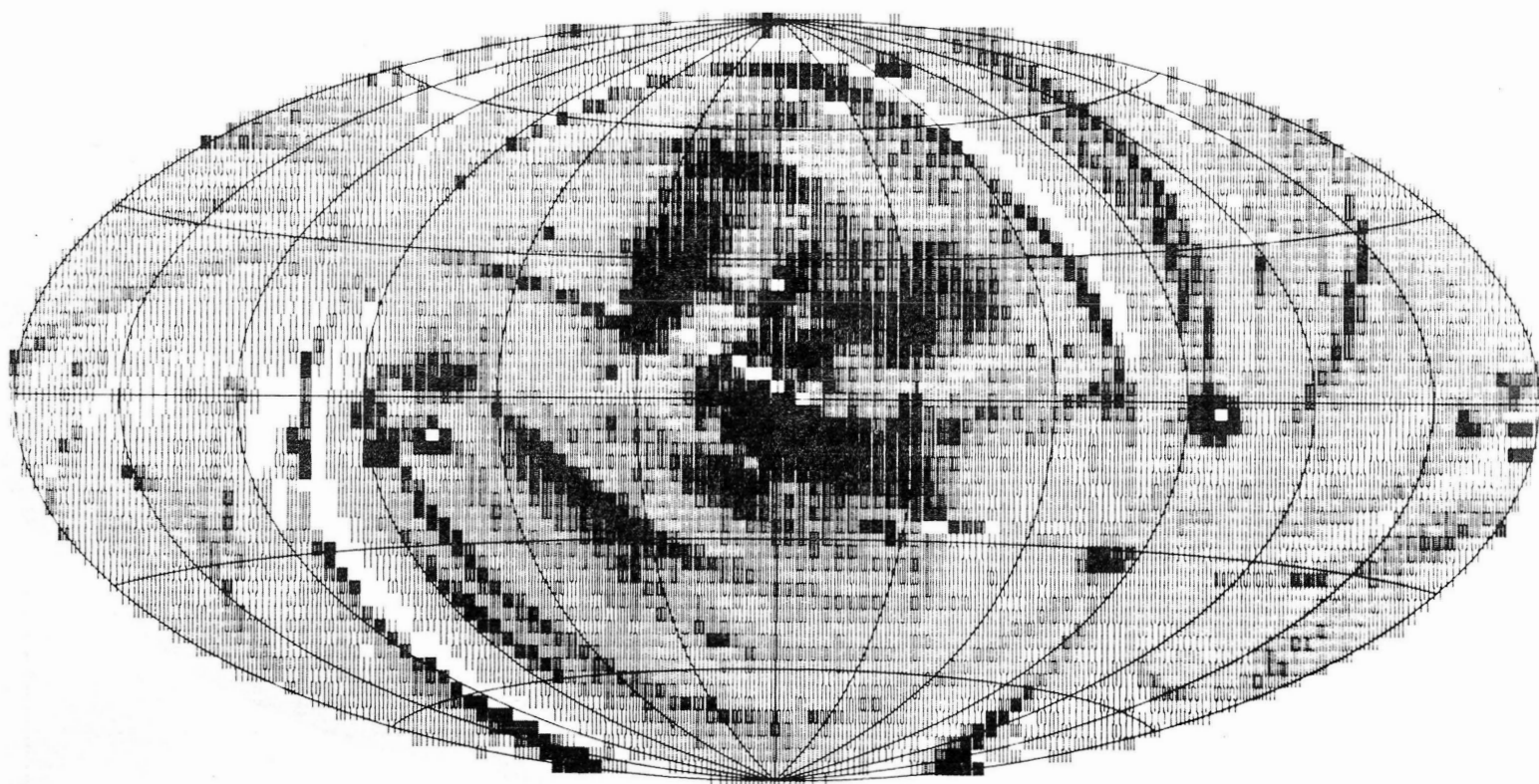


Figure 4. The  $> 0.4$  keV sky. The same description as for Figure 3.

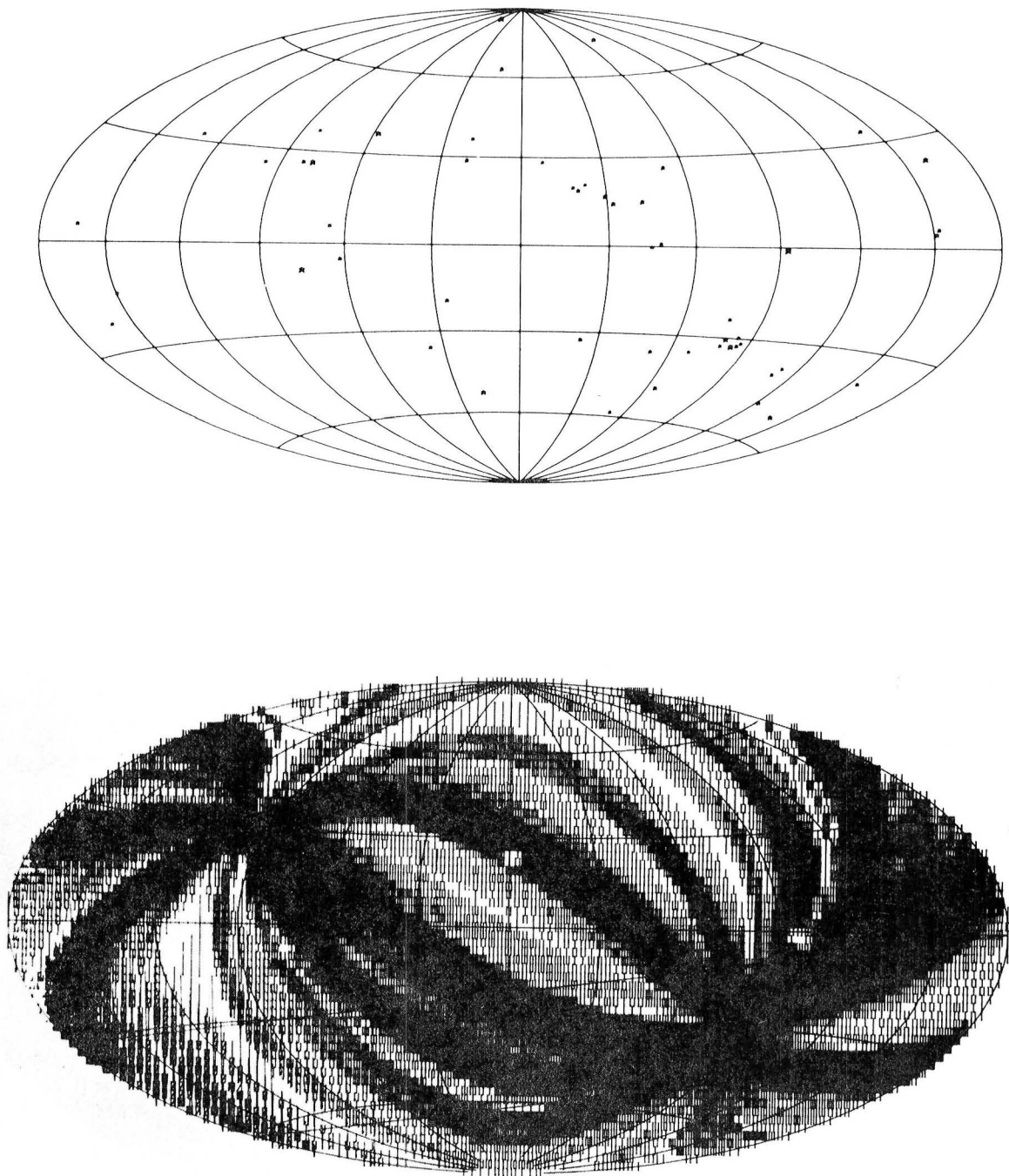


Figure 5. The upper figure is the distribution of 1/4 keV sources observed from HEAO-1. The lower curve is the exposure map, darker being more exposure. The square hole at  $0^\circ$  longitude and  $+20^\circ$  latitude is Sco X-1 and is an artifact of the way the exposure map was created.

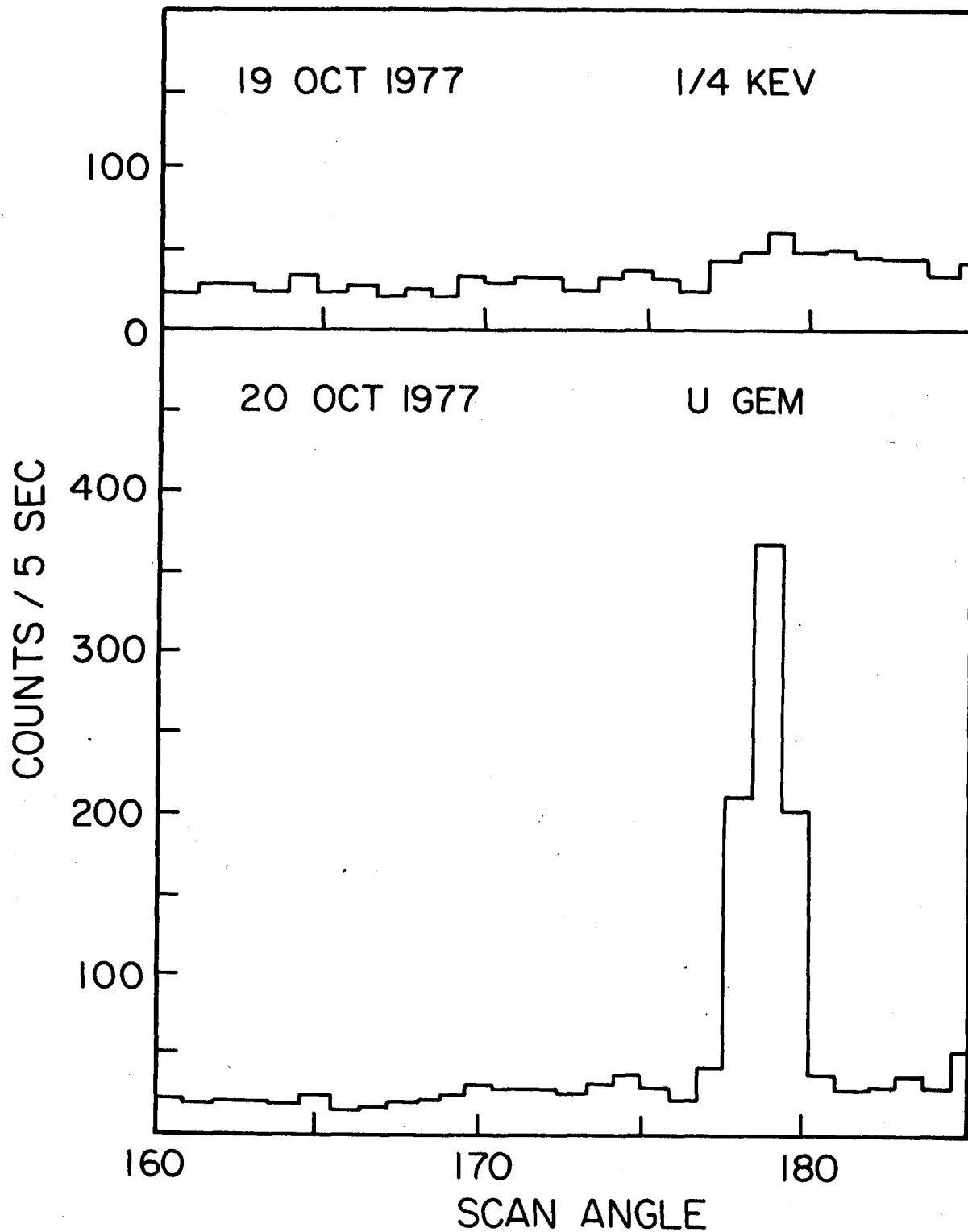


Figure 6. The upper curve is the 1/4 keV counts versus scan angle. The lower curve is the same one day later showing the tremendous increase in U Gem.

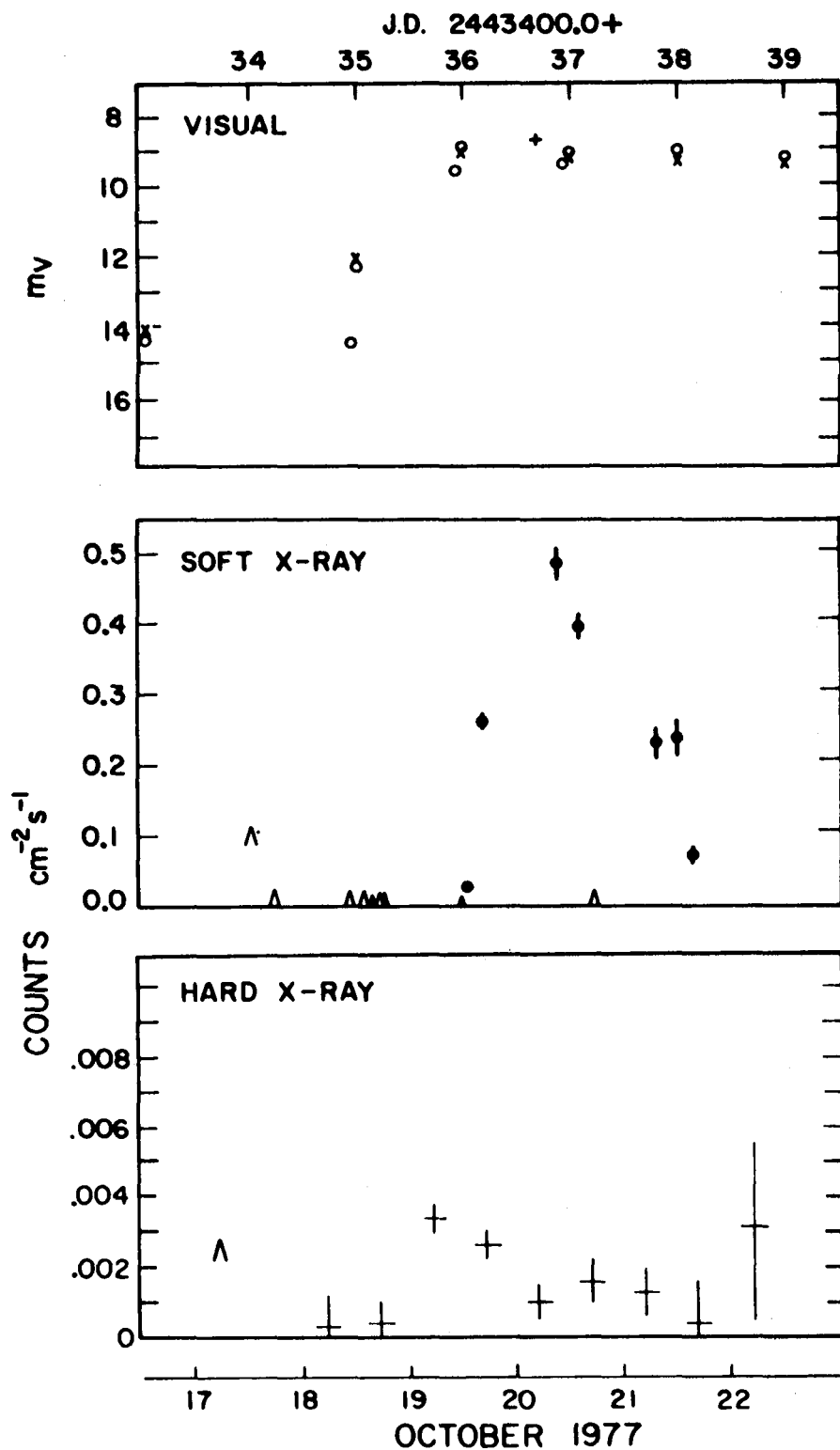


Figure 7. The visual intensity (upper), soft X-ray intensity and hard X-ray intensity of U Gem as function of time from Mason et al. (1979).

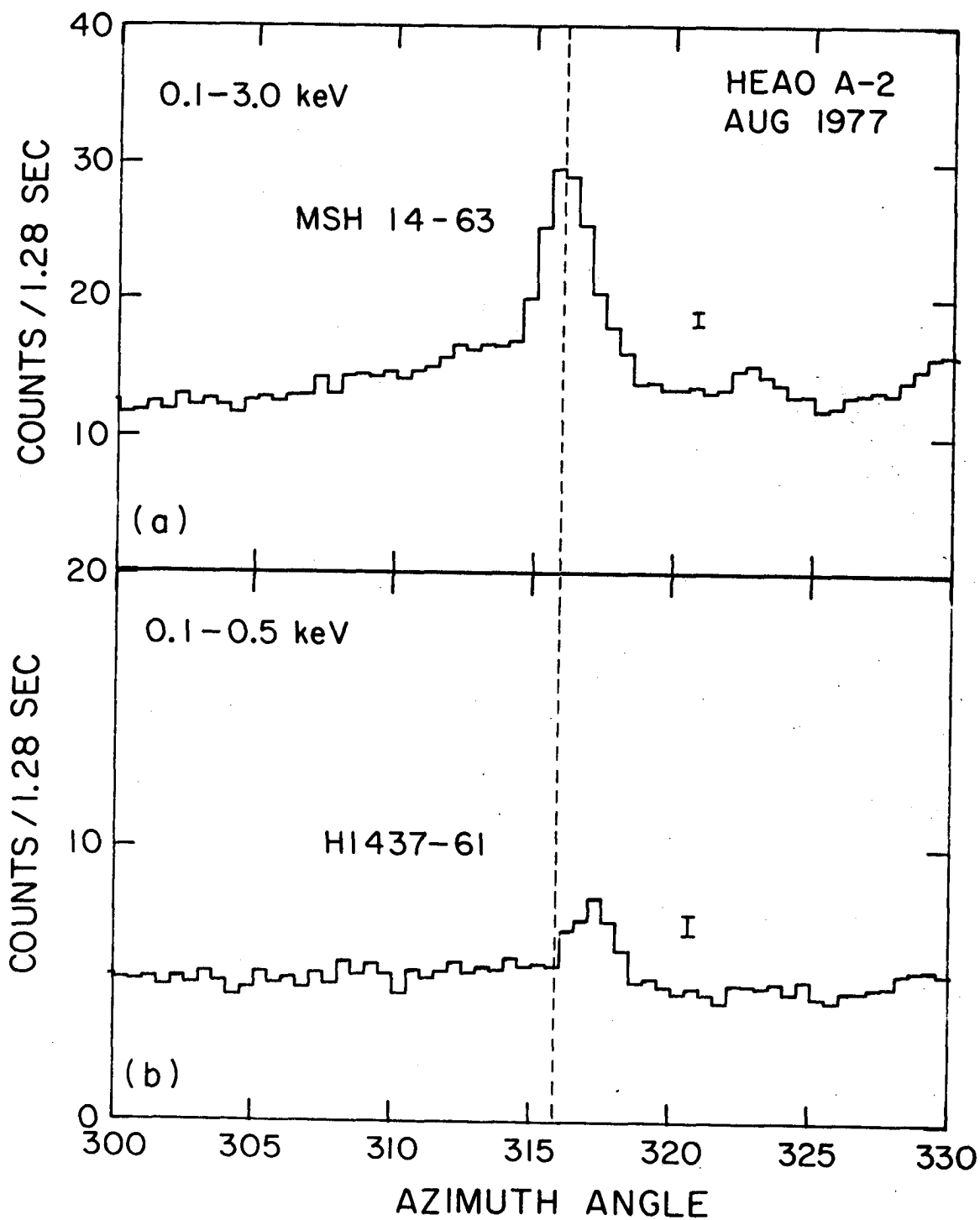


Figure 8. The scan over the region of MSH 14-63 (upper) and the displacement of the counts at low energy due to presence of a separate soft X-ray source.

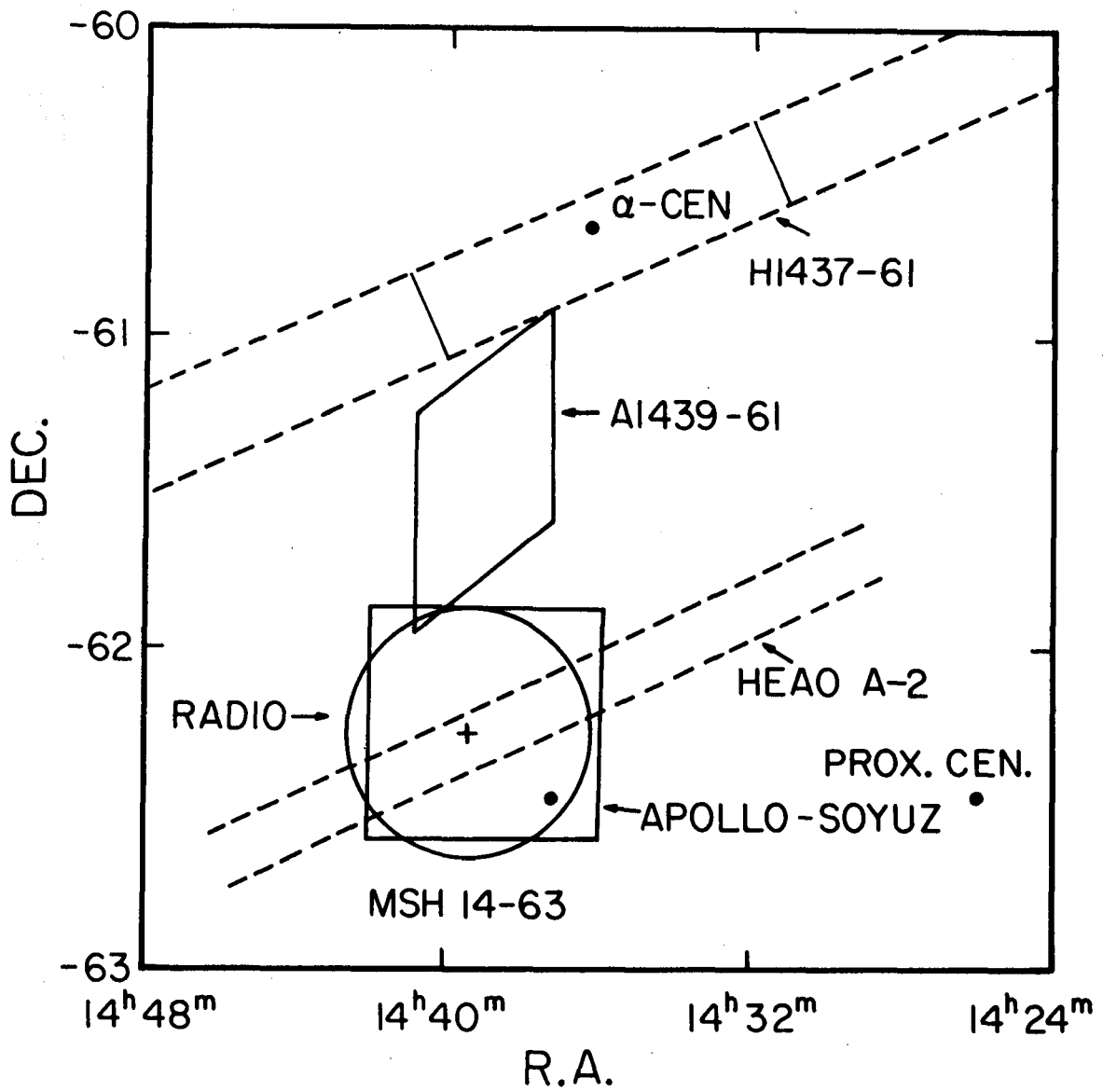


Figure 9. The position of the new soft source relative to some other sources.

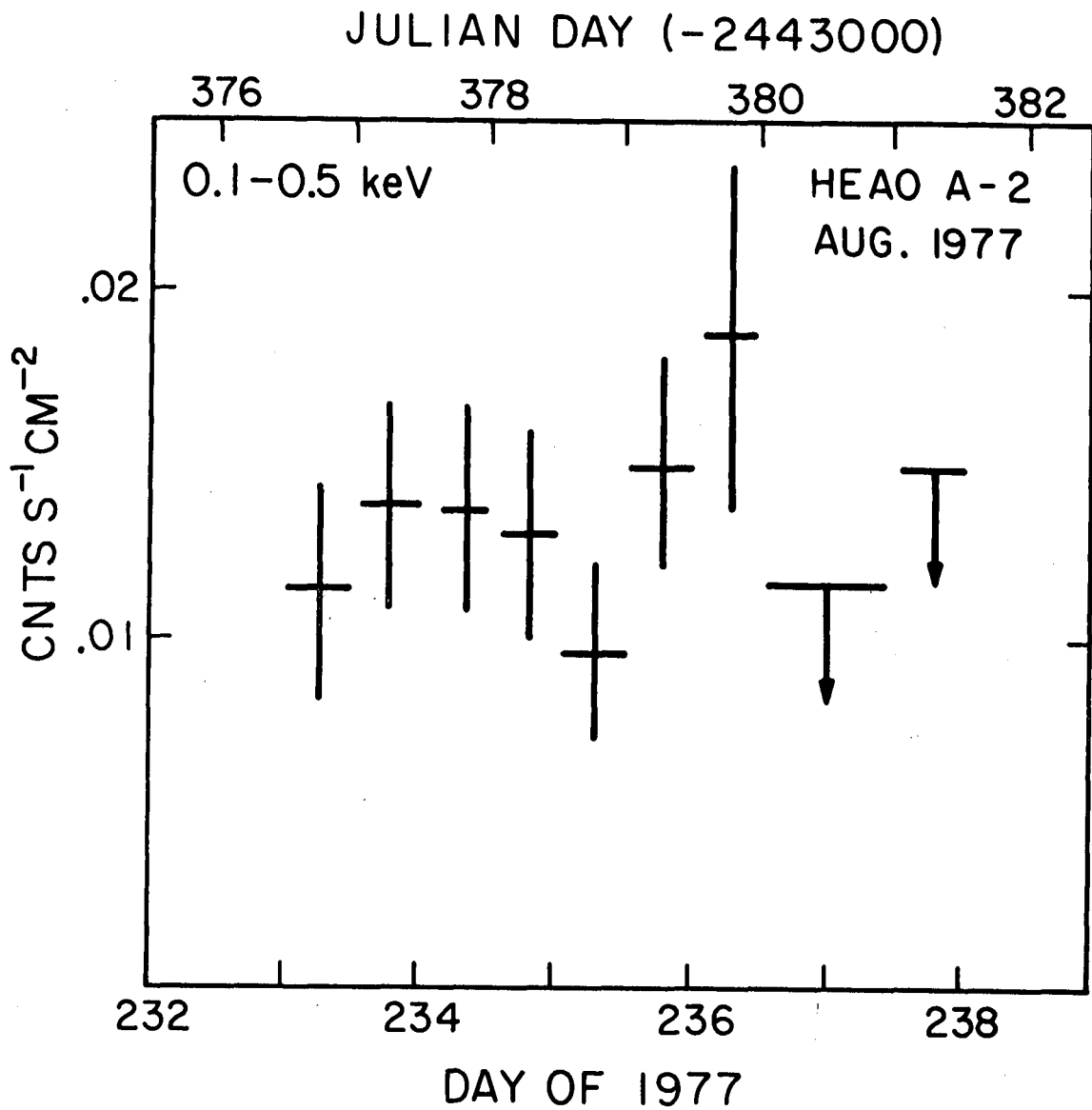


Figure 10. The intensity of  $\alpha$ -Cen as a function of time in 1977 while it was scanned.

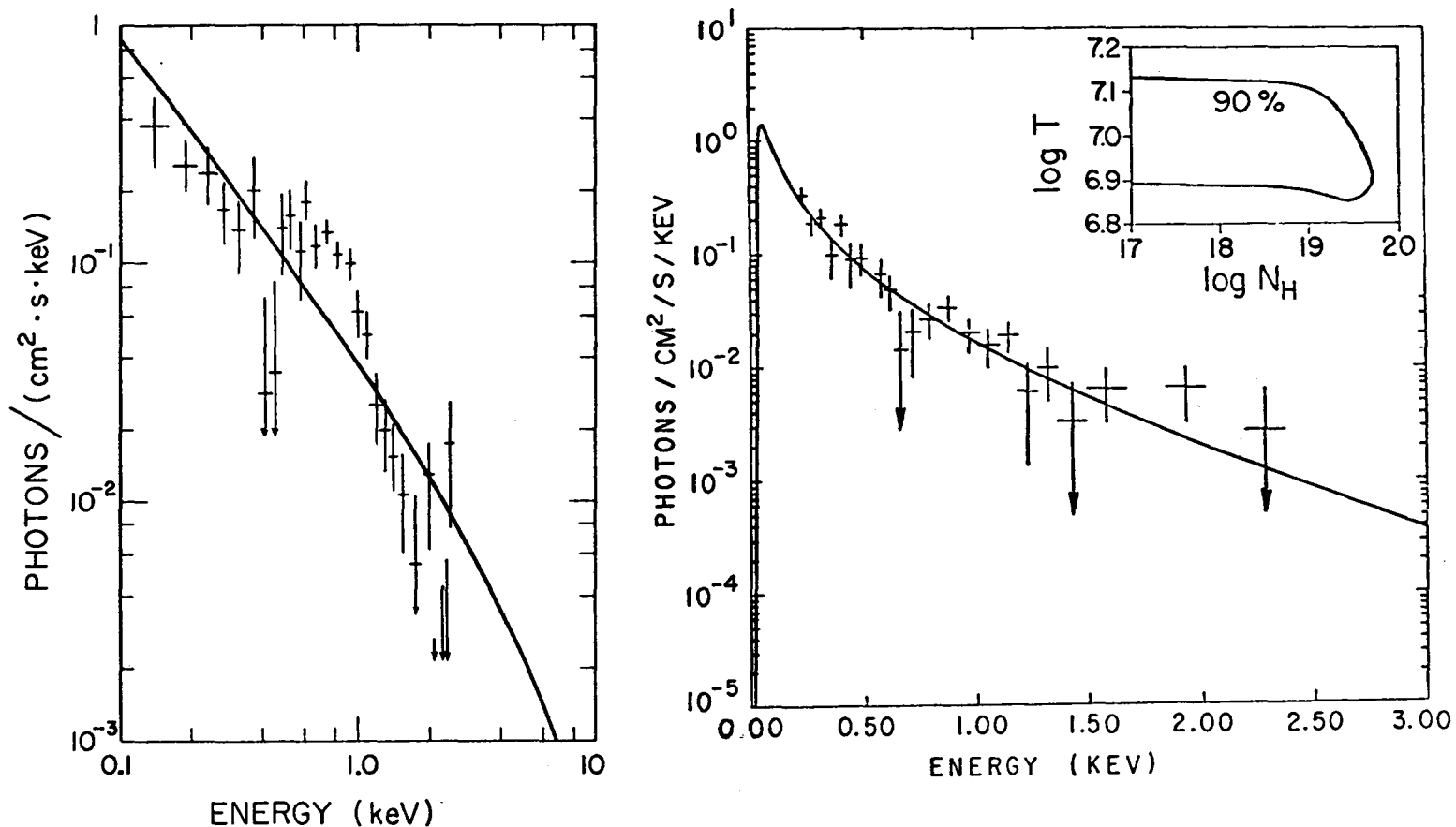


Figure 11. The Capella spectrum on the left showing the enhancement of about 800 eV due to ionized iron emission at a temperature of about  $10^7$  K from Cash et al. (1978). The right hand figure is UX Arietis showing no iron emission even though the temperature is  $\sim 10^7$  K also implying a decreased iron abundance, (from Walter et al. 1978b, Table I).



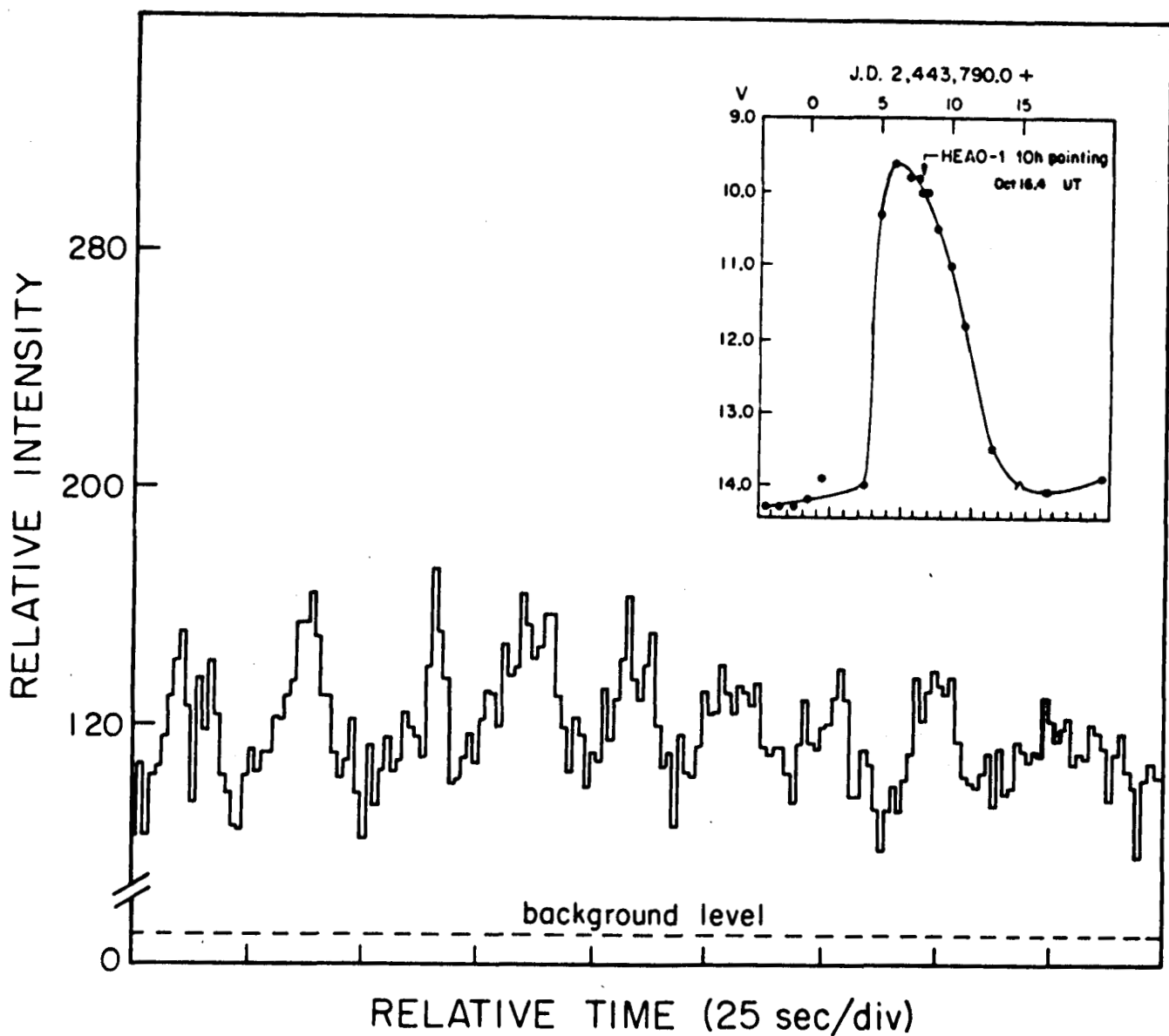


Figure 12. The pointed observation of U Gem in 1978. The inset is the optical light curve and the lower curve is a portion of the X-ray data.

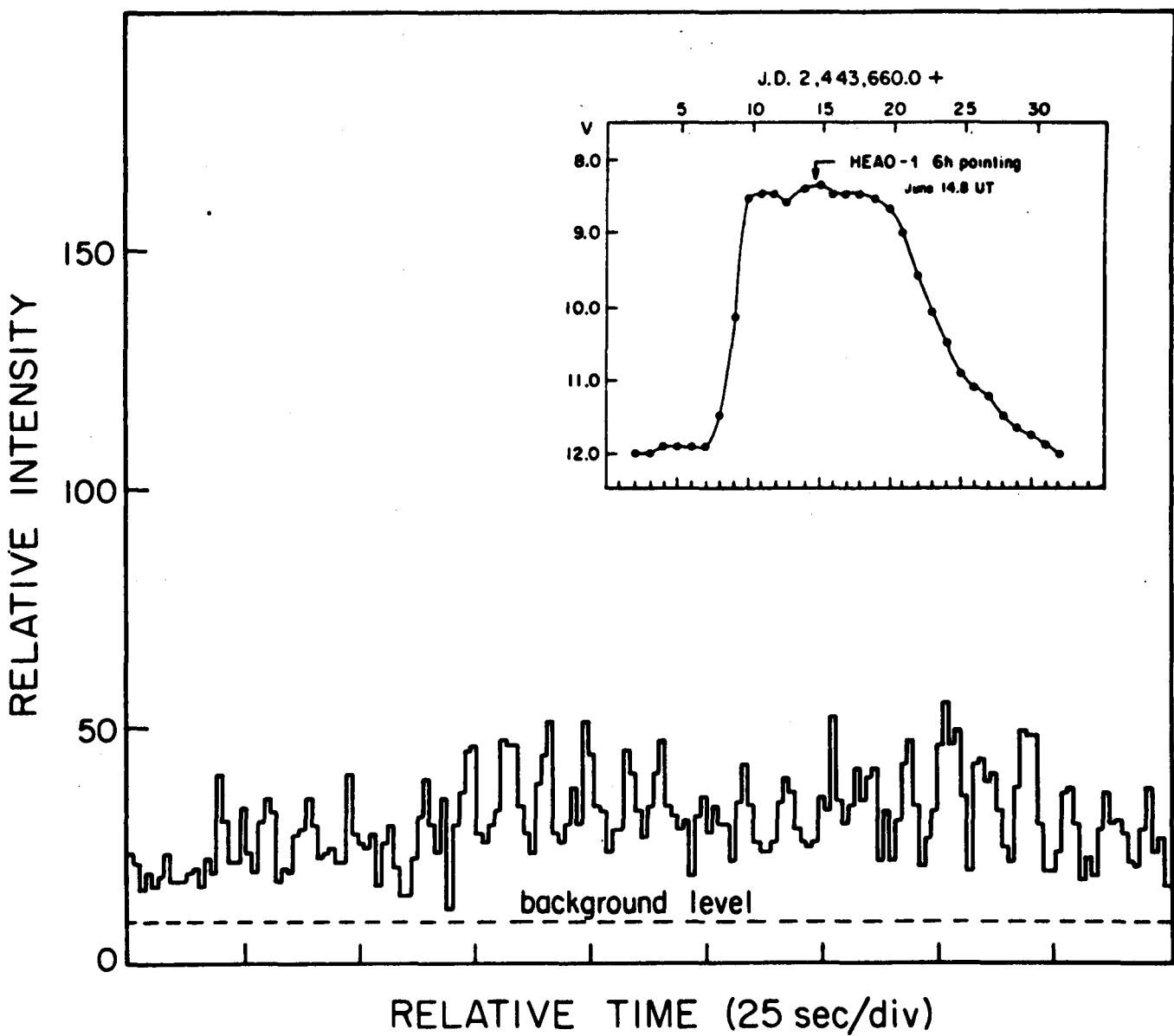


Figure 13. The pointed observation of SS Cygni in 1978. The inset is the optical light curve and the lower curve is a portion of the X-ray data.

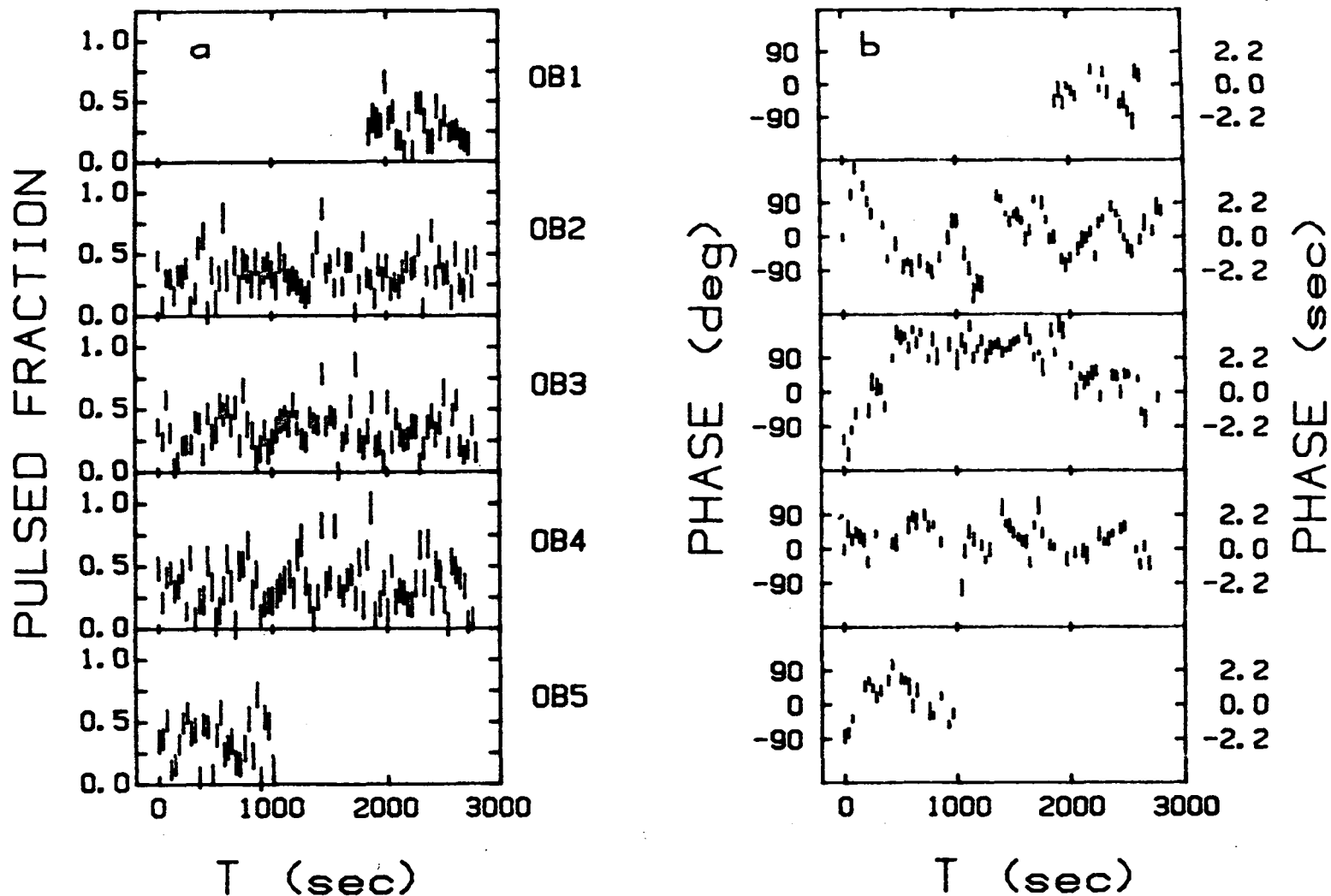


Figure 14. The pulsed fraction observed in SS Cygni (left) for each orbit binned every 41 seconds for each orbit, and the phase relative to a constant period for each orbit (right) from Cordova (1979).

# SS Cygni OB2

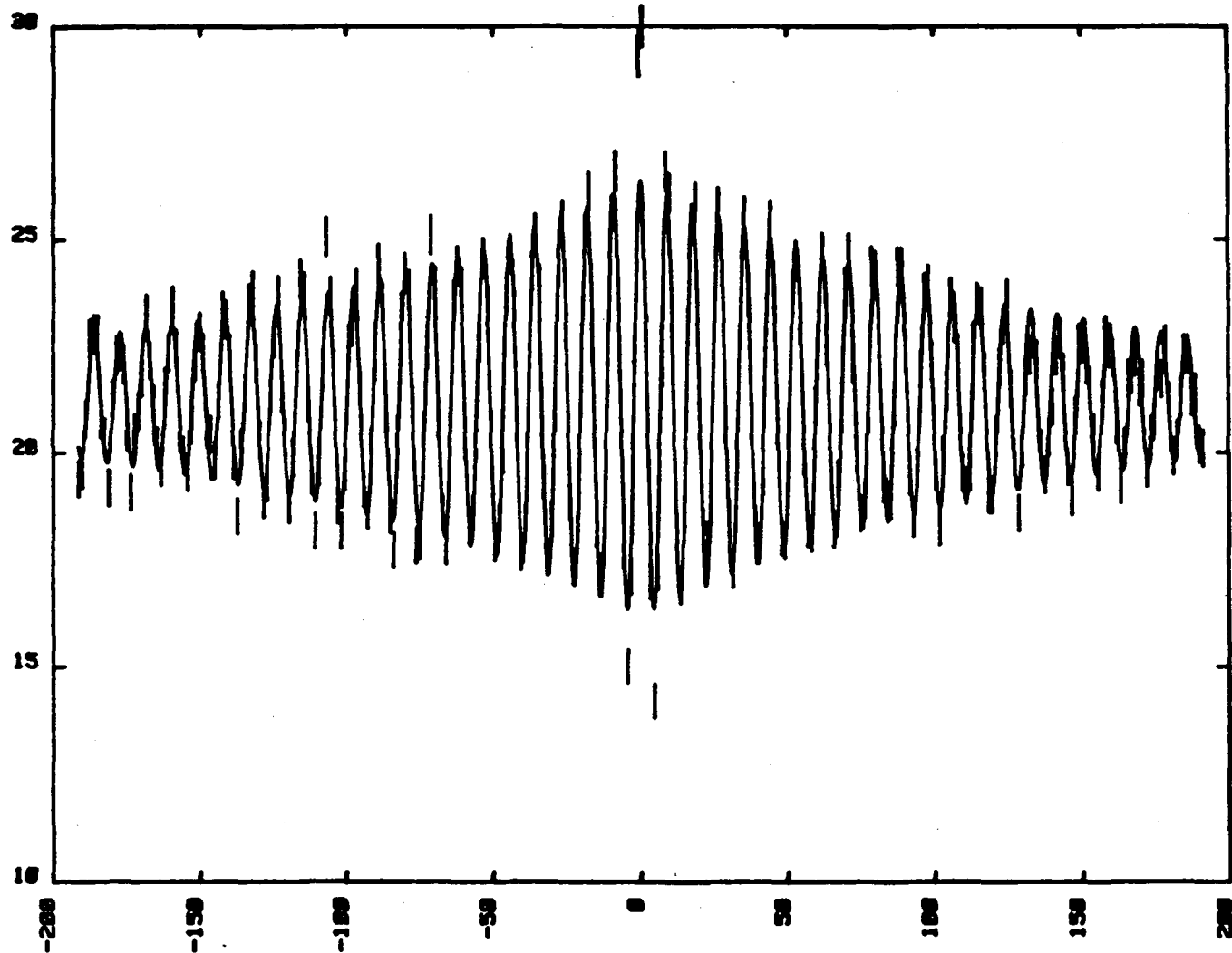


Figure 15. The superposition of pulse trains from SS Cygni. A pulse is centered with peak intensity at zero and all pulses on either side are recorded. Then the train is moved one pulse later and again all the pulses are added. A sine curve with exponentially decreasing amplitude with time is fitted to the data points.

# SS Cygni

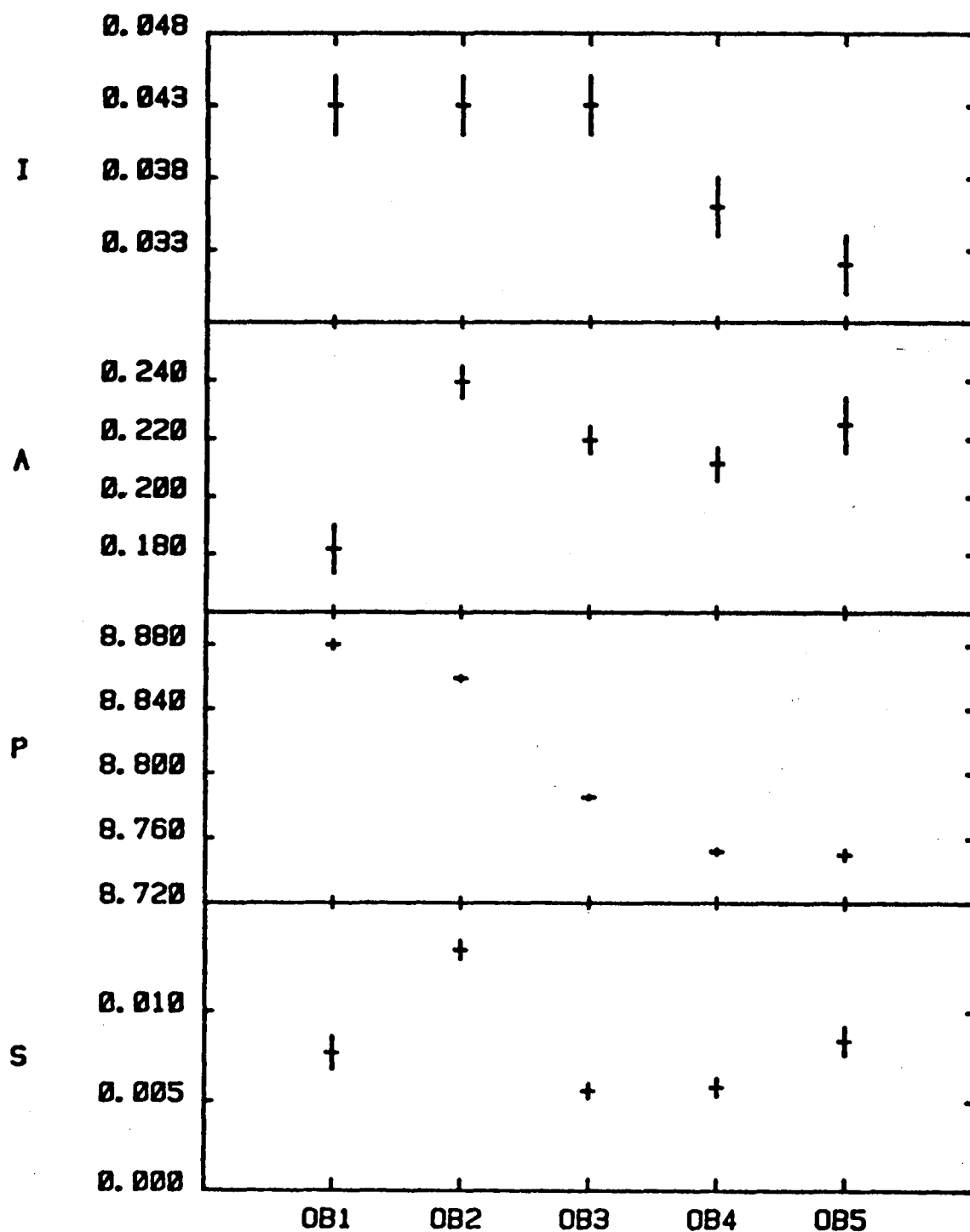


Figure 16. The intensity versus orbit number of SS Cyg (upper), amplitude of pulsations, A, period, P, and random walk strength, S.

# U Geminorum

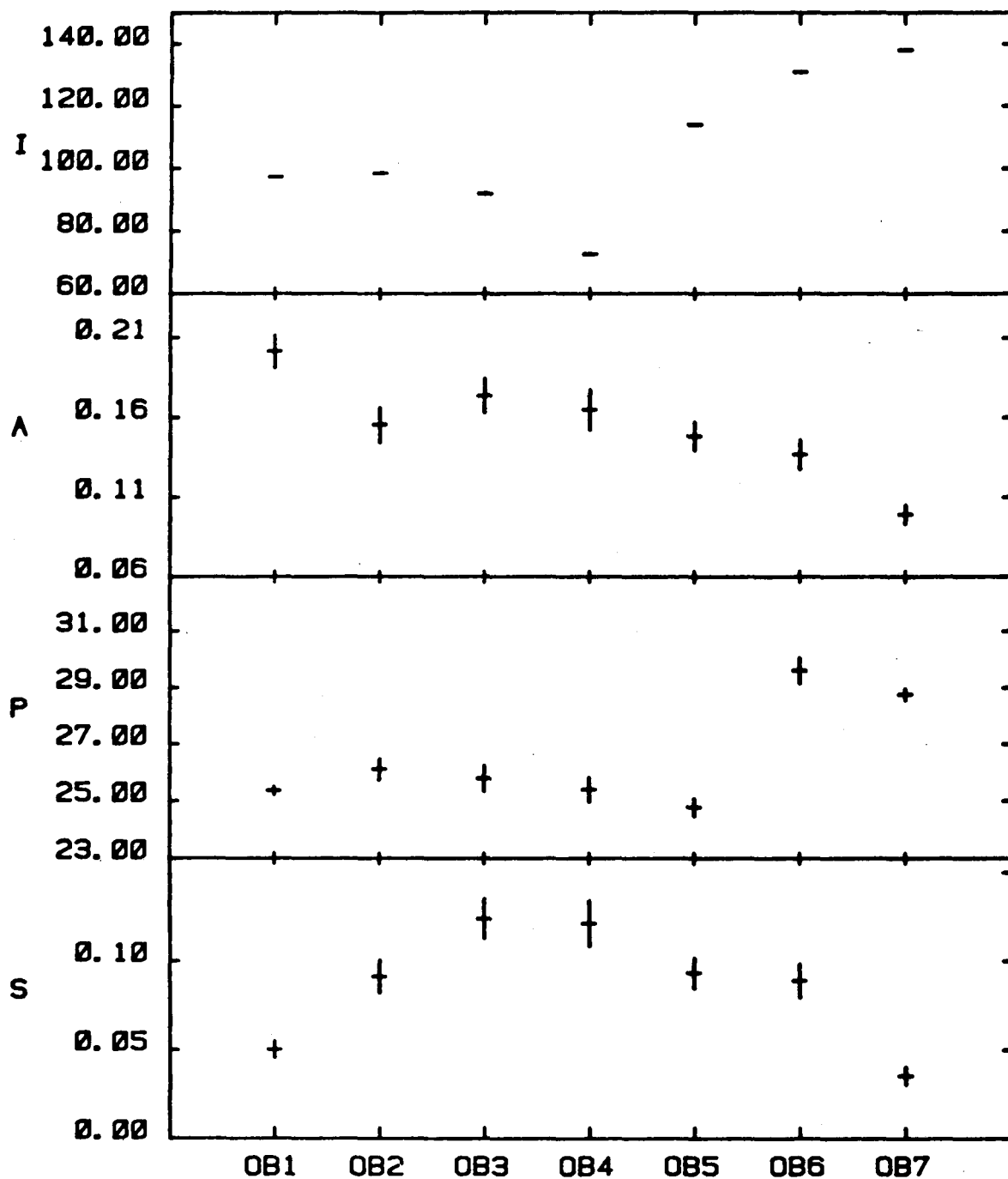


Figure 17. The intensity versus orbit number of U Gem (upper), amplitude of pulsations, A, period, P, and random walk strength, S.

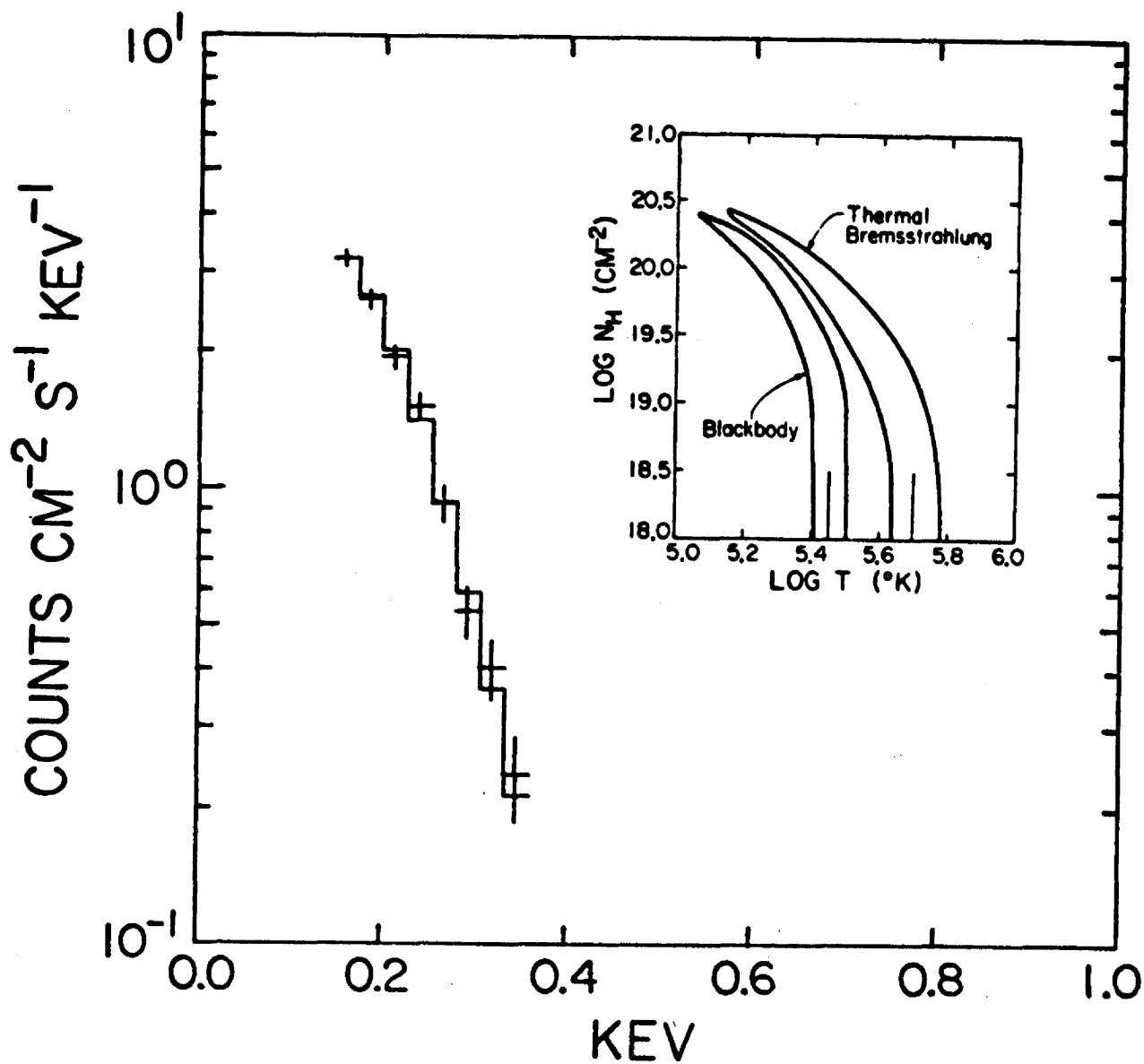


Figure 18. The pulse height spectrum of U Gem versus energy.  
The object is relatively cool.

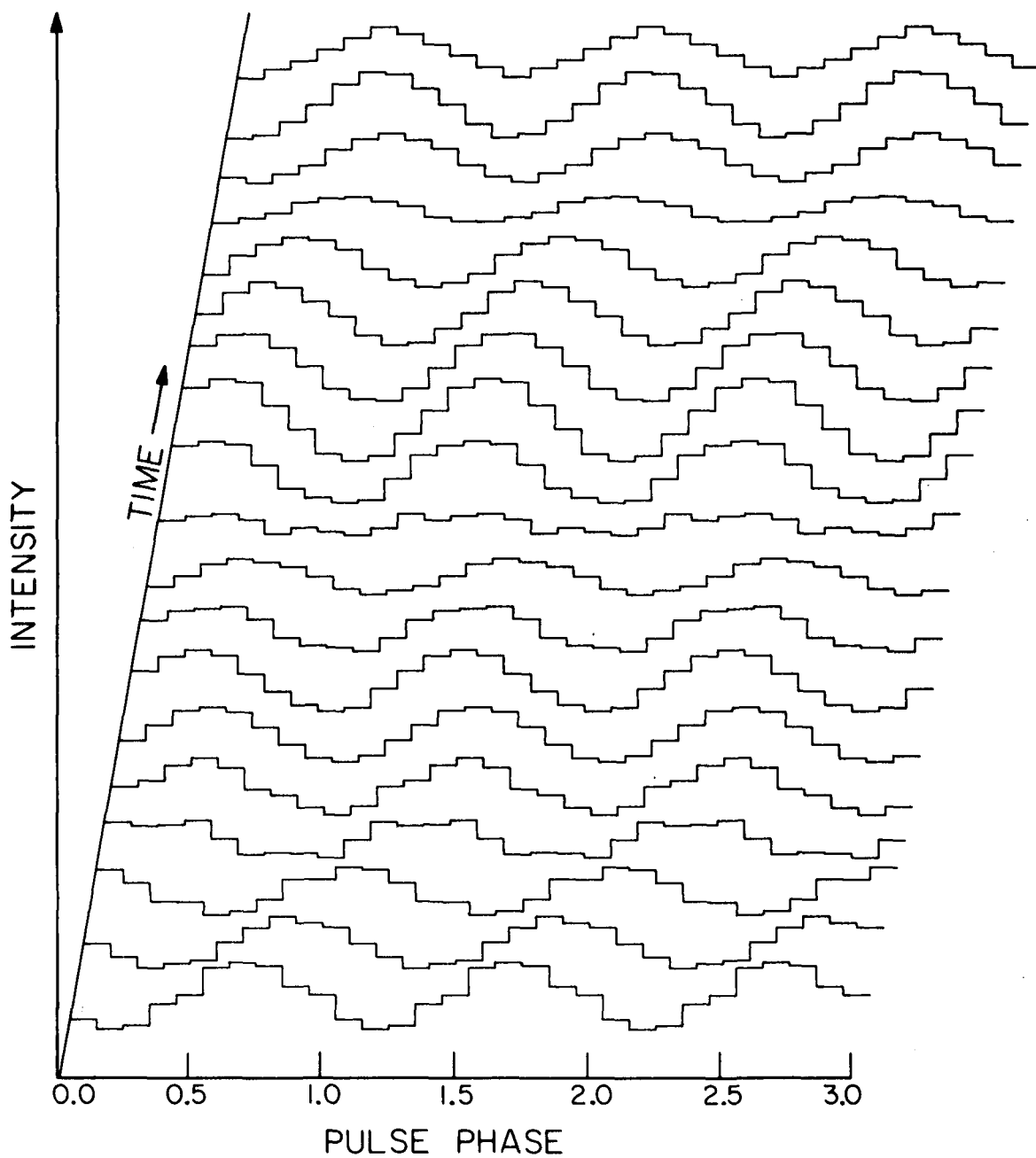


Figure 19. A plot of the SS Cygni pulsations repeated three times per line. Each line is about 15 pulses superposed at a constant period. The lines are consecutive in time.



# SPECTRAL EVOLUTION OF THE 4U1626-67 PULSE

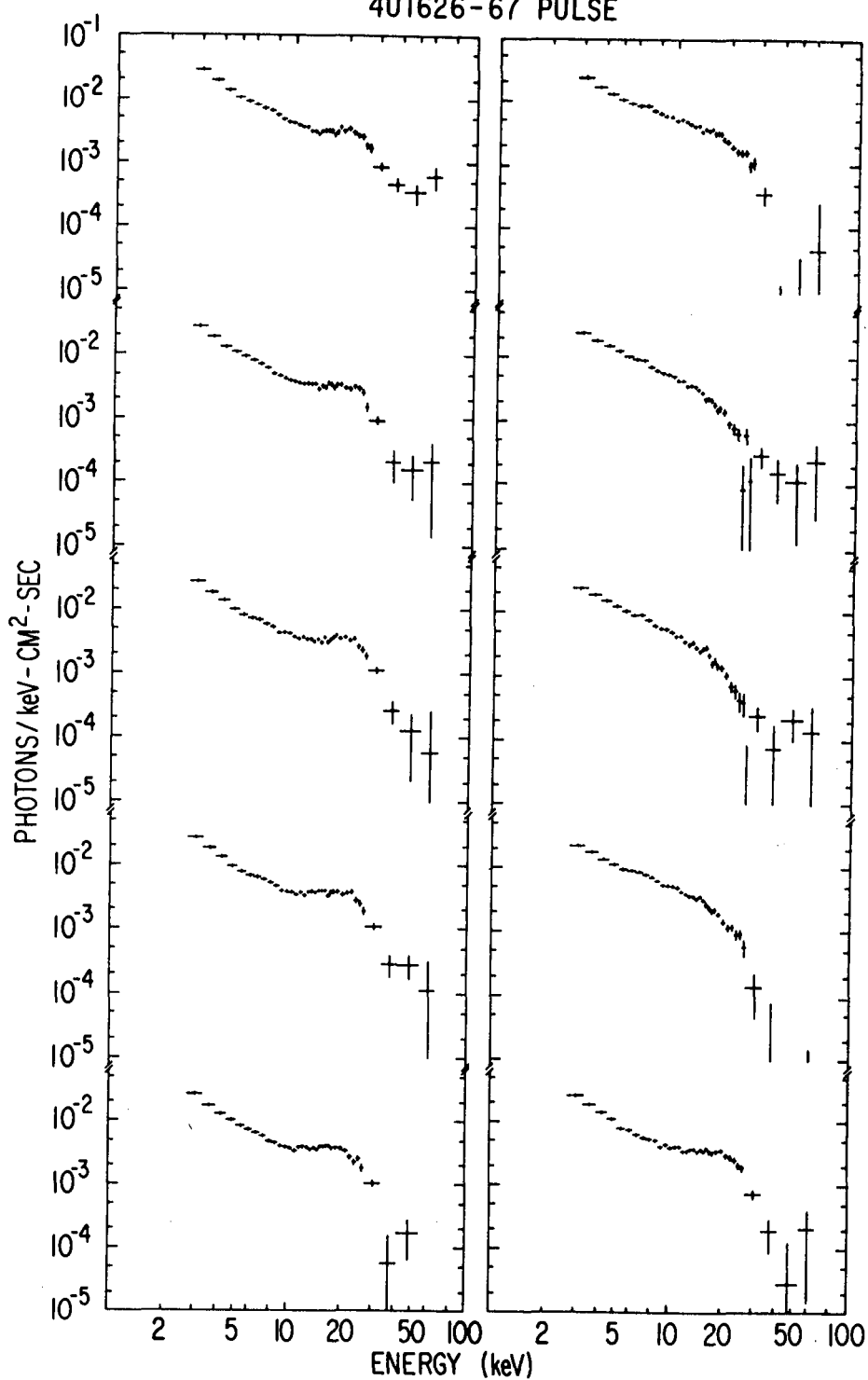


Figure 20. The pulse phase spectra of 4U 1626-67. Ten phase bins are shown representing 0.7 sec of the 7 sec period of the source. Note the feature at ~ 19 keV and the change of shape of the spectrum versus phase. Read down the first column and then down the second for the sequence.

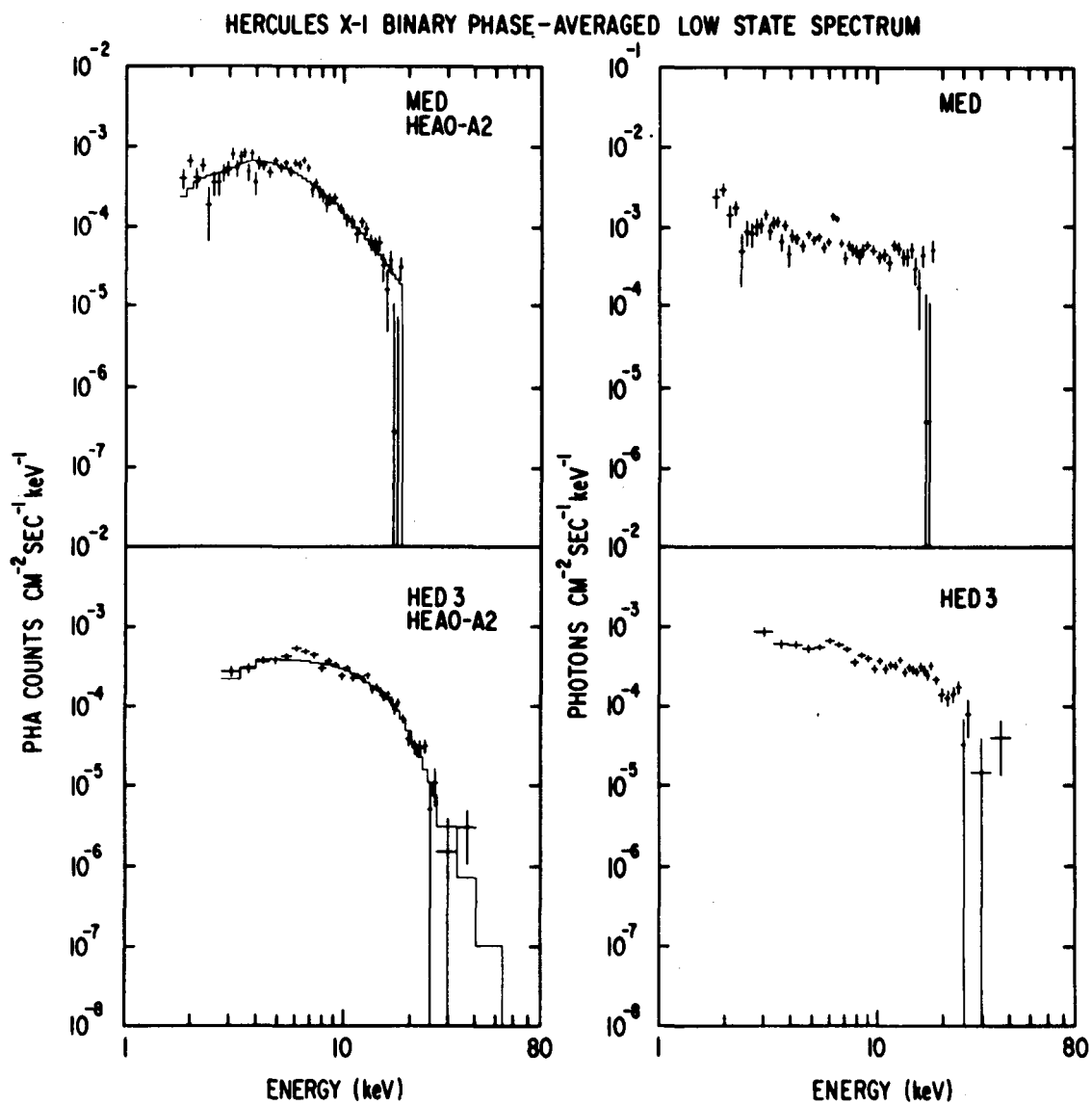


Figure 21. The low-state spectrum of Her X-1 from Pravdo et al. (1978).

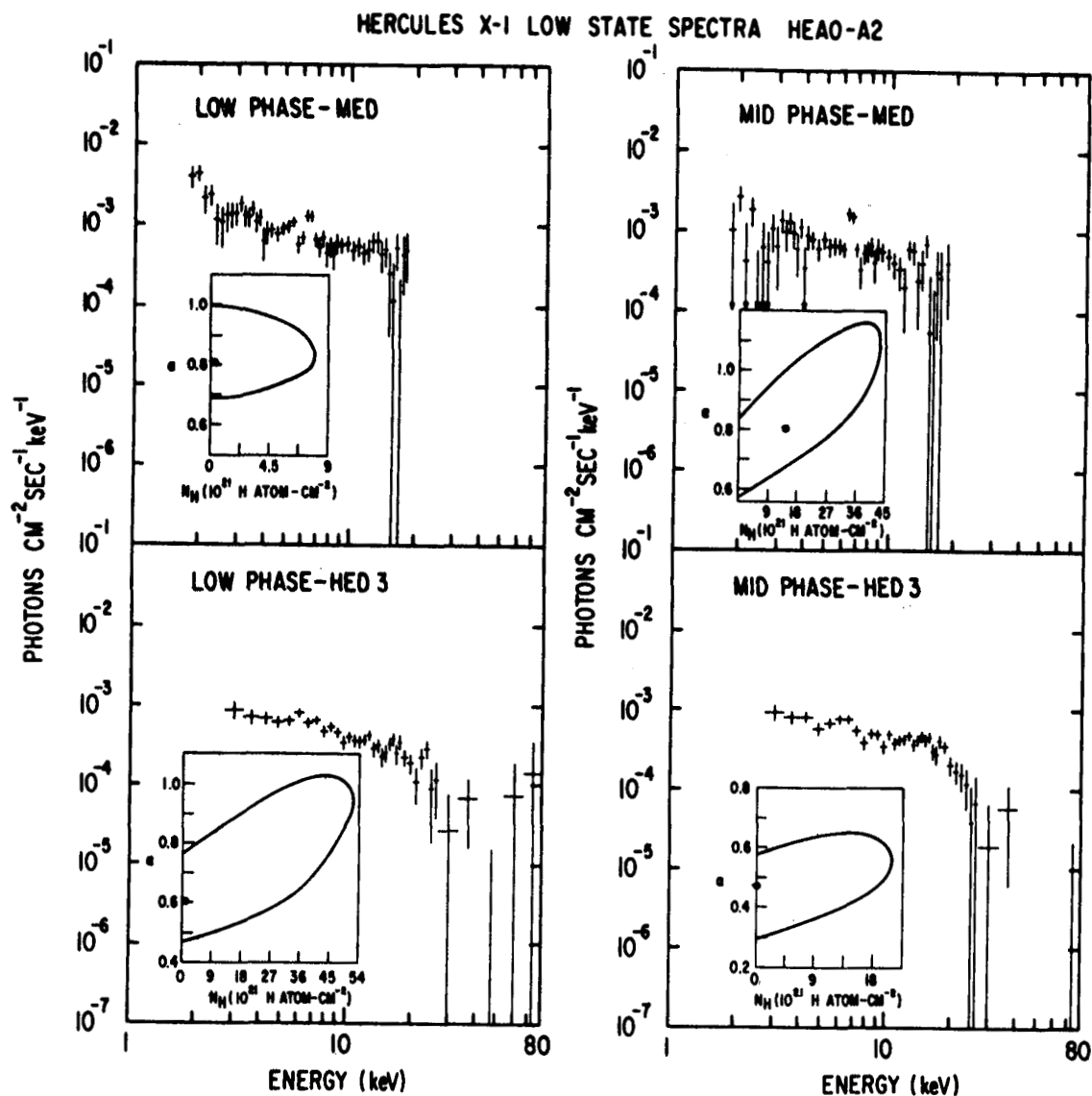


Figure 22. Fits to the low-state spectrum of Her X-1 at the beginning of the orbital binary phase (near phase zero) and toward the middle of the 1.7 day period.

X-RAY TRANSIENT 4U0115 +63  
HEAO-A2 HED

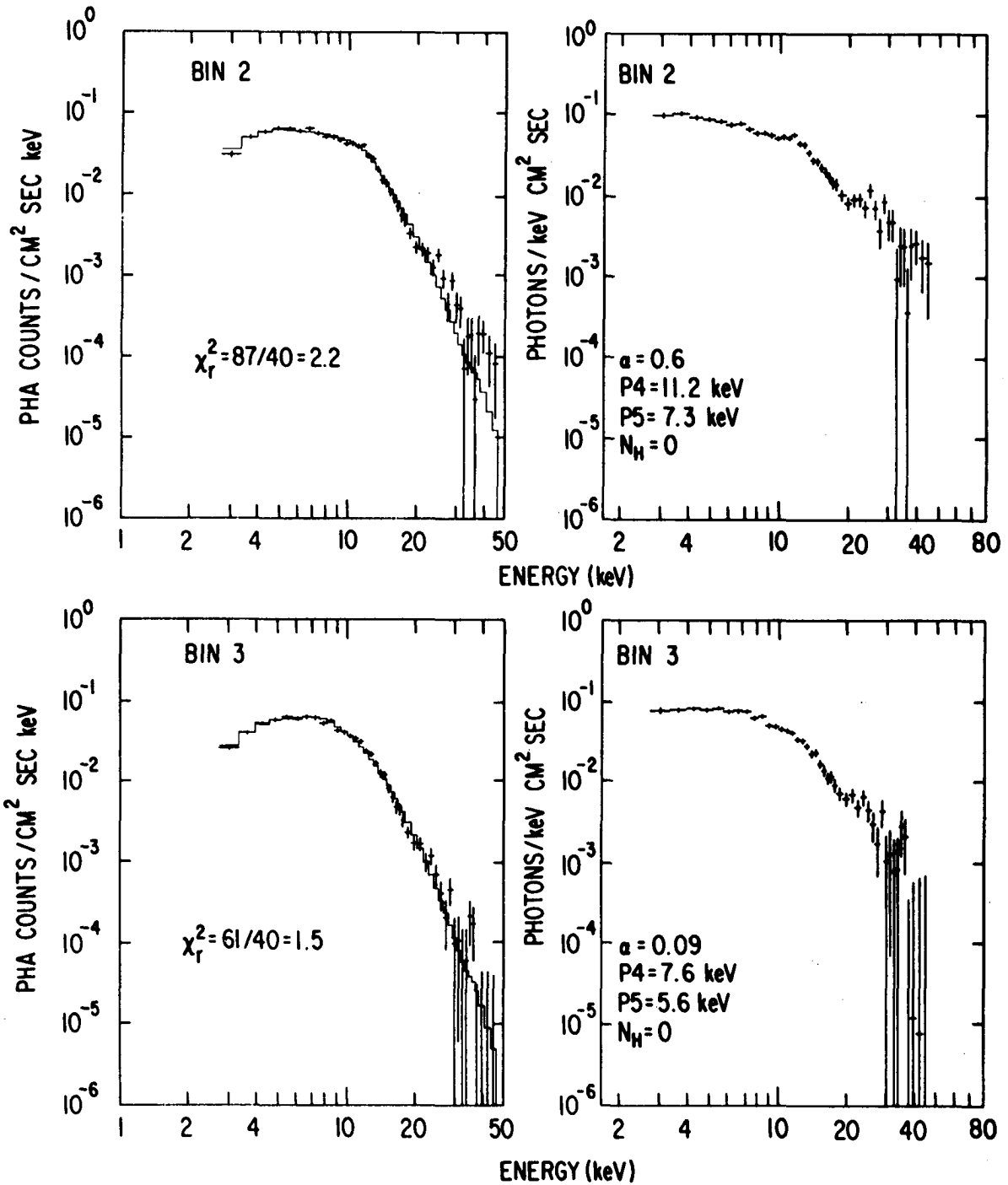


Figure 23. The spectrum of 40-0115+63, an X-ray transient with a 3.6 sec period and a hard X-ray spectrum in two of ten phase bins during the rotation of the neutron star.

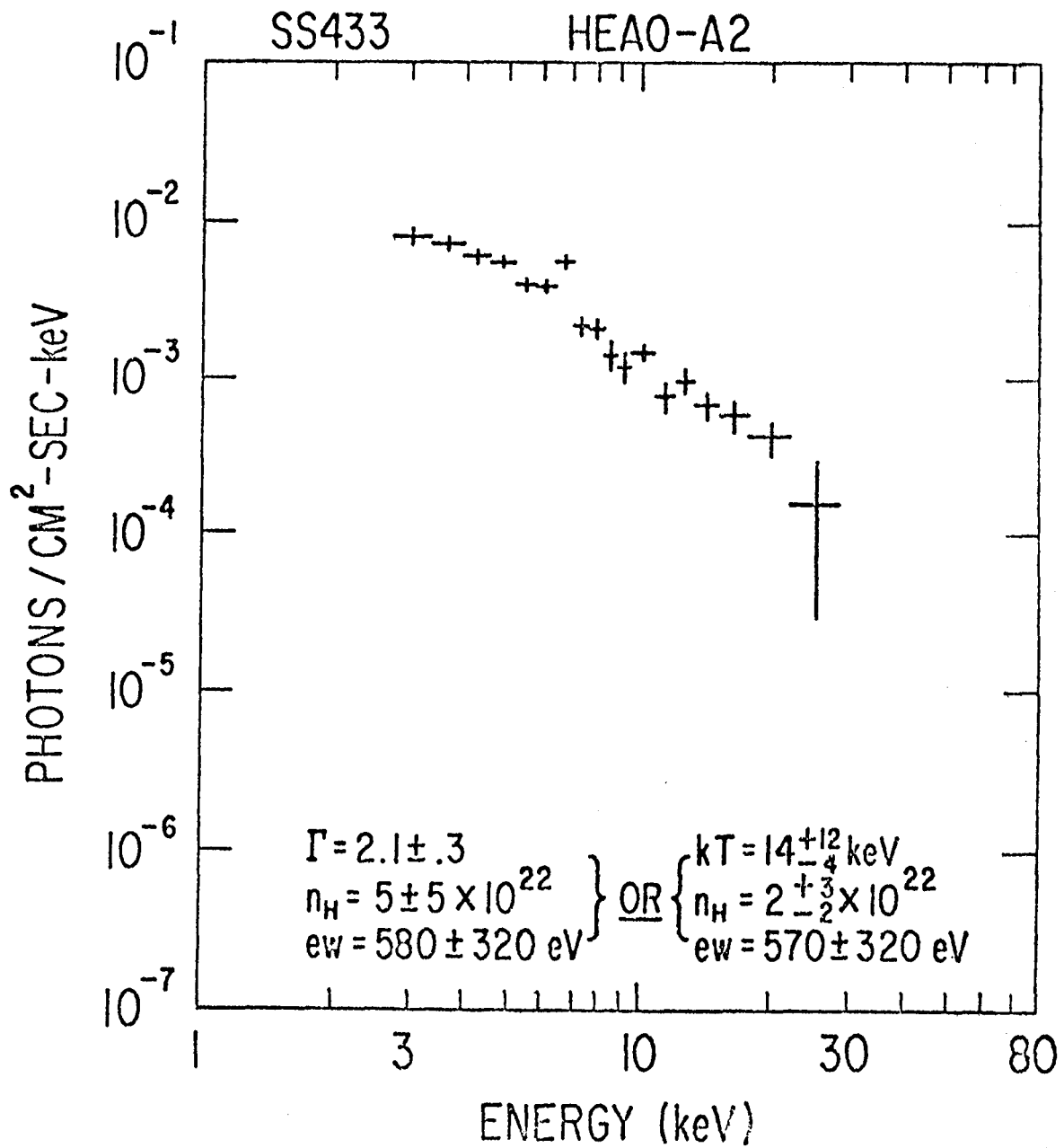


Figure 24. The deduced photon spectrum of SS433. Note the iron-line feature at 6.5 keV.

## HEAO A-2 EXTRAGALACTIC RESULTS

Dr. Elihu Boldt  
Goddard Space Flight Center

I am going to summarize some of the new things that we have learned concerning the extragalactic X-ray sky from the A-2 experiment. The first category is that of new hard X-ray sources, shown on the map in Figure 1. There are some obvious things that we can say about the new sources. First of all, most of these have been identified with extragalactic objects. In contrast to previous surveys, where clusters of galaxies have dominated the number of sources identified as extragalactic, the extended energy bandwidth of this experiment tends to single out spectra with harder components. As a result most of the identified extragalactic objects on this map are not clusters of galaxies but are isolated galaxies (i.e., active galaxies, BL Lac type objects, N galaxies). For high galactic latitudes, the number of newly identified active galaxies shown here is approximately equal to the total number of active galaxies identified as X-ray sources prior to the launch of HEAO.

Figure 2 is a map that corresponds to all the hard sources detected by the A-2 experiment in the first all-sky scan during the initial 6 months of the mission. The effective scan path of this experiment transits any given source during a limited time which is measured in days. If a particular source is off or too low during this temporal window, it is not on this map. Since source variability is quite common in X-ray astronomy this map should be considered as an all-sky "snapshot." This is our first A-2 all-sky snapshot. We are preparing a second one and most of a third.

Figure 3 presents a map of all hard sources ever detected, covering a time period of almost a decade (i.e. with data from Uhuru, Ariel 5, OSO, and SAS-3). Thus, the map consists of all sources seen prior to HEAO plus the new HEAO A-2 sources.

An important thing to notice is that, during our initial 6 month all-sky scan, we did not see many sources that had previously been seen. That is, there are well over 100 sources that were not seen with the A-2 experiment, which has an effective threshold for detection that is at least as sensitive as any of the previous scanning experiments. This result probably reflects the temporal variability of the sources that make up the extragalactic X-ray sky. We are now checking our subsequent all-sky scan for this effect. Since our experiment is extremely stable, we can compare one all-sky scan to another and get very good statistics on the overall source variability of the sky.

Figure 4 is an all-sky map of X-ray intensity; it is the first in a series that we will be developing based on the results of this experiment.<sup>1</sup> The major enhancements are associated with the galactic plane. Isolated enhancements correspond to the sources indicated on our source maps. For the most part the rest of this map is quite isotropic. We have established that galactic effects are probably less than about one percent at high galactic latitudes. This brings us to a principal goal of this experiment, which is to investigate this unresolved portion of the hard X-ray sky.

Figure 5 shows the results of an analysis on the spectrum of the unresolved X-ray background as observed at high galactic latitudes away from resolved hard X-ray sources. What is plotted here is the ratio of the observed flux to that predicted for three different thermal models. There are many different symbols used for these plots, corresponding to the fact that the A-2 instrument looked at this problem in many different ways (e.g., different detectors, different layers of different detectors) in order to minimize any systematic problems. What we see here is that the right temperature is about a half-billion degrees (i.e.,  $kT \approx 45$  keV). What seems quite remarkable is that one does get such a good fit with a single parameter spectrum. A simple power law is just not an acceptable fit to these data. The statistical error bars below about 15 keV are smaller than the size of the symbols. Hence, it is not a structured spectrum.

Now, if we search around for sources that are thermal, we must consider clusters of galaxies. The Perseus cluster is the brightest extragalactic X-ray source; Figure 6 shows its spectrum in terms of photon flux versus photon energy. This is the characteristic spectrum of a plasma at a temperature of about 80 million degrees. The luminosity of this source is about a million times the X-ray luminosity of our entire galaxy. In addition to the fact that this measurement has such fine statistics and provides such a good thermal fit, we have here finally found the first direct evidence for a higher energy transition to the K electron shell of iron (i.e.  $K\beta$  line is detected as well as  $K\alpha$ ) in a cluster source. More work on clusters has proceeded with the A-2 experiment. In particular, we have collaborated with the Institute of Astronomy of Cambridge University on this topic. Most recently additional clusters have been examined in detail and been found to have a lower temperature component in addition to a thermal component comparable to the Perseus cluster. This characteristic of two thermal components seems to be emerging in lower luminosity clusters.

Isolated galaxies with active nuclei are also strong X-ray sources but spectral information on these was really quite meager before HEAO. We now have spectra for sources representing all known classes of active galaxies, and I am now going to take you on a brief spectral tour of some of these, roughly in order of luminosity.

---

<sup>1</sup>Figure 4 is color-coded and therefore not useful in black and white reproduction. Color print available on request.

First of all, we consider the spectrum of the brightest X-ray galaxy, Centaurus A (Fig. 7). It is bright mainly because it is relatively nearby; although its luminosity is about 1000 times the X-ray luminosity of our galaxy, it is much less luminous than most active galaxies. With such good statistics we can clearly say that this is not a thermal spectrum; it is in fact a beautiful power-law spectrum. Below a few kilovolts it shows the pronounced effect of absorption by a large amount of material (an order of magnitude more than the columnar density of gas between here and our own galactic center). Since the brightest Seyfert galaxy (NGC-4151) has a similar absorption feature, this sort of spectrum was thought to be typical of active galaxies, at least prior to the launch of HEAO. For comparison, Figure 8 shows a collection of five additional Seyfert-1 spectra observed with HEAO A2. Above a few kilovolts, they all have power law spectra that have essentially the same index as the spectrum for Centaurus A. They range in luminosities from 1000 times the luminosity of our galaxy (NGC6814) up to 100,000 times the luminosity of our galaxy (MK 509). However, it is really only NGC6814 that shows any significant sort of absorption. As I indicated before, high absorption had previously been considered typical. Now we are led to the conclusion that perhaps absorption is only important for those active galaxies of lower X-ray luminosity. Figure 9 shows the spectrum of a Seyfert galaxy which was seen during a HEAO-1 point and then six months prior to that during a scan. Although the spectrum may be represented as a power-law above a few kilovolts, at lower energies one is beginning to see a new effect. The unexpected feature is a steep component which varied by a factor of two during 6 months.

Moving up in luminosity, Figure 10 shows the spectrum of an N galaxy (3C111) with an X-ray luminosity of 300,000 times that of our galaxy. Again, it has a power-law spectrum with an index approximately that of Centaurus A, but with no significant absorption. The class of strong X-ray sources identified with N galaxies was discovered with the HEAO A-2 experiment.

Figure 11 shows the spectrum of a BL Lac type object (PKS0548-322); this one has a luminosity that is about a million times the total X-ray luminosity of our galaxy. For such extragalactic sources we obtained one of the more important new effects to be seen with this experiment, that of pronounced two-component spectra. In fact, for PKS 0548-322 the luminosity below 2 keV exceeds the luminosity above 2 keV. This represents work done in a collaboration between JPL and Goddard. Similar results have been seen for MK 501 and other BL Lac type objects in a collaboration between Cal Tech and Goddard and also for MK 421 in a collaboration between Berkeley and Goddard. MK421 also shows spectral variability; in this instance, the hard component has been seen to vary most. This situation of having two variable spectra components among the highest luminosity extragalactic objects is reminiscent of Cygnus X-1, a galactic source thought to be a black hole. I think that this aspect of the subject is going to be strongly pursued theoretically in the near future.



Going up in luminosity, Figure 12 shows a BL Lac type object (PKS2155-304) which has a luminosity of 20 million times the X-ray luminosity of our galaxy; again, this is a joint project of JPL and Goddard. In this case, the hard component at the time that this was measured was not even observable (if there at all). It turns out that about 90 percent of the luminosity of this object resides below about 2 keV. The contribution of such objects to the X-ray background would necessarily be restricted to soft X-rays, such as now readily resolved with the Einstein Observatory.

Thanks to an 18-hr "ping-pong" maneuver requested by the A-4 experimenters, we were able to get a decent spectrum for a quasar (3C273), shown in Figure 13. While the number index for a single power law fit to the spectrum is 1.41 (i.e., flatter than Cen A), these data clearly exhibit that the spectrum is not that simple. Below about 8 keV, we see good evidence for a steeper component. Unfortunately, this is the only decent quasar spectrum we have available. However, we now see that steep spectral components are quite widespread among the most luminous sources, extending not only to sources like Seyferts and BL Lac type objects but at least to one quasar as well.

Now, back to the diffuse X-ray background. Given that some of the strongest extragalactic sources have now been seen to show two component spectra, we should ask whether the unresolved background also has a steep component. Above 3 keV, we see no evidence for such a component (Fig. 5). Below 3 keV further work is required on this, with this experiment and with other experiments. Do quasars such as 3C273 make a substantial contribution to the unresolved extragalactic hard X-ray flux? I cannot answer that question, but I think that the spectrum of the background already provides us with some strong constraints. We still need broadband spectra for a reasonable sample of quasars.

## BIBLIOGRAPHY

- Agrawal, P. and Riegler, G.: An Intense Soft High Latitude X-ray Source H2156-304: A New BL Lac Object. (Fig. 12), *Ap. J. (Letters)*, in press, 1979.
- Boldt, E., Marshall, F., Mushotzky, R., Holt, S., Rothschild, R., and Serlemitsos, P.: The Cosmic X-ray Background: I. The Discrete Source Component. (COSPAR) X-ray Astronomy (edited by W. Baity and L. Peterson), Pergamon Press, Oxford, p. 443, 1979.
- Boldt, E., Stottlemeyer, A., Schafer, R., Holt, S., Rothschild, R., and Serlemitsos, P.: The Cosmic X-ray Background: II. Fluctuations in (COSPAR) X-ray Astronomy (edited by W. Baity and L. Peterson). Pergamon Press, Oxford. p. 449, 1979.
- Iwan, D., Shafer, R., and Boldt, E. Surface Brightness Maps of the Hard X-ray Sky. (Fig. 4), *Bull. AAS* 11, 442, 1979.
- Marshall, F., Mushotzky, R., Boldt, E., Holt, S., Rothschild, R., and Serlemitsos, P.: N Galaxies--A New Class of X-ray Sources. *Nature* 275, 624, 1978.
- Marshall, F., Boldt, E., Mushotzky, R., Pravdo, S., Rothschild, R., and Serlemitsos, P.: New Hard X-ray Sources Observed with HEAO-A2 (Fig. 1), *Ap. J. (Suppl)* 40, No. 3; *Abstract Ap. J.* 230, 98, 1979.
- Marshall, F., Boldt, E., Holt, S. Miller, R., Mushotzky, R., Rose, L., Rothschild, R., and Serlemitsos, P.: The Diffuse X-ray Background Spectrum from 3 to 50 keV. (Fig. 5). *Ap. J.*, in press, 1979.
- Mitchell, R., and Mushotzky, R.: HEAO-A2 Observation of the X-ray Spectrum of the Centaurus and A1060 Clusters of Galaxies. *Ap. J.*, submitted, 1979.
- Mushotzky, R., Boldt, E., Holt, S. and Serlemitsos, P.: A Change in the X-ray Spectrum of MK421. *Ap. J. (Letters)*, in press, 1979.
- Mushotzky, R., Marshall, F., Boldt, E., Holt, S., and Serlemitsos, P.: HEAO-1 Spectra of X-ray Emitting Seyfert-1 Galaxies. (Fig. 8-9) *Ap. J.*, in press, 1979.
- Riegler, G., Agrawal, P., and Mushotzky, R.: The X-ray Spectrum of the BL Lac Object PKS 0548-322. (Fig. 11), *Ap. J. (Letters)*, submitted, 1979.

Rothschild, R., Boldt, E., Holt, S., Serlemitsos, P., Garmire, G.,  
Agrawal, P., Riegler, G., Bowyer, S. and Lampton, M.: The  
Cosmic X-ray Experiment Aboard HEAO-1. Space Science  
Instrumentation 4, 269, 1979.

Worrall, D., Mushotzky, R., Boldt, E., Holt, S., and Serlemitsos, P.:  
The X-ray Spectrum of 3C273. (Fig. 13), Ap. J. (Letters), in  
press, 1979.

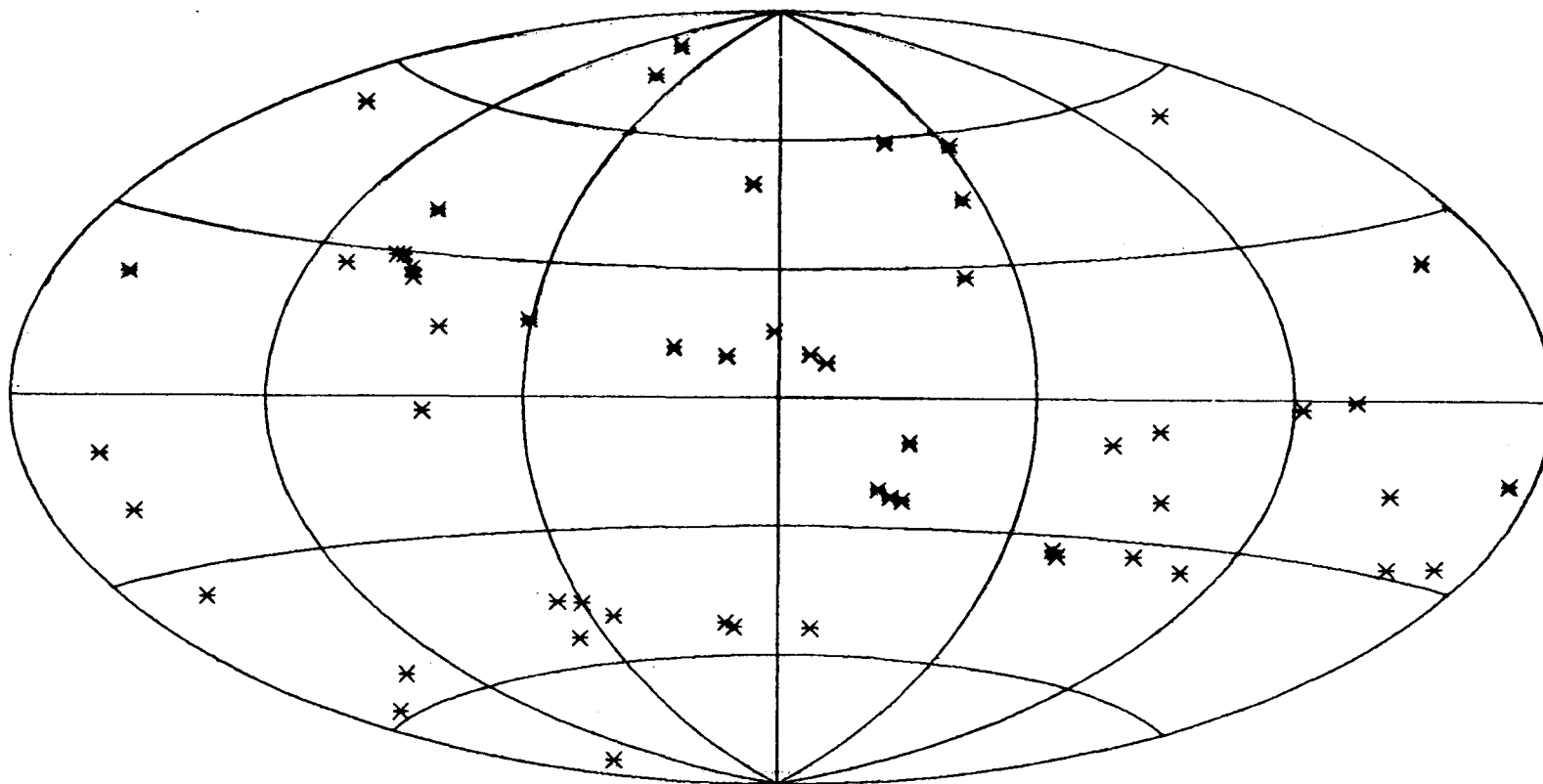


Figure 1. New hard X-ray sources (at  $> 2$  keV) discovered during the first all-sky scan with HEAO A-2. Positions are given in galactic coordinates (i.e., equator corresponds to the galactic plane).

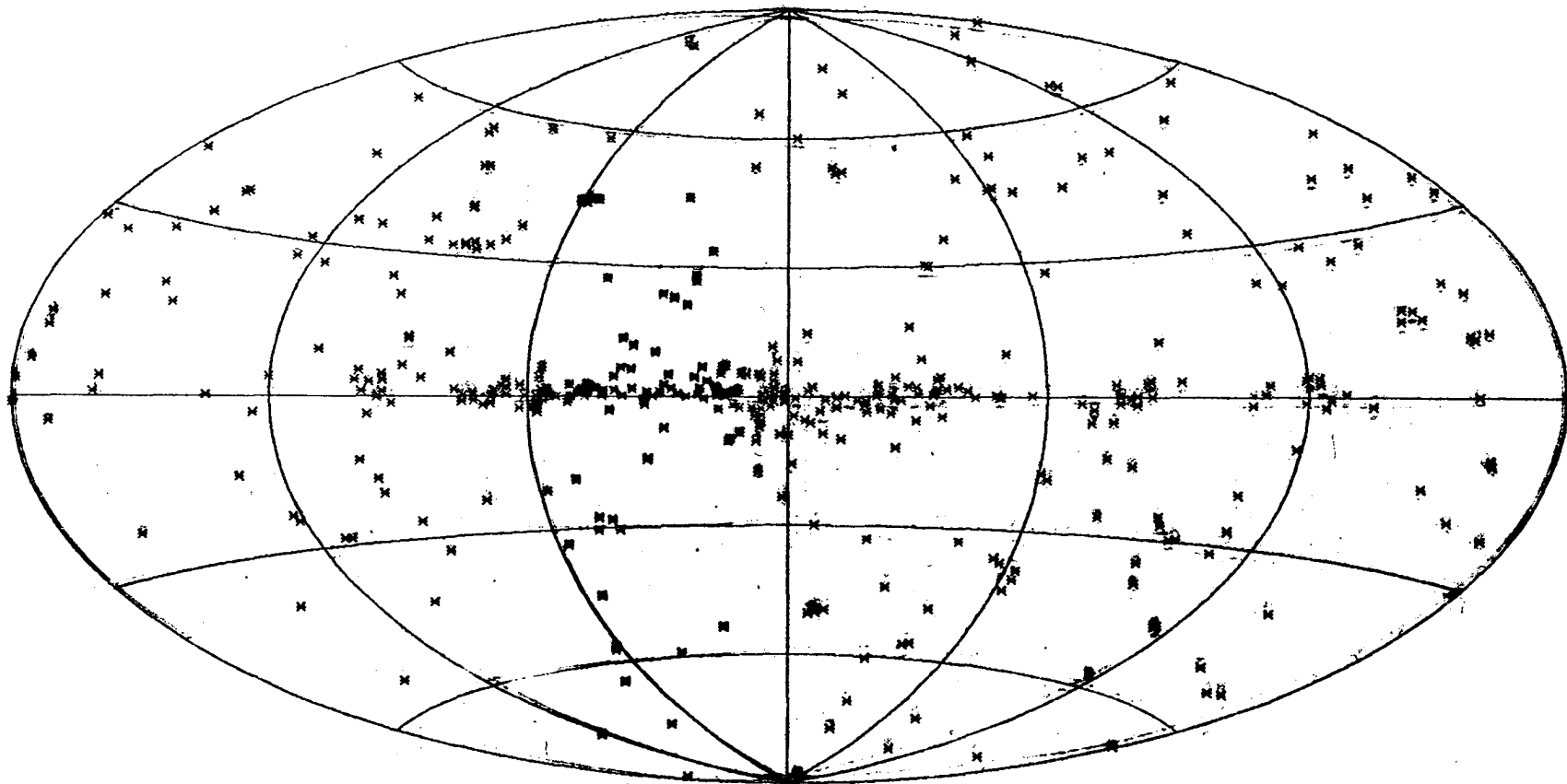


Figure 2. All hard X-ray sources detected during the first all-sky scan with HEAO A-2. Positions are given in galactic coordinates.

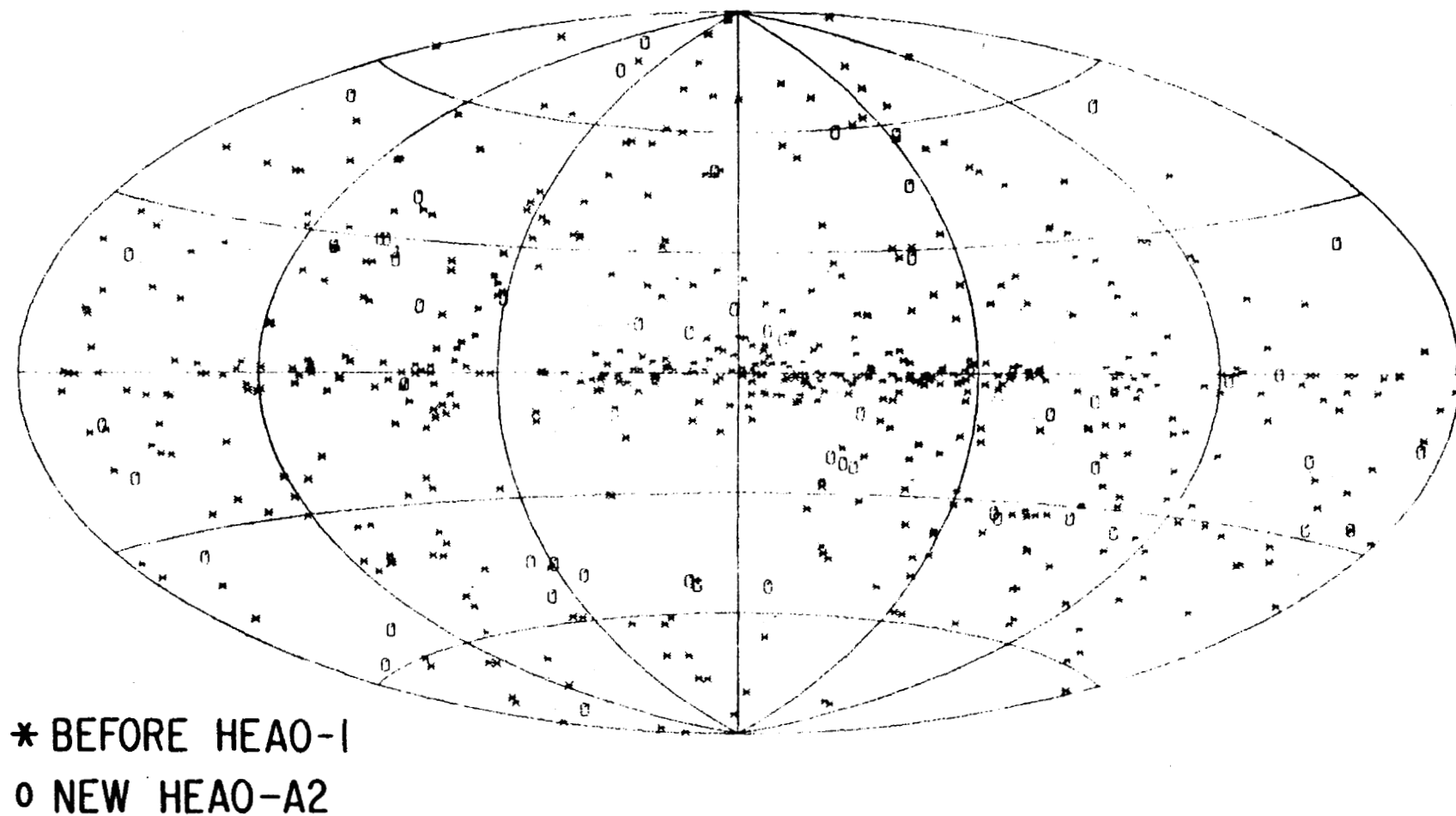


Figure 3. All hard X-ray sources ever detected. Indicated symbols distinguish new HEAO-A2 sources from those known prior to HEAO-1. Positions are given in galactic coordinates.

AVAILABLE ON REQUEST TO AUTHOR (SEE TEXT)

Figure 4. The surface brightness of the entire X-ray sky (in  $3^\circ \times 3^\circ$  pixels) as obtained with the  $1.5^\circ \times 3^\circ$  collimator section of a xenon proportional counter (HED-3 of HEAO A-2) over the band 2-60 keV. The map is presented in galactic coordinates. Intensity gradations are color-coded in the order black, blue and red (highest).

# DIFFUSE BACKGROUND THERMAL BREMSSTRAHLUNG MODEL

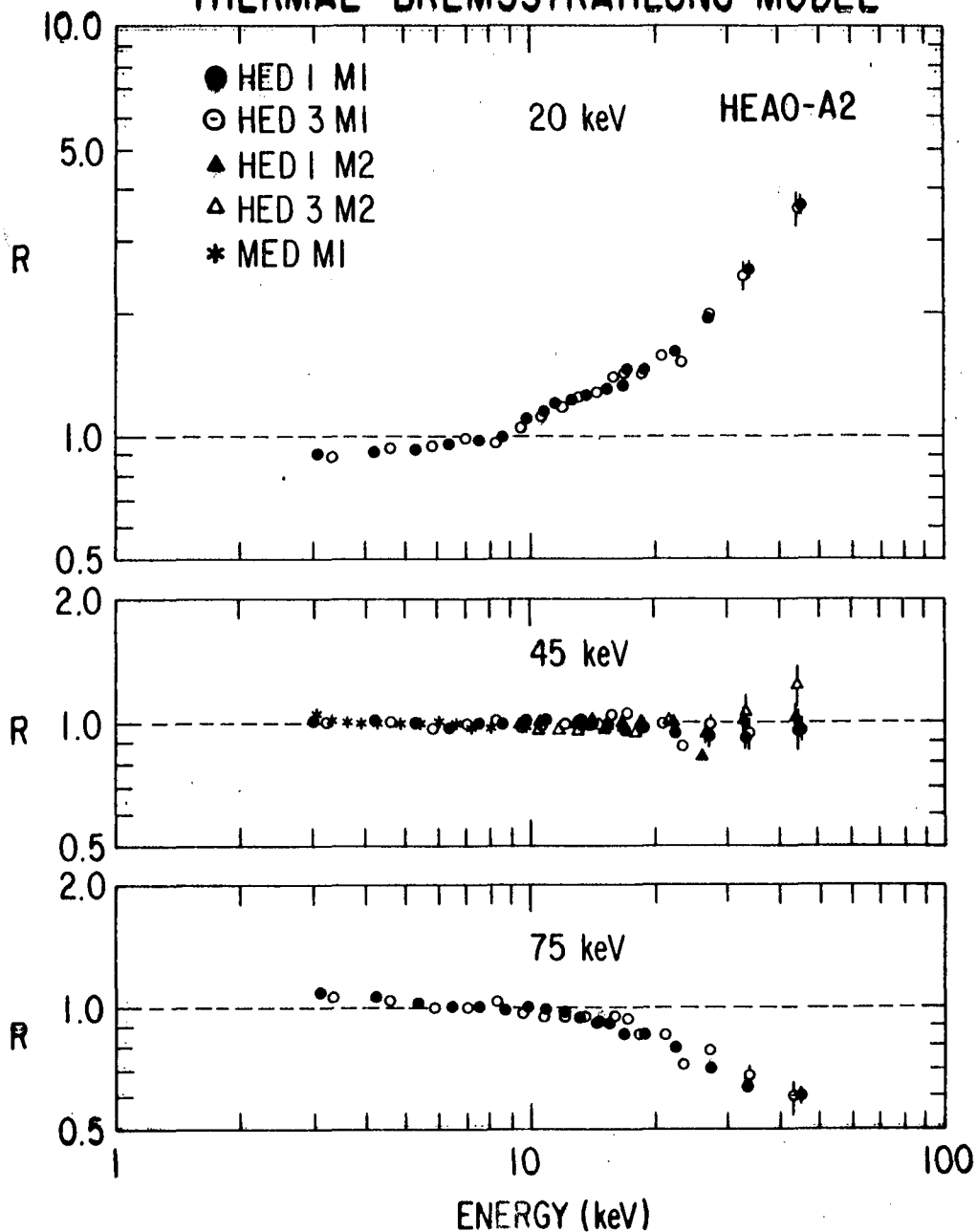


Figure 5. The ratio ( $R$ ) as a function of X-ray energy of the counts observed for the X-ray background to that predicted by convolving with the detector response function thermal bremsstrahlung incident spectra (characterized by  $kT = 20, 45, 75$  keV). Different symbols are used to represent the first layer of the MED and both layers of HED 1 and HED 3. Statistical errors are shown when larger than the size of the symbols.



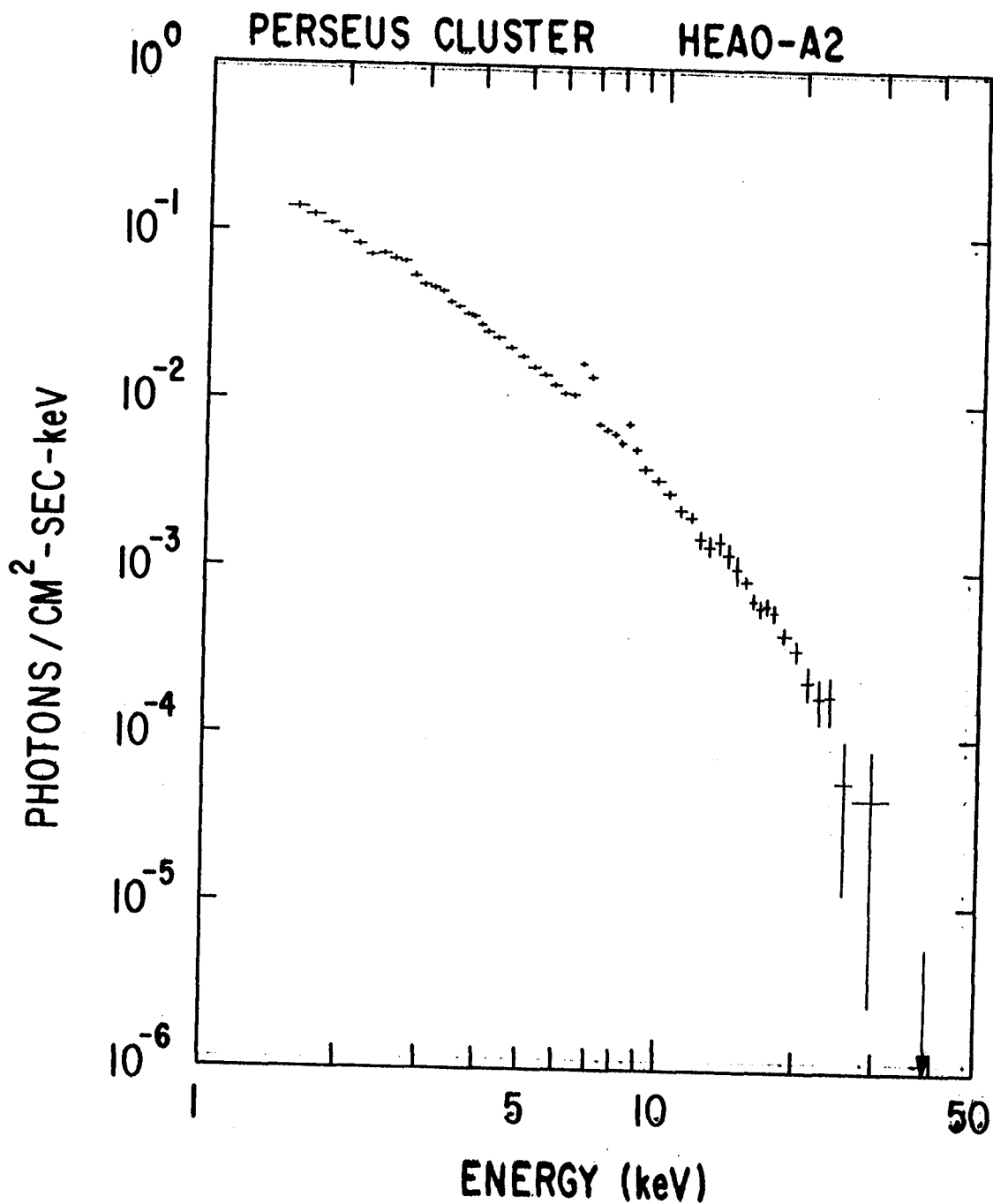


Figure 6. Incident thermal spectrum ( $kT = 6.8$  keV) for the Perseus cluster as inferred from data obtained with argon (MED) and xenon (HED) proportional counters of HEAO A2. Prominent lines in the 5-10 keV band correspond to  $K\alpha$  and  $K\beta$  transitions in iron ions having only K shell electrons.

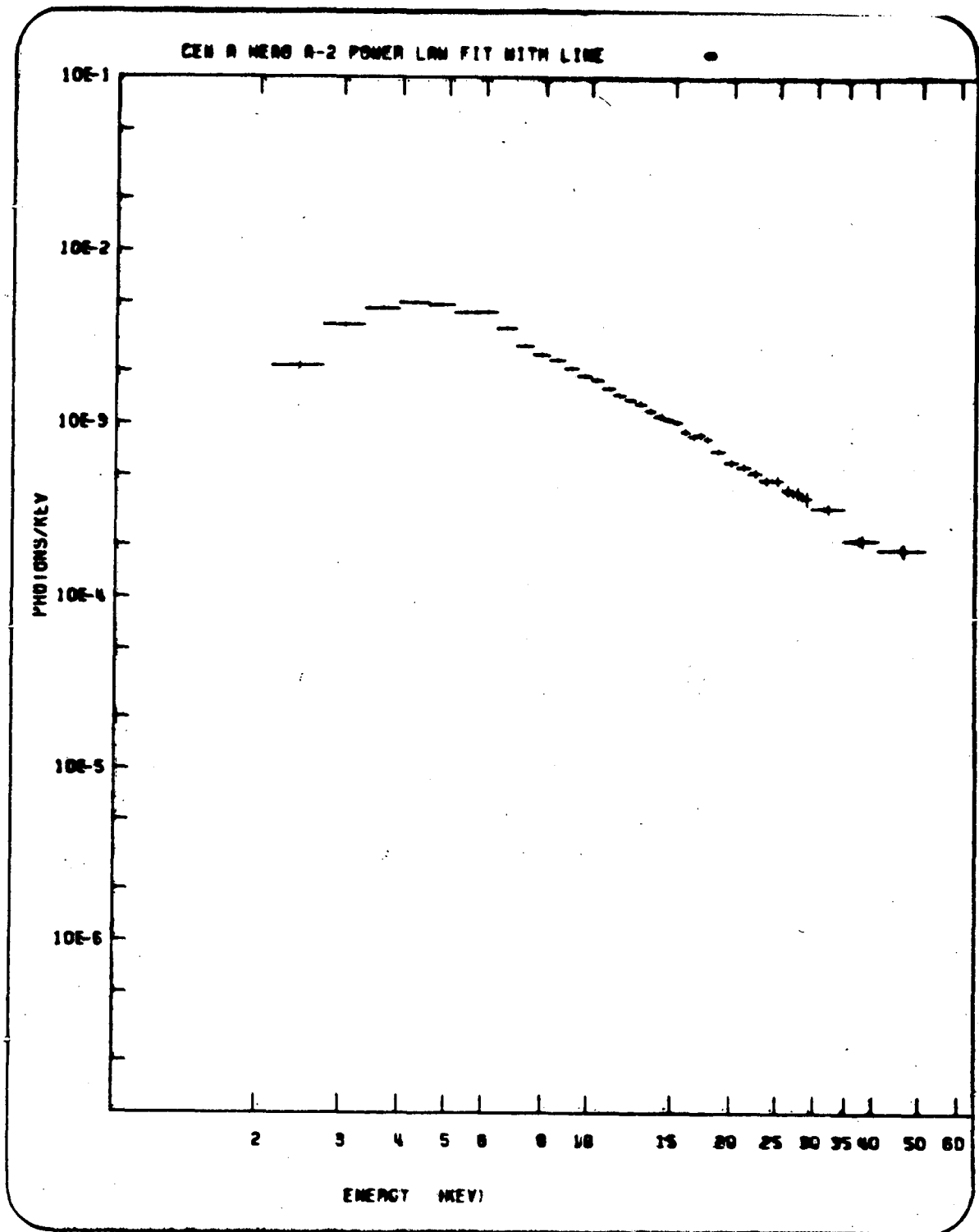


Figure 7. The X-ray spectrum for Cen A as inferred from data obtained with a xenon proportional counter (HED), using the model of a power-law spectrum at the source absorbed by surrounding ionized matter exhibiting from K fluorescence.

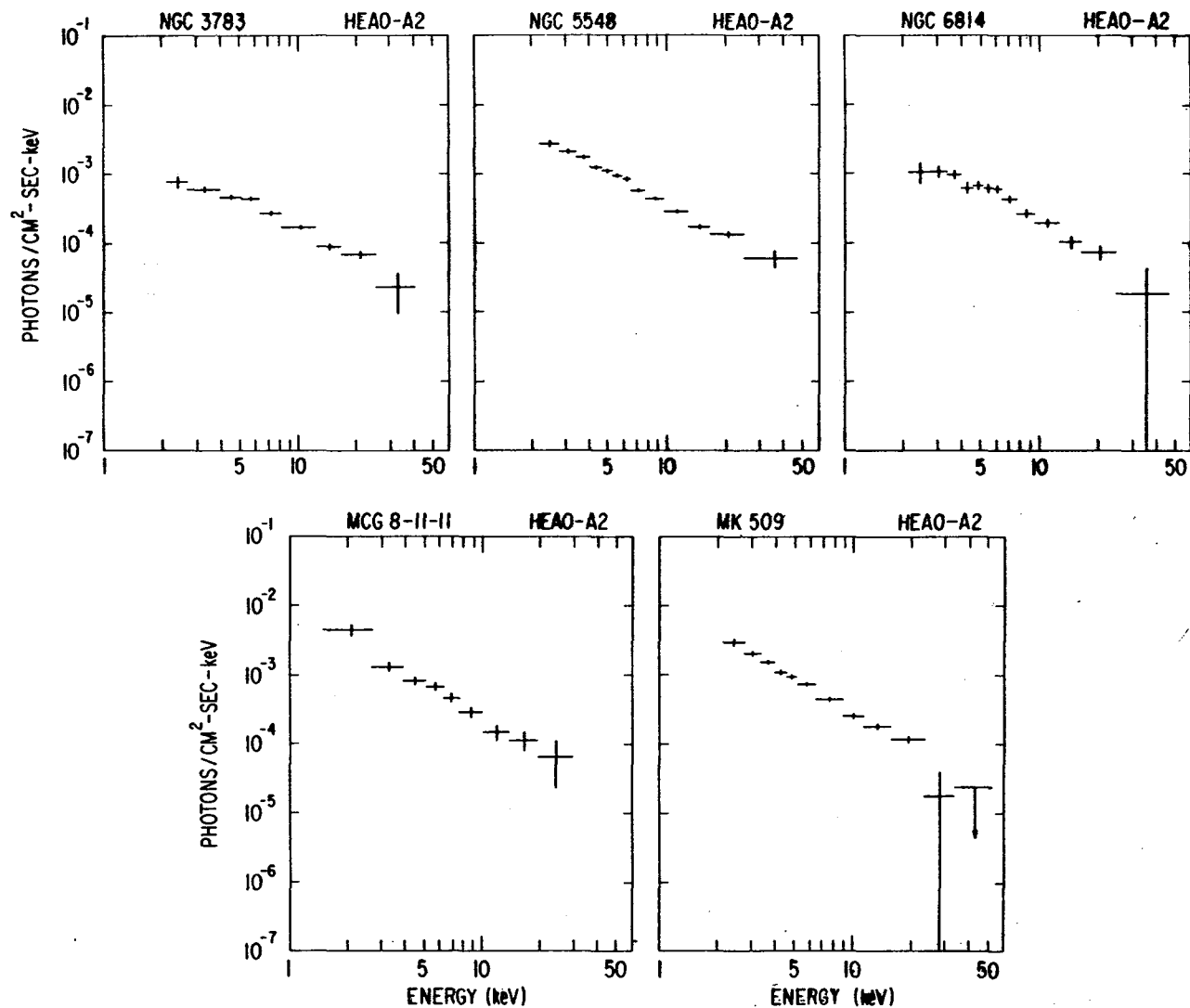


Figure 8. The X-ray spectra for 5 Seyfert-1 type galaxies as inferred from data obtained with a xenon proportional counter (HED), using the model of a power-law spectrum at the source absorbed by surrounding ionized matter. Except for MCG8-11-11, all spectra shown are from pointed data. All are consistent with a power-law spectrum of photon number index  $\sim 1.7$ ; only NGC6814 requires significant absorption to fit the data.

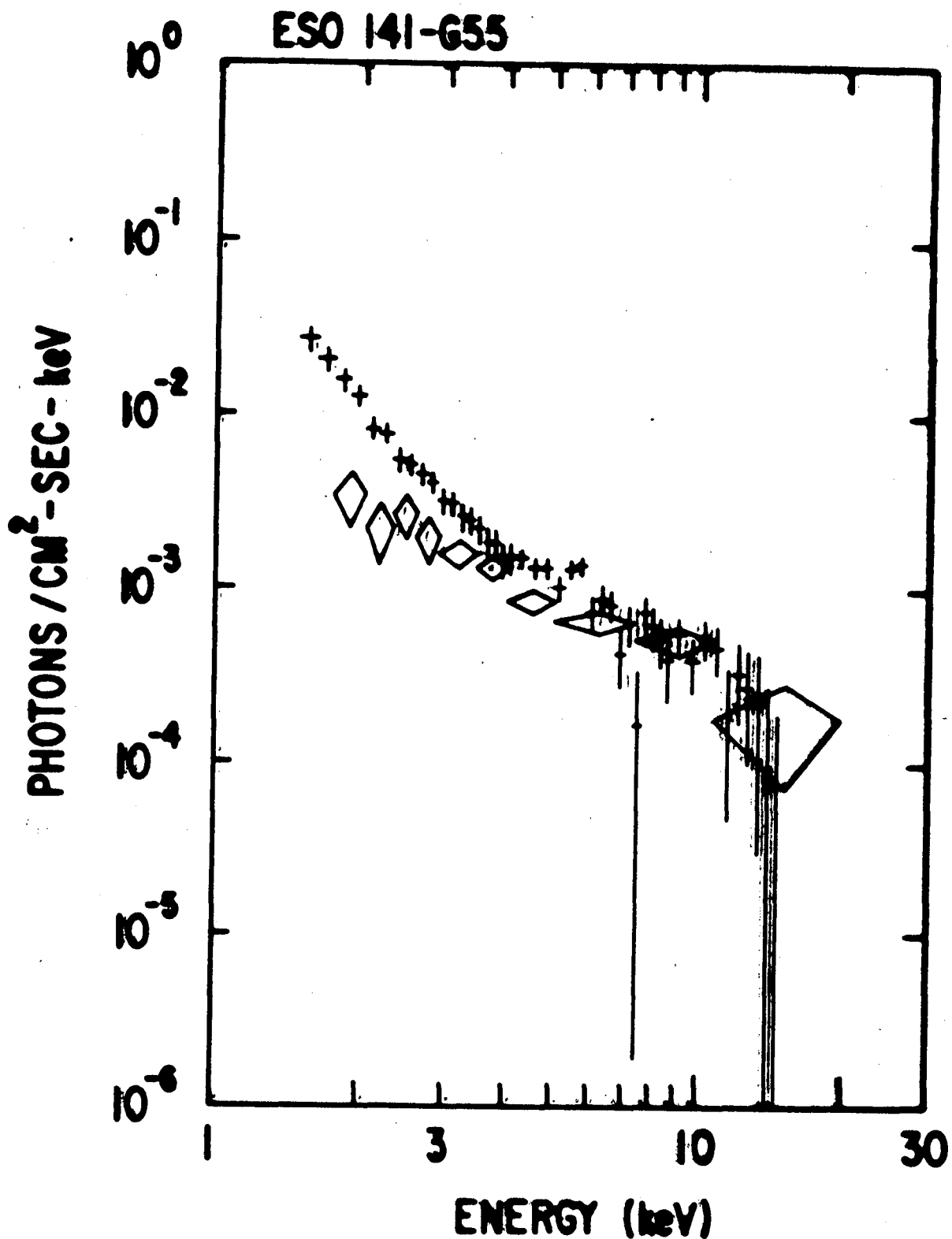


Figure 9. X-ray spectra for ESO 141-G55 inferred from data obtained 6 months apart; the initial data shown as diamonds were obtained during the normal HEAO scan while the data obtained six months later are based on a pointed observation.

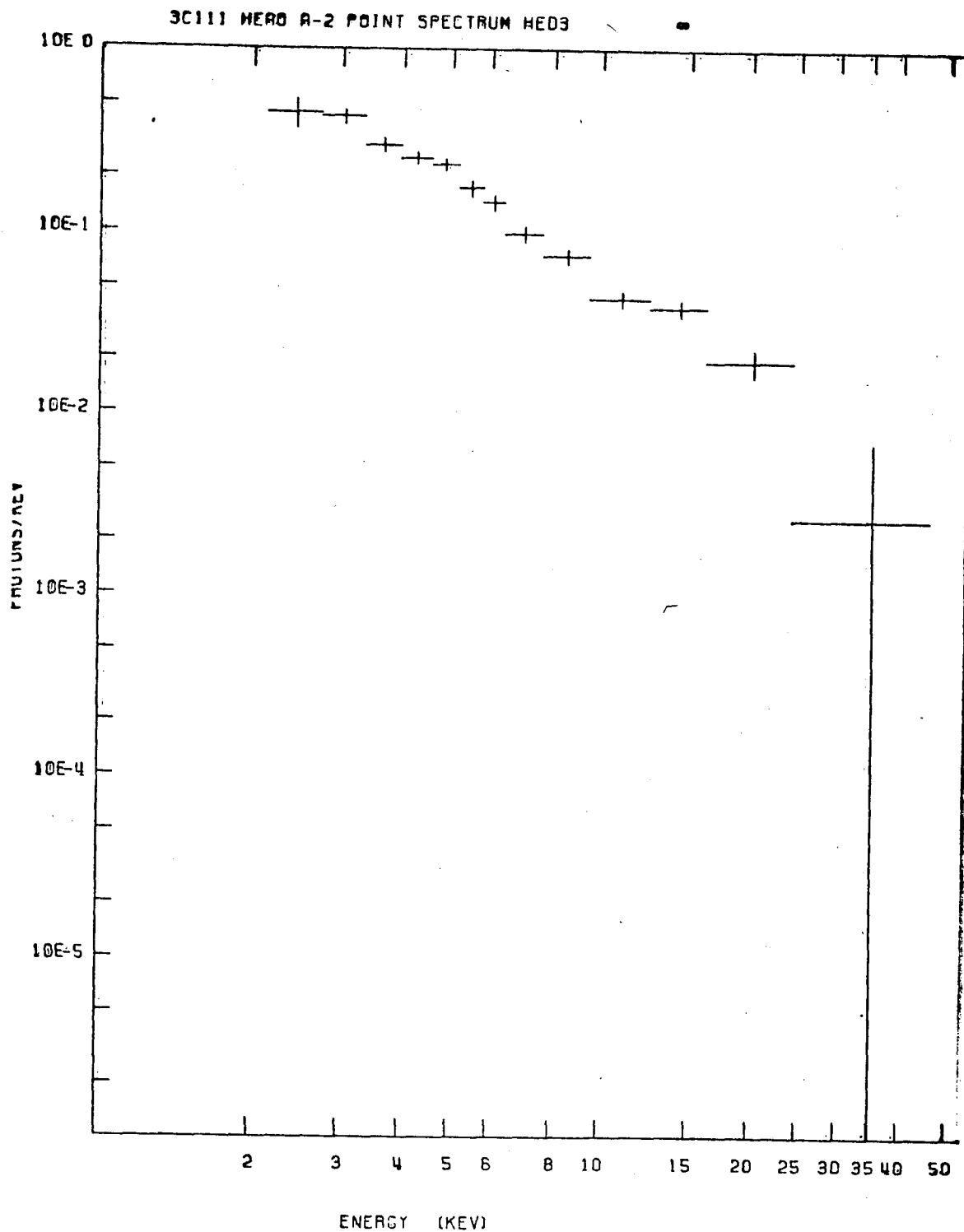


Figure 10. The X-ray spectrum for the N galaxy 3C111 as inferred from data obtained with a xenon proportional counter (HED-3), using the model of a power law spectrum.

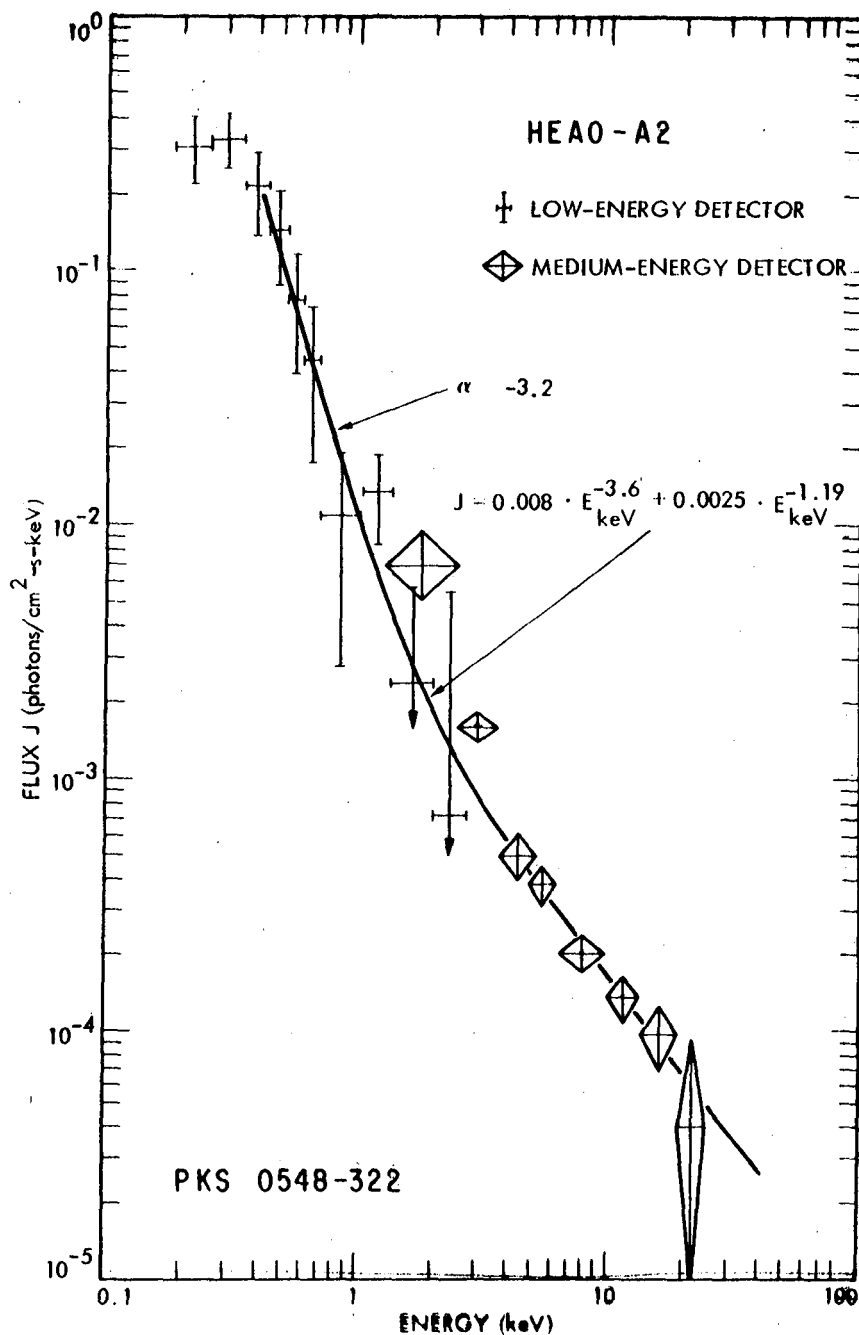


Figure 11. The X-ray spectrum for the BL Lac type object PKS 0548-322 as inferred from data obtained by a propane proportional counter (LED results from JPL indicated by crosses) and an argon proportional counter (MED results from GSFC indicated by diamonds).

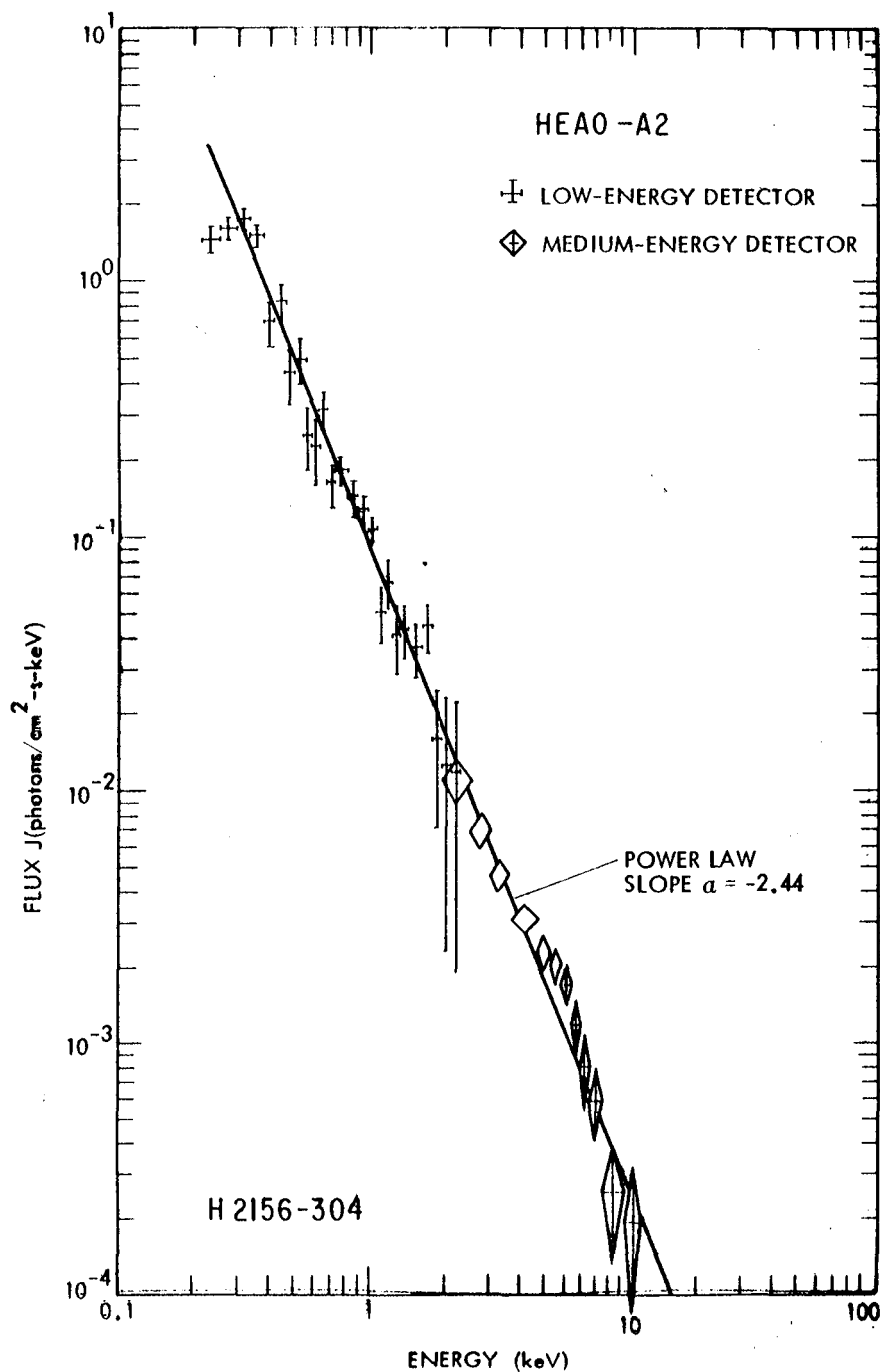


Figure 12. The X-ray spectrum for the BL Lac type object PKS 2155-304 (identified with HEAO source H2156-304) as inferred from data obtained by a propane proportional counter (LED results from JPL indicated by crosses) and an argon counter (MED results from GSFC indicated by diamonds).

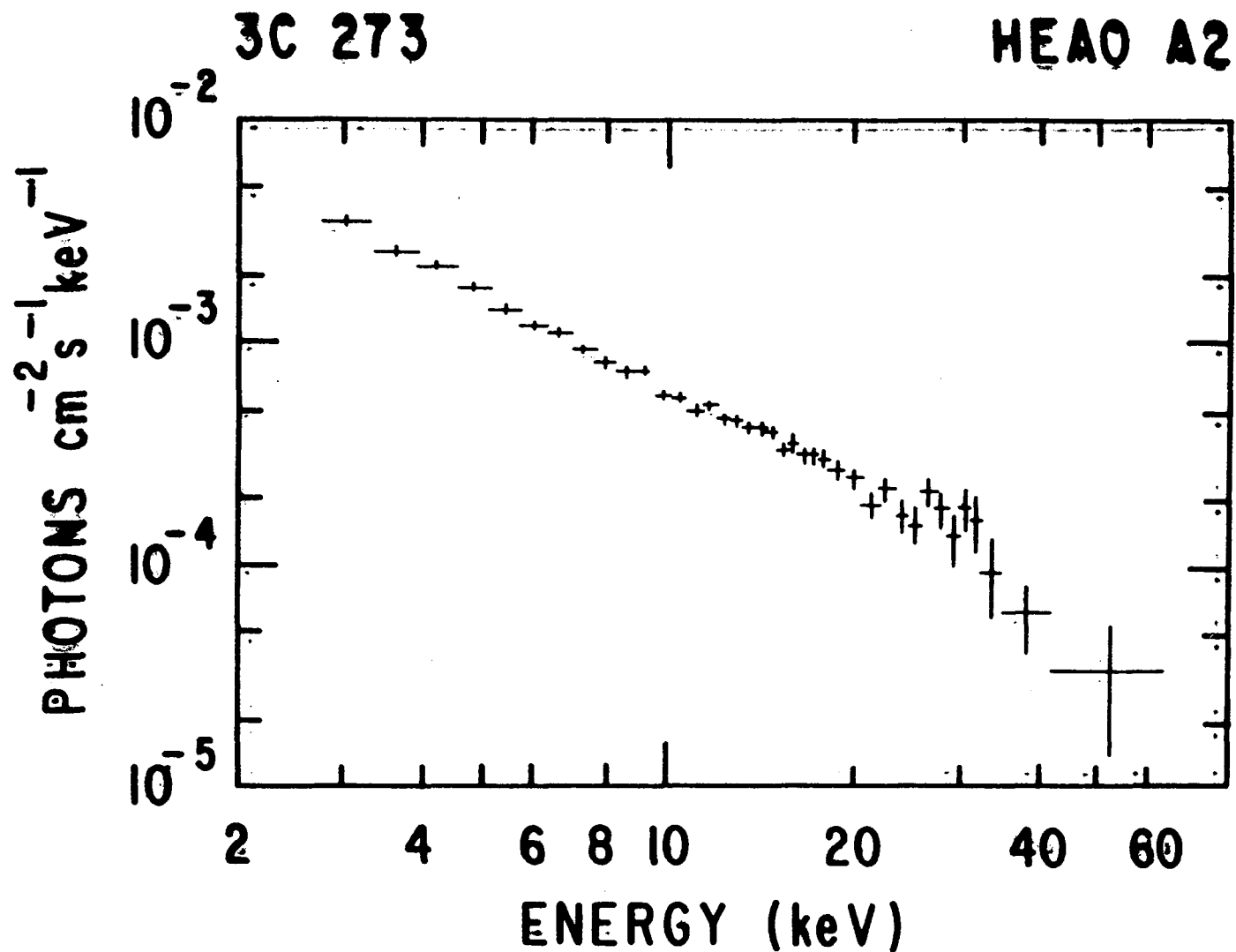


Figure 13. The X-ray spectrum for the quasar 3C273 as inferred from data obtained by a xenon proportional counter (HED) during an extended HEAO-1 point.



## A-3 SCIENTIFIC RESULTS

Roger Doxsey  
Massachusetts Institute of Technology

I would like to take this opportunity to thank the NASA personnel here at the Marshall Space Flight Center and Goddard and at NASA Headquarters for making the whole HEAO project happen. It has been quite a few years, and I guess I am a newcomer to the project since I have only been working on it since 1973. In fact, coming down here involves some nostalgia since it has been quite a while since I have been here. I can remember times when it seemed like we were coming down almost every month for various meetings and discussions during the hardware phase.

Dan and I are going to divide the discussion of A-3 results in half so I will end abruptly. I am going to discuss a little bit about the instrument and discuss results from our galactic observations and some of our results on active galaxies, and Dan will cover groups of galaxies, clusters of galaxies, and BL-Lac objects.

The purpose of the scanning modulation collimator experiment on HEAO-1 is to identify the optical counterparts of celestial x-ray sources. The optical identification and further studies at optical wavelengths can provide substantially more information about an x-ray source than is obtainable at x-ray wavelengths alone. Identification will reveal immediately whether the source is an extra-galactic object or a member of our own galaxy. The identification will usually indicate immediately whether the system is a stellar system, a supernova remnant, a galaxy, or a cluster of galaxies. Optical observations will usually lead to relatively good determinations of distance to the object and hence of the total luminosity, both at x-ray and optical wavelengths. The comparison of the x-ray and optical luminosities will tell you whether or not the x-ray emission from the source is a dominant characteristic of the source, as in the case of Sco X-1, or a minor part of the source's total emission, as in the case of our own Sun. In some cases, optical observations can provide a clue as to the age and chemical composition of the system. Detailed observation of complex sources, such as x-ray binary systems, can lead to determination of certain parameters of the system such as masses, radii, and separation of components in the binary. Probably one of the most important statements that an x-ray astronomer can make about any given particular x-ray source is to identify it with its optical counterpart.

The reason that the optical identification of x-ray sources has not been a completely trivial matter is shown in Figure 1. This shows the portion of the Palomar Sky Survey containing the x-ray source 2A1822-371.

This source was detected by both the Uhuru and Ariel 5 satellites, which were scanning missions using slit collimators. Both of these satellites determined error boxes for the source. The larger one is the Ariel 5 error box and the intermediate one is the Uhuru error box. These error boxes are typically 0.1 to several square degrees in area. It would be an impossible task for an optical astronomer to study, in detail, each of the stars in this error box to determine which is the counterpart to the x-ray source. Experience has shown, especially with galactic sources, that many of the optical counterparts are 18th, 19th, and 20th magnitude, which correspond to the faintest stars that you can see on this particular print. At high galactic latitudes one expects that the sources will be extra-galactic and hence begins by looking for cataloged, extra-galactic objects in the error boxes, as Kent Wood described the A-1 cataloging procedure. One looks for Seyferts, emission line galaxies, BL-Lac objects, clusters of galaxies, and other unusual objects. If one does not immediately find a cataloged object, one can begin doing optical studies of the galaxies in the box hoping to discover an as-yet unknown Seyfert or BL-Lac object. Many of the high latitude sources from the initial surveys, Uhuru and Ariel, have been identified in this manner. The error boxes are small enough and the surface density of unusual extra-galactic objects is low enough that the chance of getting an erroneous identification is fairly small. In particular, based on this method, Seyfert type 1 galaxies were identified as a class of x-ray sources. There are about 20 or so that were identified based on large error boxes. For any given one of them, there would be a possibility that the identification would be wrong but certainly for the class it was correct.

At low galactic latitudes the problem is more difficult because you really have to look at each individual object in the error box for unusual characteristics which would lead you to identify it as the x-ray source and, obviously, with boxes of this size, it is just not feasible to do that. From some of the original scans, astronomers began by looking at the few brightest stars in each error box to see whether they were unusual. They looked to see whether any of the brighter objects showed any unusual time variability because that is a characteristic of the optical counterparts of some x-ray sources. They especially looked for some time variability if the x-ray source had periodic variation. As you can see, what really is required is a survey with high angular resolution, one which provides relatively small error boxes. The small diamond in Figure 1 represents the HEAO A-3 error box that was obtained for this source. Phil Charles and John Thorstensen discovered a star, which is, in fact, the x-ray source, that has emission lines of Helium II  $\lambda 4686$  and CIII/NIII  $\lambda\lambda 4640-4650$  which are common lines to find in x-ray counterparts and very unusual in normal stars.

The HEAO A-3 instrument is not the first experiment to have a high angular resolution. This problem was recognized a long time ago; in fact, one of the very earliest rocket experiments was the NRL

experiment done by Dr. Friedman to use a lunar occultation to identify the Crab Nebula. There were lunar occultation measurements and some early rocket RMC flights which provided error boxes about this size for several of the brighter galactic center sources. The first high angular resolution survey that was conducted was done by the rotating modulation collimator experiment on SAS 3. This survey was primarily limited to observations of the galactic plane. This limitation was just a limitation in terms of the available observing time; it could theoretically have done the entire sky. On the scale of the HEAO instruments, it was a relatively small instrument so its sensitivity was not as good. In the galactic plane, the sensitivity of that survey was not quite as good as the Uhuru and Ariel 5 surveys. But, since it was the first high resolution survey that was carried out, it made quite a few identifications. There were many counterparts that had been proposed based on large error boxes which were either confirmed or denied by initial SAS measurements, and quite a few of the SAS circles led to new identifications and new suggestions of counterparts. There were a total of 15 to 20 of these galactic sources which were identified based on the SAS survey. The A-3 scanning modulation collimator takes advantage of the scanning nature of the HEAO-1 mission to obtain a fairly uniform all-sky coverage and it also takes advantage of the larger physical size of the spacecraft to get a larger area and hence better sensitivity, so that our survey typically gets to sensitivities comparable to the Uhuru and Ariel 5 limits of about 1 Uhuru count. In fact, in the pointed observations, we can get down to as low as a half of an Uhuru count.

Figure 2 shows a conceptual drawing of the experiment. The primary element which provides a high angular resolution is the 4 grid scanning modulation collimator. There are two of these collimators — one at the top and one at the bottom. The wires in the drawing are greatly exaggerated, the wires in the fine collimator are 5 mil diameter and in the coarse collimator they are 20 mils. The distance is about 3 ft from front to back. This provides an angular resolution for the finer of the collimators, of about 30 arc sec; and for the coarser, about 120 arc sec. The collimators basically work as shadow devices. At any instant in time, three quarters of the field of view is blocked from the proportional counter, so the counters will not detect x-rays from that part of the sky. The remaining quarter is divided into many narrow bands on the sky. The two collimators are tipped at  $\pm 10$  degrees relative to the scan direction, so that one can detect the source in both collimators and then use the intersection of the bands in the sky to derive the position. The overall field of view is limited to  $4 \times 4$  degrees to help reduce source confusion problems. The counters behind the collimators are fairly standard proportional counters operating in the range of 1.5 to 13 kV. The second primary element consists of the two image dissecting star trackers which are used in conjunction with the gyros on the spacecraft to obtain a 5 arc sec aspect solution. The accuracy is crucial to being able to derive small error boxes and hence make identifications.

Figure 3 shows the picture of one of the modulation collimators. The structure is brazed beryllium. One of the design problems with this experiment was the alignment that had to be maintained between the wires of the front grid and the wires in the back grid. This alignment tolerance was 1/10 mil and had to be maintained in all environments experienced by the spacecraft. The environments we were most worried about were the vibration of launch and the thermal cycling in orbit. The choice of beryllium in the design of the experiment was made to keep the thermal gradients as low as possible. We have no evidence of any on-orbit problems with distortions or misalignments.

Figure 4 shows the experiment as a whole, I should mention that the hardware is basically a result of the scientific direction from Herb Gursky and Dan Schwartz, originally at AS&E and then at the Center for Astrophysics, as well as Hale Bradt and myself at MIT. The hardware was built by AS&E under the direction of Phil Gray and Allen Ramsey. The experiment performed very well in orbit. We lost one of the eight proportional counters early and that reduced our sensitivity in one collimator by a small amount. We had a small problem with the thermal shields (not shown installed in the figure) which led to slightly increased gradients in the collimators, but not enough to create any distortions. Other than that the experiment worked perfectly.

Figure 5 shows how we determined source positions. The fields of view of the two collimators are shown projected on the sky. The wider triangles represent the coarser of the two collimators, which we call SMC2. There is a 16 arc min spacing between them and a 4 arc min spacing between the bands of the finer collimator, SMC1. As the collimators scan the sky, the source traverses a path across the various bands giving count rate profiles which are shown on the left. When one analyzes the data, putting it back on the sky, one gets diamonds for source positions, which are the intersections between the lines of position determined for the two collimators.

Figure 6 shows a transit through Sco X-1, normally the brightest x-ray source in the sky. The overall  $4 \times 4$  degree collimator is readily apparent, as are the differences in resolution and spacing of the two modulation collimators. Observations of bright, identified sources are used to calibrate the collimators relative to the star trackers. For most sources, the intensity is many orders of magnitude less than Sco X-1. In fact, for most sources we are really interested in, you cannot see individual transits through planes of transmission. Since we know very accurately the angular spacing between the peaks, we can fold the data modulo that angular periodicity, taking all the peaks and superposing them on top of one another.

An example of that is shown in Figure 7. This was done for an observation of a rapid burster. These data were accumulated by folding a number of scans through the source. The superposition builds up

peaks which can then be fit with triangles separately for the two collimators. Each triangle fit yields parallel lines of position, the intersections of which form the diamond shaped error boxes.

I would now like to discuss a few of the optical identifications which have been made for galactic sources. Figure 8 shows the first one, one which was very exciting at the time. This is Nova Ophiuchi 1977. There have been a number of x-ray novae in the history of x-ray astronomy. Typically, they go from being undetected or not previously known to being among the brightest x-ray sources in the sky. They rise very quickly in a few days, and then decay over time scales of months to a year or two. This particular nova appeared just prior to the HEAO-1 launch and was quite bright. HEAO-1 scanned across it in September 1977. HEAO A-1 data were used to limit which of our multiple intersections the source might be located in. The source was identified by astronomers collaborating with us in Australia. This is a "before" and "after" picture. The star which is quite bright, the brightest of the group in the "after" picture, is absent or at most barely visible on the "before" picture. One of the best ways of making optical identifications is by finding a temporal coincidence between the x-ray and optical events, as we had in this case. There are relatively few sources that are actually identified in this manner; however, most are discovered by making optical spectroscopic observations.

Figure 9 shows an optical spectrum, which happens to be of this source. Typically, one uses a relatively large telescope and a good spectral photometer and examines the optical spectrum of each star in a diamond. It turns out that there are a number of emission lines which are very characteristic of x-ray sources. In particular, the Helium II line at  $\lambda 4686$ , and the CIII/NIII blend at  $\lambda 4640$ - $\lambda 4650$  are very common. This technique has been used for most of the identifications that have been made on the basis of A-3 positions. Another way of getting a hint as to which star is the x-ray source, is to take plates at different colors; U, B, and V and to compare them looking for color differences, because x-ray sources also tend to be bluish or UV excess sources.

Figure 10 shows one of our identifications. This is the source GX339-4 which Herb Friedman discussed earlier as the one which is very similar to CYG X-1. The identification of GX339-4 was made by using an Uhuru box, an Ariel 5 circle, and our HEAO diamond. Identification was made by Josh Finley at Cerro Tololo in Chile. The star which is the candidate is a 16th magnitude star and it shows the standard emission lines which one sees from such objects.

Figure 11 shows MXB 1659-29, and again it was identified in the same way by making spectrographic observations in Chile at Cerro Tololo. This source is the burst source which for quite a while was thought not

to have a DC component. The DC component appeared in the Spring of 1978 and this HEAO measurement was made which identified the candidate.

Figure 12 is a list of the stellar sources which have been identified primarily using the HEAO A-3 positions. Most of them are very faint. The brightest one is 14th magnitude and most of them are fainter than 16th magnitude, which means that you really do need the small error boxes to identify them. Two or three of them are of particular interest. One is 4U212947 which is the first of these faint UV excess, Helium II emission stars to show very clear evidence of a binary periodicity. This will be discussed in a later session by Richard Griffiths. There have also been several confirmations. These are sources that were previously believed to be x-ray sources, and with the HEAO A-3 boxes, we substantially reduced the error box area. In particular, for the U Gem types, it demonstrates before the time correlations were known, that the hard emission is, in fact, from the same star as the soft emission. We are expecting that quite a few more identifications will be made in the next couple of weeks or months. Right now is the season when the galactic center is visible from Cerro Tololo and from Kitt Peak. There are observers there now and will be over the next few months working on identifying sources based on our positions.

Figure 13 shows the Seyfert galaxy NGC 4151. Although it is outside both the Ariel and Uhuru error boxes, it is such an unusual object (it really does not appear that unusual in the picture) that it was identified with both of these sources by those catalogs. The diamond shows the HEAO A-3 position for that source.

The situation with Seyferts was that there had been more than 20 suggested identifications for Seyfert Type 1 galaxies. We have now observed and gotten positions for 20 of these and all of the ones that we see confirmed the initial identifications. There were also a few (one or two) BL-Lacs and high excitation emission line galaxies that had been suggested as counterparts for x-ray sources. By getting positions of 5 or 6 of these in each class, we established that they do represent classes of x-ray sources and that it is not a coincidence for an object of that type to be in an error box. We have seen a total of about 30 active galaxies so far and we expect to see a few more as we continue to analyze the data.

Figure 14 shows some of the Seyfert Identifications. Most of these are from the pointed observations between last May and December. In the case of IC4329A, the SAS 3 results indicated that perhaps the source is extended or perhaps both IC4329A and its companion IC4329 are x-ray sources. Our results are not consistent with either of those suggestions. There can be no more than 1/3 the flux from IC4329 as from IC4329A and there is no evidence of any extended component.

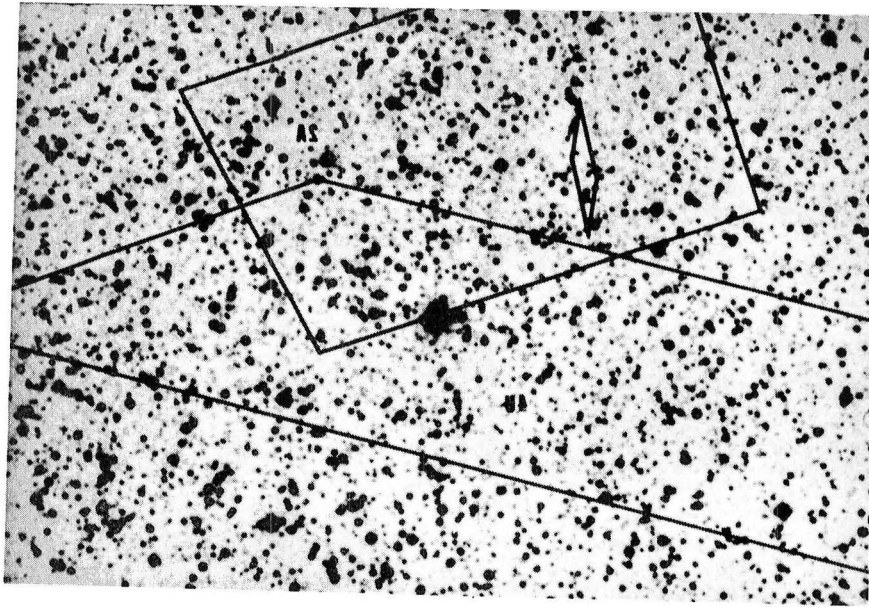
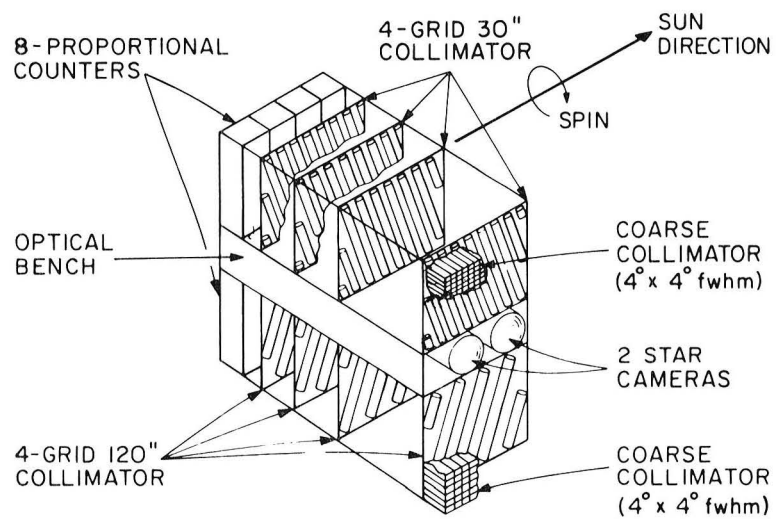


Figure 1



HEAO A-3  
SCANNING MODULATION COLLIMATOR

Figure 2

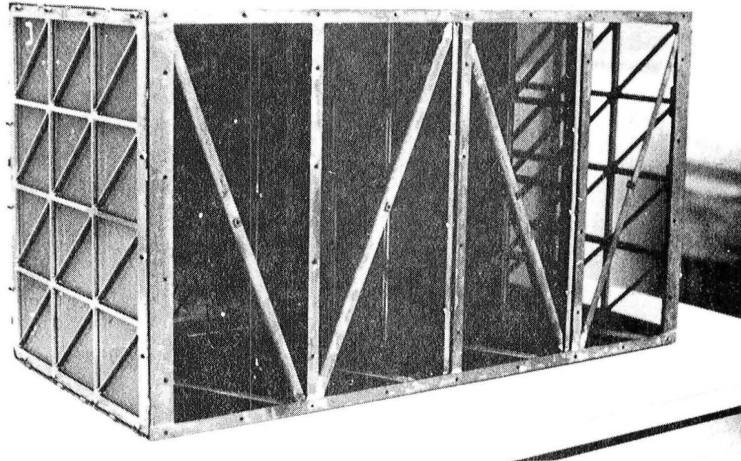


Figure 3

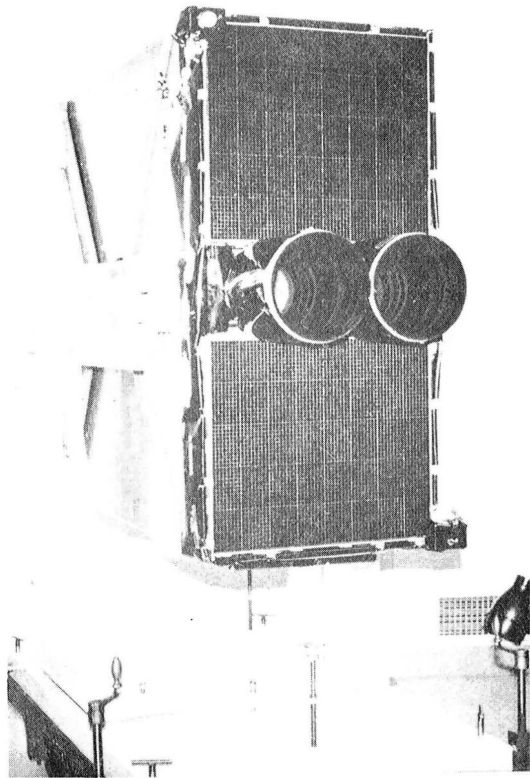


Figure 4



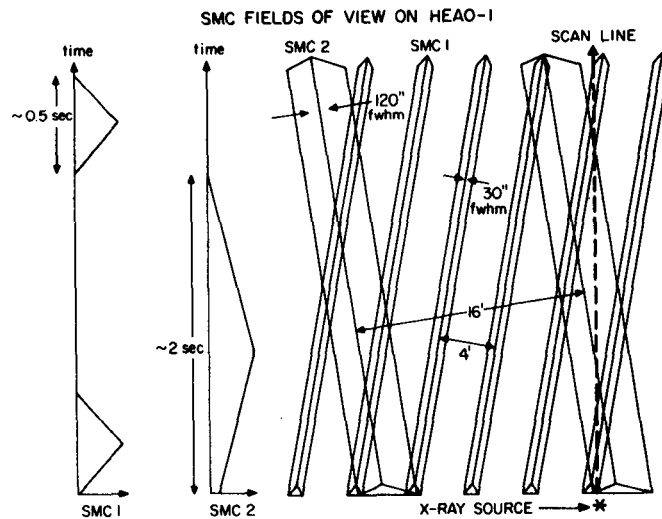


Figure 5

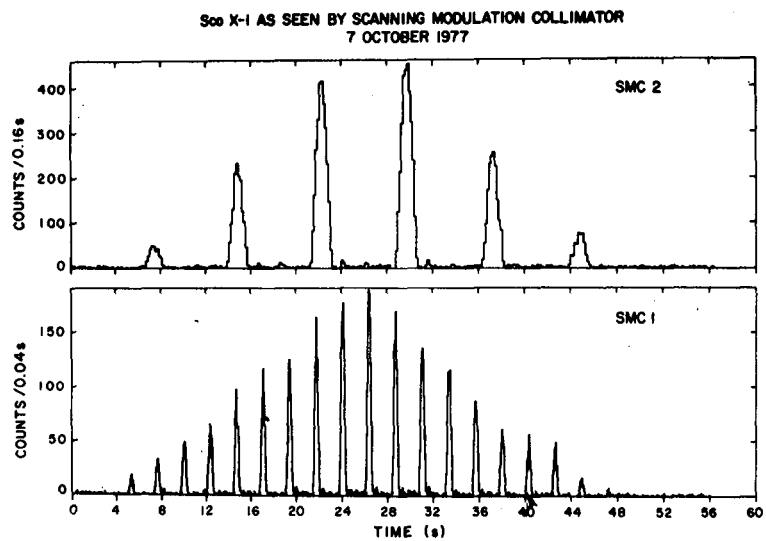


Figure 6

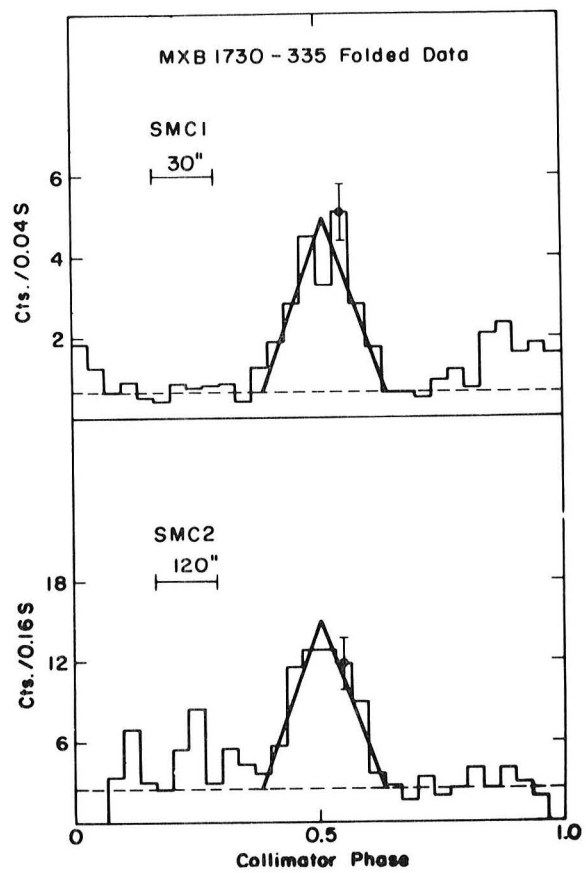


Figure 7

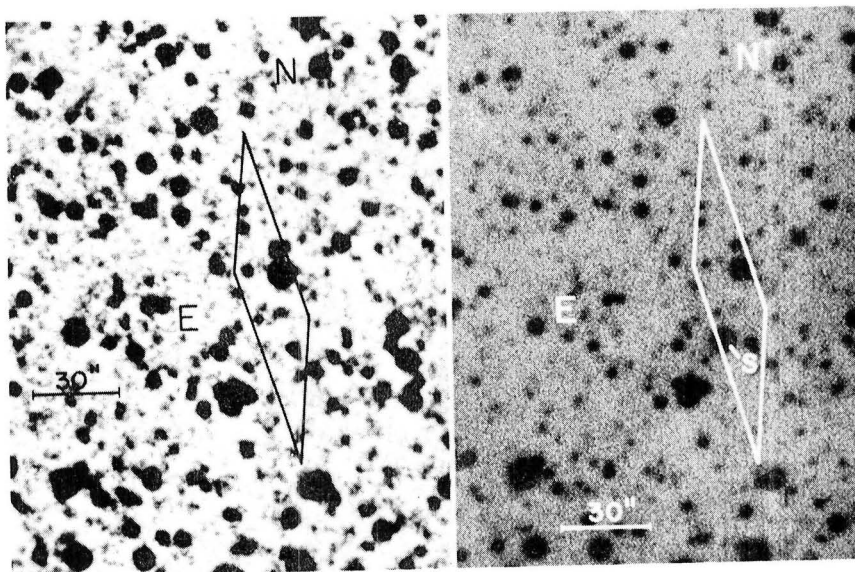


Figure 8

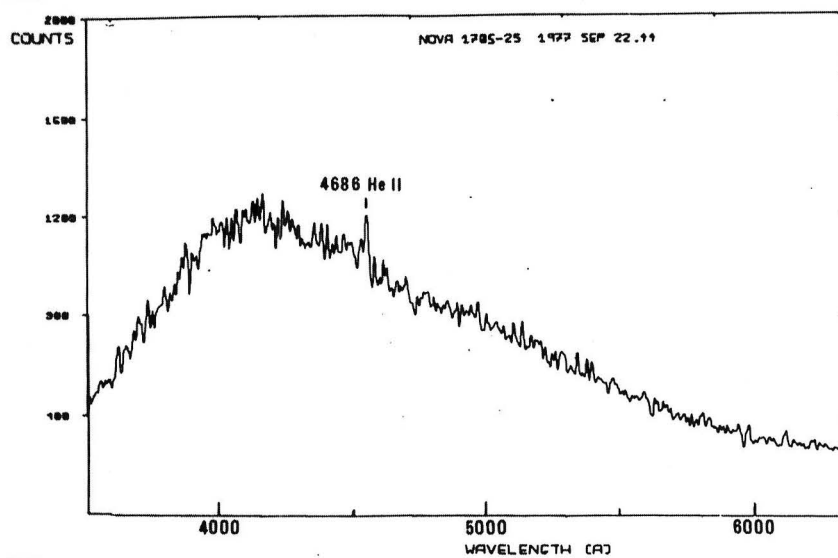


Figure 9

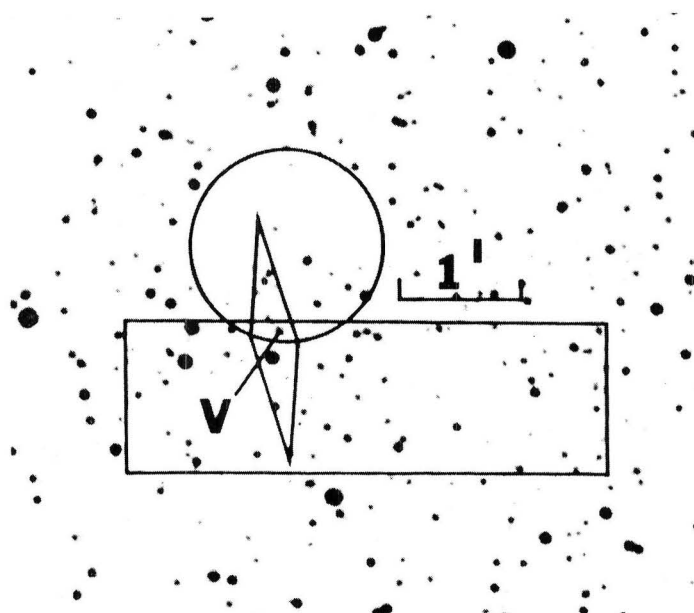


Figure 10

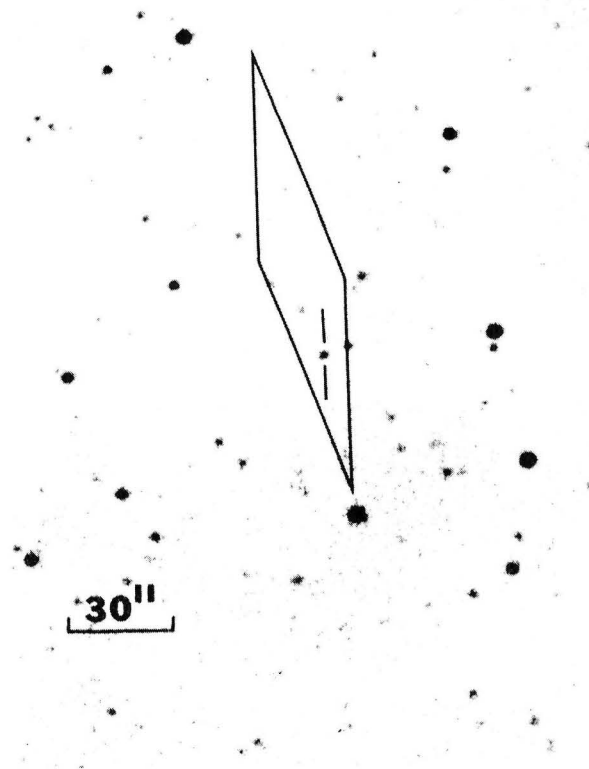


Figure 11

TABLE 1 - A-3 STELLAR OBSERVATIONS

Source	Optical Counterpart	X-ray Properties
H1705-25	Nova Oph 1977	transient
4U0115+63	B type	pulsing binary transient
4U1538-52	BOI	pulsing binary
2A1052+606	early K subgiant H $\alpha$ emission	$\leq 10^{32}$ ergs/s
4U1254-89	$m_V = 19$ HeII emission	
2A1822-371	$m_V = 16$ , HeII emission	
MXB1659-29	$m_V = 16$ , HeII emission	burster
GX339-4	$m_V = 16$ , HeII, H $\alpha$	black hole?
4U2129+47	$m_V = 16-18$ , HeII 5-hr binary	
A1916-C5	$m_V = 19$ , flat spectrum	burster
LMC X-1	B5I	$\geq 10^{38}$ ergs/s
LMC X-2	$M_V = 18.5$ , HeII emission	
LMC X-3	OB	$\geq 10^{38}$ ergs/s
A0538-66	B2 lab	recurrent transient in LMC
A1907+09	$m_V = 16$ , H $\alpha$ emission	
2A0311-227	$m_V = 15$ , many lines	AM Her type
2A0526-326	$m_V = 14$ , HeI, HeII emission	
CONFIRMATIONS:		
4U1543-624	$m_B = 20$ , UV excess	
4U1755-33	$m_B = 19$ , UV excess	
4U1608-52	variable $m_B = 18$ to $>20$	transient, burster
U Gem	U Gem type dwarf nova	
SS Cygni	U Gem type dwarf nova	
EX Hydrae	U Gem type dwarf nova	
MXB1730-335	cluster core, Liller 1	rapid burster

Figure 12

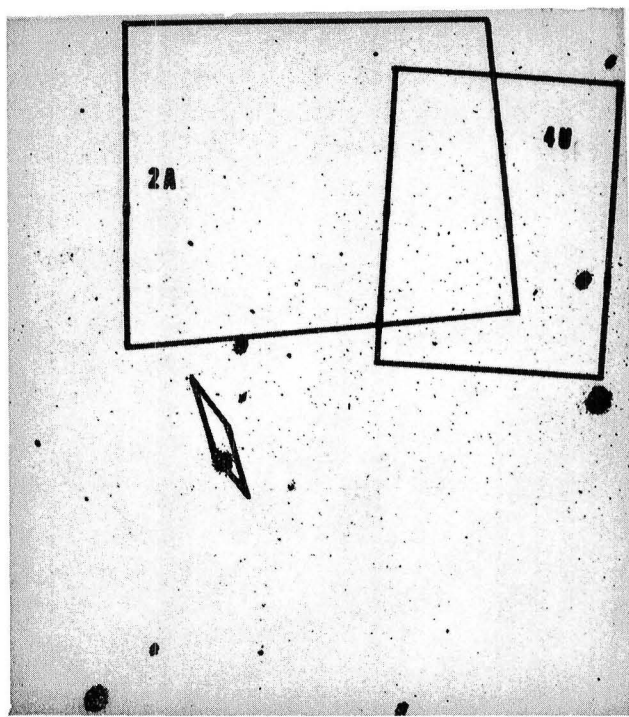


Figure 13

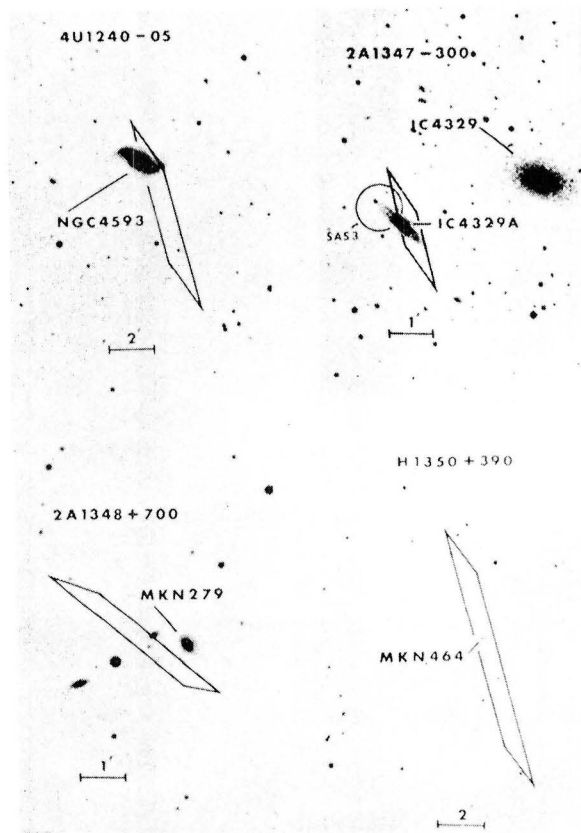


Figure 14

## A-3 SCIENTIFIC RESULTS - EXTRAGALACTIC

Daniel A. Schwartz  
Harvard/Smithsonian Astrophysical Observatory

As Roger Doxsey said, we will be splitting this talk in half, so I will start a little abruptly. I would like to discuss three specific topics in extragalactic astronomy to which the HEAO-1/A-3 experiment has made a unique contribution: first, the discovery of relatively condensed X-ray emission in the cores of those clusters of galaxies which are dominated by a giant elliptical or cD galaxy [1]; second, the discovery of extended X-ray emitting plasma in groups of galaxies [2,3]; and third, the demonstration that BL Lac objects are a new class of X-ray source [4,5,6].

What is a cluster of galaxies? Figure 1 shows the central portion of the Virgo cluster, the nearest rich cluster to our own galaxy, at about 20 Mpc.<sup>1</sup> Each of the fuzzy images is a galaxy, containing anywhere from a million to a trillion stars. Some of them are spiral galaxies like our own, others are elliptical galaxies which are distinguished by lack of gas and dust and lack of star formation. Clusterings of anywhere between 10,000 galaxies, as in the case of Coma, down to a few such as our own Milky Way and its neighbor Andromeda, are the rule rather than the exception in the universe. This imposes a stark contrast between the observation of the universe and the theories of general relativity which assume a uniform, isotropic, homogeneous universe for the scenario of the origin and nature of things. The formation and evolution of galaxies and of clusters is indeed one of the outstanding problems in astrophysics today. I will not solve this problem, but I think throughout the two days you will be hearing a lot of relevant observational data of a new kind which is now available from X-ray astronomy.

The scanning modulation collimator [7,8], because of its 4 arc min and 16 arc min periodicities, is not very sensitive to extended sources. They tend to be demodulated. In fact, we do not see most of the approximately 50 clusters known prior to HEAO-1 to be emitting X-rays, even though they are all strong enough that they formally are above our sensitivity level. The ones we do detect are of a special type. Shown in Figure 2, at the center of the cluster Abell 2199, is a so-called cD galaxy, a giant elliptical galaxy with an extended faint envelope of stars surrounding it, maybe five times the size of our own galaxy. By using previous X-ray error boxes (shown in addition to HEAO error boxes is an Ariel 5 survey [9] labeled 2A), we can typically reduce the multiple

---

1. 1 parsec (pc) =  $3.08 \times 10^{18}$  cm = 3.25 light years. 1 Mpc =  $10^6$  pc.

positions which come out of the modulation collimator experiment. In this case, we would reduce it to the region between the pair of lines on the right and identify the centroid of X-ray emission with the region right around the cD galaxy. We detect this Abell cluster only in our 2 arc min collimator, not in our 30 arc sec collimator, which is an indication of its finite size.

Figure 3 shows more clearly how we infer the finite size of extended sources. This is our typical best case result, the cluster Abell 85. In the 2 arc min collimator (MC2), we have a solid line fit to a "point" source. A point source of this strength would give a predicted counting rate as shown by the dashed line in the 30 arc sec collimator (MC1). The absence of such a response is a clear indication of finite size, about 4 arc min in this case. In general, we do not have sufficient statistics in the A-3 experiment alone to do this kind of study in the two collimators. In effect, what we do is get our predicted triangle based on previous X-ray fluxes such as catalogued by Uhuru [10] and Ariel 5 [9], and especially through a collaboration with the HEAO/A-2 experiment [1], which observes simultaneously to ours.

Figure 4 shows six cases in which we detect the cluster and locate the centroid near the cD galaxy (indicated by the arrow) and for which we measure finite size via demodulation of the signal in our detectors. We also have two other cases with the cD galaxy inside our location uncertainty, and two cases (A478 and A496) where the galaxy is outside but close to our measured position. One interesting case is A754, where the cD galaxy is very far (8 arc min) from any of our possible locations. This particular cluster may be in a very different state of evolution, or possibly we are being fooled by an extraneous point source superposed on the field.

The association of the cD galaxy with the X-ray emission has two possible interpretations. Undoubtedly both of these represent actual physical processes which are taking place in various clusters of galaxies. In one picture, both the giant galaxy and the hot X-ray emitting gas are merely being attracted to the gravitational center of the cluster and they both happen to fall there. This picture is very nice for the theory whereby the cD galaxy is actually formed by cannibalism [11] by accreting and digesting its smaller neighbor galaxies and incorporating their stars. In the second interpretation the cD galaxies are actually responsible for enhanced X-ray emission in their own right [12].

Clusters of galaxies were recognized as a class of X-ray source by Uhuru largely because of the work of G. Abell [13] whose catalog of clusters was carefully selected according to objective statistical procedures. He defined as a rich cluster anything in which there were 50 or more galaxies within a range of a factor of 6.3 (2 mag) in brightness, all within a region of 3 Mpc radius. Given X-ray emission from clusters,

there were many suggestions that groups of galaxies less richly clustered should also be X-ray sources. This is very reasonable to expect on the basis of continuity arguments. There is nothing fundamentally different about these groups compared to richer clusters as far as we know. The key observational problem was that groups were so much more numerous than clusters that their presence in a typical error box of  $1/10$  of a square degree could not be ascribed to other than chance. The situation is actually a little worse since a group of galaxies is not a well defined concept among astronomers.

Figure 5 shows locations of the X-ray source 2A0251+413. It shows how we used previous error boxes from Ariel 5 and Uhuru (with a little extent imagined for the latter) along with lines of position determined by NRL and Goddard from their HEAO-1 experiments. I also show a few of the multiple locations that we determined (with marginal statistical significance) with our 2 arc min collimator. They all focused in on the western part of the 2A location. There is another source (denoted as MX) which is undoubtedly a variable since it was very much stronger when observed by MIT on the OSO-7 [14] experiment and, therefore, could not be ascribed to a group. The fact that the modulation collimator just barely detected 2A0251+413 compared to a very strong detection from the Goddard A-2 experiment allows us to infer that it is an extended source which we identify with the Albert, White, and Morgan [15] group number 7 (AWM7). This region of the sky is shown in Figure 6 which is a blow-up of a Palomar sky survey print. This group is distinguished by the presence of a giant elliptical galaxy, NGC 1129, like those cD galaxies in the clusters which I just discussed. The dashed line indicates the finite size, an effective 9 arc min full width half maximum (FWHM) for the extent of the X-ray emission. Depending on the true profile, the X-ray centroid might be revised somewhere along this line.

The luminosity of this group of galaxies is  $10^{44}$  ergs per second, just very comfortably near the mean previously known for clusters of galaxies. Some of the other group members are designated by number in Figure 6. The most significant thing to note is the absence of spiral galaxies in this group. Perhaps the main conclusion from the discovery of X-ray emission from groups is that it looks very much like the emission from clusters of galaxies. Goddard OSO-8 results [16] on this particular X-ray source are shown in the spectrum of Figure 7. The key feature is the iron line emission at 6.7 keV, the ubiquitous signature of hot gas in clusters of galaxies which was used to prove that in fact thermal bremsstrahlung was the emission mechanism [16].

Figure 8 shows a 2 arc min collimator line of position for 4U1326+11, locating the center of X-ray emission with the Morgan, Kayser, and White [17] group number 11 (MKW 11), another group dominated by an elliptical D galaxy, NGC 5171. The other members of this group are scattered over this whole finding chart. The key thing to notice is the



absence of spiral galaxies. This fits in very well with the picture whereby spiral galaxies are stripped of their gas, as they pass through the hot gas medium that is emitting the X-rays, and with the suggestion that groups represent an older stage of the evolution of clusters. Also, if some groups do not emit X-rays, then this fits in with the empirical fact that low spiral galaxy content is correlated with high X-ray luminosity [18]. In fact, the X-ray luminosity of this group is only about  $4 \times 10^{43}$  ergs per second, within a factor of two of the weakest Abell clusters found.

The next source, Figure 9, is a very interesting case. This is the Ariel 5 source 2A0335+096. We have lines of position in the two collimators which locate the centroid of X-ray emission around a giant elliptical galaxy which has a very extended envelope. From the faintness of the galaxy (about 16th magnitude) and the size of the envelope, we can guess it is at a distance of 400 Mpc, giving this group an X-ray luminosity of about  $6 \times 10^{44}$  ergs per second — comparable with very rich clusters in Perseus and Coma (in fact, a factor of 2 or so less). We measure a finite size of about 1.5 arc min. That gives this group a rather small diameter of about 150 kpc.

I think one intriguing way to interpret emission from the groups of galaxies is in terms of the picture by Ostriker [19] whereby they represent an older stage in the evolution of clusters. In this picture, clusters with fewer galaxies evolve faster, and the central galaxy more easily accretes its neighbors and becomes a cD galaxy. The true signature if this is a valid picture of an older cluster should then be an advanced chemical age; for example, a very large iron abundance which could, in principle, be determined from X-ray measurements. Also, according to Ostriker's predictions, the group should show smaller velocity dispersions of their member galaxies since the fastest moving galaxies may have actually escaped from the group.

I would like to turn to another topic now, the so-called BL Lac objects [20]. These are named after a prototype object which had been known for a long time as a variable optical object in the constellation Lacerta. The overwhelming majority of the tens of thousands of such variable objects have turned out to be stars. However, some 30 such systems are distinguished by strong, variable optical polarization; by radio emission; and by the lack of any emission lines in their spectra. About 10 of the objects in this class are identified with distant galaxies so that we know the class does represent an extragalactic object. One of the conclusions from the X-ray discovery is that we could add an additional characteristic, namely, that they show strong and variable X-ray emission, to the definition of BL Lac objects. There are now two objects first discovered as X-ray emitters and subsequently proven to be of the BL Lacerta class.

The key interest is that these BL Lac sources appear stellar; that is, by definition they are quasi-stellar objects or quasars. Since they are so much closer and more numerous than the classical quasars, it is possible that they might be more amenable to detailed study and revelation of the internal energy conversion mechanism. In particular, if we just ask the questions, why are BL Lac objects different from quasars? why don't they have emission lines? we can look at a category of theories explaining the radiation of both quasars and BL Lac objects.

Figure 10 schematically categorizes various theories in the literature [21,22,23] as to why BL Lac objects are different from other quasars. In one class of models, it is simply a geometric difference of how the central black hole emits high energy cosmic ray particles and how those particles might intersect an irregular distribution of gas to ionize it or how the radiation transfer in this gas may present different aspects to us as we view it. The key features are that the emission from the central object is pictured as anisotropic — some sort of beaming or ejection, and that the gas is not spherically symmetric — either forming clouds as pictured or else an accretion disk. Another class of theories exploits the morphological characteristics. Seyferts and QSO's, which have many similarities, are pictured to be in spiral galaxies which are known to have gas. The N galaxies and BL Lac objects are pictured to be associated with elliptical galaxies which are deficient in gas. Perhaps a more interesting picture for future study is a very general evolutionary picture in which the clock can run in either direction, depending upon whether one considers an explosion or an accretion phenomenon. The start, for example, may be a condensed object with no gas around it and it might look like a BL Lac object. It may then explode to go through a quasar stage. Later, the gas may or may not dissipate to look like a BL Lac object again, with no gas to be ionized.

As in the case of groups of galaxies, the surveys for BL Lac objects were simply so sparse and irregular that statistical criteria for identification were not possible prior to HEAO-1. With an error box of a few tenths of a square degree, one could not be absolutely certain that a BL Lac object inside such a box was the true identification of an X-ray source. Figure 11 illustrates the source 4U 1651+39 which, in fact, was correctly identified in the Uhuru catalog [10] as X-ray emission from the BL Lac object Markarian 501. The three diamonds comprise about one-half percent of the area inside the larger box. We also used the NRL HEAO/A-1 data to select the line of multiple positions within the 4U box as the correct ones.

Figure 12 blows up this location on a Palomar sky survey. We see Markarian 501 as an elliptical galaxy. It has a measured redshift which places its distance at 200 Mpc [24]. Inside the galaxy is a variable optical nucleus, which varies by more than a factor of two on a time scale of years, and a compact radio source. It is this nucleus which is the BL Lac object itself.

As indicated in Figure 13, the source 2A1219+305 in the Ariel 5 catalog was studied by the Ariel 5 X-ray astronomers and their co-workers [25]. They obtained a revised, smaller location (denoted as 3A) and did a radio survey which found four relatively weak radio sources (denoted as numbered plus signs) in this region. They noticed that their radio source number 4 fell on a stellar object and suggested it to be the X-ray identification and the BL Lac object. In a pointed observation of the HEAO-1 satellite, we obtained the error box diamond coinciding with radio source number 4, and which contains about one percent of the total area. It is shown blown up in Figure 14 on the Palomar sky survey. It shows the stellar object which the Ariel observers picked out as the radio source, and the likely X-ray emitter. L. Chaisson of Harvard searched the Harvard Observatory plate collection from over the past 50 years and discovered that this object was in fact optically variable. Figure 15 shows about a magnitude and a half variation on a time scale of years. This is one of the key characteristics of BL Lac objects and, therefore, confirms its BL Lac nature. The A-3 team has another such case where we discovered an X-ray source and subsequently found it to be a BL Lac object. This is a more exciting one in many regards, PKS 2155-304. Richard Griffiths will discuss its properties this afternoon.

Figure 16 is an overlay of four BL Lac objects in addition to Markarian 501. Mrk 421 and PKS 0548-322 are interesting in that they are both found in elliptical galaxies with measured redshifts. Together with Mrk 501, we can have an idea of the X-ray luminosity of these objects, namely  $2 \times 10^{44}$  ergs per second, 2-6 keV, for those with measured redshifts. These are just at the bottom of the range of luminosity of X-ray quasars, and near the top of the luminosity range of X-ray Seyferts. The two sources which were originally discovered in X-rays and subsequently found to be BL Lac objects appear on the Palomar sky survey prints to be stellar-like. They therefore might be much more distant objects where we cannot see the galaxy and they, therefore, might be very much more luminous in X-rays. This remains to be demonstrated.

What is the nature of the X-ray emission from the BL Lac objects? One clue we have is to look at their radio spectra. Referring to Figure 17, typical classical radio source spectra look something like the two cases on the lower left, increasing in flux toward lower frequencies. The turnover at lower frequency seen in many sources in the left side of Figure 17 is a somewhat unusual feature which is interpreted by the radio astronomers as a source which is so small that the radio photons actually are trapped and reabsorbed by the magnetic field before they can escape from the object. Many of the classical theories of radio sources would predict that in such objects the cosmic ray electrons which are making the radio emission will scatter off the radio photons and catastrophically explode as X-ray sources [27], at least at the one

Uhuru count or  $2 \times 10^{-11}$  ergs per  $\text{cm}^2$  per second level. For the radio sources on the right side of Figure 17, which in fact are observed as X-ray sources, the spectra are somewhat less dramatic. In fact, one can construct such a model of so-called Compton self-synchrotron, or inverse Compton, for their X-ray emission. In view of the fact that the model does not work for the six sources at the top of the left column though, I would say that it is to be looked at somewhat askance. In particular, it seems that these sources are telling us that there is a self-regulating mechanism, perhaps by the X-rays, which destroys the simple radio theory geometry of uniform homogeneous point source ejection. Since we think that the ultimate energy sources of all these extragalactic active objects are gravitational accretion anyway, it is natural to look for accretion as the direct source of the X-ray emission.

We have some support for this in the A-3 data, and I know it is being exploited more fully by some of the other experiments. Figure 18 shows the spectrum of Markarian 421 as measured by the Goddard group on OSO-8 and by our pointing of HEAO-1 in June 1978, about a year after that measurement. We see very dramatic steepening of the spectrum. From a purely phenomenological point of view, it is very suggestive of both Cygnus X-1 and AM Hercules, which are in turn two very different kinds of galactic X-ray sources both of which nonetheless are well believed to be powered by accretion phenomena. I would just suggest that exploitation of the accretion disk or shock front explanation of the extragalactic sources may be very fruitful.

Let me summarize the overall results of A-3 experiment. Figure 19 shows a computer generated map showing all the X-ray sources known prior to the HEAO-1 launch. Mark Johnston and Rick Dower have this hanging in their office at MIT and diligently stick in a red push-pin for all the published HEAO/A-3 identifications, some of which are new, and some of which are confirmations, for example, of Seyfert galaxies. The blue colors represent sources for which we have accurate position from the scanning modulation collimator and which constitute the unidentified sources at present. The green colors represent some of the historical X-ray sources such as Sco X-1.

Finally, I think it would be appropriate to acknowledge the six real heroes of the A-3 data reduction effort. Figure 20 shows the data reduction and analysis support team information center, staffed by Mike Garcia, Wendy Roberts, Maureen Conroy, and Ellen Ralph, posed in front of our recent publications. Many of you receive these yellow preprints which are a joint MIT/SAO A-3 publication. And, finally, Figure 21 shows the real brains of the experiment.

## REFERENCES

1. Schwarz, J., Brief, U., Doxsey, R. E., Fabbiano, G., Griffiths, R. E., Johnston, M. D., Schwartz, D. A., and McKeey, J. D., 1979, Ap. J. (Letters), in press.
2. Schwartz, D. A., Bradt, H. V., Doxsey, R. E., Fabbiano, G., Griffiths, R. E., and Johnston, M. D., 1978, (Abstract) Bulletin of the American Astronomical Society, 10, 628.
3. Schwartz, D. A., Schwarz, J., Fabbiano, G., Griffiths, R. E., Bradt, H., Dower, R. G., Doxsey, R. E., and Johnston, M. D., Bulletin of Americal Physical Society, 24, 621.
4. Schwartz, D. A., Bradt, H. V., Doxsey, R. E., Griffiths, R. E., Gursky, H., Johnston, M., and Schwarz, J., 1978, Ap. J. (Letters), 224, L103.
5. Schwartz, D. A., Doxsey, R. E., Griffiths, R. E., Johnston, M. D., and Schwarz, J., 1979, Ap. J. (Letters), 229, L53.
6. Griffiths, R. E., Tapia, S., Briel, U., and Chaisson, L., 1979, Ap. J., 234, in press.
7. Gursky, H., Bradt, H., Doxsey, R., Schwartz, D. A., Schwarz, J., Dower, R., Fabbiano, G., Griffiths, R. E., Johnston, M. D., Leach, R., Ramsey, A., and Spada, G., 1978, Ap. J., 223, 973.
8. Schwartz, D., Schwarz, J., Gursky, H., Bradt, H., and Doxsey, R., 1978, Proceedings AIAA 16th Aerospace Sciences Conference, 78-34.
9. Cooke, B. A., Ricketts, M. J., Maccacaro, T., Pye, J. P., Elvis, M., Watson, M. G., Griffiths, R. E., Pounds, K. A., McHardy, I., Maccagni, D., Seward, F., Page, C. G., and Turner, M. J. L., 1978, MNRAS, 182, 489.
10. Forman, W., Jones, C., Cominsky, L., Julien, P., Murray, S., Peters, G., Tananbaum, H., and Giacconi, R., 1978, Ap. J. (Supplement), 38, 357.
11. Hausman, M. A., and Ostriker, J. P., 1978, Ap. J., 224, 320.
12. Fabian, A., and Nulsen, P. E. J., 1977, MNRAS, 180, 479.
13. Abell, G., 1958, Ap. J. (Supplement), 3, No. 31, p. 211.

14. Markert, T. H., Winkler, P. F., Laird, F. N., Clark, G. W., Hearn, D. H., Sprott, G. F., Li, F. K., Bradt, H. V., Lewin, W. H. G., and Schnopper, H. W., 1979, Ap. J. (Supplement), 39, in press.
15. Albert, C. E., White, R. A., and Morgan, W. W., 1977, Ap. J., 211, 309.
16. Mushotzky, R. F., Serlemitsos, P. J., Smith, B. W., Boldt, E. A., and Holt, S. S., 1978, Ap. J., 225, 21.
17. Morgan, W. W., Kayser, S., and White, R. A., 1975, Ap. J., 199, 545.
18. Bahcall, N. A., 1977, Ap. J. (Letters), 218, L93.
19. Ostriker, J., 1978, in The Large Scale Structure of the Universe, M. S. Longair and J. Einasto (editors), p. 357.
20. Stein, W. A., O'Dell, S. L., and Strittmatter, P. A., 1976, Annual Review Astronomy and Ap., 14, 173.
21. Blandford, R. D. and Rees, M. J., 1978, in Pittsburgh Conference on BL Lac Objects, A. Wolfe, Ed., (University of Pittsburgh), p. 328.
22. Colgate, S. A., and Petschek, A. G., 1978, in Pittsburgh Conference on BL Lac Objects, A. Wolfe, ed., (University of Pittsburgh), 349.
23. Shields, G. A., 1978, in Pittsburgh Conference on BL Lac Objects, A. Wolfe, ed. (University of Pittsburgh), 257.
24. Ulrich, M. H., Kinman, T. D., Lynds, C. R., Rieke, G. H., and Ekers, R. D., 1975, Ap. J., 198, 261.
25. Wilson, A. S., Ward, M. J., Axon, D. J., Elvis, M., and Meurs, E. J. A., 1979, M.N.R.A.S., 187, 109.
26. Altschuler, D. R. and Wardle, J. F. C., 1975, Nature, 255, 306.
27. Hoyle, F., Burbidge, G. R., and Sargent, W. L. W., 1966, Nature, 209, 751.
28. Grindlay, J. E., Parsignault, D. R., Gursky, H., Brinkman, A. C., Heise, J., and Harris, D. E., 1977, Ap. J. (Letters), 214, L57.
29. Mushotzky, R. F., Boldt, E. A., Holt, S. S., Pravdo, S. H., Serlemitsos, P. J., Swank, J. H., and Rothschild, R. H., 1978, Ap. J. (Letters), 226, L65.

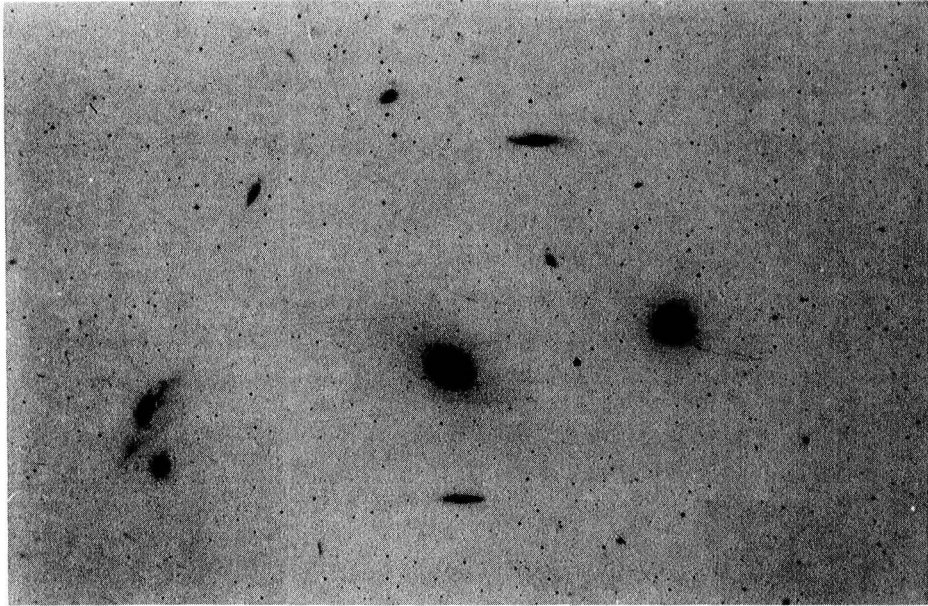


Figure 1. Central region of the Virgo cluster, showing elliptical and spiral galaxies. East is to the left and North is up on all figures.

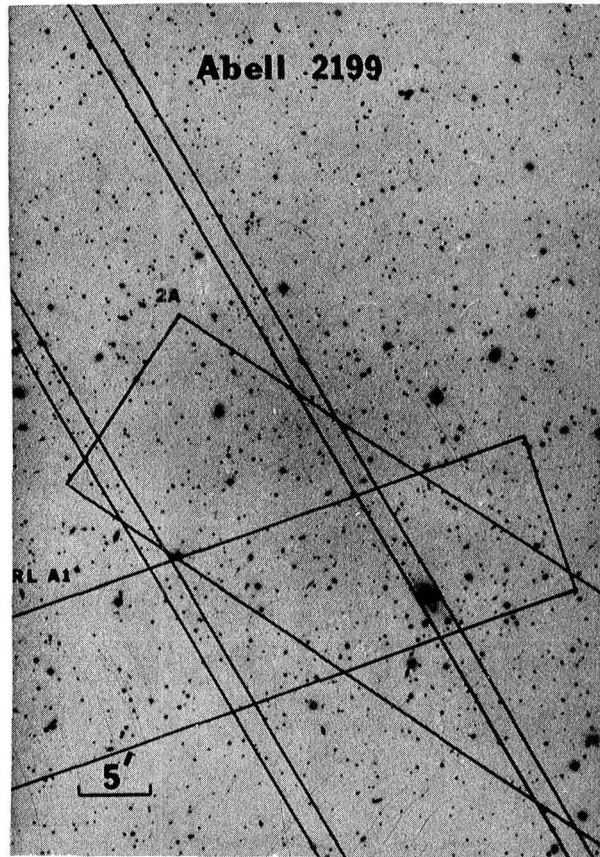


Figure 2. Location of the X-ray source 2A1626+396 = Abell 2199 cluster.  
 The X-ray source centroid must be near the cD galaxy inside the 2A,  
 NRL HEAO/A-1, and out HEAO/A-3 (long parallel lines) boxes.  
 In this and all other figures we show only a portion of the  
 extent and multiplicity of the multiple A-3 lines, which by  
 themselves would cover a  $4^\circ \times 4^\circ$  FWHM area.



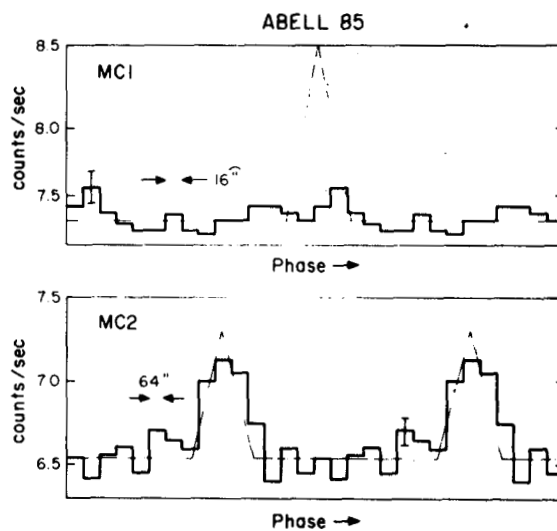


Figure 3. Response of MC2 (2 arc min FWHM) and MC1 (30 arc sec FWHM) to the X-ray source 2A0039-096 = Abell 85 cluster. Demodulation of the signal in MC1 indicates the source is extended by about 4 arc min FWHM.

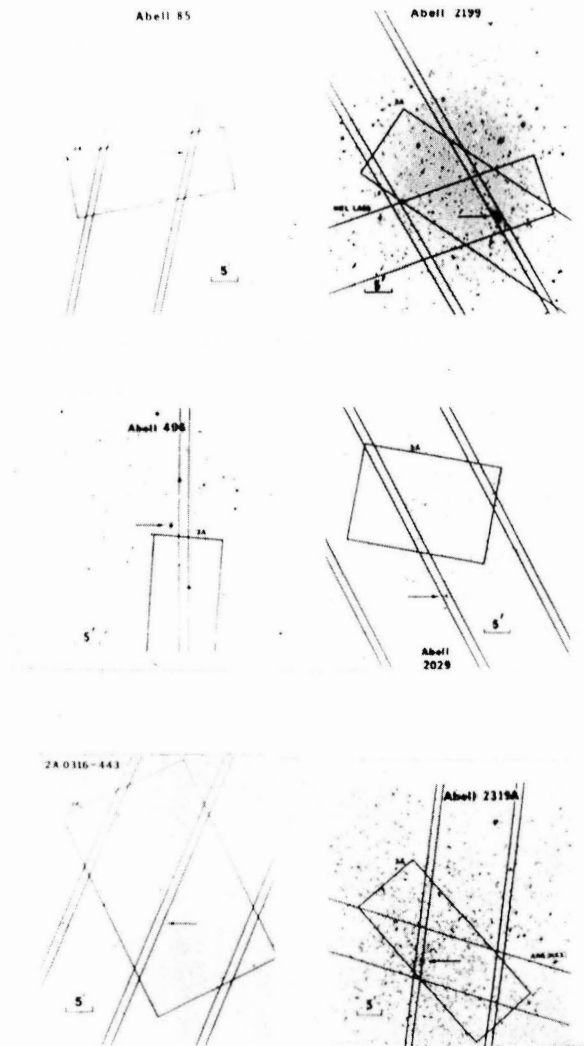


Figure 4. MC2 lines of positions for six clusters of galaxies, superposed on the Palomar Observatory Sky Survey prints along with error boxes obtained from the NRL HEAO-1 LASS, Ariel 5<sup>(9)</sup>, and the ANS Hard X-ray<sup>(28)</sup> experiments. In each case we identify the X-ray emission as extended, and centered on the cD galaxy which is marked with an arrow.

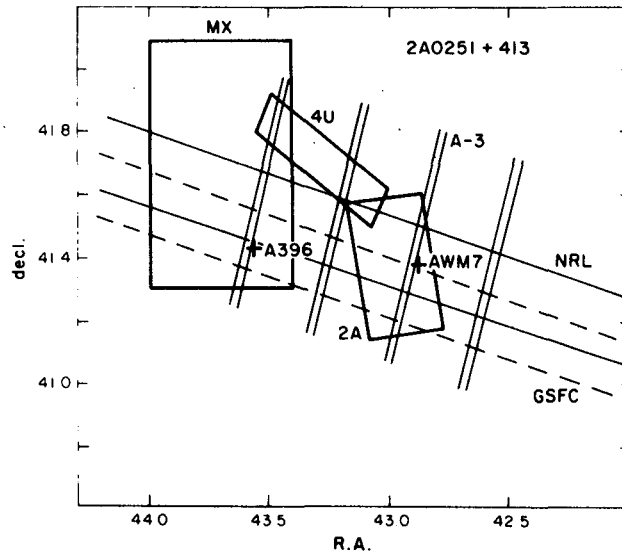


Figure 5. Locations of  $2A0251+413^{(9)} = 4U0253+41^{(10)} = AWM7^{(15)}$  group. The source  $MX0255+41^{(14)}$  is a distinct, variable source.



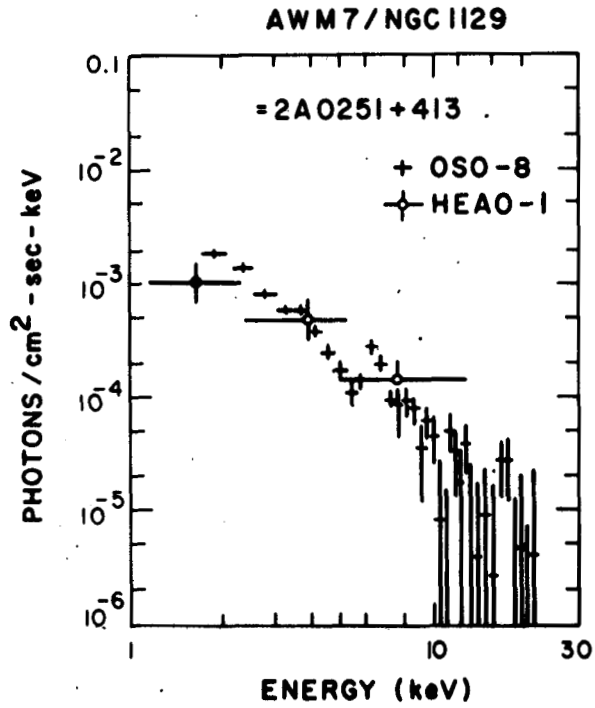


Figure 7. The X-ray spectrum of AWM 7. The OSO-8 points are from reference 16, the HEAO-1 points are our 3-channel spectral data. The iron line emission at 6.7 keV, ubiquitous in clusters of galaxies and the signature of hot gas, is clearly seen.

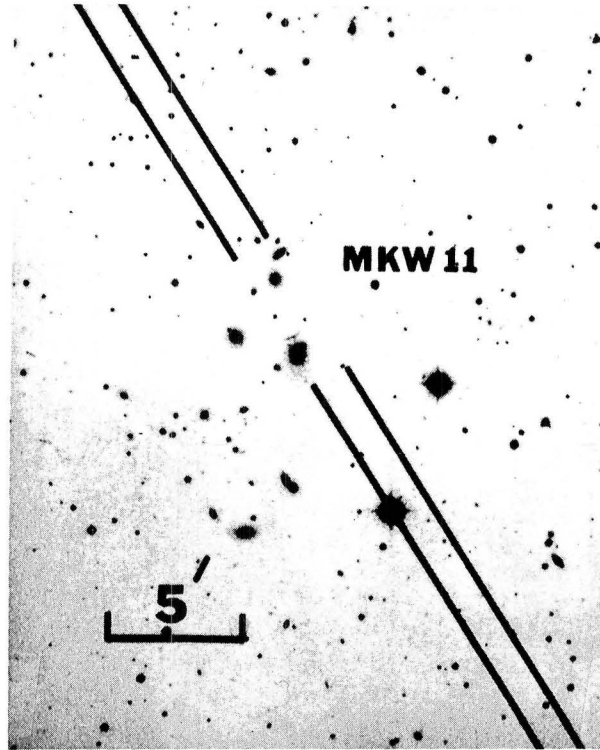


Figure 8. A portion of the MC2 line of position for the X-ray source 4U1326+11, identifying it with the group of galaxies MKW11<sup>(17)</sup>. The brightest member is NGC 5171, a D galaxy, which appears just above the break in the lower left line.

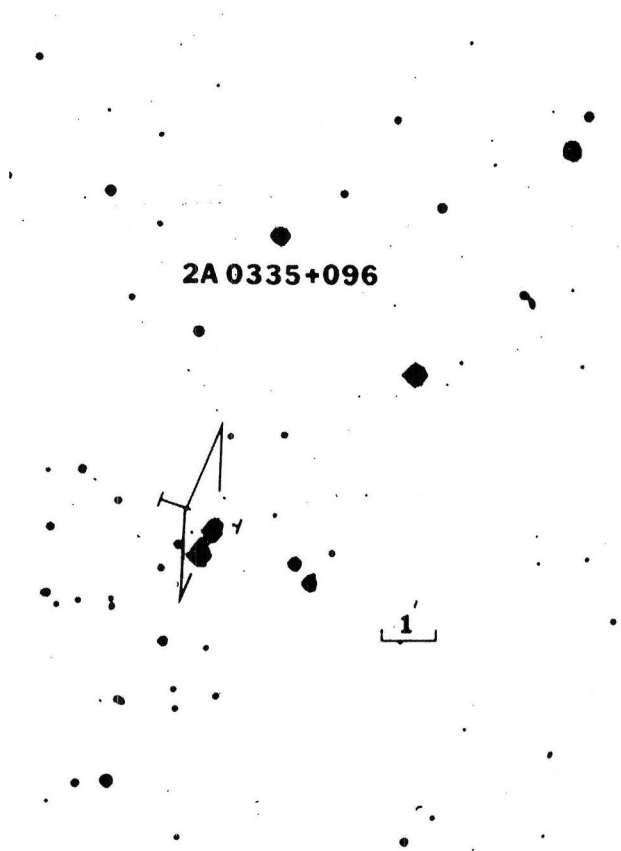


Figure 9. The A-3 location of 2A0335+096 is centered on a cD galaxy in a sparse group. The bar through our error box indicates the finite size, 1.5 arc min FWHM, inferred for this source. A foreground star of magnitude 12.2 is superposed on the SE.

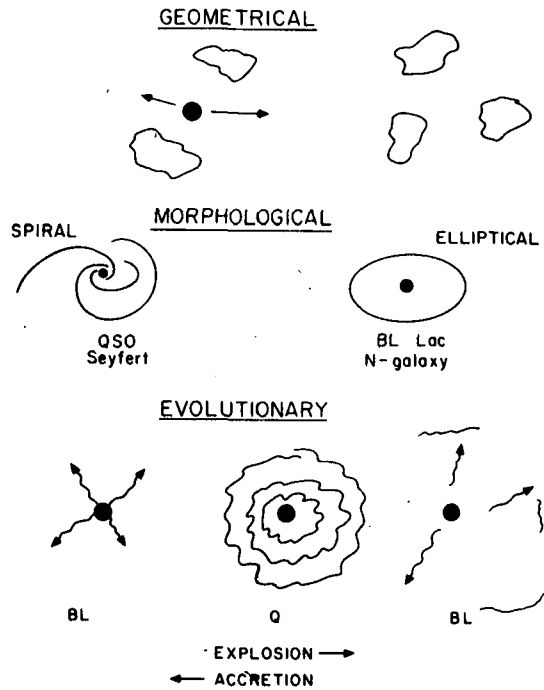


Figure 10. A schematic classification of different kinds of theories to explain the specific properties of BL Lac objects in contrast to the more general category of quasi-stellar object to which they belong. Black dots represent the ultimate energy source (black holes?). Lines with arrow heads represent particle or photon emission. Wavy lines, contours, and clouds represent gas.

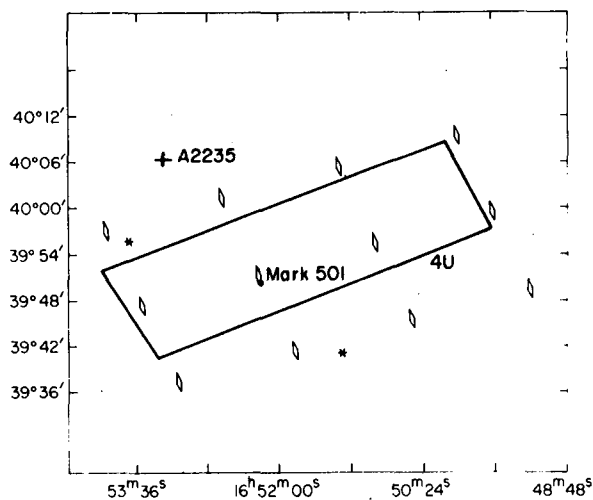


Figure 11. Location of 4U1651+39, identifying it with the BL Lac object in Markarian 501.



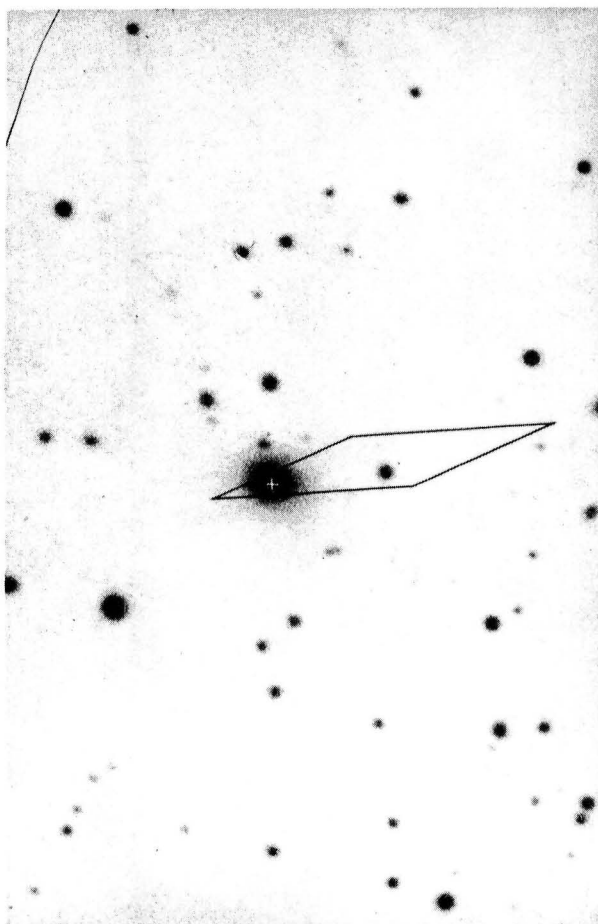


Figure 12. Superposition of one of our error diamonds on the Palomar Survey print. The white cross denotes the radio source B2 1652+396, which is the BL Lac nucleus.

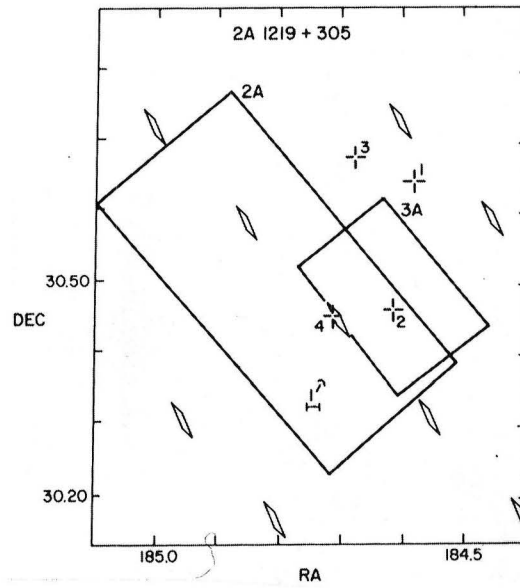


Figure 13. Locations of 2A1219+305. The only modulation collimator position allowed by the revised Ariel 5 position <sup>(25)</sup> contains the the radio source 4 suggested as the counterpart. <sup>(25)</sup>

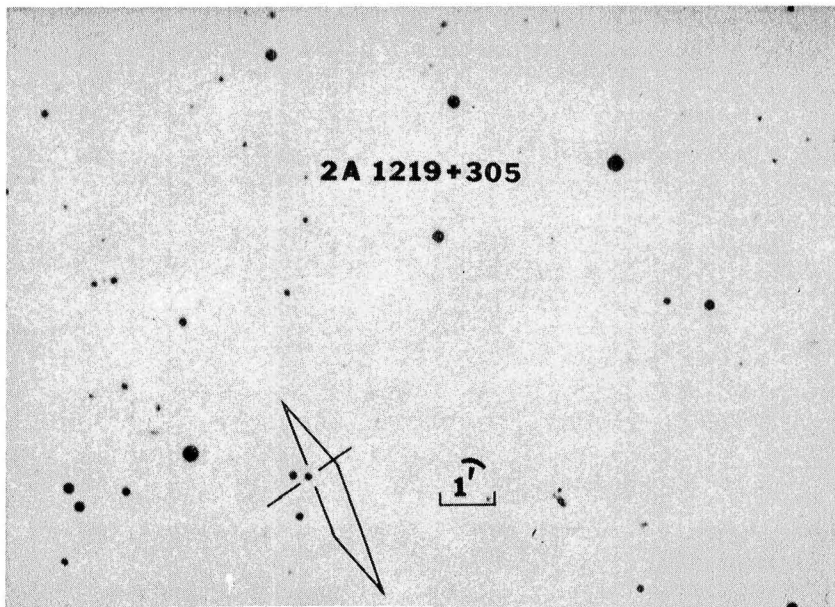


Figure 14. Superposition of the allowed MC for 2A 1219+305 superposed on the Palomar Sky Survey. The bars mark the position of the BL Lac object - the first object recognized as a BL Lac subsequent to its recognition as an X-ray source. <sup>(25)</sup>

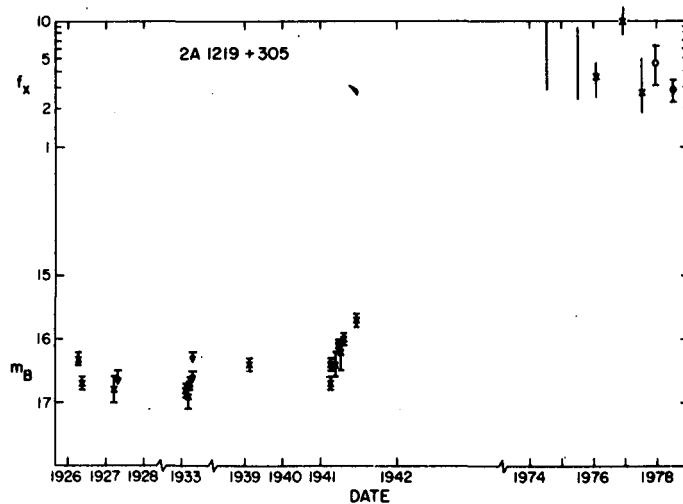


Figure 15. X-ray<sup>(25)</sup> and optical light curves of the BL Lac object 2A1219+305. For the X-ray fluxes, in  $10^{-11}$  ergs/cm<sup>2</sup> s, the straight lines give ranges observed by Ariel 5 over 6 month intervals, and the circles with error bars give our A-3 measurements. (The horizontal scale has been broken and distorted for clarity.)

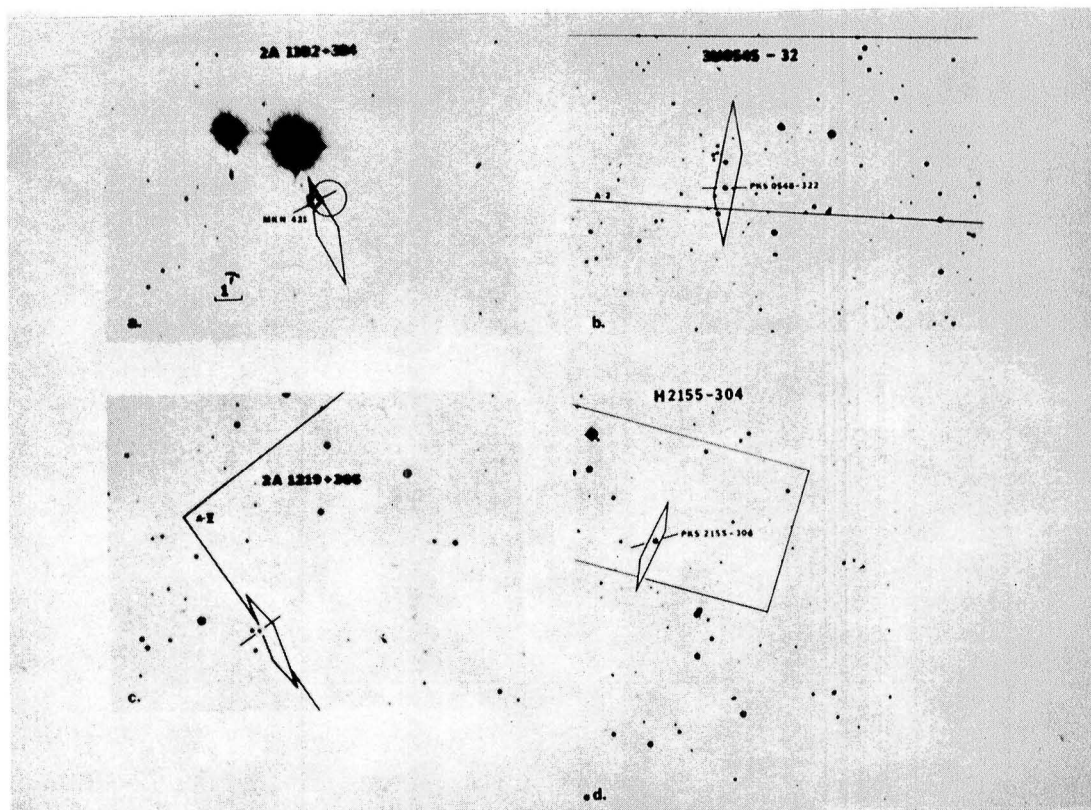


Figure 16. MC locations of 4 X-ray emitting BL Lac objects are given by the diamonds superposed on enlargements of the POSS red prints. Portions of previous X-ray locations are also shown.

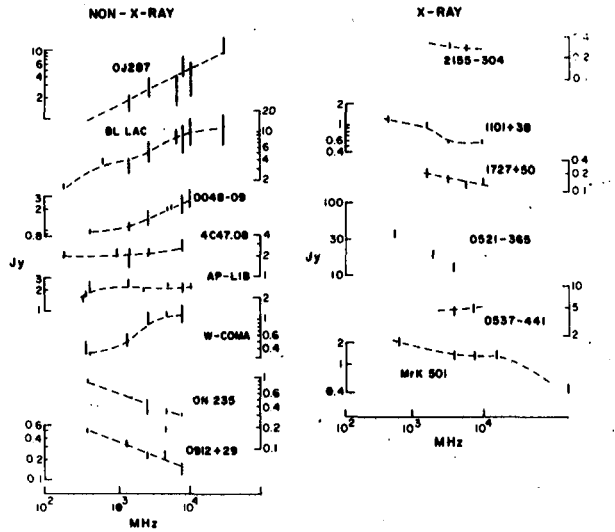


Figure 17. Radio spectra of BL Lac objects (mostly from reference 26) which do (right hand column) and do not (left hand column) emit X-rays above a threshold of about  $1 \mu\text{Jy}$  at 4 keV.

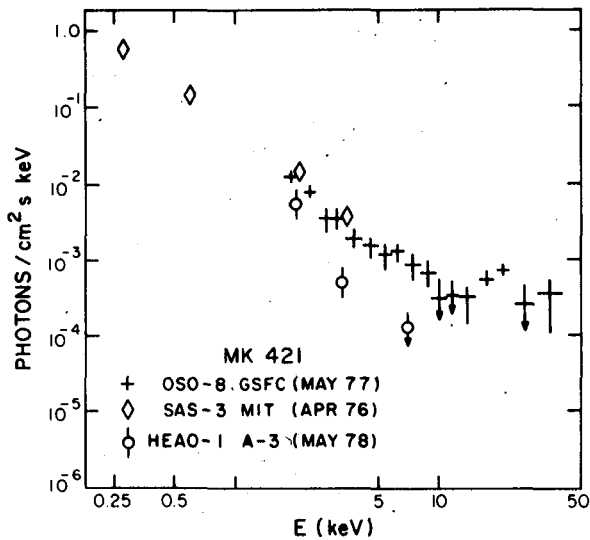


Figure 18. X-ray spectra of Markarian 421. The HEAO-1 MC data fit a power law slope  $3 \pm 1$ , in contrast to the slope  $1 \pm 0.5$  measured above 3 keV by OSO-8<sup>(29)</sup> one year previously.

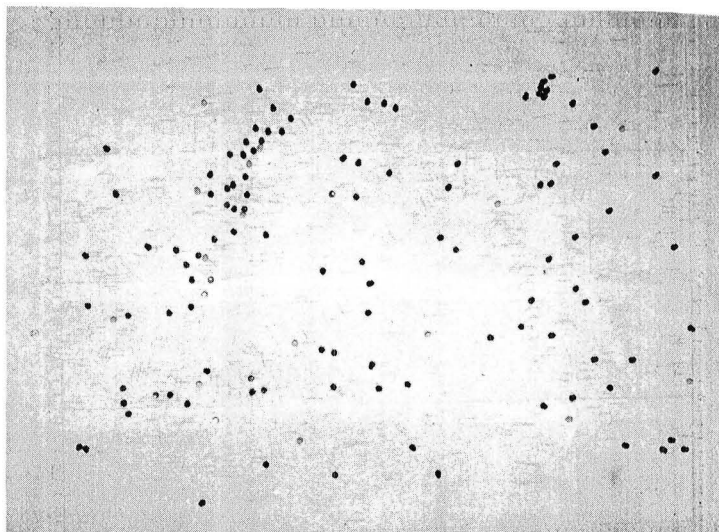


Figure 19. Computer map of all X-ray sources known prior to HEAO-1. Red pins indicate new identifications, confirmations, or structure measurements by the A-3 Scanning Modulation Collimator Experiment. Blue push-pins indicate MC locations for sources currently unidentified. Green pins are sources firmly identified prior to the HEAO-1 launch.

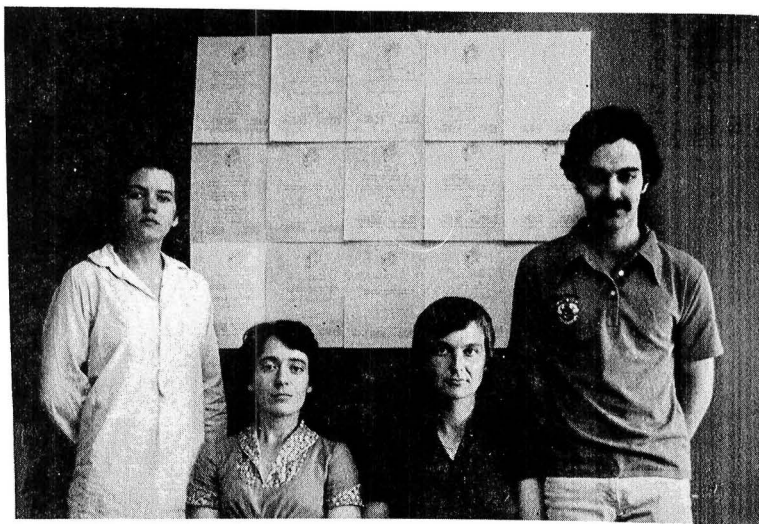


Figure 20. The Data Reduction and Analysis Support Team Information Center, staffed by (right to left) Mike Garcia, Wendy Roberts, Maureen Conroy, and Ellen Ralph, posed in front of a few of our recent publications.

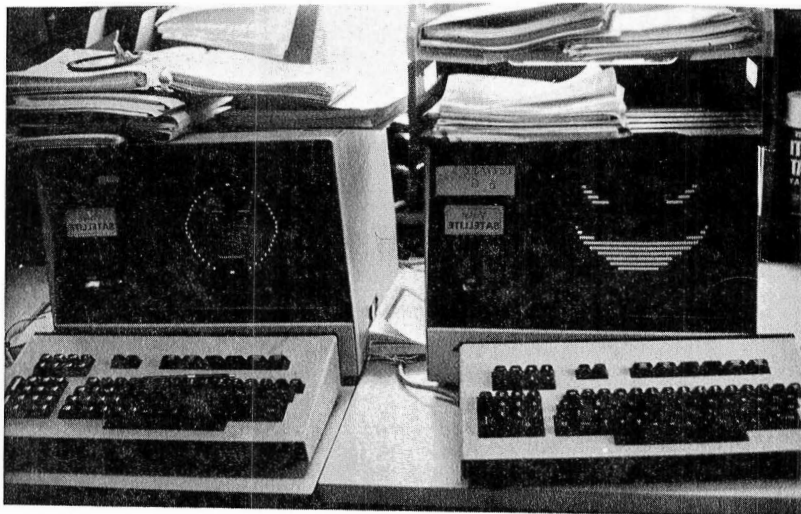


Figure 21. The A-3 computer terminals prepare to give the scientists orders for the day.

# HIGH ENERGY X-RAY RESULTS FROM HEAO-1: X-RAY PULSARS, AND THE ALL SKY SURVEY

Alan Levine  
Massachusetts Institute of Technology

I will discuss observations of high energy X-rays that were made with the University of California at San Diego/MIT instrument which was aboard the HEAO-1 spacecraft. Figure 1 shows a top view and a side view of the UCSD/MIT instrument. There were seven detectors in the instrument, five of which were sensitive to low energy gamma rays. Jim Matteson will discuss the results from those detectors. There were also two detectors which were sensitive to high energy X-rays. Each of these detectors contained a slat collimator to define the field of view. X-rays which pass through a collimator are absorbed in a sodium iodide crystal which converts the energy of each X-ray to a pulse of light which is then detected in a photomultiplier at the aft end of the instrument. The fields of view of these detectors are each  $1.2 \times 23$  degrees full width at half maximum. Note that the long direction of the fields of view were each tilted 30 degrees with respect to the perpendicular to the scan direction of the spacecraft. Figure 2 shows the full width fields of view of the high energy X-ray detectors and the scan plane for this particular orientation of the satellite projected on the celestial sphere.

Also shown in Figure 2 are the X-ray sources from the 4U catalog. In fact, hundreds of X-ray sources have been detected in the energy range 2 to 10 keV, the canonical energy range for X-ray astronomical observations. The spectrum of the typical galactic source is thermal with an exponential shape corresponding to a temperature of about 5 keV. If one extrapolates a spectrum such as this up into the energy range of the UCSD/MIT instrument, the typical source fluxes integrated over energy bands of interest are about 1000 times lower than in the 2 to 10 keV band. Therefore, if we were to have a detector that could detect the faintest sources with this spectral shape that an instrument like HEAO A-2 could detect, then we would need an enormous detector of approximately  $1 \text{ km}^2$  in area. However, this is not necessary because there are a lot of sources, such as the Crab Nebula, that do not have typical thermal spectra but have nonthermal spectra. These sources are very apparent and outstanding at our energy range and also tend to be among the most interesting sources in the sky.

The first topic will be the results of our sky survey with the high energy X-ray detectors of the A-4 experiment aboard the HEAO-1 spacecraft. The sky survey is the result of analysis of scanning data from the mission and, to make the presentation clear, we need to explain the mode of operation of the satellite during scanning (Fig. 3). During scanning, the spin axis, which is designated as the Z-axis, of the



satellite is always pointed toward the Sun. Therefore, all possible satellite orientations of spacecraft during scanning can be labeled with two coordinates. We have chosen one of these coordinates to be the ecliptic longitude of the Z-axis of the spacecraft and the other coordinate to be the azimuth of the Y-axis around the Z-axis. The north ecliptic pole is defined as the origin of the azimuth coordinate.

Figure 4 shows the fields of view pointing along the Y-axis of the spacecraft. Since we have long, narrow tilted fields of view, a high energy X-ray source which is not on the scan plane on a given day will be seen at different azimuths in the two detectors. As days go by, the scan plane will move and the azimuth at which the source is seen in each detector will change. When the scan plane crosses over the X-ray source, it will be seen at the same azimuth in both detectors.

Results from both detectors are plotted in Figure 5. What we see plotted is the average count rate of each detector averaged over all time at each possible satellite orientation. The vertical coordinate is the Z-axis ecliptic longitude; the horizontal coordinate is the Y-axis azimuth; the average count rate is encoded in intensity. Most of the hash is background, but sources, which appear at different azimuths for different Z-axis longitudes, show up as dark tilted stripes. These data cover the whole energy range from 13 to 80 keV. The bright sources which are evident include the Crab Nebula, 4U0900-40, Cen X-3, Cen A, and Sco X-1. A large number of sources near the galactic plane in the galactic center region are also evident. Sources in the Cygnus region are Cygnus X-1, X-2, X-3, and 4U0115+63. Note that the sources are tilted at different senses in the two detectors.

In Figure 6 we see data from one of the detectors in two more restricted energy ranges. The energy range of the data in the top panel is 13 to 25 keV and in the bottom panel is 25 to 40 keV. So far, by visual inspection of these data, which cover the first 6 months of the mission (2700 orbits of data), we can see about 40 sources above 13 keV and about 30 sources in the energy band of 25 to 40 keV. Immediately, one can notice spectral variations among the sources. For example, Cygnus X-2, which is prominent below 25 keV, disappears above 25 keV.

In Figure 7 we proceed to higher energy — 40 to 80 keV. This is data for the same detector. Again by visual inspection, we see approximately 15 sources above 40 keV. In fact, about five of those are still visible above 80 keV. The sources that are visible include the Crab Nebula, 4U0900-40, Cen A, and GX 339-4 — the black hole candidate which a number of other people have discussed at this meeting. Another of the sources is 4U1700-37, and also shown are Cygnus X-1 (extremely bright) and Cygnus X-3. Preliminary analysis indicates that the emission close to the galactic center must be due to at least five sources. The usually dominant hard X-ray source in the galactic center is GX 1+4, but it is by no means dominant in these data.

Since these data came from the beginning of the mission, Nova Ophiuchi 1977 was bright and, most likely, one of the strongest sources making up this hard X-ray emission. In fact, there is an indication that we detected it above 80 keV indicating that it did indeed have a hard spectrum. It is also likely that there are one or two sources whose location must be within one degree of the galactic center. We are still working on trying to precisely identify the other sources. Source confusion is a problem as one might well imagine.

There are a number of things which we would like to do with these sky survey results. One goal is to make a catalog of X-ray sources and to do that we not only want to identify strong sources (which we do by visual inspection), but to find weak sources in these data. We also want to search for time variability. A sample of that is shown in Figure 8. This is a blow-up of the 13 to 25 keV band for one detector of the region around 4U0900-40. Since the Z-axis moves uniformly around the sky with the Sun, we can interpret Z-axis ecliptic longitudes as a crude time coordinate as well. The horizontal lines are spaced at 5 degrees in ecliptic longitude and are, therefore, 5 days apart. We see a modulation in the intensity of 4U0900-40 due to the eclipses which occur every 9 days. Time variability is seen as well in a number of other sources.

The last thing we want to do is determine crude spectral parameters for a large number of these sources. One technique we have for finding weak sources is demonstrated in Figure 9. As previously mentioned, we can only find strong sources by visual inspection in our sky maps, so we perform azimuthal superpositions to look for weak sources. Note that sources stand out by visual inspection in the sky maps only if they are the equivalent of about 8 sigma or greater in statistical significance (for a 20-day integration time). Using this technique, we can set a more reasonable number such as four sigma for a detection limit. We have not systematically used this technique to study our data, but intend to do so. Figure 9 shows 20 days of data taken near the beginning of the mission. The scan plane went right over the Crab Nebula, the sharp feature at about 90 degrees. At about 270 degrees is the galactic center region. There is a hint of some emission right around the galactic center region in the 80-180 keV band, but it is only a small fraction of the intensity of the Crab. The emission above 80 keV is probably due to a superposition of the emission from two or three sources.

When we find all sources detected at the 4 sigma level of significance instead of the 6 or 8 sigma which was the detectability limit for visual inspection our sky map, and when one more year's worth of scanning data are also analyzed, we hope the number of detections will increase considerably above that which we have preliminarily noted.

We will now turn to our results of studies of X-ray pulsars. First, let us provide a brief description of an X-ray pulsar in terms of current theory. Figure 10 shows a neutron star or black hole, which is a

massive (roughly a solar mass) compact object, orbiting around a normal star. Matter from the envelope of the normal star is drawn towards the neutron star, spirals around it in an accretion disc and falls into the gravitational potential well of the neutron star. The energy released in the infall of this matter heats the infalling matter to very high temperatures, on the order of a hundred million degrees Kelvin. It, therefore, profusely emits X-rays on its way down. Figure 11 shows that the matter is confined to fall down toward the magnetic poles of the neutron star because of the presence of an extremely intense magnetic field. Thus, the X-ray emission will have an intensity which varies with direction. A pulse is observed since the neutron star is spinning about an axis and the magnetic axis is not co-aligned with that spin axis. With this theory, one can identify the pulse period of an X-ray pulsar with the spin period of a neutron star.

Figure 12 shows the pulse profile of the X-ray source 4U1626-67, in the energy range 19 to 30 keV. The energy dependence of the pulse shape is examined in Figure 13. Notice how rapidly the pulse shape varies as a function of energy. Another object which shows behavior similar to that, in that the pulse shape changes as a function of energy, is the X-ray pulsar GX 1+4, whose pulse profile is shown in Figure 14. Whereas 4U1626-67 has a period of 7 sec, the period of GX 1+4 is 116 sec. Notice the sharp spike at the top of the maximum.

An object with quite different behavior is 4U0115+63, for which in Figure 15 we show a composite light curve in the 12 to 66 keV band. The pulse period of this object is 3.6 sec. We can also examine the pulse profile of this object as a function of energy. In contrast to 4U1626-67 and GX1+4, Figure 16 illustrates that the pulse shape apparently is independent of energy between 13 and 30 keV. However, the amplitude of this pulse does not seem to be independent of energy. The pulse is strong at low energies. It seems to be pretty weak around 20 keV and is strong again at the top of the energy range.

Pulsed and unpulsed spectra as a function of energy are shown for both detectors in Figure 17. The feature just alluded to is seen as a dip in the pulse amplitude at about 20 keV. The reason it does not show up so strongly in the first detector (LED No. 1) is that this detector does not have as good an energy resolution as LED No. 2. This feature can be interpreted as cyclotron absorption occurring near the neutron star. To understand this in a very general manner, we have to understand the behavior of matter in a magnetic field (Fig. 18). The velocity component parallel to the magnetic field of a charged particle is unaffected by the presence of the field. Therefore let us just study the motion projected on a plane perpendicular to the magnetic field. The motion is circular and the energy levels of the particle are quantized such that the energy is approximately an integer times a constant times the magnetic field strength. For a magnetic field strength

of  $10^{12}$  gauss, these energy levels are separated by 12 keV. If X-rays are traveling through a medium containing ionized gas in a  $10^{12}$  gauss, magnetic field, for example, they will be more strongly absorbed if their energy is just enough to excite an electron an integral number of energy levels, 12, 24, 36 keV, etc. That is the way that a cyclotron absorption line can arise.

HEAO-1 has made quite extensive observations of perhaps the most fascinating X-ray source in the sky, Hercules X-1. The source has a 1.24 sec pulse period. In Figure 19 light curves are shown from different binary phases and different intervals. We note that the pulse shape seems to be independent of both parameters.

Figure 20 is the pulse spectrum which we have obtained for this source and it seems to be the same on at least six different occasions, at least with respect to the analysis which we have performed so far. We do not see any secondary peaks in the profile as reported by the Max Planck Institute from a balloon flight. This shape can be interpreted in any number of ways. It is a complex shape as you can see, it falls steeply, levels off somewhat, and then falls not quite so steeply. It can be fit by a continuum with an emission line at about 50 keV. It must be a broad emission line; a narrow emission line does not fit. It can also be fit with an absorption line in a continuum. It can also be fit by the sum of two continua.

To close, we will just present one additional light curve (Fig. 21). These are light curves from the object which was just discovered to be pulsing by the HEAO A-2 group. It is the 38-sec pulsar. We see it in the 13 to 25, 25 to 40, and 40 to 80 keV channels, but not above 80 keV. Hopefully, we can detect this source in scanning data within the next few weeks, and help to locate its position in the sky which is at present not well known.

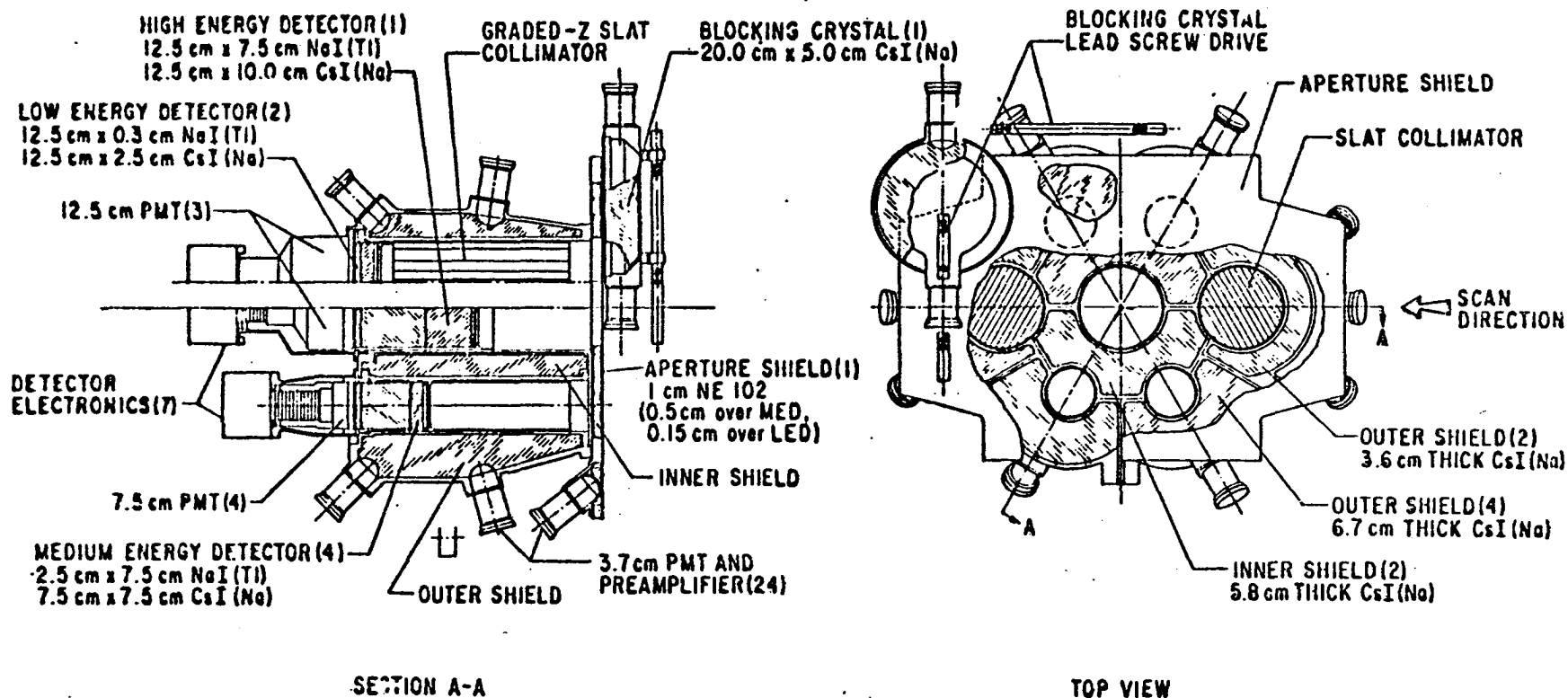


Figure 1. UCSD/MIT High Energy X-ray and Low Energy Gamma Ray Instrument of HEAO-1. Results obtained with the 2 detectors labeled "Low Energy Detector" are discussed in this article. These 2 detectors are behind the slat collimators.

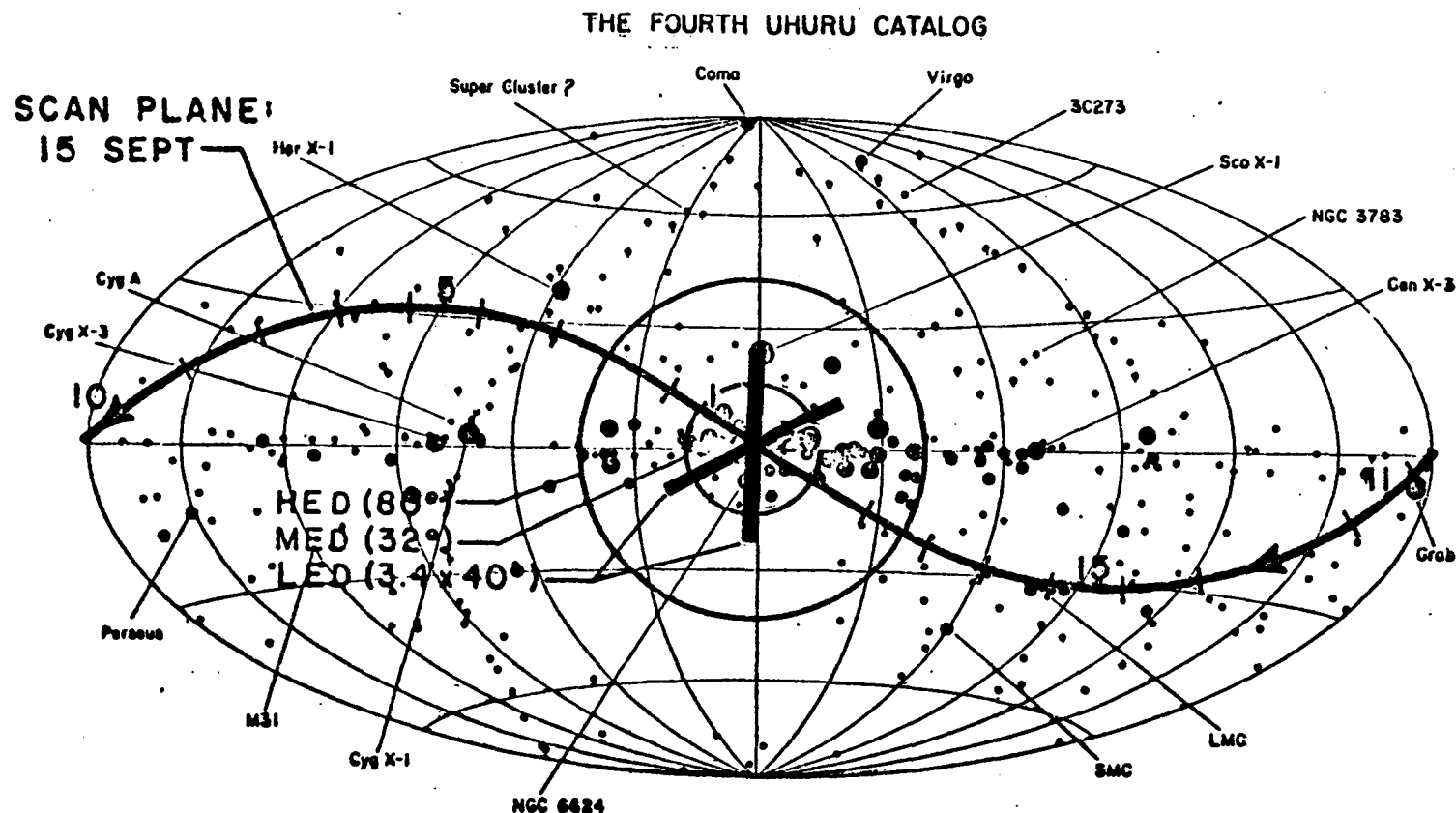


Figure 2. The full width fields of view of the high energy X-ray detectors (labeled LED) are projected onto a map of the celestial sphere in galactic coordinates. The scan plane of the satellite Y-axis for September 15 is indicated as are the X-ray sources listed in the 4U catalog.

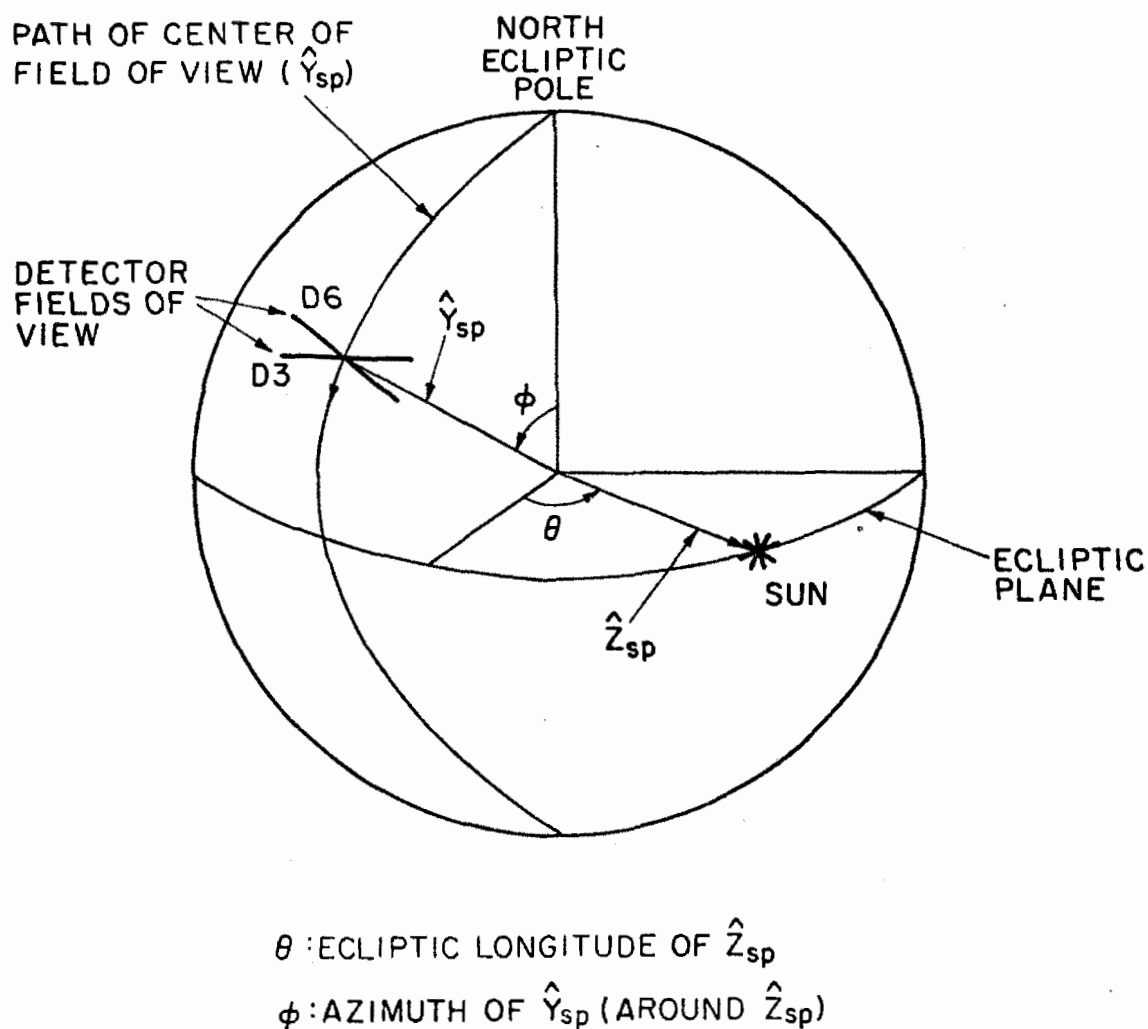
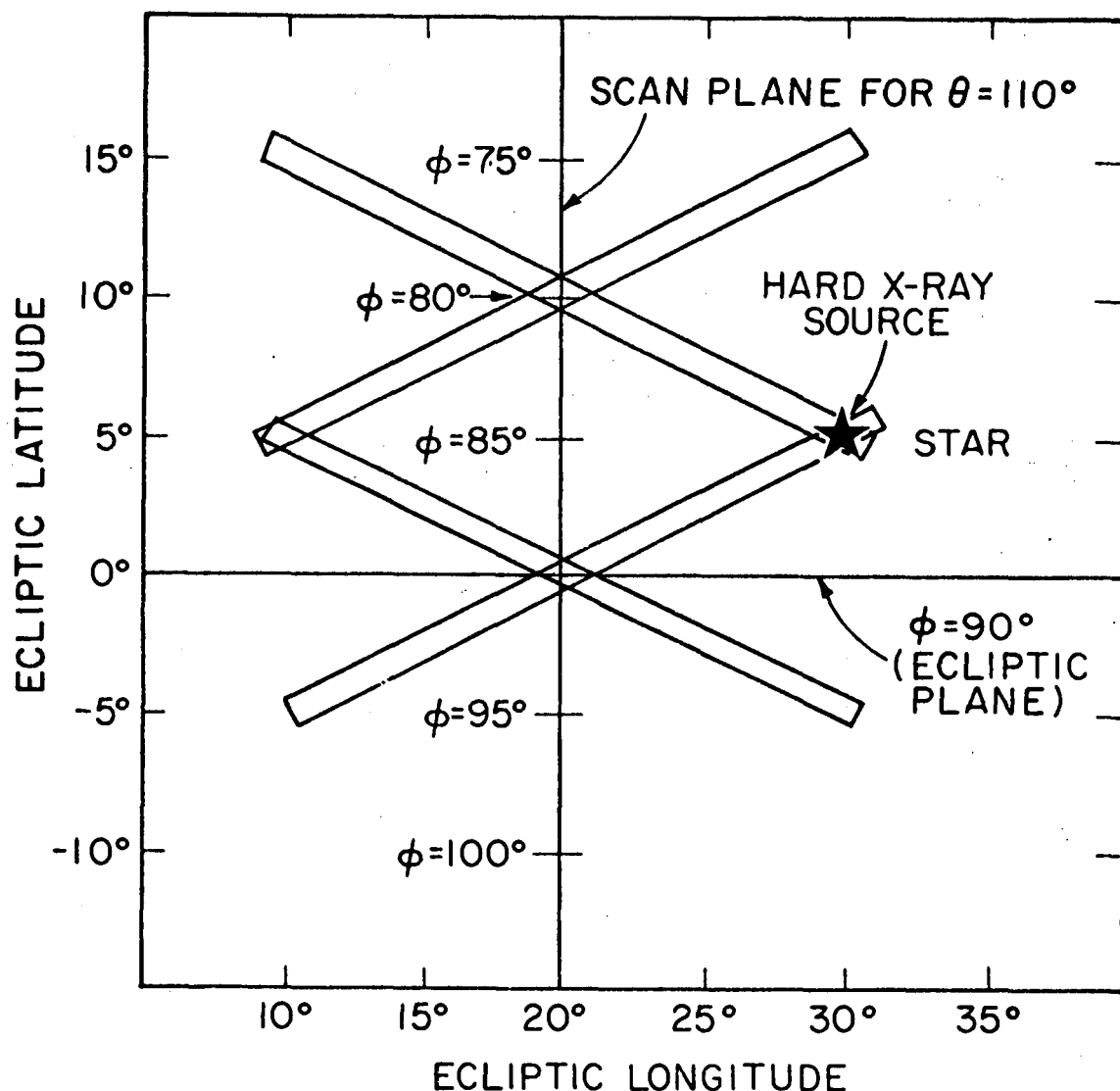


Figure 3. During scanning operations the spin axis ( $\hat{z}_{sp}$ ) of the satellite was always pointed at the sun. Therefore, the satellite orientation during scanning can be specified using two coordinates. We have chosen as coordinates the ecliptic longitude of the spin axis and the azimuth of the spacecraft Y-axis.



ALONG THE SCAN PLANE  $\theta=110^\circ$ , THE XRAY-SOURCE WILL BE DETECTED IN ONE DETECTOR AT  $\phi=80^\circ$  AND IN THE OTHER DETECTOR AT  $\phi=90^\circ$ .

Figure 4. The scan plane for a given spin axis position is projected on a small section of the celestial sphere. The FWHM fields of view of the detectors are shown at the azimuths at which an X-ray source (not on the scan plane) is detected in each of the two detectors.

Since the spin axis follows the sun around the sky, the scan plane will change with time. The azimuth at which the source is detected, by a particular detector, will therefore also change with time.



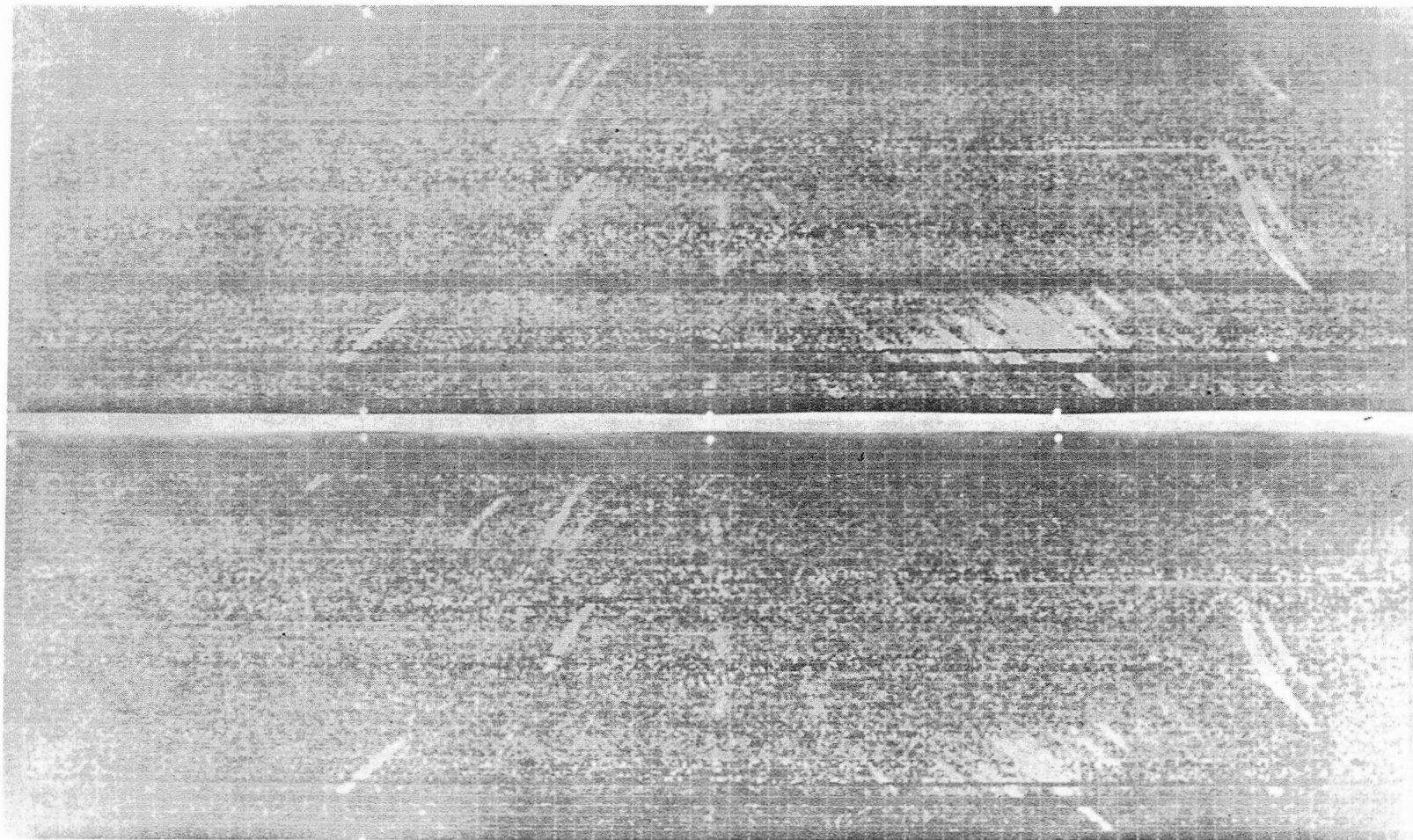


Figure 5. Top: Sky survey results from detector D3. Bottom: Results from detector D6. The average count rate for each possible satellite orientation is encoded as intensity. The satellite orientation is specified by the spin axis recliptic longitude, plotted on the vertical axis, and the azimuth of the Y-axis, plotted horizontally. On a given date the spin axis ecliptic longitude varies little while the Y-axis azimuth covers the entire  $360^\circ$  range.

Therefore, data taken on a particular date is represented on a horizontal stripe. The gray background is due both the diffuse X-ray background and non X-ray particle events in the detectors, X-ray sources show up as dark tilted stripes.

This data comprises the energy band 13-80 keV.

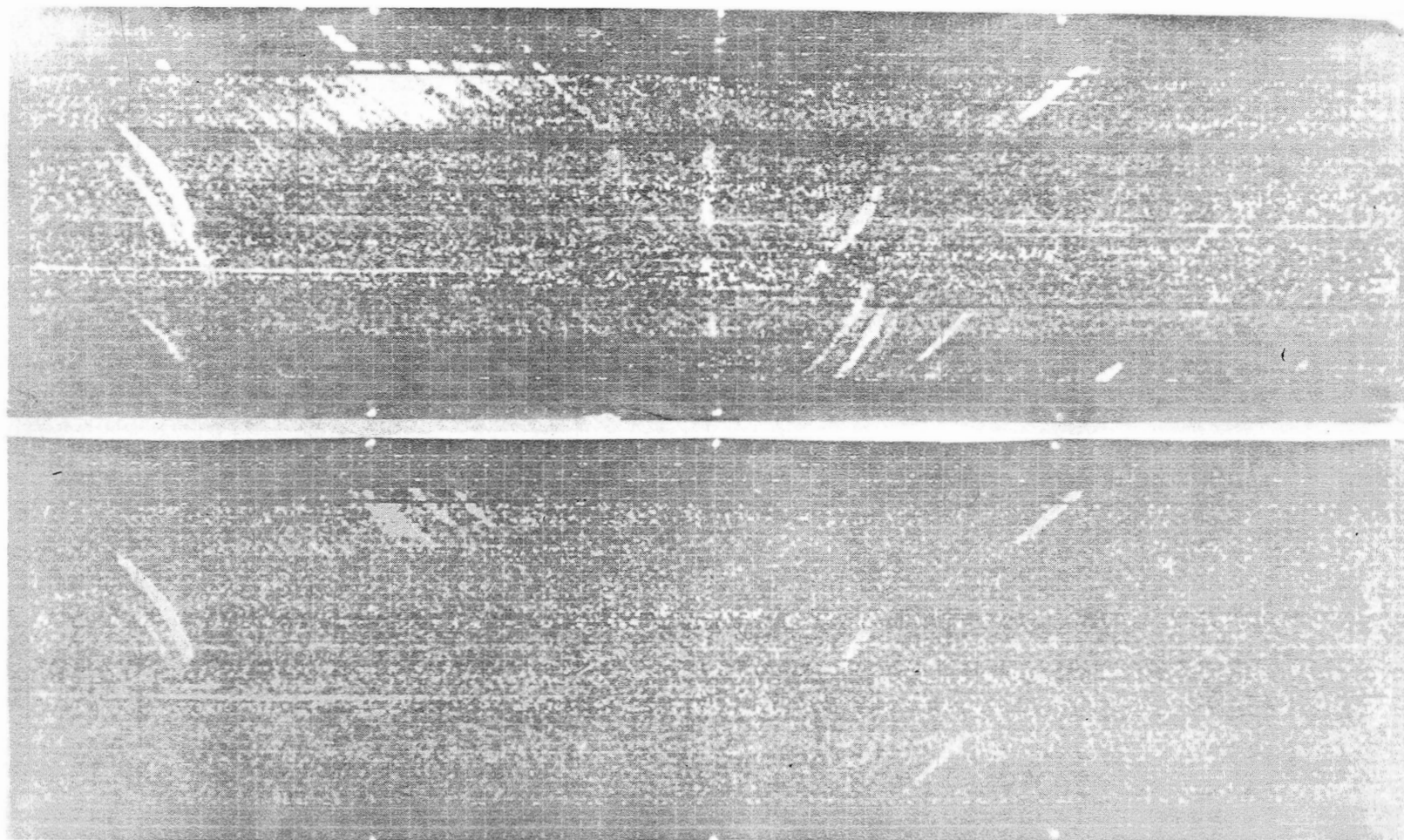


Figure 6. Sky survey results from detector D6 for the energy range 13-25 keV (top) and 25-40 keV (bottom).

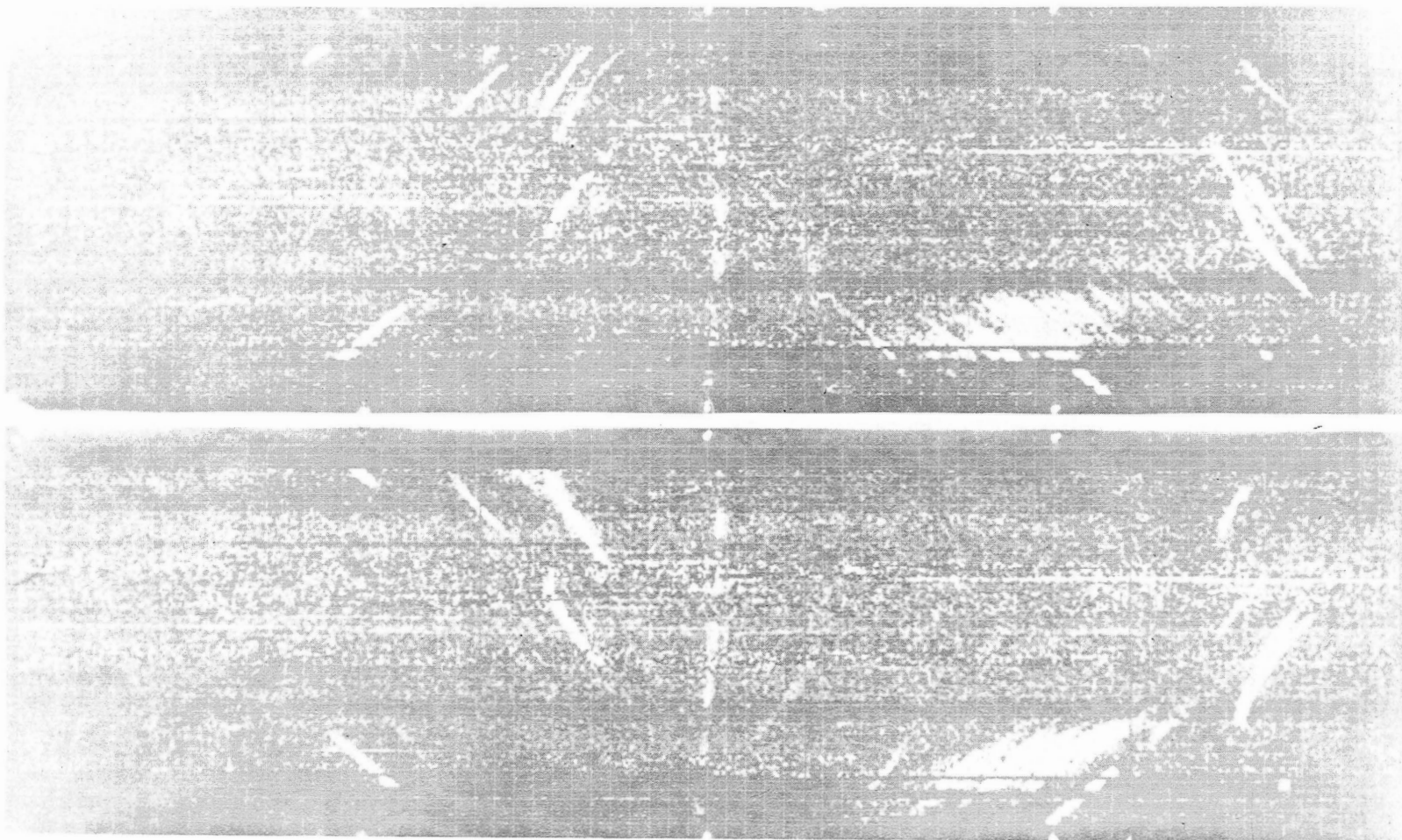


Figure 7. Sky survey results from detector D6 for the energy range 40-80 keV (top) and 13-80 keV (bottom).



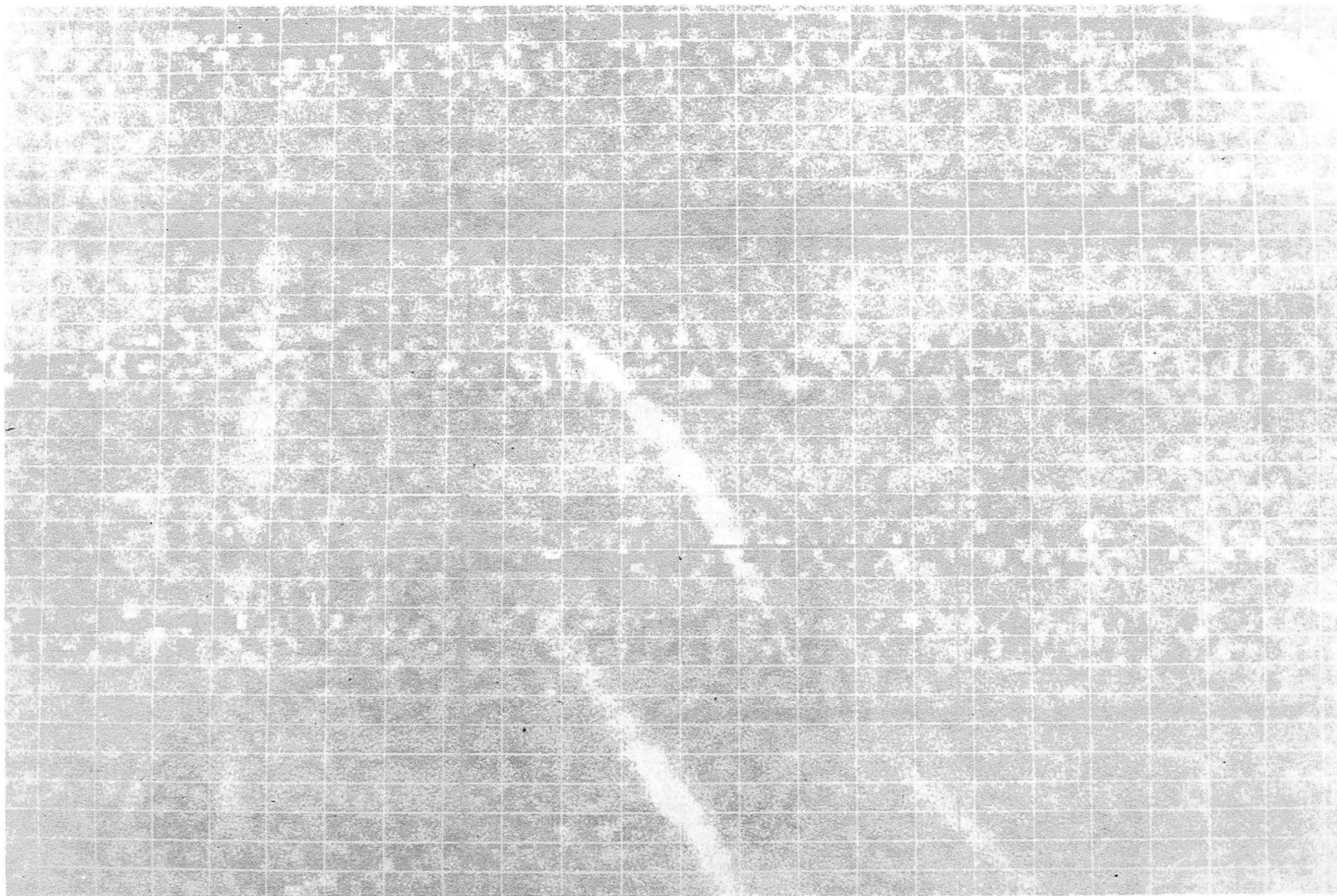


Figure 8. Blowup of the region around 4U0900-40 from Figure 6 (13-25 keV) showing the eclipses occurring every 9 days (see text).

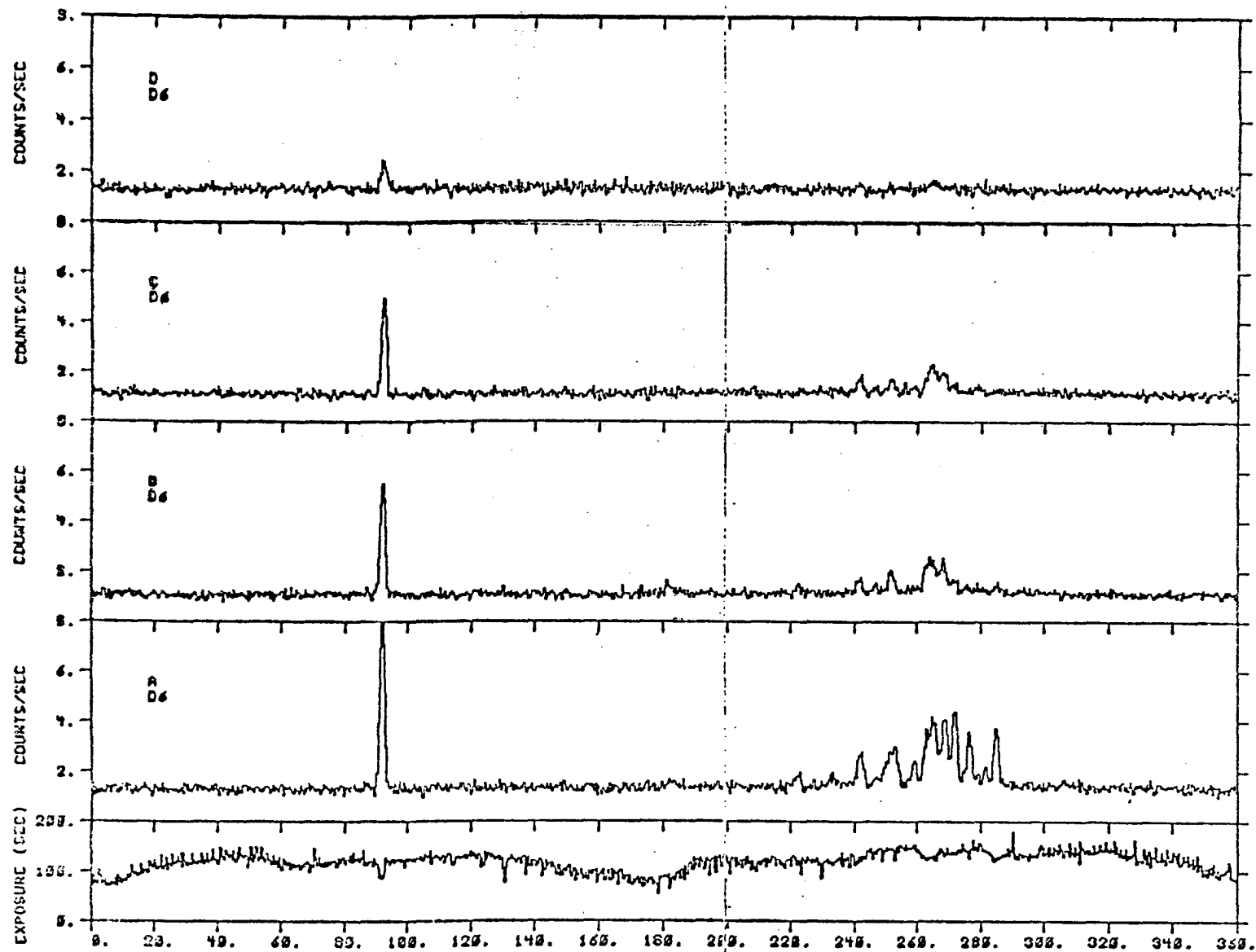


Figure 9. Count rate versus azimuth is shown in each of four energy bands for a superposition of 20 days of data from near the beginning of the HEAO-1 mission. The energy channels are: A, 13-25 keV; B, 25-40 keV; C, 40-80 keV; and D, 80-180 keV. The Crab Nebula is detected near 90° and the galactic center region is viewed near azimuth 270°.

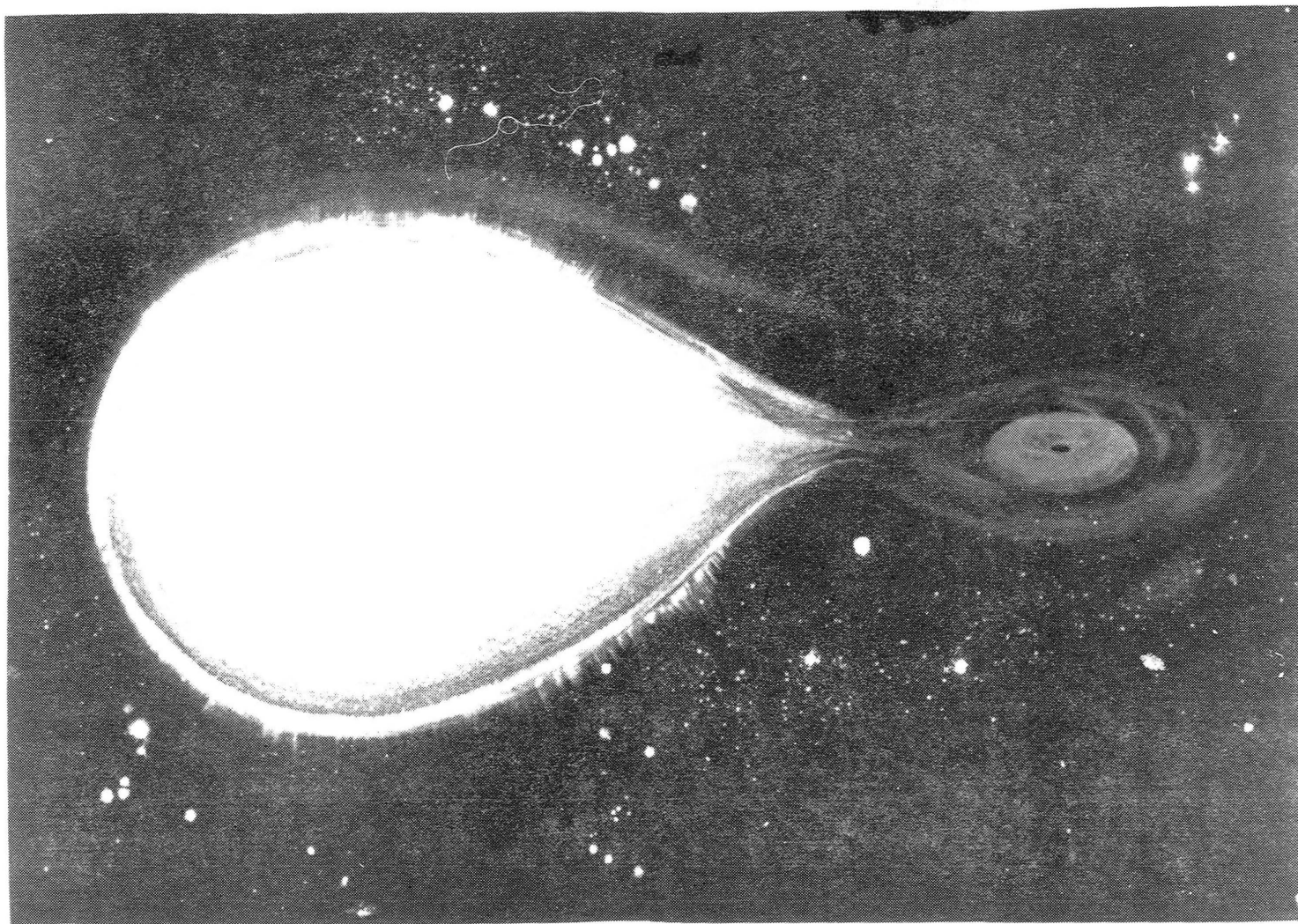


Figure 10. Artist's conception of a binary star system containing an X-ray source. A compact object accretes matter from a normal companion star. This matter forms an accretion disc from which it flows towards the compact object. In the case of X-ray pulsars the compact object is a neutron star. (Painting courtesy Lois Cohen, Griffith Observatory.)

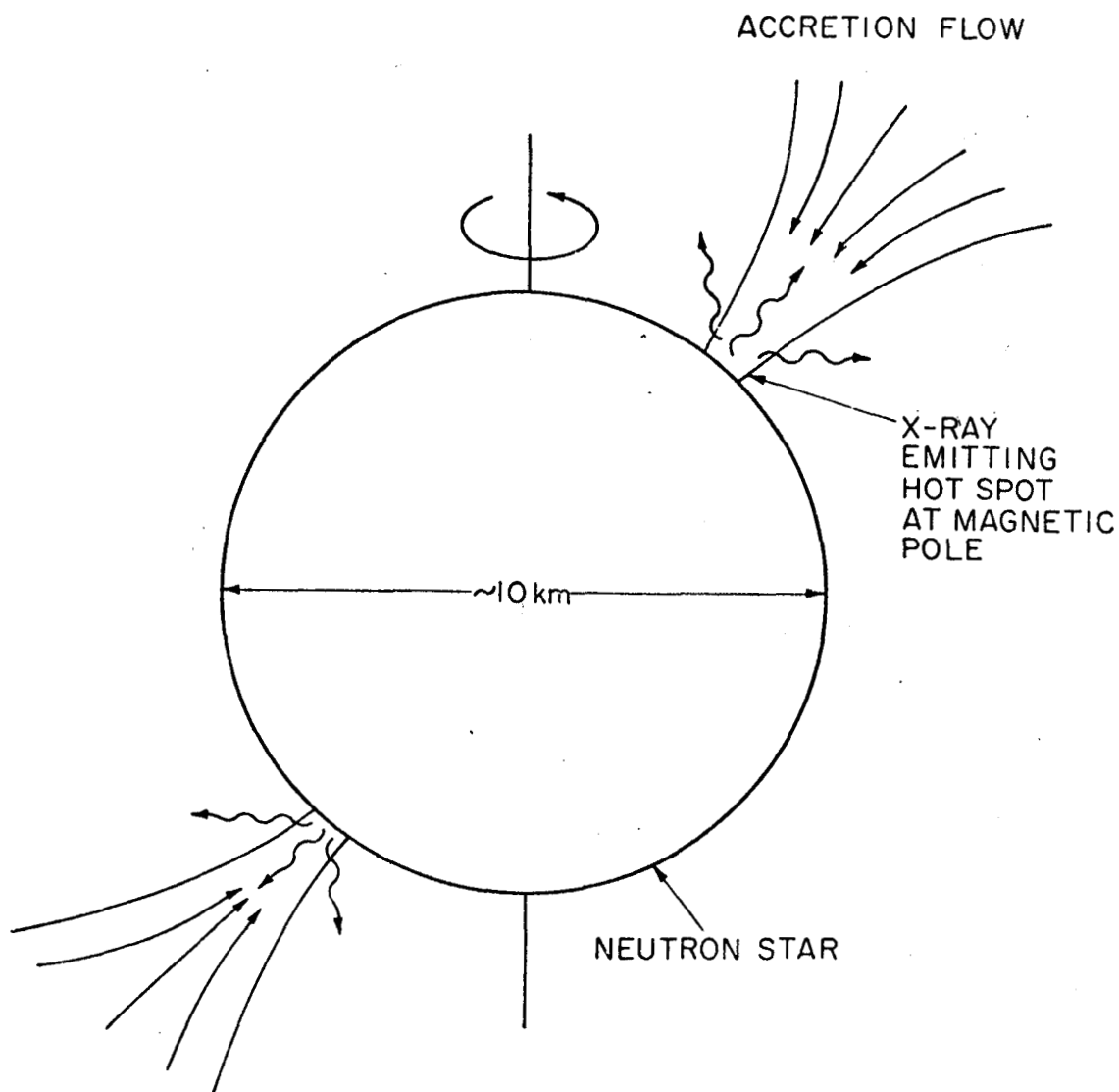


Figure 11. Schematic diagram of an X-ray pulsar. Infalling matter is confined to flow down onto the magnetic poles (which are not coaligned with the rotation axis) of a neutron star. X-rays are emitted anisotropically from hot spots at the bases of the accretion columns. Since the neutron star is spinning, the X-ray intensity varies periodically in any given direction (particularly along the line of sight to the Earth). This is the origin of the observed pulsations.

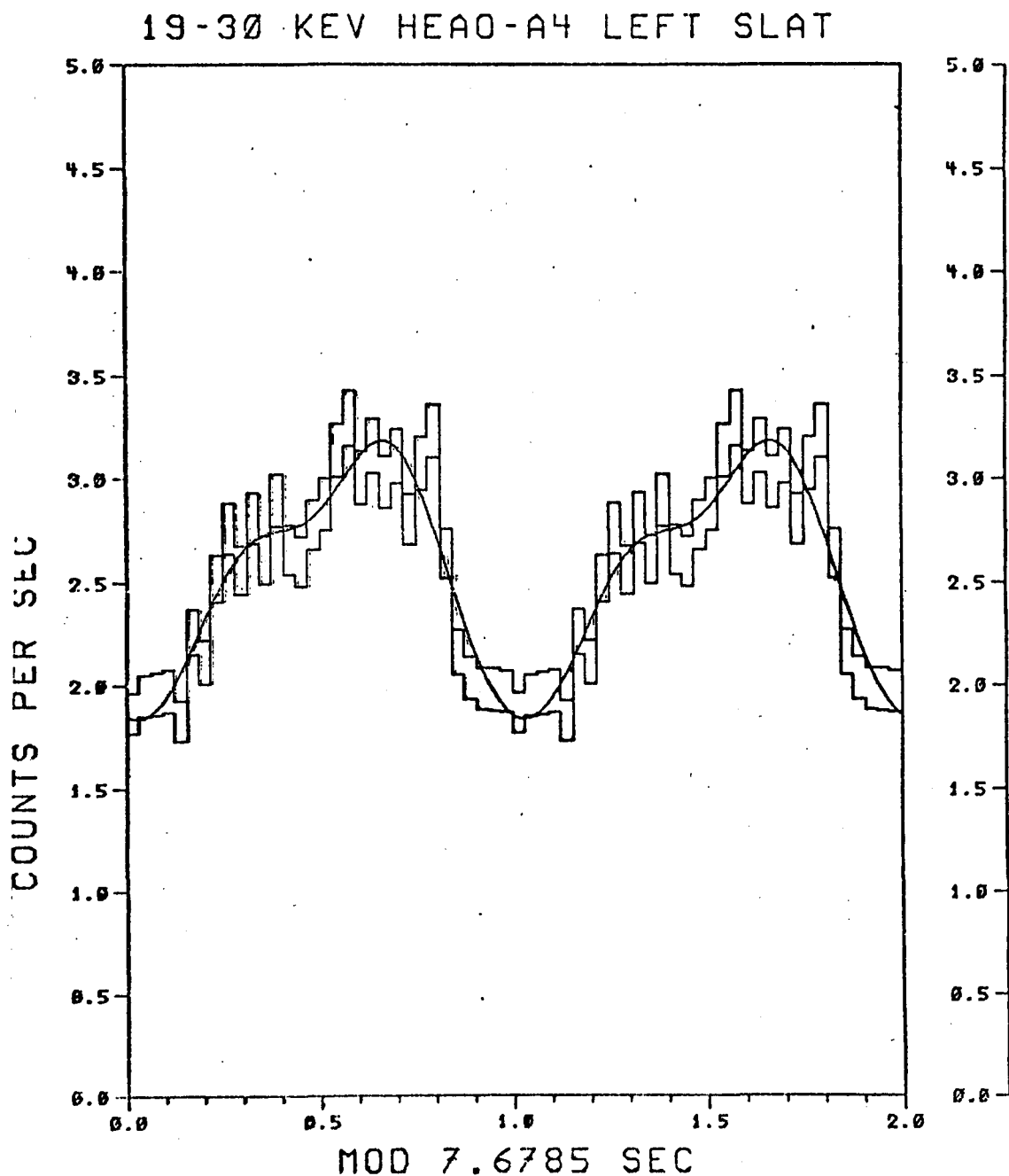


Figure 12. Pulse profile of the X-ray source 4U1626-67 shown in the 19-30 keV energy band. The  $\pm 1\sigma$  range of the profile is plotted at each phase. The smooth curve is a fit to the pulse shape. Note that the pulse is plotted twice for clarity.



1626-67

D3

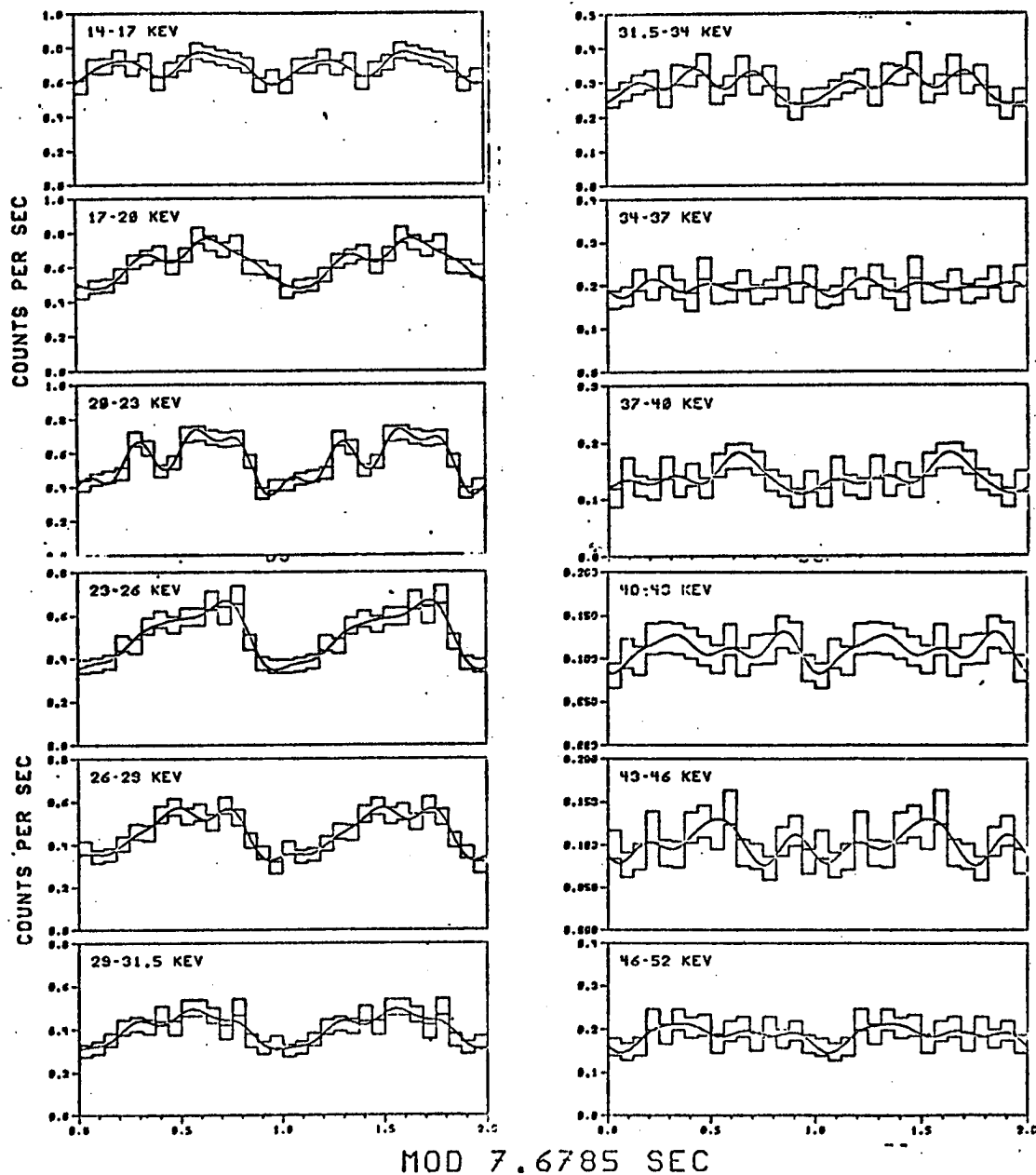
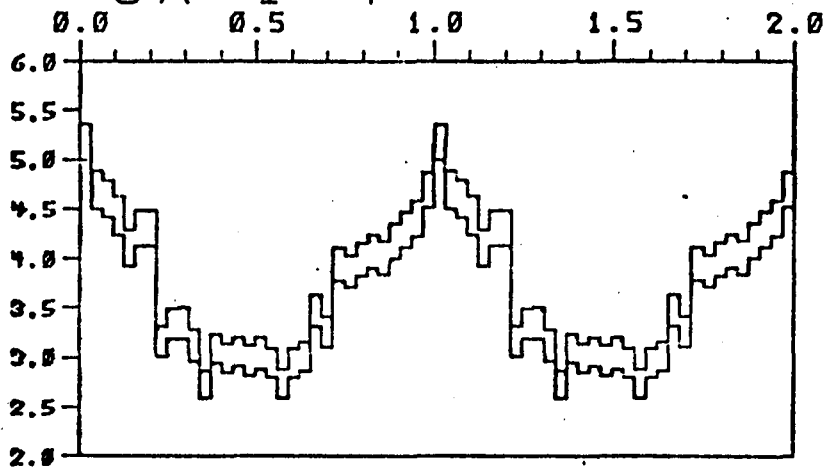


Figure 13. Pulse profile of 4U1626-67 as a function of energy. The shape of the pulse changes rapidly with energy.

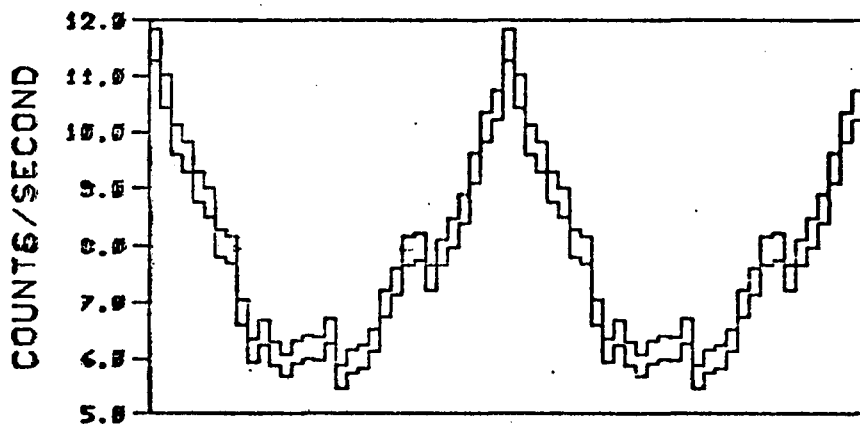
19:52:12 08/31/78

GX 1 + 4

53-98 KEV



31-53 KEV



11-31 KEV

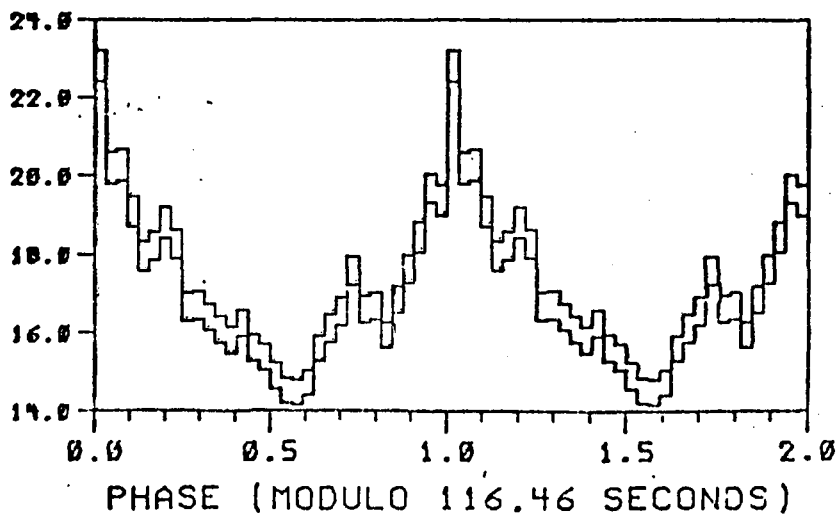


Figure 14. Pulse profile of GX1+4 for each of three energy bands. The shape of the profile of this pulsar also changes with energy.

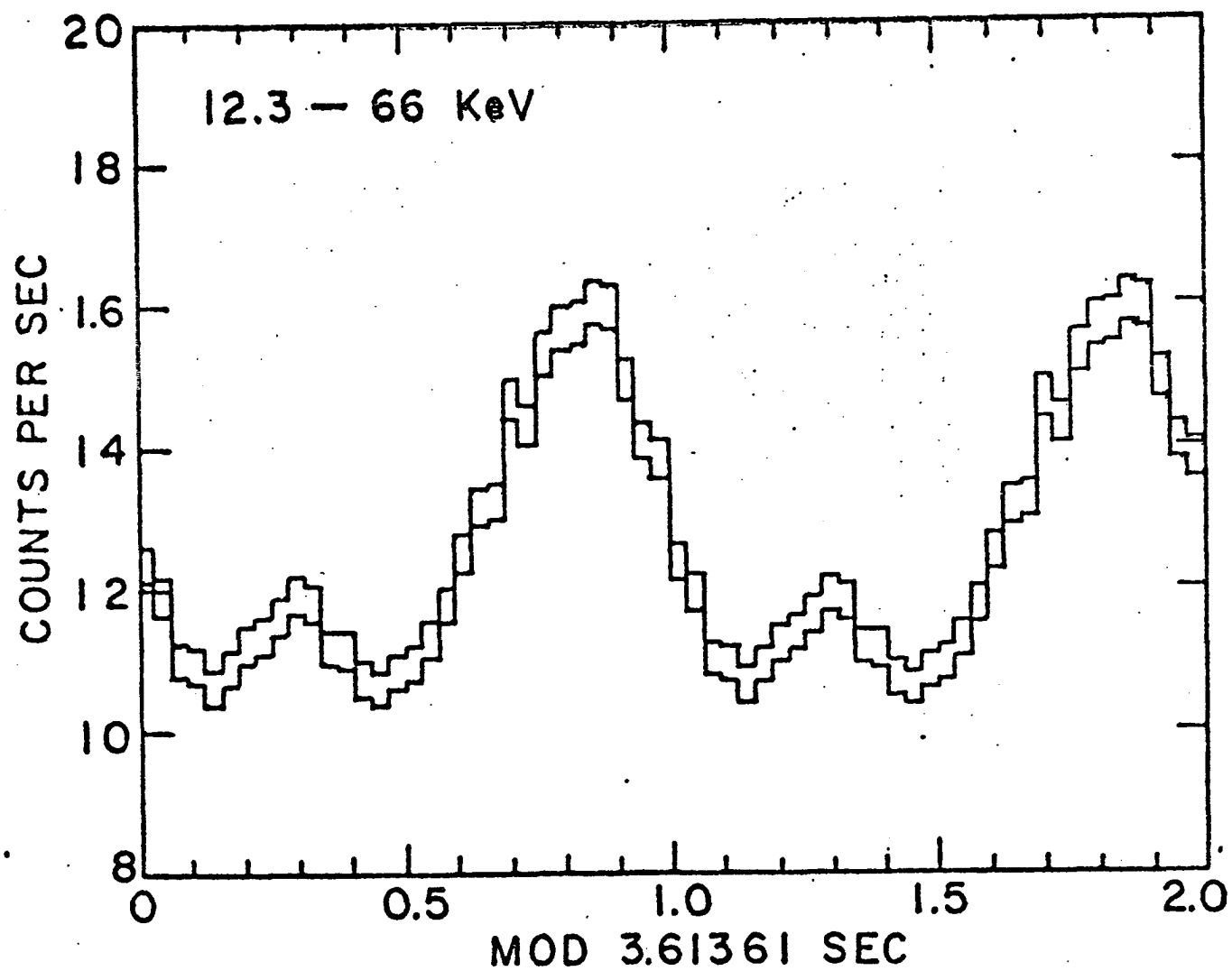


Figure 15. The pulse profile of 4U0115+63 in the energy range 12.3-66 keV.

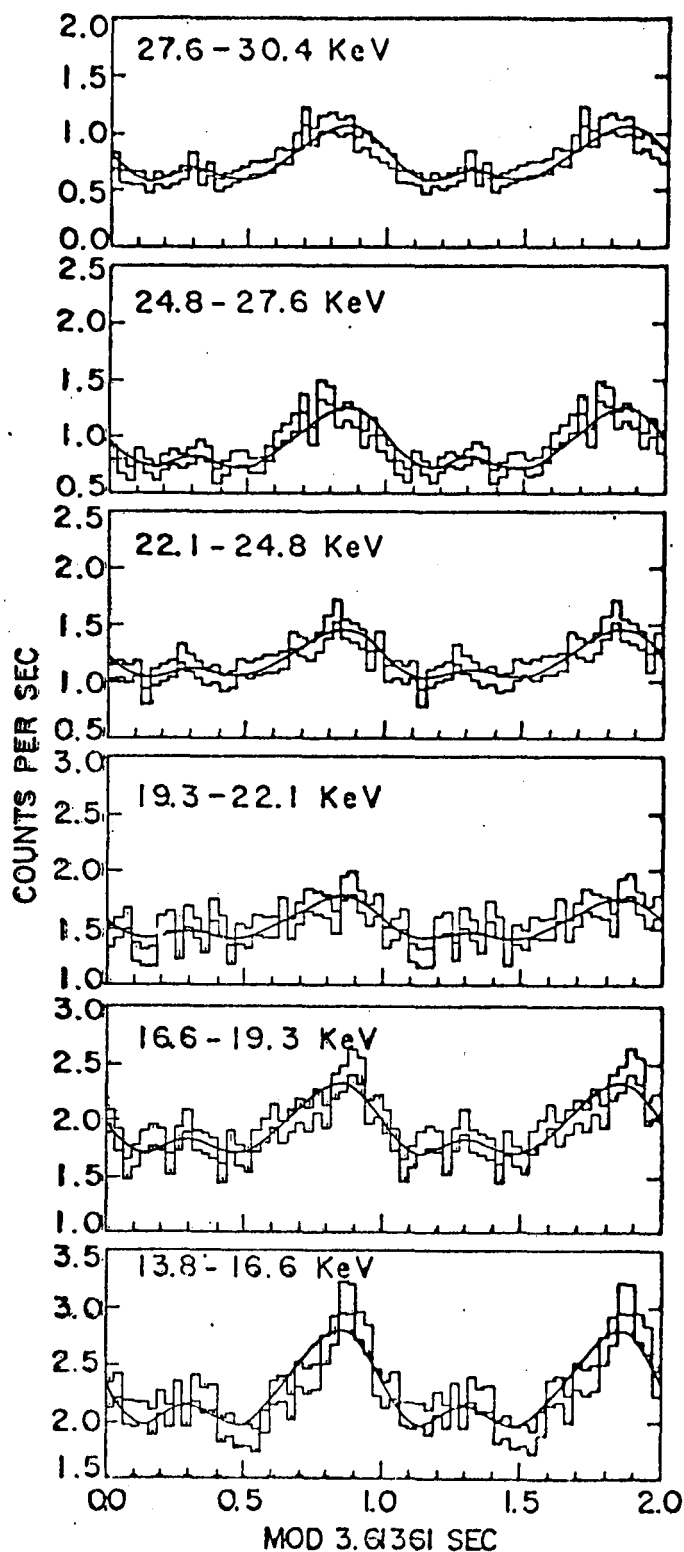


Figure 16. Energy dependence of the pulse profile of 4U0115+63. The pulse shape is independent of energy but the amplitude is not. The pulse is strong at low and high energies and is weak around 20 keV.

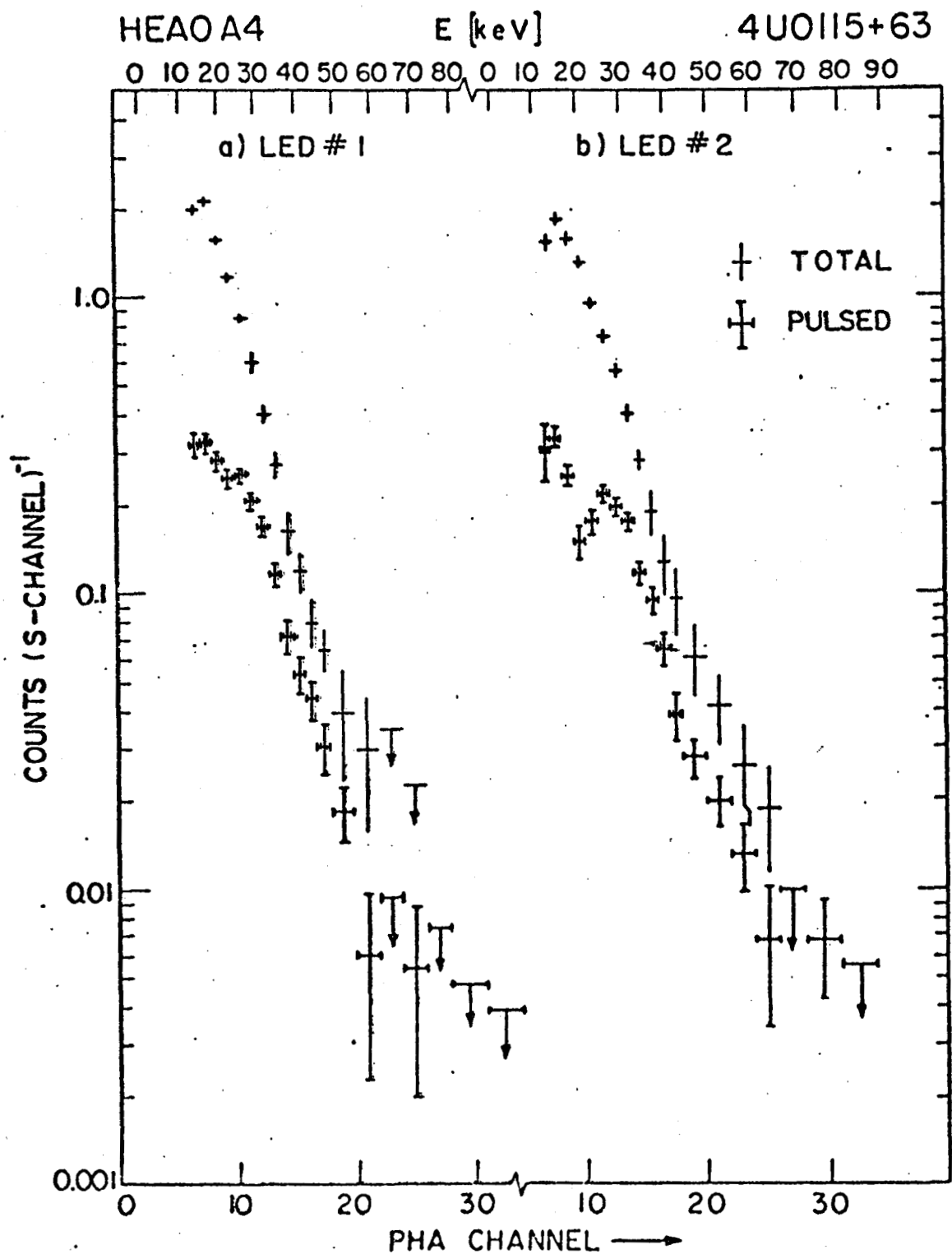
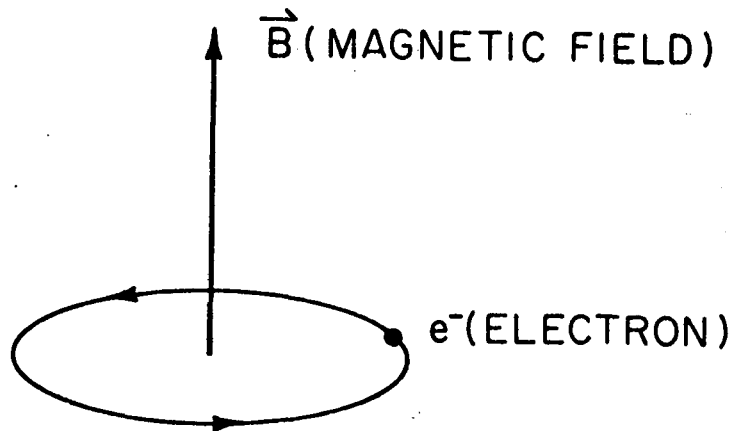


Figure 17. Total and pulsed spectra for 4U0115+63 for both detectors D3 (LED #1) and D6 (LED #2). The dip in pulse strength at approximately 20 keV is clearly evident in the pulsed spectrum from detector D6. The dip is not so evident in data from detector D3 because of inferior energy resolution.



ENERGY LEVELS  $E = n \left( \frac{e \hbar}{mc} \right) B \quad n=0, 1, 2, \dots$

$$\frac{e \hbar B}{mc} = 12 \text{ keV FOR } B = 10^{12} \text{ gauss}$$

( $B_{\text{EARTH}} \sim 0.5 \text{ gauss}$ )

Figure 18. Schematic representation of the motion of an electron in a magnetic field. The velocity component parallel to the magnetic field is unaffected by the presence of the field. The motion perpendicular to the field is circular and the energy levels are quantized. The magnetic field strength near the surface of a neutron star is expected to be of the order of  $10^{12}$  gauss.

# HERCULES X-1 PULSATION, HEAO-1

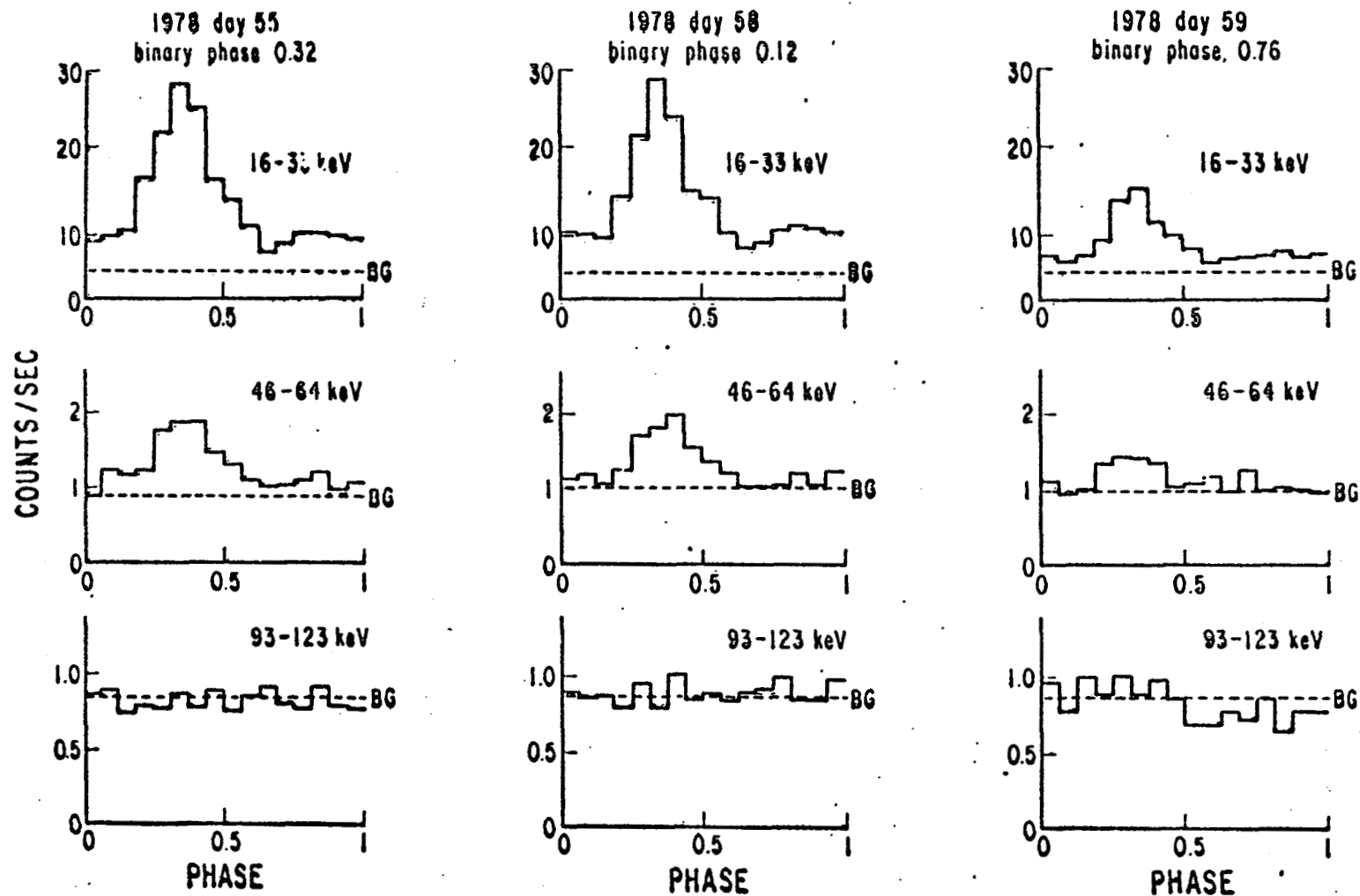


Figure 19. Pulse profiles for Hercules X-1 as a function of energy and binary phase. The shape of the pulse is seen to be constant within the accuracy of the presented data. The pulse period of Hercules X-1 is 1.24 seconds.

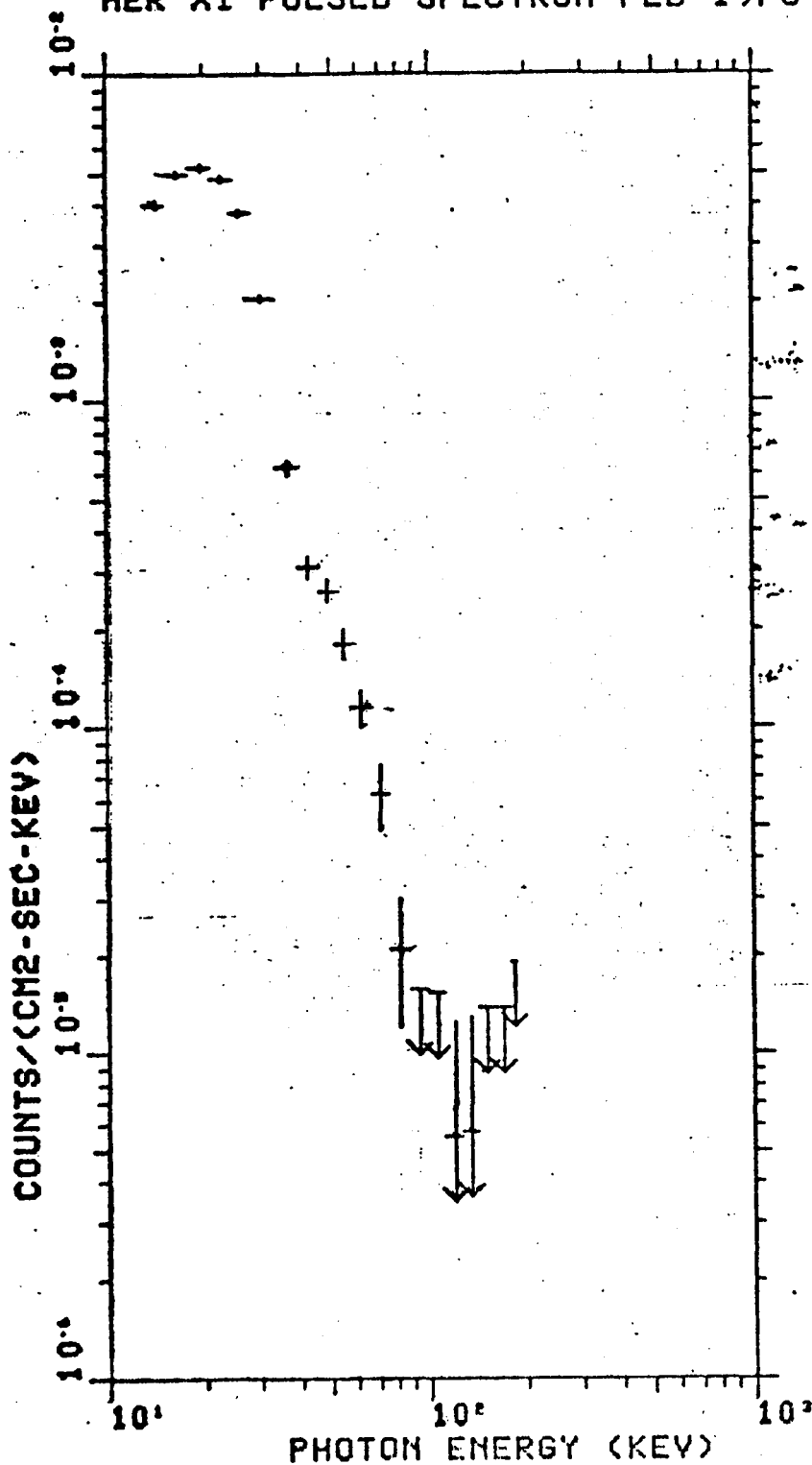


Figure 20. Amplitude of the Hercules X-1 pulse as a function of X-ray energy for the observations of February 1978. Data from both detectors are included.



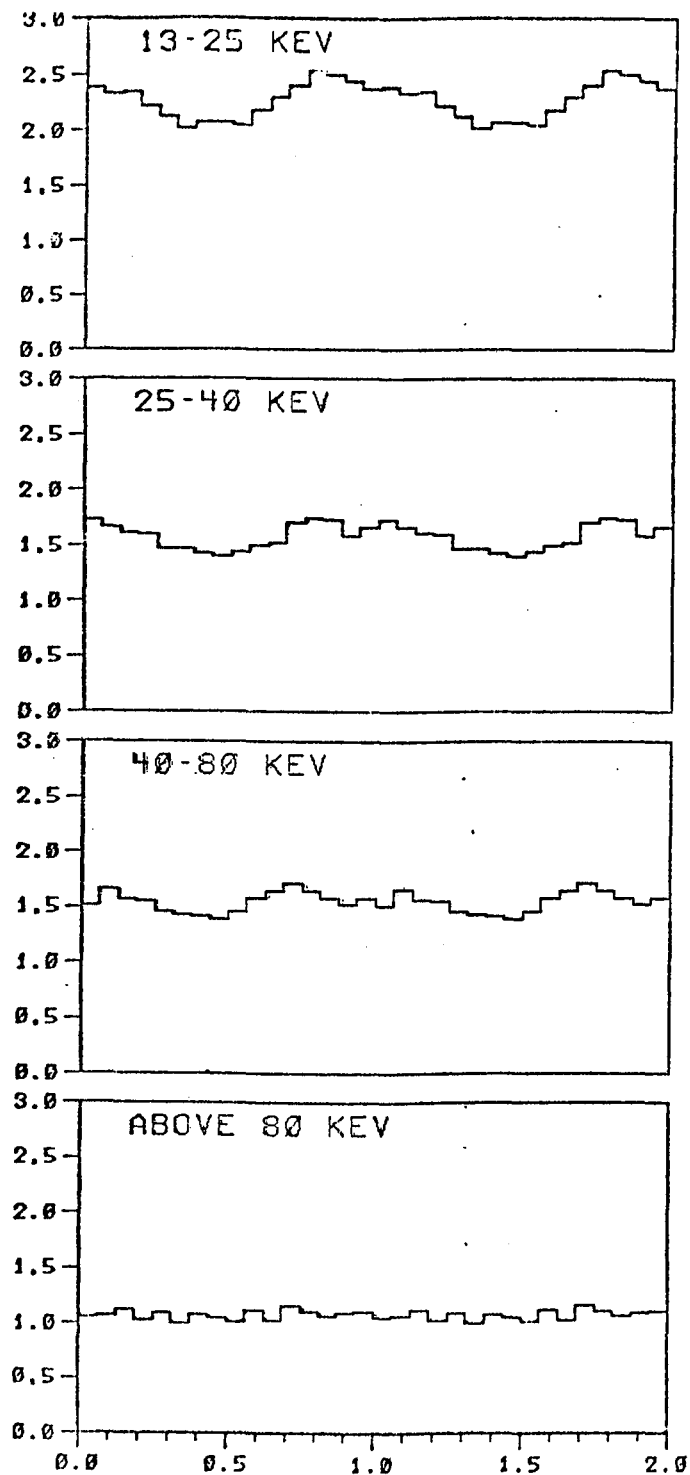


Figure 21. Pulse profile of the 38 second pulsar as a function of energy. No pulsation is detected in the data at energies above 80 keV.

## A-4 SCIENTIFIC RESULTS

James Matteson  
University of California, San Diego

In the previous paper, Dr. Levine discussed observations with the A-4 instrument below about 0.1 MeV. I would like to continue by discussing results that are for the most part at higher energies, from about 0.1 to 10 MeV, which could be called the low energy gamma-ray range or the extremely high energy X-ray range. Figure 1 shows that instrument layout. The detectors I am going to discuss are the high energy detector, located at the center of the instrument and collimated to 40 degrees full width at half maximum, and the four medium energy detectors located around the high energy detector and collimated to 16 degrees full width at half maximum. The high energy detector is designed to operate from about 0.5 to 10 MeV and the low energy detectors from about 0.05 to 2 MeV. Above about 0.2 MeV, the instrument is a first generation instrument, meaning that previous space instrumentation did not have the combination of sensitivity and angular resolution required to measure fluxes from point sources. Even in the low energy range of this instrument we could at best consider it a second generation instrument following in the paths of collimated scintillation counters flown on OSO-7 and OSO-8. Another point about the instrument I would like to make is that the requirements for extremely thick shielding to provide effective collimation above 1 MeV lead to the necessity to trade off sensitive area for shielding mass, with the result that the total instrument sensitive area is only about 500 cm<sup>2</sup> with about 300 cm<sup>2</sup> effective above 0.2 MeV. In Figure 2, I show the various fields of view that Dr. Levine showed earlier. This is to allow consideration of the instrument's ability to provide angular discrimination among the X-ray sources as we go from the highest energies, indicated by the large circle in Figure 2, to lowest energies, indicated by the crossed slats. The angular resolution improves as we go to lower energies. This allows reasonably unambiguous association of high energy flux discovered by this instrument with cataloged X-ray sources seen at low energies.

I would now like to discuss scientific results. I will not discuss the diffuse background. Our analysis of that is in work and within about a month, I think we will have something definitive to say. I also will not discuss gamma-ray pulsars and a large number of additional radio pulsars using HEAO pointings. This analysis is also in progress and results on Crab Vela pulsars should be available later this year. I will discuss some of the galactic sources, extra galactic sources, and finally, our observation of gamma bursts.

In Figure 3, I show some azimuthal scans. These are right shifted 90 degrees relative to what Dr. Levine showed you earlier and cover the 30 to 80 keV range. These data are from one of our medium energy

detectors which was intentionally operated at a slightly lower energy range to enhance the energy range overlap with the low energy detectors. The Crab Nebula and a complex of sources near the galactic center appear as strong sources. The wing to the left of the galactic center is GX 339-4 which you will recall from Dr. Levine's maps showed up as a resolved source approximately 20 degrees away from the galactic center. The fact that the low energy detectors show it is unconfused and that there are no other obvious hard X-ray sources within 10 degrees of it were used in deriving our medium energy spectrum of that source. Going to higher energies in Figure 4, I show the 79 to 150 keV range where the relative signature of the Crab Nebula and the galactic center is about the same. We also still see the wing on the left side of the galactic center due to GX 339-4. Extending up to 1 MeV in the lower part of the figure you can see a bump for the Crab Nebula and a statistically significant excess well above background for the galactic center region.

Now, I would like to discuss some of the objects associated with the azimuthal scan features in more detail. First, the Crab Nebula. Figure 5 is a spectrum of the Crab taken with medium energy detectors scanning data from a total of approximately 40 days in September 1977 and in March 1978. This is one of the most precise measurements of the spectrum of the Crab in this energy range, 25 keV to 1 MeV. Fifteen of the lower energy data points have statistical errors of only a few percent. Through extensive instrumental calibrations and Monte Carlo modeling, the systematic corrections of counts to photons also have accuracies of a few percent. The fitted spectrum has a power law index of 1.98 below 125 keV and 2.40 plus or minus about 0.1 above 125 keV. That is, we see a break in the spectrum at about 125 keV with a change in index of  $0.4 \pm 0.1$ . This is in reasonably good agreement with a recent NRL large area scintillation counter balloon observation which measured the break at slightly lower energy. That instrument was sensitive to only 180 keV, so its lever arm for establishing the higher energy spectrum was not particularly good. The dotted line in the figure is an extrapolation of the lower energy spectral fit. The large number of data points above 125 keV clearly lie well below the extrapolation. The upper limits are taken from our high energy detector data. These are  $2\sigma$  upper limits and they also lie below the extrapolation. In Figure 6, I show a different representation of the same data. It is the data of the previous figure multiplied by energy squared. This has the convenience value of making an  $E^{-2}$  power law spectrum horizontal. The data from the observation I report here are indicated as dots. Below approximately 150 keV the error bars are usually too small to show. At higher energies the individual data points obtain statistical errors which are large enough to see. The break in the spectrum clearly occurs over a remarkably narrow energy band extending from only 100 to 200 keV. Above 200 keV the data are clearly falling well below the  $E^{-2}$  extension of the lower energy points. The break is just what is required to connect the high energy X-ray spectrum with the 100 MeV gamma-ray results of SAS-2 and COS-B. They see the Crab as

between 50 and 100 percent pulsed at high energies. The data I reported are the total emission of the Crab Nebula plus the central pulsar NP 0532. Here I take the observations of the pulsar by other workers, indicated by the dashed line, and subtract it from the total in order to obtain the spectrum of the nebula. You can see that this spectrum breaks at approximately 125 keV.

In Figure 7, I show the spectrum of the Crab Nebula from low frequency radio to extremely high energy gamma-rays. The break at about  $10^{14}$  Hz is in the optical band. This break has long been taken as evidence for synchrotron radiation in the  $3 \times 10^{-4}$  gauss field of the Crab. It is the result of electron lifetime effects and the 1000 year age of the Nebula. In a  $3 \times 10^{-4}$  gauss magnetic field, an electron radiating at 125 keV would have a lifetime of only about 20 years. So, a short timescale acceleration process is required to maintain these electrons. From theoretical considerations, the Crab pulsar itself can only accelerate electrons to few times  $10^{12}$  eV due to a curvature radiation cutoff. But to radiate at 125 keV requires another 50 times increase in the electron's energy. Theoreticians have speculated that this could be due to Fermi acceleration in the inner few tens of arc seconds of the Crab Nebula. In fact, lunar occultations observed in hard X-rays show that the Nebula is extended a few tens of arc seconds. So indeed these acceleration processes and the resulting energy spectrum of the electrons may be the origin of our observed break. Whatever its cause, the spectral break at 125 keV must be intimately related to acceleration and the loss processes in the central part of the Nebula.

Turning to the galactic center, in Figure 8 I show the spectrum we observed. The continuum radiation is indicated by the large dots. GX 339-4 is not included. The total luminosity of the galactic center in this energy band, 80 keV - 2 MeV, is several times  $10^{38}$  ergs per second. Thus far we have been unable to associate this emission with a single resolved low energy detector X-ray source. As Dr. Levine mentioned earlier, it appears that the emission is due to several sources within a few degrees of the galactic center. These sources apparently form a new class of X-ray emitters with high energy X-ray luminosities up to approximately  $10^{38}$  ergs per second, ranking them among the most luminous point-like X-ray sources known. We have also searched for nuclear gamma-rays from the galactic center and have not been successful. In Figure 9, the gaussian shown at 4.4 MeV is our predicted response to a  $10^{-3}$  photon/cm<sup>2</sup>-sec flux. Gamma-rays at this energy are expected due to cosmic ray excitation of the interstellar medium and in fact, the Rice group reported an observation at about  $3\sigma$  significance at that flux level from the galactic center. We had hoped to confirm it; in fact, our  $3\sigma$  upper limits are  $3.7 \times 10^{-4}$  for a narrow line and  $5 \times 10^{-4}$  for a broader line. We conclude that either the line is significantly below the level reported by Rice or it is transient.

We performed a pointed observation of Cygnus X-1 on several occasions since it is one of the most interesting X-ray sources. Figure 10, adapted from a review by Oda, shows the geometry of the Cygnus X-1 X-ray source. A hot torus with dimension approximately 100 km surrounds the black hole and emits X-rays. Accidentally, we were once in a mode which did not give us the high time resolution we wanted, but instead gave us a good spectral resolution (Fig. 11). This was fortunate because during normal scanning there is insufficient time once a source occurs to obtain precision spectra at high energies. Notice the extremely small error bars and obvious departures from a simple power law spectrum. The spectrum steepens above 60 to 70 keV as is characteristic of Cygnus X-1. Theoreticians thinking about X-ray emission processes in Cygnus X-1 and other objects will be able to use this and similar spectra of other sources to perform detailed model testing. Figure 12 shows 160 msec timing data taken in two energy bands. The lower trace is the 14 to 32 keV band, middle is the 32 to 160 keV band, and the upper is their sum. We see flares from Cygnus X-1 occurring in both energy bands simultaneously. Intensity dips also occur. This is the first time it has been possible to do the type of high time-resolution observation required to extend shot noise and correlation analysis to energies above 20 keV. I would like to point out that about 70 percent of the power from Cygnus X-1 is radiated above 20 keV, so any theoretical understanding of the processes in this object must be biased by observations at these energies. Figure 13 shows spectra taken by randomly picking up high, low, and averaged intensity states. You see that the spectrum of Cygnus X-1 does not appear to change shape significantly over about a factor of six in intensity. Figure 14 is a more detailed analysis, showing the spectral hardness ratio over a larger range of intensity units. Below 5 units we see a slight indication of spectral softening. Here intensity is very near to background and nearly zero, so there may be a systematic effect in the data analysis.

Refer to Figure 15. We performed autocorrelations on the two energy bands and the total. They all show essentially the same form; a steep drop and then a tail. For times less than 1 sec they appear similar to previous results. The tail extending out to a few tens of seconds is new. Figure 16 shows the 14-160 keV autocorrelation in detail. Below a half second it is fitted by an exponential with approximately 0.7 sec time constant, as is often seen in 2 to 20 keV analysis of other observations. The 2.2 sec component is required to fit the data at larger times. It is persistent in 5 observations and subsets of them.

Figure 17 shows the cross correlation between low and high energy and here is where some important physics comes in. The point is to determine whether high energy X-rays lead or lag the low energy X-rays. A definite measurement of such an effect would have significant theoretical implications for the processes in the inner accretion disc. The eye says there is no obvious trend here, and an analysis by Pat Nolan, a graduate student at San Diego, shows that to about 10 msec accuracy there is no lag. What does this mean for Cygnus X-1? I think that these results

are consistent with the concept of Compton cooling which was proposed several years ago as the X-ray generation process in the inner accretion disk. Here you have  $10^9$  K electrons being cooled by Compton scattering of soft photons. High energy X-rays result. The fact that the spectrum does not change with intensity indicates that geometry of the scattering region is probably independent of the luminosity. The X-ray intensity fluctuations are possibly due to fluctuations in the soft flux which is the source of the photons which ultimately cool Cygnus X-1.

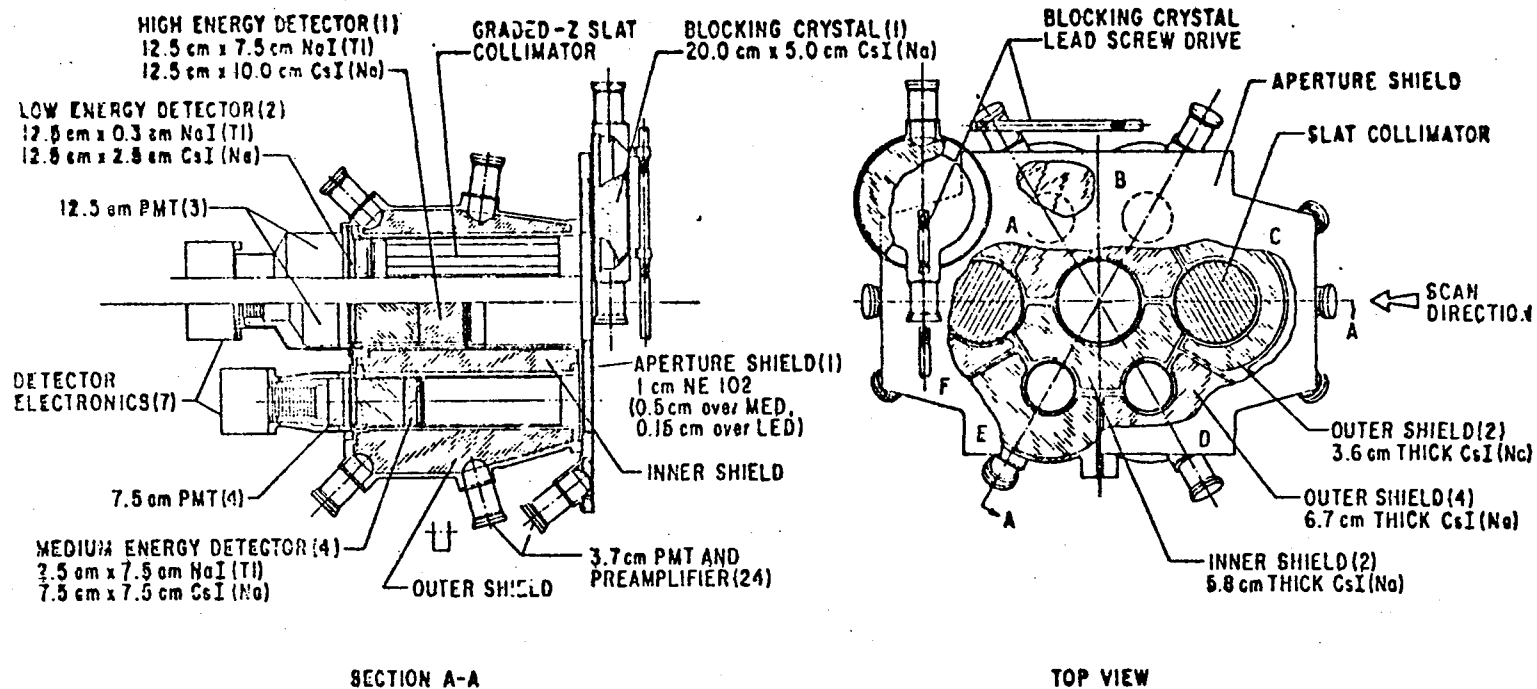
Figure 18 shows GX 339-04 which has been discussed several times earlier today as a black hole candidate due to its similarity to Cygnus X-1. The short time scale variability in two state spectrum exhibited by this object are also characteristics of Cygnus X-1. The new result we have here is an extension of its spectrum up to several hundred keV. For reference I have shown the spectrum of Cygnus X-1. They are each quite hard and have a steepening above approximately 100 keV. This is additional evidence for the similarity between these two objects. In addition, the intensity of GX 339-04 is a factor of 4 or 5 below Cygnus X-1, consistent with the estimated distances to these objects.

I next turn to extra-galactic objects. Centaurus A is the only extra-galactic object which is clearly visible in Dr. Levine's sky maps in the first 6 months of the mission. Our medium energy detector data for this object, the small dots in Figure 19, extend the spectrum up to about 700 keV, confirming the Rice balloon observation of high energy X-ray emission in this object. Since the spectrum is quite hard, about  $E^{-1.6}$  in our observation, the X-ray luminosity of Centaurus A is dominated by the highest energy where significant X-ray emission is occurring. The data which I just discussed were taken in January of 1978. In July-August 1978, we observed again. The large dots are the results. We do not have any low energy data available yet, so these are only medium energy detector results. A factor of 2 intensity decrease occurred over the 6 months and the spectrum shape stayed roughly constant, although we cannot say much about it. Centaurus A is known to have temporal and spectral variabilities in X-rays on time scales of a few years. We have now reduced that time scale to 6 months.

Turning to 3C273 (Fig. 20) I show on the right panel the data taken during the "ping-pong" pointing observations that lead to the spectrum which Dr. Boldt showed earlier, the A-2 spectrum extending from a few keV up to about 60 keV. Also on the right panel, the A-4 results are seen as the four data points from 13 to 125 keV. The motivation for the observation was that COS-B had reported a gamma X-ray flux from 3C273 at 100 Mev. Therefore, it was a good candidate for detectable X-ray emission above 100 keV. But the flux was expected to be very low, so a long duration "ping-pong" observation was spread over three periods. It paid off. The  $E^{-2.05}$  power law is capable of connecting the A-4 and COS-B results, although A-4 fitted strictly by

itself leads to a harder spectrum,  $E^{-1.7}$ . Figure 21 is the same figure which Dr. Boldt presented earlier. The crosses below 60 keV are from A-2, the diamonds are A-4 low energy detector points and the cross from 100 to 300 keV is an A-4 medium energy detector datum from scanning observations.

Referring to Figure 22, I would like to discuss two gamma-ray bursts. We have analyzed a few gamma-ray bursts. I am sure that there are many in the data. An important new observation that we have provided is the measurement of the spectrum on short time scales at high energies. For comparison purposes, the Apollo 16 burst is shown. The October 20, 1977, burst was temporal structure similar to the Apollo 16 burst except that it has a couple of peaks occurring after the main burst. These are numbered 3 and 4 and occur on approximately 10 sec centers. This may be an indication of periodicity. Also shown in Figure 22 is the November 10, 1977 burst which had only one peak, number 5. I have numbered the peaks 1 through 5. Their spectra are shown in Figure 23. For reference, the solid line is the Apollo 15 spectrum. It is not too obvious to those of you in the back of the room, but if we disregard the lowest energy point which we were having some problems with, each of these five spectra are essentially identical. They are varying in intensity but not in shape or effective temperature. From that we conclude that the intensity variations are a property of the energy source, or reservoir, for the gamma-ray burst, perhaps accretion onto some compact object and that the spectrum shape is a signature of the physics of the engine that powers these objects, perhaps the potential well into which the matter may be falling.



UCSD, MIT HARD X-RAY AND LOW ENERGY GAMMA-RAY -  
INSTRUMENT OF HEAO-1

Figure 1



# HEAD A-4 FULL WIDTH FIELDS OF VIEW

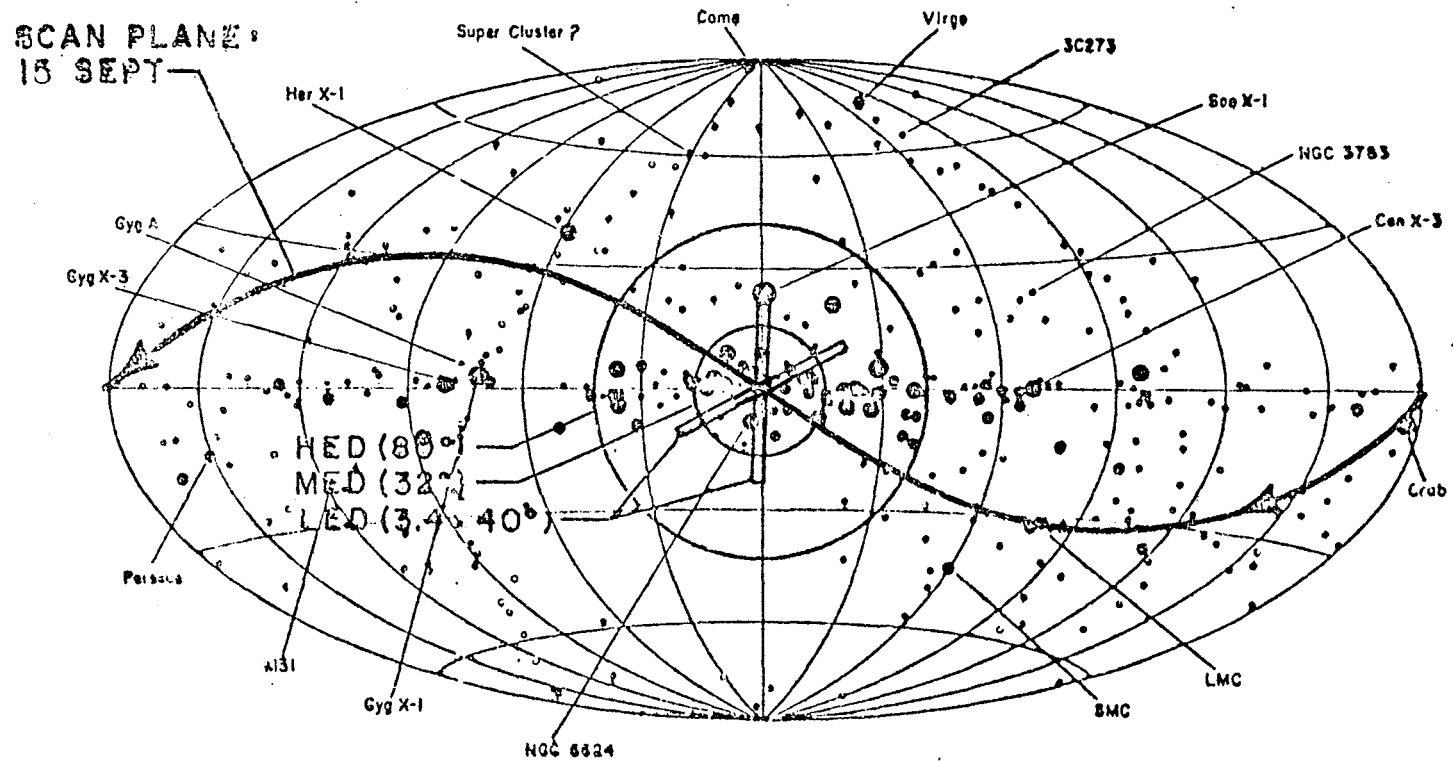


Figure 2

DETECTOR # 5

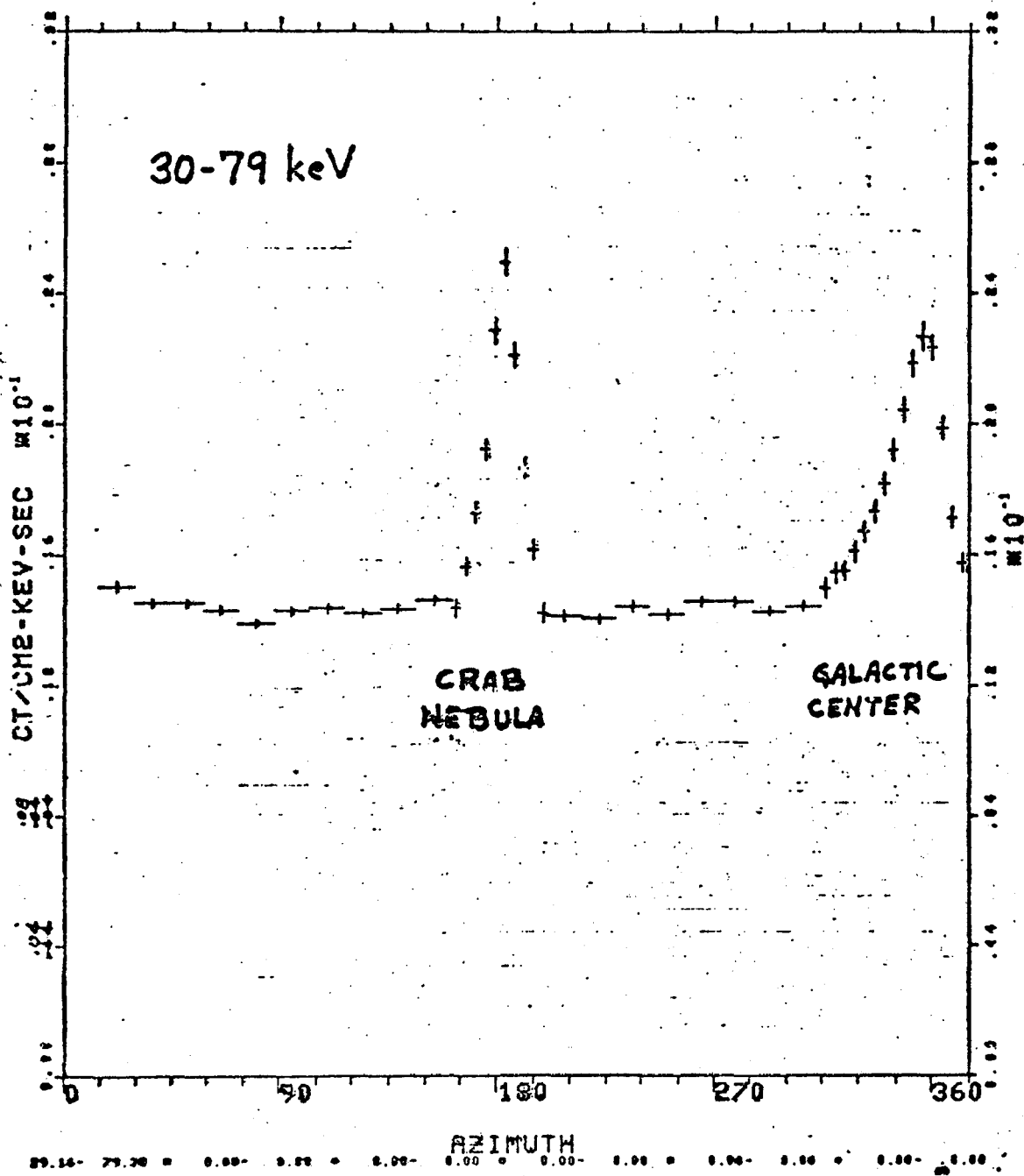


Figure 3

# DETECTOR # 2

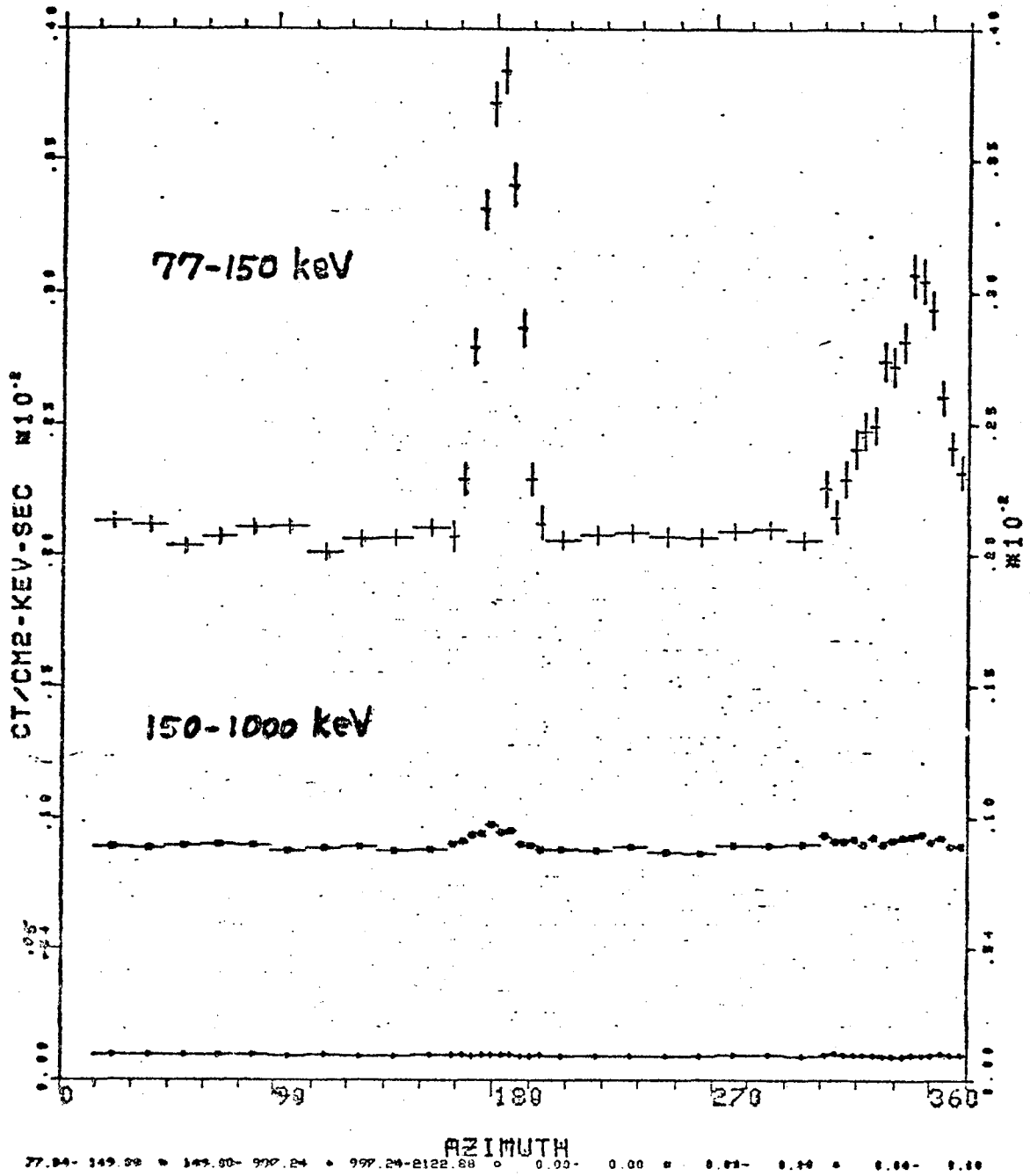


Figure 4

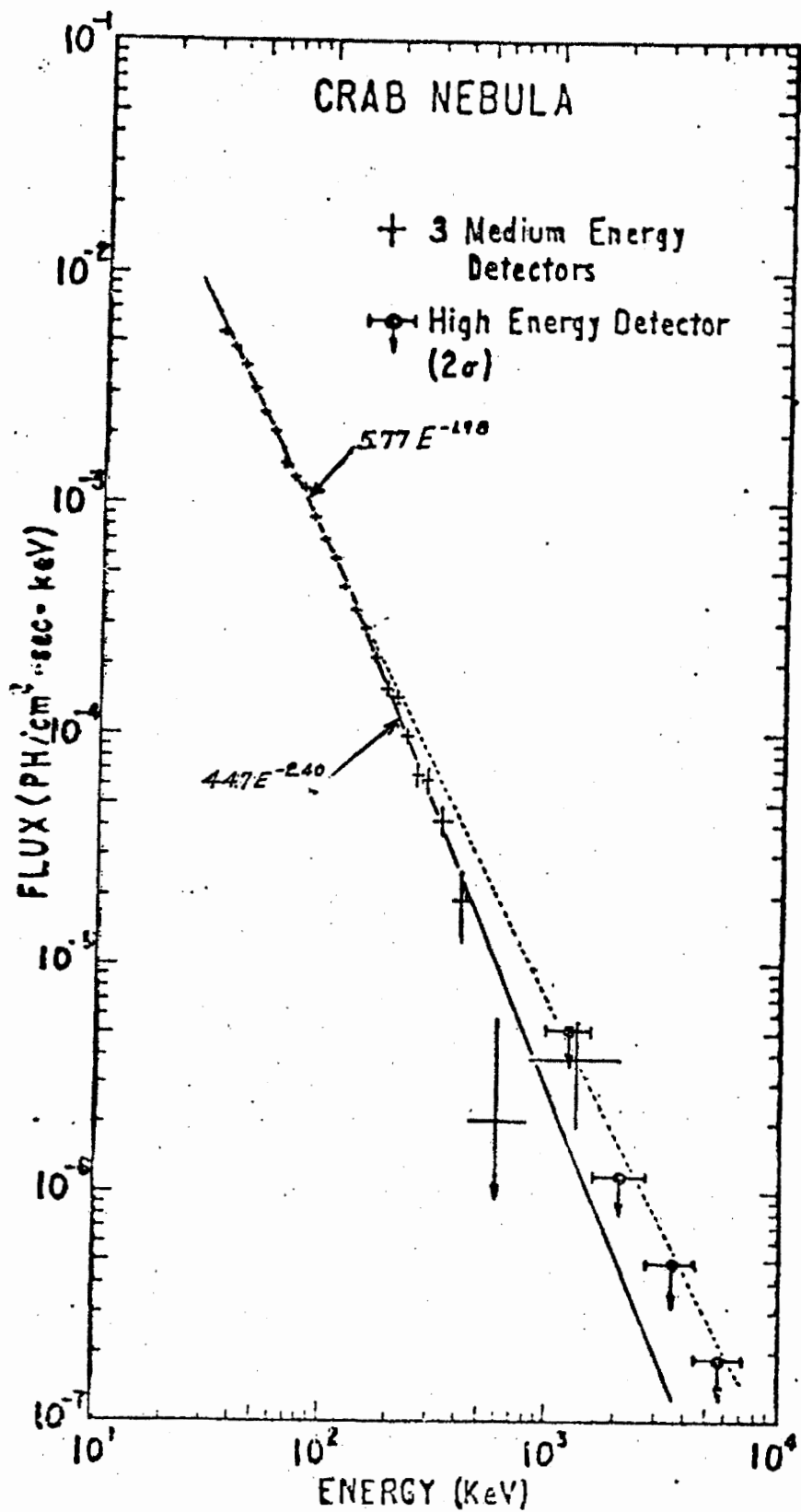


Figure 5

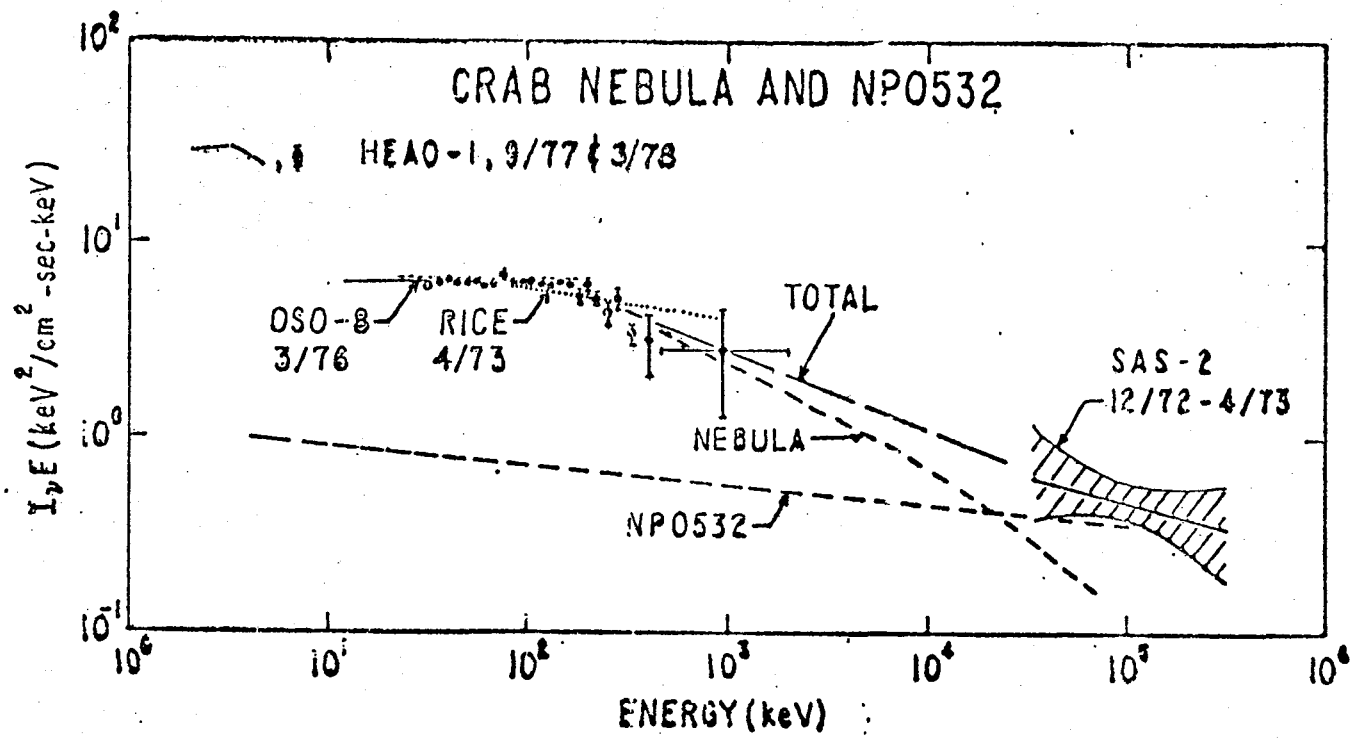


Figure 6

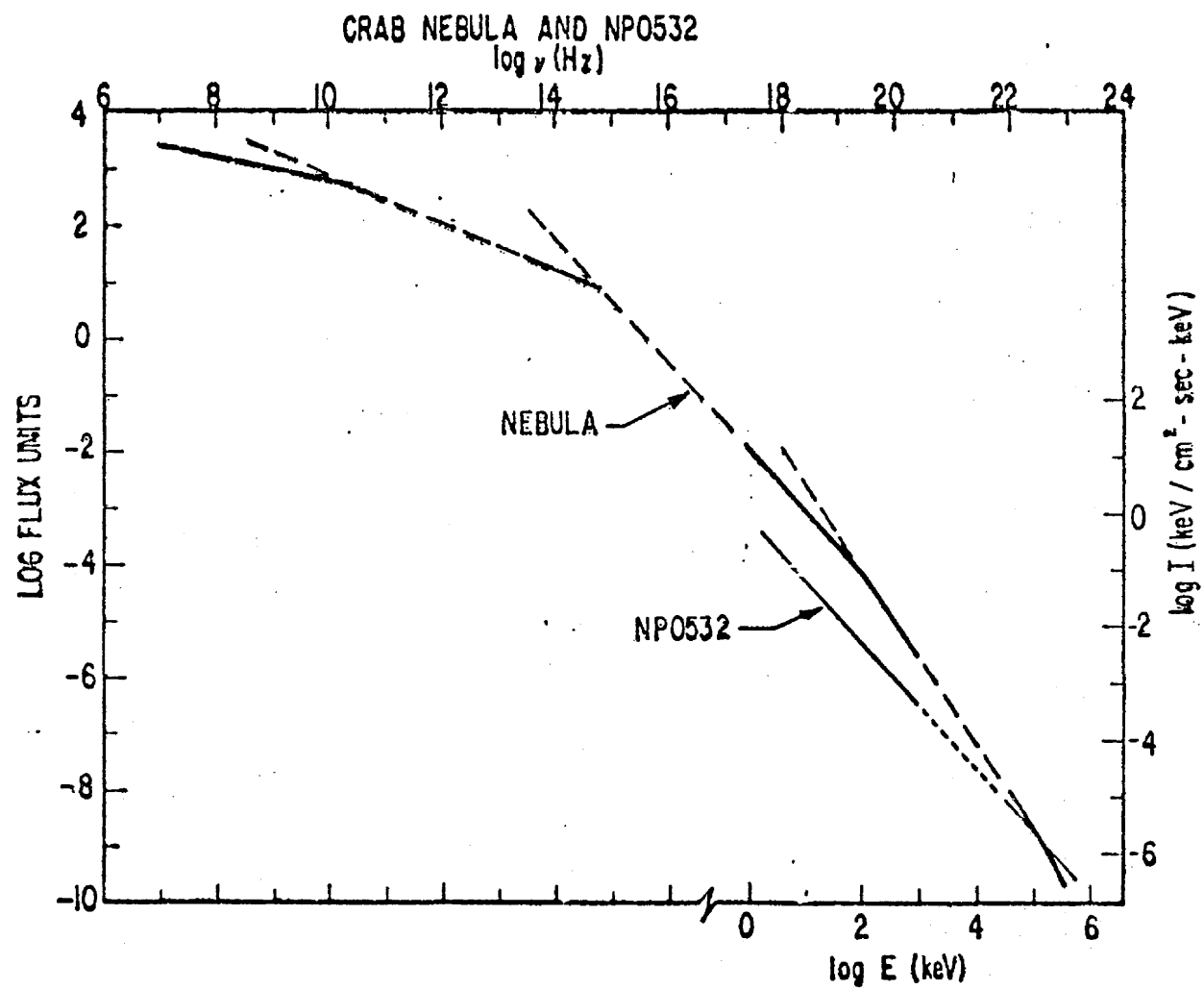


Figure 7

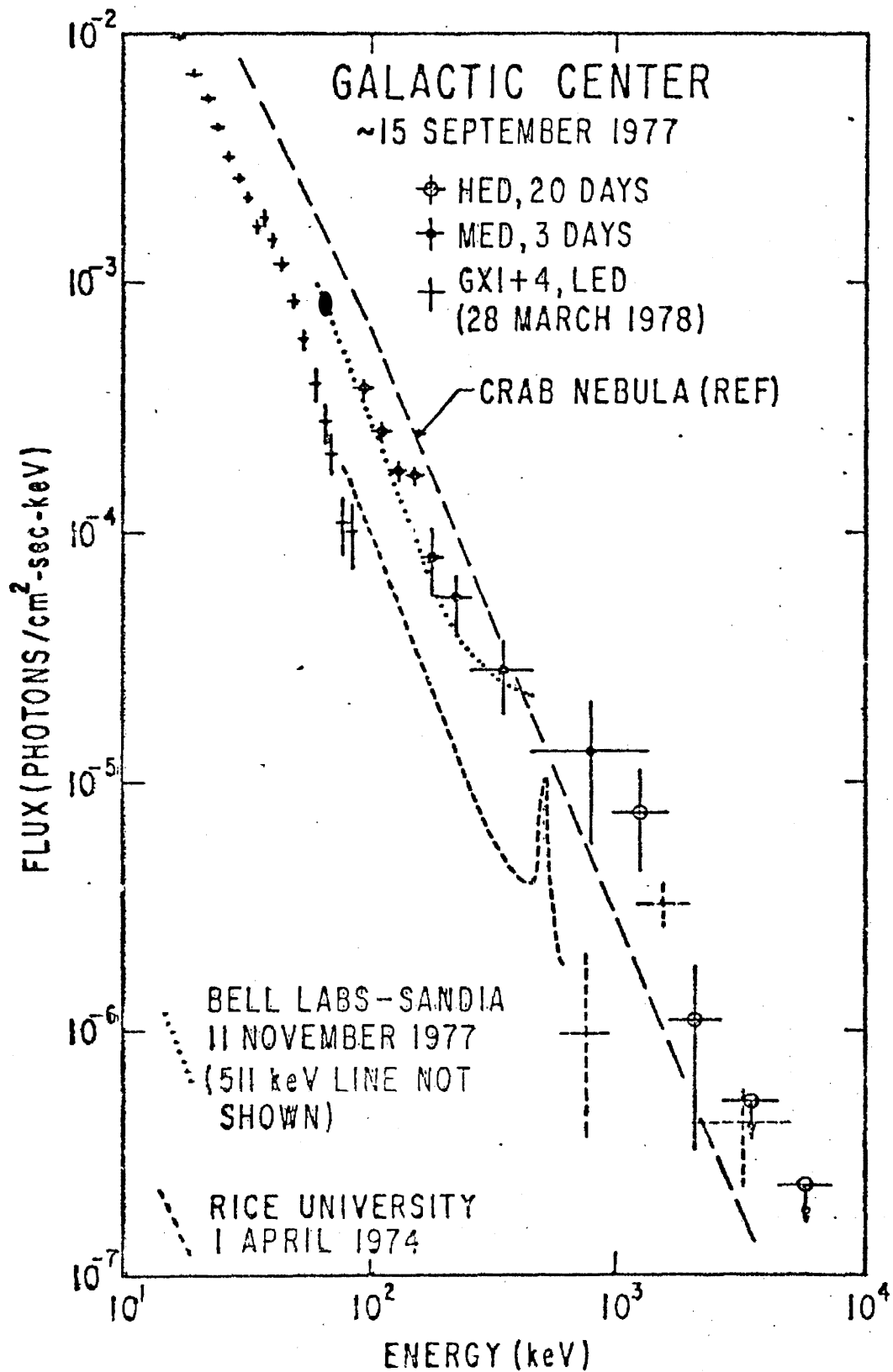


Figure 8

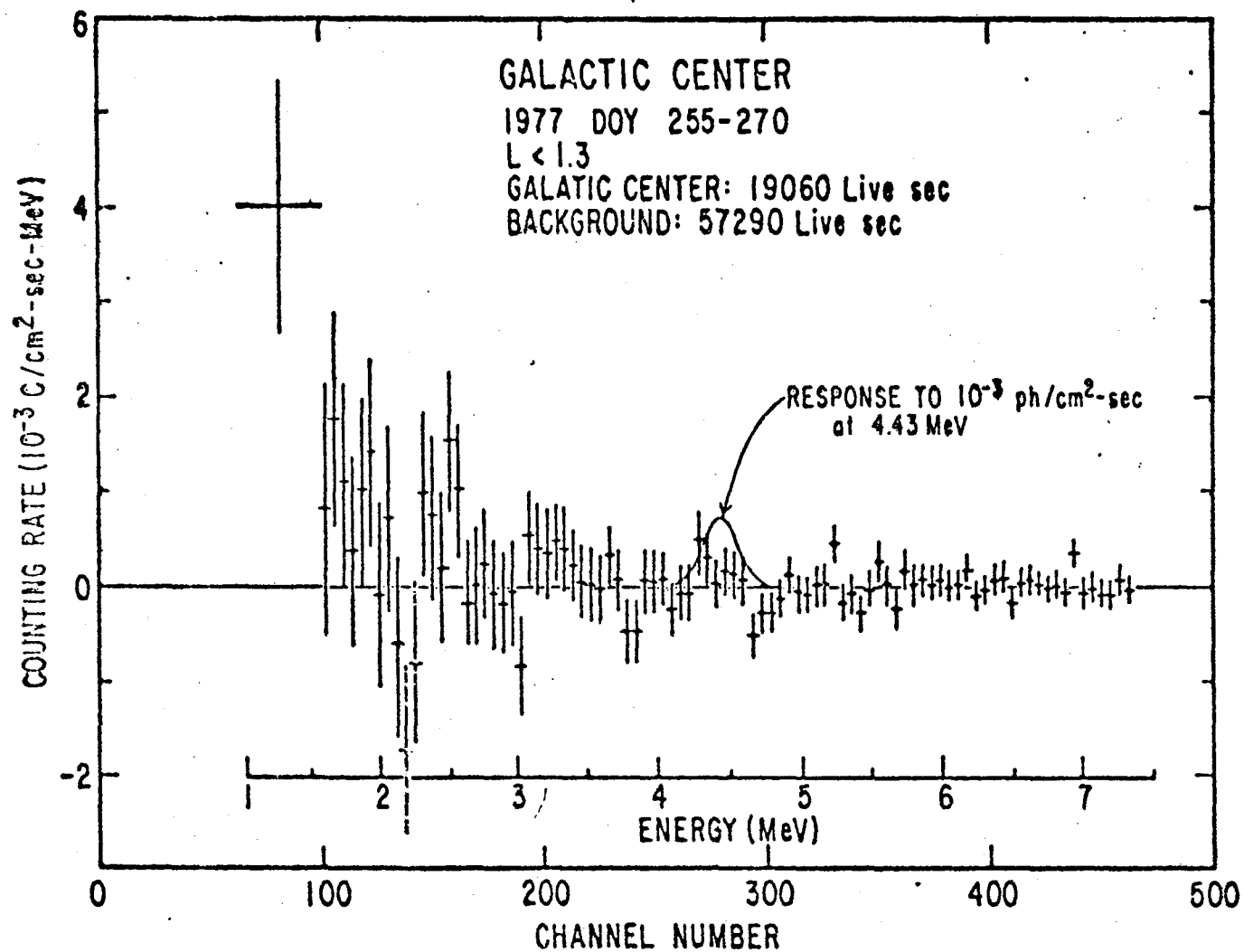


Figure 9



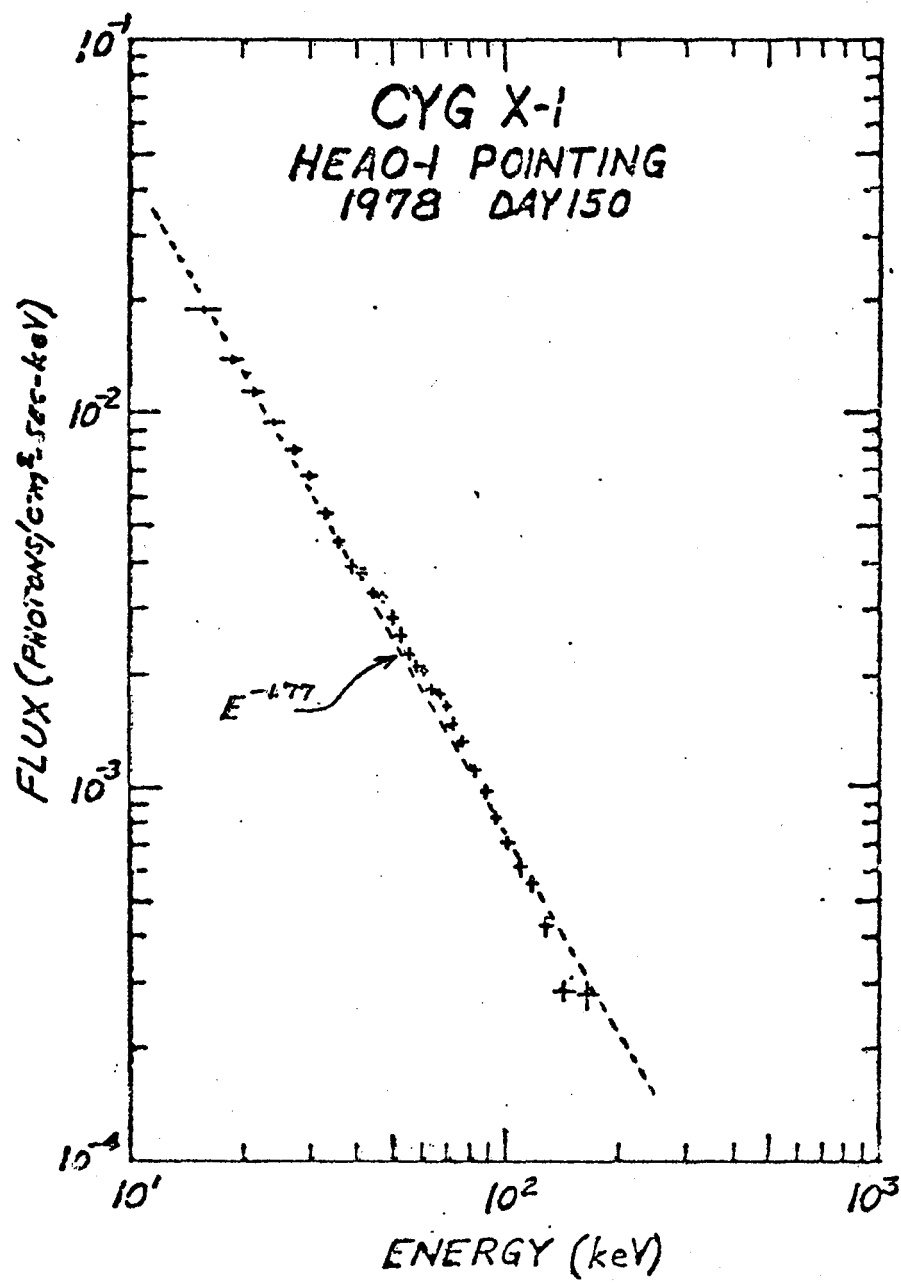


Figure 10

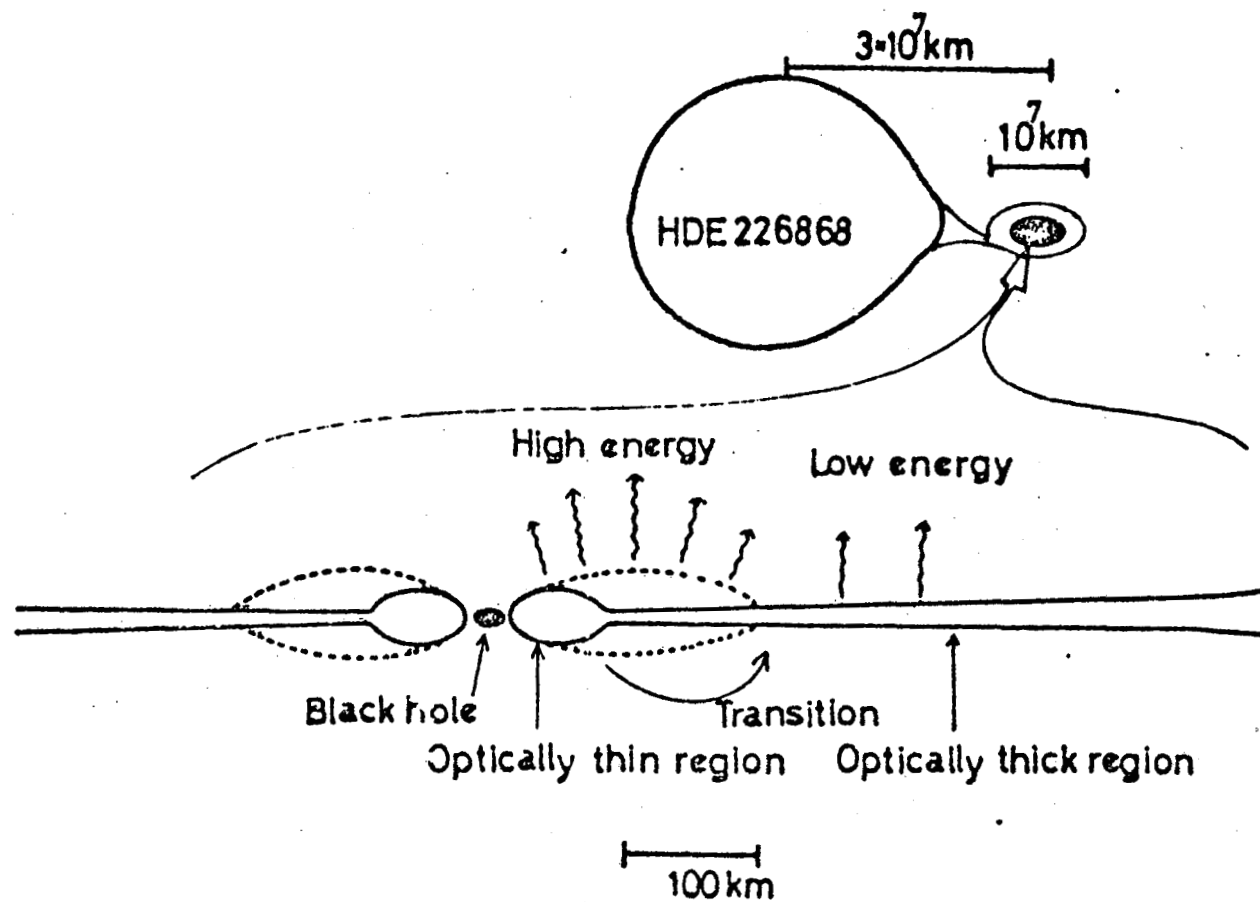


Figure 11

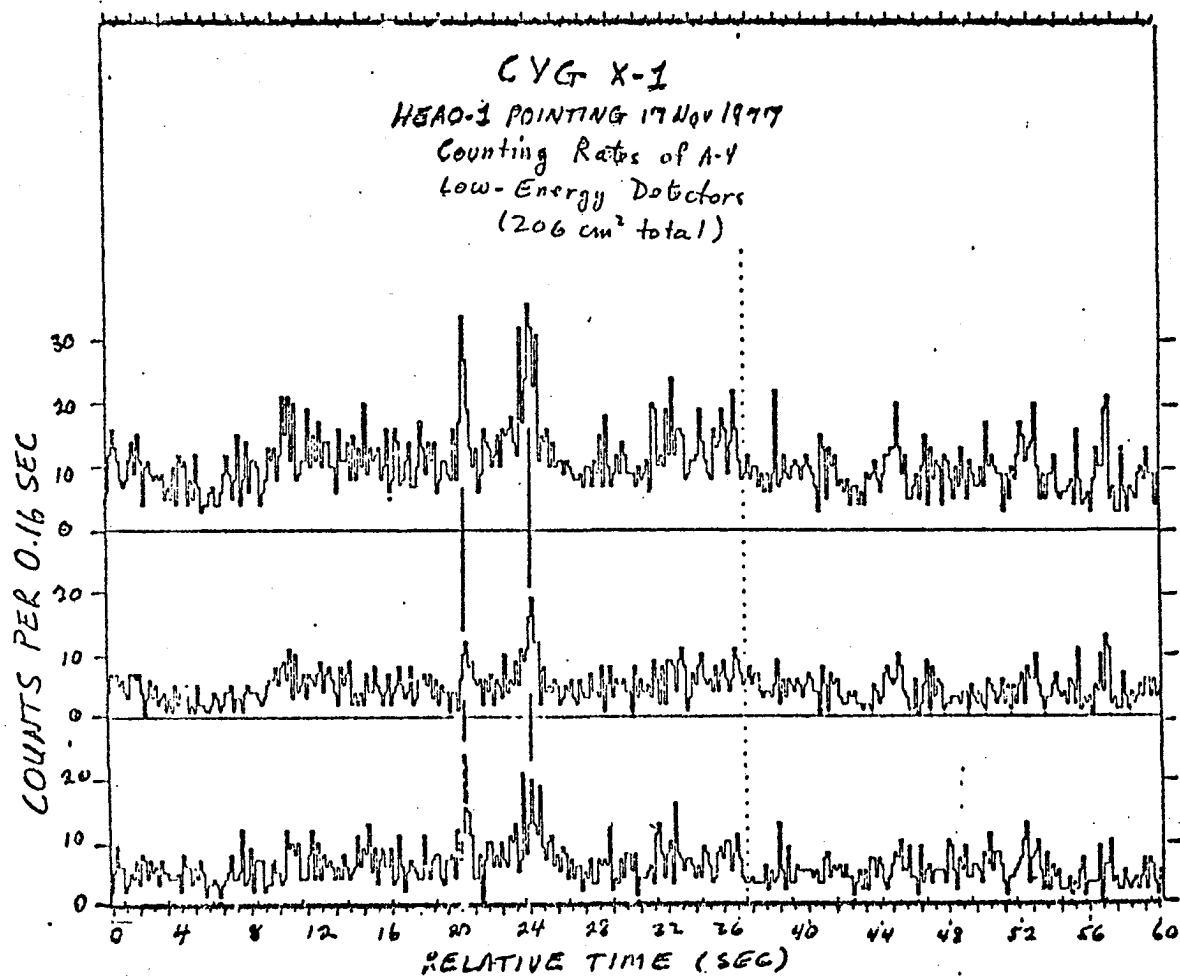
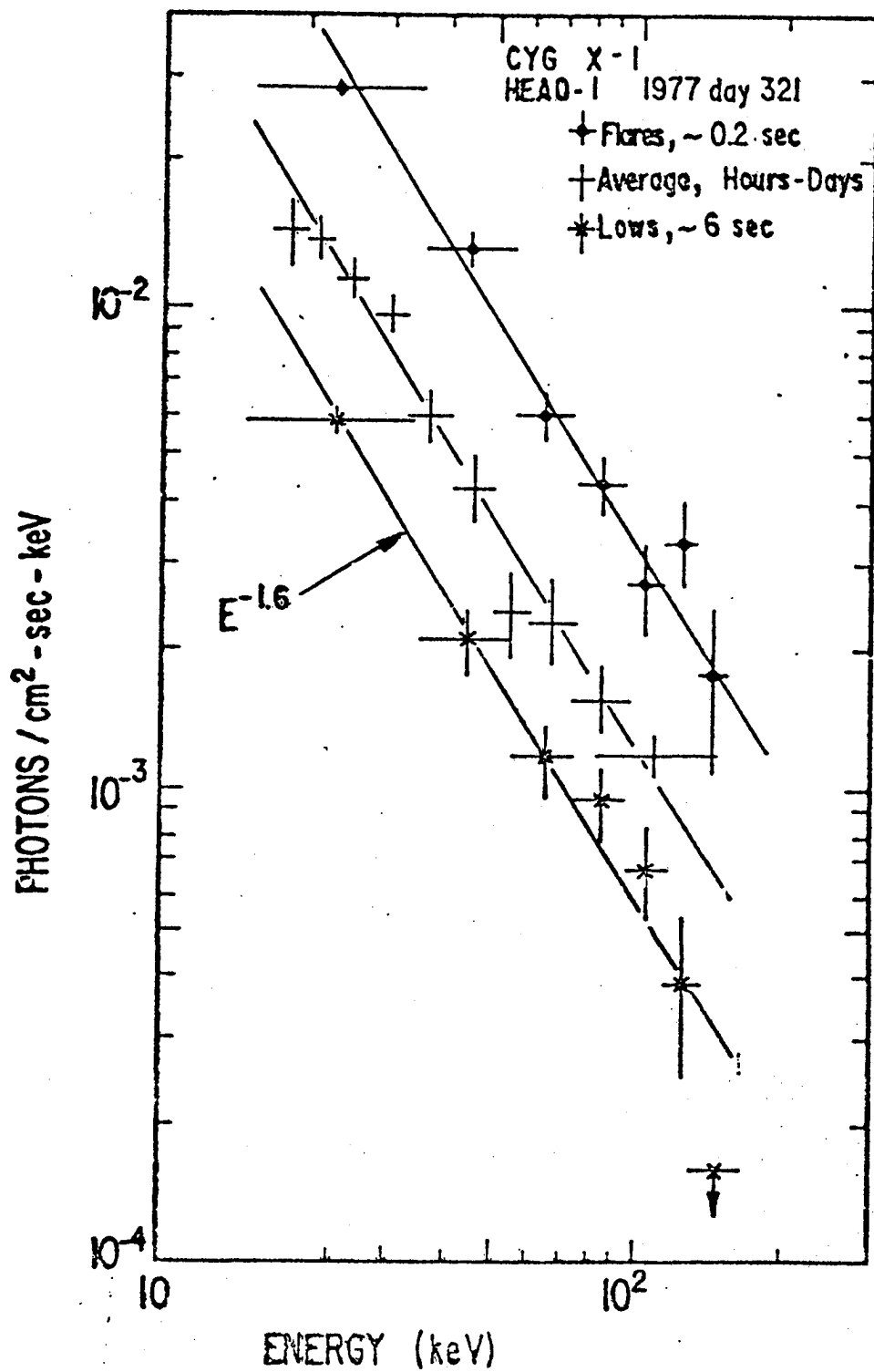


Figure 12



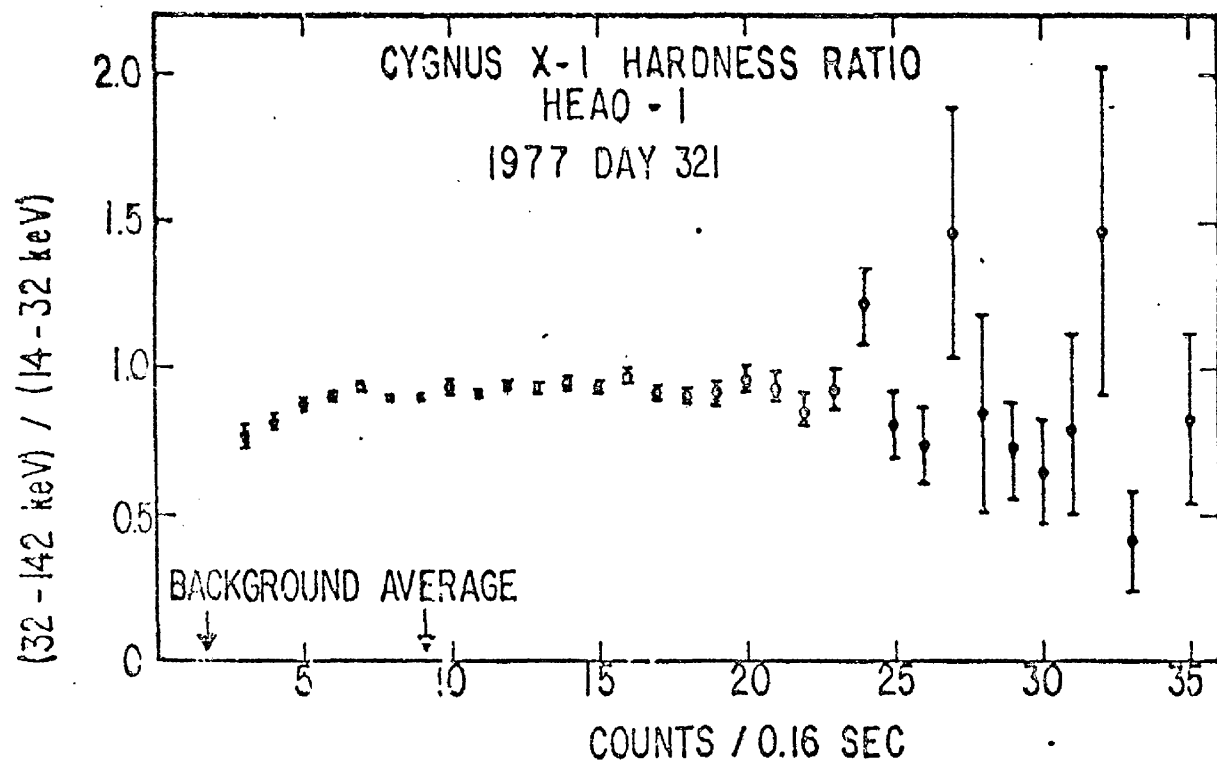
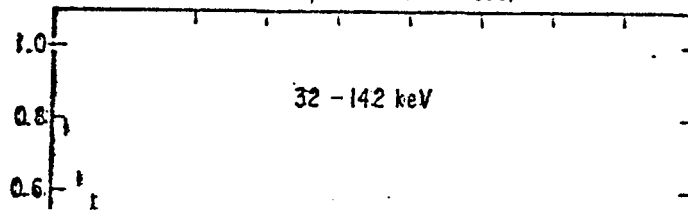
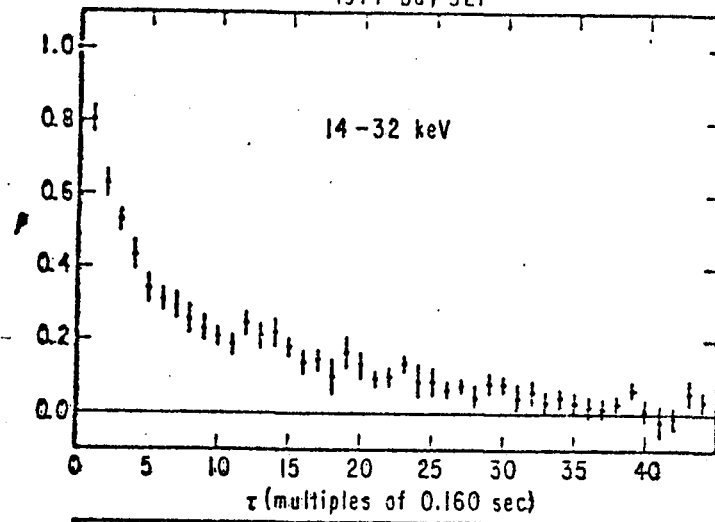


Figure 14

CYGNUS X-1  
AUTOCORRELATION FUNCTION  
1977 Day 321



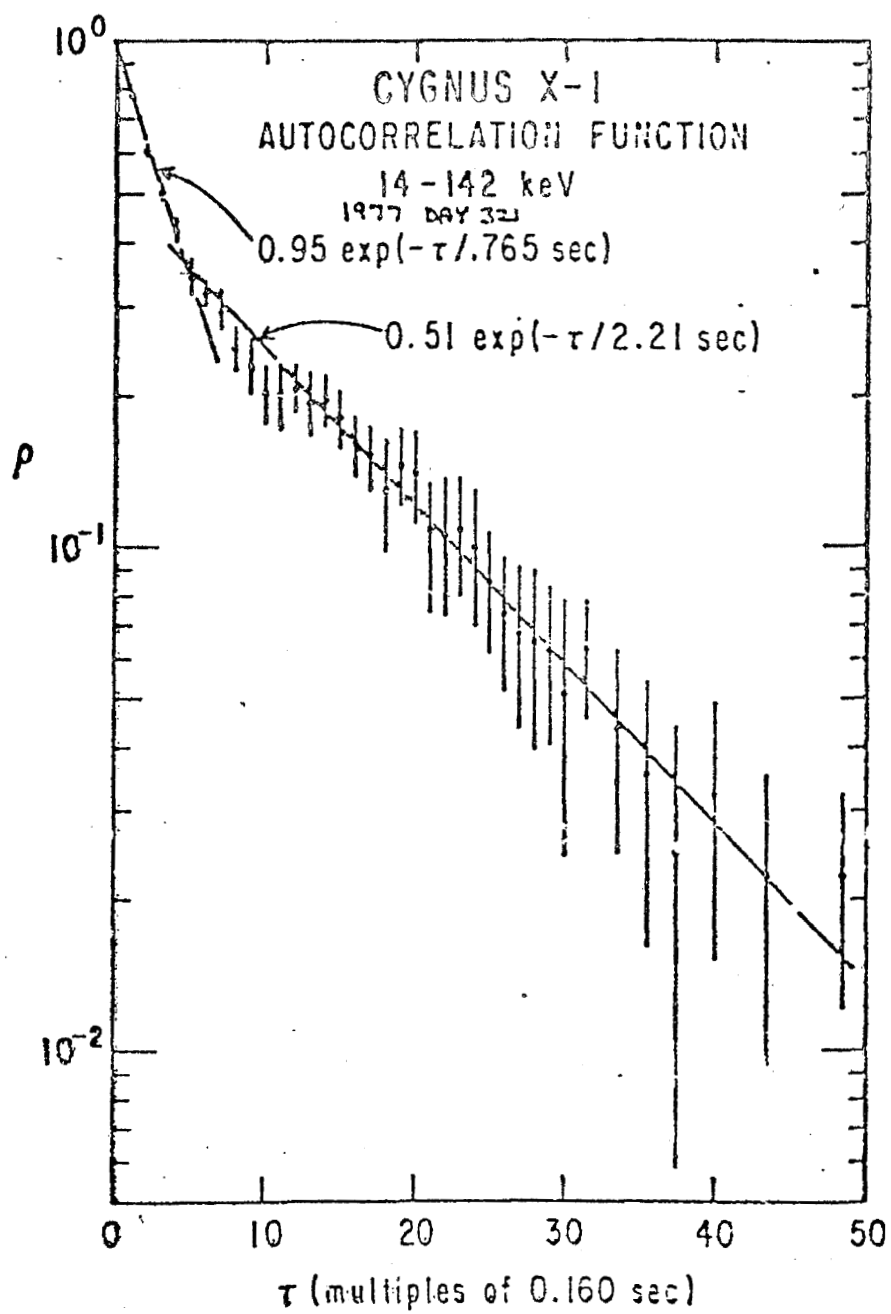


Figure 16

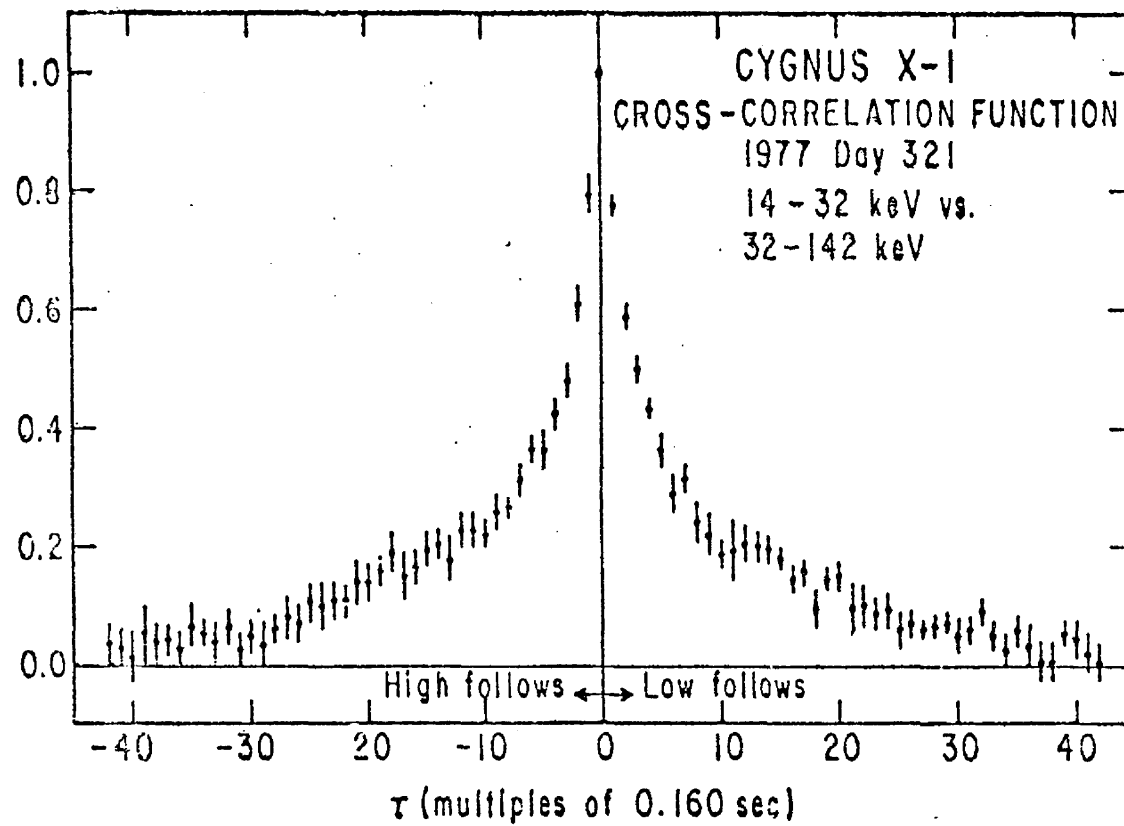


Figure 17



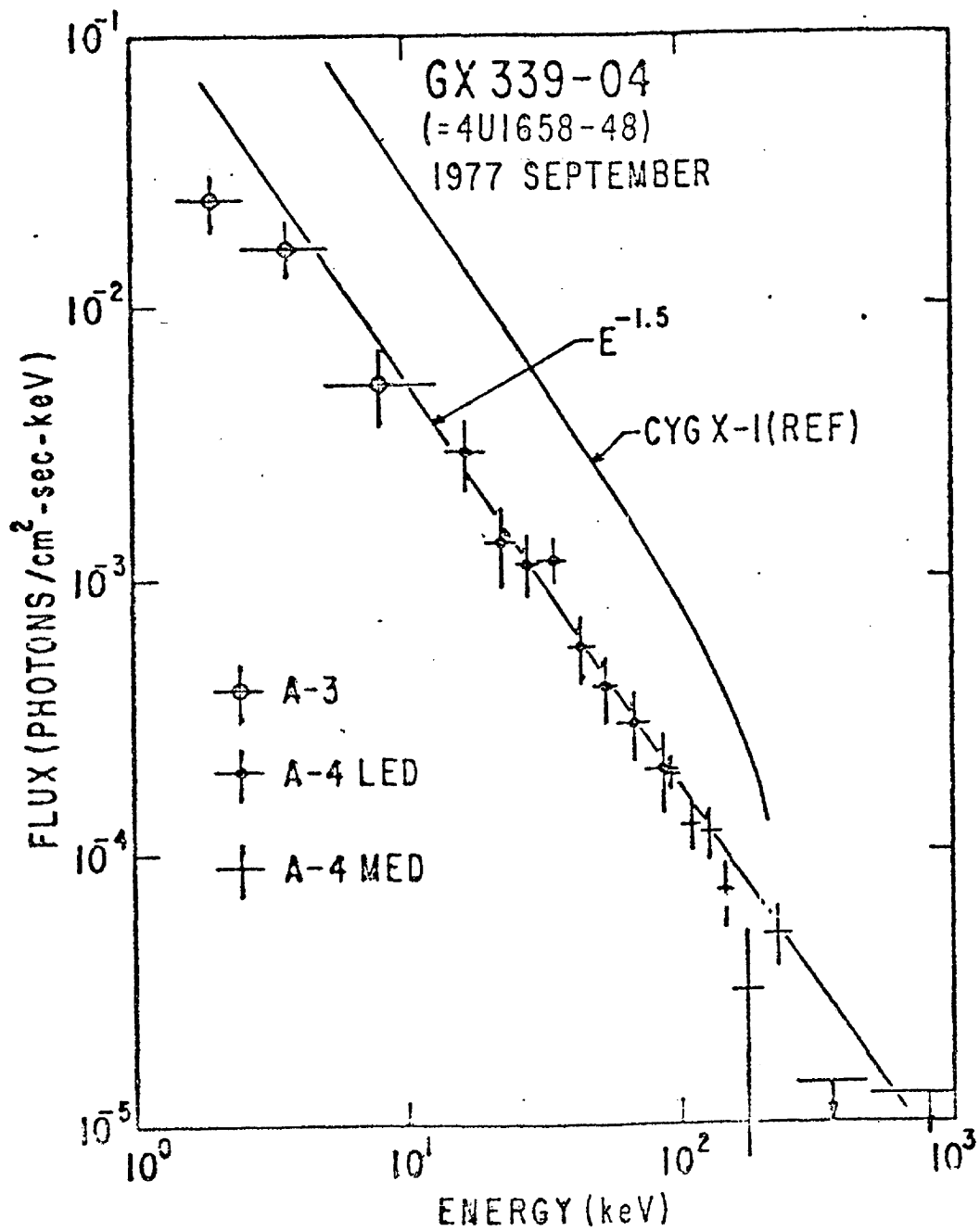


Figure 18

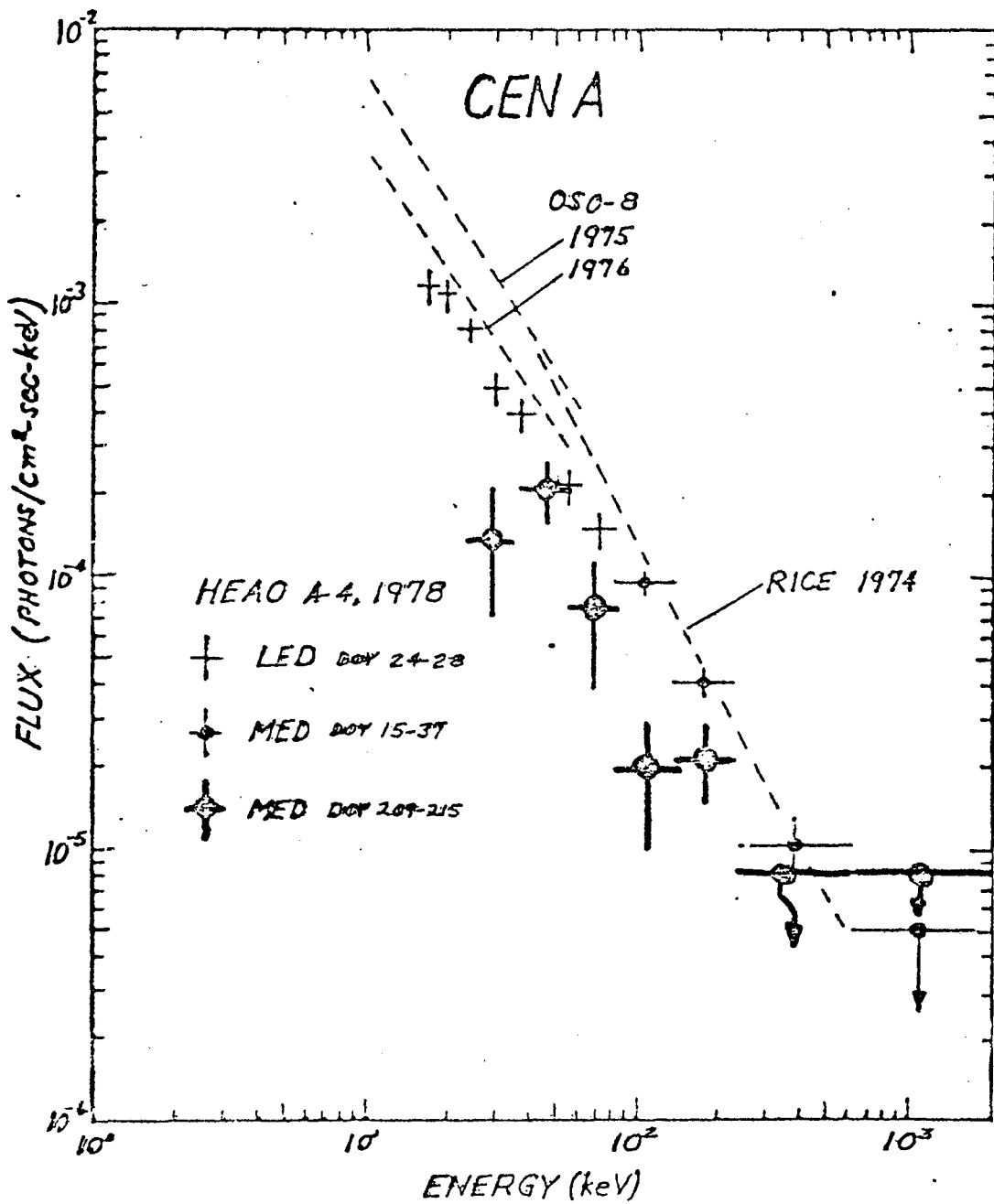


Figure 19

3C273

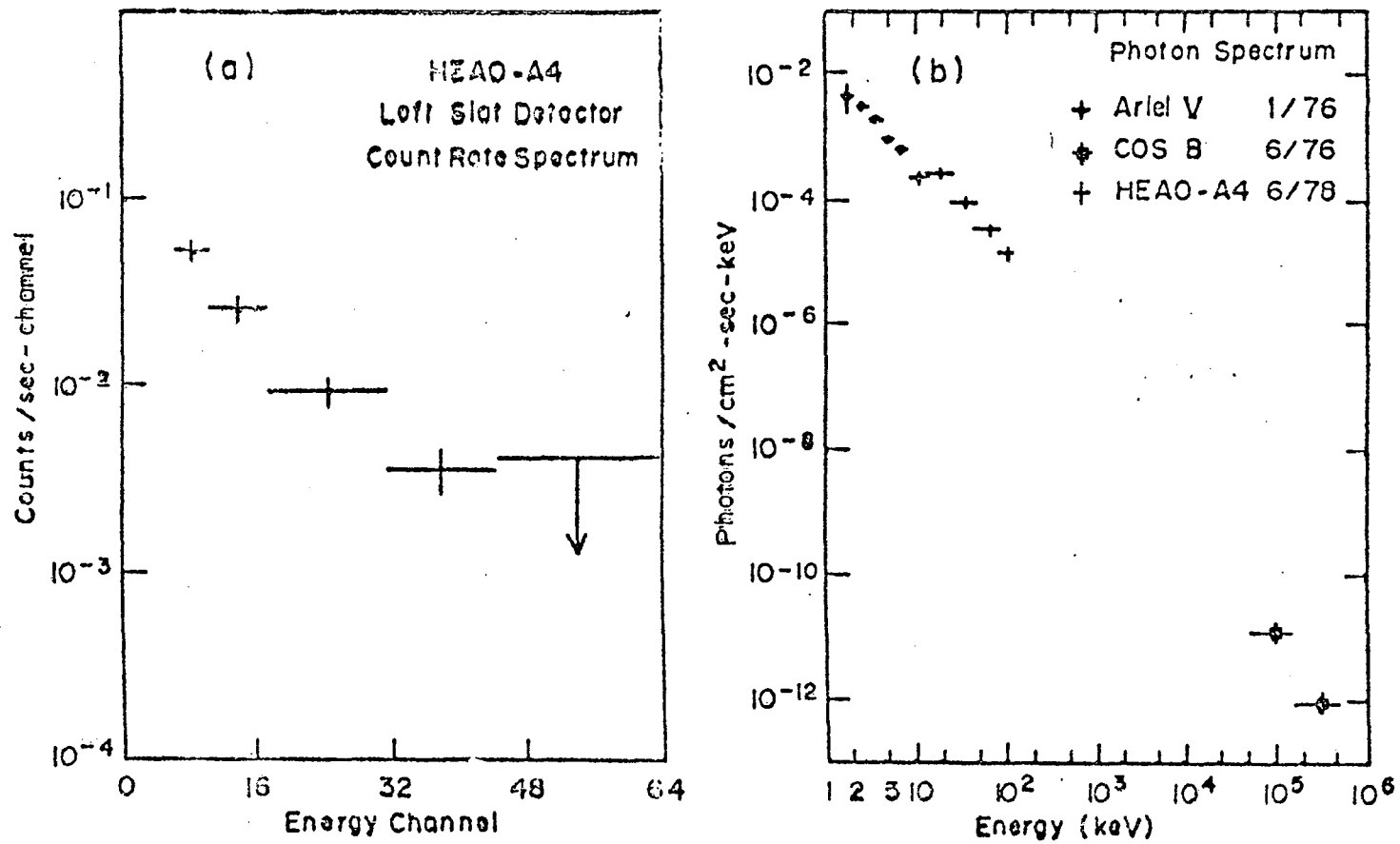
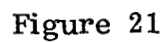


Figure 20



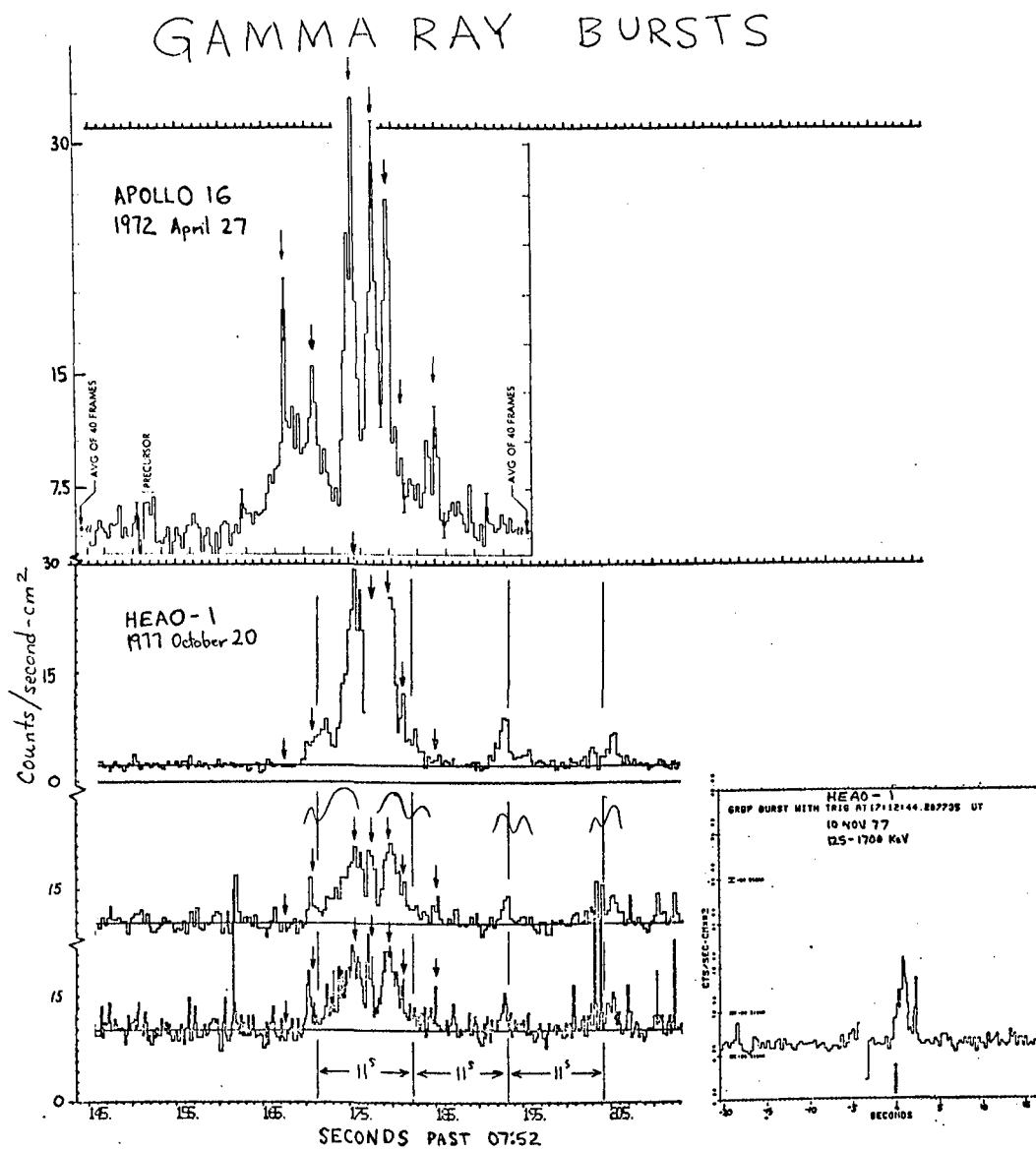


Figure 22

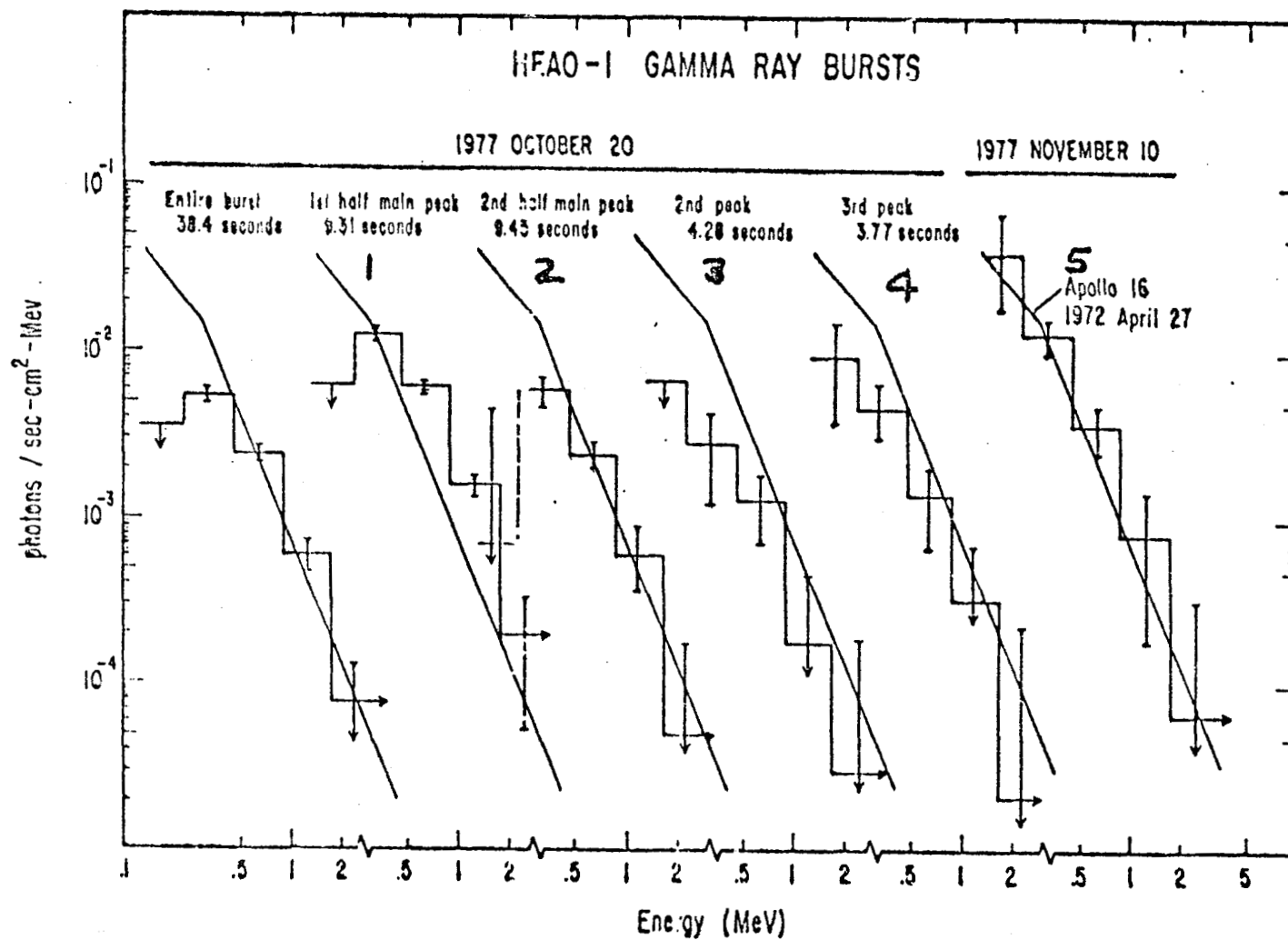


Figure 23

## SESSION II

### RESULTS FROM HEAO-1 GUEST OBSERVER PROGRAM

## HEAO-1 GUEST INVESTIGATOR PROGRAM

G. Fishman  
Marshall Space Flight Center

Before I introduce this session's speakers, I want to describe the general nature of the HEAO Guest Investigator Program and its objectives.

As shown in Figure 1, there are several objectives to the HEAO Guest Investigator program. First, it opens the HEAO results to a broad base of scientific involvement, and includes in the data analysis, not only the investigators directly involved in building the experiment, but many other investigators, as well. It is also a great aid to the HEAO principle investigators and coinvestigators. As you have seen, there is an enormous amount of data that has come down from HEAO-1. The investigators find it very helpful to have additional scientific involvement in their investigations to help to look at highly specialized studies that the PI's themselves would not have the time or the resources to go into in any detail. The Guest Investigator Program allows correlative data to be used with HEAO data. This includes ground-based data from optical, infrared and radio telescopes. Data from other spacecraft that have looked at the same objects perhaps at an earlier epoch can be correlated with the HEAO-1 results. Finally, it allows theoretical insight into new theories and models of these various X-ray sources to be tested by looking at a particular set of HEAO data.

There are three categories of participation of the HEAO investigator program (as depicted in Figure 2). The first one is cooperative research in which the guest investigator works directly with the HEAO investigators. Together, they analyze a mutually agreed upon set of data in their investigation. There are the correlative studies which involve independent observations in other spectral regions such as from ground-based optical observations. These independent observations are post-facto combined with HEAO X-ray and gamma-ray observations. Then, finally, there is a category of guest observations where the guest investigator proposes a particular object or a set of objects that would have not otherwise been looked at by HEAO. That guest investigator then receives data from that investigation to analyze and publish. The proposals for the investigator program are sent to NASA Headquarters, they are reviewed by an ad hoc committee under the chairmanship of the HEAO program scientist, Dr. Albert Opp. The project scientist and other PI's are also involved in the guest investigator selection process. As you have heard, the HEAO-1 spacecraft was primarily a survey mission and spent the majority of its time in a scanning mode with only a limited pointing capability. As such, it does not lend itself well to guest observations. In spite of this limitation, the HEAO-1 guest investigator program has been very successful and productive as you



will hear in these talks. I have listed in Figure 3 the participation in the HEAO-1 investigator program. Notice that it is somewhat incomplete. The institutions of two of our speakers are not listed: the University of Illinois and SAO. If anyone is interested, I will be glad to furnish the names of the guest investigators from these institutions and the names of their investigations. This session concerns itself primarily with the HEAO-1 guest investigator program but I would like to mention the HEAO-2 guest investigator program just now getting underway. It is meeting with overwhelming interest even though it is just in the beginning stages, literally hundreds of proposals have been received and many have already been selected. On Figure 4, I have listed the institutions of some of the HEAO-2 guest investigators who have already been selected. Most of them are from Universities. Under the category of "other," you see AAVSO which is American Association of Variable Star Observers. This is an amateur astronomy organization which is quite helpful in monitoring cataclysmic variables and other variable stars. As you can see, there is also a tremendous amount of foreign interest in utilizing the data from HEAO-2: France, Italy, India, Sweden, Canada, Germany, the Netherlands, and Japan. We expect many exciting results to come of the HEAO-2 guest investigator program. With that, I will introduce the first speaker, Dr. Richard Lamb from Iowa State University.

## OBJECTIVES

- BROADER BASE SCIENTIFIC INVOLVEMENT IN HEAO
- AID TO HEAO INVESTIGATORS
- CORRELATIVE DATA FOR HEAO
  - GROUND-BASED
  - OTHER SPACECRAFT
  - THEORETICAL INSIGHT

Figure 1. HEAO Guest Investigator program.

## CATEGORIES OF PARTICIPATION

- I. COOPERATIVE RESEARCH - WORK DIRECTLY WITH  
HEAO INVESTIGATORS IN ANALYZING DATA
- II. CORRELATIVE STUDIES - INDEPENDENT OBSERVATIONS,  
COMBINE WITH HEAO OBSERVATIONS
- III. GUEST OBSERVATION - PROPOSE AND ANALYZE DATA  
FROM A PARTICULAR OBJECT

Figure 2. HEAO Guest Investigator program.

## PARTICIPATION

### o UNITED STATES

#### UNIVERSITIES

INDIANA UNIV.

UNIV. COLORADO

UNIV. ARIZONA

COLUMBIA UNIV.

NORTHWESTERN UNIV.

UNIV. PENNSYLVANIA

UNIV. CALIF. - BERKELEY

UNIV. MARYLAND

UNIV. CALIF. - L.A.

UNIV. WASHINGTON

STANFORD UNIV.

MIDDLEBURY COLLEGE

IOWA STATE UNIV.

#### OTHER

AEROSPACE CORP.

JPL

MSFC

KITT PEAK NATIONAL OBSERV.

### o FOREIGN

U. K. - CAMBRIDGE UNIVERSITY

ISRAEL - TEL AVIV UNIVERSITY

FRANCE - CESR - TOULOUSE

Figure 3. HEAO Guest Investigator program.

o UNITED STATES

UNIVERSITIES

UNIV. VIRGINIA  
BRANDEIS UNIV.  
UNIV. ROCHESTER  
NEW MEXICO TECH.  
CAL TECH.  
UNIV. WISCONSIN  
UNIV. COLORADO  
UNIV. OKLAHOMA  
UNIV. WASHINGTON  
IOWA STATE UNIV.  
UNIV. CALIF. - BERKELEY  
UNIV. ILLINOIS  
UNIV. TEXAS

UNIV. PENNSYLVANIA  
MIDDLEBURY COLLEGE  
PRINCETON UNIV.  
UNIV. MARYLAND  
NORTHWESTERN UNIV.  
UNIV. ARIZONA  
UNIV. CALIF. - L. A.  
VIRGINIA POLYTEC. INST.  
VANDERBILT UNIV.  
VIRGINIA STATE UNIV.  
UNIV. CALIF. - SAN DIEGO  
RUTGERS UNIV.  
UNIV. MICHIGAN

OTHER

LOCKHEED CORP.  
LICK OBSERVATORY  
JPL  
AAVSO

AMERICAN SCI. & ENGR. CORP.  
JOINT INST. LAB. ASTRO.  
GSFC

o FOREIGN

FRANCE: C.E.N./SACLAY; C.E.S.R./TOULOUSE

ITALY: CNR; UNIV. PADOVA

INDIA: TATA INSTITUTE

SWEDEN: UNIV. STOCKHOLM

CANADA: UNIV. TORONTO; QUEENS UNIV; DOMINION RADIO  
OBSERV.

GERMANY: MAX PLANCK INST.

THE NETHERLANDS: LIEDEN OBSERV.

JAPAN: TOKYO UNIV.

Figure 4. HEAO-2 Guest Investigator Program - Preliminary.

## X-RAY EMISSION FROM THE REGION OF $\gamma$ 195+5

R. C. Lamb  
Iowa State University

The number of discrete celestial gamma-ray sources now stands at nearly 30, two-thirds of which are not firmly identified at other wavelengths. Figure 1 gives a breakdown of these sources. There are seven sources identified with our own galaxy — six of which are radio pulsars and Cygnus X-3, which seem to be the most luminous gamma-ray source in our galaxy by almost two orders of magnitude. There are three extragalactic sources — a quasar, a Seyfert galaxy, and a radio galaxy — all quite bright at other wavelengths and relatively close to us. Therefore as the sensitivity of new gamma-ray detectors increases, this number will surely grow dramatically as a larger volume of space is sampled.

My talk will concentrate on one of these 19 unidentified sources and our efforts to observe X-rays from it. My collaborator in this work was Diana Worrall of Goddard. I am indebted to the much larger group of people connected with the entire A-2 effort.

Our results are that we have seen some indication of X-rays from the gamma-ray source region. If that is real and if these X-rays are indeed physically associated with the gamma-ray source, then we now have a source error box about seven times smaller than it was.

Figure 2 shows the galactic plane, our milky way, in gamma-rays whose energies are greater than 70 MeV. Many of the unidentified sources are located along this plane and therefore are presumably galactic. The positions of these sources are located by arrows along this one-dimensional view below. The Cygnus region is a galactic longitude of 80 degrees. In the galactic anticenter region are the Crab pulsar and the source 195 + 5. This latter source is the one whose X-rays we are looking for. This source was first seen by the SAS-2 gamma-ray satellite. This beautiful map is from a preprint by the European Caravane Collaboration based on results from their COS-B satellite.

Figure 3 shows a close-up of 195 + 5 in the anticenter region. The SAS-2 and COS-B error boxes are shown. The other coordinate system shown here is appropriate to the satellite during late september and early October of 1977. As you know, in the scanning mode, the

HEAO-1 detectors sweep through a great circle, perpendicular to the Earth-Sun line every 30 min. For a source near the ecliptic, located at 180 degrees scan angle, the field of view moves over about 1 degree/day, moving eastward. The  $1\frac{1}{2} \times 3$  degree field of view of the X-ray detectors is also represented in Figure 3. Our plan was to locate any new source within a strip of 10 degrees in scan angle, roughly 180 to 190 degrees, and within 5 degrees in day angle, roughly day 272 to 277 centered on the gamma-ray source region. We do claim one new source within the 50 square degrees covered by this search and it is located at  $l = 195$  degrees,  $b = 5$  degrees. What is the evidence?

Figure 4 shows the accumulation of 2 days data for days 270 to 272, well away from the gamma-ray region.

Figure 5 shows two well known sources, 4U061+09 at a scan angle of 193 degrees and IC443 very near the ecliptic. As we move later in time 4U061+09 decreases considerably and we get the scan data for a 3 day interval which is centered on the gamma-ray region. Please note there has been a considerable scale change. Actually IC443 is getting weaker; you can see the probable vestiges of 4U061 in this region, but there is also another small enhancement in this region. What is its significance?

The procedure is to fit the data in this region with only IC443 and determine a  $\chi^2$ . Then allow an additional source, free to wander anywhere in scan angle and determine a new  $\chi^2$ . The position shown maximizes the  $\chi^2$  change. In this particular case the change in  $\chi^2$  is nine units, equivalent approximately to a  $2.7\sigma$  result. We have data on this region of the sky 6 months later and there is an enhancement at this identical scan angle, and therefore we believe the case is strong enough to think there may be a new source in this region, in that we see the source on two different occasions. The statistics are summarized in Figure 6. The overall probability that the effect is only a statistical fluctuation is  $2 \times 10^{-3}$ , about equivalent to a  $3.1\sigma$  result.

Figure 7 shows the intensity of the source as a function of the observing day for the 1977 data. The points are the observed intensity. The staircase is the collimator response fitted to the points. The fit is certainly acceptable. There is no gross evidence for either strong variability or for a source which is extended in this angular dimension.

The error box determined from the 2 observations is shown in Figure 8. Its area is 1.4 square degrees approximately seven times smaller than the size of the gamma-ray error region. The significance of the COS-B error box has not been stated; however, I think it is reasonable to assume that its significance is comparable to the SAS-2 result. Therefore we claim the position of the X-ray source is consistent with both gamma-ray error boxes.

Figure 9 gives the parameters relating to the source's intensity and spectrum. The energy flux from 2-6 Kev is  $1.5 \times 10^{-11}$  ergs  $\text{cm}^{-2}\text{s}^{-1}$  or approximately 0.9 Uhuru counts/sec. You can calculate the probability of seeing by chance, an unrelated X-ray source, of this intensity or stronger anywhere within the immediate 10-square degree vicinity of the gamma-ray error boxes, based on what is already known about the density of X-ray sources of a given strength. That chance probability is calculated to be 9 percent. This number is small enough to indicate that the X-ray source may well be associated with the gamma-ray source.

The spectrum of the source was determined from data when the detectors were pointed at the source for 6 hr. The spectrum is fit equally well by either a power law or by simple thermal bremsstrahlung with the parameters shown in the slide.

Figure 10 shows a comparison of the X-ray source spectrum with the gamma-ray spectrum. To make this comparison I have taken the SAS-2 integral flux value and assumed a power law exponent for the number spectrum of -1.5. If one makes the assumption that the X-ray source and the gamma-ray source are indeed related, then the following observations are relevant. The best fit power law of the X-ray source falls below the gamma-ray by about four orders of magnitude; that is, there does not seem to be a simple extrapolation to the gamma-ray point. Also the level of hard X-ray emission and low energy gamma-rays suggested by this slide are not very encouraging to experimenters seeking to fill in the gap. For example at 100 keV the energy flux density of  $10^{-4}$  keV/ $\text{cm}^2\text{-sec-keV}$  is less 1/100 of the total emission from the Crab at the same energy. On the plus side we believe that this detection may represent an important first step in identifying  $\gamma 195+5$ .

Certainly, the smaller error box will guide future identification efforts with the Einstein Observatory and at other wavelengths. The region will be studied with the Einstein Observatory in August or September of this year.

#### DISCRETE $\gamma$ RAY SOURCES

	TYPE	NUMBER
1.	GALACTIC	
	PULSARS	6
	CYGNUS X-3	1
2.	EXTRAGALACTIC	3
3.	UNIDENTIFIED	<u>19</u>
	TOTAL	29

Figure 1

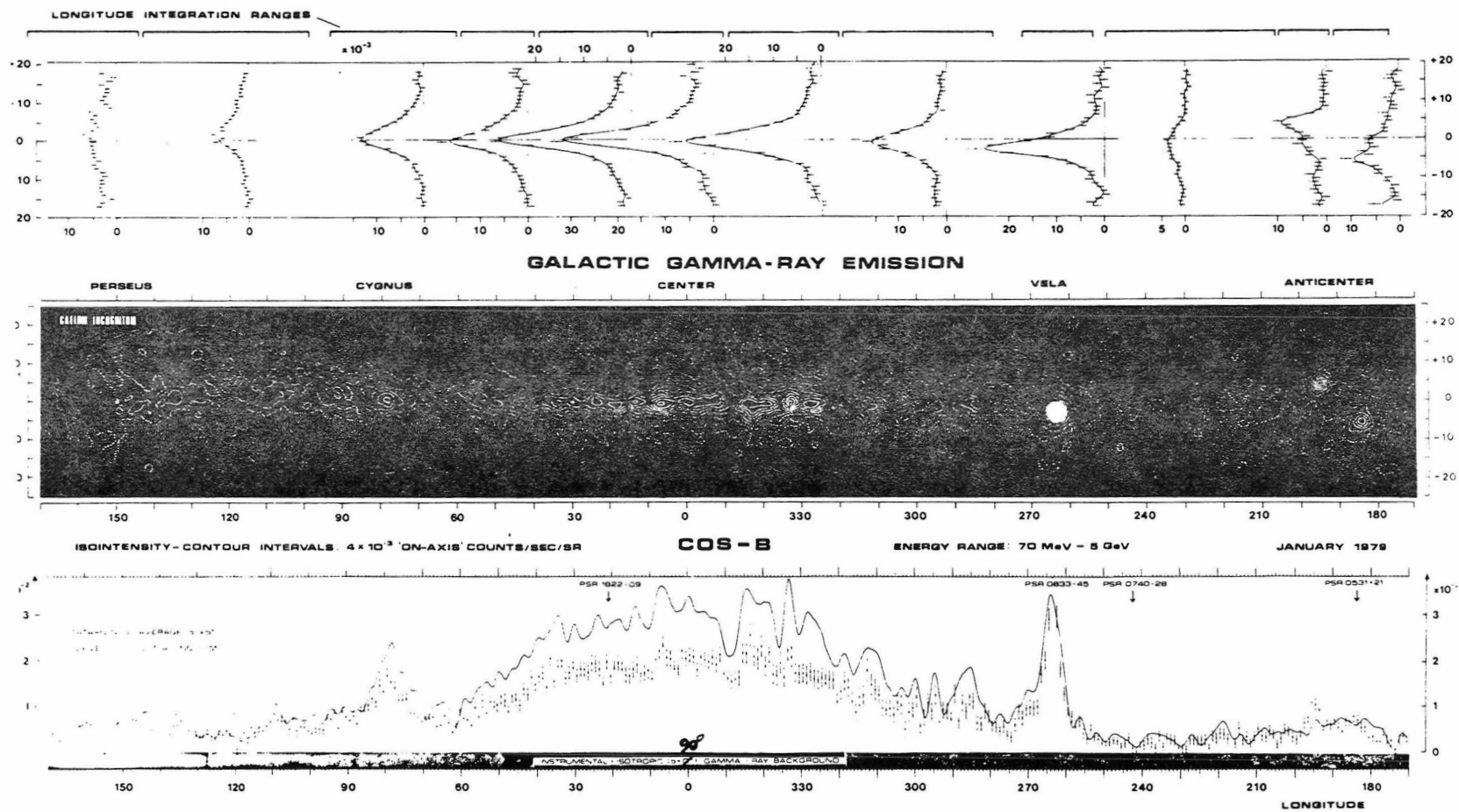


Figure 2



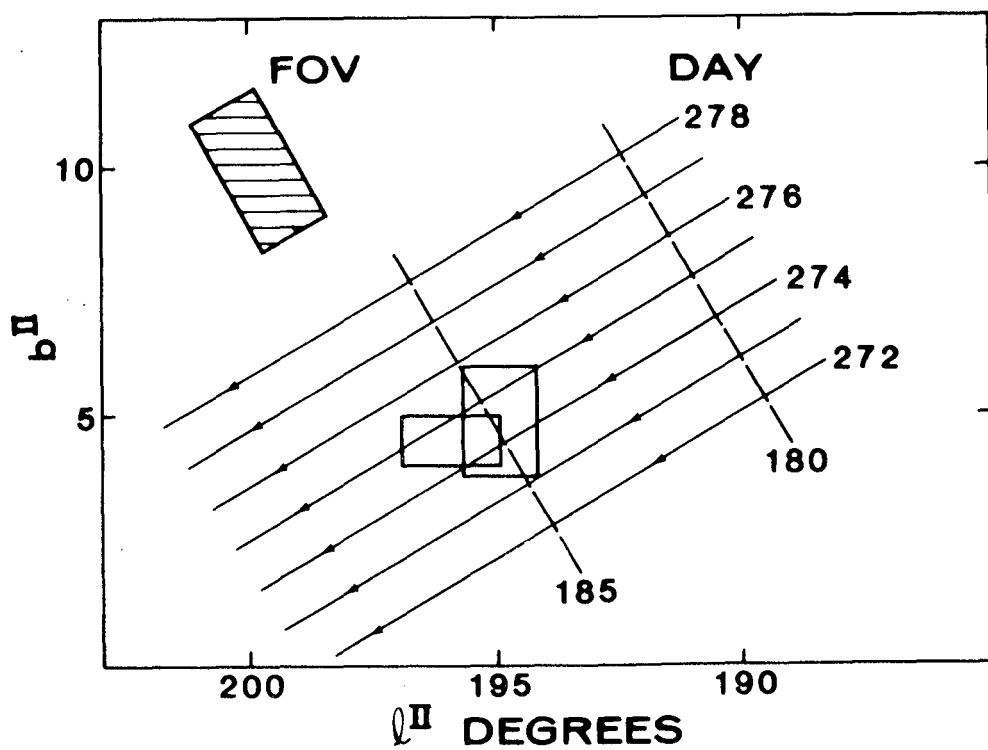


Figure 3

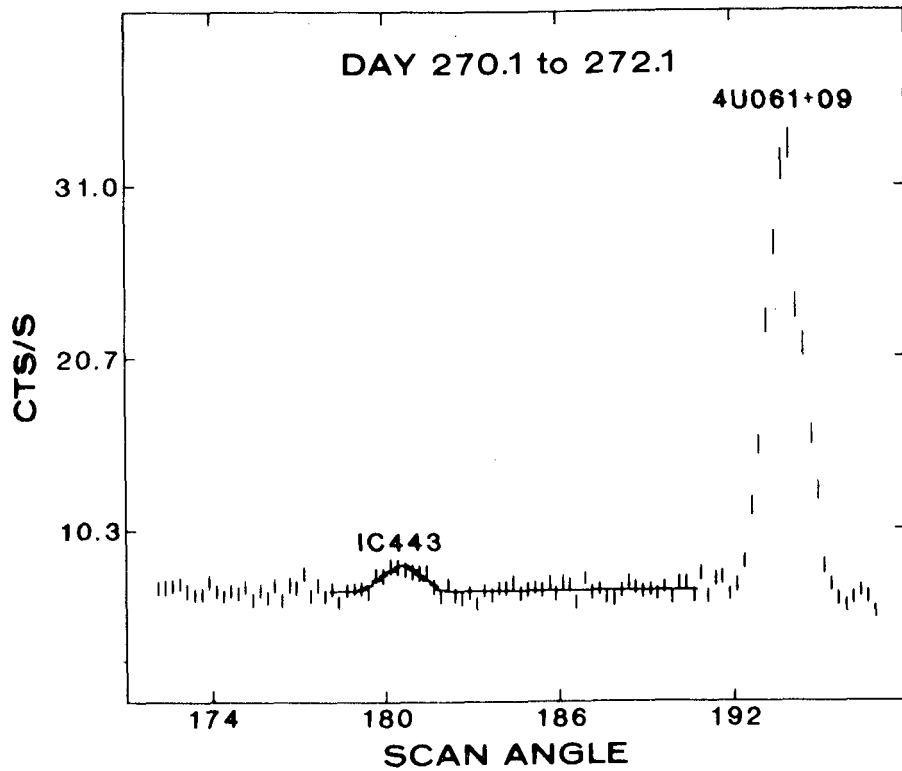


Figure 4

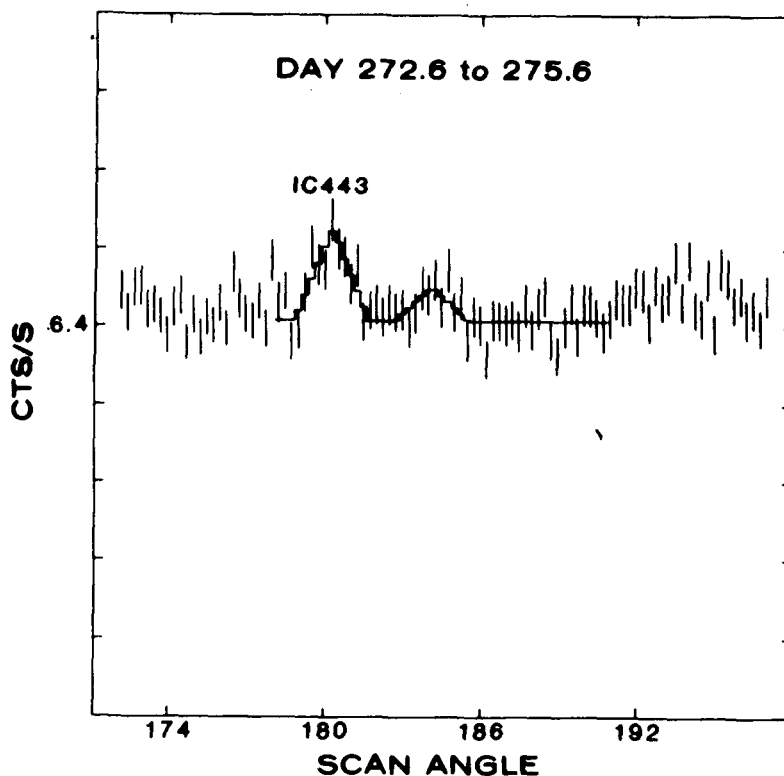


Figure 5

#### STATISTICAL SIGNIFICANCE

DATA SET	$\Delta x^2$	PROBABILITY THAT THE EFFECT IS A FLUCTUATION
OCTOBER 1977	8.9	$0.8 \times 10^{-2}$
MARCH 1978	5.0	$5 \times 10^{-2}$

THE POSITIONS OF THE TWO SOURCE DETERMINATIONS ARE IN GOOD AGREEMENT:

$$\Delta(\text{SCAN ANGLE}) = 0^{\circ}02 \pm 0.38$$

$$\Delta(\text{DAY ANGLE}) = 0^{\circ}65 \pm 0.61$$

THE COMBINED PROBABILITY THAT THE EFFECT IS A FLUCTUATION IS:  $(0.8 \times 10^{-2})(5 \times 10^{-2}) = 4 \times 10^{-4}$ .

THE NUMBER OF RESOLVABLE POSITIONS IN THE IMMEDIATE VICINITY OF THE  $\gamma$ -RAY ERROR BOXES IS  $\approx 5$ . THEREFORE, THE OVERALL SIGNIFICANCE IS:

$$5 \times 4 \times 10^{-4} = 2 \times 10^{-3} \quad (3.1\sigma)$$

Figure 6

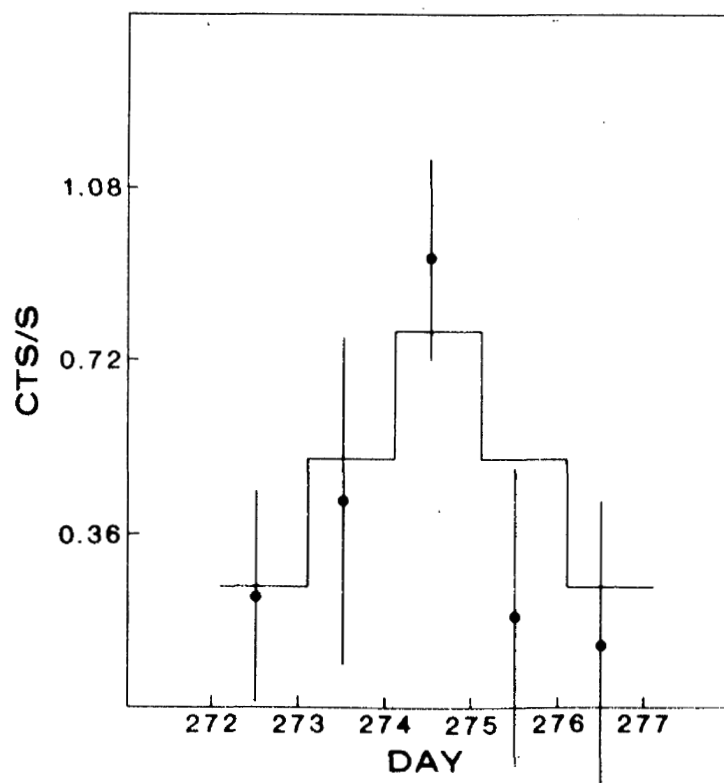


Figure 7

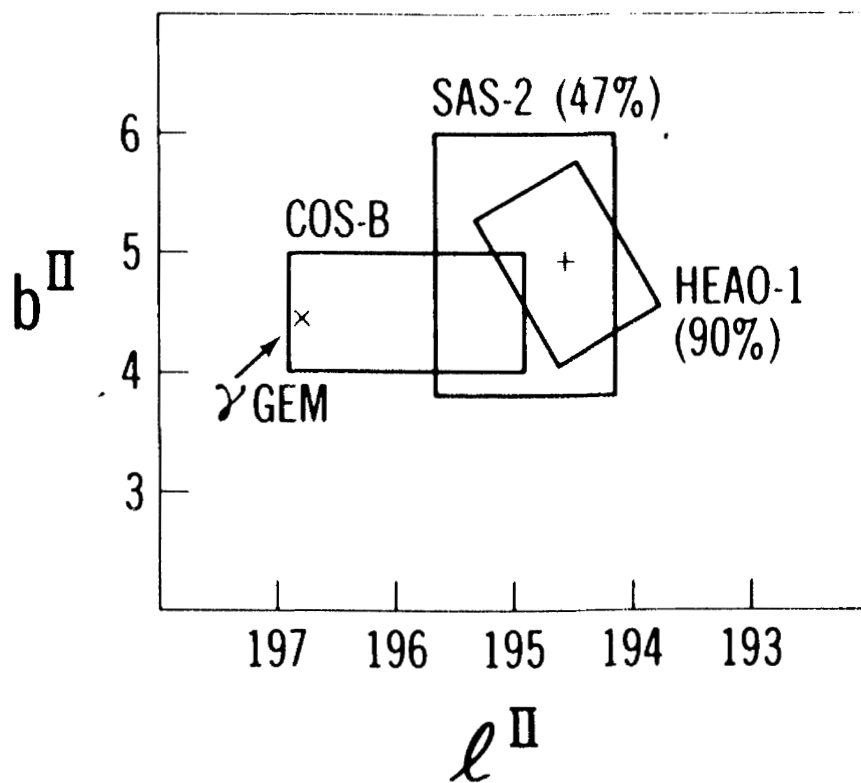


Figure 8

# SOURCE INTENSITY (2-10 KeV)

PHOTON FLUX  
( $\text{CM}^{-2} \text{S}^{-1}$ )

$$(3.2 \pm 1.0) \times 10^{-3}$$

ENERGY FLUX  
( $\text{ERGS CM}^{-2} \text{S}^{-1}$ )

$$(2.1 \pm 0.7) \times 10^{-11}$$

## SPECTRUM

### POWER LAW

$$\text{DN/DE} \propto E^{-\alpha}: \alpha = 2.6^{+0.7}_{-0.6}$$

$$\text{ABSORPTION} < 7 \times 10^{22} \text{ (H ATOMS CM}^{-2}\text{)}$$

### THERMAL BREMSSTRAHLUNG

$$kT = 6 \pm 3 \text{ KEV}$$

$$\text{ABSORPTION} < 4 \times 10^{22} \text{ (H ATOMS CM}^{-2}\text{)}$$

Figure 9

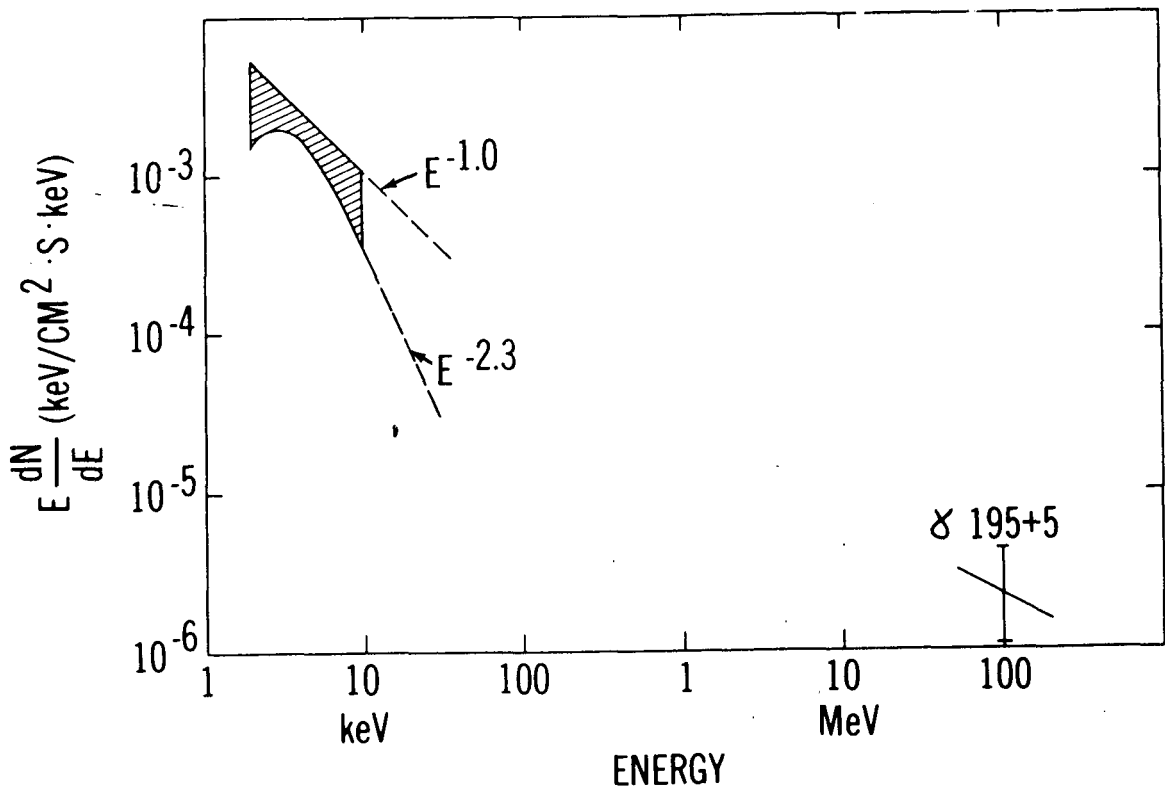


Figure 10

## DIFFUSE X-RAY EMISSION FROM ABELL CLUSTERS

Dr. Melvin Ulmer  
Northwestern University

Thank you. I must say it is my first visit to Huntsville after nearly 13 years of X-ray astronomy. I may have set a record for not coming here and I really appreciate the opportunity to take part in the guest observer program. It has given me an opportunity to continue in X-ray astronomy without having my own multimillion dollar satellite program. What I am going to talk about today are basically the Abell clusters of galaxies: Abell 401 and Abell 399. I will then talk about the follow-up work that can be related to the study of these objects.

Figure 1 is the map of the Abell 401, Abell 399 region. We actually had two sets of observations: one was the lunar occultation pointed observation in which we had two orbits in which to look at this region while the moon scanned over it and the other was a scanning observation through the area. The disc shows the size of the moon, the sloping line shows the apparent path of the moon in front of the region for the second set of data and the horizontal line shows the path of the moon for the first orbit. For reference this (dot,  $\alpha \sim 44.0$ ,  $\delta \sim 13.4$ ) is the optical center determined by Neta Bahcall. This (open dot,  $\alpha \sim 44.0$ ,  $\delta \sim 13.47$ ) is the cD galaxy which Abell had originally assigned as the optical center and this position down here is the optical center of Abell 399 as determined by the cD galaxy which is there also.

Figure 2 shows the data from the satellite. The background has been subtracted and the aspect corrected by determining the position which also minimizes  $\chi^2$ . The solid lines show the best fit to a single diffuse model for the X-ray emission, the upper curve shows the apparent distance of the moon from the center of the emission region, so you can see in the first path (a), the moon was actually moving away from the center of the emission region, and in the next portion (b) it was coming down to the center of the emission region and then starting to move away.

We actually had more data but these were the data that we felt had the least contamination, the least problems with variation of the background. We varied the length of the data we selected and put in all kinds of fancy models for the background, and showed that the X-ray emission was insensitive to any kind of arbitrary variation so I am fairly confident of these results. In the lower portion of the figure (c), we show the scanning data. You can see indeed there is a signal. This is the center of the emission region which does come out in between Abell 401 and Abell 399.

Refer again to Figure 1. Here is the position that we determine from the lunar occultation data (solid ellipse), this position (lower left rectangle) is determined from the scanning data, 4U error box here and the Ariel 5 error box. Taking both of these, I do not know how democratic you want to be but anyway by taking a weighted vote if you will, I like to think the center of the emission region is somewhere in here ( $\alpha = 43.95$ ,  $\delta = 13.15$ ). Notice it seems to be fairly well centered in between Abell 401 and Abell 399. Now as far as the models go for the emission, there are 2 basic kinds of models that work; one is a large diffuse emission region that covers both of these (one uniform disc), and the other is a double source model, a diffuse model in which one diffuse component is here and maybe another down here is equally as good as a diffuse model plus a point source somewhere else in the field. However, a 2 point source model does not fit the data well at all. We showed this by determining the lower limits to the size of the diffuse emitting region around here at 10 min of arc even assuming a point source somewhere else in the field of arbitrary strength and position.

Refer to Figure 3. At the bottom is Abell 399. There is a cD galaxy there. At the top is Abell 401, and its cD galaxy. The white circles demonstrate the two most interesting choices that were interpretations of our data: a huge diffuse gas cloud centered on here; or two separate gas clouds. Either of these interpretations will suggest that perhaps clusters like to form binary systems, if you will, just as stars like to form binary systems in our galaxy. I do not know whether that kind of formation law scales up; I'll leave that to theoreticians. But I believe that is an interesting suggestion. Now if you take the large single gas model, it is possible assuming it to be fairly diffuse and not too clumped to get quite a large amount of gas, in fact,  $10^{15} - 10^{16}$  solar masses depending on how far out you want to run your model. Now if that interpretation is correct and if such phenomena are common, it opens up the possibility that we can close the universe, which is always nice to do because we do not want our errors to propagate forever. I do not know whether it is really opened or closed, but in any event, it is certainly an exciting interpretation of the results. Now we also did a survey of clusters of galaxies that Kent Wood alluded to this morning and in that survey of some 70 clusters of galaxies we found 2 in which there is certainly evidence for extended emission (see Figure 4). This is the point source response and the diffuse source response. You see the point source just does not work well at all. These are distance class 6 clusters and if indeed they are at the distance implied by that inferred red shift (to my knowledge there's no real measurement of the red shift of these clusters), then the linear extent of these things is even larger than the Abell 401, Abell 399 region. This one corresponds to about 10 Mpc and this about 5 in radius. So they are pretty large regions. I must admit they are awfully weak, which introduces the possibility of source confusion, which is why I used the words "evidence for" even though the data looked okay. In this survey, we also found

3 binary cluster systems, in which at least one member was an X-ray source. They are Abell 508, 509, 2177, 2178, 2204, and 2210. In conclusion then these binary cluster systems and/or large extended regions seem fairly common and I believe these kinds of studies (we've only looked at 1/9 the sky so far) should lead to much better understanding or a better model for the formation and evolution of clusters of galaxies and at most they will even be able to close the universe.

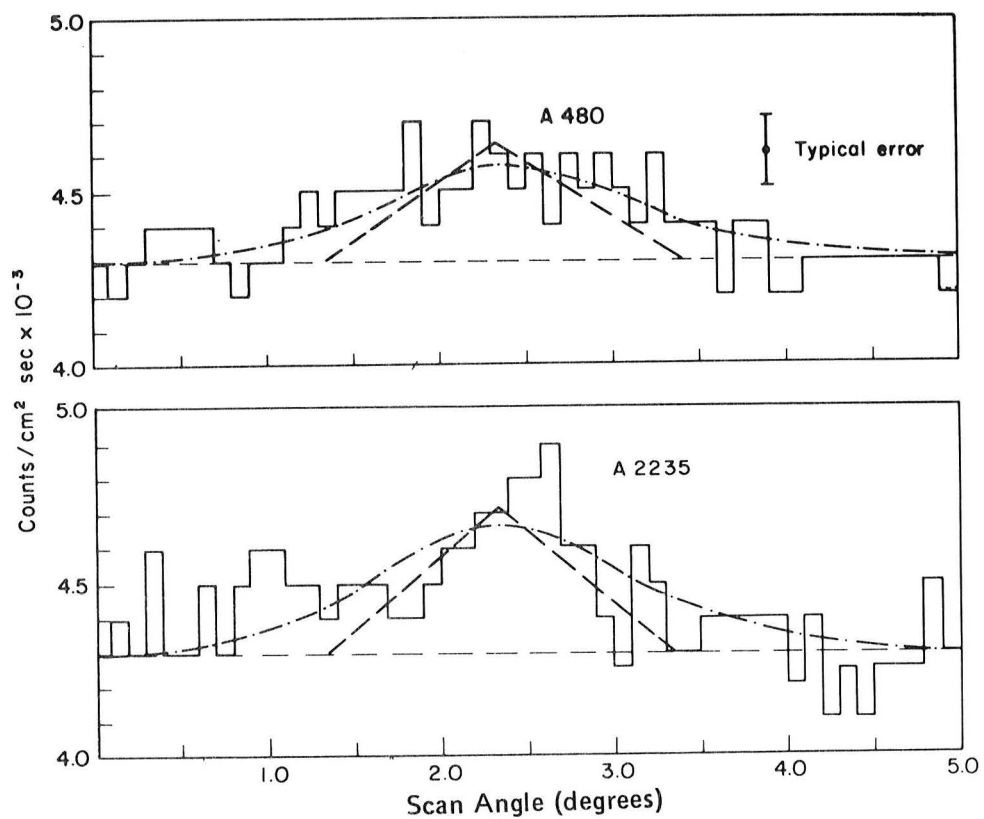


Figure 1

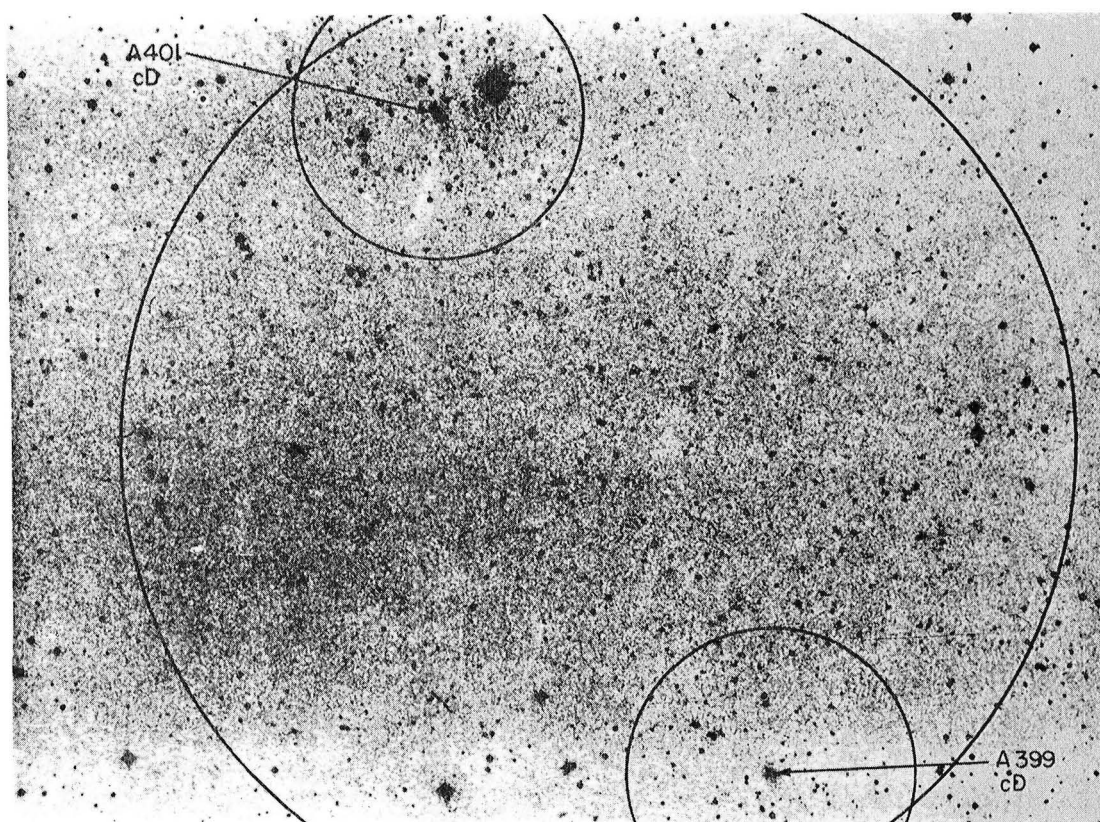


Figure 2



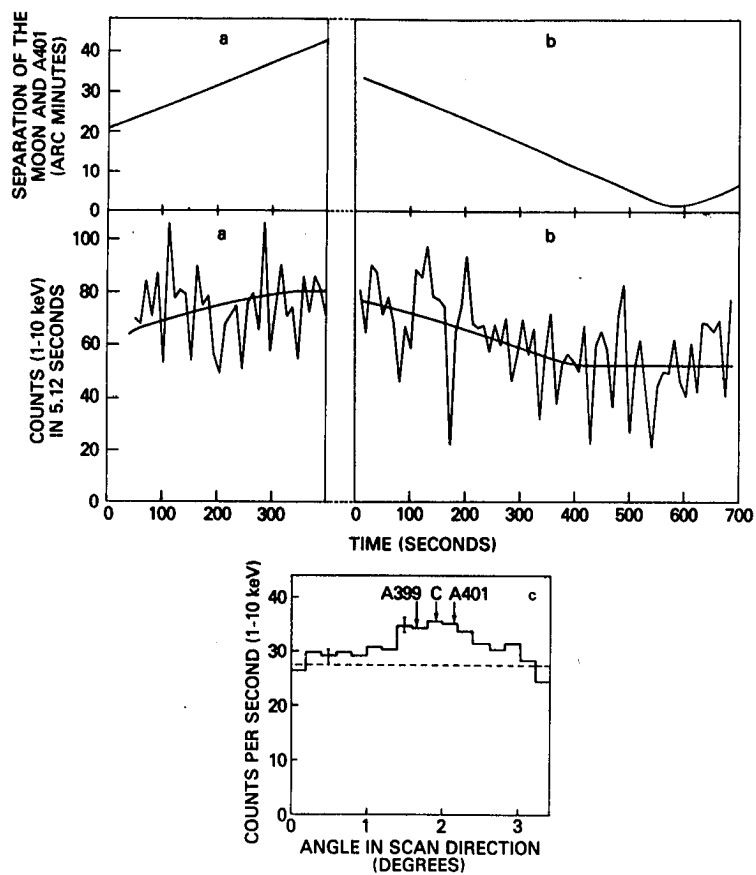


Figure 3

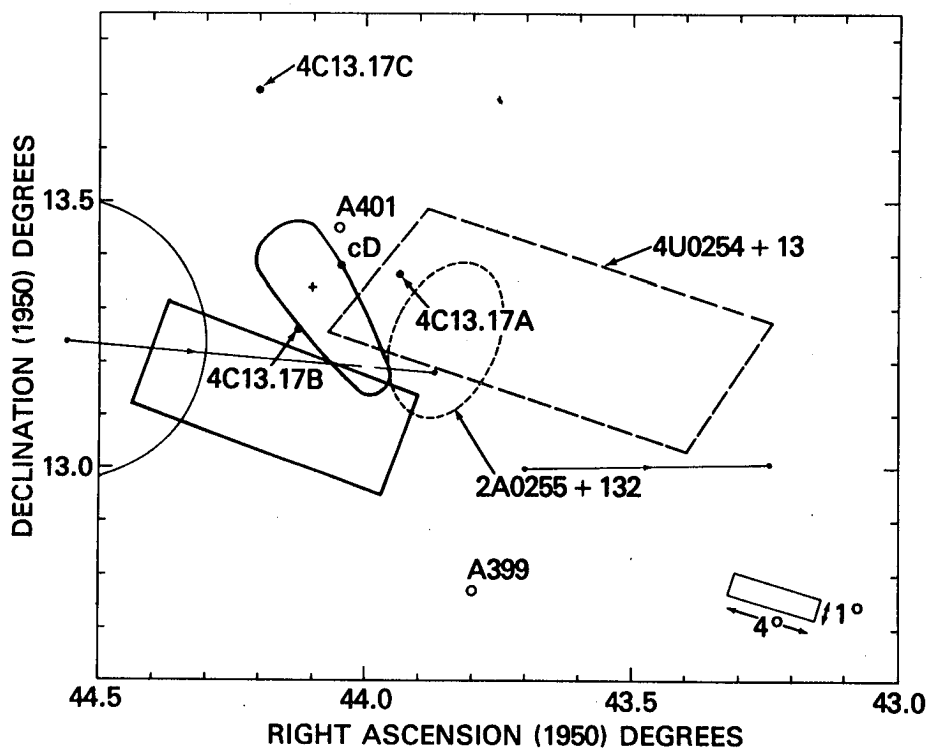


Figure 4

## CORRELATED GROUND BASED OBSERVATIONS IN SUPPORT OF THE HEAO-1 X-RAY OBSERVATORY

Stewart Mufson  
Indiana University

In this program our intent was to explore the physics associated with cosmic X-ray sources. Our objective was to be achieved by combining X-ray fluxes obtained by the A-1 experiment aboard the HEAO-1 observatory with ground based optical and near infrared photometry and optical spectroscopy. The objects whose properties we have chosen for our study fall into two categories: (1) energetic, compact extragalactic sources, and (2) compact, galactic X-ray emitters like X Persei. In our investigation of the program sources, we observed UBVRI fluxes, and at times optical spectra, during periods chosen to coincide with observations made by the HEAO-1 satellite. In addition to simultaneous experiments, a significant effort was made to monitor the sources. Since HEAO-1 only observes objects near dawn and dusk, we utilized the remainder of our observing sessions to establish optical baselines against which longer term X-ray variability could be compared.

The photometric data obtained during the HEAO-1 mission represent observations made on 53 nights, extending back to the date originally planned for the HEAO-1 launch, April 1977. These data include 11 simultaneous X-ray and optical experiments performed during the HEAO-1 mission. In addition, we have obtained seven nights of high time resolution optical spectroscopy in connection with our program. These data include three simultaneous experiments. In many cases we are currently continuing our optical observations of the program objects.

In Figure 1 we show our UBVRI photometric data for BL Lacerta, an example of one type of compact, extragalactic source we have studied. Optical emission lines are absent in this source, so our optical photometry, like X-ray photometry, is directly sampling the central engine without complications introduced by intervening gas [1]. An average straight line has been drawn through this compilation of our photometric data. Clearly BL Lac has a predominantly nonthermal spectrum. The triangles are a set of observations obtained on one night, a snapshot, in which the spectrum was thought to be like the average spectrum, and the x's are a snapshot of the spectrum when it was considerably different from its average. As is usual in BL Lac objects, the spectral shape

varies quite considerably in the course of time. The variations in the intensity of optical emission with time scales of days suggest the central engine in this source is quite small.

In Figures 2 and 3 we see two low energy BL Lac objects, Markarian (Mrk) 421 and Mrk 501, which have been identified with X-ray sources. The mini-lacertids in both these objects are embedded in giant elliptical galaxies [2]. These optical spectra are again predominantly nonthermal. Mrk 421 shows especially large variations in optical activity. The notation in these figures is the same as that used in Figure 1, where triangles mark a snapshot of an average spectrum and the x's show an example of a peculiar spectrum. In his talk this morning, Dr. Schwartz made a very interesting point. From May 1977 to May 1978, the continuous X-ray spectrum of Mrk 421 was seen to steepen quite considerably [3,4]. In Figure 2, the x's represent the optical spectrum of Mrk 421 in May 1978 and the average line is representative of the optical spectrum in May 1977. From May 1977 to May 1978 the optical spectrum, like the X-ray spectrum, was seen to steepen considerably. This correlated X-ray and optical behavior is what one would expect from a synchrotron-Compton source [5].

The combined UBVR photometry for another BL Lac object we have studied closely — B2 1308+32 — is shown in Figure 4. The intensity variations seen in this source are enormous. Our observational record also shows the optical spectrum has often changed its shape. A cosmological interpretation of its  $z = 0.996$  redshift [6] implies B2 1308+32 has a peak luminosity of  $10^{48}$  ergs/sec; this luminosity is near the maximum observed in the most energetic quasars [7]. On the first pass by HEAO-1, the A1 experiment found only an upper limit to the X-ray flux in the energy range  $\frac{1}{2}$ –20 keV. But as can be seen in Figure 5, the combination of our B band photometry with other published values shows that the source was very quiescent during this satellite observation, and so not likely to have been seen in the X-ray. This figure also shows that B2 1308+32 flared very brightly in 1974 and 1977, flared moderately in 1975 and 1978, and was probably quite weak in 1976 and 1979. We suggest the source will again be brightly flaring in 1980, and so will be an excellent candidate for a combined X-ray and optical study.

The characteristic form of an optical burst has been followed now through almost three cycles. In Figure 5, the optical emission can be seen to rise slowly to a maximum, and then abruptly fall off. During spring 1978, such an outburst was particularly well marked. In Figure 6 we display our UBVR photometry during this burst using flux values normalized with the frequency independent units of energy flux (ergs/cm<sup>2</sup>-sec). The energy flux rises more slowly than it falls at all colors. The radio emission at 15 GHz during this outburst (H. Aller and T. Balonek, private communications) also rises gradually to a maximum in June. But the radio emission falls off far more slowly than the optical.

In Figure 7, we show the UBVRI energy flux measurements during one night of monitoring observations. Variations at all colors can easily be seen. However, variations at different colors do not appear to be correlated. As seen in Figures 4 through 7, our optical studies so far imply the existence of two engines in this source — one for the long term intensity variations which are correlated from radio to optical wavelengths, and one for the emission of the rapid, uncorrelated intensity fluctuations observed at all colors.

In Figure 8 we give our photometric data for the X-ray quasar 3C 273. Our data for December 22, 1978 (x's) — near both HEAO-1 and HEAO-2 observations — shows that 3C 273 was brighter than any time since 1965 [8]. Even on December 27, at the time of HEAO-A1 pointed observations, this source was significantly brighter than average.

Finally, in the second phase of our program, we have been investigating the photometric and spectroscopic properties of X Persei, an unusual Be star associated with an intrinsically weak X-ray source. Both its X-ray and optical emission show complex variability on many different time scales. At X-ray wavelengths the flux is observed to vary with a period of 13.9 min [9]; there is in addition some evidence for a period of 22.4 hr. A period of 580 days is well observed in the radial velocity of the Balmer lines [10]. X Persei is most often interpreted as a BOe star with a neutron star companion.

On August 23, 1978 we monitored the  $H\alpha$  emission line during a HEAO-A1 pointed observation. The spectroscopic observations were made at the Goethe Link Observatory of Indiana University using an I-SIT spectrograph. The spectral resolution of this instrument is  $2 \text{ \AA}$ , and each observation lasted 90 sec. In Figure 9 we show the equivalent width of  $H\alpha$  versus time for the two dates August 23, 1978 and September 25, 1978. Our optical spectroscopy recorded a remarkable event during the simultaneous experiment. Between 9:28 and 9:31 UT the equivalent width dropped from 7.3 to 3.3  $\text{\AA}$ . This was followed by a more extended event of 540 sec duration in which the equivalent width dropped from 7.7 to 2.6  $\text{\AA}$ . Standard stars were observed and the event does not appear to be instrumental in origin. During this event, the central wavelength increased and the line widths became narrower. This suggests a weakening of an unresolved, blueshifted line component. In the past observations of similar events have been reported [11,12]. The X-ray data from this experiment is not yet available. On September 25, 1978 the equivalent width was higher (10.2  $\text{\AA}$ ) and showed only a hint of variability over a three hour period.

## REFERENCES

1. Stein, W. A., 1978, in Pittsburgh Conference on BL Lac Objects, A. M. Wolfe (ed.), Pittsburgh: University of Pittsburgh Press, p. 1.
2. Ulrich, M. H., Kinman, T. D., Lynds, C. R., Rieke, G. H., and Ekers, R. D., 1975, Ap. J., 198, 261.
3. Schwartz, D. A., Doxsey, R. E., Griffiths, R. E., Johnson, M. D., and Swarz, J., 1979, Ap. J. (Letters), 229, L53.
4. Mushotzky, R. F., Boldt, E. A., Holt, S. S., and Serlemitsos, P. J., 1979, preprint.
5. Jones, T. W., O'Dell, S. L., and Stein, W. A., 1974, Ap. J., 188, 353.
6. Miller, J. S., French, H. B., and Hawley, S. A., 1978, in Pittsburgh Conference on BL Lac Objects, p. 176.
7. Moore, R. L., Angel, J. R. P., Rieke, G. H., Lebofsky, M. J., Wisniewski, W. Z., Mufson, S. L., and others, 1979, Ap. J., preprint.
8. Bradt, H. J., Doxsey, R. E., Johnson, M. D., Schwartz, D. A., Burkhead, M. S., Dent, W. A., Liller, W., and Smith, A. G., 1979, Ap. J. (Letters), preprint.
9. White, N. E., Mason, K. D., and Sanford, P. W., 1976, M.N.R.A.S., 176, 201.
10. Hutchings, J. B., Cowley, A. P., Crampton, D., and Redman, R. O., 1974, Ap. J. (Letters), 191, L101.
11. Murdin, P., Penston, M. V., and Penny, A. J., 1976, M.N.R.A.S., 176, 233.
12. Campisi, I. E., and Treves, A., 1976, M.N.R.A.S., 176, 225.

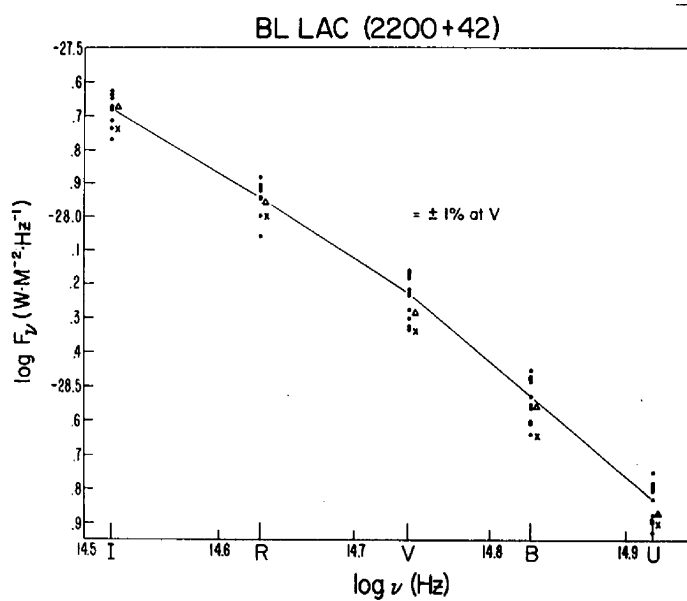


Figure 1

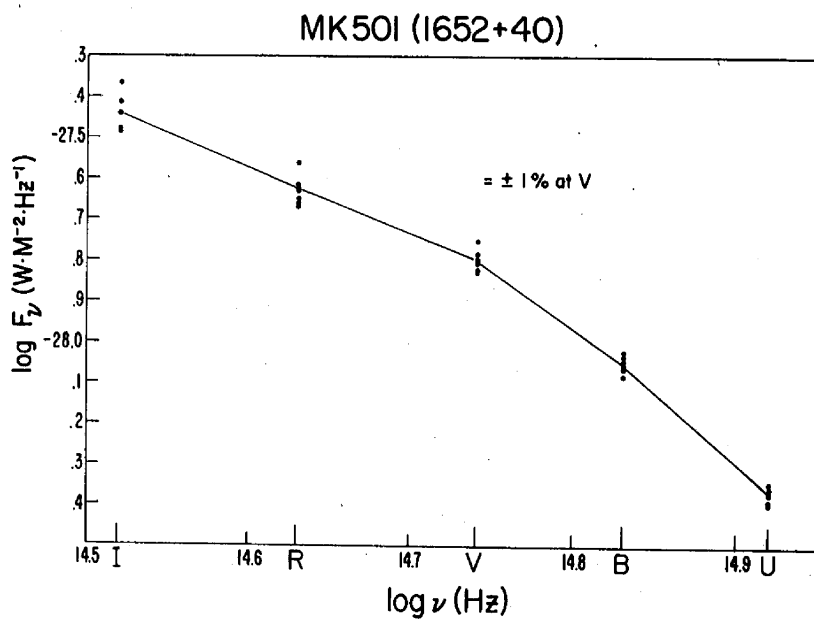


Figure 2

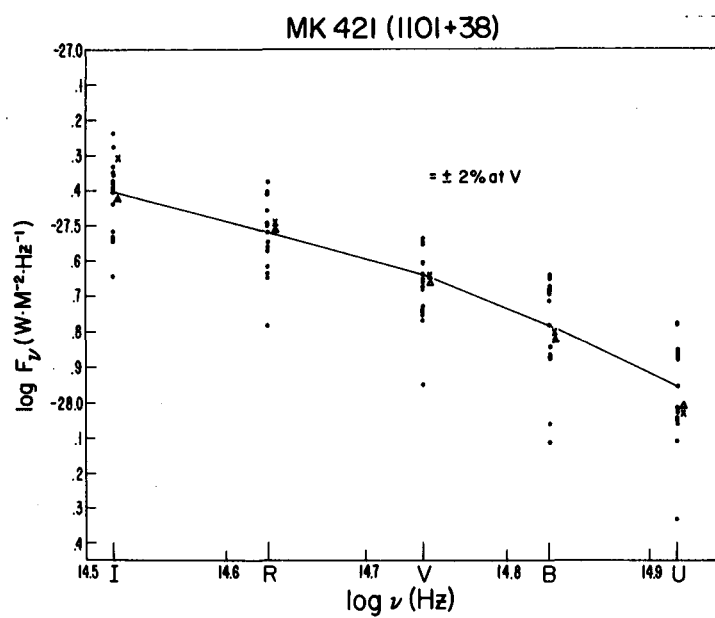


Figure 3

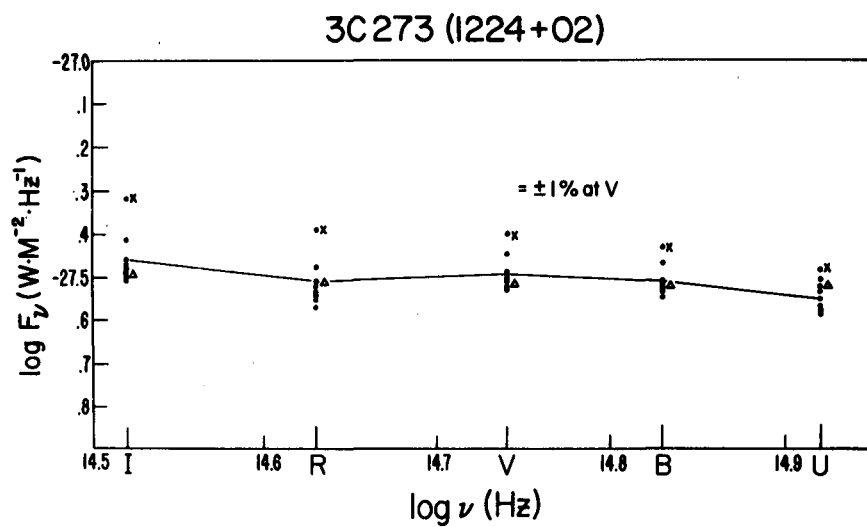


Figure 4

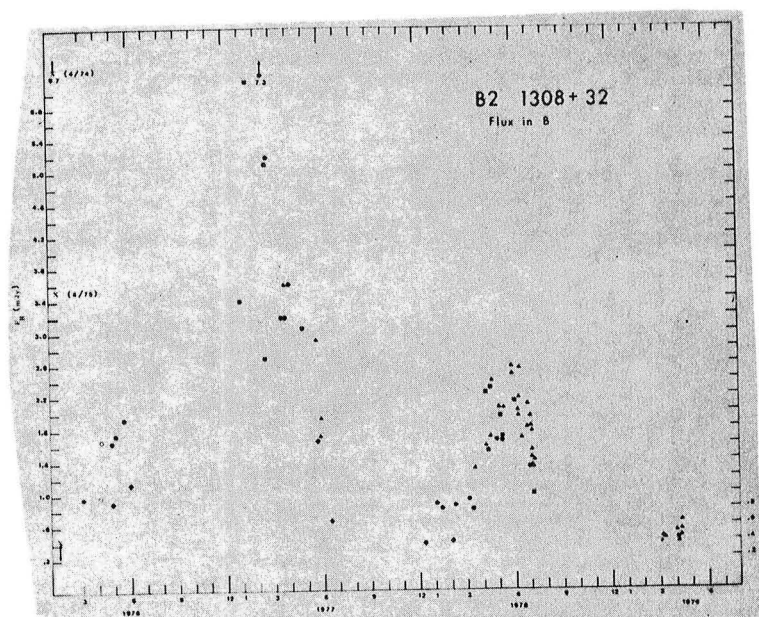


Figure 5

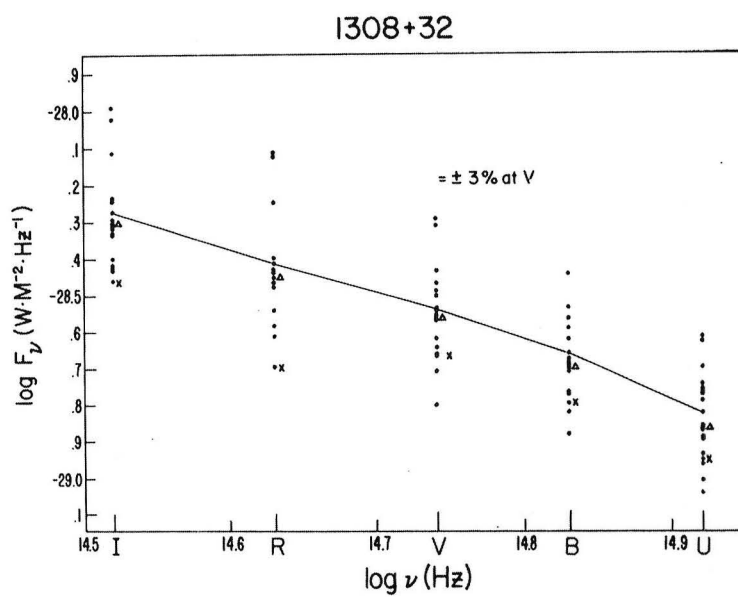


Figure 6



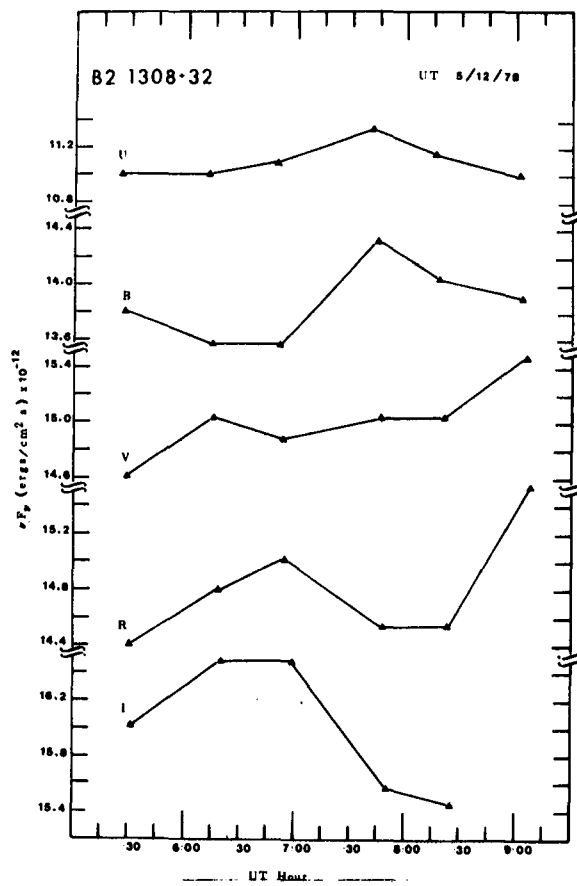


Figure 7

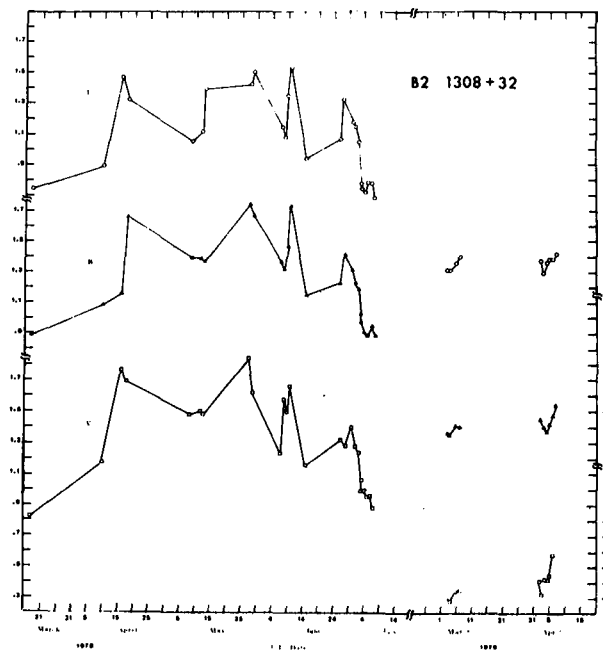


Figure 8

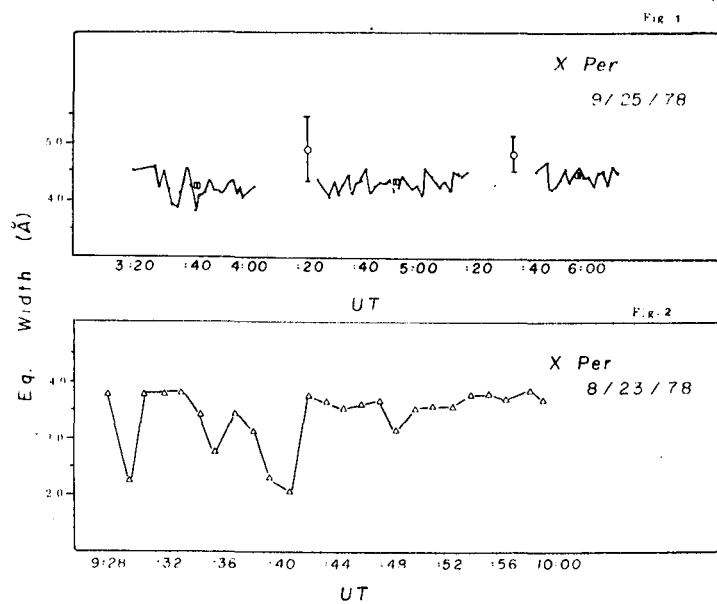


Figure 9

# THE HEAO-1 NEUTRON STAR TIMING EXPERIMENT

F. K. Lamb  
University of Illinois

## INTRODUCTION

I have been asked to describe the HEAO-1 neutron star timing experiment, even though the analysis and interpretation of this experiment are still in progress. The investigators who are participating in this experiment with me are Paul Boynton and John Deeter at the University of Washington, Steve Pravdo and Nick White at Goddard Space Flight Center, and Kent Wood at the Naval Research Laboratory. In this progress report I will describe briefly the scientific motivation for the experiment, the reasons for our choice of Her X-1 and Vela X-1 as promising sources to study, our methodology, and the current status of the experiment.

## SCIENTIFIC MOTIVATION

The basic scientific goals of the experiment are summarized in Table 1. There are two basic thrusts: first, to improve our understanding of the internal structure of neutron stars, and second, to obtain more information about accretion flows. The way that we hope to address both questions is to study in detail the changes in the pulsation periods of Her X-1 and Vela X-1. These changes are thought to be due to changes in the angular momentum, and hence the rotation period, of the neutron star crust. According to current ideas, the change in period over a sufficiently long time is due to the action of the external accretion torque (Pringle and Rees 1972; Lamb, Pethick, and Pines 1973), while period fluctuations on shorter time scales may be caused by fluctuations in either the external accretion torque (Elsner and Lamb 1976) or the internal torque exerted on the crust by the superfluid neutron liquid interior (Lamb, Pines, and Shaham 1978). Some possible sources of internal and external torque fluctuations are listed in Table 2.

The external torque depends on the flow pattern of the accreting plasma, while the internal torque depends on the strength and nature of the coupling between the liquid interior and the crust. The response of the neutron star to a torque acting on the crust, whether external or internal, depends on the dynamical properties of the star: the "applied signal" represented by the torque is, in effect, "filtered" by the coupled crust-superfluid system to produce an "output" represented by changes in the pulsation period. Thus, a detailed study of period

changes in a given X-ray source can provide information both about the properties of the accretion flow onto the star and about the properties of the star itself.

In the following subsections I first describe why measurement of short-term fluctuations in the pulse phase and X-ray flux is the most promising approach to use in such studies. I then outline how one can extract information about the internal structure and dynamical properties of the neutron star from such measurements and describe briefly how they can also be used to determine the accretion flow pattern and to test accretion theories.

### Advantages of Studying Short-Term Behavior

The interpretation of any particular period change is complicated by the fact that the response of the neutron star interior is not known a priori. Hence, such a change might be due either to the internal and external torques acting at the time, or to the response of the star to previous values of these torques. If the change in the rotation rate were smooth and the total observing interval were long, the likelihood that the star was still responding to an earlier value of the torque would be less, but the interpretation would still be ambiguous. In fact, the period changes in those sources that have been studied carefully are observed to be highly irregular.

Recently, Lamb, Pines, and Shaham (1978) pointed out that if the torque fluctuations that cause the short-term period variations can be described by a simple noise process, then these interpretational difficulties can be overcome by using the period variations themselves to determine the dynamical response of the neutron star. These authors further suggested that either white or red torque fluctuations are physically plausible models and showed that the available data on Her X-1 and Cen X-3 are consistent with either type of torque noise. Motivated by these studies, Boynton and Deeter (1979) used the Uhuru data on Her X-1 to compute the power density spectrum of the pulse phase fluctuations in this source. They find that the torque fluctuations in Her X-1 are describable as white noise over a wide range of frequencies and derive significant constraints on the dynamical response of the neutron star from their analysis. Thus, this method of determining the neutron star response appears quite promising. Use of this method requires a dense, regular sequence of pulse phase measurements.

Measurements of the short-term behavior of the pulse phase and X-ray flux also provide the best type of data for determining the accretion flow pattern and the large-scale structure of the magnetosphere (see Ghosh and Lamb 1979b). First, accretion theory predicts that the change in spin period between two observations depends sensitively on

the behavior of the accretion luminosity  $L$  during the interval. If  $L$  is highly variable, as it often is, spot checks at widely-spaced times may lead to very large errors in the inferred luminosity history  $L(t)$ . Such errors can be minimized by measuring the period and flux at frequent intervals. Second, theoretical models necessarily include a number of adjustable parameters, such as the mass, radius, effective moment of inertia, and magnetic dipole moment of the star. Although the dependence on these parameters does not permit one to fit every possible value of  $P$ ,  $\dot{P}$ , and  $L$ , in practice the possibility of adjusting these parameters introduces a substantial degree of freedom. If only the average values of  $\dot{P}$  and  $L$  are known, there is often not enough information to test the theory. However, once these parameters are determined there is no more freedom, so that additional measurements of  $P$ ,  $\dot{P}$ , and  $L$  provide a quantitative test of the theory. Finally, since the effective inertial moment of the star generally is not constant, one must combine the theoretical equation for the accretion torque as a function of the mass accretion rate with the observed luminosity behavior  $L(t)$  and a dynamical model of the neutron star crust and core in order to solve for the predicted period behavior  $P(t)$  of the neutron star crust. Only then can a comparison be made with the observed period behavior. This procedure can only be carried out if a dense, regular sequence of period and flux measurements is available.

In summary, only frequent, regular measurements of the pulse phase and flux of neutron star X-ray sources can provide the type of data required to confront current theoretical models of their magnetospheres and interiors.

### Probing Neutron Star Interiors

The actual response of a neutron star to fluctuating torques acting on its crust is expected to be quite complex. A key question is the coupling time between the solid crust and the rest of the star, which then determines the effective inertial moment involved in angular momentum changes on various time scales. X-ray timing observations of pulsating sources can measure, or at least severely constrain, the moment of inertia,  $I_c$ , of that part of the star which responds quickly to torque variations; the moment of inertia,  $I_s$ , of that part which responds only more slowly; and the coupling time,  $\tau$ , between them. Such measurements can be made by observing the fluctuation of the angular velocity of the crust and then computing the power density spectrum of the fluctuation. If the spectrum obeys a power law at both high and low frequencies, a description of the torque fluctuations in terms of a simple noise model is possible; the index of the power law then indicates the dominant type of noise. The power law region of the spectrum is expected to extend over many decades in frequency, and defines the range of time scales and

frequencies that can be searched for evidence of the crust-core coupling time  $\tau$  and the frequencies of any internal modes.

In the absence of an internal mode with a frequency within the range covered by the power spectrum analysis, the two-component model predicts a shoulder in the power spectrum at  $\omega \sim 1/\tau$ , with the power at higher frequencies enhanced by the factor  $(I/I_c)^2$ , where  $I = I_s + I_c$  is the total moment of inertia of the star. This is because the lower frequency torque fluctuations drive both the crust and superfluid whereas the higher frequency fluctuations drive only the crust. An example of this type of power spectrum is shown in Figure 1a, which displays the response of a two-component neutron star to white torque noise.

The ratio of inertial moments,  $I/I_c$ , is a sensitive function of the mass of the neutron star and the equation of state, ranging from 1 for the lightest neutron stars and the stiffest equations of state to greater than 100 for the maximum mass neutron stars given by soft equations of state. Thus the shoulder in the power spectrum at  $\omega \sim 1/\tau$ , which is proportional to  $(I/I_c)^2$ , may be quite prominent. The detection of such a shoulder would provide the first evidence for the existence of superfluid neutrons in X-ray sources. It would also help to pin down the correct equation of state of matter at very high densities, and to stimulate further theoretical work on the nature of the coupling between crust and core (see Lamb 1977 and references therein).

In the presence of an internal mode of frequency  $\omega_0$ , the generalized two-component model predicts a peak in the power spectrum at  $\omega = \omega_0$  with a width  $\Delta\omega \sim 1/\tau$ , where  $\tau$  is the relaxation time of the mode. Such a spectrum is shown in Figure 1b for the case of a lightly damped mode ( $\omega_0 \tau \gg 1$ ) excited by white torque noise. The spectrum shows a sharp notch in the spectrum at  $\omega = (I_c/I)^{1/2} \omega_0$ , as well as the enhancement of the power at higher frequencies already seen in Figure 1a. Detection of internal resonant modes would allow a direct comparison with theoretical work on the dynamics of the degenerate electron-proton plasma and the superfluid neutron liquid (see Lamb 1979 and references therein), and would provide an important stimulus to this work.

### Probing Accretion Flows

As noted earlier, one possible explanation for a fluctuating neutron star spin rate is the presence of fluctuations in the mass accretion rate, which will produce correlated changes in the pulse period and X-ray flux. Clearly, however, the extraction of information concerning the accretion flow from observations of period fluctuations requires some care. First, in order to study the accretion flow in this way the period fluctuations

must be shown to be due to fluctuations in the accretion torque rather than the internal torques. Second, the response of the neutron star must be considered in interpreting the data, since the response time of the liquid interior may be comparable to the time scale for changes in the accretion torque.

Accretion torque fluctuations can potentially be identified by searching for correlated changes in the pulse period  $P$  and the X-ray flux  $F$  at earth, since accretion theory predicts that fluctuations in the mass accretion rate will cause fluctuations in both the accretion luminosity and the accretion torque; correlated changes in  $P$  and  $F$  are much less likely if the period change is caused by internal torque fluctuations. Fluctuations in the accretion rate appear quite natural and can easily produce torque variations large enough to account for the period wandering observed in the well-studied pulsating sources (Lamb, Pines, and Shaham 1978; Ghosh and Lamb 1979b). I shall therefore focus on torque variations that arise in this way.

To the extent that the torque variations can be described by a simple noise process, one can disentangle the variations in the torque from the time-dependent response of the star in the manner described above. Once this is accomplished, a sequence of pulse period and X-ray flux measurements can potentially be used to (1) determine whether the source is fed by a Keplerian accretion disk or by some other accretion flow pattern, (2) test quantitatively the theory of disk accretion, (3) confirm that the X-ray source is indeed a neutron star, (4) determine accurately the dipole moment of the X-ray star, and (5) establish the nature of the accretion torque fluctuations.

The first step in achieving these goals is to construct a theoretical relation between the X-ray flux  $F(t)$  at earth and the pulse period  $P(t)$ . Such a relation can be constructed if one has available (1) a relation between  $F$  and the accretion luminosity  $L$ , (2) a relation between  $L$  and the mass accretion rate  $\dot{M}$ , (3) a relation between  $\dot{M}$  and the torque  $N$ , and (4) a model for the change in the rotation of the neutron star crust caused by  $N$ . Assuming that the X-ray flux at earth accurately reflects the X-ray luminosity and that the latter is essentially the accretion luminosity  $L$ , then  $F = L/4\pi D^2$ , where  $D$  is the distance to the source, while  $L = \dot{M}(GM/R)$ . One can then turn to accretion theory for a relation between  $\dot{M}$  and  $N$ . Finally, the stellar properties required to determine the change in the rotation period  $P$  of the neutron star crust produced by the torque  $N$  are fixed by the power density spectrum of pulse phase fluctuations.

Once a theoretical relation between  $F(t)$  and  $P(t)$  has been constructed, it can be tested by comparison with a sequence of X-ray flux and pulse period measurements. As an example of how this approach can be applied, consider the case of disk accretion, for which a

quantitative theory has recently been developed (Ghosh and Lamb 1978, 1979a,b). Figure 2 shows the dependence of the accretion torque on the mass accretion rate which is predicted by this model. The dashed curve shows the torque that would occur if the transition zone between the disk and the magnetosphere were narrow, whereas the solid curve shows the torque given by the broad transition zone predicted by the theory. This illustrates how measurements of the accretion torque can furnish information about the accretion flow. If the neutron star responds like a rigid body with a constant effective moment of inertia  $I_{\text{eff}}$ , then this torque curve predicts that for a star of given mass and magnetic moment,  $\dot{P}$  is a function only of  $PL^{3/7}$ . The character of this relation is shown in Figure 3. For large values of  $PL^{3/7}$ , the star is a slow rotator and  $-\dot{P}$  scales as  $(PL^{3/7})^2$ . Thus, if  $\log(-\dot{P})$  is plotted versus  $\log(PL^{3/7})$ , the theoretical spin-up curve is a straight line of slope 2 in the region of slow rotation. As  $PL^{3/7}$  decreases, the fastness  $\omega_s$  increases and  $\log(-\dot{P})$  falls below the extrapolation of this line. Finally, at the value of  $PL^{3/7}$  for which  $\omega_s$  reaches a certain critical value,  $\dot{P}$  vanishes and  $\log(-\dot{P})$  diverges. The value of  $PL^{3/7}$  at which the spin-up curve begins to fall below the extrapolated straight line depends sensitively on the magnetic moment of the star, as shown.

If observed values of  $P$ ,  $\dot{P}$ , and  $L$  are plotted on such a graph and are qualitatively represented by the theoretical curve, this would constitute strong evidence that the X-ray source is a neutron star which is disk-fed. The shape of the curve would then give the size of the dipole magnetic moment, while a detailed comparison of the data with the theoretical curve would provide a quantitative test of the theory. Finally, a detailed comparison of the time history of the pulse period and X-ray flux with the theoretical model would establish whether the torque noise is caused by fluctuations in the mass accretion rate.

### The Current Evidence

We have just seen that sequences of accurate period and flux measurements can establish unambiguously many properties of neutron stars and accretion flows. Unfortunately, such sequences are not yet available. Nevertheless, some information can be extracted from the current data by comparing theoretical spin-up curves with the time-average values of  $P$ ,  $\dot{P}$ , and  $L$  available at present, and by comparing neutron star response models with the pulse phase fluctuations observed in Her X-1. One should, however, keep in mind the ambiguities that arise in working with such a limited set of data.



If we consider a collection of pulsating X-ray sources, the theory of disk accretion predicts that they would all lie on the same curve  $-\dot{P} = f(PL^{3/7})$  if they all had (1) the same mass  $M$  and (2) the same magnetic moment  $\mu$ . Although all pulsating X-ray sources are not expected to have identical masses and magnetic moments, observed values of  $-\dot{P}$  should be correlated with observed values of  $PL^{3/7}$  if the variation of the mass and magnetic moment from source to source is not too large. Figure 4 shows a plot of observed values of  $-\dot{P}$  against  $PL^{3/7}$ . Such a plot tends to order the sources according to their fastness, since for fixed  $M$  and  $\mu$  the fastness parameter is a function only of  $PL^{3/7}$ . Shown are the theoretical spin-up curves for three stellar masses, assuming a magnetic moment of  $0.48 \times 10^{30}$  gauss cm<sup>3</sup> and the tensor interaction (TI) neutron star models of Pandharipande, Pines, and Smith (1976). The curve for  $M = 1.3 M_{\odot}$  is a rough best fit to the observations. Except for Vela X-1, all the sources lie in the shaded region spanned by the curves corresponding to values of  $M/M_{\odot}$  in the range 0.5 - 1.9.

Even though wind theory is not sufficiently advanced to predict the behavior of  $\dot{P}$  as a function of the physical conditions in any single source, the wind hypothesis does, under some conditions, predict a correlation between  $PLT_s$  and  $P_{orb}$  (Ghosh and Lamb 1979b). Here  $T_s$  is the spin-up time scale and  $P_{orb}$  is the binary orbital period. Figure 5 shows the currently available data for seven well-studied X-ray sources on a plot of  $\log(PLT_s)$  against  $\log(P_{orb})$ . Also shown in the figure is the theoretical relation for one plausible set of binary system parameters. Although the observed values of  $PLT_s$  lie within an order of magnitude of the values expected theoretically, there is little evidence for any correlation with  $P_{orb}$  (the  $22^h$  X-ray variation sometimes observed in X Per is shown in the figure, even though it probably is not the binary period of the source; if this point is given a low weight, there is no evidence for any increase of  $PLT_s$  with  $P_{orb}$ ).

If one assumes that all nine sources are disk-fed, one can estimate the magnetic dipole moment of each star by adjusting  $\mu$  so that the theoretical spin-up curve passes through the datum of the star (Ghosh and Lamb 1978, 1979b). The inferred moment depends weakly on the mass and equation of state of the neutron star. Acceptable fits are possible for all nine sources, for a mass of  $1.3 M_{\odot}$ , the TI neutron star models of Pandharipande, Pines, and Smith (1976), and magnetic moments in the range  $3 \times 10^{29} - 4 \times 10^{32}$  gauss cm<sup>3</sup>. Indeed, one can find a set

of solutions with magnetic moments all lying within the relatively narrow range  $\sim 5 \times 10^{29} - 5 \times 10^{39}$  gauss cm<sup>3</sup> that is consistent with the data on all the measured sources except Vela X-1. A magnetic moment  $\sim 10 - 10^2$  times larger than that inferred for the other sources is required in order to fit the relatively long spin-up time scale of Vela X-1. While such a large magnetic moment is certainly allowed by our current understanding of neutron star magnetic fields, the fact that Vela X-1 alone requires such a large value of  $\mu$  suggests the alternative possibility that Vela X-1 is wind-fed rather than disk-fed (Lamb 1977), in which case it could have a relatively long spin-up time scale even if its magnetic moment were similar to those of the other sources.

Turning to the problem of the dynamical properties of accreting neutron stars, Boynton and Deeter (1979) have used the Uhuru data on Her X-1 to compute the power spectrum of pulse phase fluctuations in this source. They find that this neutron star responds like a rigid body to torque fluctuations on time scales ranging from  $1^d$  to  $100^d$ . Thus, either the crust-superfluid coupling time in Her X-1 is shorter than  $1^d$  or longer than  $100^d$ , or the superfluid moment of inertia must be less than or comparable to that of the crust.

The good agreement between the predictions of disk accretion theory and the observed average spin-up rates of the currently measured sources together with the apparent absence of any correlation between  $PLT_s$  and  $P_{orb}$  suggests that at least 8 of these sources are disk-fed and that the theory is qualitatively correct. This good agreement also argues that these sources are indeed neutron stars with canonical masses, radii, moments of inertia, and magnetic moments. However, given our present limited information on magnetic moments, wind conditions, and binary system parameters, these conclusions are necessarily very tentative, a situation which underscores the importance of the HEAO-1 experiment.

## THE EXPERIMENT

In the following subsections I outline the nature of the HEAO-1 experiment, describing briefly the utilization of HEAO-1 capabilities, the reasons for choosing to study Her X-1 and Vela X-1, and the planned types of studies.

## The Contribution of HEAO-1

The HEAO-1 satellite provided the particular combination of capabilities best suited to carry out this pulse timing mission, for

- 1) The large detector area and pointing ability provide the high average count rate necessary to minimize the counting statistics noise level in the sequence of pulse arrival times;
- 2) The precision aspect correction associated with pointed observations allows the study of possible correlations between variations in flux and angular velocity; and
- 3) The long lifetime of the HEAO-1 mission enables exploration of the power spectrum to sufficiently long periods (at least 100 days) to allow a credible test of power law behavior and an adequate frequency range in which to search for dynamical behavior of the neutron star.

The results of this prototype experiment will provide information which is essential for the design of future instrumentation and observing programs to pursue studies of this type.

## Choice of Sources

1. Theoretical Motivation. There are specific theoretical expectations of possible differences between the sources of torque fluctuations in fast rotators and slow rotators. Internal torque fluctuations may be more important in the case of slow rotators (Lamb, Pines, and Shaham 1978). However, if the sources are disk-fed, the torque contribution from the region of magnetic coupling between the disk and the star is especially important in fast rotators (Ghosh and Lamb 1978, 1979b). For these reasons, it is important to select examples from both classes for observation and study.

2. Observational Motivation. Because of the extensive observing time required for even a modest characterization of the angular velocity noise in the strongest sources, we have decided to concentrate our initial studies on only two objects, one short period source, Hercules X-1, and one long period source, Vela X-1.

Preliminary analysis of Uhuru data on Hercules X-1 has already indicated the presence of measurable torque noise in this source (Boynton and Deeter 1979). This fact makes the Hercules source a prime candidate for further study. The HEAO-1 data will allow us to carry out on this source the crucial flux-angular velocity correlation analysis discussed below.

Among the long period sources, Vela X-1 provides the best opportunity for torque noise studies. There are preliminary indications that the noise strength characterizing angular velocity fluctuations in this source is roughly  $10^3$  times larger than that measured in Her X-1 (Becker et al. 1978; Joss 1978). This means that the HEAO-1 observations of Vela X-1, supplemented by previous HEAO-1 and OSO-8 data, should allow us to recover information from the power spectrum over roughly the same frequency range and with roughly the same signal-to-noise ratio as was possible with the Uhuru data on Her X-1.

### Types of Studies

1. Power Spectrum Analysis. In this type of study, one constructs a library of pulse arrival times. A polynomial expression for the arrival times is then fit to the observed sequence, and the residuals are used to calculate the power density in pulse phase fluctuations. If torque noise is detected, one can place significant constraints on the internal structure of the neutron star by fitting theoretical stellar response functions to the measured power spectrum. If there are features in the response power spectrum, one can determine directly neutron star structure parameters such as  $I_c/I$ ,  $\omega_0$ , and  $\tau$ . Because  $I_c/I$  is a sensitive function of the equation of state, its value together with an estimate of the stellar mass can be used to constrain the equation of state at high densities. The value of the crust-superfluid coupling time  $\tau$  can be compared directly with theoretical estimates, while the value of  $\omega_0$  can be compared with the frequencies of expected internal modes.

2. Studies of X-ray Flux and Angular Velocity Correlations. In this approach, both a sequence of pulse arrival times and a corresponding sequence of X-ray flux determinations are obtained. As emphasized in § II, such a set of paired measurements is a crucial diagnostic tool for establishing the source of any torque fluctuations, since observation of a correlation between the flux and the rate of change of the angular velocity would indicate that the source of the torque fluctuations is external rather than internal. Moreover, the nature of this correlation could then be compared with the detailed predictions of accretion theory to test that theory. If correlations are adequately described by the theory, it would then be possible to distinguish between disk and spherical accretion. In the case of disk accretion, further analysis could lead to an estimate of the neutron star magnetic moment and could even provide constraints on the equation of state of neutron matter. The knowledge of the neutron star response function obtained from the power spectrum analysis is essential to carry out this second phase of analysis, since without knowing the stellar response, it is impossible to determine the torque by working backwards from the crustal angular velocity changes.

3. Searches for Individual Torque Events. In this type of study, one searches the pulse arrival times for relatively rare, very large pulse phase changes. If such events are found, the torque noise process has been at least partially resolved. By resolving the noise process, one can determine the sign distribution of the torque excursions, their characteristic rise and fall times, and their mean rate of occurrence as a function of size. This information can then be compared with the expected properties of accretion and internal torque fluctuations. Again, a knowledge of the neutron star response is essential.

## CURRENT STATUS

A total of 11 pointed observations of Vela X-1 were made by HEAO-1 during November and December of 1978. A further pointed observation of Vela X-1 was contributed by SAS-3 in January of 1979, after HEAO-1 pointing capability was lost. These observations were carefully arranged to allow us to construct a pulse phase power density spectrum of the type described in § IIb, with a minimum number of pointings. In addition, arrangements have been made to supplement this data set with several days of OSO-8 observations obtained earlier by the Goddard Space Flight Center X-ray group and HEAO-1 observations obtained by that group during May 1978. The Goddard Space Flight Center group are also contributing several days of OSO-8 observations of Her X-1 and HEAO-1 observations of Her X-1 during February and August 1978.

Some 10 hours of the Her X-1 data from HEAO-1 observations during February 1978 have been furnished to the guest investigators and have been analyzed by Boynton and Deeter. The torque noise power spectrum constructed for Her X-1 with this new data included is shown in Figure 6. The flat spectrum at low frequencies is the white torque noise indicated by the Uhuru data. The three highest frequency points are those obtained from the first HEAO-1 data. They are in the counting-noise-dominated part of the spectrum, but lie somewhat higher than expected for counting noise alone. This indicates that there are indeed pulse shape changes in Her X-1 on time scales of 10 minutes or so. Other evidence for such changes has been reported previously by the Goddard group.

Analysis programs have been developed over several months, and plans have been made to analyze rapidly the remaining observations as they become available.

It is a pleasure to acknowledge useful discussions with Paul Boynton, John Deeter, Steve Pravdo, Nick White, and Kent Wood.

## REFERENCES

- Becker, R. H.; Rothschild, R. E.; Boldt, E. A.; Holt, S. S., Pravdo, S. H.; Serlemitsos, P. J.; and Swank, J. H., 1978: *Ap. J.*, 179, p. 585.
- Boynton, P. E. and Deeter, J. E.; 1979: in *Compact Galactic X-Ray Sources*, Proc. of the Washington, Workshop on Observing Compact Objects, ed: F. K. Lamb and D. Pines (Physics Department, University of Illinois), p. 168.
- Elsner, R. F. and Lamb, F. K.; 1976: *Nature*, 262, p. 356.
- Ghosh, P. and Lamb, F. K.; 1978: *Ap. J. (Letters)*, 223, p. L83.
- Ghosh, P. and Lamb, F. K.; 1979a: *Ap. J.*, 232, p. 259.
- Ghosh, P. and Lamb, F. K.; 1979b: *Ap. J.*, 234, in press.
- Joss, P. C.; 1978: private communication.
- Lamb, F. K.; 1977: *Proc. 8th Texas Symp. Relativistic Ap.*, *Ann. Ny Acad. Sci.*, 302, p. 482.
- Lamb, F. K.; 1979: in *Compact Galactic X-Ray Sources*, Proc. of the Washington Workshop on Observing Compact Objects, ed: F. K. Lamb and D. Pines (Physics Department, University of Illinois), p. 143.
- Lamb, F. K.; Pethick, C. J.; and Pines, D.; 1973: *Ap. J.*, 184, p. 271.
- Lamb, F. K.; Pines, D.; and Shaham, J.; 1978: *Ap. J.*, 224, p. 969.
- Pandharipande, V. R.; Pines, D.; and Smith, R. A.; 1976: *Ap. J.*, 208, p. 550.
- Pringle, J. E. and Rees, M. J.; 1972: *Astr. Ap.*, 21, p. 1.

TABLE 1  
GOALS OF THE HEAO-1 TIMING EXPERIMENT

As a probe of neutron stars:

- Determine mass, radius, inertial, and magnetic moments
- Search for evidence of neutron superfluidity
- Determine ratio of inertial moments of crust and core
- Search for internal resonant modes
- Search for evidence of internal torque fluctuations

As a probe of accretion flows:

- Determine flow pattern (disk-fed or wind-fed)
- Test accretion theory quantitatively
- Investigate fluctuations in flows

TABLE 2  
POSSIBLE SOURCES OF TORQUE FLUCTUATIONS

External	Internal
Fluctuations in $\dot{M}$	Crustal fracture
Fluctuations in flow pattern	Vortex unpinning in crust
Flow reversals	Stochastic spin-up of superfluid core

TABLE 3  
COMPARISON OF CHOSEN SOURCES

Her X-1	Vela X-1
Detectable white torque noise is present	Evidence for torque noise with a strength $\sim 10^3$ that in Her X-1
Fast rotator	Slow rotator?
Disk-fed	Wind-fed?



TABLE 4  
METHOD OF DATA ANALYSIS

Power Spectrum Analysis

Confirm statistical description

Determine torque noise spectrum

Measure or constrain  $\tau$  and  $I_s/I_c$

- First evidence for superfluid in X-ray stars
- Compare  $\tau$  with theory
- Help choose correct equation of state

Measure or constrain  $\omega_0$

- Compare with theory

$\dot{P}$ /Flux Correlation Analysis

Establish character of torque noise (external or internal)

Construct observed  $\dot{P}(L)$  curves

- Flow pattern
- Test theory
- Determine magnetic moment
- Constrain  $M$ ,  $R$ ,  $I$

Pulse Shape Analysis

New evidence concerning pulse formation

Resolve Noise Process

Rise and fall times

Event size versus frequency

Event sign distribution

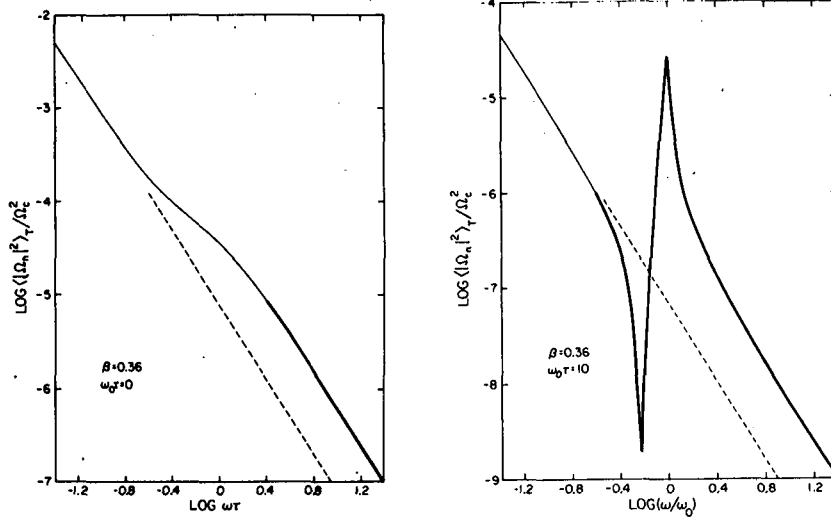


Figure 1. Power density spectra of fluctuations in the crustal angular velocity excited by white torque noise for (a) a neutron star with no internal modes and (b) a neutron star with a single internal mode. From Lamb, Pines, and Shaham (1978).

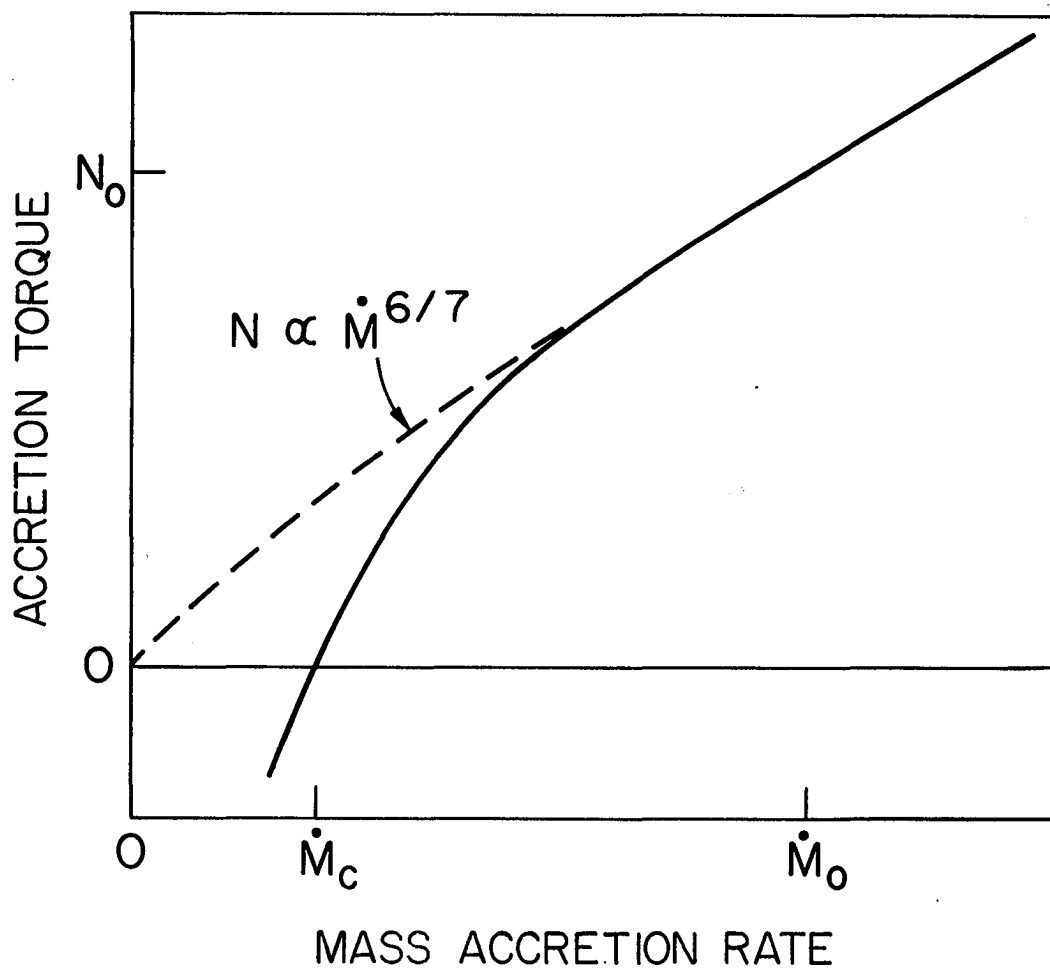


Figure 2. Torque curve predicted by disk accretion theory.  
From Lamb (1977).

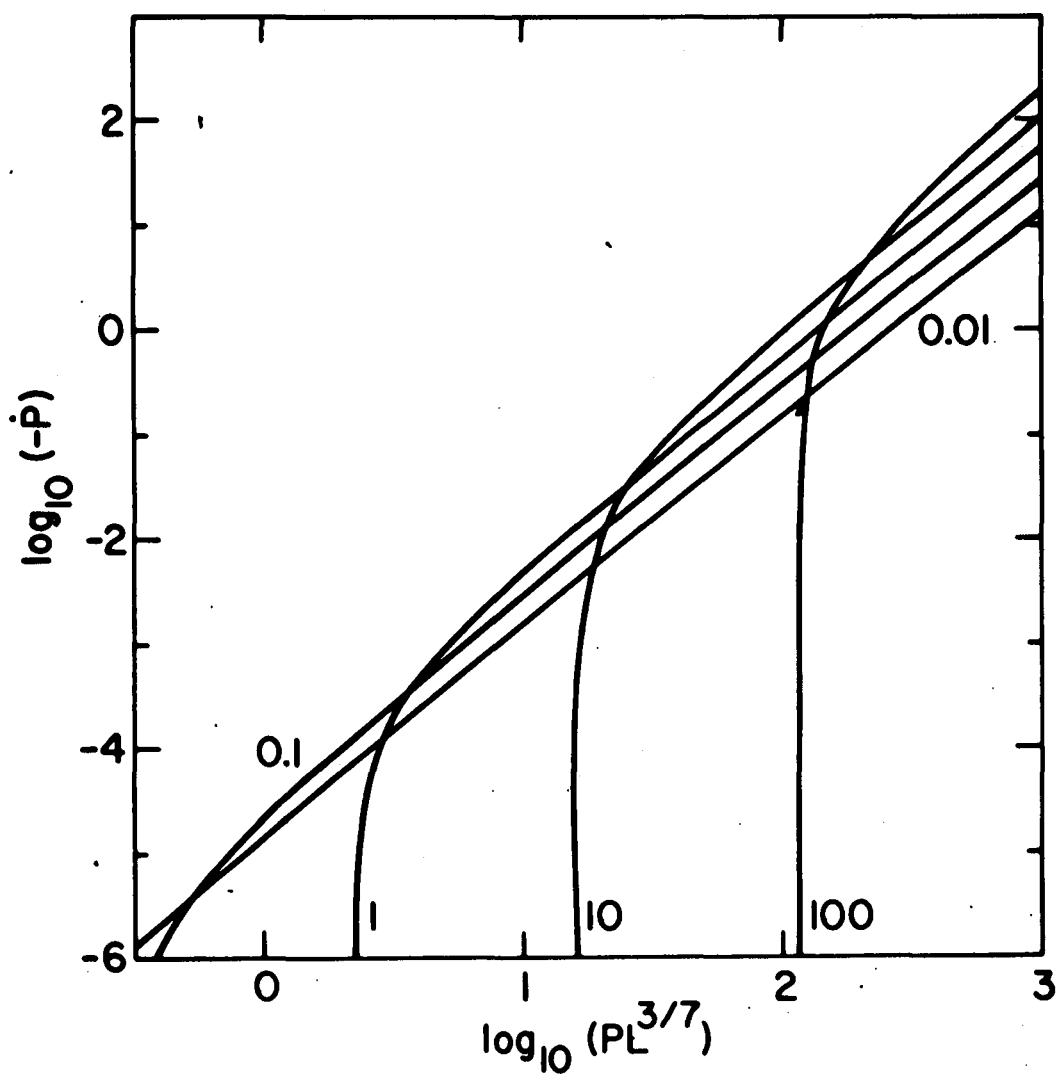


Figure 3. Spin-up curves for a neutron star with a constant effective moment of inertia and various magnetic moments, in units of  $10^{30}$  gauss cm<sup>3</sup>. From Ghosh and Lamb (1979b).

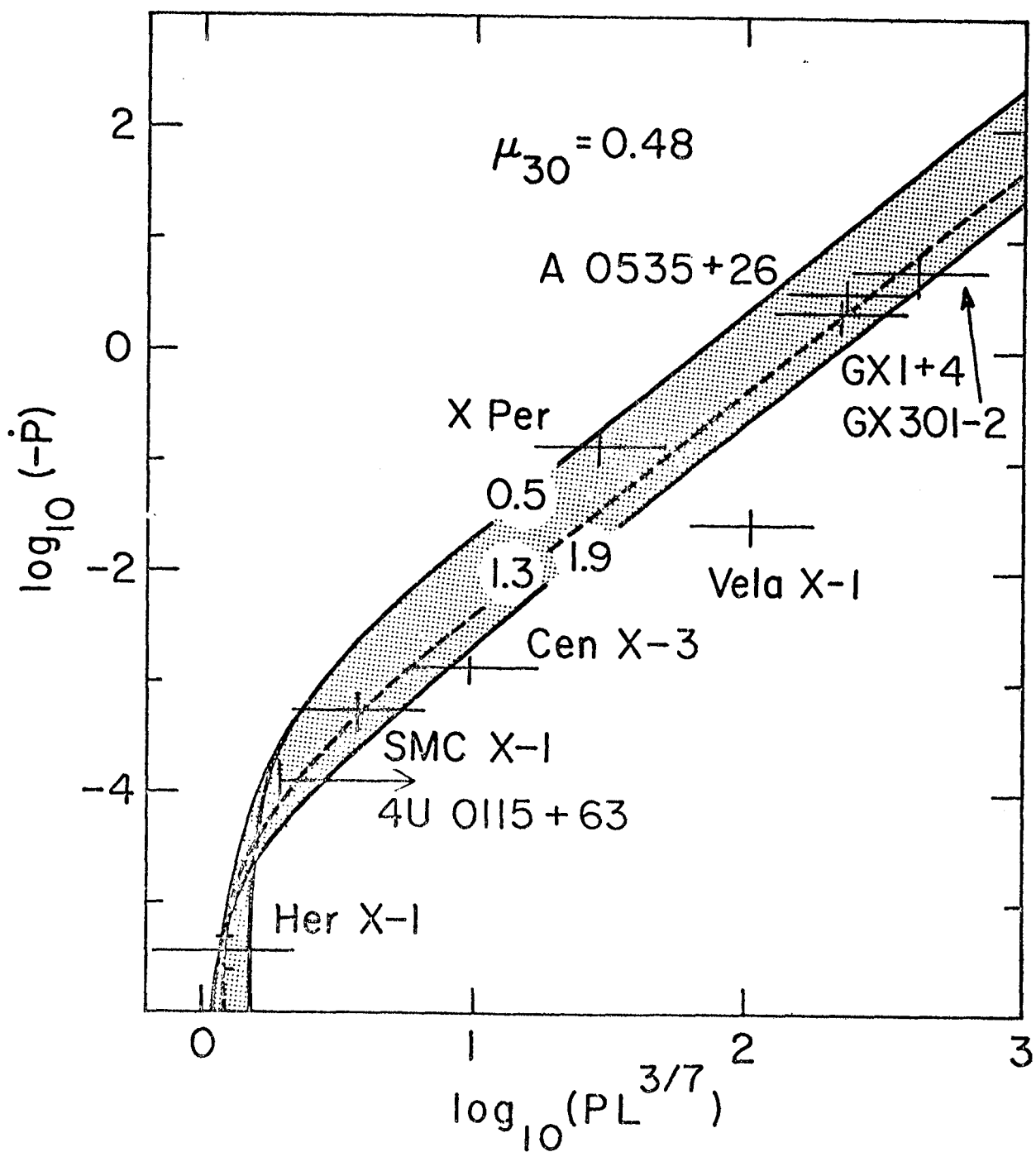


Figure 4. Spin-up curves for three neutron star masses, superimposed on the average values of  $-\dot{P}$  and  $PL^{3/7}$  for 9 sources. From Ghosh and Lamb (1979b).

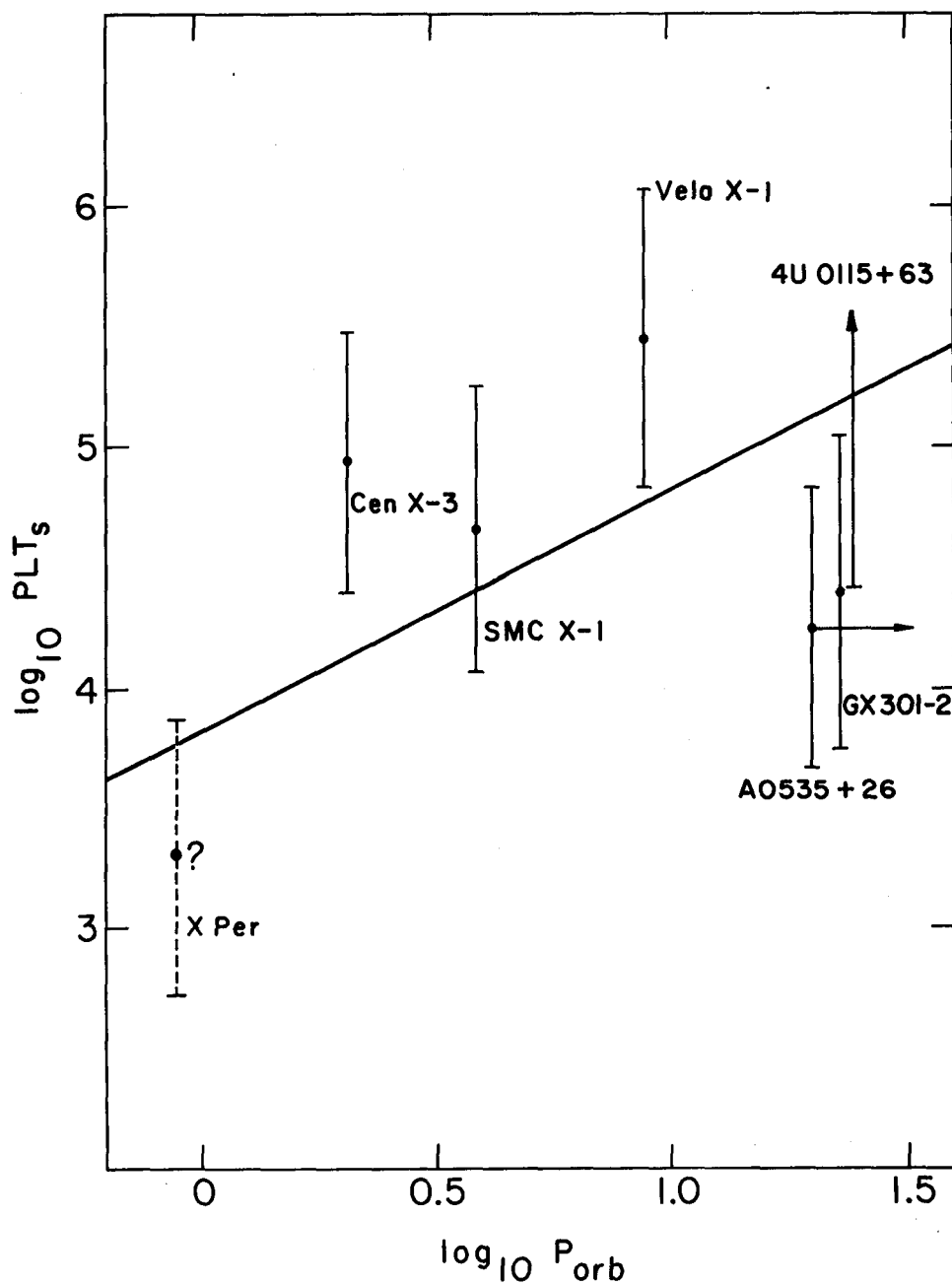


Figure 5. Observed values of  $\text{PLT}_s$  plotted against observed values of  $P_{\text{orb}}$  for 7 sources. The straight line is the theoretical relation expected for wind-fed sources under certain conditions.  
From Ghosh and Lamb (1979b).

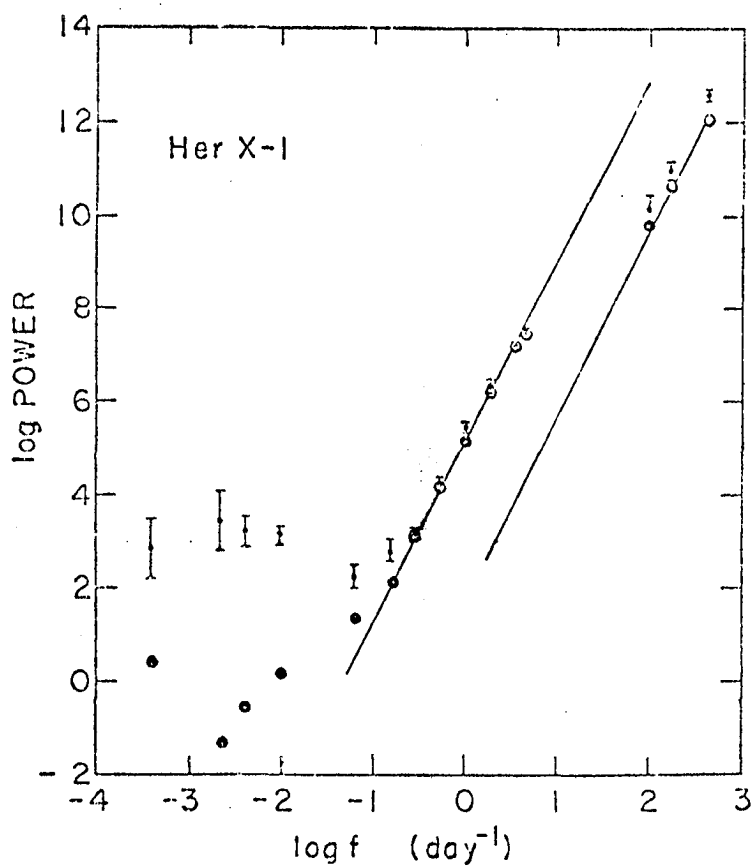


Figure 6. Power density spectrum of fluctuations in crustal angular accelerations in Her X-1, constructed from Uhuru and HEAO-1 A-2 data. From Boynton and Deeter (1979).

## X-RAY IRON-LINE EMISSION FROM THE SN 185 REMNANT

P. F. Winkler  
Middlebury College

Most of the results that we have been hearing about today are very recent ones. The story of the object which I would like to talk about begins quite a long time ago. The earliest supernova event which was recorded historically occurred in the year 185 AD; the chief point of the work which we carried out is to try to show that the supernova remnant RCW86 is in fact the remnant of this historical event.

This remnant has the galactic designation G315.4-2-3; the non-thermal radio source is known as MSH 14-63, and the optical filaments are designated RCW86. It is thought to be at a distance of about 2.5 kiloparsecs, determined by Westerlund (1969) who established its association with a group of OB stars at about that distance. Westerlund went on to suggest that the supernova was probably a type II event because of the association with early-type stars, which are generally believed to give rise to type II supernovae.

The association of this remnant with the supernova of 185 AD has long been suggested. Clark and Stephenson (1977) reviewed the evidence for this association, which I would characterize as good, but not certain. RCW 86 is the best candidate among four known supernova remnants in the vicinity of the historically recorded event.

The radio and optical appearances of this object are shown in Figure 1. The optical picture is from a broad-band red plate taken by Robert Kirshner and myself at the CTIO 4-m telescope. Superimposed on it are 5 GHz radio contours as measured by Caswell, Clark and Crawford (1975). The size of the radio shell is about 40 arc min which corresponds to a diameter of about 28 par sec at a distance of 2.5 kiloparsec. The optical nebulosity consists primarily of two groups of filaments, one at the north and another near the southwestern edge of the radio shell.

The situation in X-rays is that there is an X-ray source coincident with the supernova remnant RCW86 which was first discovered by Naranan, et al (1977) from the NRL experiment on the Apollo-Soyuz. It is very bright at about 1 keV. This was independently observed by the MIT OSO-7 experiment above 2 keV where it has a flux of about 7 Uhuru counts (Winkler 1978). This source has been tentatively identified with the supernova remnant, but its location near the galactic plane makes an identification based on positional coincidence alone less than positive.



The results I am reporting today make the identification much more definite. These are based on data from a 3-hour pointed observation of RCW86 with HEAO-1, carried out in March 1978. Data from the Medium-Energy Detectors of the A-2 experiment are shown in Figure 2. These are raw pulse-height data which have been untouched except for background subtraction. Attempts to fit the data points with a spectrum consisting only of a thermal continuum fail; but if we allow the computer to add a single line to the thermal spectrum, a successful fit is obtained. The statistical significance of the line is  $\geq 10\sigma$ . Furthermore, the line energy, left as an adjustable parameter in the fit, is fixed by the computer at 6.7 keV. This corresponds to K-line emission from highly ionized states of iron similar to lines which have been observed in other supernova remnants such as Cas A and Tycho. The thermal spectrum of lines plus continuum indicate that we are definitely observing hot plasma in this source and reinforces the identification of the X-ray source with the supernova remnant.

In Figure 3, we have the same spectrum which has now been unfolded through the response of the detector to give us an incident spectrum. One sees the iron line standing up very dramatically. The best-fit temperature here is 5.9 keV. If we assume that the hot plasma has been heated by a shock wave, then the shock velocity must be very high, about  $2000 \text{ km s}^{-1}$ . This indicates that the supernova remnant must be young, because if we run the picture backwards (just extrapolate backwards to when the supernova must have gone off) then the explosion occurred about 2000 years ago. We feel that this establishes the identification with the 185 AD event beyond all reasonable doubt.

Also shown in Figure 3 is the low-energy flux as determined by the NRL group. The remnant is very bright at about 1 keV and falls sharply at higher energies. It is impossible to fit all these data with a thermal model at a single temperature, which suggests that plasma components at more than one temperature are present in this remnant. The spectral parameters are summarized in Table 1.

The equivalent width in the iron line (a measure of the line strength relative to the continuum) is about 780 eV. This can be compared with what would be expected from a hot plasma with cosmic abundances. I have indicated the predicted equivalent width based on two models for a plasma at the measured temperature. The difference between the two predictions lies primarily in different choices for the iron abundance.

The iron line we observe falls within the range predicted by the models. This indicates that the iron abundance, assuming thermal equilibrium, is consistent with the cosmic abundance of iron.

We may interpret the X-ray emission above 2 keV within the context of the canonical blast-wave model, with a shock wave expanding outward, heating swept-up interstellar material, and producing X-rays. We obtain the results which are shown in Table 2 for the age, the density of the interstellar medium, and the energy required for the supernova explosion. Since the distance is somewhat uncertain, I have indicated how these parameters scale with distance. In the right hand column I have scaled these so that the explosion occurs in the year 185 AD. The results are similar to what is observed for other supernova remnants, except that the blast energy is somewhat higher than for most of the other cases in which it has been determined.

In summary, we first find that iron-line emission at 6.7 keV definitely stems from this source, which confirms that the X-ray source is indeed associated with the remnant. Second, the temperature measured from HEAO-1 is about 6 keV, (for the hard X-ray component at any rate) which requires a shock velocity of at least  $2000 \text{ km s}^{-1}$ . This indicates that the remnant must be a young one and leads to our conclusion that the identification with the 185 AD event is correct. And third, the equivalent width which we observe is consistent within the uncertainties with a cosmic iron abundance.

I would like to thank everyone involved in the HEAO project for the opportunity to participate as a guest investigator. In particular, I would like to thank Steve Pravdo, Rich Mushoteky, Elihu Boldt and the other members of the X-ray astronomy group at Goddard Space Flight Center with whom I collaborated on this work.

#### REFERENCES

- Bahcall, J. N. and Sarazin, C. L.: 1978, Ap. J., 219, 781.
- Caswell, J. L., Clark, D. H., and Crawford, D. F.: 1975, Australian J. Phys. Suppl. No. 37, 39.
- Clark, D. H. and Stephenson, F. R.: 1977, The Historical Supernovae, Oxford, Pergamon Press.
- Naranan, S., Shalman, S., Yentis, D., Fritz, G., and Friedman, H.: 1977, Ap. J. (Letters), 213, L53.
- Raymond, J. C. and Smith, B. W.: 1977, Ap. J. Suppl., 35, 419.
- Westerlund, B. E.: 1969, A. J., 74, 879.
- Winkler, P. F.: 1978, Ap. J., 221, 220.

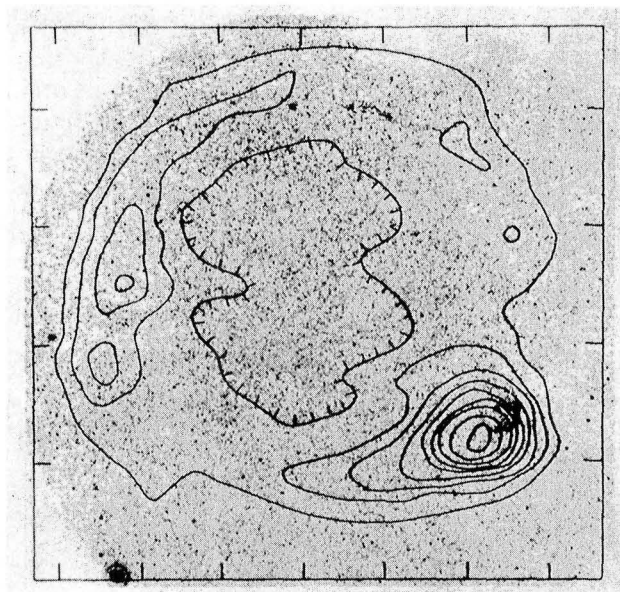


Figure 1. Radio contour map of MSH 14-63 - RCW 86  
(from Caswell, Clark and Crawford 1975)  
superimposed on a broad-band red 4-m plate.

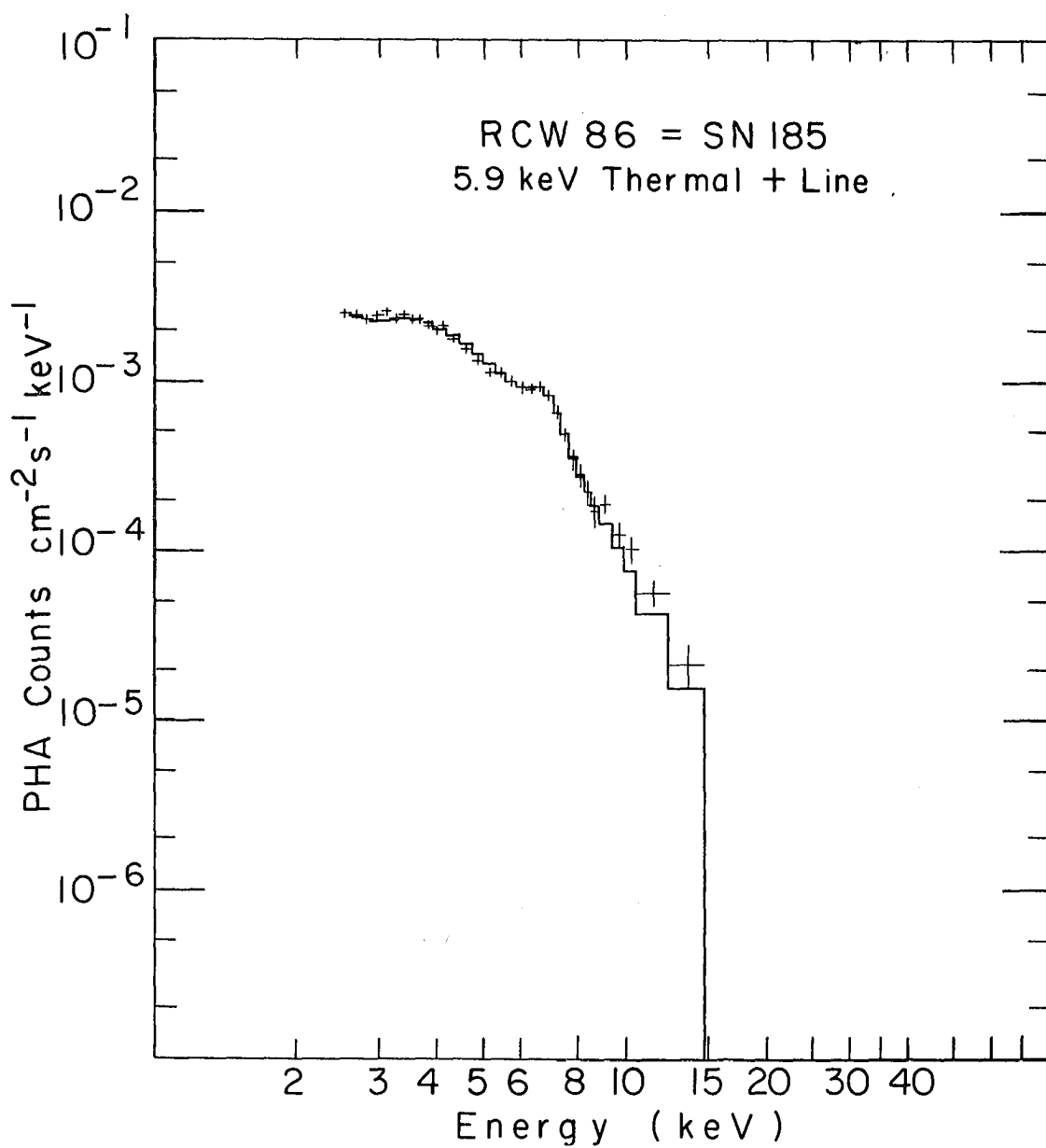


Figure 2. Raw pulse-height spectrum of RCW86 from HEAO A-2 Medium Energy Detectors. Solid line indicates best fit to the data.

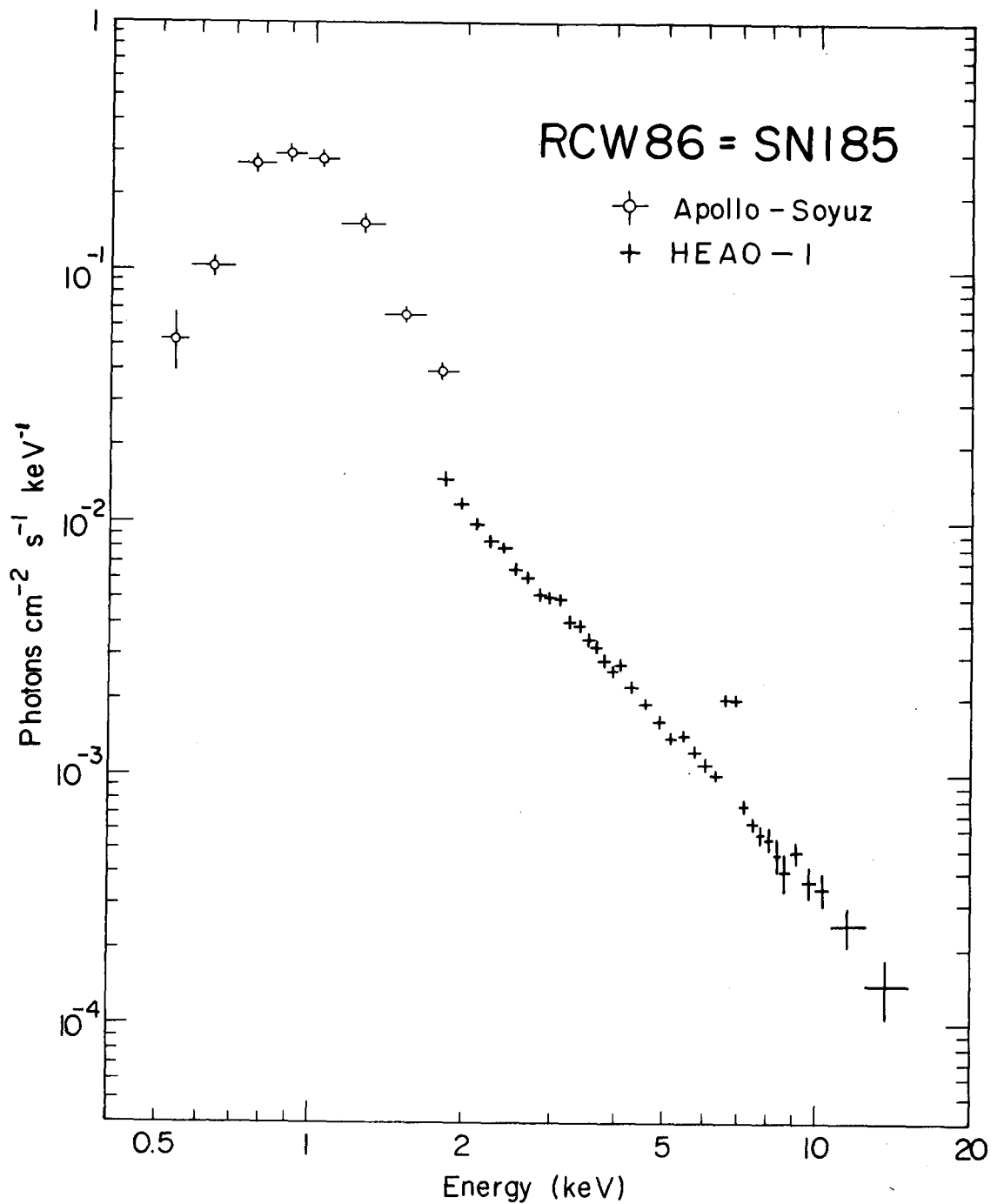


Figure 3. Deconvolved incident spectrum of RCW86. Apollo-Soyuz data are from Naranan et al. (1977); HEAO-1 is this work. Note strong line at 6.7 keV.

TABLE 1. G315.4-2.3 HEAO-1 (A-2) SPECTRUM

Continuum:	Thermal, $kT = 5.9$ keV Flux (2-10 keV) = $1.1 \times 10^{-10}$ ergs $\text{cm}^{-2} \text{s}^{-1}$ Additional Low-T Component (Apollo-Soyuz)
Line:	$\langle E \rangle = 6.75$ keV Flux = $6.7 \times 10^{-4}$ photons $\text{cm}^{-2} \text{s}^{-1}$ EW = 0.78 keV
Predicted EW (Cosmic Abundances):	
	Raymond and Smith (1977): 1.41 keV Bahcall and Sarazin: 0.74 keV

TABLE 2. G315.4-2.3 BLAST-WAVE MODEL

	General ( $d_* \equiv d/2.5$ kpc)	Age-Scaled
Age (Sedov)	$2900 d_*$	1793 years
Luminosity (2-10 keV)	$9.2 \times 10^{34} d_*^2$	$3.6 \times 10^{34}$ ergs $\text{s}^{-1}$
Density	$0.11 d_*^{-1/2}$	$0.14 \text{ cm}^{-3}$
Blast Energy	$2.5 \times 10^{51} d_*^{5/2}$	$0.8 \times 10^{51}$ ergs
Swept-Up Mass	$34 d_*^{5.2}$	$10 M_\odot$

## OPTICAL IDENTIFICATION AND SPECTROSCOPY OF X-RAY SOURCES PRECISELY POSITIONED WITH A-3

Richard Griffiths  
Harvard/Smithsonian Astrophysical Observatory

As we heard in this morning's review by Roger Doxsey and Dan Schwartz, the main purpose of the scanning modulation collimator on HEAO-1 is in the optical identification of X-ray sources by means of precise positioning. Figure 1 shows a list of those optical observers who collaborated with us in obtaining optical identifications. In particular I would like to draw your attention to the work of Phil Charles and John Thorstensen of Berkeley, who have observed on multiple occasions at Lick and at Cerro-Tololo Inter-American Observatory in Chile and have obtained several galactic counterparts. The same is true of Josh Grindlay working with Claude Canizares and Jeff McClintock of MIT, also working at the CTIO and partly at Kitt Peak. Bruce Margon of UCLA has also observed at Lick on a number of occasions in collaboration with us, Andrew Wilson, Martin Ward, and others at the Anglo-Australian telescope and also at Kitt Peak. We have collaborated with optical observers at all major telescopes in the southern hemisphere, that is telescopes in the 4 meter class, viz. those at Cerro-Tololo, the Anglo-Australian telescope, and the European Southern Observatory (also in Chile). In the northern hemisphere we collaborated with people largely at Lick, Kitt Peak, and partly at the Royan Greenwich Observatory.

Rather than try to summarize the optical identifications that we have made so far, I would rather describe a couple of the more interesting galactic identifications, 4U2129+47 and 2A0311-227. The error box for the 4U source is shown in Figure 2: the plates were taken at Lick observatory by Charles and Thorstensen. You will immediately notice that the object indicated here has an ultraviolet excess (these are the blue and ultraviolet plates). Further plates established that the indicated star is in fact variable and monitoring the source with the Lick 3 meter reflector and image tube scanner for 5 hours on September 8 last year clearly resulted in a sinusoidal type of modulation, establishing it as a binary with a 5.2 hour period (Fig. 4). Folding the photographic photometry data with this period, the same result is apparent with a peak-to-peak amplitude of just over 1 magnitude in B. A typical spectrum from the image tube scanner is shown in Figure 3. The object has a rather blue continuum with the characteristic emission lines from a galactic X-ray source; that is, helium II and the CIII/NIII blend. The optical light curve in Figure 4 is interpreted as due to the changing aspect of a late type star which is heated by the X-ray emission from the compact object, that is, the neutron star or white dwarf nearby.

The finding chart for 2A0311-227 is shown in Figure 5. The error box prefers the indicated star although we could not absolutely rule out two others. The indicated one did in fact turn out to be the counterpart. Lola Chaisson assembled the long term light curve from the Harvard plate stacks, and this is shown in Figure 6. There is clearly variability during the years plotted, with a peak at 15th magnitude and a minimum at about 17th. There was some difficulty in assembling this light curve because of proximity of the star just 18 arc sec to the west of the candidate. A spectrum of the candidate taken at the Anglo-Australian telescope late last year (78) (Fig. 7) shows that it is in fact one of the richest emission line spectra of any galactic X-ray source with the exception of AM Herculis, with which it is in fact identical. The Balmer series of hydrogen is seen very strongly in emission from  $H\alpha$  down to  $H9$  and 10 with a strong Balmer continuum. There are also lines of helium I, carbon II and the usual CIII/NIII blend. What is most unusual about this spectrum is the ratio (the Balmer decrement) of  $H\alpha:H\beta:H\gamma$ .  $H\alpha$  is normally 2 or 3 times as strong as  $H\beta$ . This anomaly has been explained in AM Herculis and is likewise explicable in 2A 0311-227 as due to collisional processes in a plasma with electron densities of approximately  $10^{13} \text{ cm}^{-3}$  in a region near the accretion column of a magnetic white dwarf. AM Herculis has of course been studied optically over the past two years and it has been established to be a magnetic white dwarf in a binary system.

Figure 8 shows the first extragalactic object, viz. NGC 526a which was also observed at the Anglo-Australian telescope (Fig. 9) and appears to be a Type 1 Seyfert galaxy, based on the fact that the  $H\alpha$  emission line has broad wings. It also has forbidden oxygen III lines and  $H\beta$  is relatively weak. Figure 10 is the spectrum of another Seyfert for which the X-ray source has been positioned by HEAO A-3. In fact, we thought it was a Seyfert nucleus in an elliptical galaxy since it has absorption lines characteristic of an elliptical but plate material from CTIO by Mark Philips has shown that it is, in fact, an SO galaxy.

Lastly, I am going to talk about Parkes 2155-304. Figure 11 shows the only A3 error box inside the NRL error box which Herb Friedman mentioned this morning. We asked Hjellming and others at the Very Large Array to obtain an improved position for the radio source which was initially catalogued approximately 30 arc sec north of the stellar object shown here. The refined position from the VLA shows the radio source to be coincident with this 14th magnitude optical object to within approximately 3 arc sec. We also collaborated with Santiago Tapia of the University of Arizona on this object to show that the object is polarized; polarization, in fact, varying as a function of time from about 7 percent in the blue in October 1978 down to about 3 percent in December (Fig. 11). Tapia also obtained a red plate of the object which shows diffuse emission, which you can just see on either side of this optical object (Fig. 11, right), but this diffuse image is not visible on the UK Schmidt



blue plate (left). This diffuse emission on the red plate is apparent when you compare it with the diffraction spikes which are barely visible on the two stars at the lower right. The long term light curve of this object, again assembled by Lola Chaisson, shows variability which is characteristic of BL Lac objects. The problem with BL Lac objects, however, is that it is very difficult to observe spectroscopic optical features. Figure 13 is a spectrum obtained on the 3.9 m AAT with integration time of about half an hour and showed nothing in the way of either emission or absorption features. Phil Charles may, however, have been more successful. He claims to have seen forbidden oxygen III in this spectrum, at a red shift of about .17. If the red shift is confirmed, this makes it one of the most luminous X-ray sources yet observed at approximately  $10^{47}$  ergs/sec. The overall spectrum is shown on the final slide (Fig. 14) from the radio through to the X-ray region. Most of the data points were taken around November-December last year, with HEAO-A-2 data from November 1977. It is tempting to fit the overall spectrum with one smooth curve but until we get more data filling in the emission regions it is difficult to establish an overall mechanism.

<u>OBSERVER</u>	<u>INSTITUTE</u>	<u>OBSERVATORY</u>
P.A. Charles J. Thorstensen	University of California, Berkeley	Lick, CTIO
D. Crampton	Dominion Astrophysical Observatory	DAO
M. Davis J. Huchra	Center for Astrophysics	SAO (Mt. Hopkins)
J. Grindlay C. Canizares J. McClintock	Center for Astrophysics M.I.T.	CTIO, KPNO, McGraw Hill
A. Longmore D. Malin	Royal Observatory, Edinburgh	UK Schmidt (Australia)
W. Liller	Center for Astrophysics	CTIO
B. Margon	University of California, Los Angeles	Lick
S. Mayo J. Whelan B.A. Cooke I. McHardy	Institute of Astronomy University of Leicester	AAT, RGO
P. Murdin	Anglo-Australian Observatory	AAT
S. Tapia	University of Arizona	Steward Observatory
R.M. Thomas J. Greenhill D. Watts	University of Tasmania	AAT
J. van Paradijs	MIT, University of Amsterdam	ESO
M. Ward J.C. Blades A.S. Wilson	Institute of Astronomy Anglo-Australian Observatory University of Maryland	AAT, Mt. Stromlo KPNO

Figure 1



Figure 2

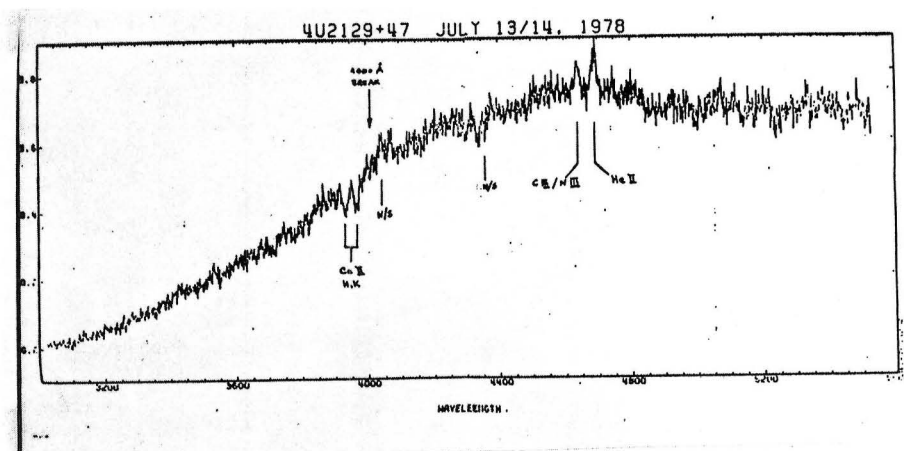


Figure 3

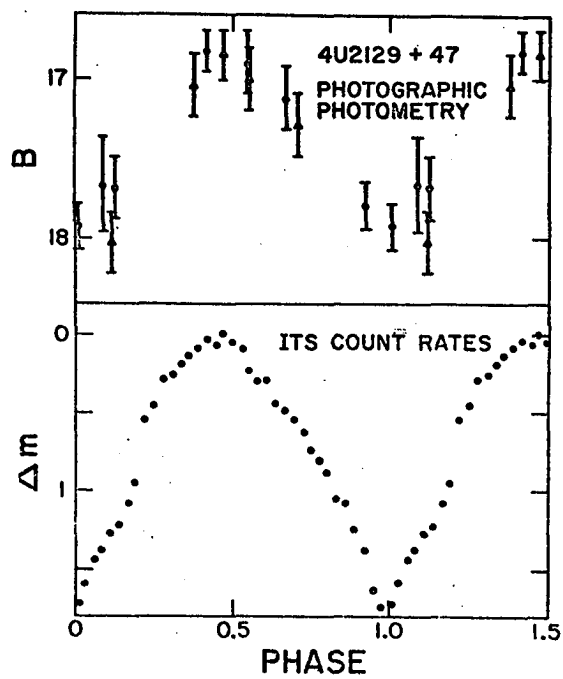


Figure 4

**2A 0311-227**

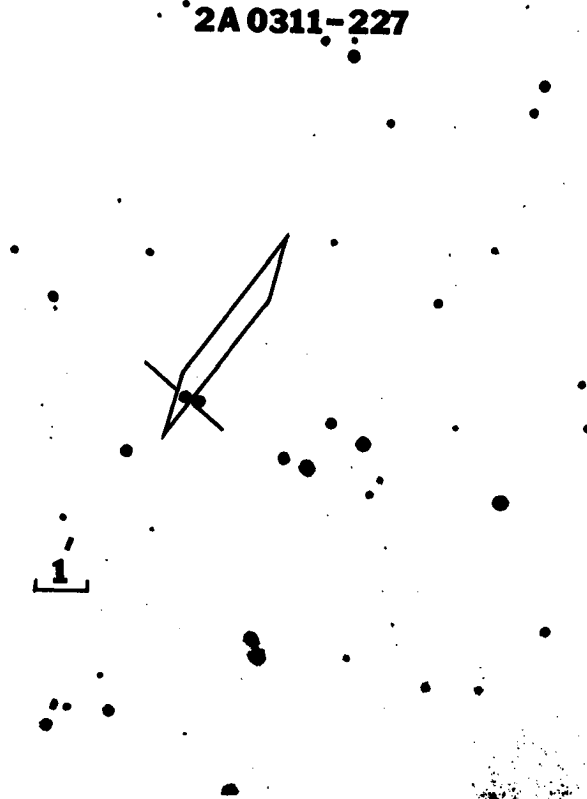


Figure 5



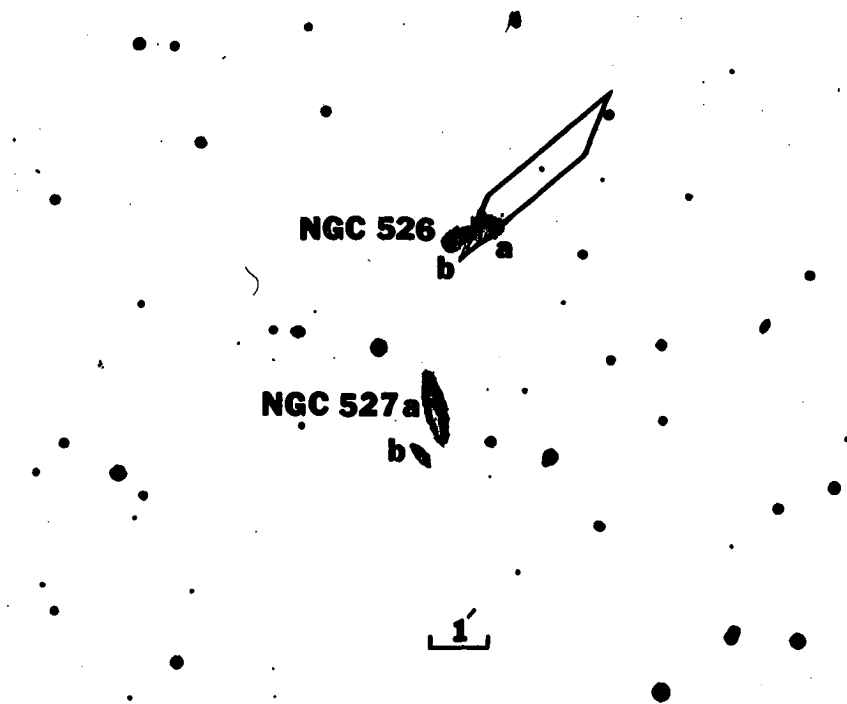


Figure 8

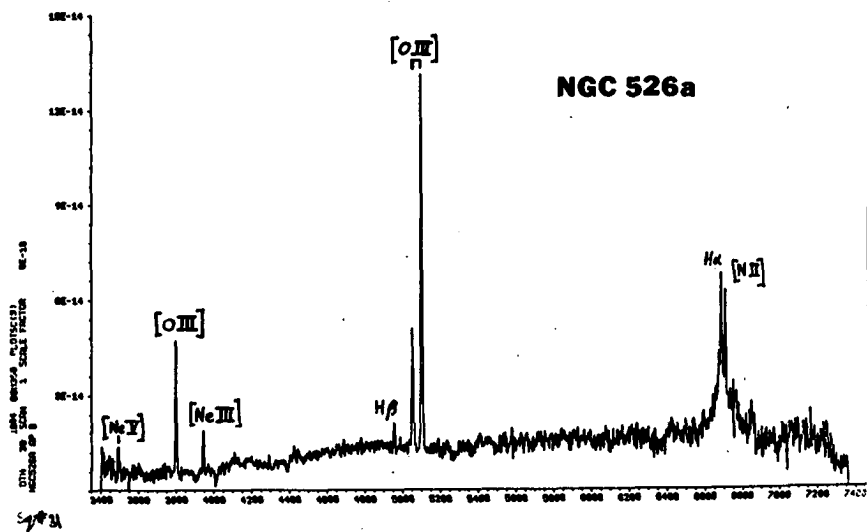


Figure 9

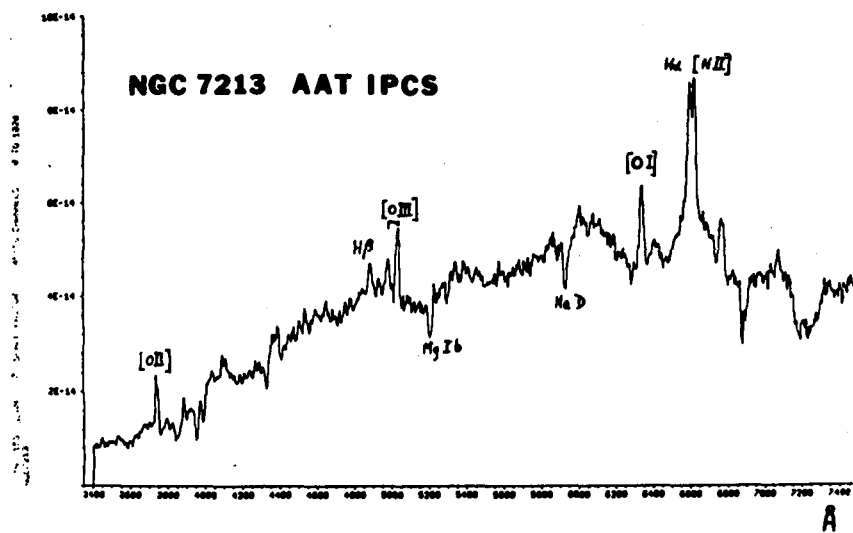


Figure 10

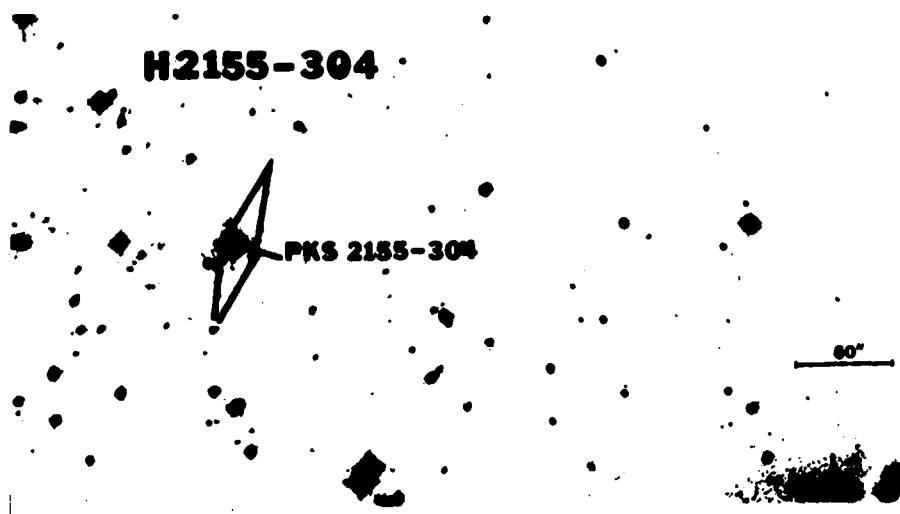


Figure 11

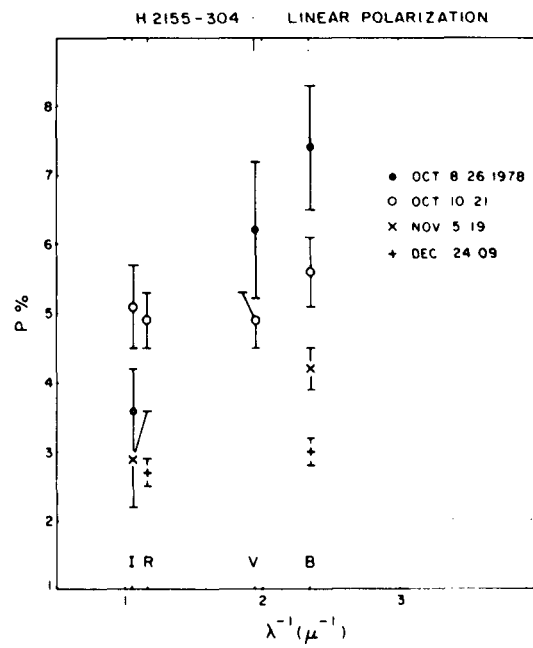


Figure 12

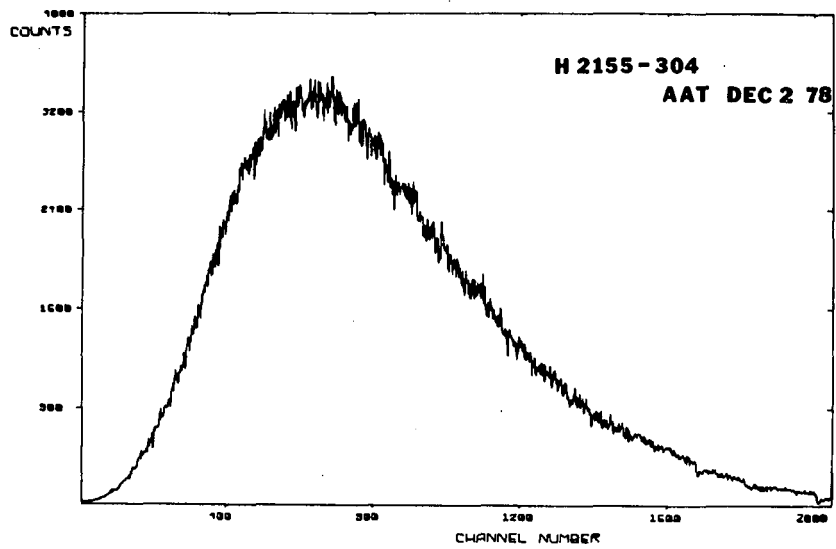


Figure 13

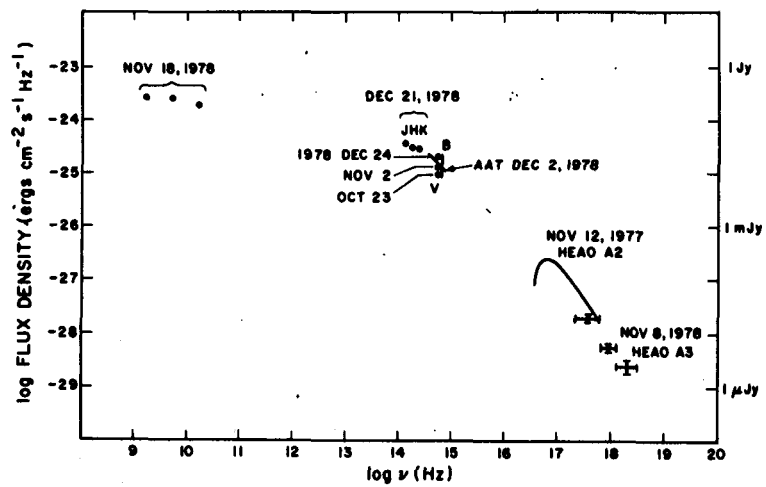


Figure 14



## SESSION III

### RESULTS FROM HEAO-2 NON-IMAGING INSTRUMENTS

# A HIGH ENERGY ASTRONOMY OVERVIEW

Riccardo Giacconi  
Harvard/Smithsonian Astrophysical Observatory

## INTRODUCTION

The growth of extrasolar X-ray astronomy in the years since the discovery of the first X-ray star has provided one of the most exciting new windows to study high energy phenomena in the universe. As the instrumentation grew in sophistication and sensitivity from the very modest instruments carried aloft by short duration rockets, to dedicated orbiting X-ray observatories — first, of the Uhuru class, and finally of the HEAO-1 size, hundreds of galactic sources and many tens of the nearest extragalactic objects in each class were detected in X-rays (Fig. 1). As the body of observational data grew, it became apparent that X-ray observations revealed to us new phenomena or unsuspected aspects of known objects.

To mention only a few of the many results, the discovery of binary X-ray sources containing a collapsed companion has permitted us to measure, for the first time directly, the mass of neutron stars and to obtain the strongest experimental evidence to date for the existence of black holes. The discovery of the intergalactic medium through the detection of thermal bremsstrahlung emission from intracluster gas clearly demonstrated the unique role of X-ray observations in studying a previously undetected component of the universe containing as much mass as represented by all other known objects.

As exciting and scientifically rewarding as this progress was for many of us it fell far short of achieving the full potential of X-ray astronomy in the study of the more common galactic objects, such as main sequence stars, as well as in the study of objects at cosmological distances.

In order to achieve these aims, a radical improvement in instrumentation was necessary — something comparable to the step taken in visible light astronomy going from Tycho to Galileo.

That grazing incidence X-ray telescopes could in fact provide the means for this radical improvement had been clear to some of us since 1960 when I published with Bruno Rossi an article pointing out the great advantages of using this technique in the study of celestial objects. The fact that, although designs for microscopes had existed since the study by Wolter in 1952 (Fig. 2), no such device had ever been realized, coupled with the fact that no X-ray sources had yet been discovered, may help explain the lack of overwhelming enthusiasm our proposal

received at the time. It took approximately 8 years of laboratory developments of telescopes of increasing collecting area and resolution to obtain in 1968 devices suitable for the study of our nearest star: the Sun. Although my first proposal for a large (1.2 m) X-ray telescope to study the stars was made to NASA in 1963, it took the clear demonstration of the capabilities of this technique, shown in Figure 3, to convince NASA to proceed. A study was undertaken under NASA sponsorship for the use of an X-ray telescope in 1968 by groups at Columbia, Goddard Space Flight Center, MIT, and by my own group now at the Harvard-Smithsonian Center for Astrophysics. We formed a consortium in 1970 to successfully propose an integrated X-ray astronomy observatory, centered on the use of an X-ray telescope as part of the HEAO program. Notwithstanding the severe difficulties that draconian fiscal cuts imposed on the program, and the consequent reduction in experimental capabilities, we succeeded in placing in orbit on November 13, 1978 the most advanced X-ray astronomy facility ever flown. The radical improvement in technical approach can be appreciated if one considers that the thousand-fold gain of sensitivity with respect to the very largest arrays of counters ever flown was achieved with a mirror collecting area only one-half as large as that of the Uhuru detectors.

Such qualitative improvements in observational capabilities occur but rarely in science and it is indeed a privilege to be part of this program and to share with you the preliminary findings of the Einstein Observatory.

In a project of this magnitude credits should go to literally hundreds of people in government centers, industry and academic institutions. Although I cannot even begin to do this properly, I would like to emphasize the sense of obligation that all of the scientists most directly involved in the program feel. Although carried out as a principal investigator experiment, the Einstein Observatory has assumed a national significance; we have therefore waived our rights in the matter of observing time and data to permit an ever increasing share of the scientific results to go to investigators in other institutions from all over the world. In the first 5 months of the mission, 150 guest investigator proposals have been approved and are being implemented.

#### THE EINSTEIN OBSERVATORY

The observatory (Fig. 4) consists of a 0.6 m X-ray telescope, an optical bench, a lazy Susan capable of positioning cameras or spectrometers at the focus, an attitude control system to point us in the sky and a spacecraft to house it, power it and transmit data to the ground receiving stations. The project was carried out under MSFC management; TRW designed and built the spacecraft; AS&E was responsible for many of the observatory common instruments and integration. Perkin-Elmer built the mirror. I will not go into details of the instrumentation which

will appear in the June issue of the Astrophysical Journal; I will only recognize some of the great technical feats which we tend now to take for granted:

- 1) The development of the largest and best X-ray telescope ever built: a 0.6 m, 3.5 arc sec FWHM resolution telescope in which Leon VanSpeybroeck, of CFA, played such a key role (Fig. 5).
- 2) The development of a high resolution X-ray TV camera at CFA, aided by the University of Leicester (England) group.
- 3) The development of a large format IPC detector.
- 4) The development of transmission gratings by the University of Utrecht group.
- 5) The development of a cryogenically-cooled solid state spectrometer by Goddard Space Flight Center.
- 6) The development of a high resolution Bragg crystal spectrometer by MIT.
- 7) The development of a sophisticated software system, including interactive image displays, which allows us to reduce and analyze data in near real time.

Each day the Einstein Observatory is pointed on the average to 10 different fields. In the first 5 months of the mission some 1500 different fields have been examined; about half of them with imaging cameras. In each field there is at least one source (the object pointed at) but more often several. More than 1500 X-ray sources have therefore been studied with the Einstein Observatory, most of them previously unknown.

The sources range in intrinsic luminosity from the weakest X-ray sources ever detected in our own galaxy at  $10^{27}$  erg sec<sup>-1</sup> in the 0.1 to 3 keV range to the most luminous X-ray objects, the very distant quasars, at  $10^{47}$  erg sec<sup>-1</sup>. The diversity of physical conditions and objects represented in these two decades of intrinsic luminosity is as great as found in all of astronomy and soon it will be almost impossible to give an overall review of our findings.

In dealing with the subject I have therefore chosen to highlight some representative topics.

## STARS AND STAR ASSOCIATIONS

Among the first delightful surprises of the Einstein Observatory returns, the discovery of X-ray emission from O-B associations is certainly noteworthy. The nature of the observations can be exemplified by the picture of Eta Carinae obtained with the IPC (Fig. 6). Eta Carinae had been known as a weak X-ray source possibly coincident with a supernova remnant, which had been claimed to exist in the region — its relation to the object Eta Carinae itself being unclear. Figure 6 shows no evidence of a SN, but a number of discrete sources in the field accompanied by diffuse emission. One source coincides with the object Eta Carinae, others with a Wolf-Rayet star and O stars. The dark lanes so prominent in visible light can be seen in the X-ray image as well, indicating that the source of the X-ray diffused emission is at the same location as the optical emission, possibly as a result of an ancient SN explosion. When we observe this field with the HRI, we can see greater details of the emission from each source (Fig. 7).

Eta Carinae is a very strange object whose nature is not fully understood. It has been classified as a supernova because it underwent in the 1840's an outburst which made it one of the most luminous objects in the sky. However, the maximum of light lasted for about 20 years and did not at all resemble an SN. Today Eta Carinae is the strongest IR source in the sky. If its radiation is interpreted as coming from a single star, this star would have to be one of the most massive objects in our galaxy. Fred Seward, who has been analyzing this field, finds that the X-ray emission from the O stars in the field is consistent with a point; but that from Eta Carinae is extended. We may be seeing the results of the blast of 1840, as well as the object itself behind the obscuring dust and gas cloud (Fig. 8). The fact that severe upper limits can be placed on the size of the emission region of the O stars puts into question models for X-ray emission in which the emission is due to stellar wind collision with the surrounding medium. Models which invoke a compact object orbiting the O star and accreting from it have been suggested. The small intrinsic luminosity  $10^{+30}$  erg sec $^{-1}$  of these objects, as compared to the classical binaries emission at  $10^{38}$  would be due to the different state of evolution of the primary. As the primary evolves from the main sequence onto the supergiant branch, gas accretion and hence X-ray emission would increase. Although the sample is still small, there is no correlation between X-ray emission and evolutionary state of the O and B stars observed. This then leaves us with the possibility that what we are observing is coronal emission. This is not a trivial finding in that it does not fit well in the current picture on the energy transport mechanisms in the interior of stars. To transport energy from the center of a star to the cooler outer region convection and radiation can be invoked. Noise associated with convection is thought to be responsible for the formation of coronas. Convection occurs efficiently, however, only under particular conditions which depend on

the composition and evolutionary state of a star. In a simple picture which has been extremely successful in explaining qualitative characteristics of stars, it was understood that stars earlier than F5 would not sustain convection. This explained the sharp change in rotation velocity around F5. Stars later than F5 have coronas and extended fields which interact with the surrounding medium to slow down rotation while earlier stars would not. Stars earlier than F5 are known to produce radiation driven winds which were thought to be cool. The only possibility for X-ray emission under these conditions would be thermalization of the wind by interaction with the interstellar medium creating a bubble of large dimension. Such simple theories were already having difficulty due to the findings of solar research as well as hints of hot winds in early stars from optical and UV studies.

With Einstein the discrepancies are made much more acute due to the observation not only of F2, F0, A and B stars, but O stars as mentioned above. In fact, one can consider that X-ray observations of coronas from main sequence stars will form the new foundation on which theories will have to be recast. It is an amusing turn of events that with this most powerful of the extrasolar X-ray observatories, we may end up learning much about stars like our own Sun.

An interesting speculation is whether OB associations not only in Eta Carinae, but in Cyg and Orion as well, appearing to contain bright X-ray sources may be connected with events such as shedding of magnetic fields and angular momentum characterizing the birth of stars.

Ultimately, Vaiana and others at CFA are engaged in constructing the X-ray equivalent of an H-R diagram which hopefully will contribute significantly to our understanding of stellar evolutionary processes.

## SUPERNOVAS AND PULSARS

If we turn now from stars being born to the results of stellar collapse, a different and interesting aspect of the Einstein Observatory research is found.

First, observe the classical pulsars in Crab and in Vela (Fig. 9). The emission from the Crab pulsar, which is being studied by Tananbaum, can be clearly separated in the image from that of the surrounding nebula. The pulsar emission is observed to pulse at the well-known 33 m sec period. We are in the process of assessing the presence of any non-pulsed component which may be due to black body emission. High energy particles accelerated in the pulsar and streaming in the surrounding magnetic field presumably give rise by synchrotron radiation to the main filament which we see at the NE. This filament coincides with the main filament observed in polarized light. It is puzzling that the region of maximum X-ray emission in the nebula should not be symmetric with

respect to the pulsar. A similar picture is found by Harnden for the Vela pulsar with two main differences. No pulsations are observed at the 1 percent level and the source of X-ray emission centered on the pulsar appears extended; we have no ready explanation for this phenomenon.

The usefulness of the imaging capabilities of the Einstein mission is clearly demonstrated by the X-ray picture of other supernova remnants, which are being analyzed by groups led by Pye, Gorenstein and Murray. Figures 10, 11, and 12 show SN 1006, Tycho and Cas A. The steep gradient of the X-ray emission propagation of a shock from the explosion itself. The detailed filamentary structures observed in Cas A correspond to the evaporation of material heated within the shock from fragments of the stellar envelope flung out in the explosion. Spectral measurements with the solid state spectrometer of GSFC detect the presence of Fe, Mg, S, Ca, Argon, etc., with Fe abundance currently estimated to be twice solar.

Although it is widely believed that the enrichment of low Z materials occurs in the interior of the stars, and that SN explosions are the means of injection of the enriched material in the interstellar medium to form new generations of stars, here we appear to be witnessing the actual mechanism by which the material is dispersed. It is quite puzzling that no pulsar is detected near the center of these remnants. Current knowledge of pulsar velocities predicts that the pulsar cannot have moved far from the center of these historical supernovas. Current theories on cooling rates of supernovas also predict that the pulsars should retain temperatures of a million degrees at the present epoch. Black body emission from such an object would be readily observed with Einstein instruments. Their absence could be explained in one of two ways: either pulsars are not always formed as the residue of SN's, or they cool faster than expected. The first explanation further worsens the problem of explaining the large number of pulsars observed, in view of the relatively low frequency of SN explosions. The second requires new cooling mechanisms, such as pion cooling, to play an important role and requires substantial revisions of our theoretical picture of the constitution of a pulsar. The observational program of SN research with Einstein has just begun. Even so, the observations to date include the detection of the remnants of the 14 known supernovas in the large Magellanic Cloud which have been observed to have higher average flux than supernova remnants in our own galaxy by the Columbia group. The study of the characteristic of supernovas phenomena for stars evolved in different conditions of galactic composition and evolution promises to be extremely interesting.

## BURSTERS AND GLOBULAR CLUSTERS

The discovery of X-ray bursts by J. Grindlay and H. Gursky has opened one of the exciting new chapters of X-ray astronomy in recent years. Their relation to globular cluster sources and the nature of the underlying system have not yet been fully resolved. On the one hand, the explanation that they are low mass binary systems containing neutron stars explains conveniently many of the observational phenomena; on the other hand, their binary nature has not been directly observed. Models invoking accretion onto massive black holes arising from collapse of cluster cores have difficulty in explaining sources outside of globular clusters and may be difficult to reconcile with some of the optical data on the candidate counterparts. It is hoped that detailed measurement of the position of such sources with respect to the center of the globular cluster gravitational potential well may lead to conclusive evidence in favor of one or the other model. Figure 13 shows how a globular cluster burst source appears to Einstein in four successive 2.5 min exposures of Terzan 2. The identification of the steady source, with the burst source and with the globular cluster which had been suggested by Grindlay, is clearly established. Some eight additional cluster sources have been examined. Most of the X-ray sources appear to cluster within 1 or 2 arc sec of the center (Fig. 14) with one exception, NGC-1851 which is found at 7 arc sec from the center. Although it is too early to fully evaluate systematic and statistical errors and draw strong conclusions on the mass limits for the sources, it is clear that X-ray observations have the potential of probing in detail the mysterious central region of these star clusters.

### M-31

Einstein observations have been extended to galactic X-ray sources in M-31. Three IPC exposures are necessary to cover the entire galaxy and 1 HRI exposure of the center has also been obtained. The X-ray source M-31 which at 1 UFU was approximately the limit of detection for previous survey, dissolves into 70 or more discrete sources (Figs. 15 and 16). The optical galactic center appears to be an X-ray source at approximately  $10^{37}$  erg sec<sup>-1</sup>, and the remainder of the sources are presumably supernova remnants, classical binary X-ray source or globular clusters. (In fact, 4 sources have already been identified with globular clusters and several others with bright optical counterparts which may turn out to be classical binaries containing a supergiant.) Their division in galactic arms and bulge sources is much more clearly revealed than in our own galaxy. Leon VanSpeybroeck has undertaken detailed studies on the relation of X-ray source formations to the evolutionary and dynamical history of different galactic settings.



## VIRGO CLUSTER

Weak external galaxies emitting as little as  $4 \times 10^{38}$  erg sec<sup>-1</sup> have been detected with Einstein at distances as large as 20 Mpc. This means that a study of galaxy morphology versus creation of strong X-ray emitting sources is quite feasible and can be carried out both by studying individual galaxies in clusters where one can observe many types of objects within a single field, and by studying field galaxies whose emission would be free from obscuring contributory effects due to gas in the cluster. The second approach is that carried out in the deep surveys and the first has been initiated by W. Forman in the detailed study of the Virgo Cluster. Figure 17 shows an X-ray isointensity contour super-imposed on a portion of the Virgo Cluster containing M-86 and M-84. In addition to a diffuse emission from the cluster gas gradually decreasing as we move away from M-87, we see emission arising from around the giant elliptical galaxies M-84 and M-86 as well as from a narrow emission line galaxy (very similar to NGC-2992) and from a tidally disrupted spiral.

It is clear that the emission about M-86 ( $\sim 5 \times 10^{41}$  erg sec<sup>-1</sup>) is extended and we can compute gas density and temperature yielding parameters not too dissimilar from those found in M-87. This phenomenon of clumping of cool gas about massive individual galaxies in a cluster is found in Einstein observations to be a general feature of many clusters and help us significantly in understanding cluster properties.

## CLUSTERS OF GALAXIES

Several independent efforts led by Christine Jones, Pat Henry, and Steve Murray, of CFA, are proceeding to study cluster morphology and evolution. Although but a small fraction of the Einstein observing program has been completed and only preliminary analysis of the data has been carried out, certain characteristics seem already to emerge. Clusters seem to show a great diversity of morphological shapes exemplified by the IPC pictures of Cluster A-1367 and A-85. Figure 18 shows the X-ray contours superimposed on the optical data. In addition to the broad X-ray distribution, amounting to approximately  $10^{46}$  erg sec<sup>-1</sup> which for an isothermal sphere model extends over about 0.5 Mpc, we see now that the emission is highly clumped. About  $2 \times 10^{42}$  erg s<sup>-1</sup> are associated with the radio emitting galaxy 3C264. Also, two galaxies, NGC-3842 and NGC-3841, which do not lie near the center of the cluster, have X-ray luminosities of  $3.4 \times 10^{41}$  erg s<sup>-1</sup> and  $5.5 \times 10^{41}$  erg s<sup>-1</sup>, comparable to M-86. Other apparent X-ray peaks do not correspond to bright galaxies. If there is a relationship between X-ray enhancements and mass concentration, these bright spots may indicate the presence of previously undetected mass in the cluster. Both Virgo and A-1367 have relatively low velocity dispersion for the galaxies, suggesting that the binding of gas by the potential of individual galaxies is a more important factor than the cluster central potential well.

Figure 19 illustrates the very different picture that we obtain for the cluster A-85. Here the one-dimensional projections show a very strong central peaking as well as an overall smoother X-ray distribution. The isothermal sphere core radius for this cluster is about half that which we obtained for A-1367, the X-ray luminosity is  $\sim 10^{45}$  erg s<sup>-1</sup>, and the temperature is  $\geq 8$  keV (or 100 million deg).

Generalizing our cluster observations, we see that clusters whose emission is broadly spread and clumped around individual galaxies tend to be rich in spiral galaxies, have low velocity dispersions, and X-ray temperature in the few keV range. Clusters which are smooth X-ray sources with well-defined central peaks are spiral poor, have larger velocity dispersions, and have higher X-ray temperatures. These observations can be understood in the framework of cluster evolution models, such as that of Peebles, if we allow clusters in different stages of evolution to be present at a given epoch. Peebles has shown that a cluster begins as a large cloud of galaxies, collapses, and finally reaches equilibrium with an extended halo around a high density core. The broad, highly clumped clusters could be interpreted as clusters in their early evolutionary stages.

Clusters in this early stage would be expected to have a lower density of hot intracluster gas, and therefore, a higher fraction of spirals than in more evolved clusters in which the ram pressure of gas can strip the galaxies of their interstellar matter, transforming them into SO's and perhaps elliptical galaxies.

During the collapse or second phase of cluster evolution, a high density core is formed, thereby enhancing the chances for building a central dominant or cD galaxy at the cluster center, either by dynamical friction leading to galaxy capture, or by tidal stripping of galaxy halos. So far all of the clusters we have observed, which show a strong X-ray peaking, such as A-85, are Bautz-Morgan type I clusters with cD galaxies. The increased X-ray central surface brightness and higher temperature are probably due to the increased gas density at the center, bound by the cluster potential well.

A consequence of these observations is that the previous extended X-ray emission reported by Forman et al. for at least two clusters, A-1367 and A-2666, no longer need be interpreted as evidence for a massive halo outside the isothermal core. Instead, the extent can be understood in terms of broad, highly clumped emission, with negligible total mass.

The observation of distant clusters may also shed light on their evolution, if we assume that the more distant clusters will be observed earlier in their development than the nearby clusters. The dynamic cluster potential models of Perrenod predict a strong evolution in the cluster gravitational potential, with luminosities at a redshift of 1, predicted to be only 1/10 of those at redshifts near 0. Also, the distant

clusters provide more tests for the ram pressure gas stripping models or for the evaporative stripping models for converting spirals to SO's or ellipticals after cluster collapse (Peebles' Phase 2). Since Butcher and Oemler have observed many blue, rather than red galaxies in several centrally condensed clusters near  $z = 0.4$  in contradiction to this simple picture, one possible way out was to suggest that these clusters do not have the intergalactic medium or gas needed to do the stripping.

Our observation of the redshift 0.46 cluster 3C295, with Einstein IPC, shows that the source has a finite angular extent of 0.6 arc min which corresponds to a core radius of 0.5 Mpc. With this core radius, the measured X-ray luminosity of  $1.3 \times 10^{45}$  erg s<sup>-1</sup>, and an assumed temperature of 7 keV, we obtain a central ion density of  $2 \times 10^{-3}$  cm<sup>-3</sup>. Only through X-ray measurements such as these can the hot gas be directly observed and thereby the density determined. This density is sufficiently high that the stripping models predict that contrary to the observed colors, there should be few, if any, spiral galaxies in this cluster. It is possible that the cluster has just recently collapsed and the stripping has not had time to process. Alternatively, Gisler has recently suggested that gas injection from the stars in the galaxies may also be capable of removing momentum from the intergalactic gas, thereby avoiding the stripping process.

With respect to the question of luminosity evolution, we again find a complex situation. This is caused by the large, >100, spread in cluster luminosities as shown in Figure 20. This is a plot of the spectral density received at our detector at an energy corresponding to 2 keV at the cluster, plotted versus redshift. OSO-8 data of Mushotzky et al., and Einstein data are shown. Closed symbols refer to Bautz-Morgan type I and I-II with cD galaxies to which the remainder of the discussion is confined. The smooth curves represent the expected flux versus redshift for an average  $7 \times 10^{44}$  erg s<sup>-1</sup> B-M type I cluster. Two curves for deceleration parameter 0 and 0.5, but no evolution are indicated as is a curve which evolves according to one of Perrenod's dynamic potential models. The high redshift cD clusters observed so far appear to favor such a model, but clearly more data are required for a definitive test.

## QUASARS

We are carrying out a program of observations of known quasars with a wide variety of radio and optical properties, over a significant range of redshifts (>3). Prior to Einstein only quasars at redshift <0.2 had been observed in X-rays. New quasars are also being discovered through optical identification of X-ray sources detected in the deep surveys. Five such quasars have already been identified in Einstein deep surveys with  $0.5 < Z < 2.6$ .

Figure 21 is a 10,000 sec exposure for the quasar 0537-286 at  $z = 3.1$  which emits more than  $10^{47}$  erg  $s^{-1}$  in the 0.5 to 4.5 keV band. Other objects detected in the field include a 5.3 magnitude F2 star and a 7 magnitude F5. The other objects are as yet unidentified and correspond to optical candidates fainter than 15 magnitude.

The ease with which we observed QSO 0537-286 and a second quasar, 0420-388, at redshifts of 3.1, indicate that we can expect to detect still more distant quasars. An interesting question is whether in fact still more distant quasars exist. Since the quasars are the first known aggregates to condense from the expanding big bang "gas," the epoch at which they first formed is a most intriguing issue. Have the optical observations to date been limited by instrumental effects as many have suggested, or did the quasars only form at the epoch given by redshift 3.5? Since our X-ray deep surveys are capable of detecting and locating sources much weaker and hence possibly much more distant than we have discussed, we should be capable of detecting these more distant quasars if they exist.

A second important question about the quasars concerns the long-standing question of the nature of the underlying energy mechanism capable of producing luminosities up to  $10^{47}$  ergs  $s^{-1}$ . The X-ray observations may be able to provide a unique insight into this question by studying time variability of QSO emission. Figure 22 shows our observations of the quasar OX-169, which is a weak X-ray source, but nonetheless, easily detected by our telescope. The figure shows the data we obtained for six orbits of HRI observations. The observed intensity variation in  $\leq 100$  min corresponds to a decrease in absolute luminosity from 2.0 to  $0.6 \times 10^{44}$  erg  $s^{-1}$ . The probability that the event is due to random fluctuations of a steady source is quite small, although more careful analysis is required to precisely define the size and time scale of these variations.

Observations of time variability, such as we see in OX-169, may be a signature of the ultimate energy source in the nuclei of quasars. For a process involving conversion of a mass into energy, rapid variations in a powerful emitter require a high efficiency, supporting models involving release of gravitational energy through accretion onto a compact object. If one assumes that the X-ray emission is powered by accretion onto a massive black hole and that the Eddington luminosity is not exceeded, the luminosity and time scale for variability can be used to obtain bounds on the mass of the black hole. The short time scales involved in the emission from OX-169 confirm the expectation on theoretical grounds that the X-rays are produced very close to the central source and may therefore provide the means for ultimately understanding the machines powering the quasars and active galaxies in general.

Figure 23 summarizes some of our observations of the quasars. We have plotted the 0.5 to 4.5 keV X-ray luminosity for the individual sources as a function of redshift. The three nearby quasars known prior to the launch of Einstein are shown, as are the Einstein observations now extending to a redshift of 3.1. The luminosities range from  $10^{44}$  erg s $^{-1}$  to  $10^{47}$  erg s $^{-1}$  with no obvious dependence of luminosity on redshift. The absence of low luminosity, high redshift quasars is primarily a measure of the instrument sensitivity limit for a several thousand second observation.

Our observations to date clearly do not satisfy the statistical requirements for a complete sample; for example, they are strongly biased towards radio quasars indicated by filled circles on the slide.

In the meantime, we can use optical luminosity functions for quasars plus a tentative correlation between the optical and X-ray fluxes in order to estimate the possible contribution of the quasars to the X-ray background. We define the quantity  $\alpha_{ox}$  which is the slope of a power law connecting the optical data (at 2500Å) with the X-ray data (at 2 keV).

The resulting values of  $\alpha_{ox}$  range from 0.95 to 1.71 and show no obvious dependence on redshift or, for example, on radio emission properties. We also note that the range in observed  $\alpha_{ox}$  corresponds to a factor of 100 in the ratio of optical to X-ray luminosities. Even though this is a substantial range, we can attempt to use an average value of  $\alpha_{ox}$  plus an optical luminosity function to estimate the contribution of the quasars to the X-ray background. Averaging the X-ray luminosities and the optical luminosities, we find an average  $\alpha_{ox}$  of 1.5, where the result is dominated by the most luminous quasars.

Neither the optical luminosity function for quasars, nor the rate of evolution are fully determined at present. In our calculations we used recent results of Braccetti et al. (1979) who analyzed all the available data on optically selected quasars. With a Friedmann cosmology and deceleration parameter  $q_0 = 0$ , they found that the number versus magnitude relationship for optically selected quasars implies a strong evolution rate, [with density increasing as  $(1+z)^8$ ] up to  $z = 2.5$ , followed by less rapid evolution at higher redshift.

Using this formalism, together with the average  $\alpha_{ox}$  of 1.5, we can estimate the contribution of quasars to the X-ray background. The result depends on the limits of the integration and we have assumed that the optical luminosity function is valid over a range which corresponds to limits of  $10^{44}$  to  $10^{46}$  erg s $^{-1}$  for the X-ray luminosity. The calculation leads to an immediate contradiction, since the computed background

is 2.5 times the observed "extragalactic" background. Therefore something must be wrong. X-ray luminosity may evolve less rapidly or the  $L_x/L_{op}$  ratio we find is the result of sample selection. It is interesting to note as an aside that the observations can be reconciled with a local theory of QSO only if the local distance scale is assumed to be of 500 Mpc which then is essentially equivalent to a cosmological interpretation of the redshifts.

## THE DEEP SURVEYS

I would like to turn to another aspect of Einstein research: the deep surveys. The long-standing question of the diffuse or discrete origin of the X-ray background can be approached directly with Einstein observations by extending the Log N versus Log S curve, or by imaging it at the limit of sensitivity. Given the fact that Einstein deep surveys have achieved already 500 times the sensitivity of any previously reported experiment, we expect for a  $3/2$  power law extension of the number intensity relation found with Uhuru to be able to observe several million sources in the sky or several tens of sources per square degree. At this source density not only is imaging essential to avoid source confusion, but in fact the IPC is just about confusion limited with 2 arc min resolution and the HRI takes over with 4 arc sec resolving capabilities. We point at selected regions of the sky where we have optical and radio coverage and cover the region with a mosaic of exposures as shown in Figures 24 and 25. Given the fact that we are navigating in unknown lands, we tend to observe everything at least twice with the IPC and use cross-correlations to reassure us about the validity of our automated detection techniques. In Figures 26 and 27 are two examples of superposition of HRI fields in exposures from 10,000 to 50,000 sec in Draco and Eridanus. Several sources can be immediately seen. I have chosen to summarize the results by showing the 4-meter blue plates of the regions obtained by W. Sargent at Kitt Peak and by W. Liller at CTIO with the sources superimposed (Figs. 28 and 29).

HRI positions are marked by the hatched lines while circles define a standard 1 arc min radius error box adopted for IPC position. Several nearby stars can be seen as the optical candidates of the X-ray sources in the pictures. As described above we detect stars of classification F0, F2, G and K<sub>8-9</sub> in these two fields.

We wish to separate the contribution of nearby stars from extragalactic objects to evaluate the contribution of such discrete objects to the background. This can be done either by direct measurement of the redshifts of the objects, identifying QSO's and compact galaxies, by their optical and radio morphology, or in the case of faint counterparts which may be QSO, BL Lac objects, or white dwarfs, by directly measuring their proper motions over a 25-year span. Some fields appear completely empty, although in one case both a 21.5 magnitude object possibly

a cD galaxy and a cluster of galaxies of magnitude 22-23 were observed at the X-ray location with CCD cameras by Westphal and Kristian. Only about one-third of the objects can be stars belonging to known classes of objects. We can then proceed to estimate the contribution of such objects to the background by estimating their number at our limiting sensitivity. We select for this purpose only sources within the central 30 arc min of the field and whose intensity is known better than 5 standard deviations to reduce possible errors due to uncertainty in the intensity of the sources and other effects. The data point on Figure 30 is placed where the number of sources per steradian (of intensity greater than  $S$ ) is plotted at the survey sensitivity. The Uhuru Log  $N$  - Log  $S$  curve has been obtained by extrapolating the results in the 2-6 keV range to the 1-3 keV range of this Einstein measurement. The background envelope has been also similarly derived by extrapolating the  $E^{-1.4}$  power law valid at energies below 20 keV. The differential contribution of the sources is of order 13 percent. Their integral contributions extrapolated to 1 UFU with a  $3/2$  power law is 30 percent. Finally, extrapolation to the limit of sensitivity of our current survey or to the limits of known quasars (with X-ray intensity a factor of 4 below the 5 sigma limit) may yield integral contributions of 50 to 60 percent, respectively. Once the point is made that a significant fraction of the background is due to discrete sources, it becomes very interesting to find out both the nature of the objects and the expected turn-over of Log  $N$  - Log  $S$ . This type of measurement may give us a very useful different approach to the study of QSO evolution.

#### CONCLUDING REMARKS

It should be clear that the Einstein mission has given X-ray astronomy observational capabilities not too different in their power from those available in the visible or radio range — particularly in the study of objects at cosmological distances. In fact, the Einstein mission has opened for X-ray observation all known classes of stellar and extragalactic objects. X-ray observations have unique capabilities in studying high energy processes, whose fundamental importance in the dynamic and evolution of the universe is becoming increasingly better understood through astronomical observations at all wavelengths.

X-ray astronomy has moved from the consideration of problems intrinsic to the discipline to the study of the great problems of formation and evolution of cosmic objects which are and have been the fundamental questions in astronomy. Yet this observational capability rests entirely on the Einstein mission, which will be over in two short years. I am convinced that just as ST and VLA are essential to modern astronomy, equally essential is the establishment of a permanent orbiting X-ray telescope. I believe this task has the highest priority for all of astronomy in the 1980's.

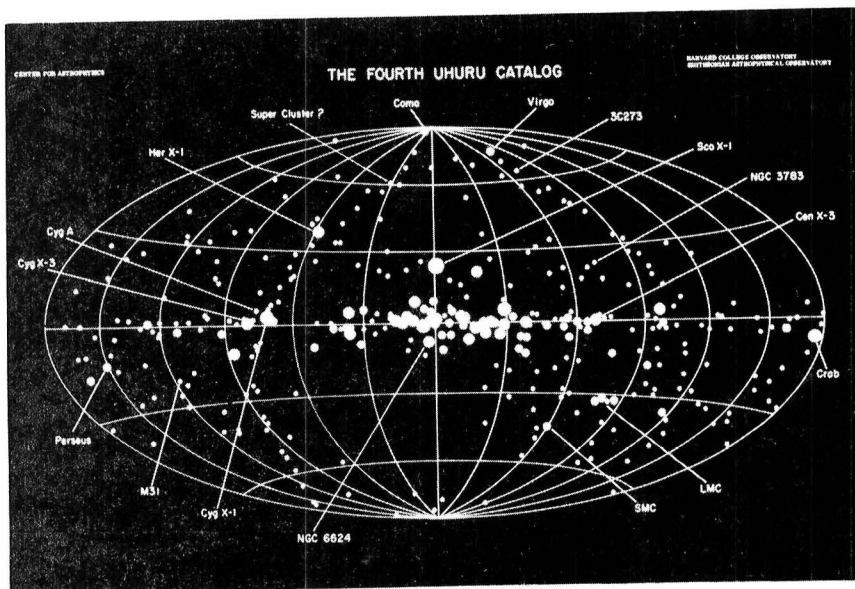


Figure 1

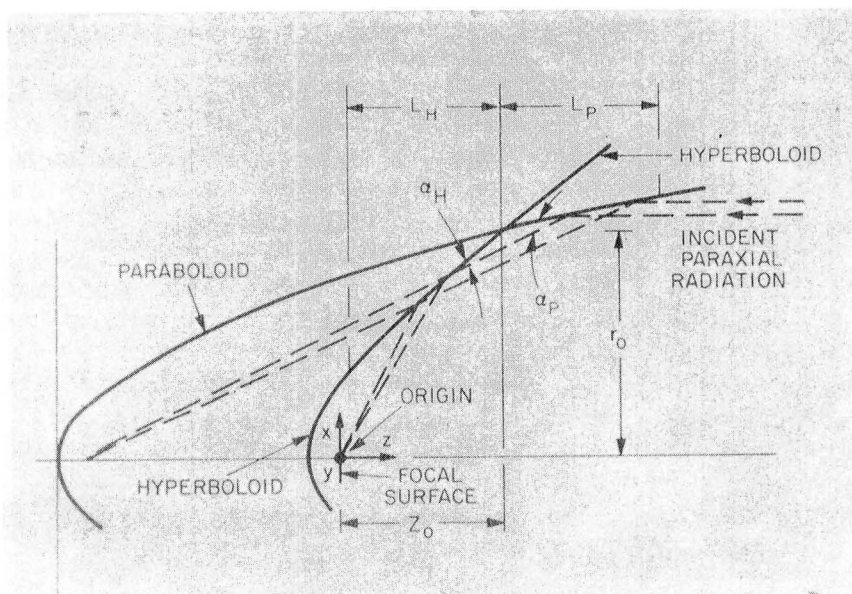


Figure 2



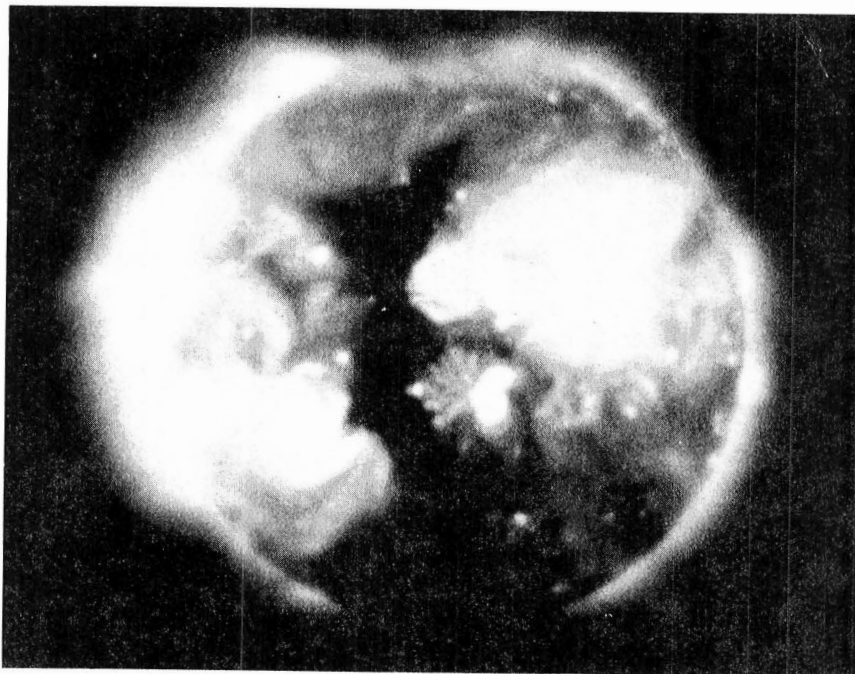


Figure 3

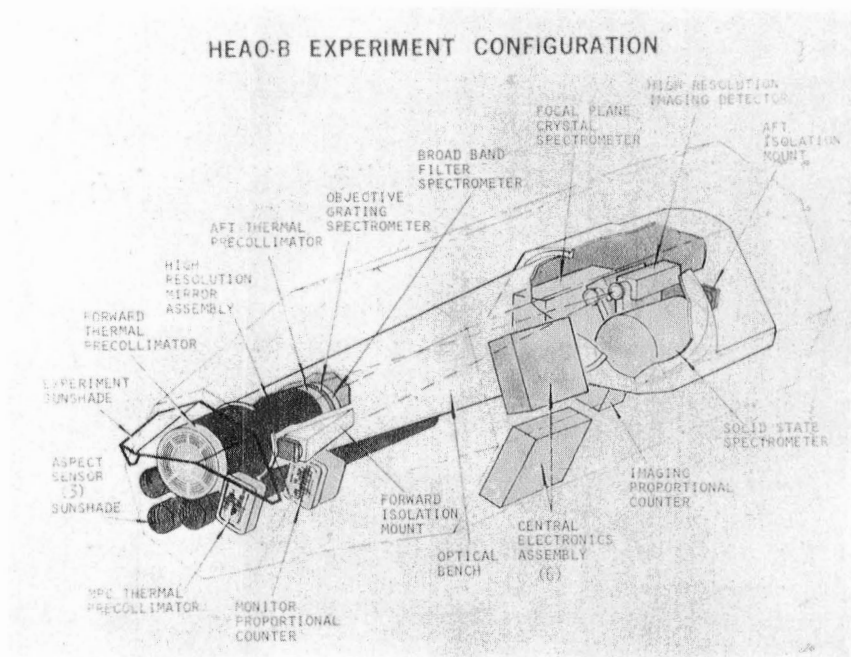


Figure 4

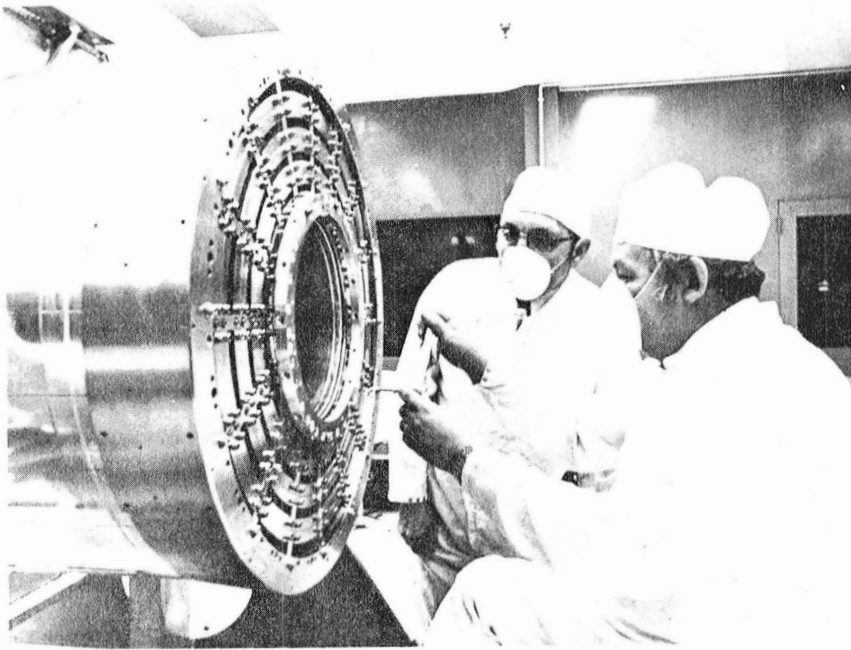


Figure 5

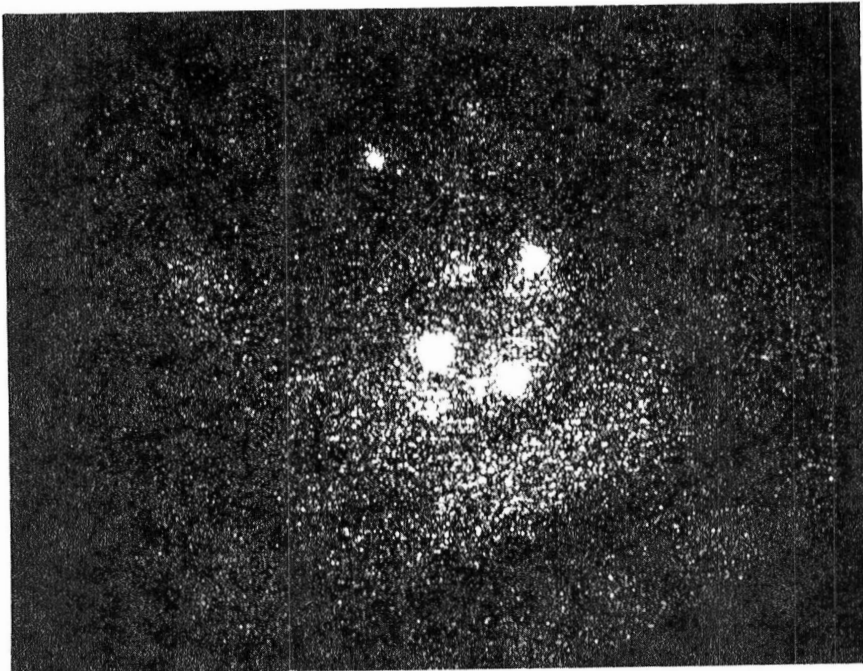


Figure 6

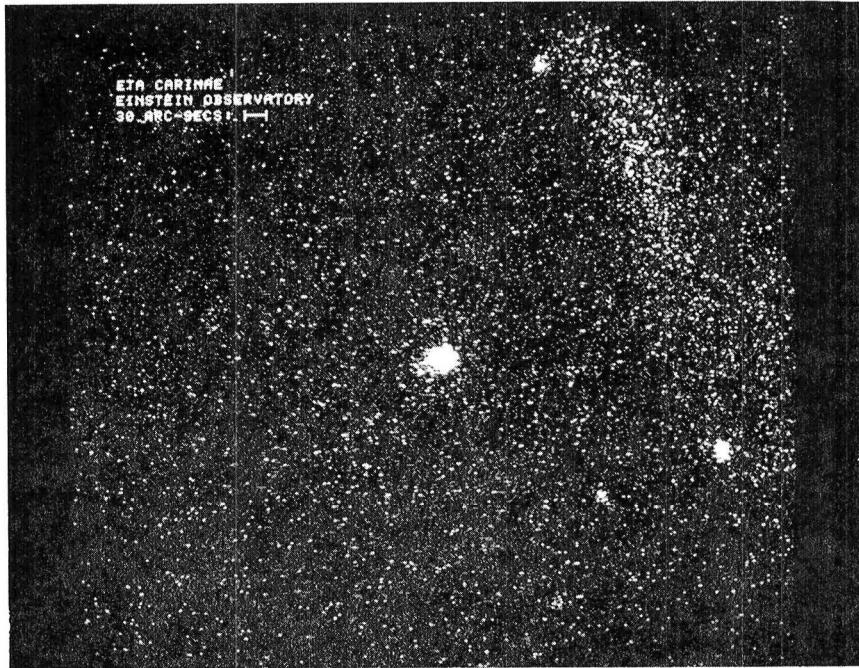


Figure 7

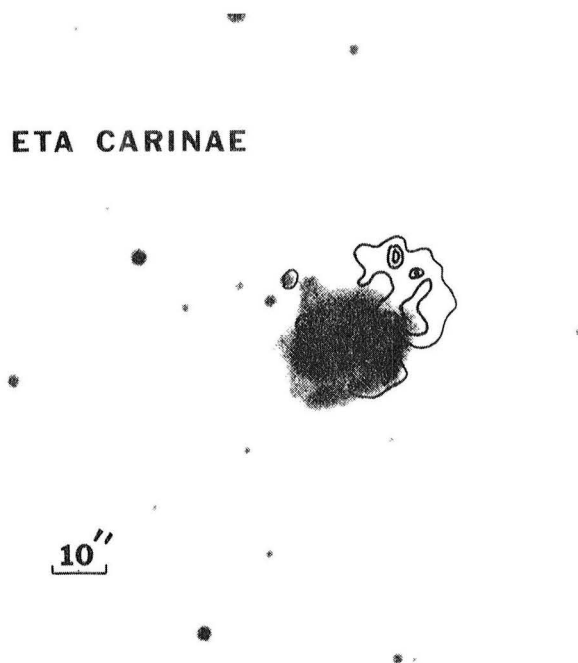


Figure 8

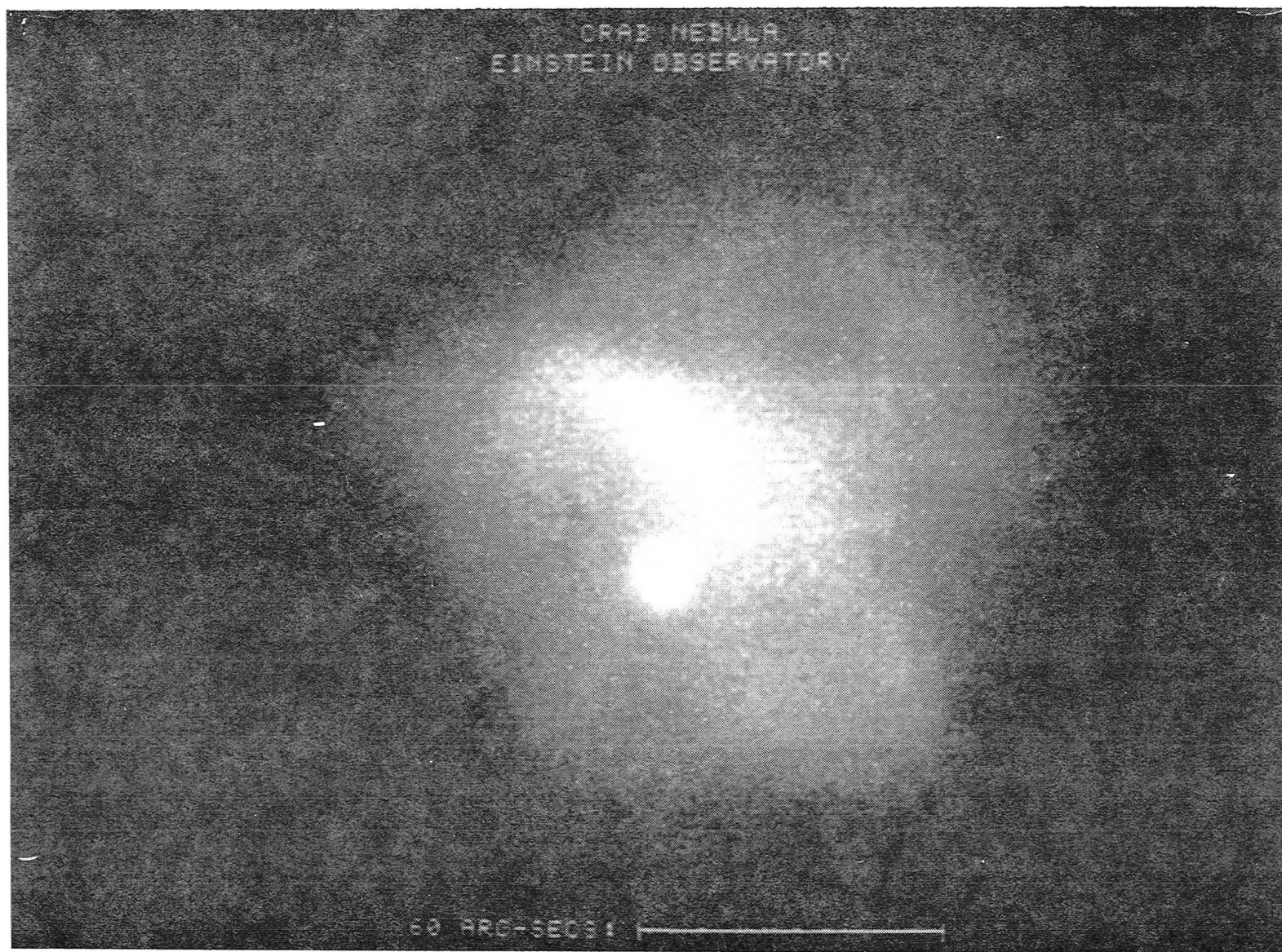


Figure 9

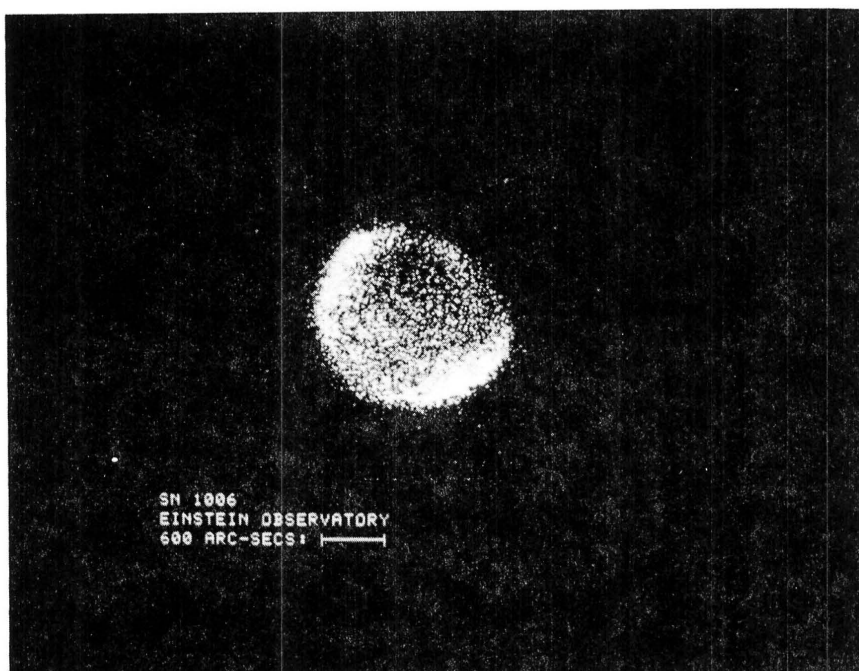


Figure 10



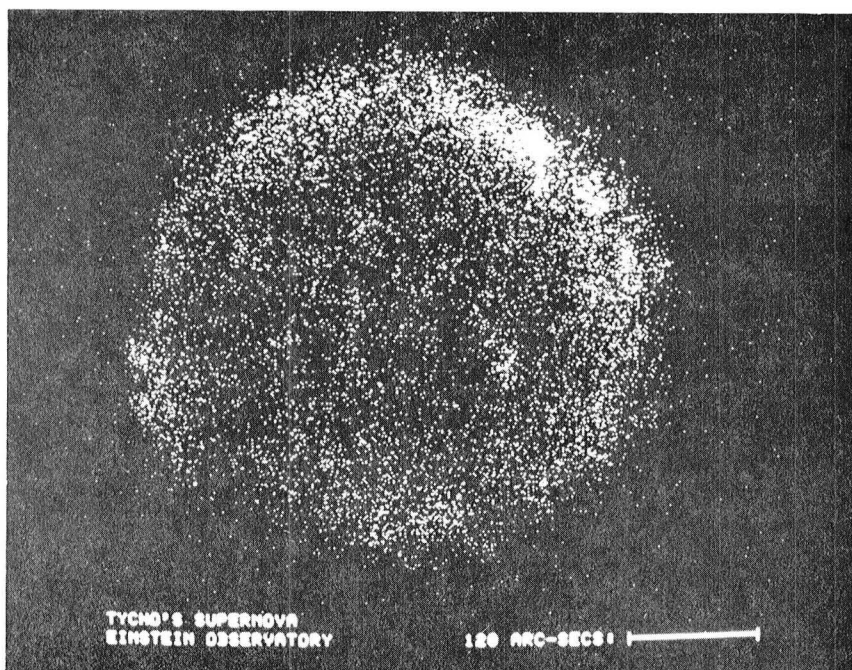


Figure 11

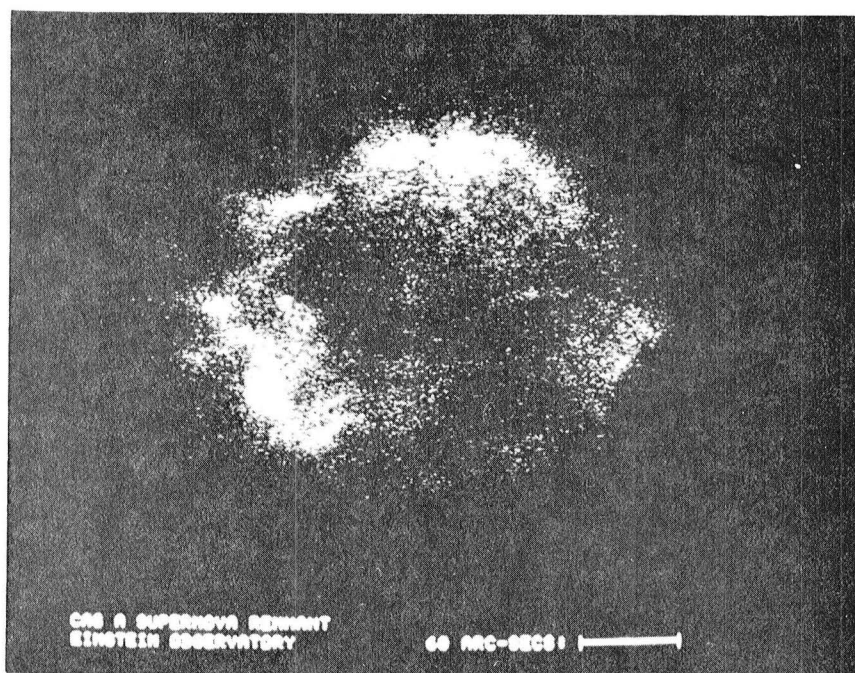


Figure 12

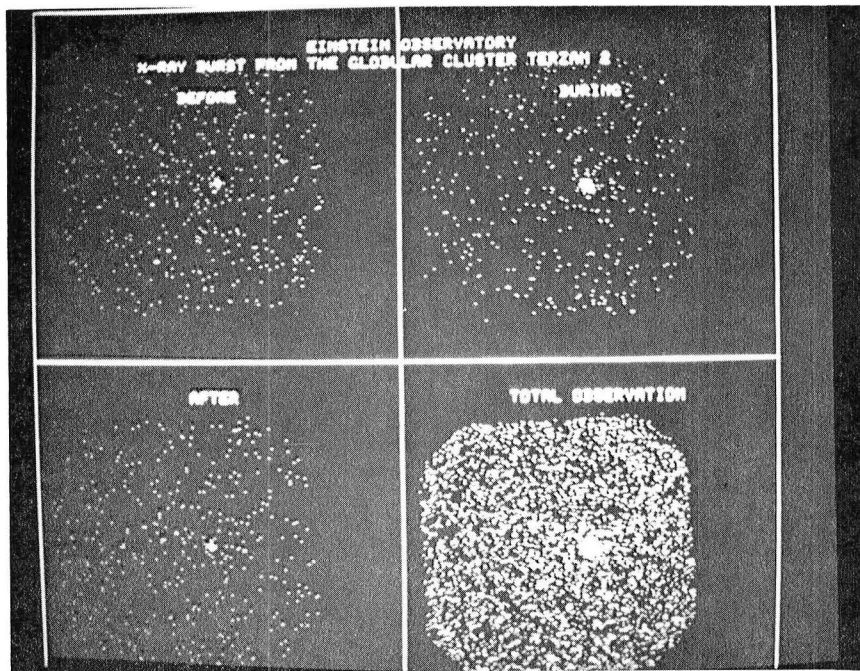


Figure 13

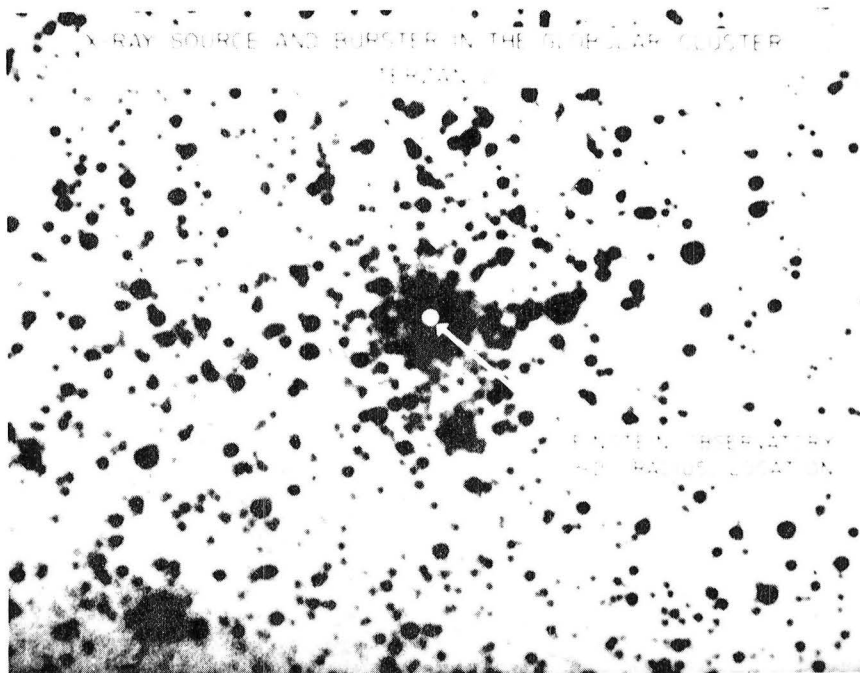


Figure 14

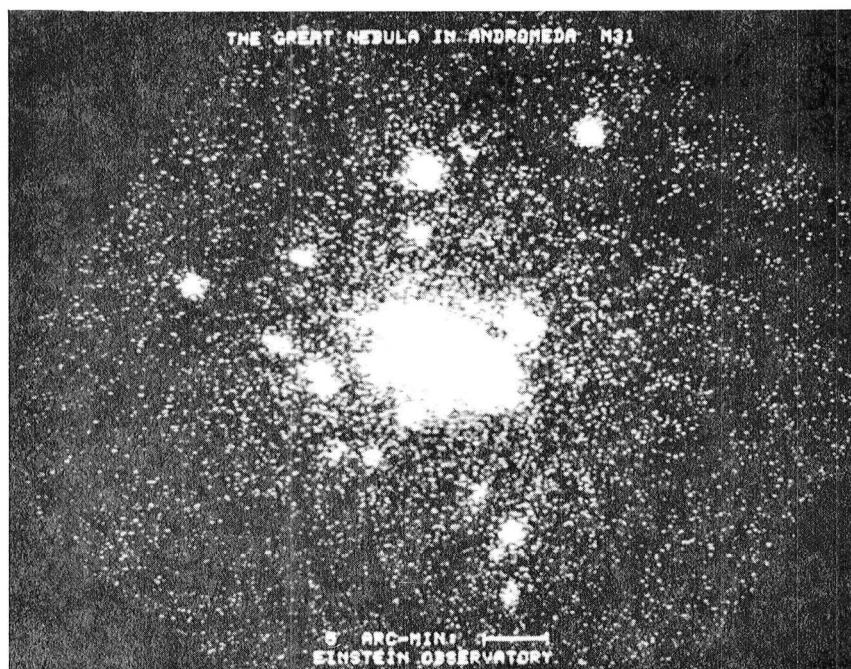


Figure 15



Figure 16



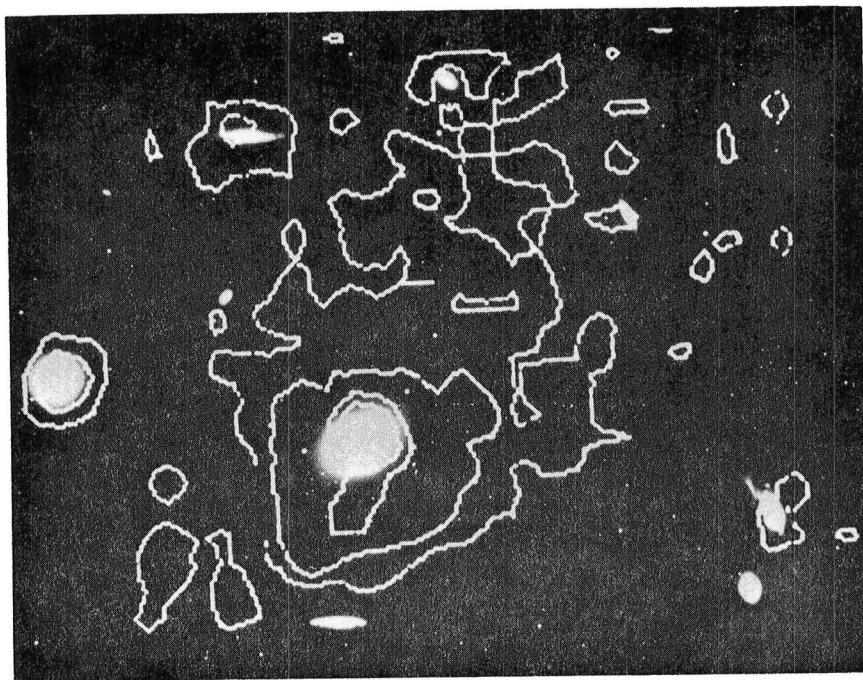


Figure 17

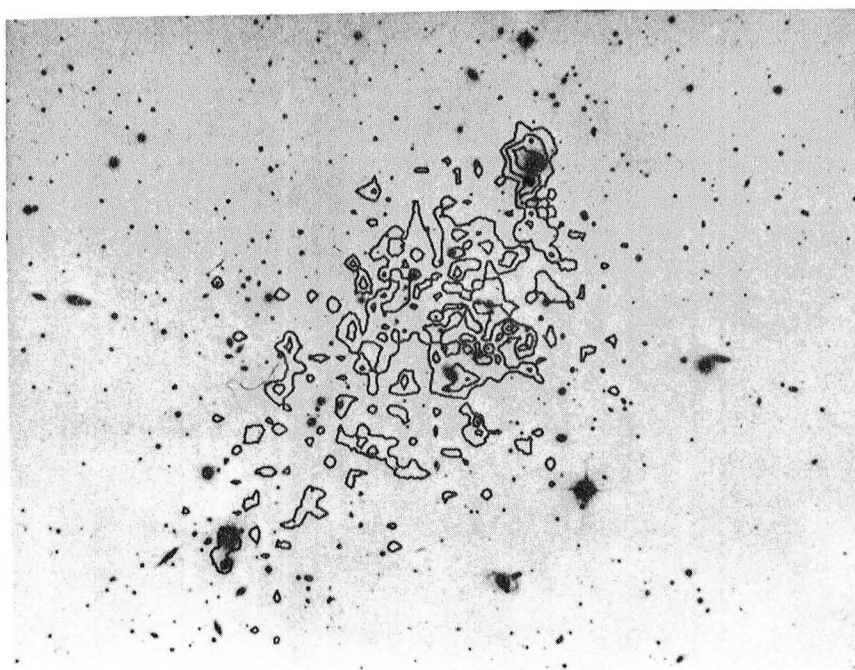


Figure 18

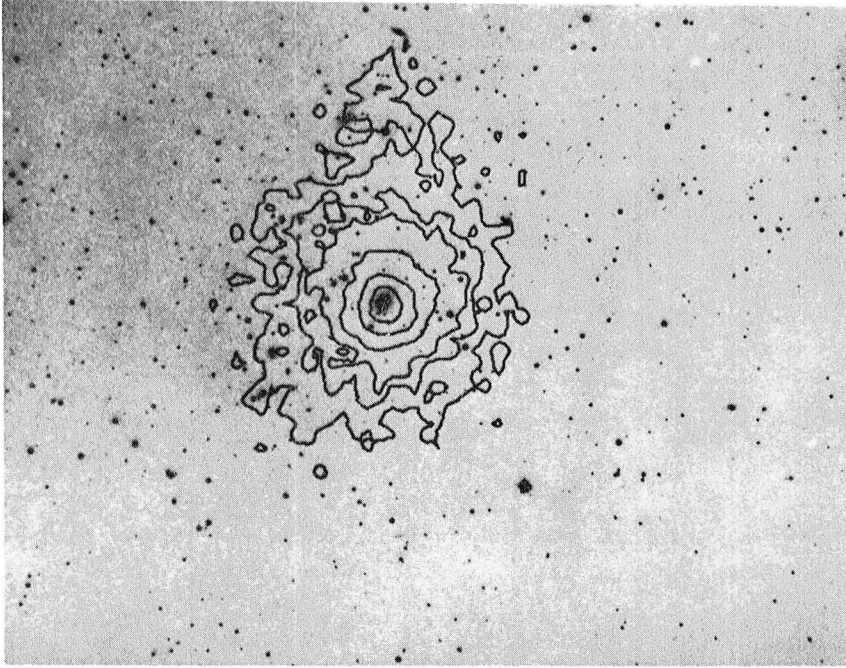


Figure 19

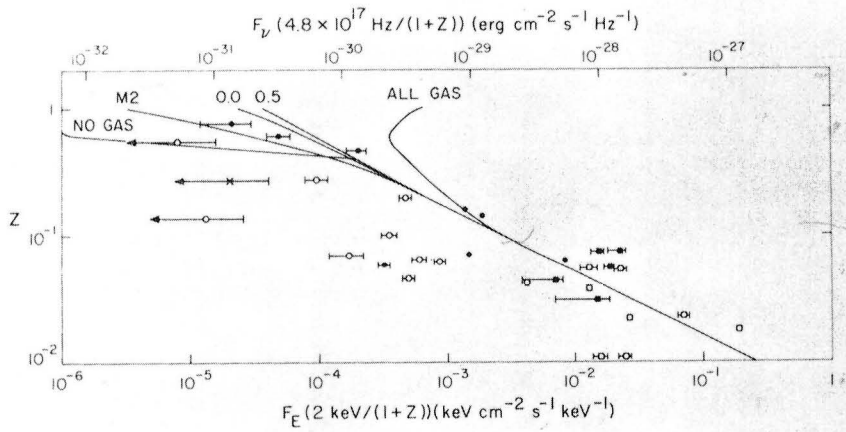


Figure 20

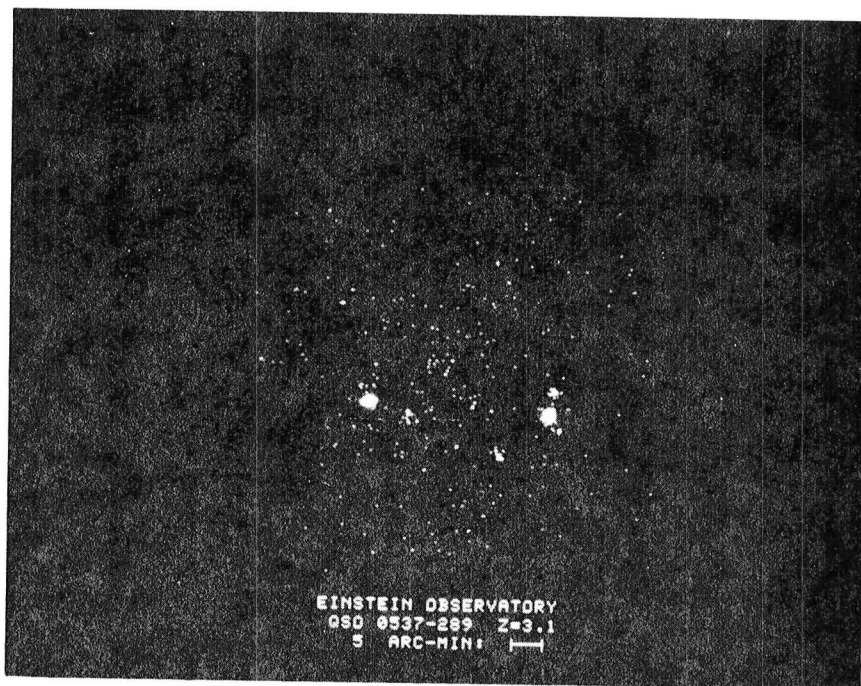


Figure 21

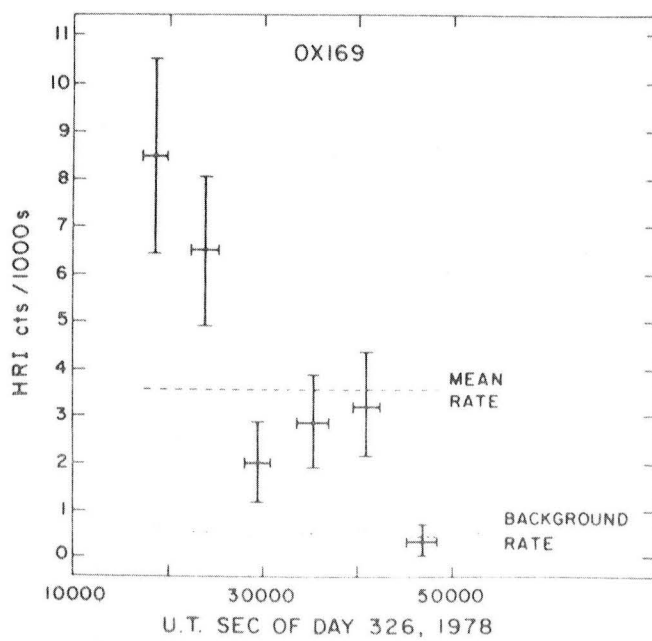


Figure 22

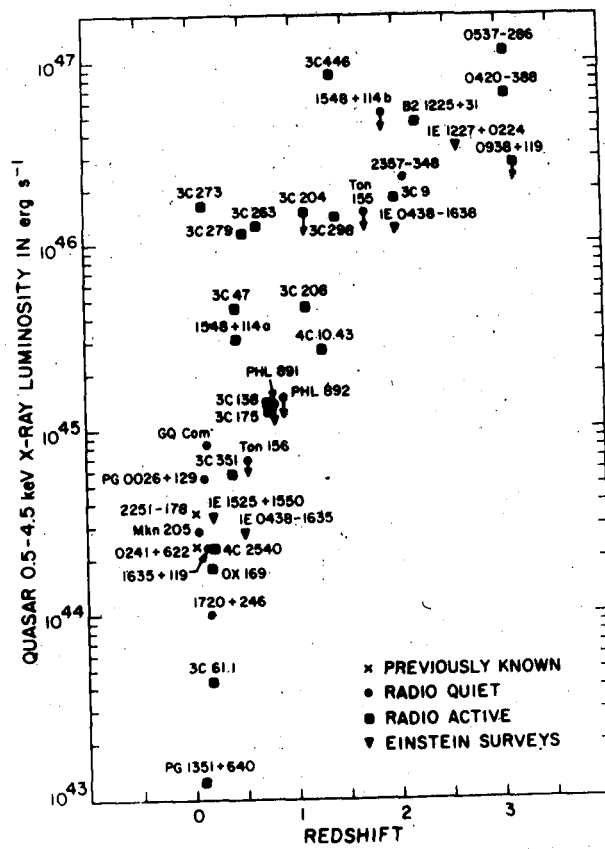


Figure 23

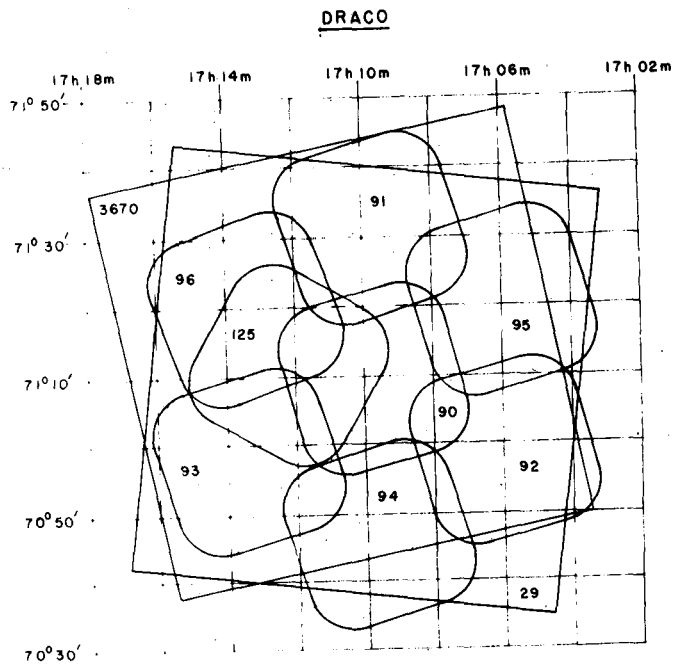


Figure 24

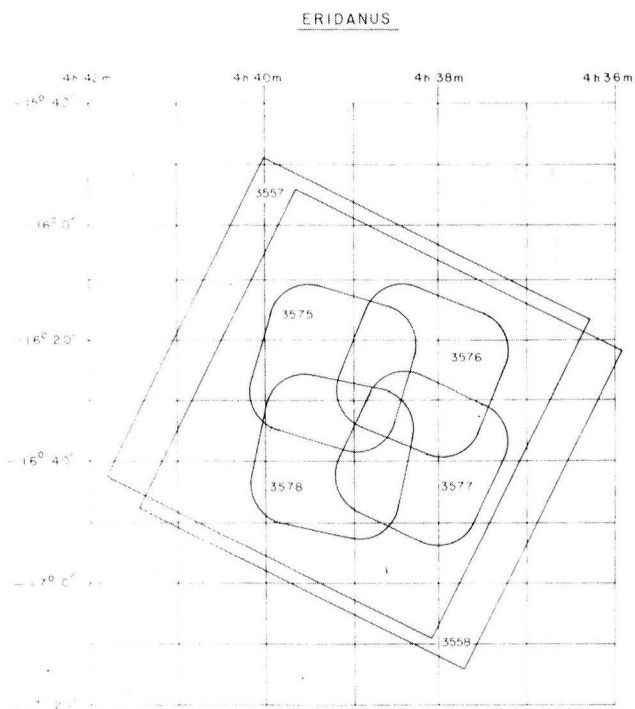


Figure 25

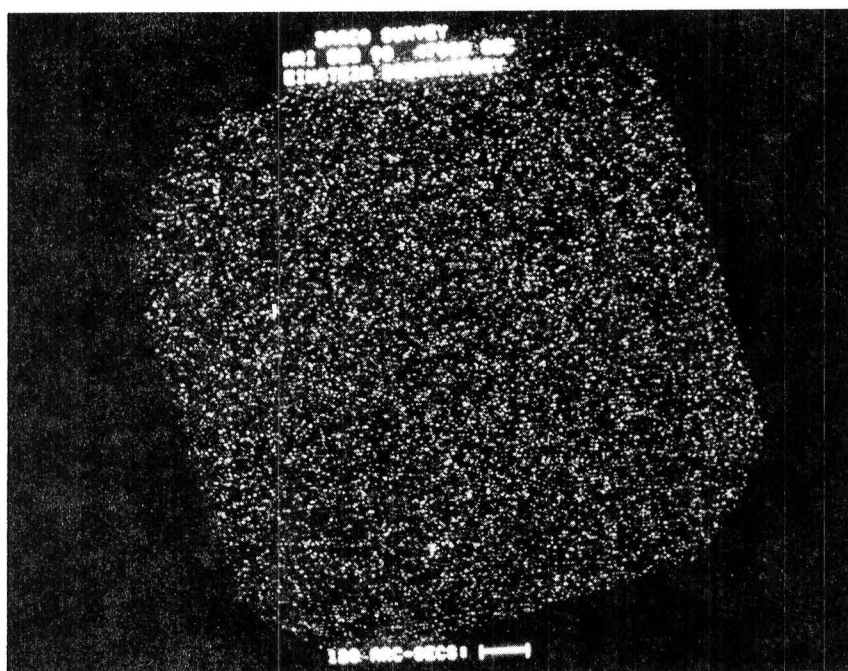


Figure 26

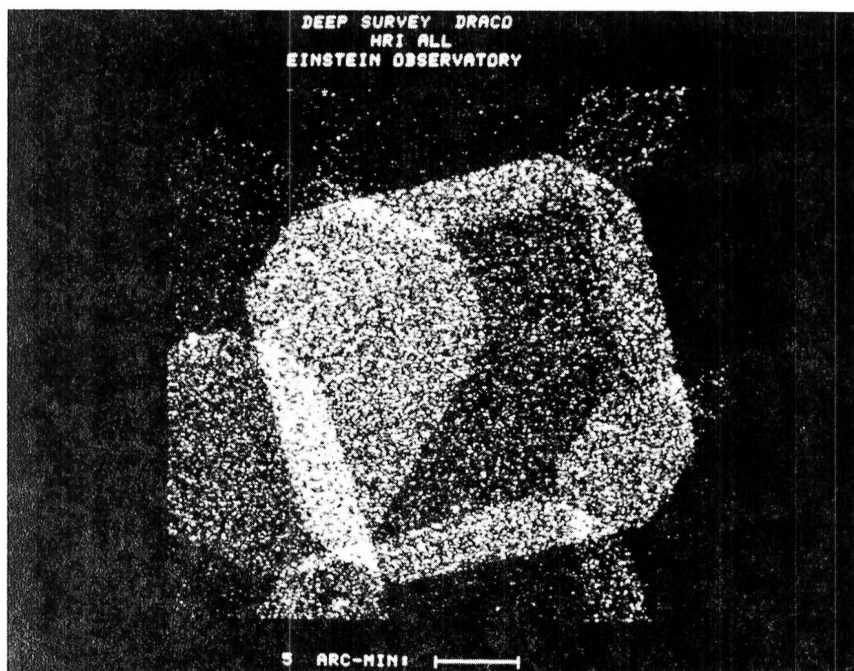


Figure 27

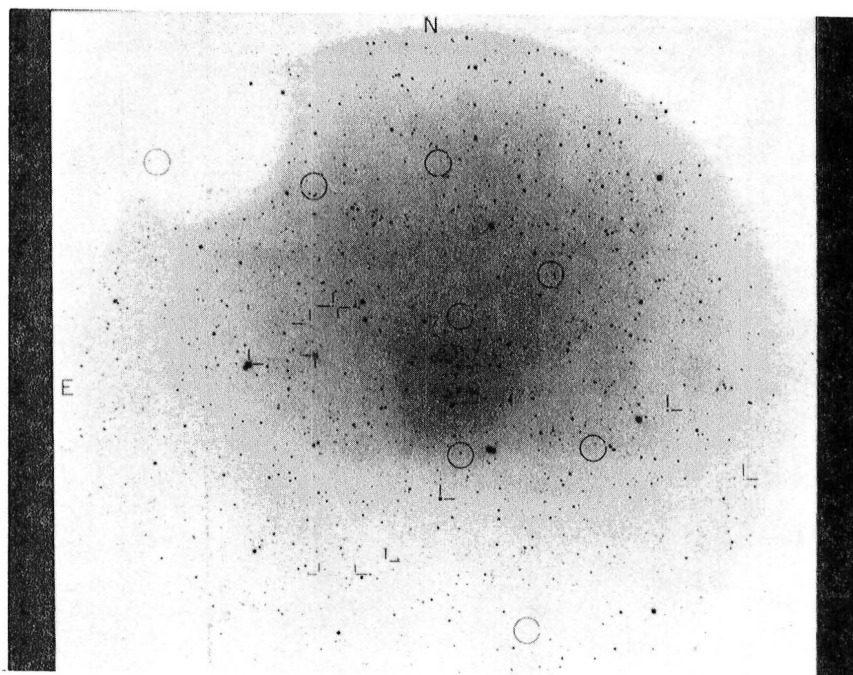


Figure 28

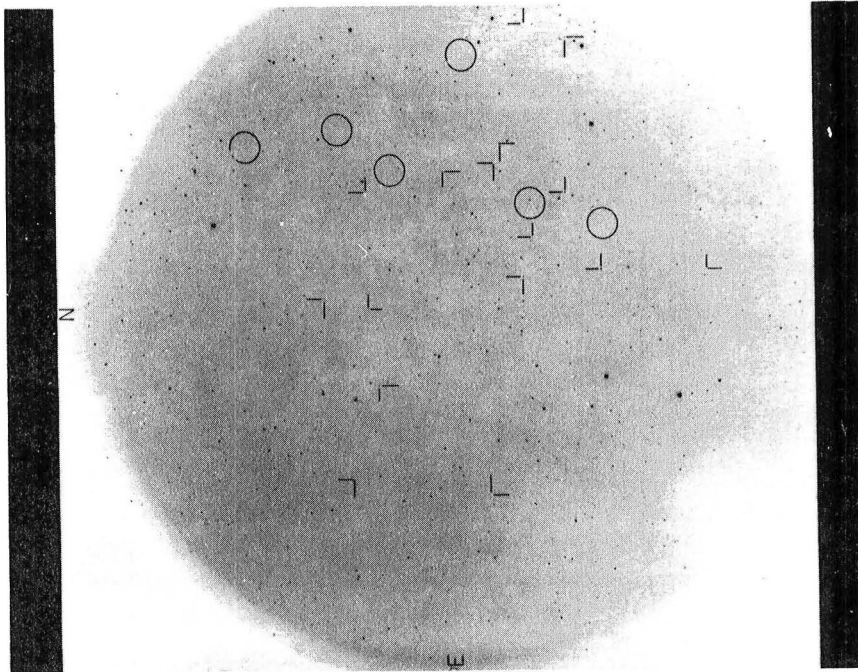


Figure 29

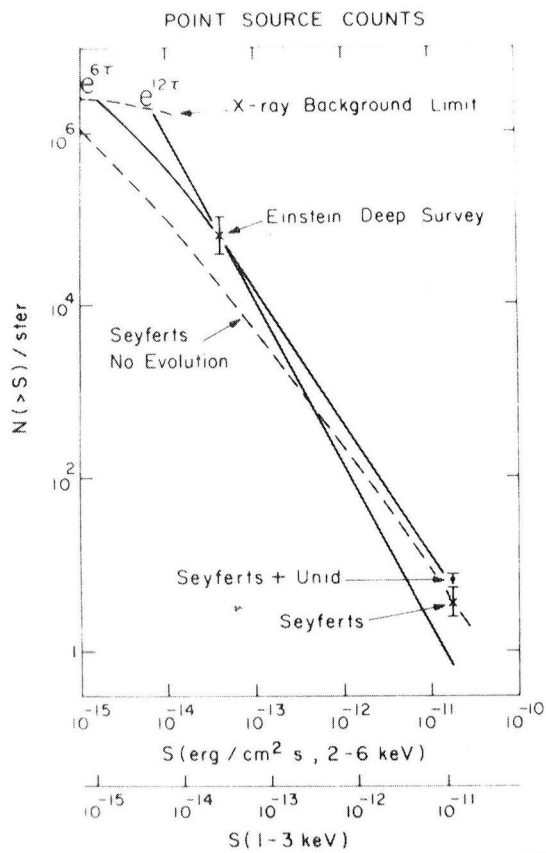


Figure 30



# NONDISPERSIVE SPECTROSCOPY OF CELESTIAL X-RAY SOURCES

S. Holt  
Goddard Space Flight Center

I am going to begin the discussion of spectroscopy aboard the Einstein Observatory. First, I would like to thank the many people here at Marshall to whom we owe such a great debt. It may sound obligatory for us to come up and say these things, but I assure you that the gratitude which the scientists have for the project personnel is truly sincere. They did a magnificent job.

With respect to spectroscopy aboard Einstein, the consortium members took the point of view that if we were going to do the best job we could on X-ray sources, we should really pursue two separate approaches: one to take advantage of the highest possible resolution we could obtain with dispersive techniques, and two, to take advantage of the maximum amount of area possible, because many X-ray sources are just too dim for us to successfully use the resolution possible with dispersive techniques.

Table 1 indicates what the prospects were prior to the launch of the observatory for doing spectroscopy. The first column lists, in very broad categories, the various flavors of X-ray sources which we knew about (exotic binaries mean binaries which have neutron stars or potential black holes within them). The column labelled  $L_x/L_\odot$  is the logarithm of the X-ray luminosity relative to the total luminosity from the Sun. The Sun, in fact, would be  $-6$  on this scale because its X-ray luminosity is only about 1 millionth of its total luminosity. The middle column exemplifies the high efficiency we had to attain to do spectroscopy on a large number of sources. Shown there is the logarithm of the counting rate resulting from a detector with a gross area of  $100 \text{ cm}^2$  and 100 percent efficiency (typical of what we can get from Einstein). Most of the sources we expected to look at would give us something like 1 count per second with such a system. If we were using a dispersive technique, it would approximate 1 count per 1000 sec. The last column, which is particularly relevant for an estimate of how useful spectroscopy might be, is a measure of the temperature of these sources. The temperature of  $10^6$  deg, which is characteristic of the solar corona, is really too low to see a substantial amount of structure from Einstein. At  $10^7$  deg (approximately 1 keV) the structure is clearer and elements between neon and calcium are either hydrogenic or helium-like. Therefore we expected extensive cooling in these plasmas from line emission in that energy range. However, once you reach  $10^8$  deg, or when the logarithm becomes two, all the species of mid-Z elements are completely ionized and are no longer visible. So the best things for us to look at are items in the third column which have an approximate value of 1, corresponding to  $10^7$  deg.



In addition, however, there might be features other than thermal which might be seen from optically thick or non-thermal sources, such as fluorescent lines or different kinds of spectral features.

Now, having decided to do the nondispersive spectroscopy because of the efficiency advantage it gives, we will discuss the selection of the spectrometer. Shown in Figure 1 are traces of real data obtained with an Fe 55 laboratory source, with a K-capture X-ray of about 6 keV. The first peak is the best resolution we can get with a proportional counter. The center peak is resolution which we can get with a device called a gas scintillator which was not available at the time we designed Einstein, but which is basically just a proportional counter without the last stage of amplification, so the noise from that last stage is suppressed. The peak on the right is what we get from a system which is identical to the one which actually flies aboard Einstein. This is a solid state spectrometer, and the small bump which is just coming out of the gas scintillator spectrum is, in fact, a separate line feature from the Mn 55 which results from the K-capture decay. The reason we decided to use a solid-state spectrometer was simply because it was the best available, but there is a very good reason to be enthusiastic about this kind of resolution, which is about 160 eV FWHM. If we look at the separation between line features that we might expect to see, this is just about what we need to be able to separate those features. Figure 2 shows this full-width half-max resolution compared to expected lines from each of the even-Z elements; shown is the energy of Lyman alpha from each of these hydrogenic ion species, the resonance line from helium-like species of these ions, and K alpha from the neutral atom. As you can see, the resolution is just about typical of the separation for most of the atoms. For thermal plasmas in the neighborhood of a few tens of millions of degrees, we expect to see features like these. In addition, we might see some from the odd-Z elements, which are not quite as abundant. The last feature I want to bring to your attention is that a variety of temperature-dependent L-transitions in iron, which has its K transitions at much higher energy (above 6.5 keV), will be present below about 1.5 keV in any thermal spectra we see.

Figure 3 shows the effective area which we can apply using the Einstein telescope and a very small solid-state detector, much smaller than a square centimeter. We get about 100 cm<sup>2</sup> net from the telescope magnification. Figure 3 was prepared just prior to launch. We have two detectors with the one in standby redundancy having a slightly thicker gold contact on the front surface. The one we actually use is shown by the solid line, but we found out some 6 months prior to launch that we were accumulating water ice on the detector surface, reducing our sensitivity at low energy. To try to do something about it at that time would have meant a delay of probably a year in the launch, so we devised a way to operate around it. It means that we have to give up some fraction of the efficiency of the instrument at the lowest energies,

but from about 0.8 keV up, we operate virtually unaffected. So, all things considered, we are quite happy with the way things have turned out. We have lost the ability to look at oxygen, but everything else seems to be all right.

Before talking about the Einstein data, let me show you the last of the HEAO-1 data that you will see today. Figure 4 shows an MED CAS A spectrum with the logarithmic actual raw counts plotted, not corrected for anything or folded backwards through the detector response, but just raw counts as a function of logarithmic energy. You can see that there is a clear indication of iron K emission such as we can typically find with HEAO A-2, but that to the left of the heavy vertical line there are no features which are discernible in the raw data. In fact, if you try to fit the totality of these data, which is what the solid line through the data represents, you find that it is necessary to have at least two temperature components. However, the line contributions at lower energies cannot be seen in the raw data. What we can observe with Einstein is the portion of the spectrum from the heavy vertical line at 4.5 keV leftward, so, let me now show you what we see with the solid state spectrometer (Fig. 5).

There are very obvious features in the raw data which we can ascribe unambiguously to helium-like transitions in silicon and in sulphur, but in addition there are many many more little bumps and wiggles which might look tempting but which in fact are a lot more than that. We do not try to replicate the data by fitting some continuum and then just finding lines to stick in. We actually take models which insist that there be collisional equilibrium in the whole source, so that just choosing the temperature defines the positions of the lines. The magnitudes of the lines are then determined solely by the abundances. I can demonstrate some of the things which I have just said. First, if you use the best two-temperature fit which the computer determines and just throw away all the elements above neon, Figure 6 is the contribution from the lower-Z elements. That is, this is closer to the continuum than are the low points between the line features in the raw data. What I am going to do now is synthesize the data by adding one element at a time. Iron L is responsible for most of the excess at the lowest energies (Fig. 7). Figure 8 adds the contribution from magnesium. Figure 9 accounts for the helium-like and hydrogen-like transitions due to silicon, and I can do the same thing for sulphur in Figure 10. There are still features which are, in fact, unambiguously ascribable to argon and calcium, as you can see from Figure 11. Virtually all the young supernova remnants we have seen, with the exception of the ones (like the Crab) which are never going to snow plow up enough material from the interstellar medium to be thermal X-ray sources, have spectra that look like that in Figure 11. There are about 12 of them now which we have seen.

Figure 12 shows Tycho, which is just one example. Tycho is bigger than our whole field of view (while Cas A just about fills it). So we will be able to look at four quadrants of Tycho and see what the subtle differences in the temperature and the abundances are between them. What we are finding is that in the case of Cas A, the abundances for the mid-Z elements which are due to oxygen burning such as silicon and sulphur are about a factor of 3 higher than solar. We are pretty sure that the trend is correct; we are not so certain, however, that the absolute numerology is correct. The reason for that is that the models we are using are strictly collisional equilibrium models and we are sure in all these cases that we have higher temperature components which are not contributing very much to these lines, but which are necessary for the continuum at higher energy. The second point is that the collisional equilibrium models themselves are in the process of being changed all the time, because more and more detailed atomic physics are going into them which can change the best-fit abundances. The shapes do not change very much but the abundances do, and John Raymond and Barry Smith are both, in fact, working on such refinements right now. I guess I should point out that not all the spectra we see have lines. Figure 13 shows the Crab Nebula, which is very very bright and has no line features whatsoever. This is the raw spectrum once again, and its shape just replicates the detector response to a power law. In this case I felt it was fair to invert the spectrum because there should be no pronounced spectral discontinuities in the source spectrum (Fig. 14). The only features observed are a little dimple at about 1.8 keV which is due to interstellar silicon, and the interstellar medium is responsible for the increasing absorption at lower energies. That is something that we see for almost every object.

Sources other than supernova remnants have exhibited thermal line emission as well, although the line emission is not quite as intense. Figure 15 shows the star Capella; it is only 14 parsecs away and is a G star in a binary system. The lines which can be seen are due predominantly to material at less than 10 million degrees but to get the continuum at high energies, it is necessary to introduce a component which goes out to about 50 million degrees or so. We cannot uniquely specify what the whole range of temperatures is, but we can insist, because of the iron, magnesium, silicon, and sulphur features we see, that there has to be a dominant component below  $10^7$  degrees, and lesser emission out to at least 30 million degrees.

Quite a different kind of object is M-87 (Fig. 16) which is a giant elliptical galaxy at the center of the Virgo Cluster. Here we fit with a single temperature, but the features are not as apparent because the temperature is much higher. The M-87 fit is to about 20 million degrees, and as we go up in temperature the line features will not only shift to higher energies, corresponding to higher ionization states, but will also become less prominent as the continuum takes a larger responsibility for cooling the source.

Going yet higher in temperature (Fig. 17), NGC 1275, a Seyfert galaxy at the core of the Perseus cluster, has a temperature corresponding to almost 50 million degrees. At 50 million degrees, we should not be able to see any more line features, but in fact the bumps and wiggles which the model demands to get an acceptable Chi-square are at energies prescribed by some contamination from material closer to about 10 million degrees. Finally getting up to higher temperatures, Figure 18 shows dwarf novae which have such high temperatures that we can only measure the flat continuum; they have temperatures corresponding to about 8 kV which is almost 100 million degrees. In the case of SS Cygni, it is difficult to see but in fact there are very slight bumps and wiggles even for temperatures this high, but certainly nothing is very obvious. For EX Hydrae, which has the large fraction of its energy in this very high temperature component, there is much more significant spectral structure. This means that less than 1 percent of the total X-ray energy has to be at a temperature of about 10 million degrees or so to account for these very obvious bumps and wiggles. I don't think that we realized the full significance of that until we started looking at sources which we thought were distinctly nonthermal. For example, Figure 19 is a HEAO A-2 photon spectrum of MK 501, inverted so that you can see that it really does look like a straight line on log-log paper. That is the BL Lac object you have heard quite a bit about this morning. We have got an SSS spectrum from it taken at a different time (Fig. 20) so perhaps the fact that the spectral index is about the same is coincidental because you have already heard that it varies, but this is over a smaller dynamic range. We don't see any line features from Mk 501; it just looks pretty flat, with the low-energy turn-over corresponding to just as much gas as it would take to see the object through the  $3 \times 10^{21}$  or so hydrogen atoms per square centimeter in our own galaxy between us and the object.

In general, we have been disappointed when we have looked at compact extragalactic sources (3C 273 does not have any apparent features either); however, remembering that it takes just a very small contamination in terms of total energy from low temperature stuff to stick out, let's look at Figure 21, which is the spectrum we see from the unusual Seyfert galaxy 3C120. This again is the raw data fit with the best power law that we can get. You can see there is some obvious structure which we can't quite match; in fact, we can't get an acceptable fit at all. What I have shown in Figure 22 is exactly the same continuum just lowered by a few percent to illustrate the possibility that what we are seeing is some lines superposed on that power law spectrum. In fact, if we ask a computer to find the positions of possible lines which could be in there, the results are shown in Figure 23. The most prominent proto-line happens to correspond to exactly the helium-like feature in silicon 13 which we see from most of the thermal sources which we have looked at, red shifted by a  $Z$  of 0.033, which is the accepted red-shift of the object. Also found is a feature corresponding to a

slightly lower ionization state of sulfur, and the lowest energy feature can't really be associated with anything sensibly at that red shift, but there are ways that we can get it just by suitably absorbing a thermal spectrum. This analysis has not been properly performed yet. We can red shift thermal models properly now, but there are a variety of parameters which are still uncertain, and the final analysis will be performed when all the response function uncertainties are resolved in the production data. But it certainly looks very very tantalizing. What it means is that we might be able, with just an infinitesimal contamination by a thermal component at about 10 million degrees corresponding to a tenth of a percent or a hundredth of a percent (in terms of a total energy) from nonthermal X-ray sources, to unambiguously get their red shifts in X-rays.

There is a source, called Cygnus X-3, which to those of us who have done some spectroscopy in X-rays with proportional counters is sort of our favorite because it has the largest amount of iron line emission. In fact, the iron line emission of Cygnus X-3 alone ranks in the top 30 or so sources in the whole sky, in terms of apparent luminosity. We would have expected then, because we ascribed that emission to fluorescence, that if any object was going to give us the opportunity to observe silicon or sulfur fluorescence, which should be down by about a factor of 20 in equivalent width from what iron is, it would be Cyg X-3. It would take me a long time to explain how we went from the lower trace of Figure 24, which didn't fit at all well, to the top trace (which fits much better). Below about 1.2 kV, we don't see any X-rays at all from the source, and the data points plotted below 1.2 keV just correspond to incompletely collected charge from photons which entered at much higher energy. The spectral feature can be fit quite precisely by insisting that there has to be both fluorescence and a thermal component from sulfur. We have been successful in finding fluorescence from sulfur from Cygnus X-3, but the prospect of doing it for other sources is not too good.

In addition to looking for fluorescence, the more general thing we have been doing with pulsars for a long time now is the phrase you heard this morning called "pulse-phase spectroscopy." Figure 25 shows data, again from the solid state spectrometer, from the pulsar Hercules X-1, which has a period of 1.24 sec. The data all plotted twice for clarity, and the resolution enable us to unambiguously separate the energy ranges chosen. The lowest trace looks identical to pulse profiles which you have seen before from Hercules X-1 from 2 to 6 or 2 to 20 keV. and we have always supposed, based upon looking at those higher energy spectra, that the portion of the main pulse was the closest look we had at what we called the intrinsic pulse. This is because the spectrum of the pulse here was hardest, and we assumed that most of the emission at other phases was due to scattering from lower temperature material surrounding it. If we looked at the hardest energies, therefore, we

were seeing something corresponding to the raw pulse, or something close to it. Each of the traces if normalized such that the average value is in the middle, and the total range is from zero to twice the average value. As you can see, the pulse between 1.6 and 4.5 keV is almost 100 percent pulsed. Between 1 and 1.6, it is pulsed at only about half that, but the features correspond very well. At the lowest energies, however, what we had presumed was the hard part of the pulse lines up exactly with where the minimum in the soft flux is. So it looks like our supposition really wasn't too bad, and the maximum in the soft flux corresponds, in fact, to something very close to the minimum in the hard flux.

In summary, then, we think that the higher energy curve is our best measure of the raw pulse; and the lower energy trace arises from reprocessing in the sense that it is probably Compton-scattered near the Alven surface. Looking in a little bit more detail at these spectra, Figure 26 is just the raw spectrum obtained near the maximum in the hard pulse. If we compare that with Figure 27, the spectrum from the same source normalized exactly the same way during the portion of the spectrum where the soft flux is at a maximum, then we see that the two cross at about 1.2 kV. We expect that all the reprocessed emission is x-radiation from which, if we had the sensitivity, we could see fluorescence lines, and we are working very hard trying to find them. The expectation for the equivalent width of these features, particularly from silicon, is less than 10 eV. I think it is premature to talk about whether or not we have detected it because we are still refining our response function, but it looks possible for at least silicon. From anything else I am afraid it doesn't look quite so hopeful.

The last example of preliminary indications of the kind of spectroscopy which we can do shows an attempt to measure interstellar features. Figure 28 displays the spectrum of a transient source, called the Norma transient 1608-52; again the raw counts are plotted, and the dimple near 2 keV is what I would like to call your attention to. It is the silicon absorption feature from the interstellar medium. This feature is completely consistent with the column density to the source, but Figure 29 is apparently fit with exactly the same spectrum. The star with which it has been identified is a highly reddened object which is behind the Coalsack Nebula, so that if any star in the X-ray catalog is going to have more dust in the line of sight relative to the gas in the line of sight, then it is going to be 1258-61. The gas which is implied by the low energy absorption in 1608-52 is just about the same as the gas that it takes to fit 1258-61; however, where there is a very very small dimple in the curve for 1608-52 corresponding to exactly what the model tells us is interstellar absorption due to silicon, in 1258-61 there is, in fact, a much more pronounced dip, at least 3 times more silicon relative to hydrogen as required for 1608-52 and it occurs in exactly the right place, 1.83 kV.

What I have tried to do today is to show you some examples of the kinds of thermal features we see, the kind of nonthermal features we see, and the very exciting possibility of seeing small traces of thermal features in either much higher temperature objects or nonthermal objects. Our analyses are still quite preliminary, and we expect to go once more around the sky before the cryogen disappears, so that we are going to look at those objects which have been most interesting for us the first time to get better statistics, as well as those objects we haven't looked at yet which look like promising candidates for non-dispersive spectroscopy.

TABLE 1. X-RAY SOURCES

Class	"Typical" $\log_{10}$		
	$L_X/L_O$	$(100 \text{ cm-sec})^{-1}$	$T/T_6$
Stars	0	<0	0
Dwarf Binaries	1	0	2 (thick)
Supernova Remnants	2	1	1
"Exotic" Binaries	4	2	2 (thick)
Compact Galaxies	11	0	Non-thermal
Clusters of Galaxies	13	0	2

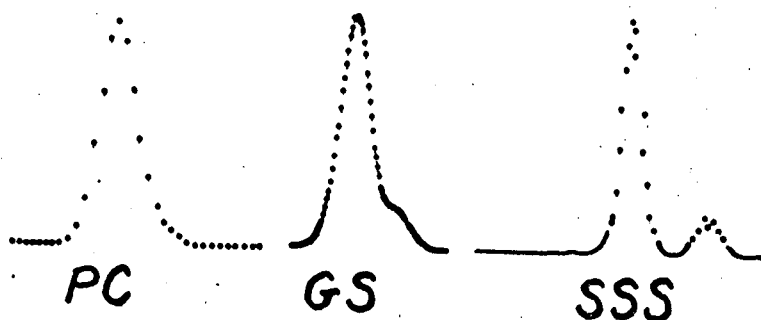


Figure 1



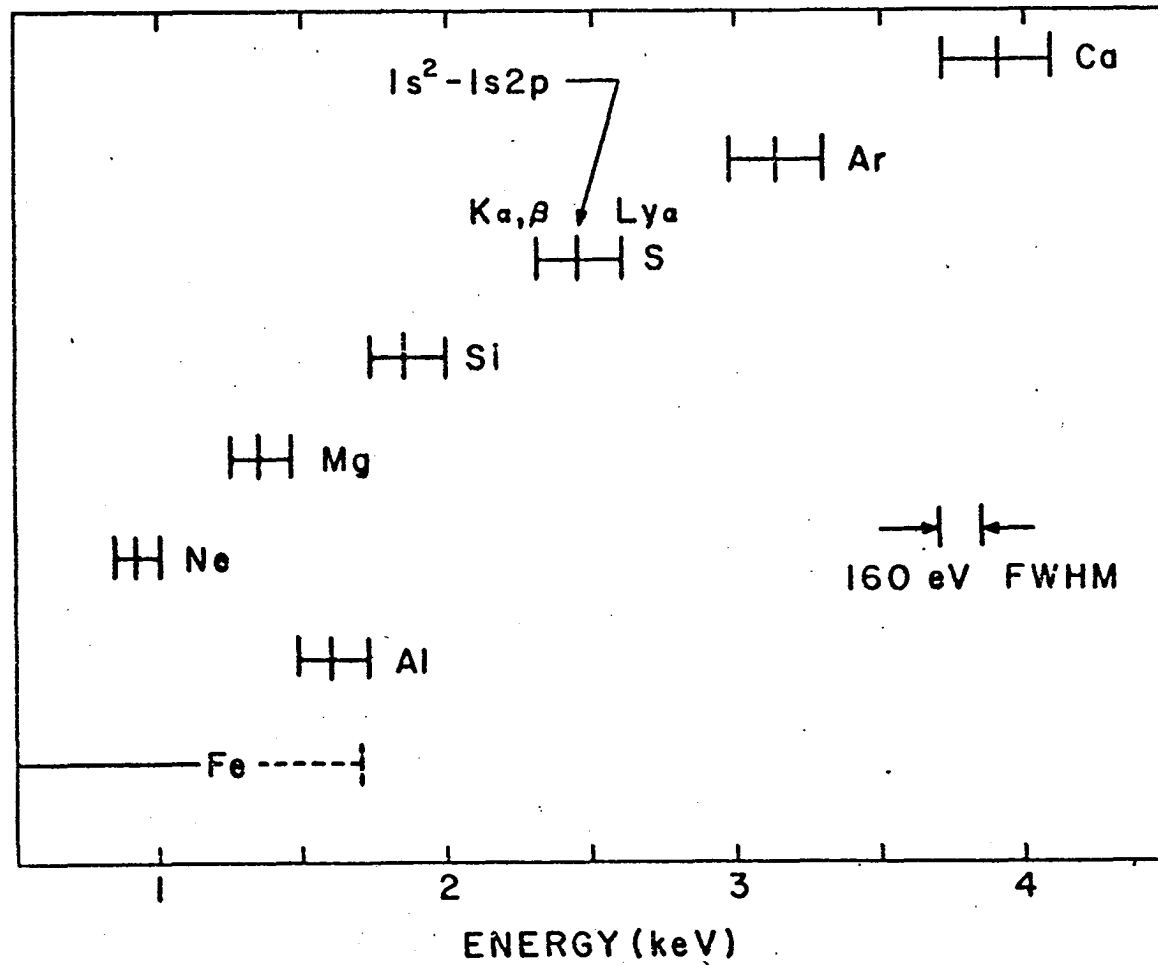


Figure 2

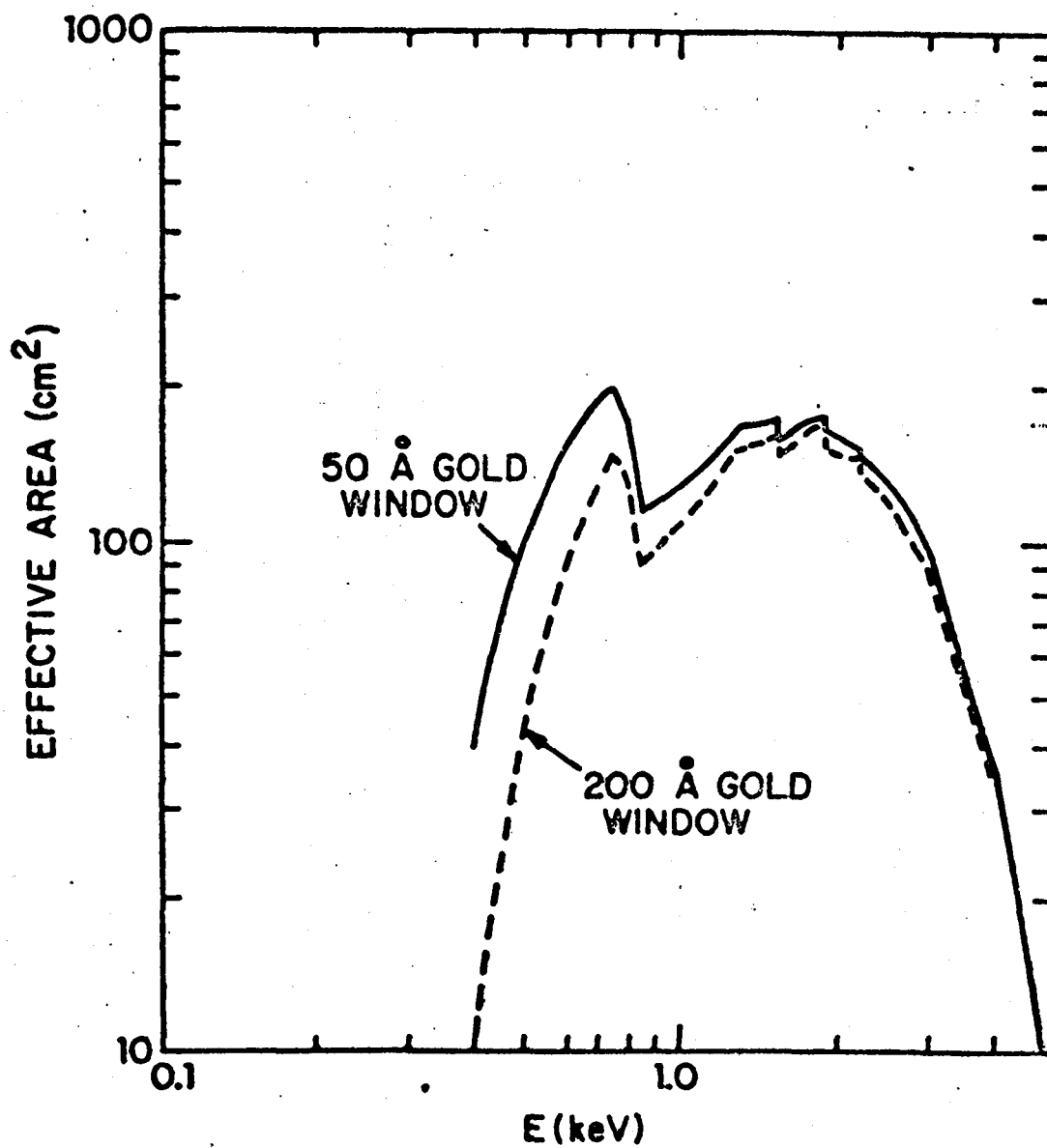


Figure 3. SSS effective area.

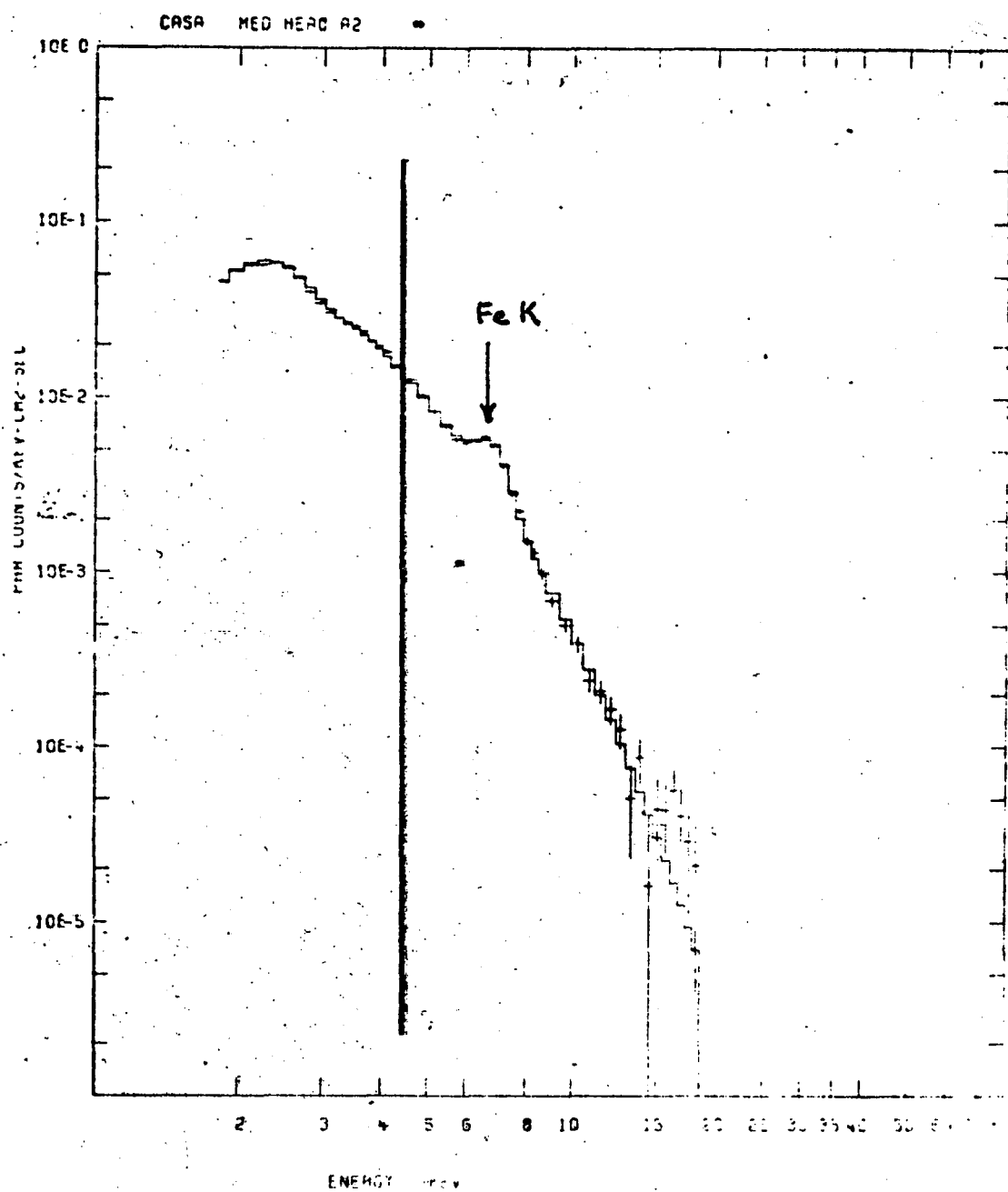


Figure 4

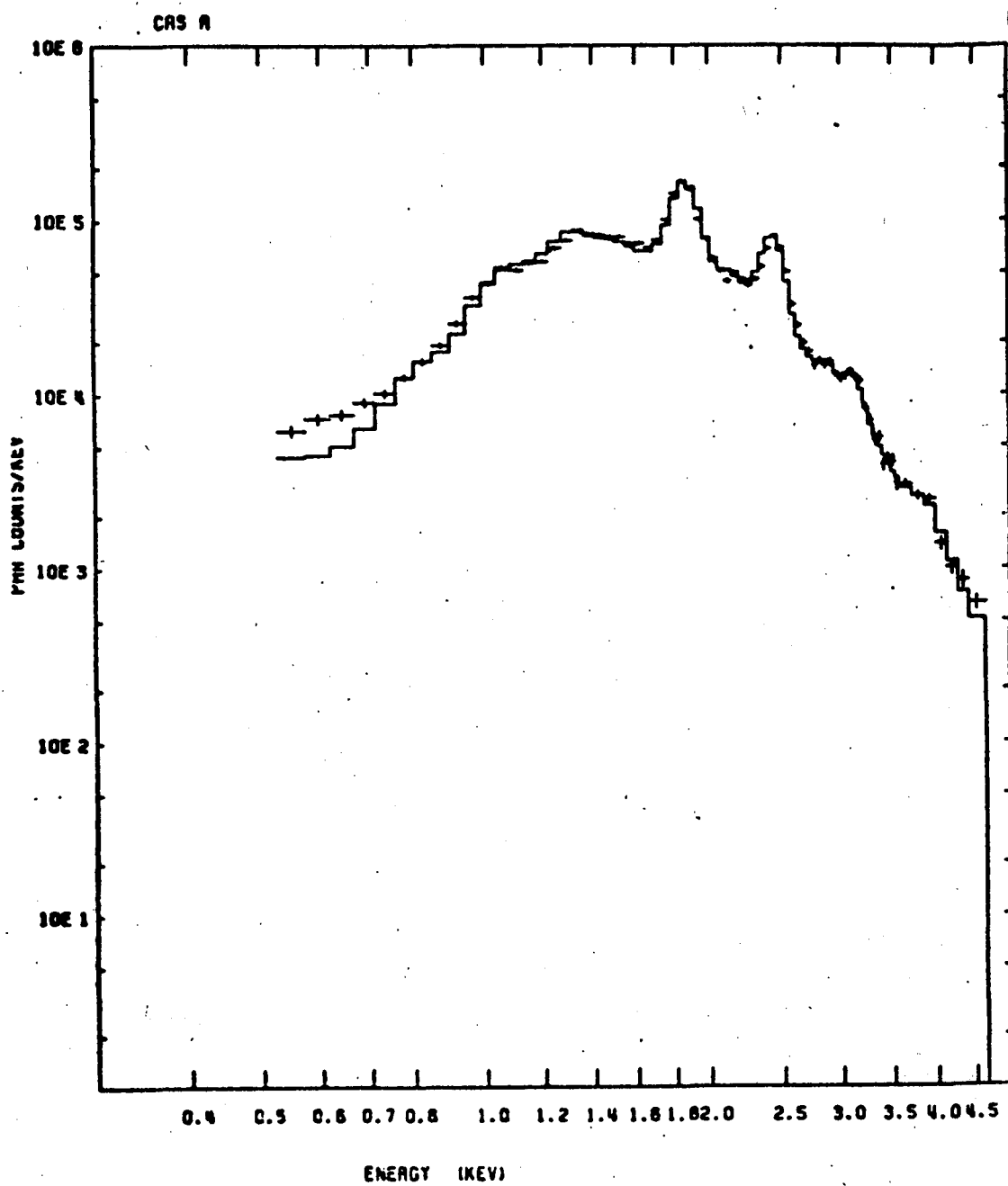


Figure 5

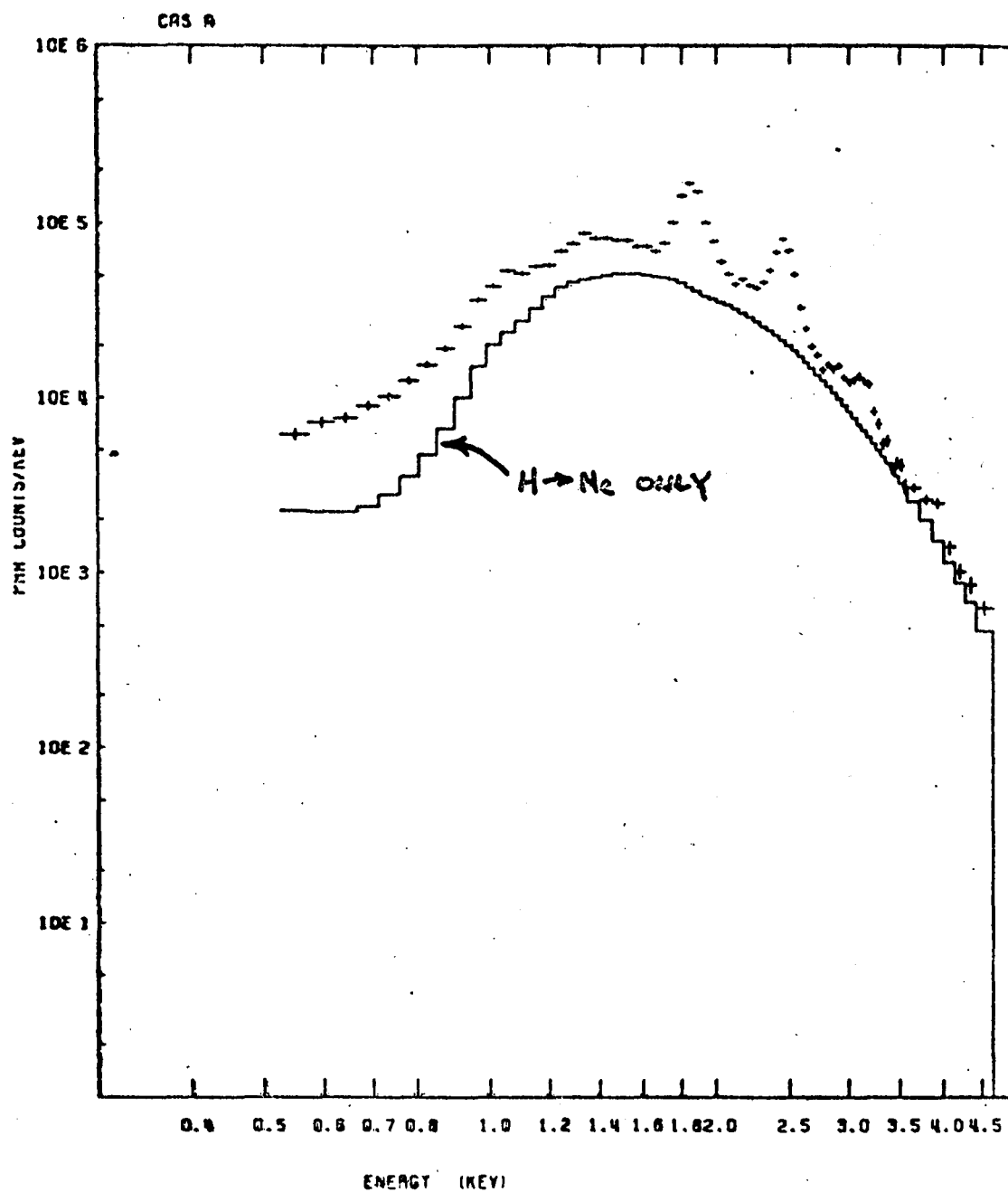


Figure 6

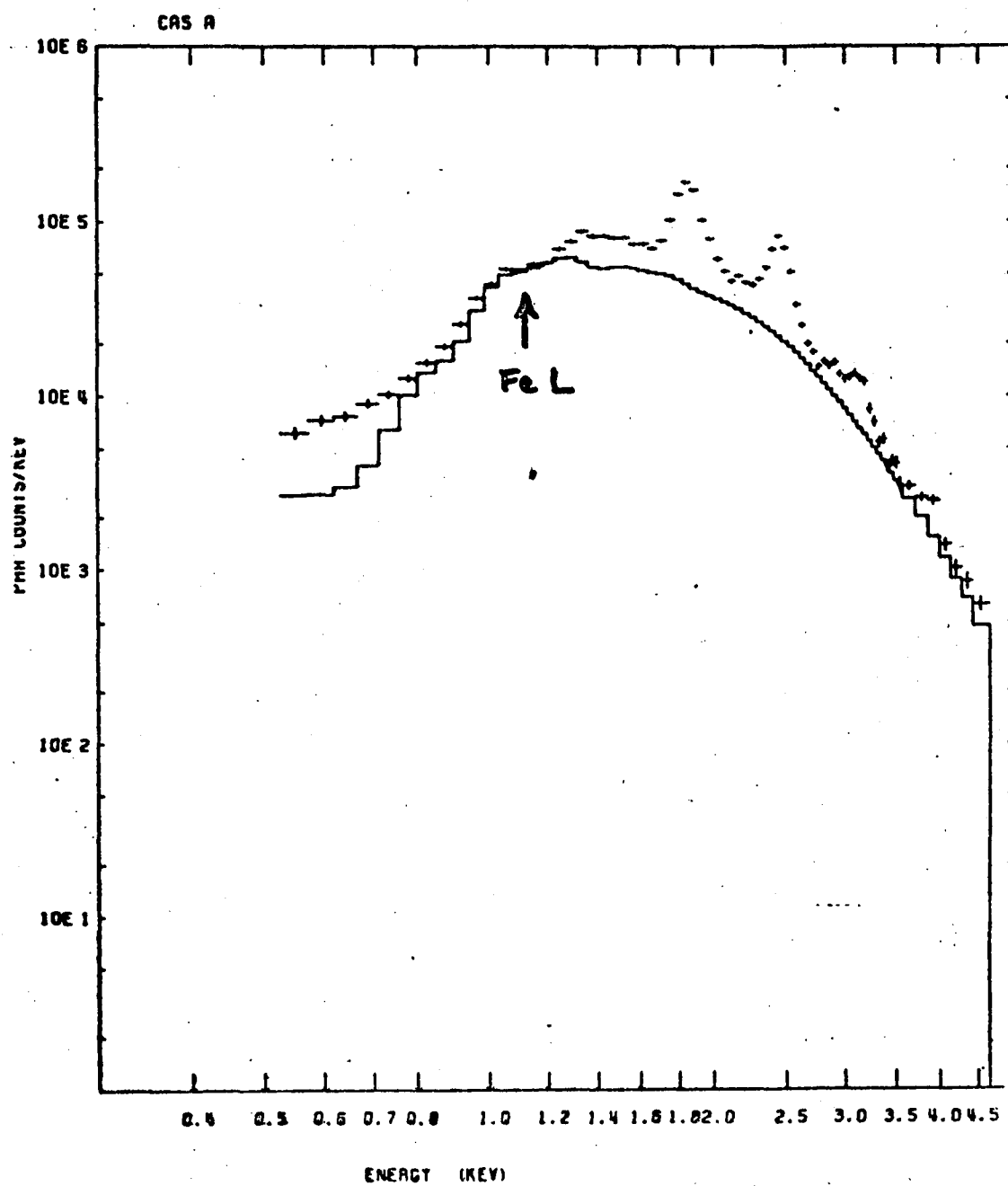


Figure 7

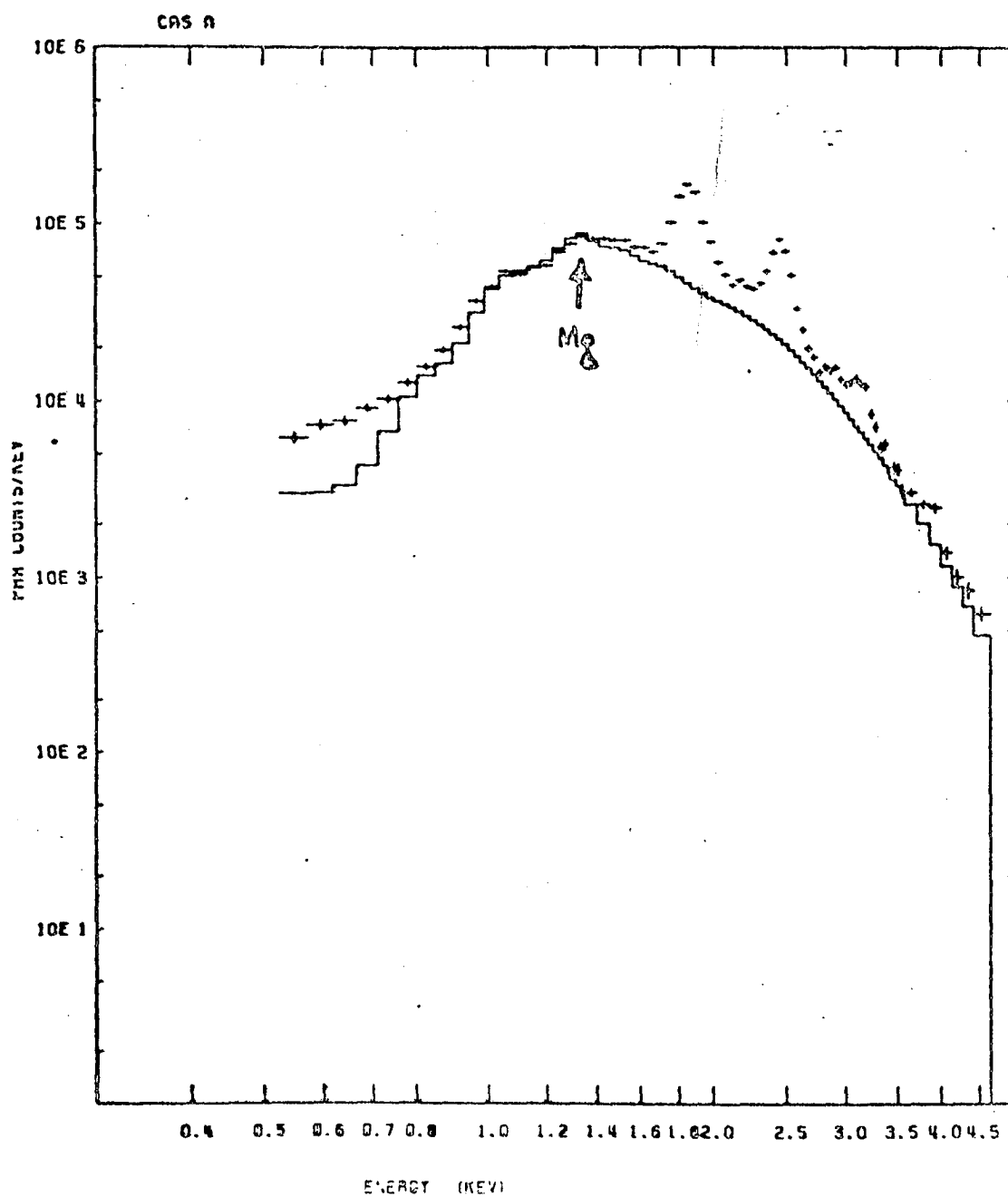


Figure 8

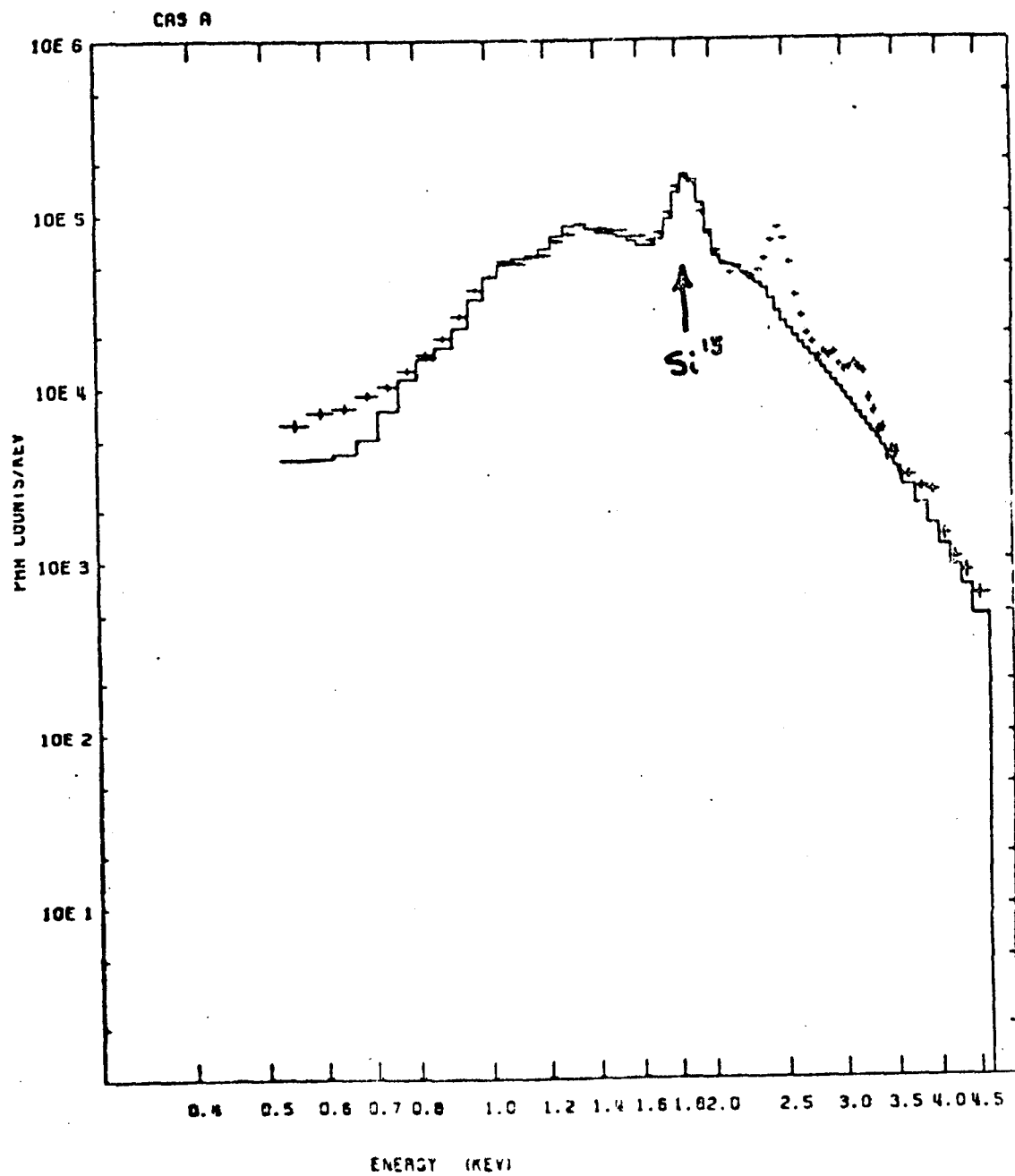


Figure 9



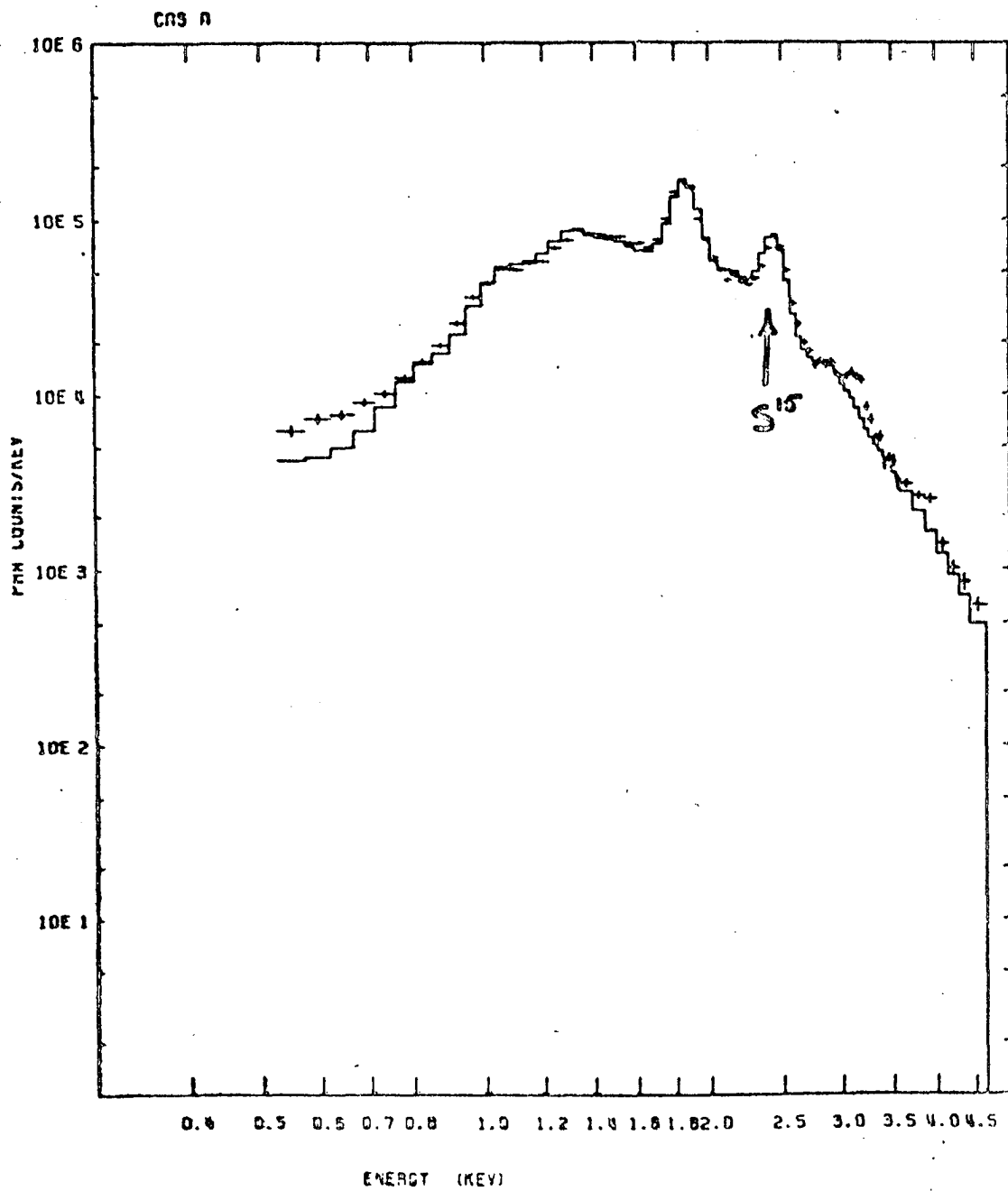


Figure 10

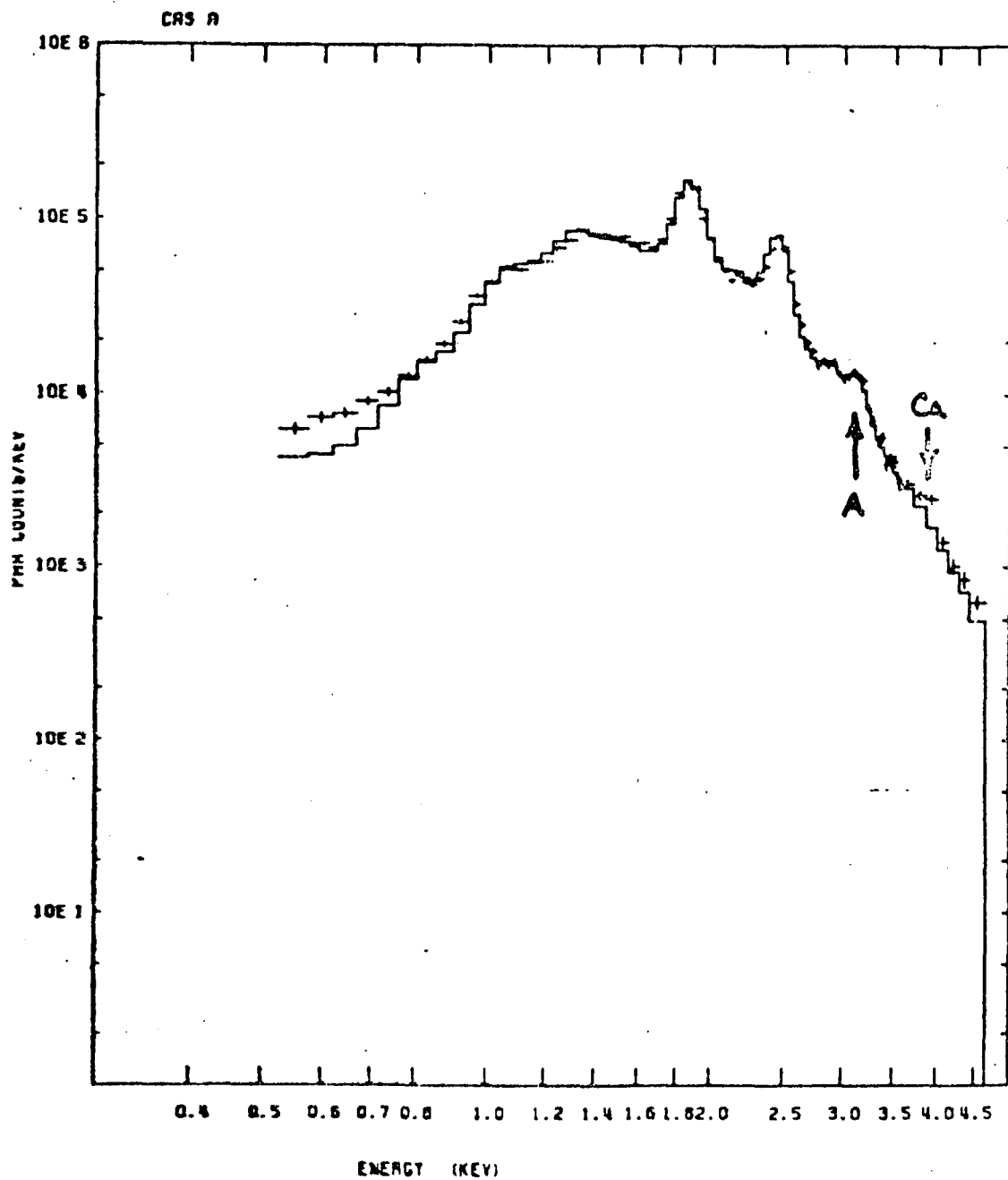


Figure 11

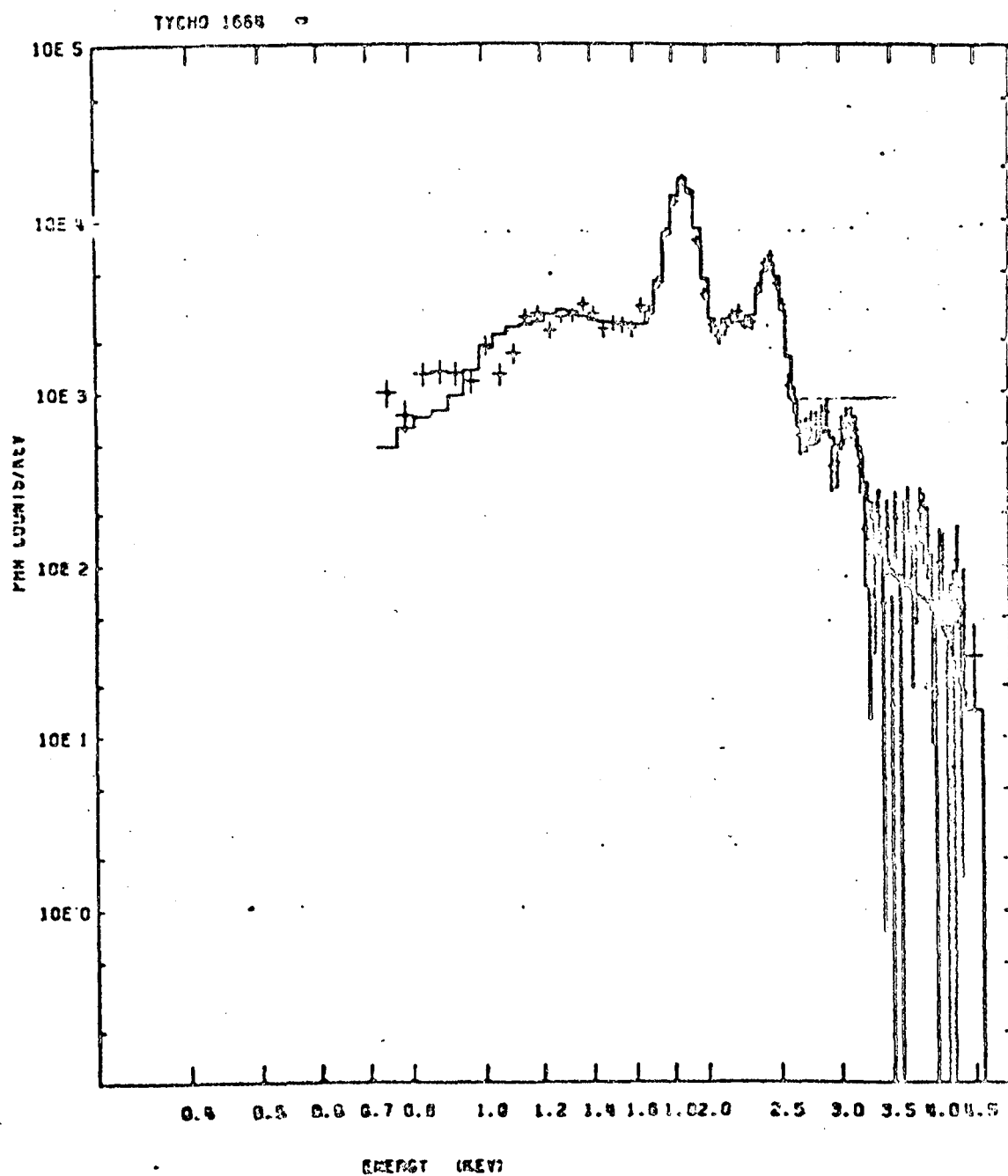


Figure 12

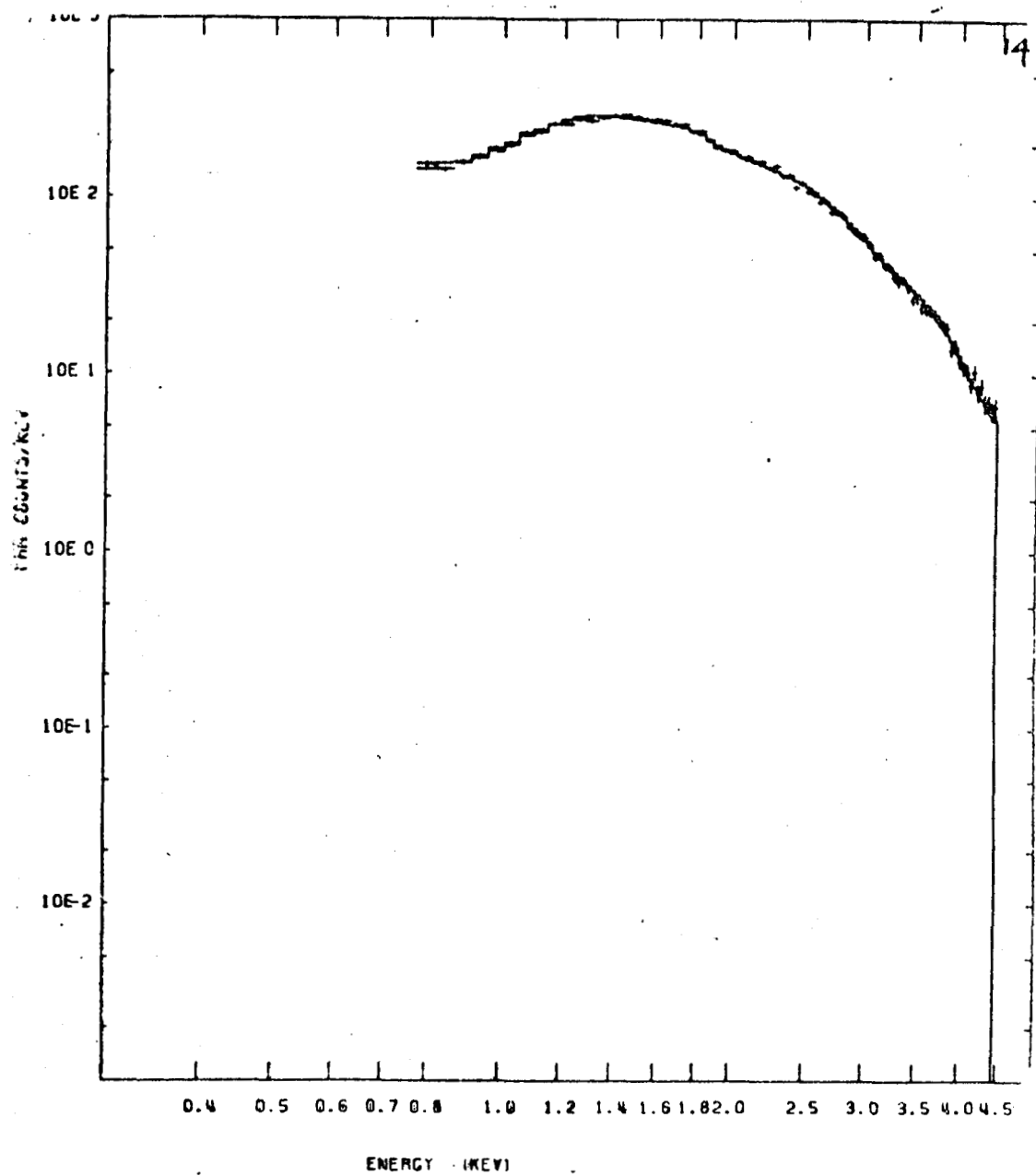


Figure 13

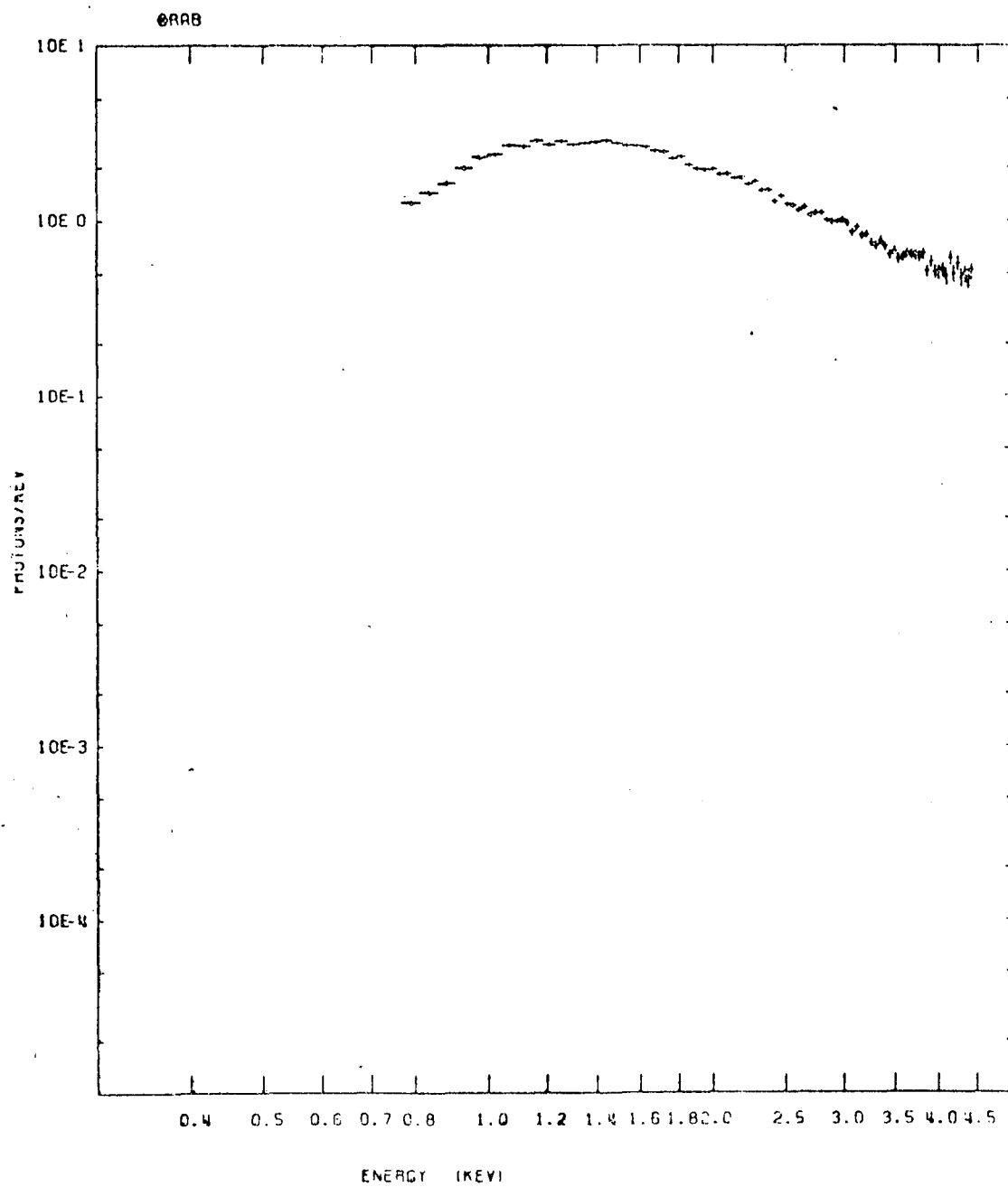


Figure 14

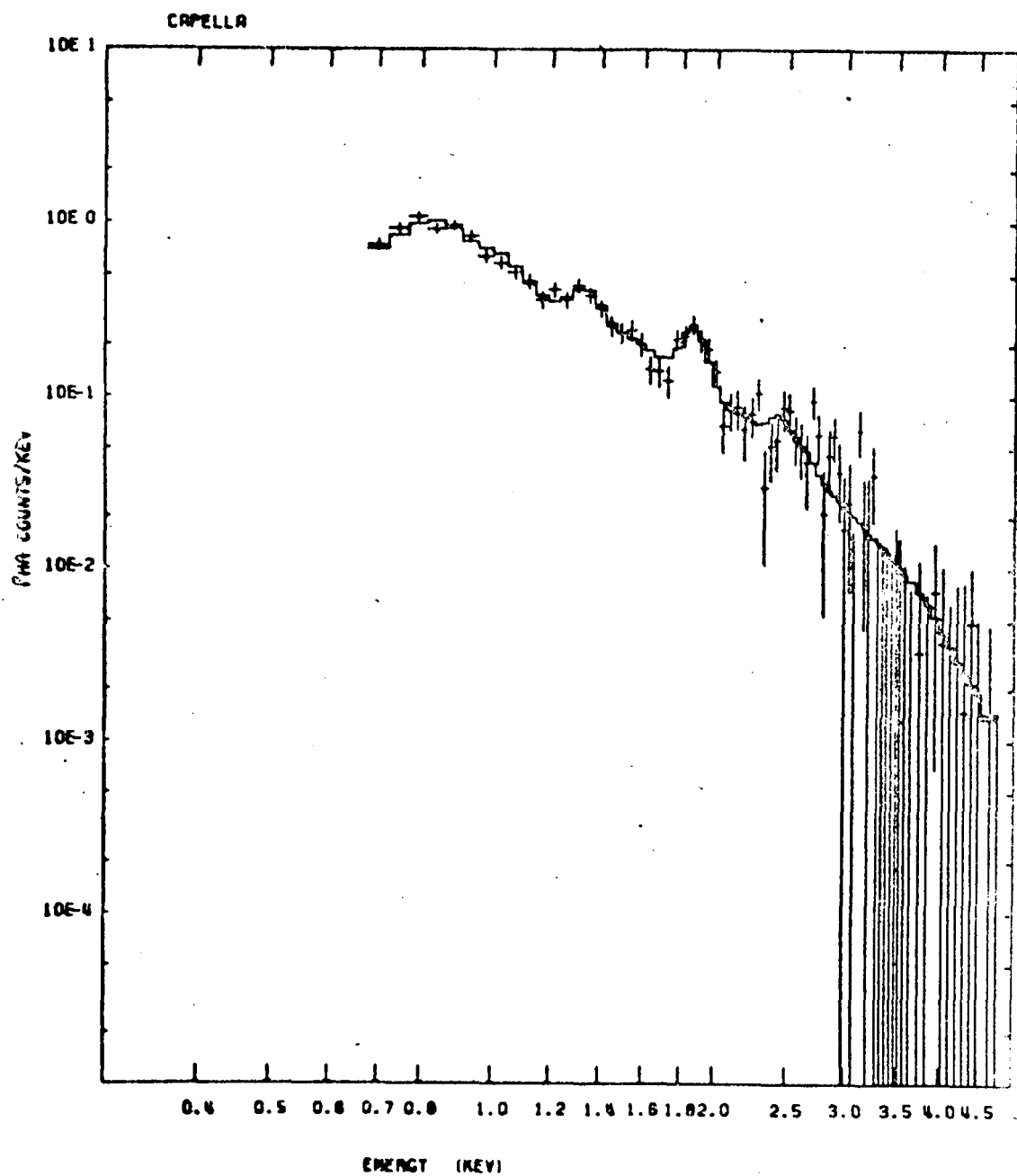


Figure 15

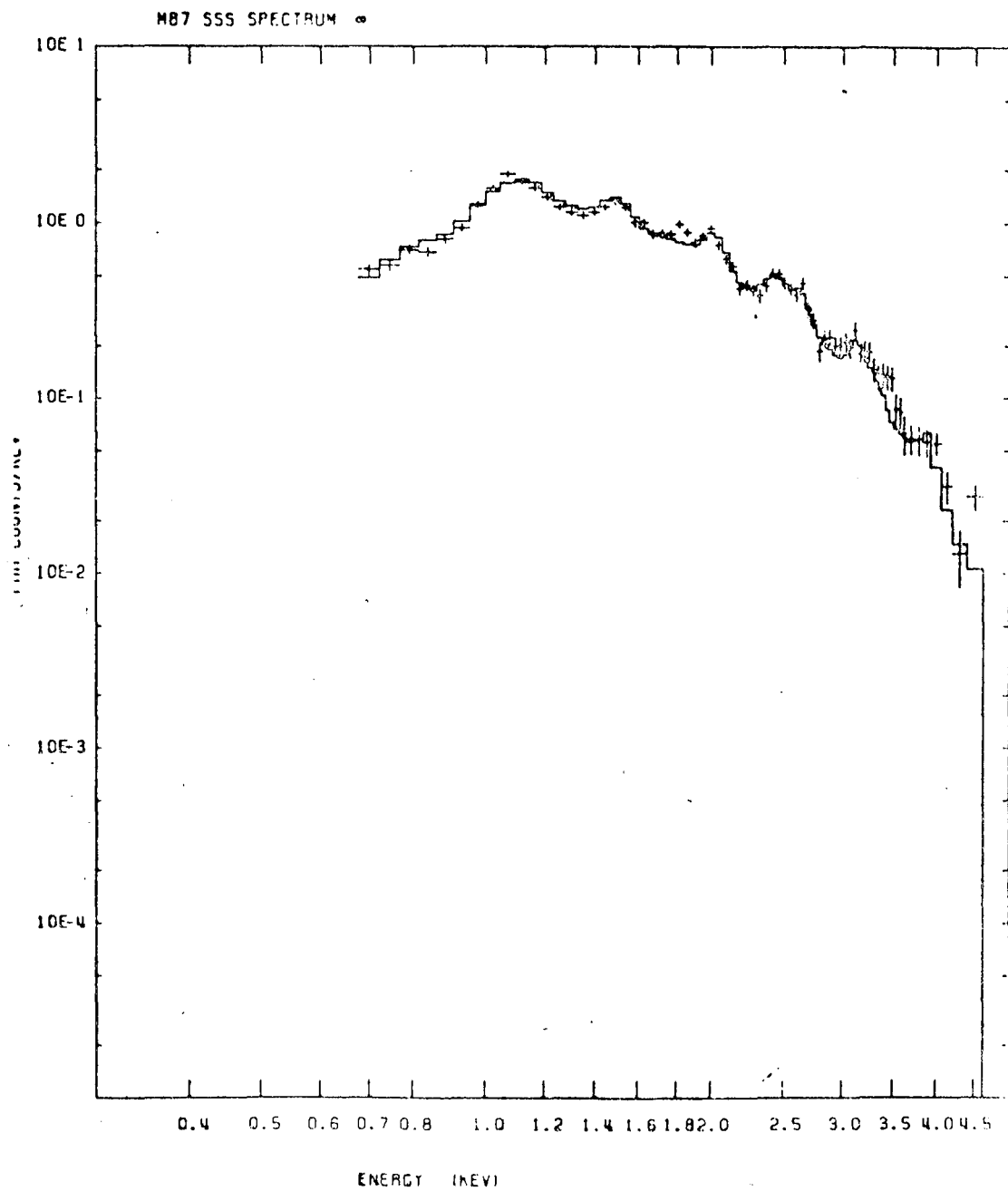


Figure 16

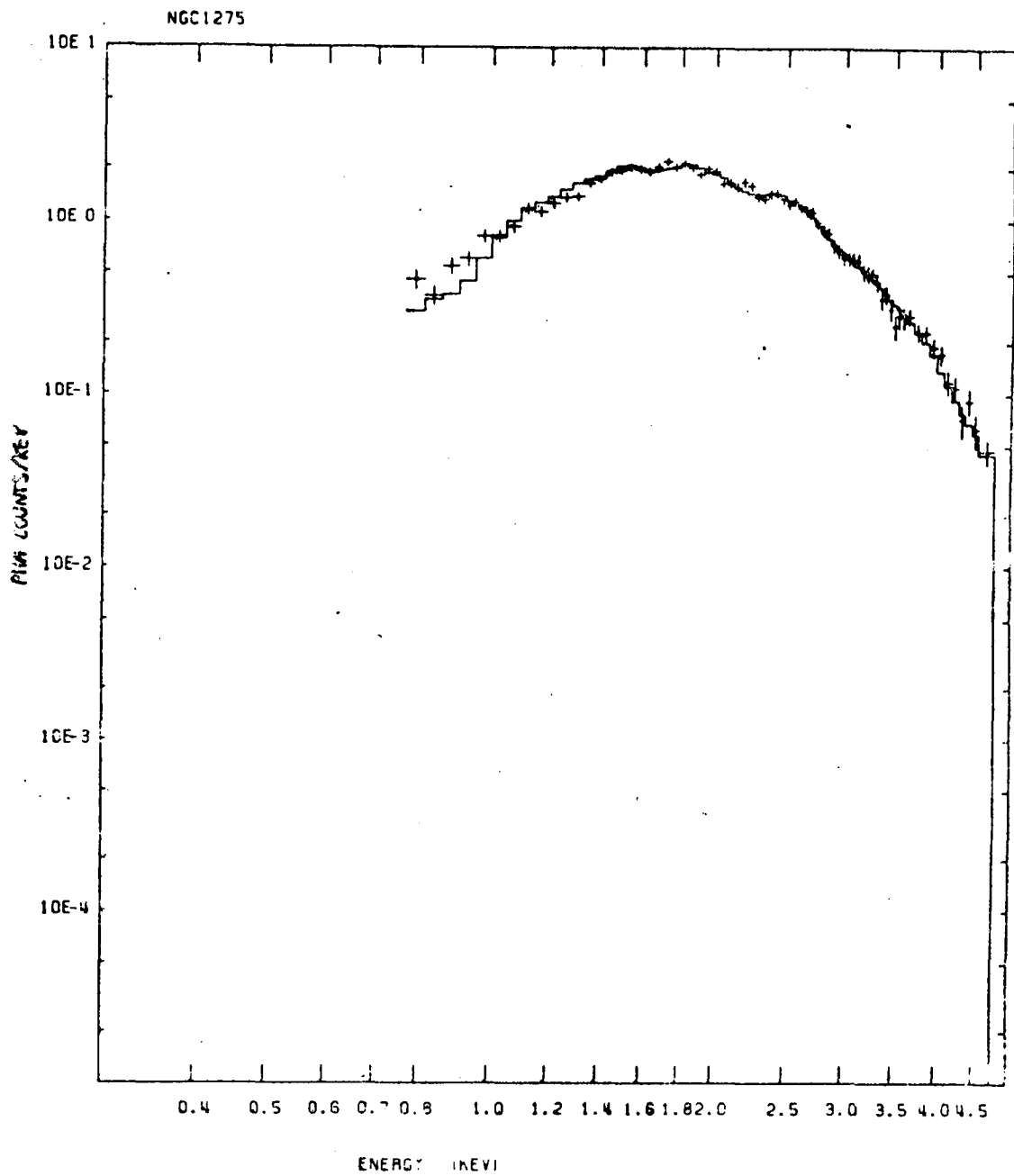


Figure 17



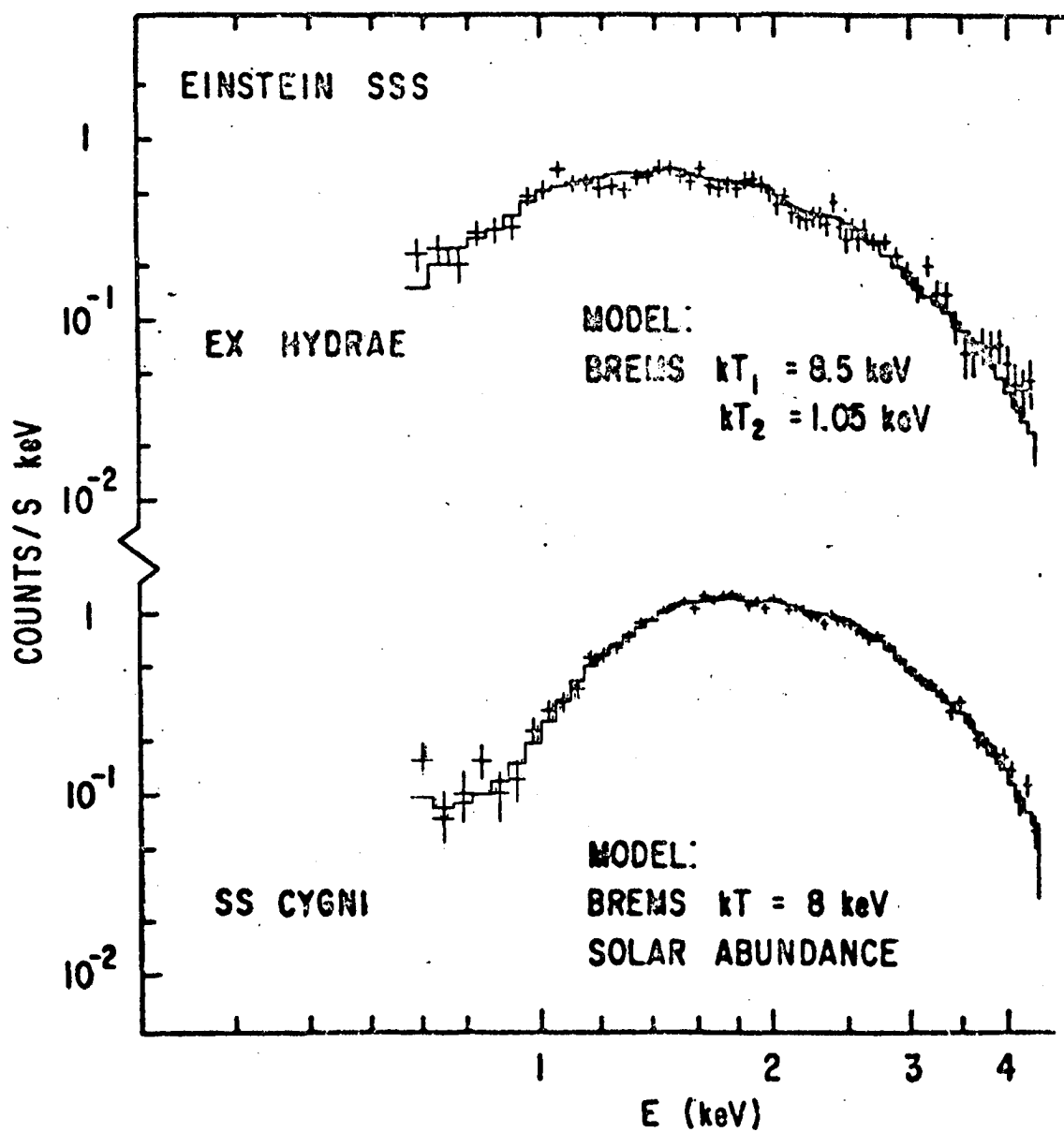


Figure 18

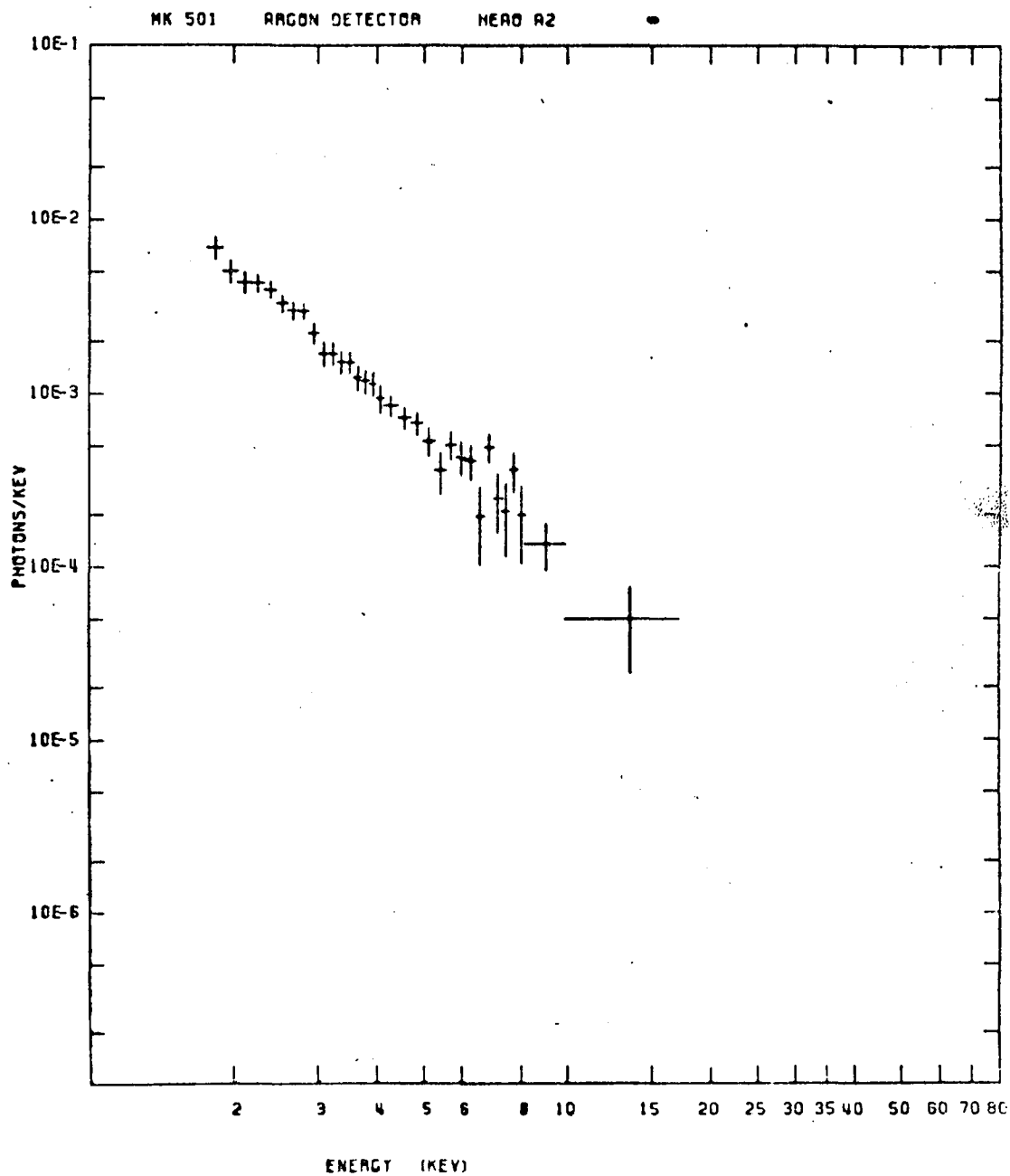


Figure 19

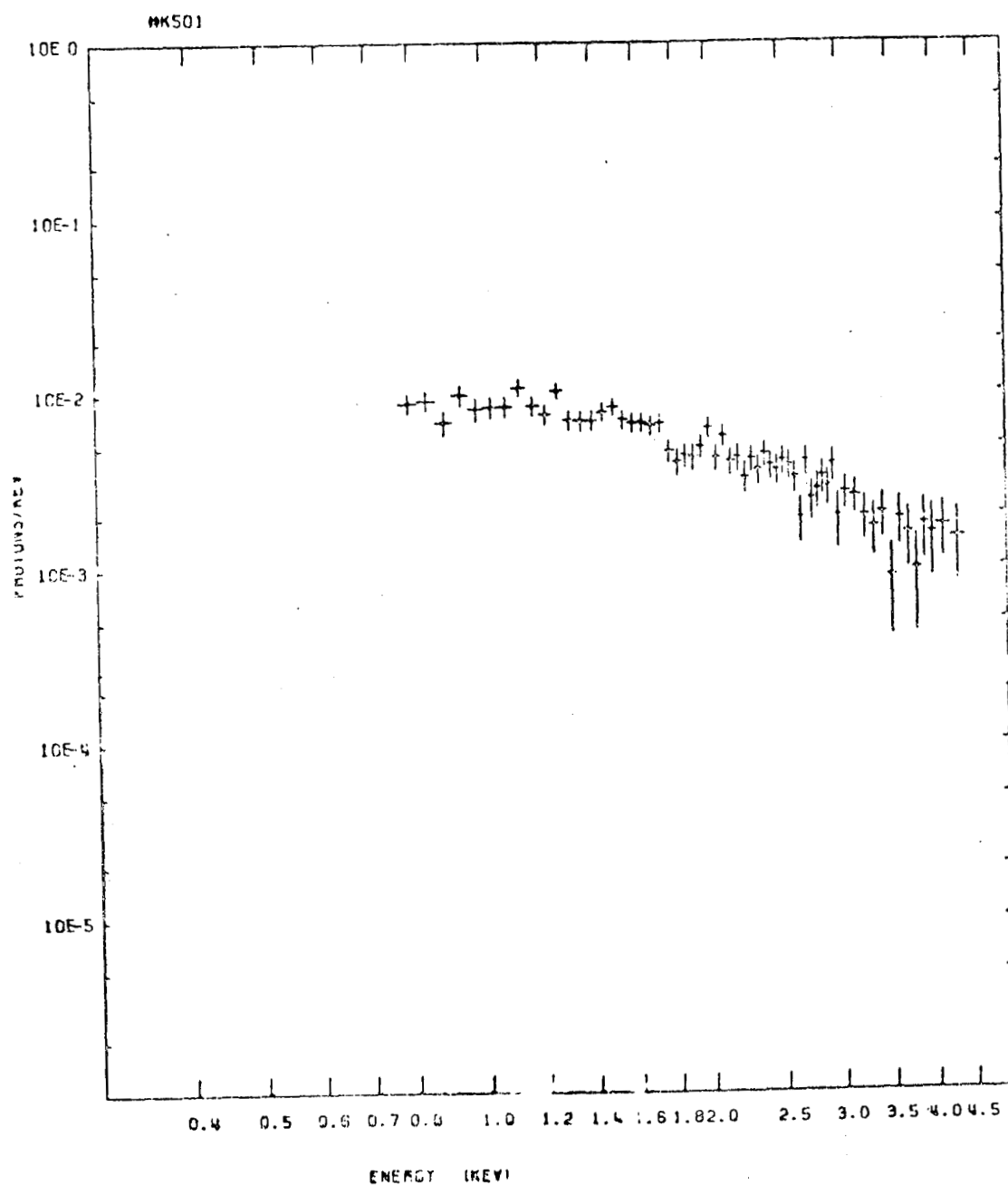


Figure 20

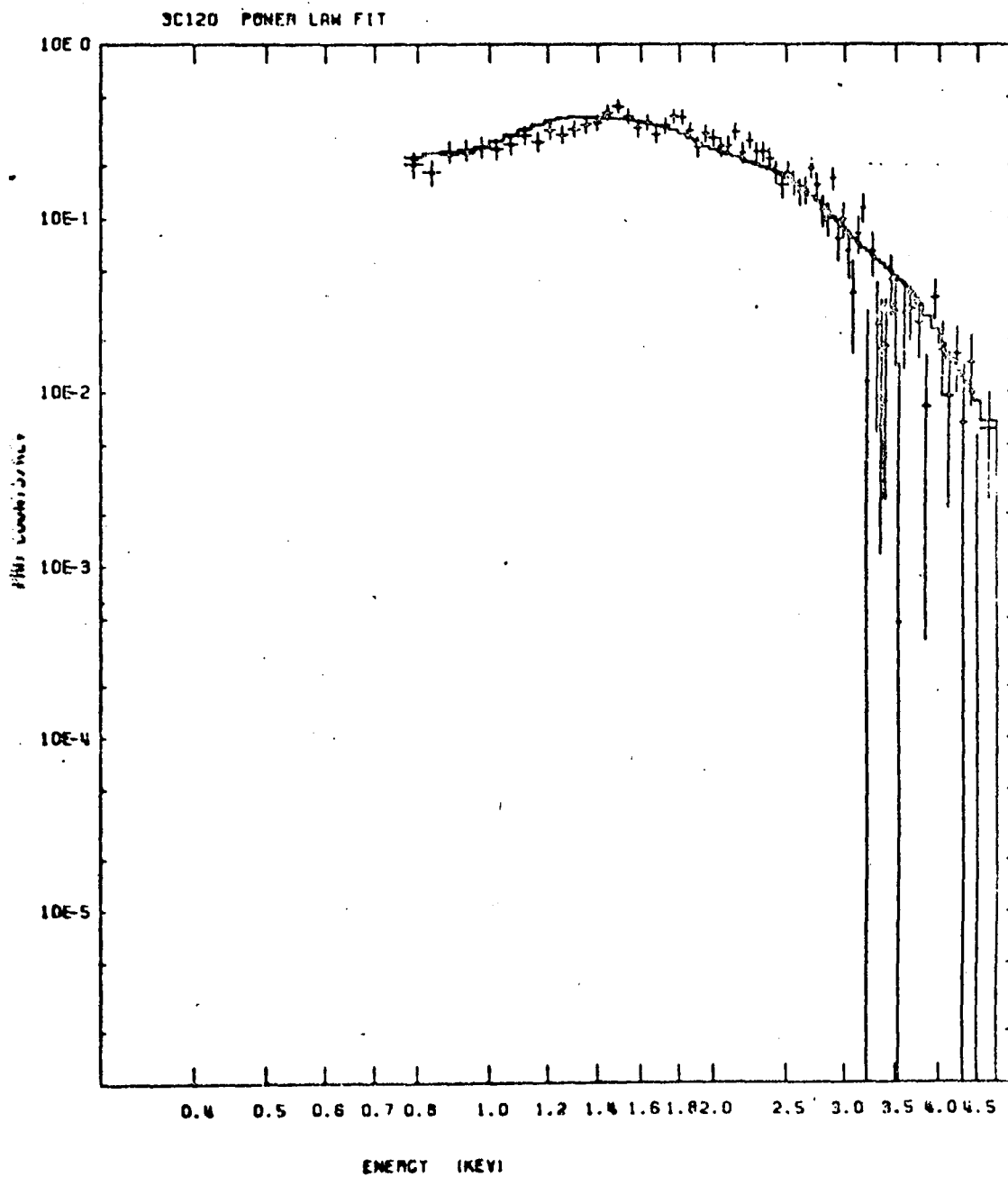


Figure 21

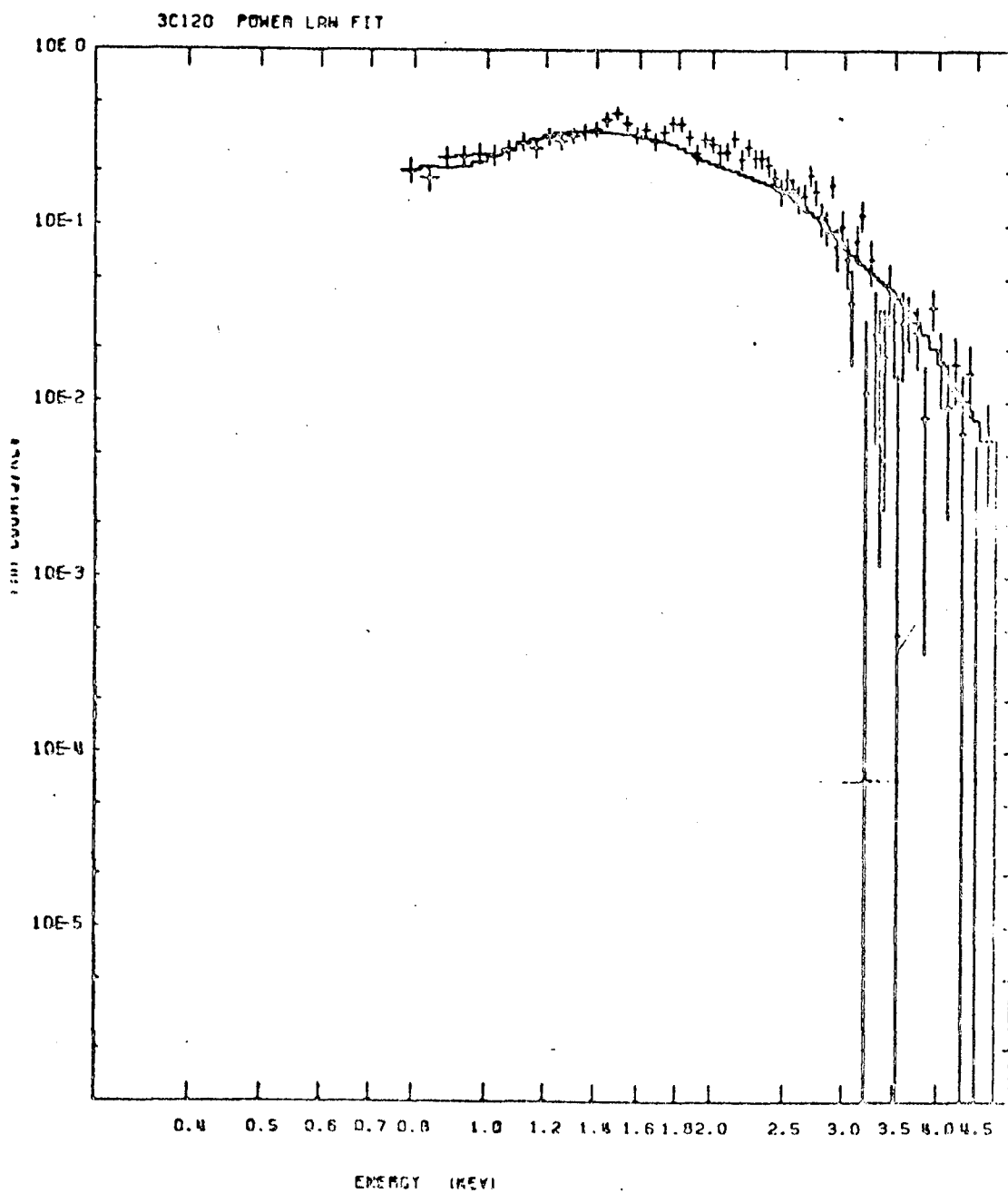


Figure 22

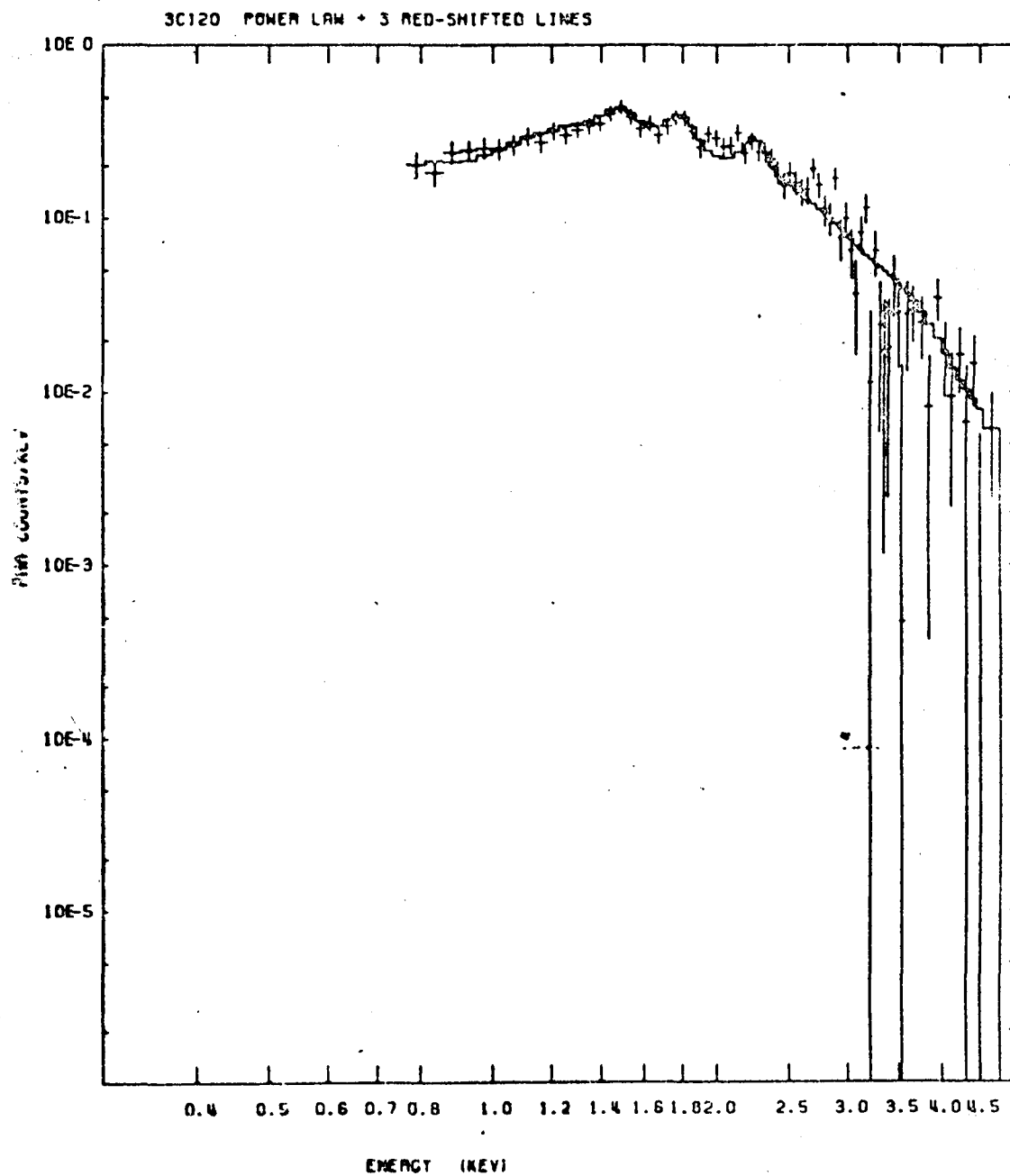


Figure 23

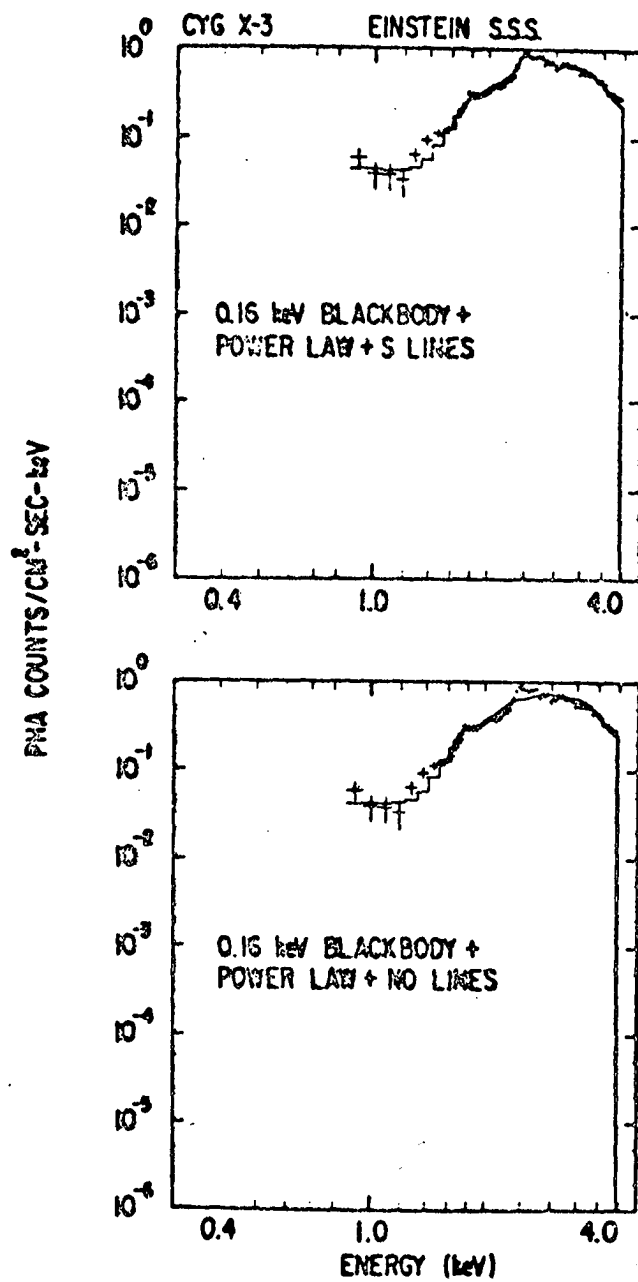


Figure 24

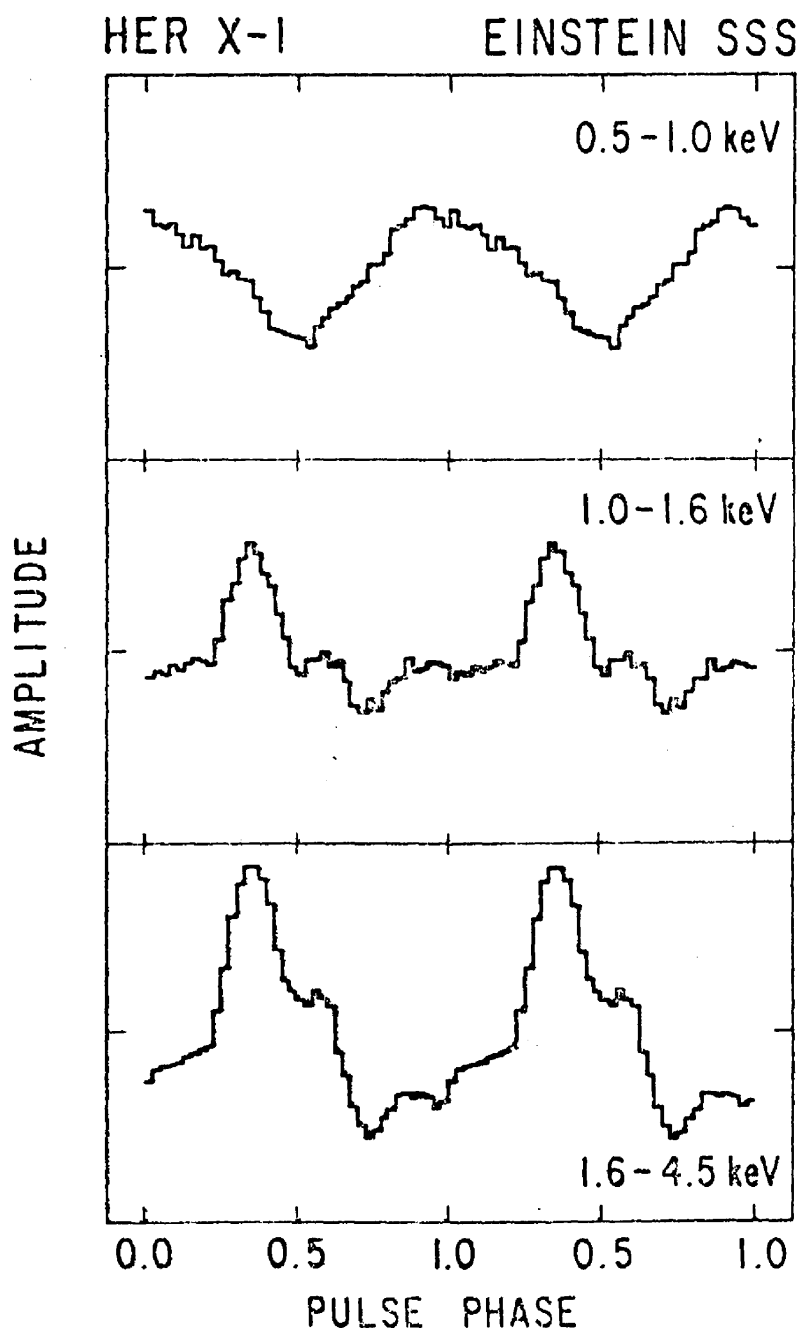


Figure 25



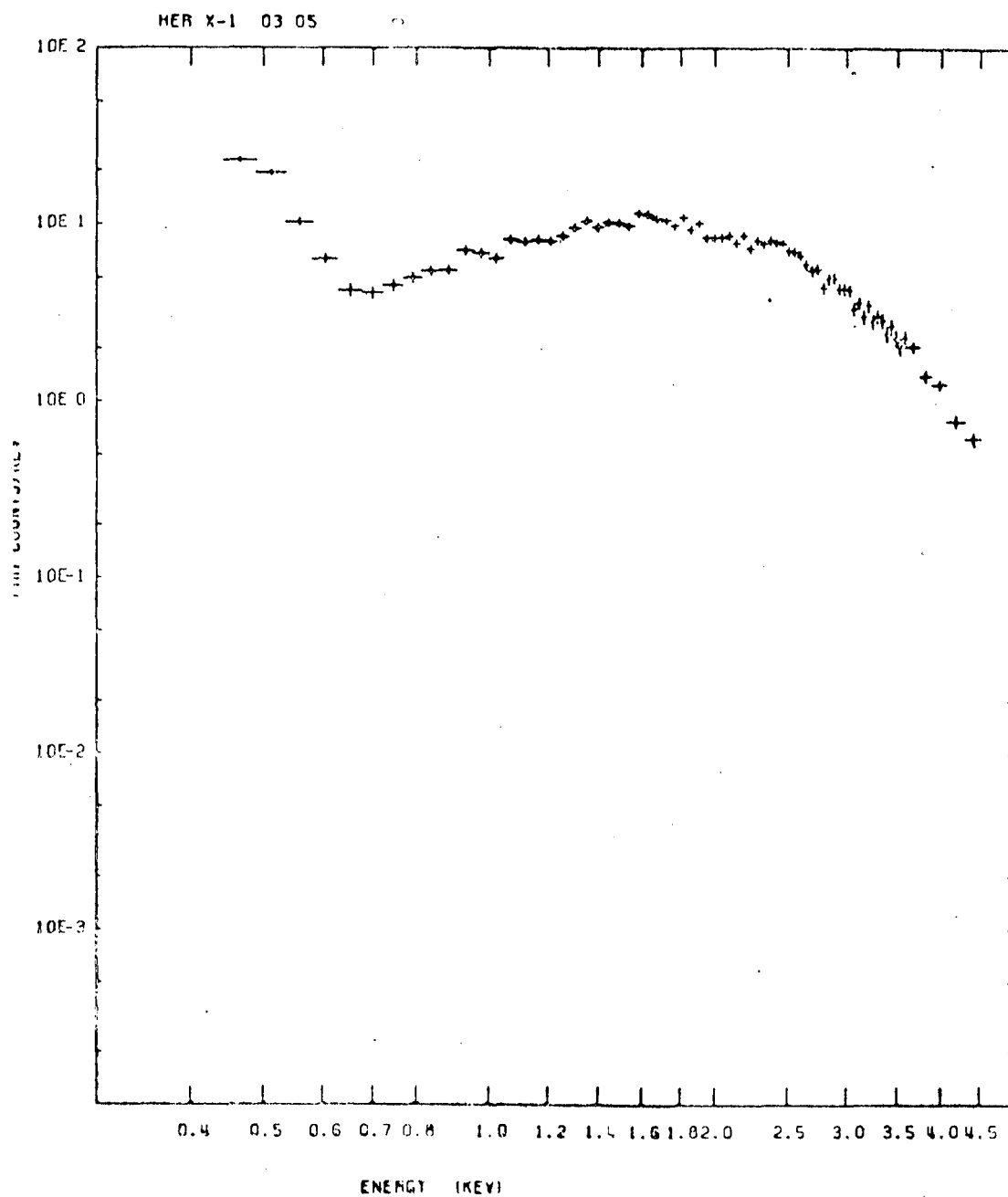


Figure 26

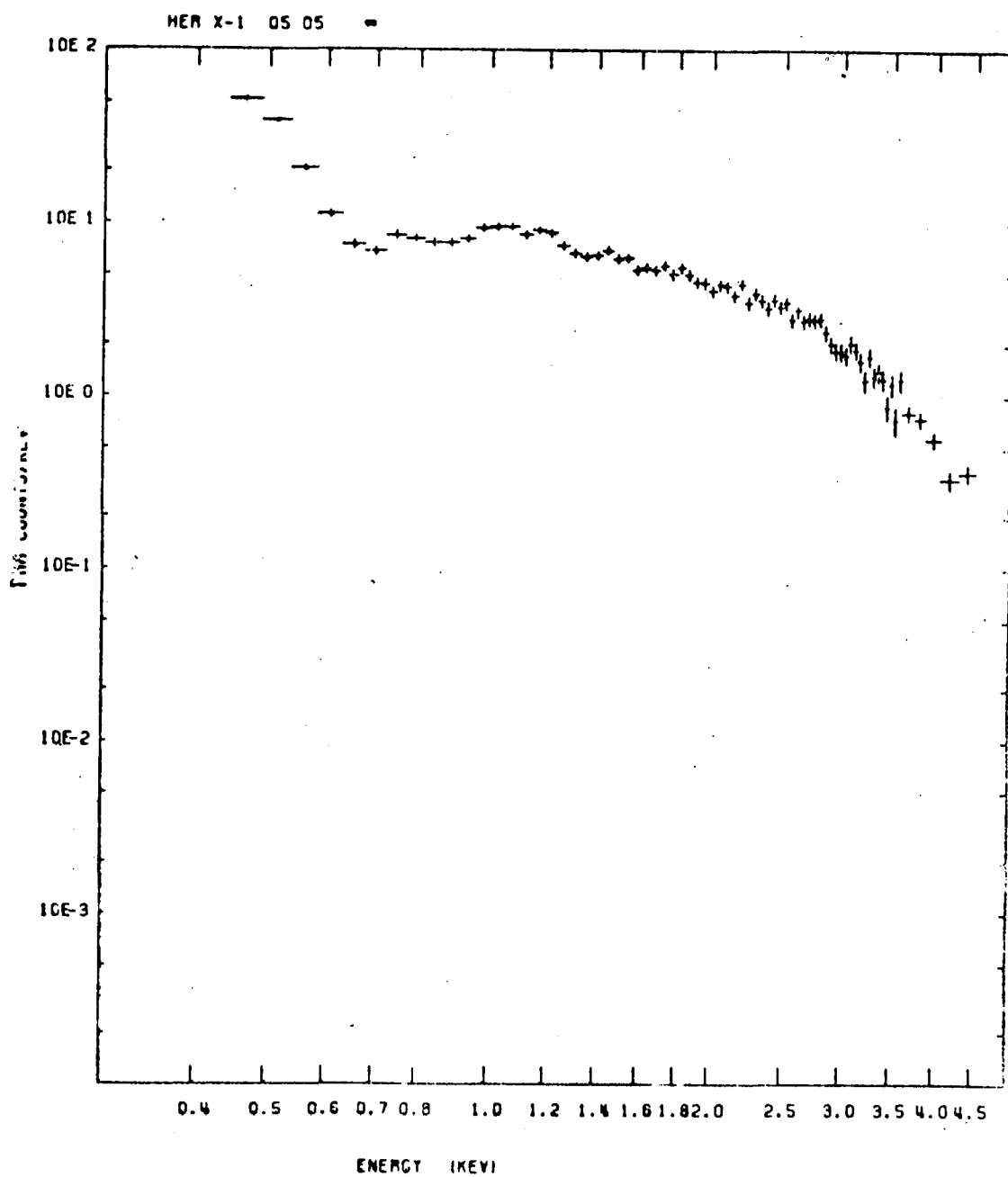


Figure 27

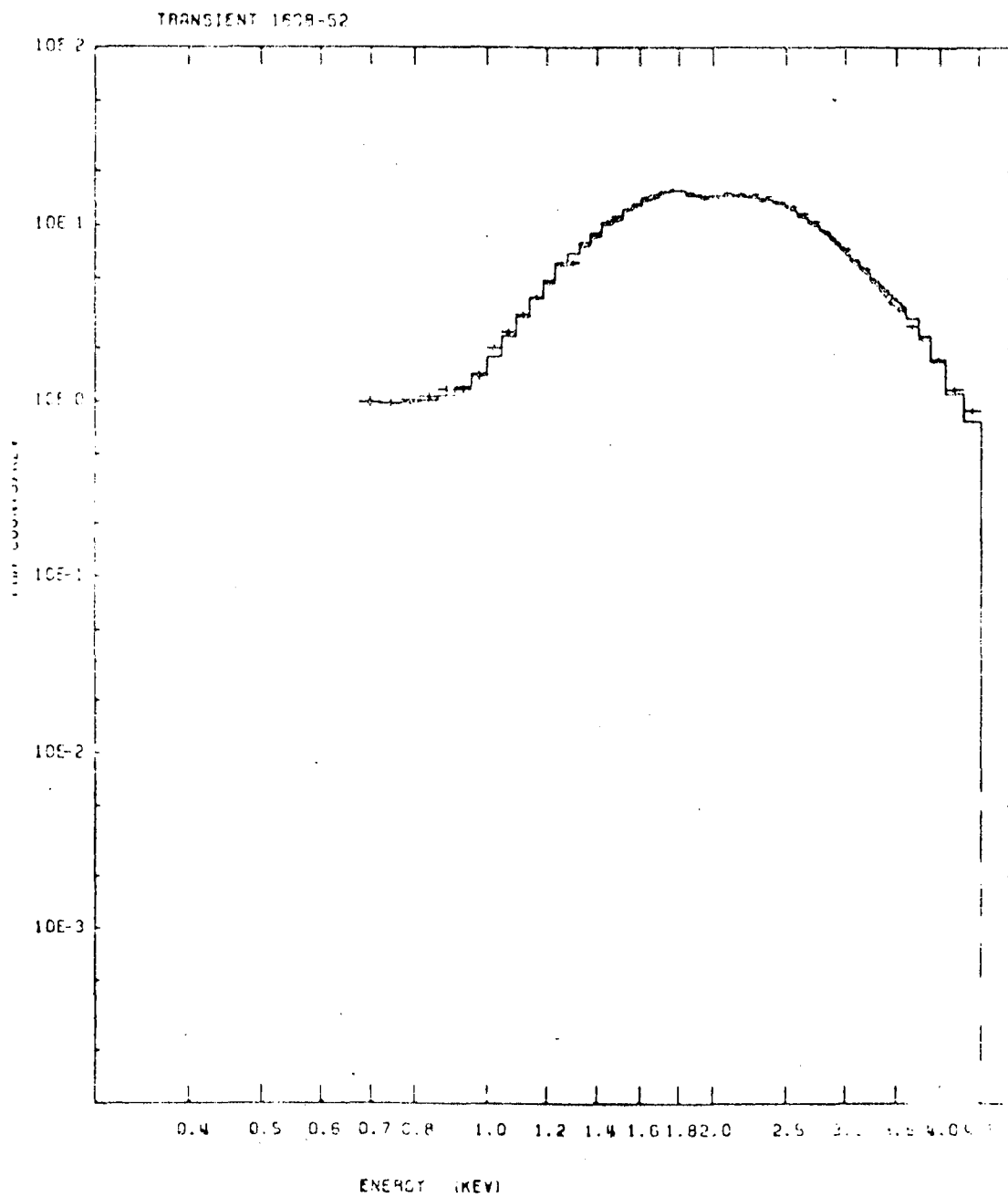


Figure 28

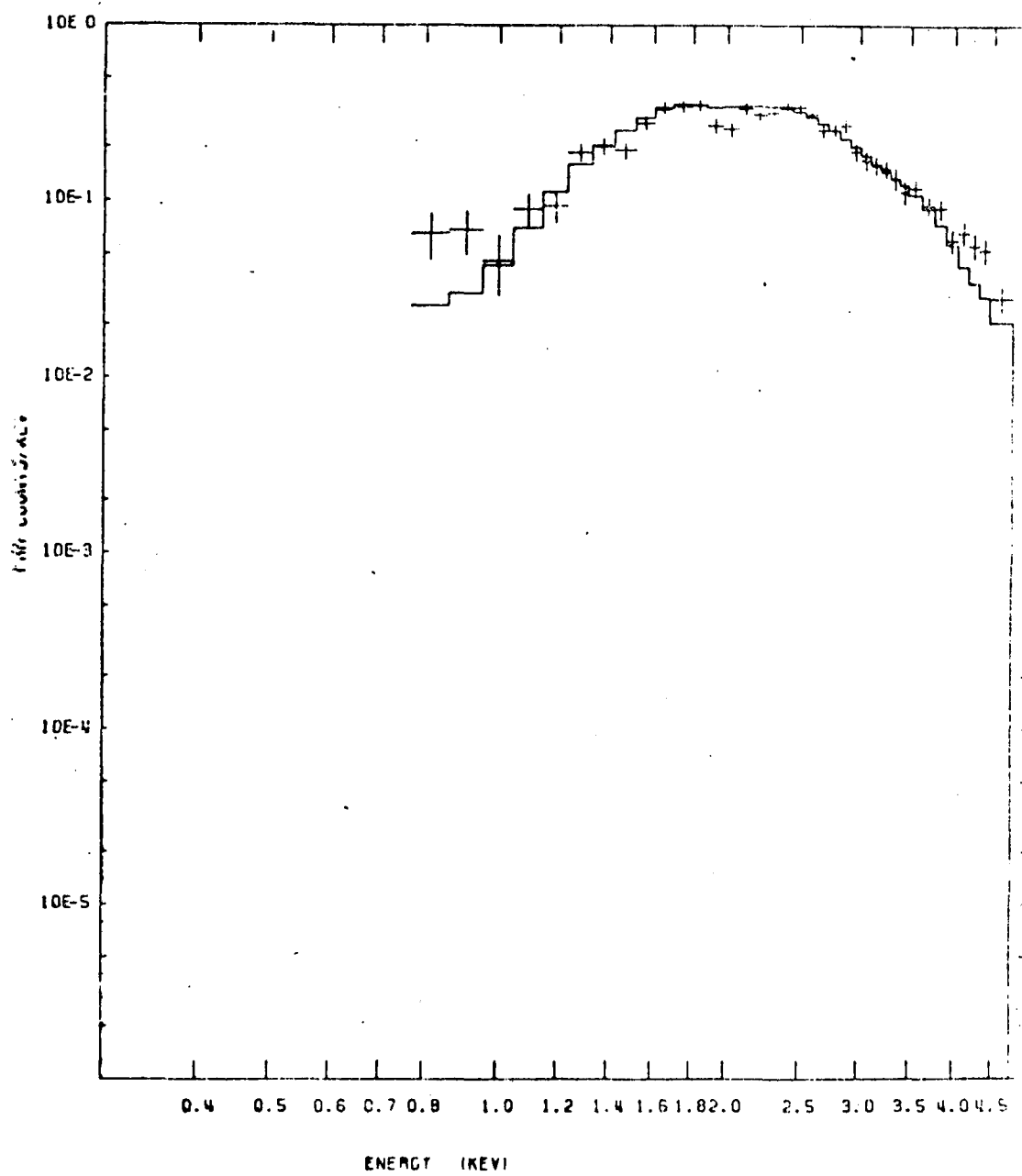


Figure 29

## HIGH RESOLUTION X-RAY SPECTROSCOPY ON THE EINSTEIN OBSERVATORY

George W. Clark  
Massachusetts Institute of Technology

My first trip to Huntsville was in 1959 when work began at the Redstone Arsenal on NASA's first astronomy satellite, Explorer XI, with a payload developed at MIT for detecting high energy gamma rays. It is a pleasure to return to Huntsville once again to join in the celebration of the success of NASA's most recent astronomy satellite, HEAO-2, and to tell about the early results from the Focal Plane Crystal Spectrometer (FPCS) developed at MIT for the Einstein Observatory.

Since the early days of X-ray astronomy it has been realized that detection and measurement of emission lines in X-ray spectra offer the prospect of new and detailed understanding about the physical conditions in X-ray sources. In the results from the Einstein Solid State Spectrometer, we have seen how emission features can be detected and identified by moderate resolution spectroscopy. However, many of these features undoubtedly have significant structure which can only be resolved by instruments with higher resolutions. For example, the features attributed to the helium-like ions of silicon and sulfur are expected to be composed of three separate lines whose relative intensities are a measure of the density and equilibrium state of the emitting plasma. The broad feature near 1 keV are attributed to a complex of L lines of the various ions of iron. Resolution of these lines and measurement of their relative intensities would provide a composition-independent measure of the source temperature.

These possibilities and others have motivated numerous efforts to achieve high resolution spectroscopy of cosmic X-ray sources. Much success has been achieved in the case of the Sun which is near and bright. Figure 1 presents the spectrum of a solar flare obtained by Bragg reflection spectrometry in a rocket observation by Walker and Rugge (1970). The latter shows the triplet structure of the emissions from helium-like ions of sulfur XV and silicon XIII.

To measure these interesting details of spectra, one needs resolutions of more than 100, i.e.,  $E/\Delta E \gtrsim 100$ . Only Bragg reflection from crystals affords such resolutions in the energy range above 0.5 keV where most of the interest lies. Bragg reflection occurs for only a very narrow range of wavelengths about the value given by the Bragg formula  $\lambda = (2d/n) \sin \theta$ , where  $d$  is the lattice spacing,  $\theta$  the grazing angle of incidence, and  $n$  an integer (generally 1). Thus Bragg reflection acts like a filter with a very narrow pass band. To observe a line one must scan this pass band back and forth over the wavelength of the line by

rocking the crystal through a small range of angles. The result is inevitably a low average throughput of line photons. Unfortunately, the brightest extrasolar sources are much fainter than a typical solar flare so that high resolution spectroscopy of extrasolar sources is much more difficult to achieve. Even with the Einstein telescope very long exposures are necessary to achieve adequate statistics.

During the 10 years since development of the FPCS began, more than 12 rocket and satellite observations of extrasolar sources with Bragg spectrometers were carried out. Two positive results were reported. One was evidence for the Lyman alpha line of Oxygen VIII in the Puppis A supernova remnant, reported by Zarnecki and Culhane (1977). The second was detection of K-alpha emission from highly ionized iron in Cygnus X-3 by the Columbia Group (Kestenbaum et al., 1978) working with their instrument on the OSO-8 satellite.

The Einstein Observatory has now provided two capabilities essential to achieving the full potentialities of high resolution spectroscopy. One is focusing optics which permits the use of an imaging spectroscope. This gains the benefits of the large collecting area of the primary mirrors while bringing the Bragg reflected X-rays to a focus on a small area of detector, thereby achieving a high ratio of signal counting rate to detector background counting rate. The other essential capability is accurate and sustained pointing which achieves long and efficient exposures. With these capabilities the FPCS attains sensitivities which are orders of magnitude greater than those achieved by previous instruments.

Table 1 summarizes the spectral resolutions required to attain various scientific objectives. Spectral features can be identified with resolutions of 10 to 30. Resolution of the helium triplets and identification of the ions responsible for lines in the L-line complex of iron requires resolutions of 100 to 300. Measurement of Doppler shifts due to bulk motions in supernova remnants need resolutions in the range 100 to 1000. The effects of thermal broadening require resolutions in excess of 1000 which are not yet attainable.

The FPCS was developed at MIT for the purpose of obtaining this new kind of astrophysical data. Herbert Schnopper and Kenneth Kalata contributed to the instrumental concept. Claude Canizares has been responsible for the scientific development of the instrument and scientific coordination of the project. Thomas Markert has been in charge of the prelaunch calibration measurements, the mission planning and the orbital operation. Garrett Jernigan supervised development of the data system. Frank Winkler has played a key role in developing the observing program, particularly the part devoted to supernova remnants. John Donaghy was in charge of the engineering effort carried out at the MIT Laboratory for Space Experiments.

Figure 2 illustrates the operation of the instrument: X-ray photons diverging from a point in the focal plane and having wavelengths near that defined by the Bragg formula for the given angle of incidence are reflected from the curved crystal to an astigmatic image in the form of a narrow line in the position sensitive proportional counter. The crystal curvature compensates for the divergence of the X-ray beam so that the angles of all rays striking the crystal are nearly the same. X-rays diverging from a different point in the focal plane, horizontally displaced from the other point, strike the crystal at a different angle, and are selectively reflected to a displaced parallel line image. Thus the instrument achieves both spectral resolution and one dimensional spatial resolution. This spatial resolution is useful in the study of extended sources such as supernova remnants.

For the spectrometer to function as described, the entrance aperture, curved crystal and detector must lie on the circumference of the "Rowland Circle." This condition is achieved for any desired angle of incidence on the crystal with gears and slides driven by stepping motors controlled through telemetry according to procedures incorporated in the mission operation program. The instrument is mechanically complex; however, it has functioned flawlessly since launch. An assembly drawing is shown in Figure 3, and a list of its properties is given in Table 2.

Figure 4 shows the profile of the line image at the spectrometer detector of a distant point source of 1.5 keV aluminum K-alpha radiation obtained during calibration tests here at MSFC. Selecting only those events detected in the image, we plot their frequency as a function of the angle of incidence on the crystal. The result is the "rocking curve" shown in Figure 5. It shows the response of the instrument to a narrow spectral line.

I turn now to the results obtained so far on three very different kinds of X-ray sources: a compact X-ray star, a diffuse supernova remnant, and an extended halo around an external galaxy. The compact X-ray star is Sco X-1, the brightest persistent X-ray source in the sky, and therefore a favorite target of previous efforts at Bragg Spectrometry. Those efforts have shown no evidence of line emission and have placed upper limits on such emissions which are far below the line strengths expected for an optically thin plasma with solar composition at the temperature of Sco X-1. This has led to the conclusion that Sco X-1 is an optically thick source in which multiple electron scatterings alter the wavelengths of escaping photons and thereby broaden emission lines to the point of undetectability. Sco X-1 was an early target of FPCS observations carried out by Christophe Berg. Figure 6 is the Bragg reflected image of Sco X-1 near the wavelength of the iron L-lines. Figure 7 is the pulse height distribution of the X-ray photons recorded in the image. There are two peaks corresponding to the energies of the first ( $n = 1$ ) and second ( $n = 2$ ) order Bragg reflected photons. Figure 8

is the rocking curve in the wavelength range of the iron L lines. No lines are seen and from this we have further reduced the upper limits on the line emission from Sco X-1 (Table 3).<sup>1</sup>

We have examined several supernova remnants including Cas A which has been shown by the Solid State Spectrometer to have strong lines of the helium-like ions of silicon and sulfur. Figure 9 shows the FPCS rocking curve of the sulfur XV line which has been analyzed by Frank Winkler. It is clearly broader than the aluminum K-alpha line observed during the calibration tests. The various possible contributions to the line width are indicated in the figure. The effects of spatial extent obscure the intrinsic structure of the line so that we have not yet determined the relative strengths of the triplet components.

Last week we received the first data from the observation of the Puppis A supernova remnant. Figure 10 is the rocking curve for the Lyman alpha line of Oxygen VIII. The curve on the bottom is the exposure as a function of the Bragg angle. This is a crucial part of every analysis. Data are accumulated from many observations during which the crystal is rocked slowly back and forth. We therefore must keep an accurate account of the exposure we have at each Bragg angle to make sense out of the observed numbers of events. The rocking curve shows a very strong emission line. Only about one-sixth of the supernova remnant image was included in the aperture of the spectro-scope. If one multiplies the apparent line emissivity by the ratio of the total area of the remnant to the area that was examined, one finds a line intensity which is consistent with that found previously by Zarnecki and Culhane.

Finally, I turn to the study of M-87 which is a giant elliptical galaxy with an X-ray emitting halo whose overall spectrum has been characterized as that of an optically thin plasma with a characteristic temperature of 2.6 keV. The K line of iron has been detected previously in the X-ray spectrum. This was clear evidence for the presence of heavy elements in the region around M-87 and led to the conclusion that the emitting gas is not primordial, but rather that it was stripped out of other galaxies in the Virgo cluster and is now falling into the potential well of M-87. As it falls, its kinetic energy is converted into heat, and as the density rises the rate of cooling by radiation increases. Model calculations have been made to predict the temperature profile across the halo region. The observed intensities of various emission lines can be used, in principle, to test the validity of such a temperature profile. The Lyman alpha line of oxygen VIII should be particularly useful in such a test because it is strong at temperatures lower than 2.6 keV. Figure 11 shows the discovery of this line in the rocking curve obtained

---

1. Since this report was given a broad OVIII line has been detected.



by Claude Canizares. The observed line flux implies a luminosity at the source of  $1.2 \times 10^{42}$  ergs s<sup>-1</sup>. A search was also made for the L lines of ionized iron, but only upper limits have been obtained so far. The measured intensity of the oxygen VIII line is more than seven times greater than expected for an isothermal gas with the cosmic abundance ratio of oxygen to iron at 2.6 keV. The results show that substantial amounts of cooler gas at temperatures of 10<sup>7</sup> K or less are present in the vicinity of M-87.

Only a fraction of the production data from the long FPCS exposures has been received so far. Thus we have only begun our exploration of what promises to be a highly productive new area of research in X-ray astronomy.

Note: As of July 11, 1979 a total of nine emission lines had been detected in the spectra of galactic and extragalactic objects by the FPCS and there were strong indications of the presence of an additional seven lines.

## BIBLIOGRAPHY

Kestenbaum, H. L.; Ku, W. H. M.; Long, K. S.; Silver, E. H.; and  
Novick, R., 1978, Ap. J., 226, 282.

Walker, A. B. C. and Rugge, H. R., 1970, Astron, Astrophys., 5, 4.

Zarnecki, J. C. and Culhane, J. L., 1977, Mon. Not. R. Astr. Soc., 178,  
57P.

TABLE 1. COSMIC X-RAY SPECTROMETRY

Purpose	Required Resolutions ( $E/\Delta E$ )
Element Identification	10 - 30
Iron Ion Abundances (temperature)	>100
Helium Triplet Intensities (densities and equilibria)	>100
Doppler Shifts in SNR	100 - 1000
Thermal Broadening	>3000

TABLE 2. EINSTEIN OBSERVATORY FOCAL PLANE  
CRYSTAL SPECTROMETER

Range	0.2 - 3.0 keV
Resolving Power ( $E/\Delta E$ )	50 - 500
"Effective Area"	$\sim 0.5 \text{ cm}^2$ (single line)
Required Observing Times	$10^4 - 10^5$ sec

TABLE 3. SCO X-1

Line	$3\sigma$ Upper Limit Equivalent Width (eV)	Model
Fe 23/24	1.0	Thermal
Fe 17 (11Å)	2.5	Thermal
Fe 17 (15Å)	1.7	Thermal
O VIII Recombination	1.0	Nebular Fluorescence
O VIII Ly $\alpha$	1.3	Nebular Fluorescence
Fe 1	1.3	Stellar Fluorescence

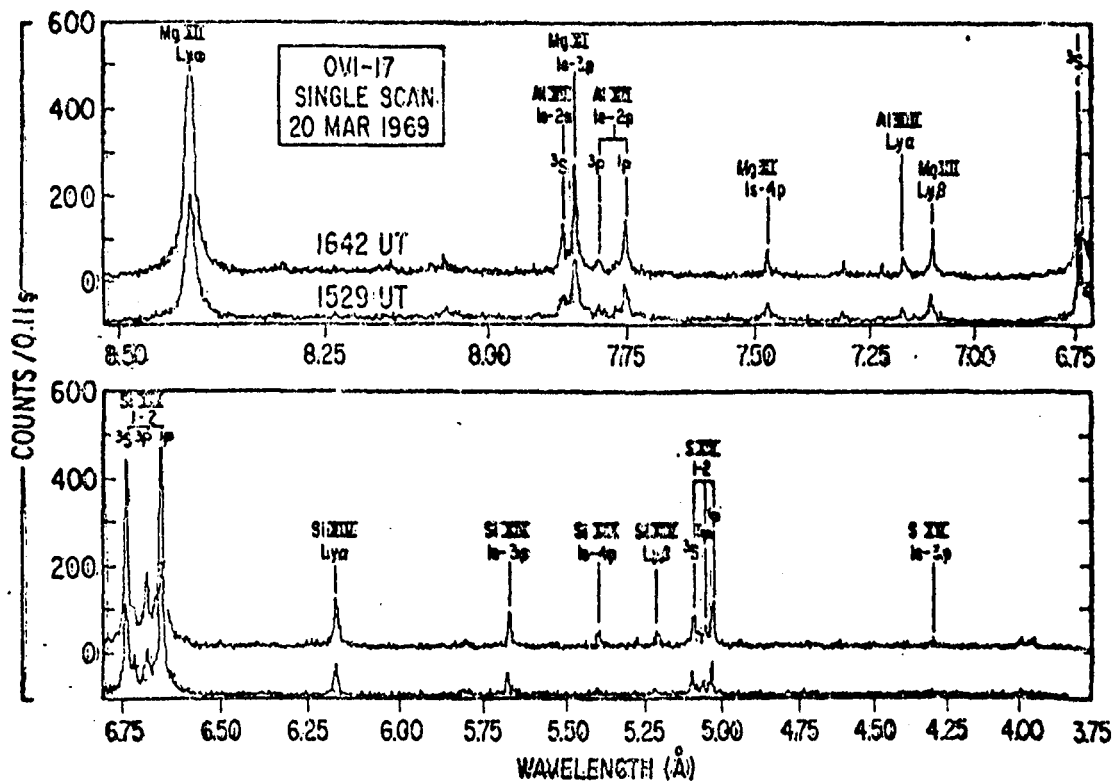


Figure 1. Solar X-ray spectrum between 4 and 8.5 Å during a period of high solar activity obtained by a rocket-borne Bragg reflection spectrometer by Walker and Rugge (1970).

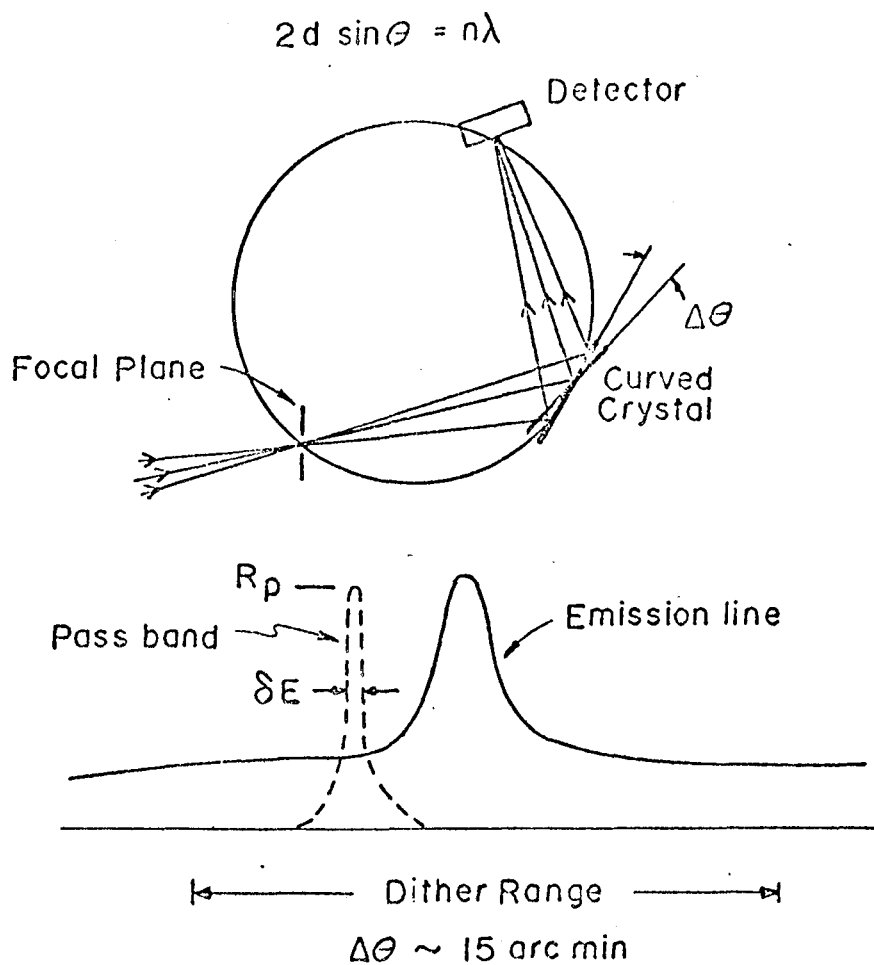


Figure 2. Schematic diagram of Bragg spectrometer.

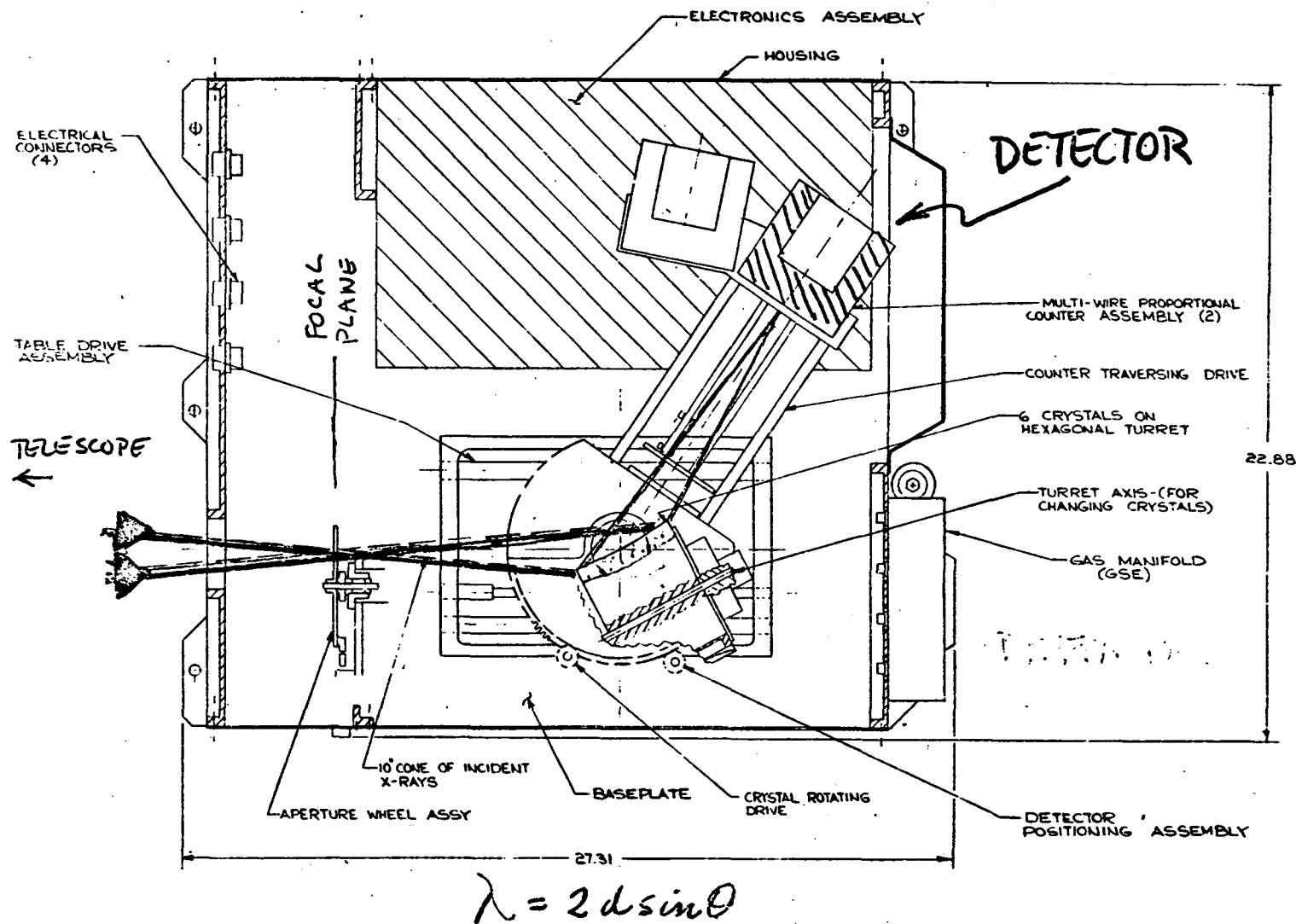


Figure 3. Assembly drawing of the MIT Focal Plane Crystal Spectrometer.

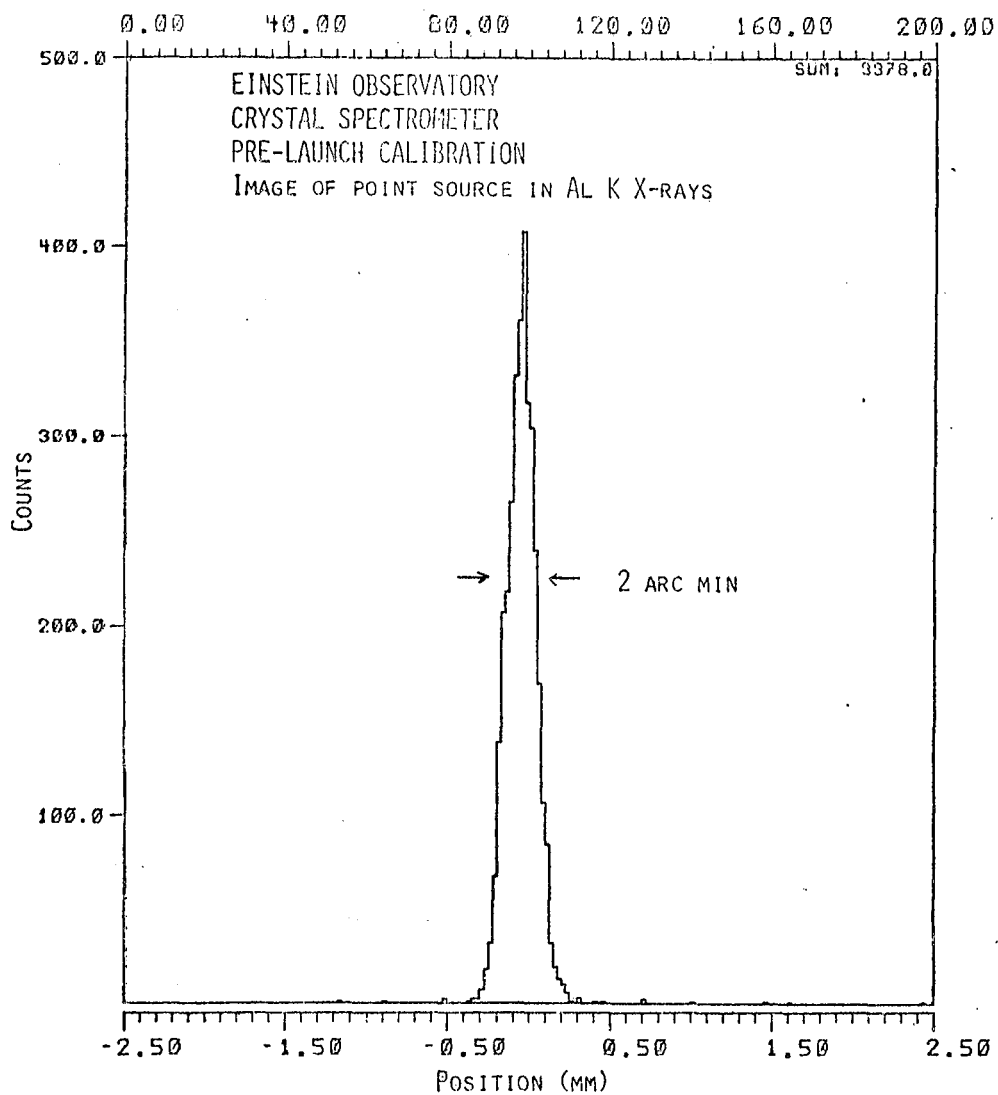


Figure 4. Bragg-reflected image of a point source of Al K X-rays obtained during prelaunch calibration tests.

-B3  
24/24/79  
-L

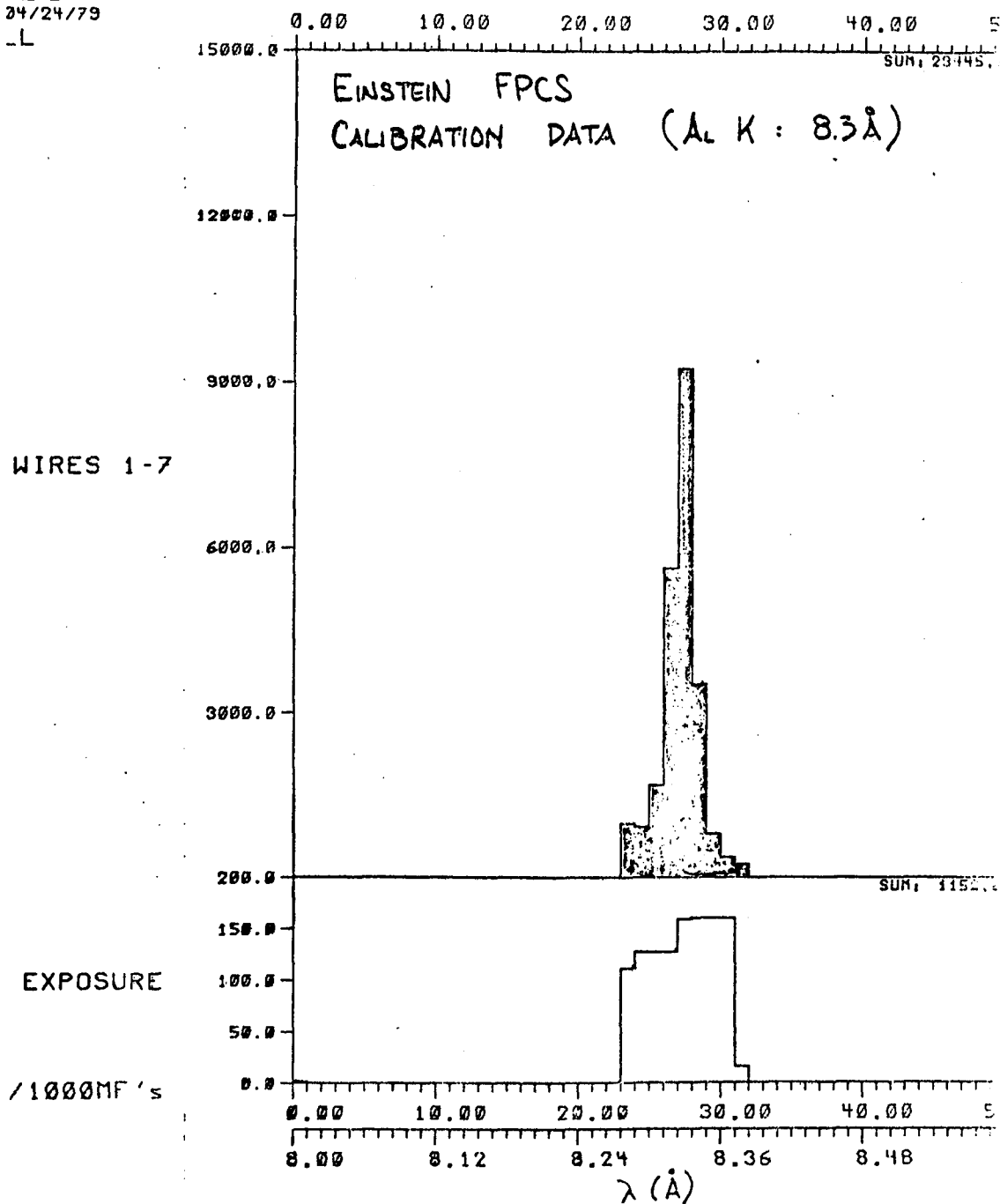


Figure 5. Rocking curve of Al K X-rays obtained during prelaunch calibration tests.



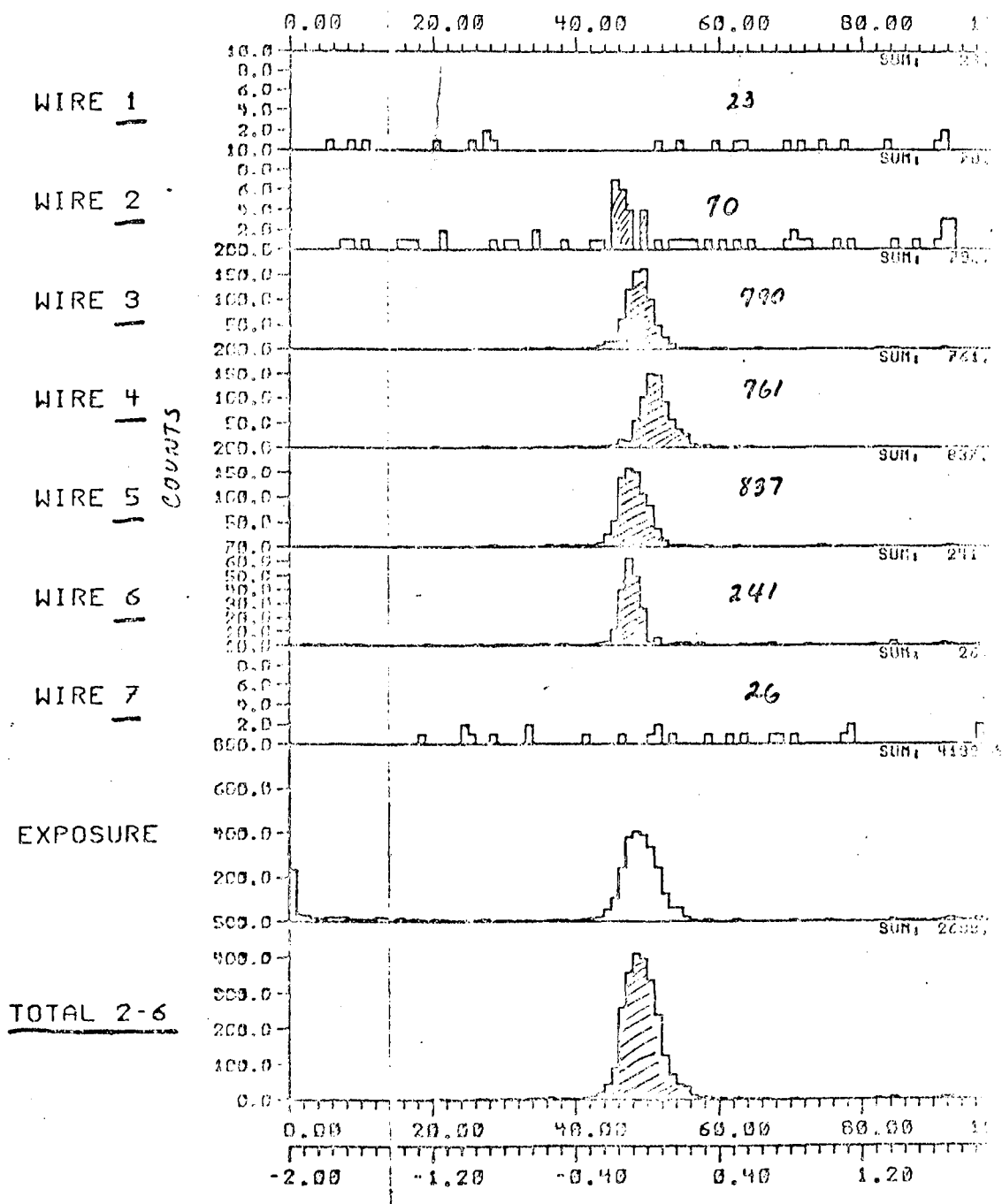


Figure 6. Bragg-reflected image of Sco X-1 near 1 keV.

33

7/24/79

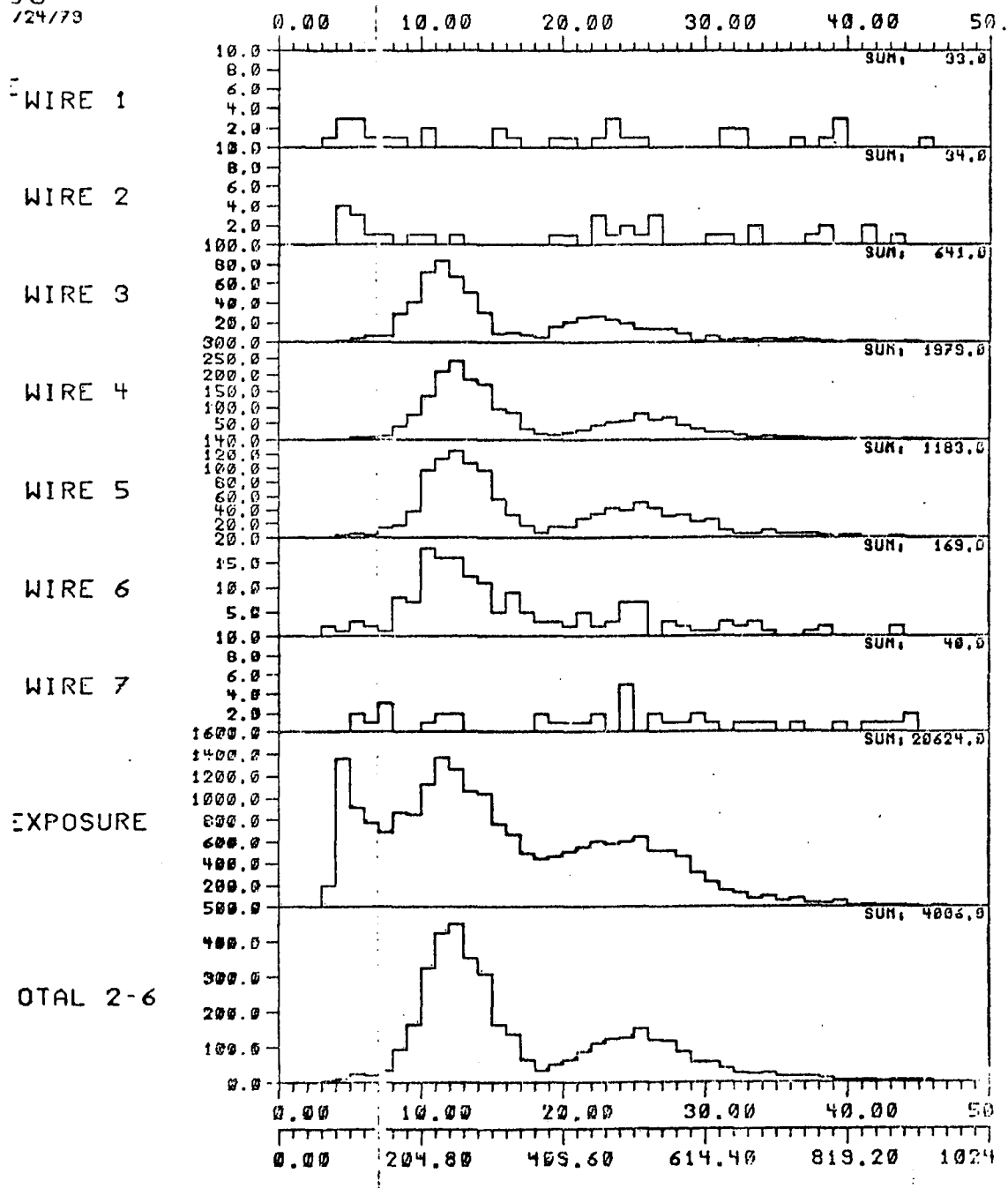


Figure 7. Pulse height distribution of Bragg-reflected X-rays.

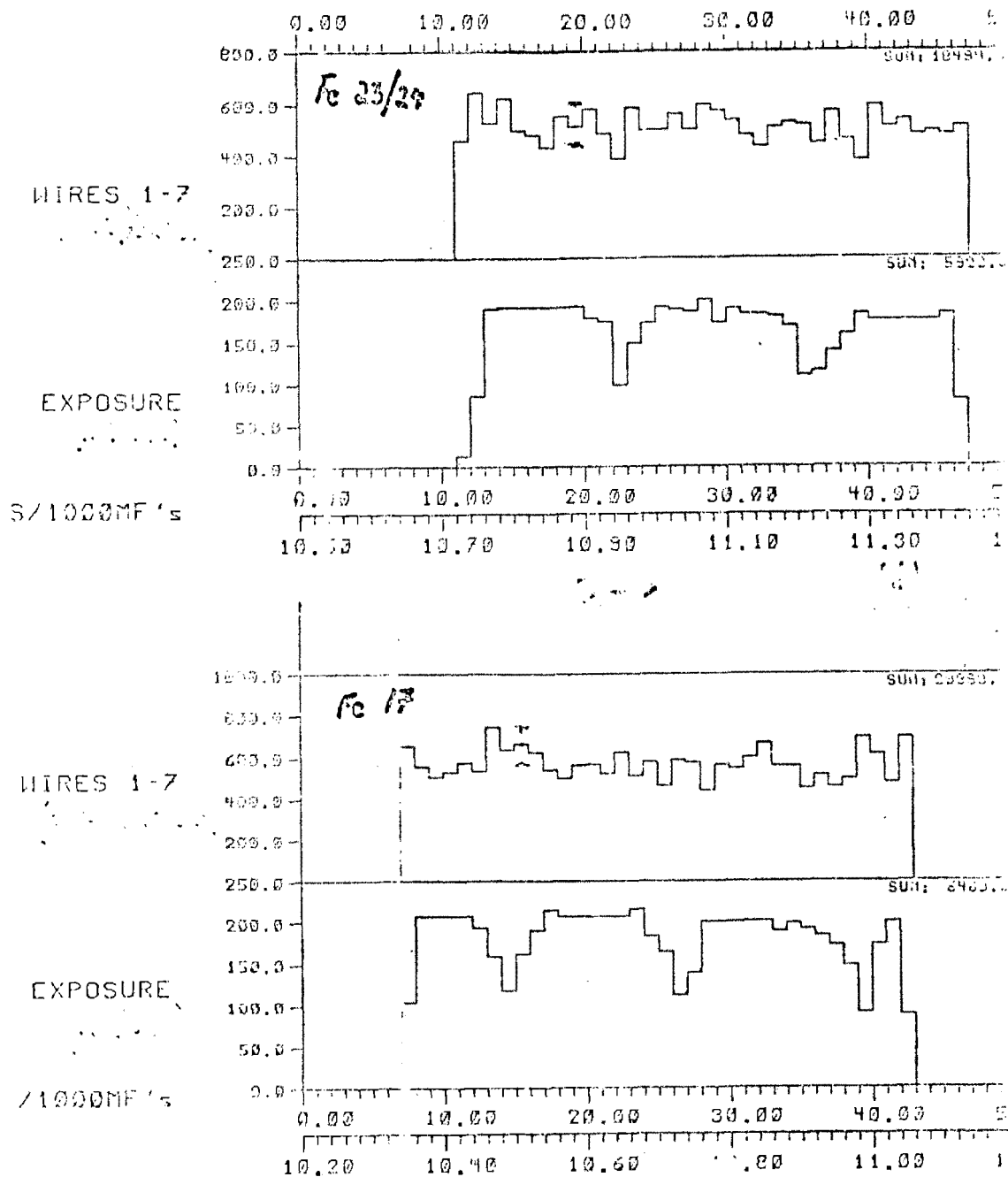


Figure 8. Rocking curve of Seo X-1 spectrum of wavelengths of iron L lines.

B3  
4/24/79  
L

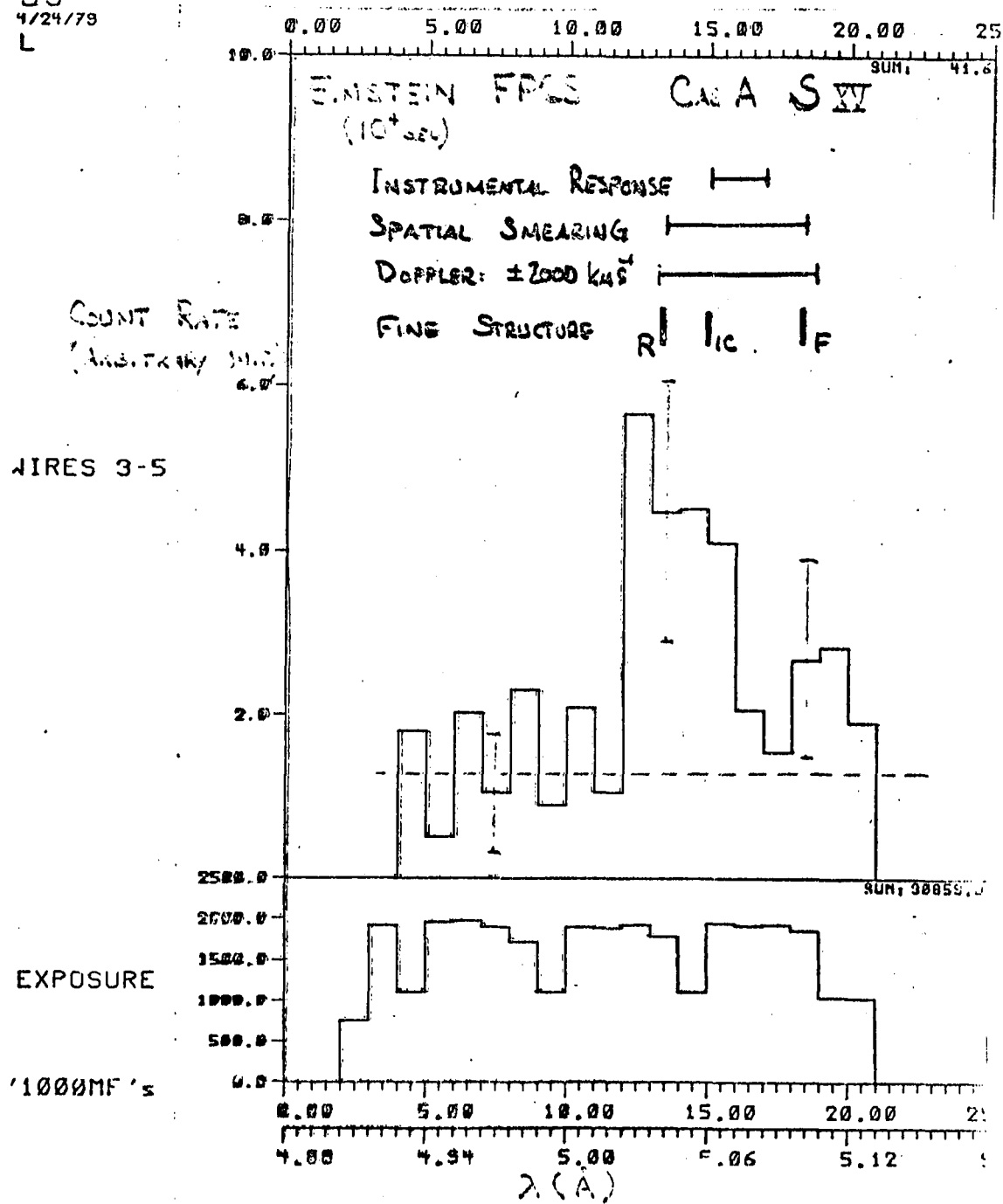


Figure 9. Rocking curve of sulfur XV line in Cas A.

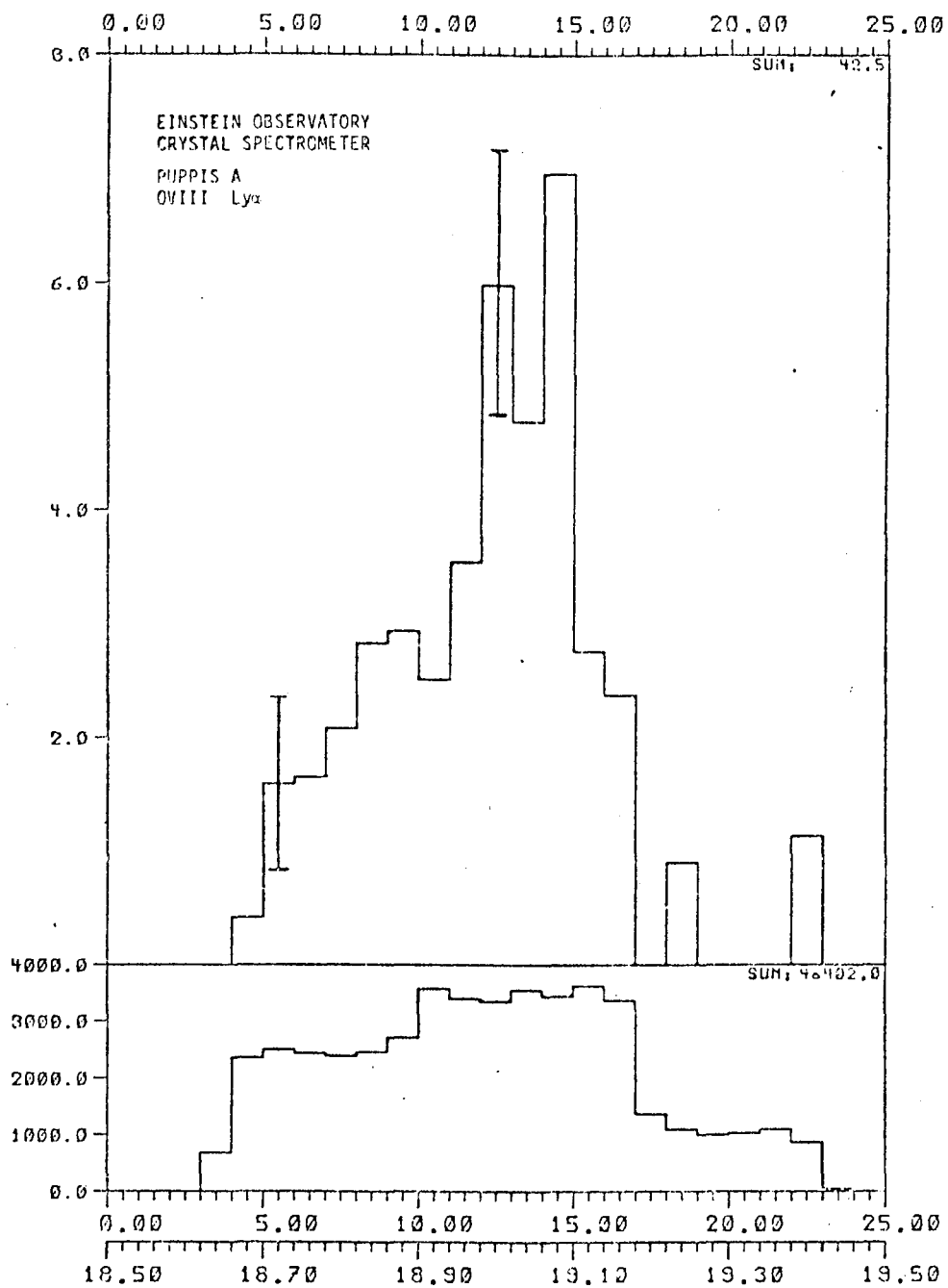


Figure 10. Rocking curve of oxygen VIII Lyman alpha line on Puppis A.

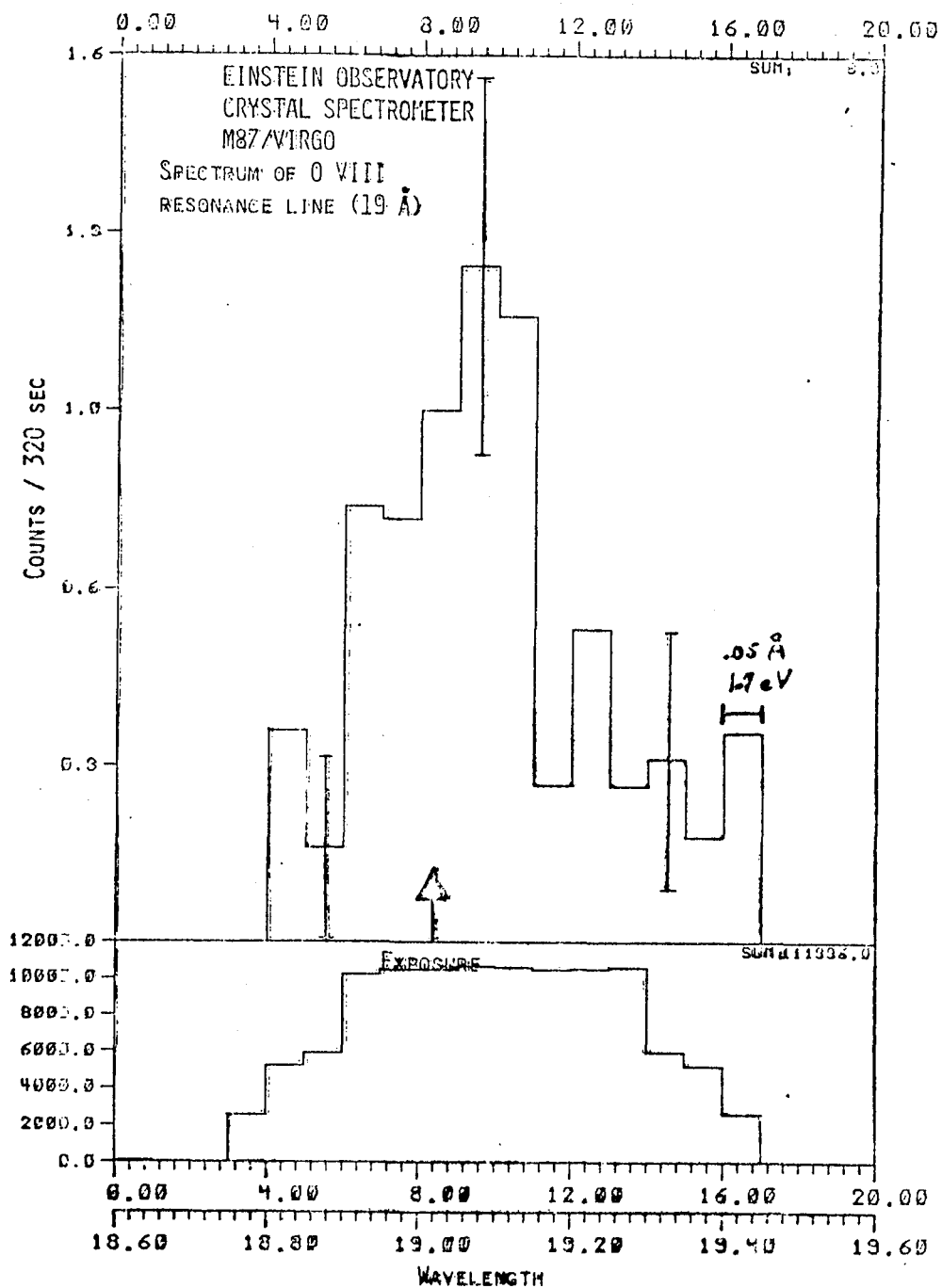


Figure 11. Rocking curve of oxygen VIII Lyman alpha line in M-87.

# MONITOR PROPORTIONAL COUNTER

M. C. Weisskopf  
NASA, Marshall Space Flight Center

## INTRODUCTION

One of the instruments on the HEAO-2/Einstein Observatory is the Monitor Proportional Counter (MPC). The MPC and its associated electronics have been described in detail elsewhere (Gaillardetz et al., 1978 and Giacconi et al., 1979) and will only be reviewed briefly here. The MPC is an Uhuru class Ar-CO<sub>2</sub> gas-filled proportional counter sealed with a 1.5 mil beryllium window and sensitive to X-rays in the energy bandwidth from 1.5 to 22 keV. Both pulse shape discrimination and anticoincidence cells are used to limit the background counting rate to 20 c/sec in favorable portions of an Earth orbit. The efficiency for detection of X-rays is such that with the Crab Nebula and Pulsar at the center of the 42 min field of view (FWHM) the counting rate is 1350 c/sec.

The MPC detector electronics are configured to accumulate an eight channel pulse height spectrum every 2.56 sec. In addition a time interval processor (TIP), measures the time between events (independent of energy over the 1.5 to 22 keV band), with a time resolution of a few microseconds. To accomplish the latter, an on-board memory serves as a buffer between the TIP and the telemetry system. As long as the counting rate is sufficiently low, the TIP is always operational. On the other hand, if the X-ray counting rate is high enough so that the memory fills entirely, the TIP becomes inactive until the memory is completely emptied by the telemetry. Except when the crystal spectrometer is in the focal plane, the counting rate which fills the memory is 33 c/sec. For counting rates above this threshold there will be gaps in the data stream which last for 2.56 sec. When the crystal spectrometer is in use, the threshold is 100 c/sec and the gaps last for 0.82 sec.

The MPS is coaligned with the X-ray telescope and takes data as a normal part of the Observatory operation. One of the specific research programs of the Observatory is to make use of the MPC data to prepare a time variability catalog of the brighter galactic and extragalactic X-ray sources. I would like to present a few of the results that have been obtained thus far in this program. Before doing this I would like to emphasize that this work is being performed in collaboration with several people at three institutions. My collaborators are listed in Table 1. I would especially like to take this opportunity to underscore the contributions of one of the unsung heroes of this program, Mr. Ross Lippman. Ross, an undergraduate at Harvard, must have, by now, developed a permanent crick in his neck from balancing a telephone while at the same time typing in changes to computer programs as we worked via long-distance late into the night.

## THE TREE

The MPC, with its high time resolution ( $10\ \mu\text{sec}$ ), together with the long continuous observing time afforded by the Observatory, presents a challenging problem in the analysis of the data. In a thousand second observation, for example, there are  $10^8$  potentially interesting time scales corresponding to the number of statistically independent frequencies. Examination of such a data set for periodic behavior is in and of itself a major undertaking because of the computer time involved. Furthermore, searches for periodicity address only one aspect of the time variability of the X-ray sources. One of the most interesting aspects of X-ray astronomy has been the discovery of erratic time variations ranging from long time scales as in the case of the transient X-ray sources, to medium time scales as from the X-ray bursters, to subsecond variability as for example in the case of the blackhole candidates. Because of this aspect of the time variability and because of the need to minimize computer time we have developed, or more accurately refined, a technique for rapidly searching for and isolating erratic time variations. An example of the result of the application of this technique is illustrated in Figure 1 and I would like to take a few minutes to describe the procedure before discussing the observations.

The procedure is based on binning the data on an extremely fine time scale, calculating the variance with respect to the mean, and comparing the calculated variance to that expected on the basis of counting statistics. There is no guarantee that such a calculation will detect any time variability, even if present, as the binning time scale may be much too fine as compared to the time scale of any features in the data and/or the particular feature, such as an X-ray burst, may only span a small fraction of the total time and thus be lost as only a single contribution to the total variance. To try to account for the former effect one can consider rebinning the data on coarser and coarser time scales and recalculating the variance each time. To account for the latter effect one can repeat these calculations on subsections of the entire data set. Examination of the equations involved shows that if both the binning time scales and the subsection time scales are chosen to be integral powers of two of the finest time scales involved, then explicit binning of the data and calculation of the variance need only take place once for each subsection of data on the finest time scale. The remaining variances can then be calculated by algebraic manipulation.

Figure 1 is a graphical illustration of the results of this type of calculation, which we refer to as the "tree." The vertical bar (= branch) at the top of the tree represents the calculation for the data treated as a whole. The highest point is based on the variance of the entire data set binned on the finest time scale which in this example is 0.191 msec. The points below this, but still within the single vertical bar correspond to the finest time scale multiplied by two, by four, by eight, etc.,



until the number of bins is four. The two vertical bars immediately below the top of the tree represent the same calculation, but now for each half of the total data separately. Below this are the results for each  $1/4$ ,  $1/8$ ,  $1/16$ ,  $1/32$  of the data. The quantity plotted is the statistical significance of the departure of the measured variance from that expected from counting statistics; the darker the display the higher the statistical significance. For a steady source, the entire tree would appear as seen in the 24 rightmost branches at the bottom. In the example shown in Figure 1, however, a transient event has been detected and isolated to a particular portion of the data. In this example 1600 sec of data with  $66 \times 10^3$  events were examined for time variability over time scales covering a range of  $8 \times 10^6$  in 30 sec of (UNIVAC 1108) computer time.

## TERZAN 2

The example discussed previously clearly demonstrates the detection and isolation of a single transient event. (Note the three dark branches at the bottom of the illustration in Figure 1.) This activity was detected during the HRI observation of the globular cluster, Terzan 2. As noted by Professor Giacconi, we were fortunate that J. Grindlay was at the HEAO control center during the two thousand seconds devoted to this particular experiment. His presence seems to guarantee that X-ray burst phenomena will be detected. This is only the second burst detected from the cluster, which now is unambiguously identified as the source of the X-rays, thanks to the HRI observations which have isolated the source to lie within 2 arc sec from the cluster center.

Figure 2 shows the entire time history of the burst in 2 sec intervals of TIP data. The previous burst from Terzan 2 was detected by the Goddard experiment on OSO-8 (Swank et al. 1977). Qualitatively the second burst from Terzan 2 is very similar to the first. A weak steady source is seen, in our case at an intensity approximately equal to the background counting rate. The flux is then observed to increase by almost a factor of 80 followed by what appears to be an exponential decay and lasting several hundred seconds.

Figure 3 is a plot of the major burst activity with the data binned on a time scale of 120 msec. This figure serves not only to illustrate more clearly the time development of the burst but also, unfortunately, to emphasize the gaps in the TIP data due to memory overflow. All the high time resolution observations of bursts from this source have been plagued with sampling problems. The OSO-8 experiment provided coverage of the source for 160 msec every 11 sec. That experiment was unable to determine the burst rise-time, setting an upper limit of 10 sec. Since the overall burst length from this source is much longer than that from other bursters, it is assumed that the burst rise-time was also long, of the order of several seconds. This is not the case. Figure 4 shows

the details of the rising portion of the burst. The next data point in time (not shown) occurs 2.56 sec later and is at the maximum counting rate we observed, 1345 c/sec. If we take this rate, after subtracting background, to correspond to the peak luminosity, then the results shown in Figure 4 indicate a rise to 70 percent of the peak in under 0.3 sec.

Figures 5 and 6 show the time evolution of the burst plotted in two second intervals. The first 14 sec appear saturated at a constant rate, but this may be misleading as they are based on only five samples each of 0.2 sec duration separated in time by 2.56 sec. As the counting rate decreases, however, the "on" time increases and the frequency of occurrence of the gaps decreases. At least three time constants characterize the falling portion of the burst. From 14 sec to about 34 sec the flux decreases exponentially with a time constant of 11.8 sec. This time scale was not identified in the OSO-8 burst but may not have been detectable given that they sampled the burst only once every 11 sec. At 24 sec after burst onset the decay follows a 32.0 sec e-folding for at least 50 sec. The final decay can be described by a time constant of 85.9 sec. Both of the latter time constants (32.0, 85.9) are similar to, but shorter than, those seen in the first burst of Terzan 2, i.e., 44.8 sec and 215.7 sec.

As stated earlier the peak detected luminosity to preburst luminosity ratio is 80. The energy in the burst is approximately 40 times greater than the peak luminosity which corresponds (very) approximately to  $5 \times 10^{36}$  ergs/sec at a distance of 1 kpc. The distance to Terzan 2 being approximately 7 kpc (Grindlay, 1978), this would put the flux at the Eddington limit for a two solar mass object. A spectral analysis of the data is currently in progress and the results will be presented at the Wellesley meeting of the AAS.

### CYGNUS X-3

The light curve of the MPC TIP observations of Cygnus X-3 is shown as the histogram in Figure 7. These observations were performed when Cygnus X-3 was in an extremely low state. The MPC energy bandwidth extends to 20 keV and the energy spectrum was extremely hard during these observations, yet our mean counting rate was much lower than the minimum (2-6 keV) seen during the early Uhuru observations. The dots in the figure are the individual data points obtained during the 2.4 days of observation, and indicate the variability in the flux above and beyond that expected on the basis of counting statistics above. The two sigma error bars on individual data points are approximately the same size as the symbols shown.

Using the technique of the tree, we have examined the counting rate as a function of time and have discovered several interesting features.

Figure 8 shows one such feature, a fairly long flare which was observed on the falling portion of the light curve. A similar feature shown in Figure 9, but weaker, was again observed in the next 4.8 hr period of this source but somewhat earlier in phase. The energy spectrum of these features has not as yet been analyzed.

Figures 10, 11, and 12 illustrate the second type of feature observed in the data. This feature is referred to as a "sudden" transition, where the counting rate changes suddenly and significantly on the time scales to 10 to 20 sec. Two such transitions separated in time by approximately 500 sec are shown in Figure 10. Five 4.8 hr periods later, again two such transitions were observed, and are shown in Figure 11 but now separated in time by 1100 sec and at different phases in the 4.8 hr period than the first pair. Finally, as shown in Figure 12, at least one and possibly two transitions were observed in the 11th 4.8 hr cycle. The times and phases refer to the 4.8 hr period and the amplitudes of these features are summarized in Table 2. In general, there was insufficient coverage at all phases to establish whether or not these transitions were always present during the rising portion of the light curve, however, no sudden transitions were ever observed in either the peak or the falling portion of the light curve.

It should be noted at this point that although we have ruled out the possibility that these features are due to an attitude maneuver, we have not, as yet, examined enough data from other X-ray sources to conclusively eliminate the possibility that the sudden transitions are a manifestation of some type of systematic effect not associated with the X-ray source. Thus, our current efforts have concentrated on, not an interpretation of these features, but rather on understanding the Cygnus X-3 system as a whole. In this regard we have puzzled about the obvious asymmetry in the 4.8 hr light curve which is apparent not only in our data, but also in the majority of the historical light curves. The asymmetry can, clearly, be produced for a variety of reasons such as an anisotropic distribution of circumstellar material or an eccentric orbit. The smooth curve in Figure 9 is the light curve one would observe in the case where the modulation is due to absorption in a stellar wind with Cygnus X-3 in an eccentric orbit. In the calculation shown in the figure the eccentricity was 0.3, the inclination angle 24 degrees, and the longitude of periastron at 95 degrees. This calculation (which considered only a pure absorbing atmosphere) and the resulting parameters are not meant to be taken as an exact description of the Cygnus X-3 system; they indicate that the suggestion of an elliptical orbit can, at least in this simple model, lead to acceptable light curves which fit the data.

One consequence of the elliptical orbit hypothesis is that one might expect to see changes in the apparent shape of the light curve due to apsidal motion. Since no reversals in the asymmetry of the light curve have been observed in the 5.5 years since the source's discovery the

period would have to be long, at least of the order of 20 years. Such periods imply a companion to the X-ray source much more centrally condensed than a main sequence star. In addition, the companion must have a mass loss rate which can provide enough circumstellar matter to produce the observed X-ray modulation. This rules out compact companions (i.e., degenerate dwarfs or neutron stars) and makes it very likely that the companion is a highly evolved state filling its Roche Lobe.

## REFERENCES

Gaillardetz, R., Bjorkholm, P., Mastronardi, R., Vanderhill, M., and Howland, D., 1978: I.E.E.E. Trans. on Nucl. Sci., NS-25,437.

Giacconi, R., Barnduardi, G., Briel, U., Epstein, A., Fabricant, D., Feigelson, E., Forman, W., Gorenstein, P., Grindlay, G., Gursky, H., Harnden, F. R., Henry, J. P., Jones, C., Kellogg, E., Koch, D., Murray, S., Schreier, E., Seward, F., Tananbaum, H., Topka, K., van Speybroeck, L., Holt, S. S., Becker, R. H., Boldt, E. A., Serlemitsos, P. J., Clark, G., Canizares, C., Markert, T., Novick, R., Helfand, D., and Long, K., 1979: Ap. J., 230, 540.

Grindlay, J. E., 1978: Ap. J. (Letters), 224, L107.

Swank, J. H., Becker, R. H., Boldt, E. A., Holt, S. S., Pravdo, S. H., and Serllimitsos, P. J., 1977: Ap. J. (Letters), 212, L73.

TABLE 1. COLLABORATORS ON THE TIME  
VARIABILITY PROGRAM

NASA/George C. Marshall Space Flight Center
W. Darbro
R. Elsner (NAS/NRC)
P. Ghosh (NAS/NRC)
M. C. Weisskopf
McMaster University
P. G. Sutherland
Harvard-Smithsonian Center for Astrophysics
P. Hertz
J. E. Grindlay
G. S. Vaiana

TABLE 2. SUMMARY OF THE OBSERVATIONS OF THE SUDDEN  
TRANSITIONS IN CYGNUS X-3

Time of Occurrence (Day of 1978) (sec)		4.8 hr Phase	Percent Change in Intensity
350	22329	0.253	15
350	22841	0.283	25
351	2650	0.120	15
351	3756	0.184	11
352	19359	0.097	14
352	20843	0.183	9

MAJOR FRAME 237805  
TERZAN 2  
MAXIMA

,000191 SEC. RESOLUTION  
1598.09682 SECONDS  
65939 EVENTS

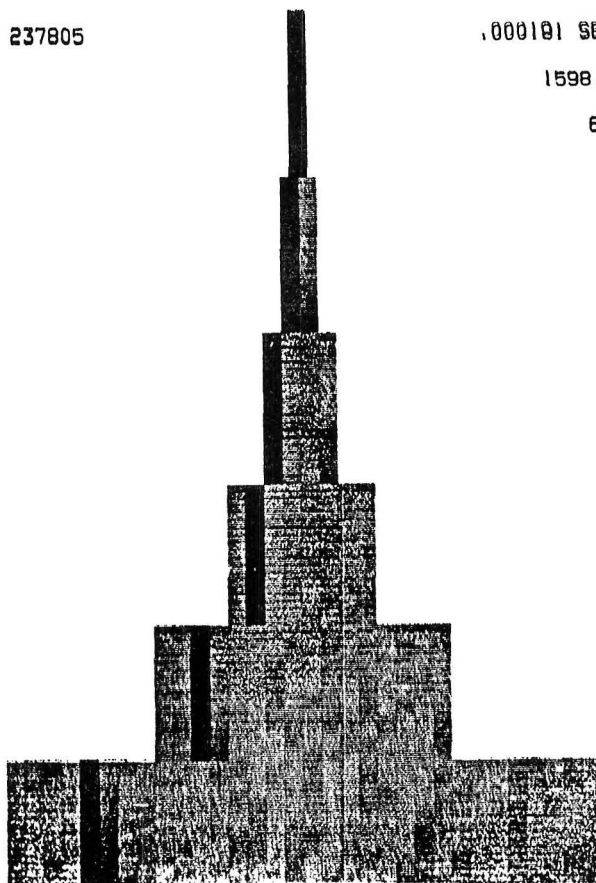


Figure 1. Graphical representation of the tree. The figure is discussed in detail in the text in Section II.

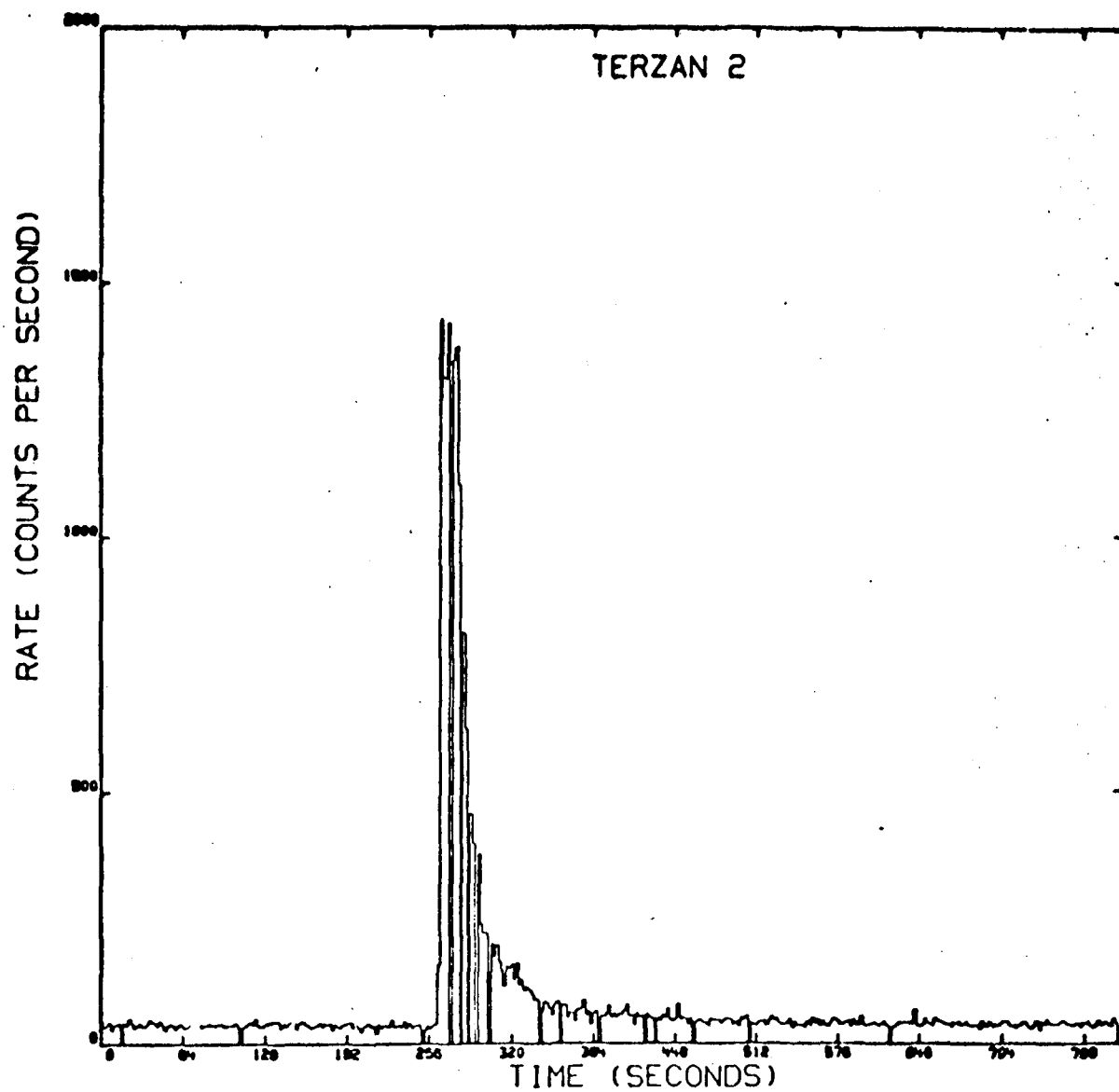


Figure 2. Counting rate versus time during the TIP observation of Terzan 2. The data are binned in 2 sec intervals.



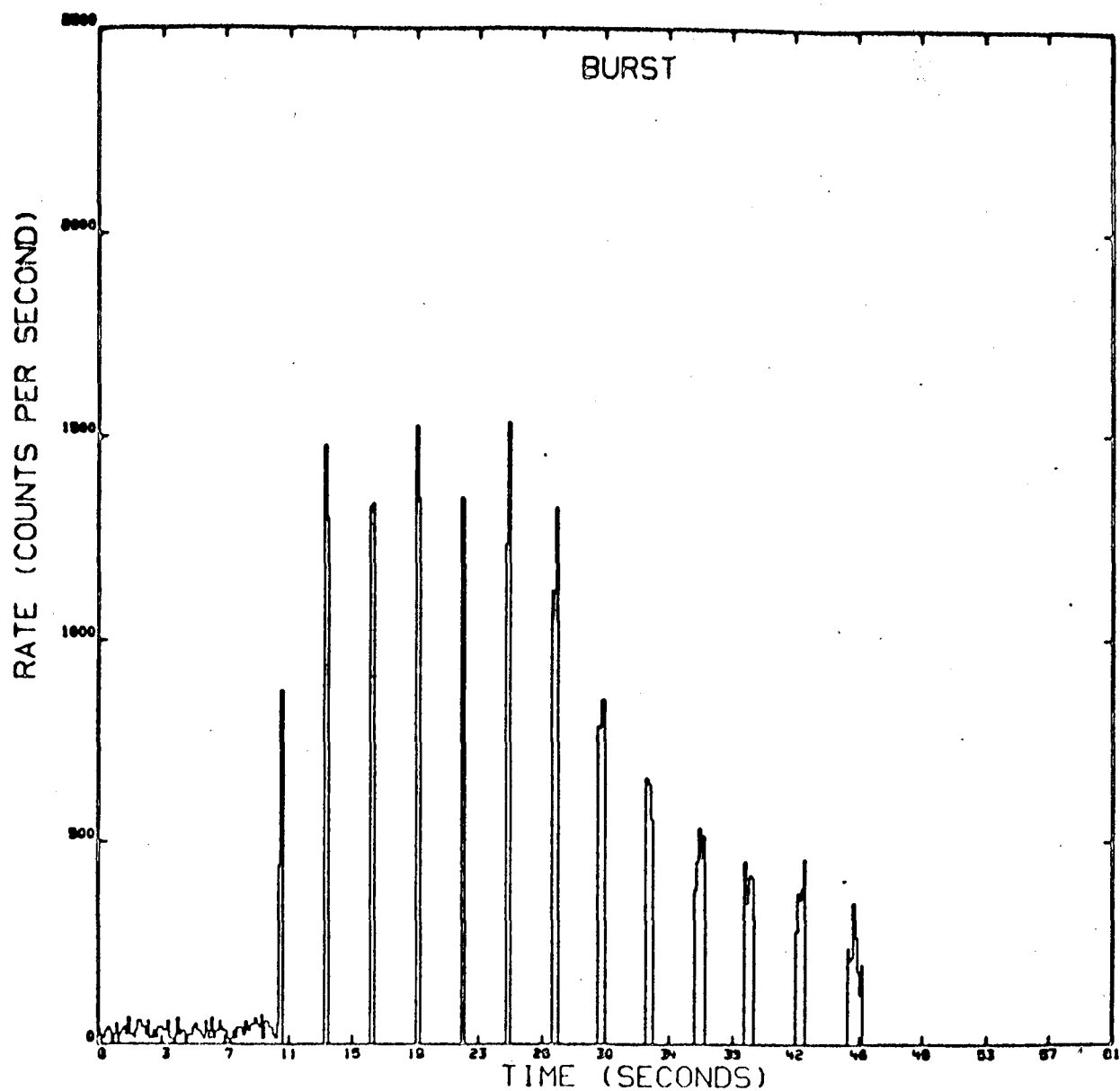


Figure 3. Forty-eight seconds of TIP data including the onset of the burst from Terzan 2. The data are binned in 0.12 sec intervals.

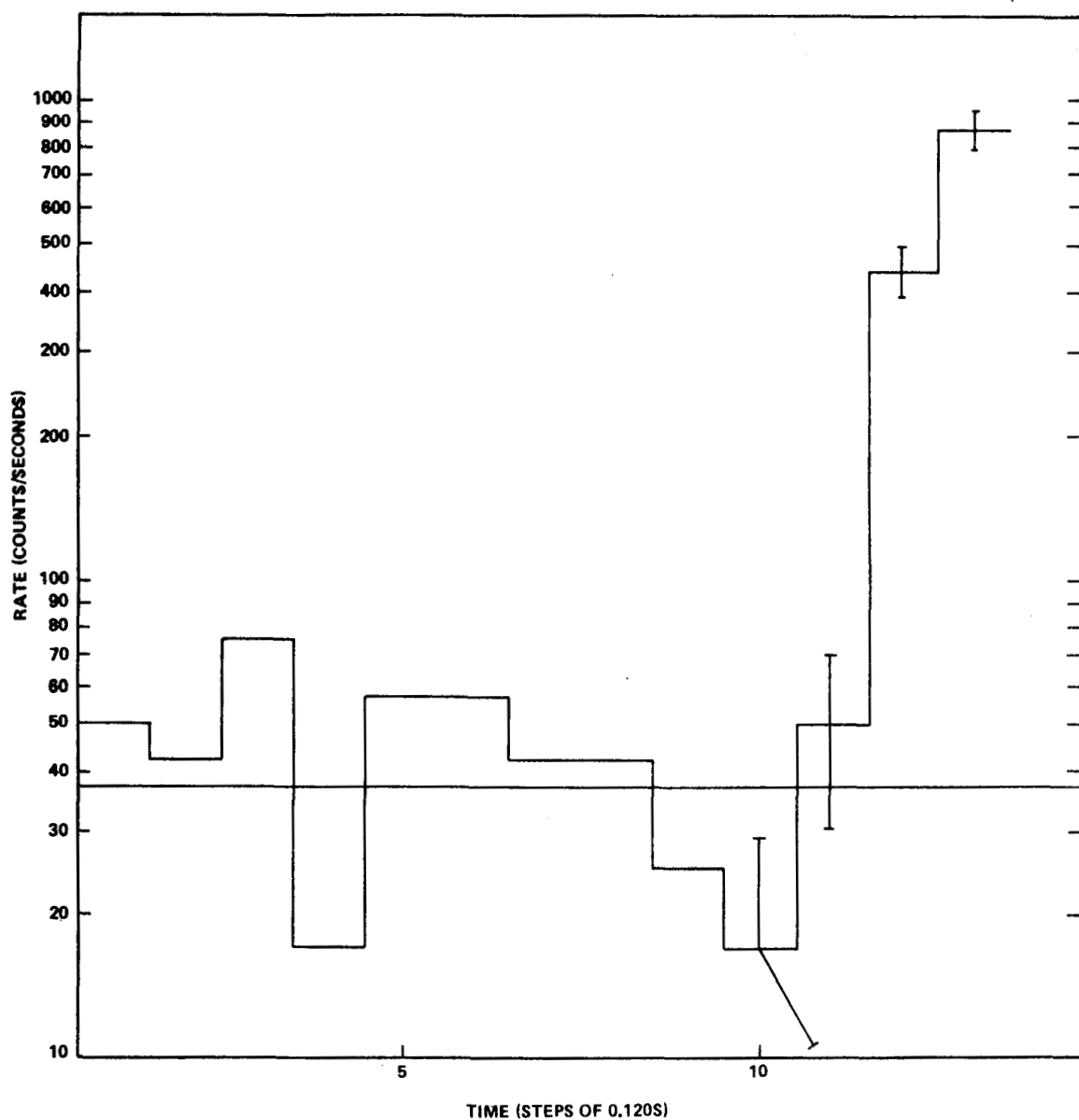


Figure 4. Burst onset. The data are binned in 0.12 sec intervals.  
 The solid line is the mean preburst counting rate including  
 20 c/sec of background.

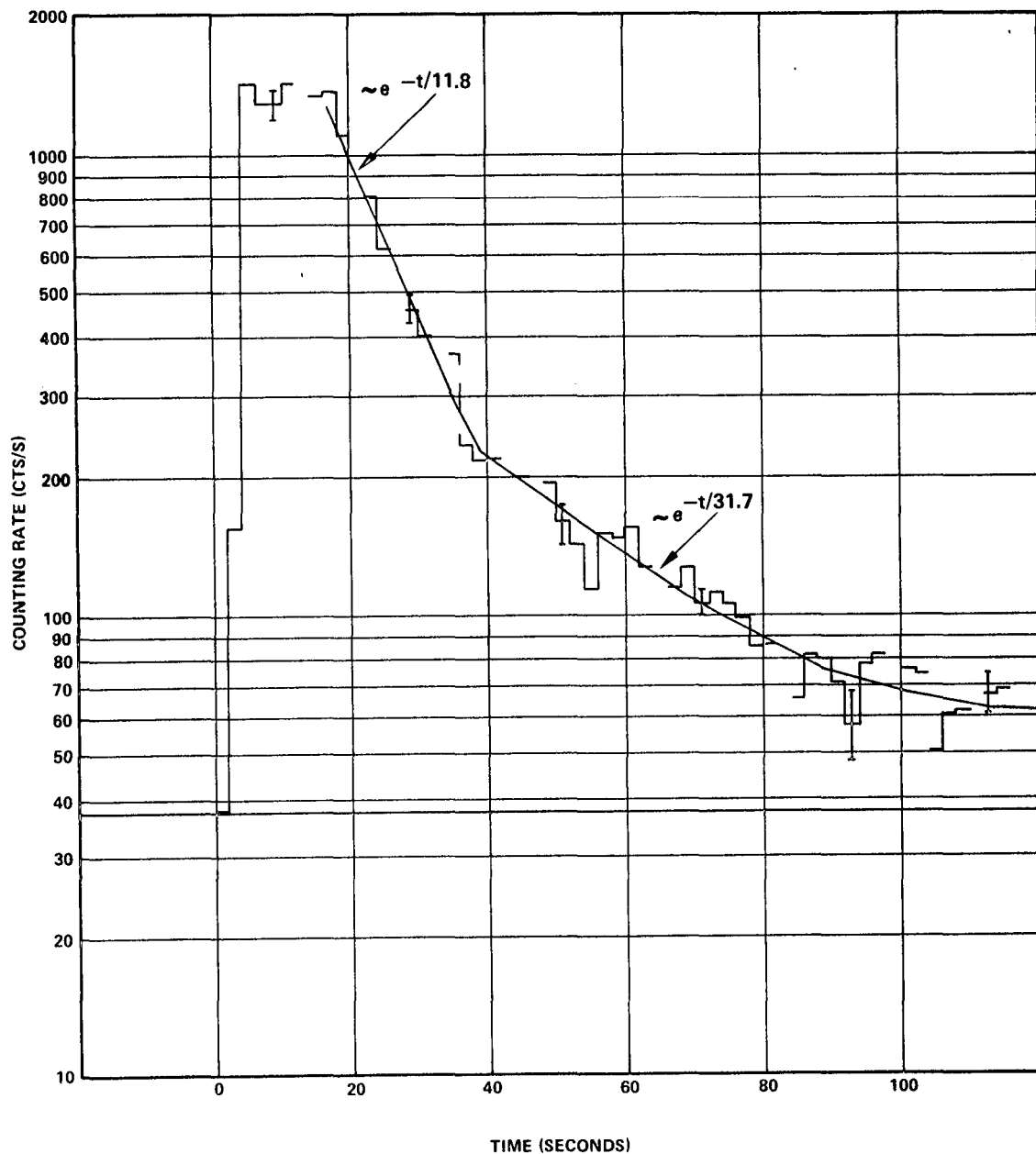


Figure 5. The time evolution of the burst from Terzan 2 plotted in 2 sec intervals. The solid line is the mean preburst counting rate including the non X-ray background.

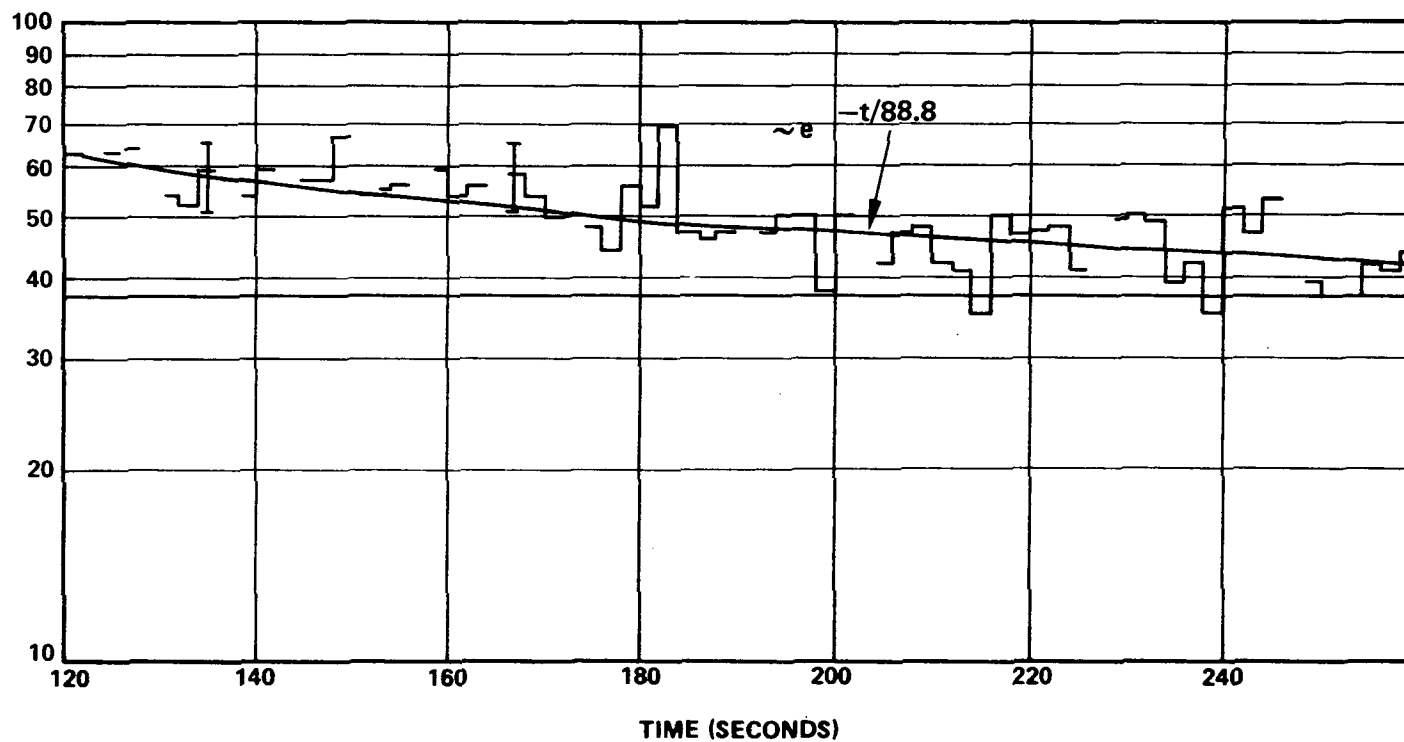


Figure 6. The time evolution of the burst from Terzan 2 plotted in 2 sec intervals. The solid line is the mean preburst counting rate including the non X-ray background.

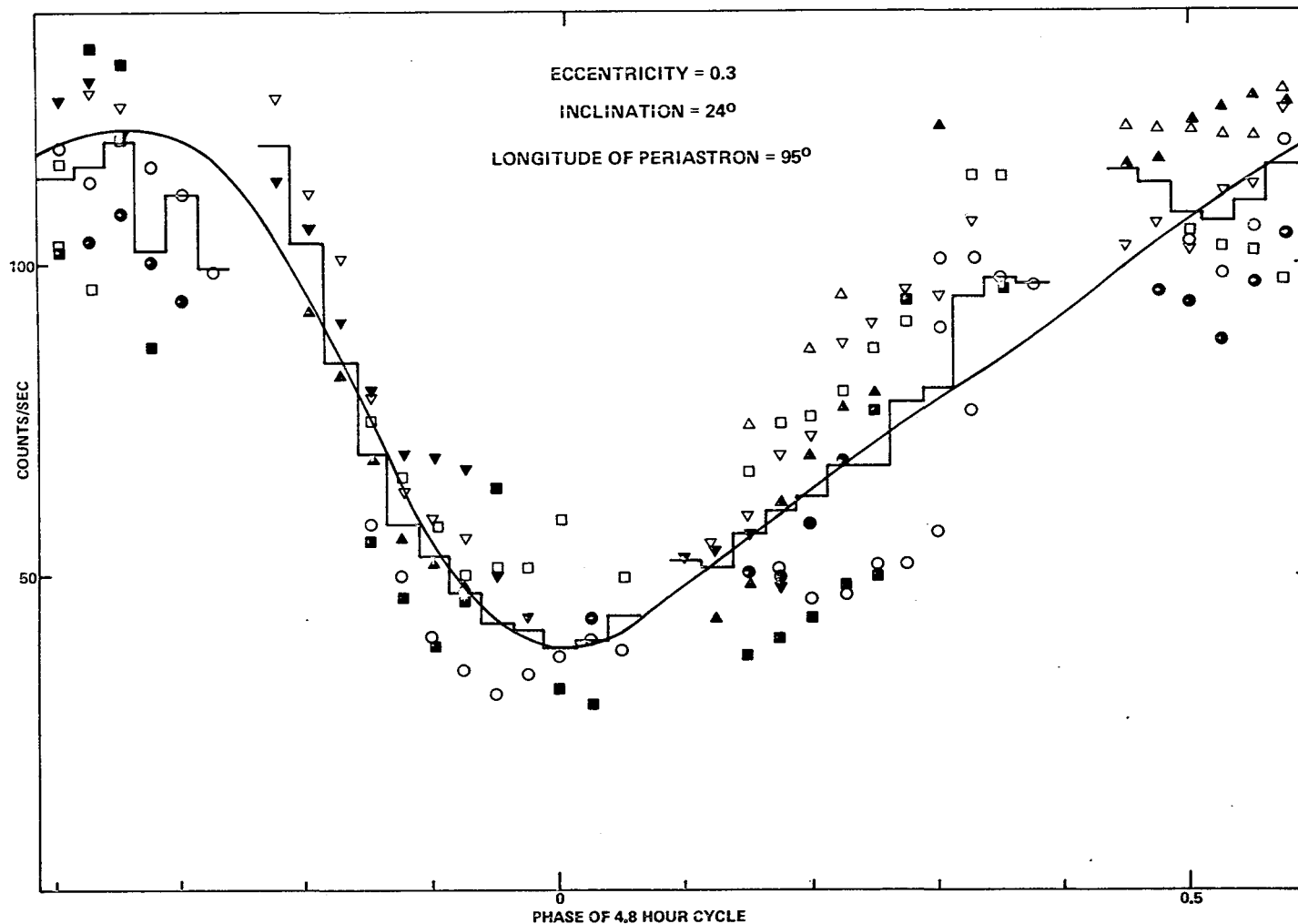


Figure 7. TIP observations of Cygnus X-3 folded modulo the 4.8 hr period. The histogram is the mean light curve. The points are the contributions to the mean from each 4.8 hr cycle. In both cases the errors due to counting statistics are approximately the size of data points shown. These data are shown with background subtracted and corrected for aspect. The solid line is the light curve expected from a pure absorbing atmosphere produced by a stellar wind with the X-ray source in an elliptical orbit.

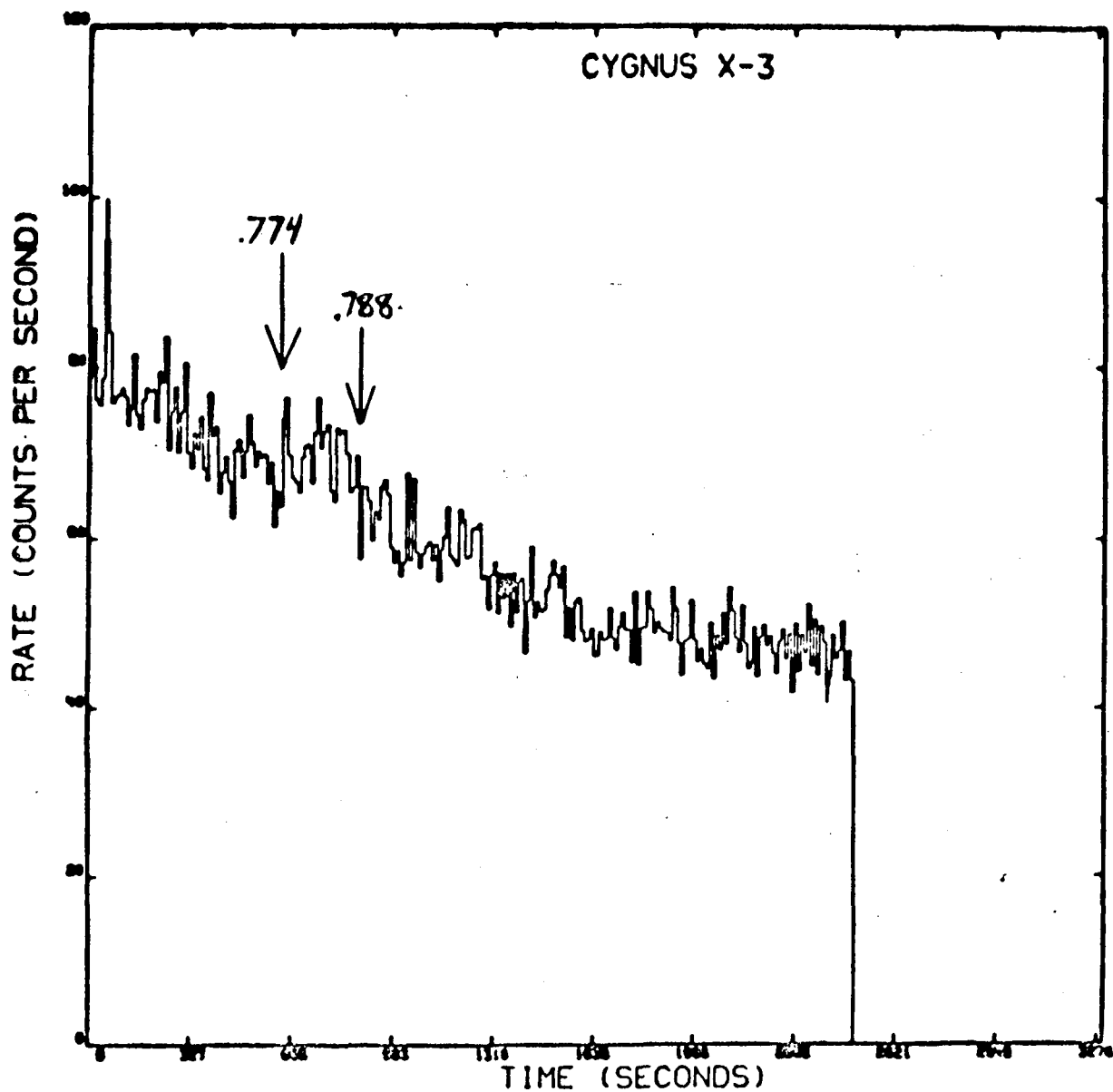


Figure 8. An X-ray flare from Cygnus X-3 detected in the falling portion of the light curve during phases 0.774 to 0.778 of the 4.8 hr period. The data are binned in intervals of 10.24 sec and are uncorrected for background and aspect.

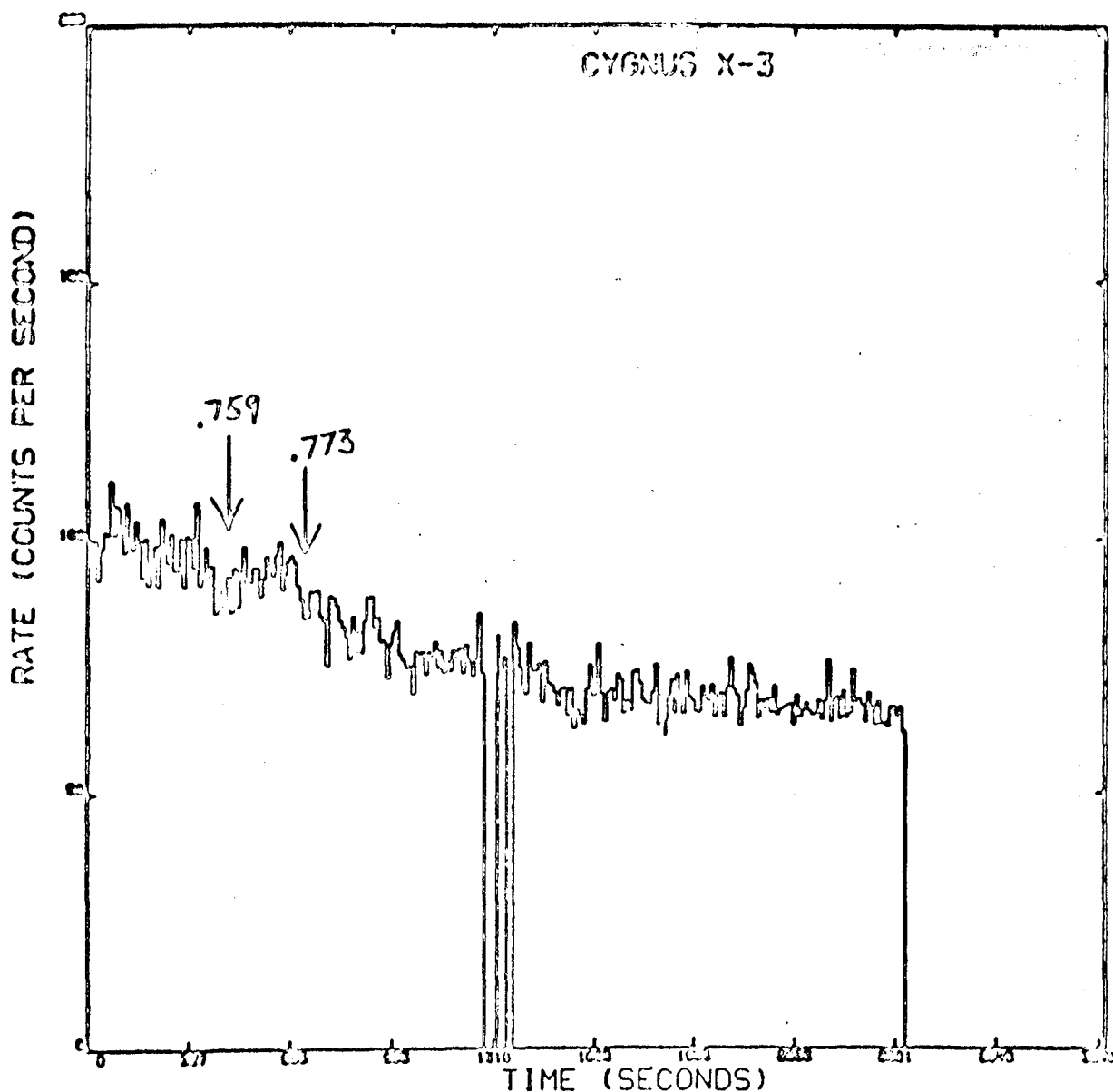


Figure 9. An X-ray flare from Cygnus X-3 detected in the falling portion of the light curve in the 4.8 hr period subsequent to the one shown in Figure 8. This could well be the same flare reappearing due to e.g. binary motion. Note that the phase of occurrence lies in the interval 0.759 to 0.773.

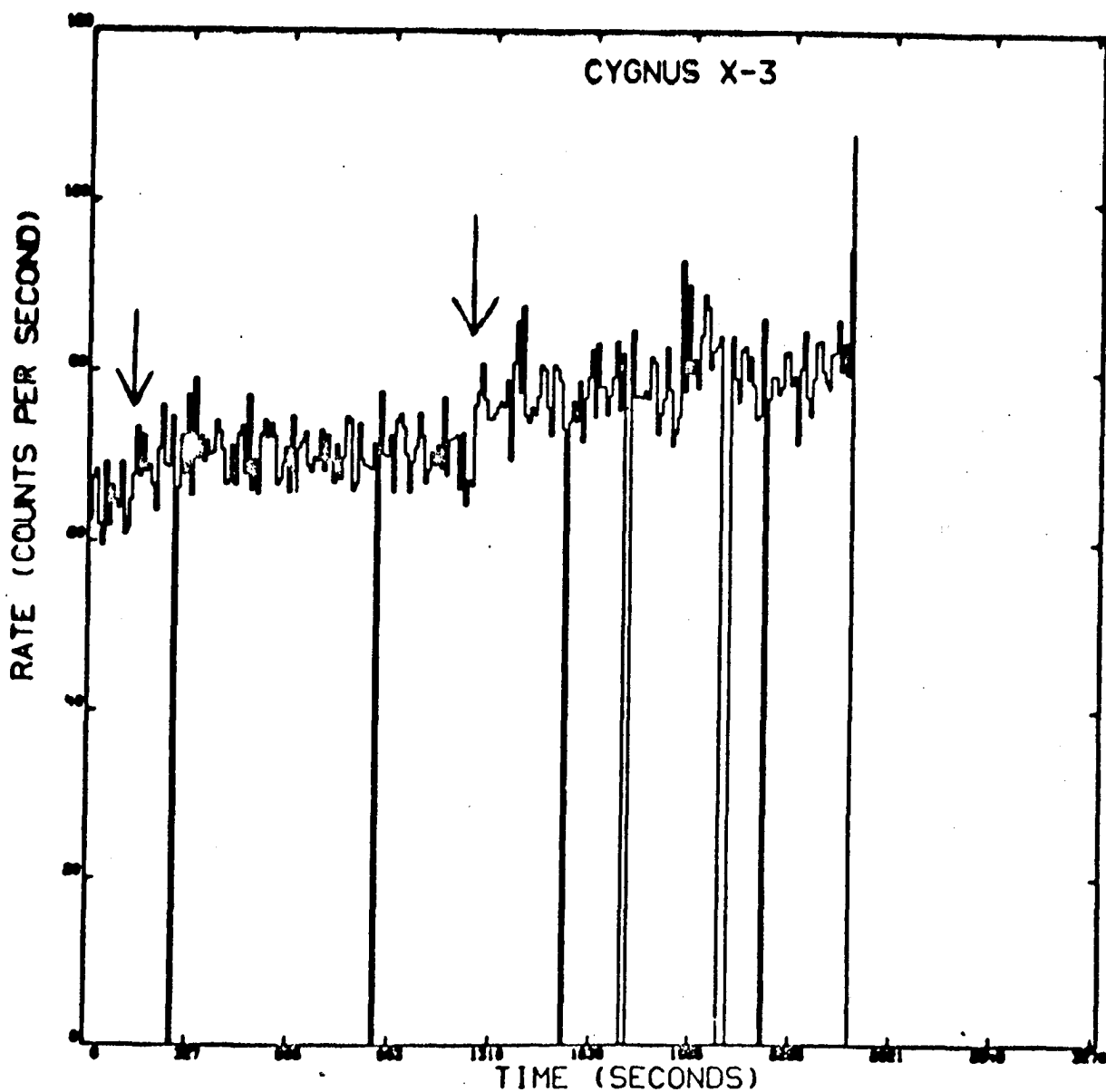


Figure 10. Sudden transition in the counting rate versus time during the TIP observations of Cygnus X-3. The data are binned in intervals of 10.24 sec and are uncorrected for background or aspect. There were no attitude maneuvers during the observations shown. The observations are summarized in Table 2 of the text.



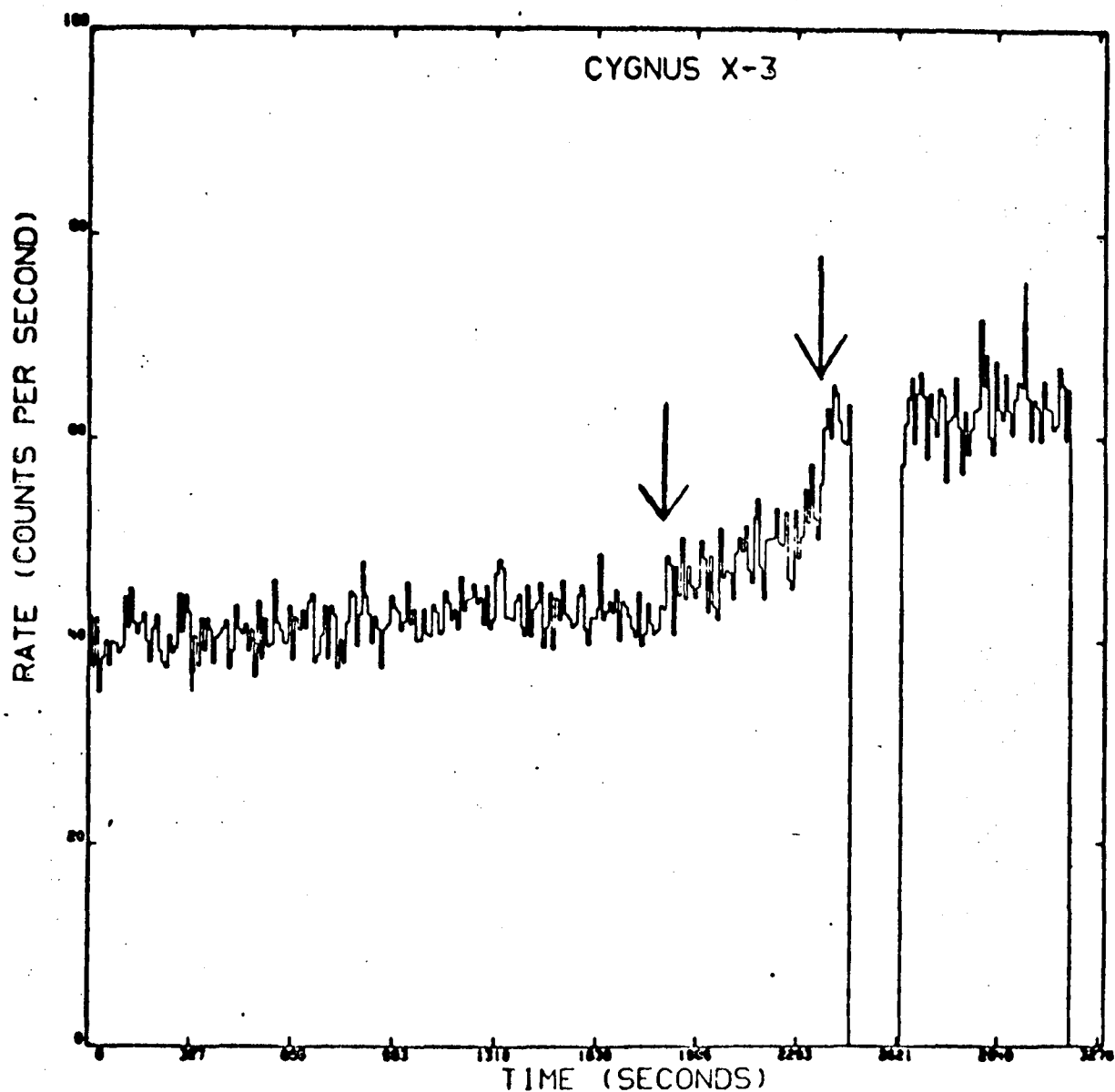


Figure 11. Sudden transition in the counting rate versus time during the TIP observations of Cygnus X-3. The data are binned in intervals of 10.24 sec and are uncorrected for background or aspect. There were no attitude maneuvers during the observations shown. The observations are summarized in Table 2 of the text.

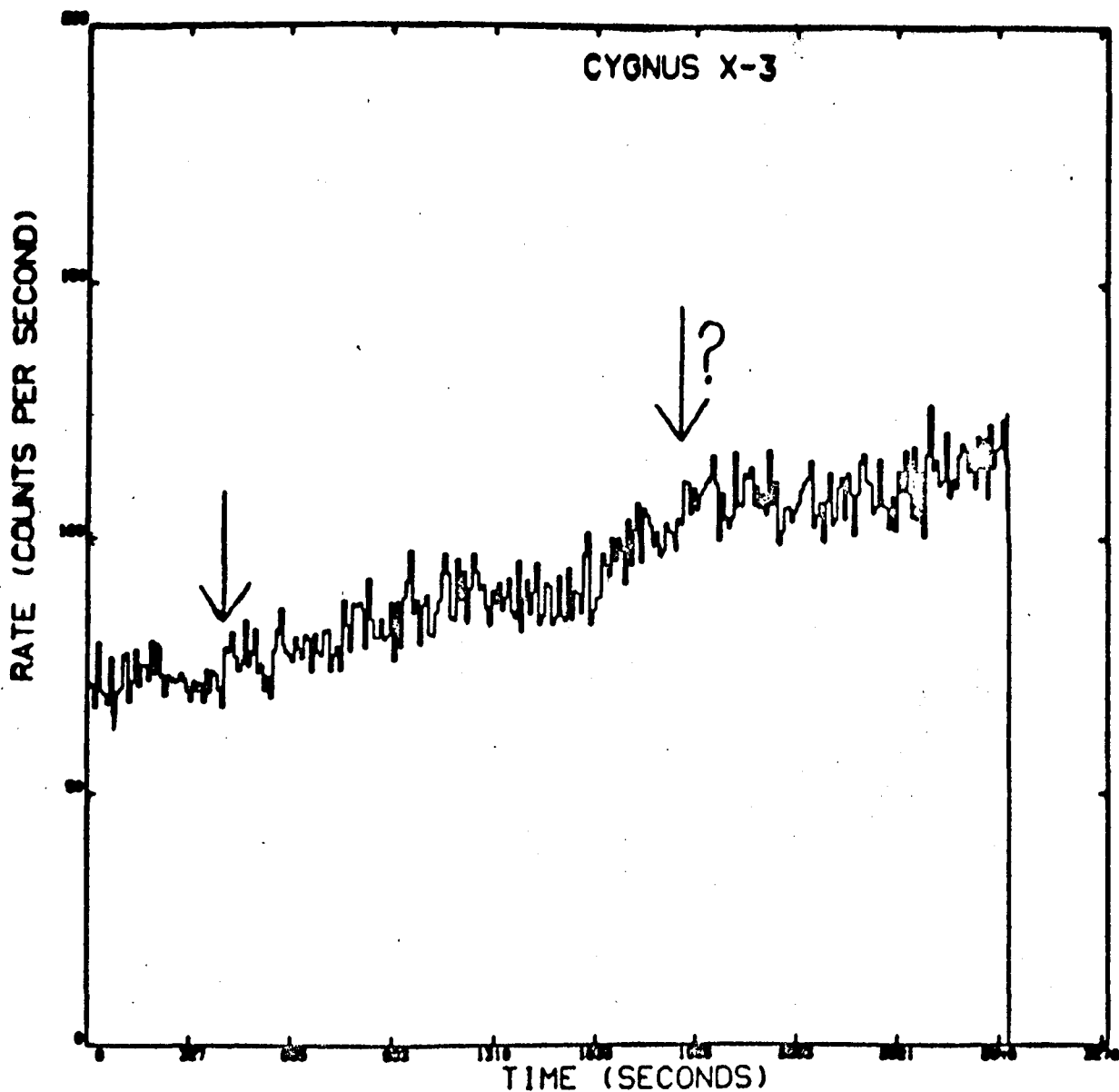


Figure 12. Sudden transition in the counting rate versus time during the TIP observations of Cygnus X-3. The data are binned in intervals of 10.24 sec and are uncorrected for background or aspect. There were no attitude maneuvers during the observations shown. The observations are summarized in Table 2 of the text.

## SESSION IV

### RESULTS FROM HEAO-2 IMAGING INSTRUMENTS

# EINSTEIN OBSERVATIONS OF EXTENDED GALACTIC X-RAY SOURCES

F. D. Seward  
Harvard/Smithsonian Astrophysical Observatory

## I. INTRODUCTION

With the X-ray optics of the Einstein Observatory, it is now possible, for the first time, to "see" X-ray sources. Previously known extended sources have been resolved: sometimes into several sources, sometimes into clouds of diffuse emission with perhaps knots and filaments. Spatial resolution of the X-ray pictures is comparable to that of radio and optical observations, and we can now compare the X-ray morphology of a source with that observed at other wavelengths.

This paper presents some early results. Since analysis of these data has just started, this is not a formal presentation of scientific conclusions, but rather a discussion of the basic features of the X-ray pictures.

Let us first consider supernova remnants. A supernova is caused by the explosion of a massive star. The central regions of the star collapse, releasing an enormous amount of gravitational energy. The explosion ejects the outer layers of the star at high velocity and much of the energy goes into kinetic energy of the moving debris. This material plows into the interstellar medium, at first expanding freely, then after hundreds of years accumulating an appreciable mass of interstellar material and slowing down. The kinetic energy of the expanding debris is turned into thermal energy and will eventually appear as a shock wave moving outward through the interstellar medium. This blast wave is the same phenomenon as that produced by a large explosion in the atmosphere.

A supernova remnant consists of the expanding debris, the blast wave, and the remains of the imploded stellar core (probably a neutron star). Supernova remnants are studied to learn about the supernova explosion itself. It should be possible to derive the initial energy release, the mass of the pre-supernova star, and the composition of the material produced in the explosion. Observation of the expanding shell and the blast wave also yields information concerning the interaction of this material with the interstellar medium and the interstellar medium itself.

Each supernova remnant has its own personality. It is obvious that some are very young and some ancient. However, it is somewhat difficult to arrange the various observations to illustrate an evolutionary sequence. Often emission from one feature is so strong that fainter

features of interest are obscured. Nevertheless, we present here five supernova remnants arranged approximately in order of increasing age.

Recall that the Einstein Observatory carries two imaging detectors, the Imaging Proportional Counter (IPC) having a resolution of 1 arc min and a field of view approximately 1 degree in diameter, and the High Resolution Imager (HRI) with spatial resolution of 3 arc sec and a field of view 25 arc min in diameter (Giacconi, et al. 1979). The energy range covered by both instruments is 200 eV - 3 keV. The IPC is capable of determining the photon energy, and it is possible to obtain IPC pictures in three broad X-ray energy ranges.

## II. CAS A

The youngest supernova remnant observed is Cassiopeia A. Although the optical event was not witnessed, the motion of the expanding material can be followed backwards in time to the point of origin. The date of the explosion has been estimated by van den Bergh and Dodd (1970), with an accuracy of a few years, as 1667. The Einstein observation of Cas A has been described by Murray, et al. (1979), and Figure 1 shows the HRI picture. The diameter of this remnant is 4 arc min. The brightest parts are probably regions containing the actual debris from the stellar explosion. Optical pictures of Cas A show many faint fast moving knots of material (van den Bergh, et al. 1973). Optical spectra of these knots show very strong emission from oxygen and sulphur indicating that the material has been enriched in heavier elements.

Figure 2 compares X-ray, optical, and radio maps of Cas A taken from Dickel and Greisen (1979). The spatial regions containing fast moving knots are identical with the brightest regions in the X-ray picture. The X-rays must come from a plasma at a temperature of approximately  $10^7$  degrees. This material has been heated either by the original supernova explosion or by friction with the interstellar medium. There is a faint X-ray halo just outside of the bright regions. This faint outer shell is real and is interpreted as a shock wave moving just ahead of the expanding debris.

The X-ray spectrum shows at least two thermal components with many emission lines. The generally accepted picture is that the blast wave is hotter than the debris. The solid state spectrometer on the Einstein Observatory shows strong emission lines from silicon, sulphur, argon, calcium, and iron proving beyond doubt that most of the X-rays are from a thermal source and strongly indicating that the material has been enriched in heavy elements (Holt, et al. 1979).

The radio picture of Cas A (which is an extremely strong radio source) shows a shell virtually identical in size and shape to the X-ray shell. Some knots of emission appear in both radio and X-ray pictures, but in general the regions of strongest X-ray emission are not prominent in the radio picture.

There is no sign of a pulsar in the central regions of the supernova remnant. The X-ray picture shows nothing obvious which might correspond to the remnant of the core of the imploded star.

### III. TYCHO

The supernova was observed by Tycho Brahe in 1572. The light curve was typical of Type I supernovae. Various estimates have been given for the distance, and we have used 3 kpc in our calculations.

Figure 3 shows the HRI picture of this remnant. This was a 10-hr exposure requiring approximately 1 day of Observatory time. The appearance of the remnant is an almost circular shell with diameter 8 arc min. It shows limb brightening varying from a maximum in the northwest to a minimum in the southeast. The center is filled with emission which the HRI resolves into patches or knots.

Figure 4 shows a 6 cm Westerbork radio map taken from Duin and Strom (1975). Radio and X-ray emission come from shells of equal diameter. The correlation is remarkably good in places, particularly in the eastern part of the shell where there is a projection or discontinuity with two knots of emission. There is also a knot of emission to the north of this feature in radio and X-rays. The radio bright region on the northeast limb is identical with the X-ray bright region, but the brightest part of the X-ray picture, the northwestern limb, is not a strong radio source.

From this picture, we can measure characteristics of the X-ray emitting shell. The measured features are real, the detector resolution is better than the observed thickness of the shell. The sharpness of the edge of the shell is not limited by the detector resolution. The shell thickness is on the average 0.3 of the radius. It is 0.1 of the radius where the emission is maximum in the northwest. There is no indication of a shell at all in the southeast.

One might interpret this spherical shell as a blast wave. However, the knots of emission and the discontinuity in the western part of the shell are inconsistent with this hypothesis. We are probably seeing the ejected material. It may be immersed in a blast wave or producing local shock waves closely associated in space with the material itself. Again, the SSS spectrum of Tycho's remnant shows very strong emission lines, proving thermal emission from hot gas and being highly suggestive that the emitting gas has been enriched in heavy elements.

We can derive the density of the emitting gas from the observed surface brightness of the material. The average electron density in the northwest part of the shell where the limb is brightest is about 6 electrons/cm<sup>3</sup>; the density in a bright knot is about 15 electrons/cm<sup>3</sup>. The thermal energy in the hot gas is approximately 10<sup>50</sup> ergs, the kinetic

energy of the expanding shell is approximately  $3 \times 10^{51}$  ergs, and the total mass of the shell is approximately  $6 M_{\odot}$ . The nonuniformity of the shell indicates spatial asymmetry in the ejected material or density variations in the interstellar medium.

Once more, there is no sign of a pulsar or other X-ray emitting remnant of the imploded core.

#### IV. THE SUPERNOVA OF 1006

In the year 1006, a very bright supernova was seen in the constellation Lupus. Figure 5 shows the IPC picture of the remnant. It is 30 arc minutes in diameter, almost exactly the apparent size of the full moon. Optically, very little is seen at the position of this remnant. The radio map (Milne 1971) looks quite similar to the X-ray picture showing an approximately spherical shell with brightest emission from two opposing faces in the east and southwest. This remnant looks more like the expected blast wave. There are no resolved bright knots indicating regions of high density of material. The expanding debris has probably picked up an appreciable amount of interstellar material, more of the kinetic energy has been thermalized, and the hot gas appears as a shock wave moving outward. Once again, no pulsar is seen.

#### V. THE CRAB NEBULA

The Crab Nebula is the remnant of a supernova explosion of 1054 AD. Although about the same age as the remnant of SN 1006, the Crab is radically different in appearance. Figure 6 shows an optical picture of the  $5 \times 7$  ft Nebula. The entire shell is laced with red filaments emitting mostly line radiation from hydrogen atoms. The central regions are filled with an amorphous diffuse continuum which appears blue in contrast to the red filaments. Figure 6 shows the continuum radiation clearly whereas the filaments appear only faintly.

The southwest member of the double star seen in the center of the nebula is a pulsar. This neutron star, spinning at 30 rps, is the most rapid pulsar known and is visible clearly at all frequencies: radio, optical, X-ray and gamma-ray. Figure 7 shows the Einstein HRI picture of the Crab Nebula. The pulsar is seen as a point source surrounded by a patch of diffuse X-ray emission approximately 2 arc min in extent. The strongest diffuse emission comes from a region located northwest of the pulsar, corresponding closely with the region of maximum optical emission.

The diffuse emission, both X-ray and optical, is caused by extremely high energy electrons moving in a weak magnetic field. These electrons are probably created at the pulsar and accelerated in the strong electric and magnetic fields of the rotating pulsar. The apparent X-ray

point source at the pulsar location is due to pulsed X-rays. These X-rays are created very close to the pulsar analogously with the pulsed optical and radio emission observed from this object. The reason for the asymmetrical location of the diffuse synchrotron source with respect to the pulsar is not understood.

The Crab Nebula as an X-ray source is completely dominated by the pulsar. If there is any thermal radiation from the expanding envelope or from a blast wave, it is completely swamped by the powerful synchrotron source in the center of the Crab. The Crab could be surrounded with a weak envelope identical to that of the supernova remnant of 1006, and it would be extremely difficult to see with our detectors. We are presently searching the data very carefully for this effect.

## VI. NEUTRON STARS

The Crab Pulsar is the brightest neutron star seen in the X-ray data. Strong pulsed radiation is seen from the pulsar itself which appears as a point source to the Einstein detectors. The diffuse synchrotron source associated with the pulsar is a second manifestation of the neutron star in the X-ray data.

A third source of X-rays from pulsars might be blackbody radiation associated with high surface temperature. Theoretically, pulsars are born with high temperatures and cool as they age. Even though only 10 km in radius, if the surface temperature were  $10^7$  degrees, blackbody radiation from the surface would peak at soft X-ray frequencies and the neutron star would appear very bright to the Einstein telescope. The fact that no pulsars are seen in the vicinity of several SNR allow us to set upper limits on the surface temperatures. An upper limit of  $2 \times 10^6$  degrees can be set on possible neutron stars associated with Cas A and Tycho's remnant, and a limit of  $1 \times 10^6$  degrees can be set on any neutron star in the vicinity of the remnant of SN1006. We expect these limits to constrain models of the internal composition of neutron stars, perhaps requiring the existence of pions in the core to explain the apparent rapid cooling observed (Helfand, et al. 1979).

Another area that must be investigated, however, is the assumption that the neutron star surface is a blackbody. Because of extremely high magnetic fields at the surface, all states are not possible to electrons. For a given temperature, the radiation emitted may be considerably less than that predicted under the assumption that the surface is black.

## VII. VELA X

This is a very old remnant (age approximately  $10^4$  years) in the constellation Vela at a distance of approximately 400 pc. The blast wave has cooled and left an array of filaments quite visible in the optical



band (Miller 1973). The remnant has a diameter of 5.5 degrees and is a source of strong radio and X-ray radiation. We are mapping this region with the IPC. It takes 27 pointings to complete this mapping and only 6 have been accomplished. Figure 8 shows the results of three pointings. These are IPC pictures covering fields 1-degree square. The detector is shadowed by window support ribs which form a tic-tac-toe pattern obscuring some of the diffuse X-rays.

X-ray emission from Vela X is patchy. The inside of the remnant contains wisps and blobs of hot gas which show strongly in the X-ray pictures. The Vela remnant also contains a pulsar which is an X-ray source. In contrast to the Crab, the X-ray picture of the Vela remnant is dominated by thermal radiation. These X-rays are very soft and most of the energy appears as photons with energies of a few hundred eV. Pulse height spectra from the IPC are shown on the right hand side of Figure 8 to illustrate this. The upper spectrum shows the soft diffuse X-rays from one of the bright patches of emission, the lower spectrum is that of the pulsar. By restricting the picture to only high energies, the pulsar appears more clearly as is also shown in Figure 8.

Figure 9 shows an HRI picture centered on the pulsar. The pulsar appears as a point source surrounded by a weak diffuse nebula of diameter 1 arc min. In comparison with the Crab pulsar, this diffuse radiation is much, much weaker and the apparent point source is not pulsed. This apparent point source is either a small diffuse region surrounding the pulsar and too small to be resolved by the Einstein telescope, or it is radiation from the surface of the pulsar. If this is the "blackbody" radiation, the surface temperature implied is  $1.5 \times 10^6$  degrees.

### VIII. THE ETA CARINAE NEBULA

Now let us consider a region where new stars are forming. The Eta Carinae Nebula is a bright emission nebula approximately 2 degrees in extent. It contains many bright early stars and the region is permeated with gas clouds having densities approximately  $10^3$  atoms/cm<sup>3</sup>. A prominent V-shaped dust lane traverses the lower part of the nebula. Eta Carinae itself is a unique object. It is now a 6th magnitude, almost stellar object, but in 1843 there was an outburst during which it brightened briefly to magnitude -1. It remained bright for 20 years and then declined to approximately its present level.

Eta Carinae forms the central part of an optical nebula, the homunculus, of dimension  $10 \times 15$  in. which contains several knots of luminosity and is expanding with a velocity of approximately 600 km/sec. This material was probably generated during the great outburst. The homunculus is surrounded by a faint outer shell of dimension  $20 \times 30$  in. (Walborn 1976).

Eta Carinae itself is now the brightest extrasolar infrared source at a wavelength of  $20\ \mu$ . At a distance of 2600 pc, the bolometric luminosity is approximately  $2 \times 10^6$  solar luminosities. The infrared emission comes from a shell of dust with dimension approximately that of the homunculus, and it is generally accepted that the energy source is a massive central object(s) obscured by the dust.

We obtained two X-ray pictures, both centered on Eta Carinae, both 3 hour exposures (Seward, et al. 1979). Figure 10 shows the IPC X-ray picture and Figure 11 shows contours of constant X-ray emission overlaid on a near UV photograph of this region. The X-ray picture is remarkably similar to the optical. Several bright sources are imbedded in diffuse emission. The western dust lane is seen in absorption. The brightest apparent point sources are Eta Carinae, a Wolf-Rayet star, and a cluster of O stars, Tr 14. The other sources have all been identified with O stars.

Eighty percent of the emission from this region is diffuse, coming mostly from the optically bright region, but not completely. This diffuse X-ray emission probably comes from hot gas. The region is 40 pc in extent and the temperature is about 5 million degrees. The total X-ray luminosity is approximately  $10^{35}$  erg/sec. The derived gas properties are: density approximately  $0.4\ \text{electrons/cm}^3$ , lifetime approximately  $10^7$  years, total thermal energy approximately  $10^{50}$  ergs. The western dust lane is seen clearly in the X-ray data and has a width of approximately 5 pc. The assumption of a comparable depth and a density of material the same as that of the optical emission nebula gives sufficient path length of cold material to absorb the X-rays.

This diffuse hot gas is probably the result of past supernova explosions or strong stellar winds. The O stars in this region are known to have strong winds, and these winds interacting with the surrounding dense material might give rise to X-ray emitting gas. Alternately, since the lifetime of O stars is short, a region such as this is expected to generate a supernova explosion approximately every million years. The diffuse emission might be part of an ancient supernova remnant or remnants, so old that it has lost its original characteristic shell-like structure.

Figure 12 shows the HRI picture. The diffuse feature in the northwest corner is an instrumental effect, not a real X-ray feature in the sky. Several point sources are seen: The Wolf-Rayet star, HD 93162, and three O stars. Eta Carinae itself is seen to be an extended source. There is a small bright horseshoe with weak emission extending to the southeast. Figure 13 shows Eta Carinae expanded. The contours of constant X-ray emission have been overlaid on an optical picture. The Homunculus (the IR source) forms the overexposed central part of this region and, in this photograph, has blended with emission features

attributed to the outer shell. Most X-ray emission is associated with this outer shell, and there appears to be a point source at the center of the Homunculus coincident with the brightest part of the nebula. If we assume that this X-ray emitting shell is a blast wave from an explosion, we can use the observed X-ray luminosity ( $3 \times 10^{33}$  ergs/sec) and size (0.2 pc) to estimate the initial energy of the outburst, and the gas density. These are  $E_0 = 10^{46}$  ergs and  $N_0 = 20/\text{cm}^3$ . These numbers are not compatible with the hypothesis that the 1843 outburst was a slow supernova. The energy released and the amount of material in the expanding shell are orders of magnitude too small to be the result of a supernova outburst.

The point source in the middle of the nebula is exciting. Perhaps this is the underlying massive object which supplies energy for the infrared source. This has been postulated by Davidson (1971) to be a star with mass approximately 100 solar masses. Such a star is expected to rapidly consume the nuclear fuel in its core and to end its brief extravagant life as a supernova.

Now we come again to Cassiopeia A, the remnant of a supernova which was unusual in that the optical event was not seen. One explanation given is that the exploding star was surrounded with a dense cloud of material and the optical radiation was attenuated to the point where it was not bright enough to be noticed by 17th century astronomers. Eta Carinae gives every sign of being an extremely massive star surrounded by a dense shell. Perhaps in the not too distant future (astronomically speaking) it too will explode as a supernova and leave a remnant similar to Cas A.

You should appreciate that the entire Eta Carinae region is only a weak X-ray source having an intensity of 3 Uhuru flux units. The Einstein pictures resolve this weak source into the peculiar object, Eta Carinae, at least seven stars, and diffuse emission. We are also observing the structure of Eta Carinae itself.

To those of us who a few years ago were doing X-ray observations with small rocket borne detectors, progress has been amazing. We are now seeing things undreamed of before the launch of the Einstein Observatory.

## REFERENCES

- Davidson, K. 1971, MNRAS, 154, 415.
- Dickel, J. R. and Greison, E. 1979, submitted to Ast. & Ap.
- Duin, R. M. and Strom, R. G. 1975, Ast. & Ap., 39, 33.
- Giacconi, R., et al. 1979, to be published Ap. J. (Letters).
- Helfand, D. J., Chanan, G. A., and Novick, R. 1979, submitted to Nature.
- Holt, S., et al. 1979, to be published Ap. J. (Letters).
- Kamper, K. W. and van den Bergh, S. 1976, Ap. J. Supp., 32, 351.
- Miller, E. W. 1973, PASP, 85, 764.
- Milne, D. K. 1971, Aust. J. Phys., 24, 757.
- Murray, S., et al. 1979, to be published Ap. J. (Letters).
- Seward, F. D., et al. 1979, to be published Ap. J. (Letters).
- van den Bergh, S. and Dodd, W. W. 1970, Ap. J., 162, 485.
- van den Bergh, S., Marscher, A. P., and Terzian, Y. 1973, Ap. J. Supp., 26, 19.
- Walborn, N. R. 1976, Ap. J. (Letters), 204, L17.

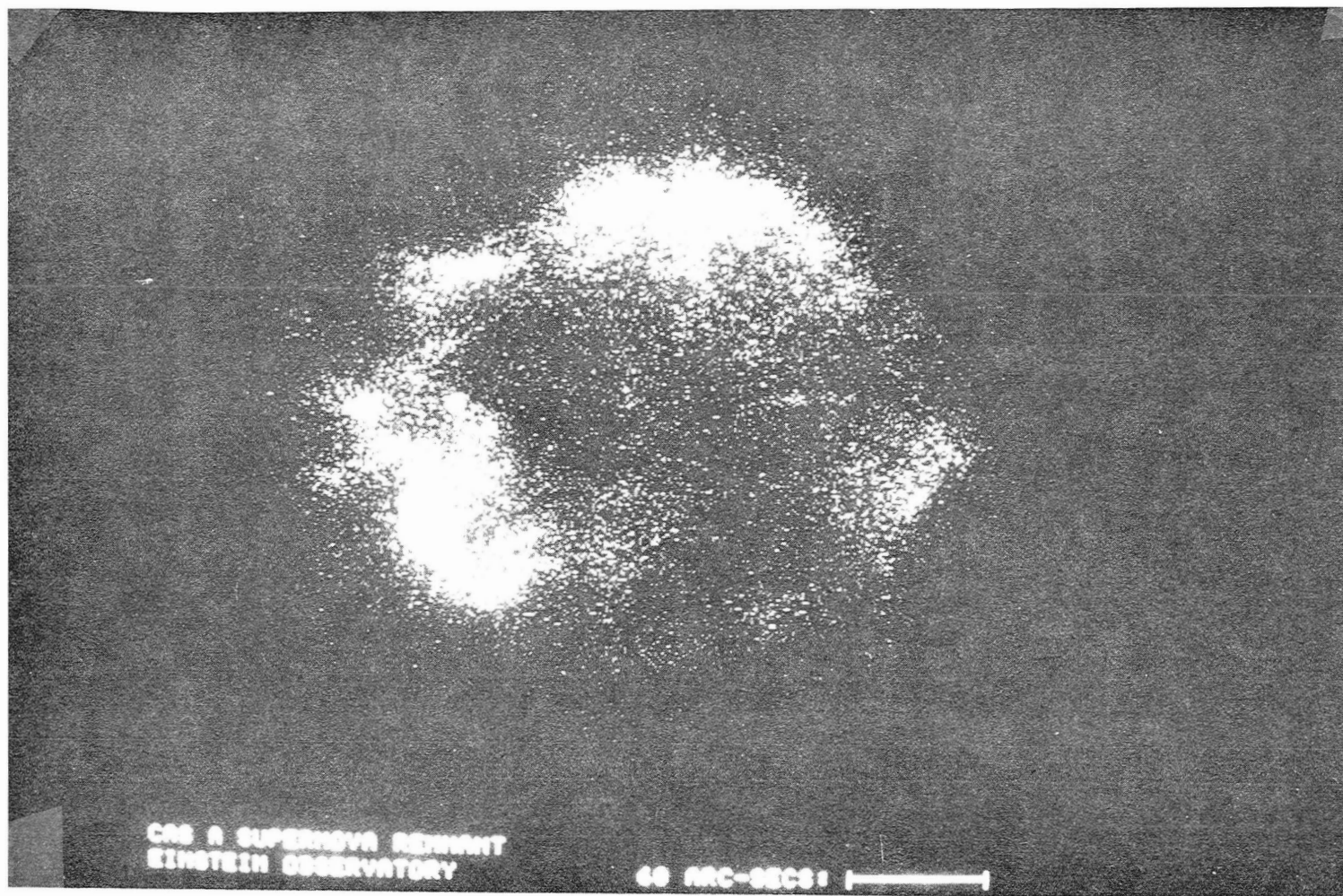


Figure 1. HRI picture of Cas A. Exposure approximately  $3 \times 10^4$  sec.

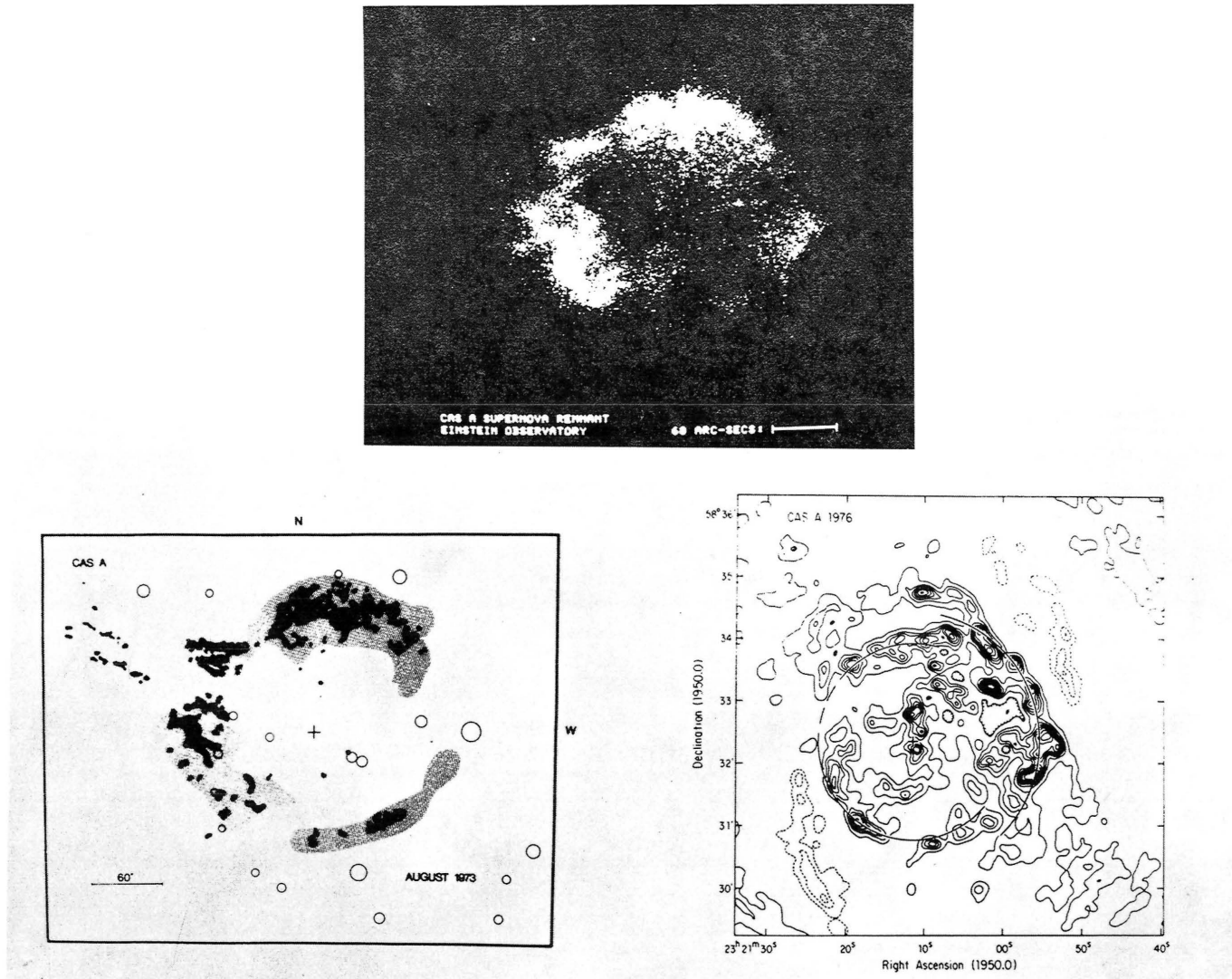


Figure 2. Cas A: X-ray picture, schematic of optical features from Kamper and van den Bergh (1976), and 6 cm radio map from Dickel and Greisen (1979).

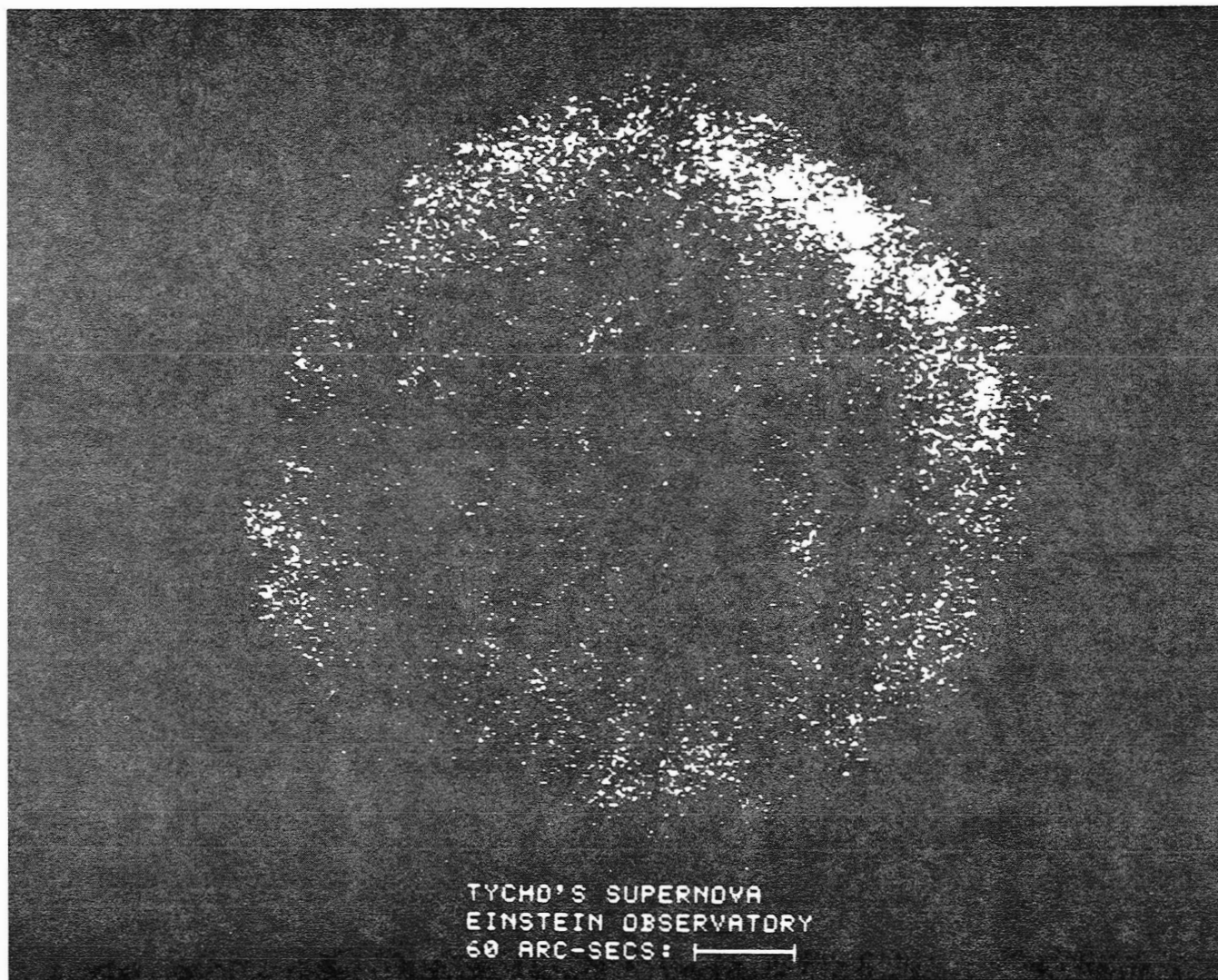


Figure 3. HRI picture of Tycho SNR. Exposure approximately  $4 \times 10^4$  sec.



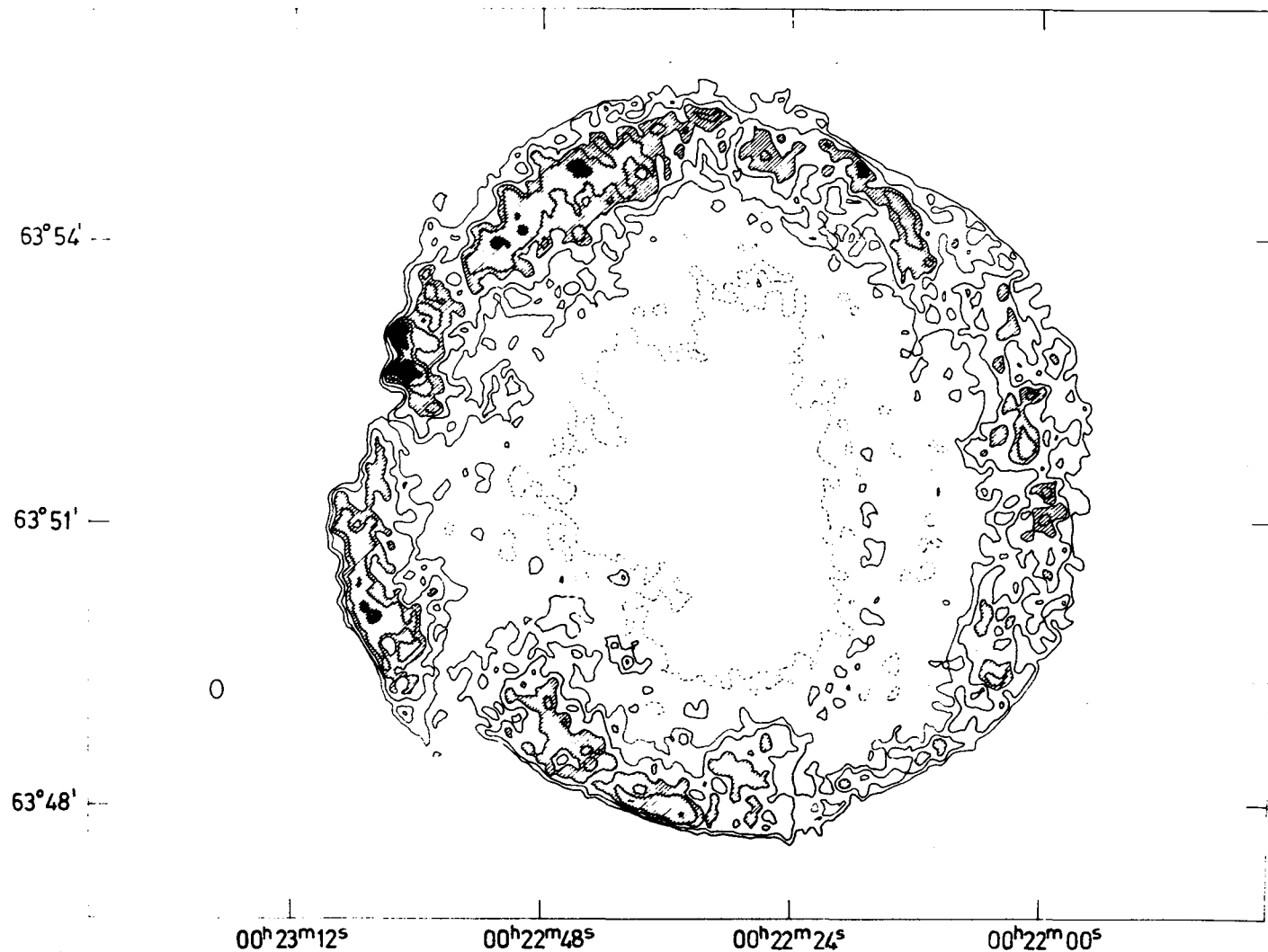


Figure 4. Tycho SNR: 6 cm radio map from Duin and Strom (1975).



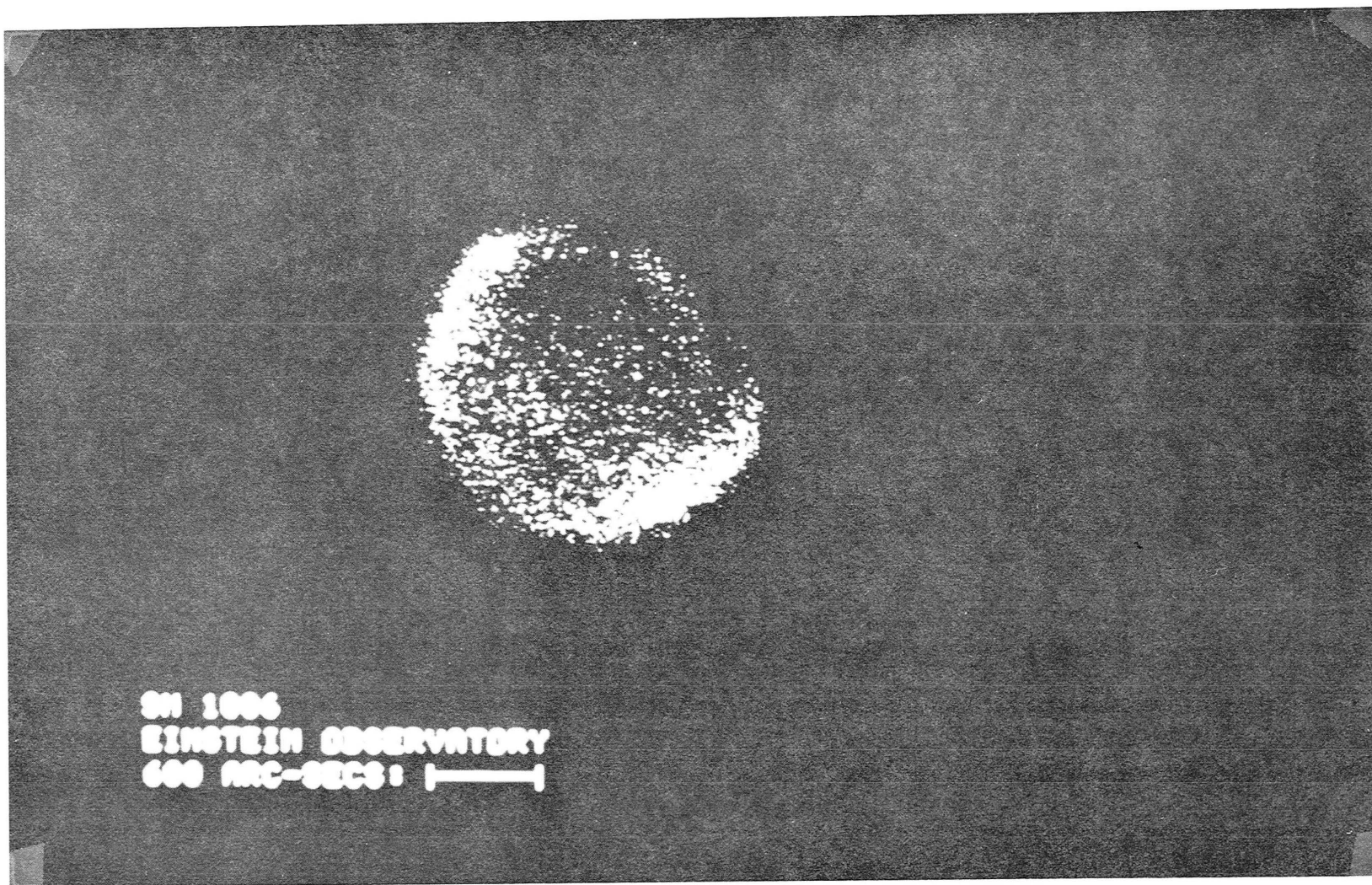


Figure 5. IPC picture of SNR 1006. Exposure approximately 3000 sec.

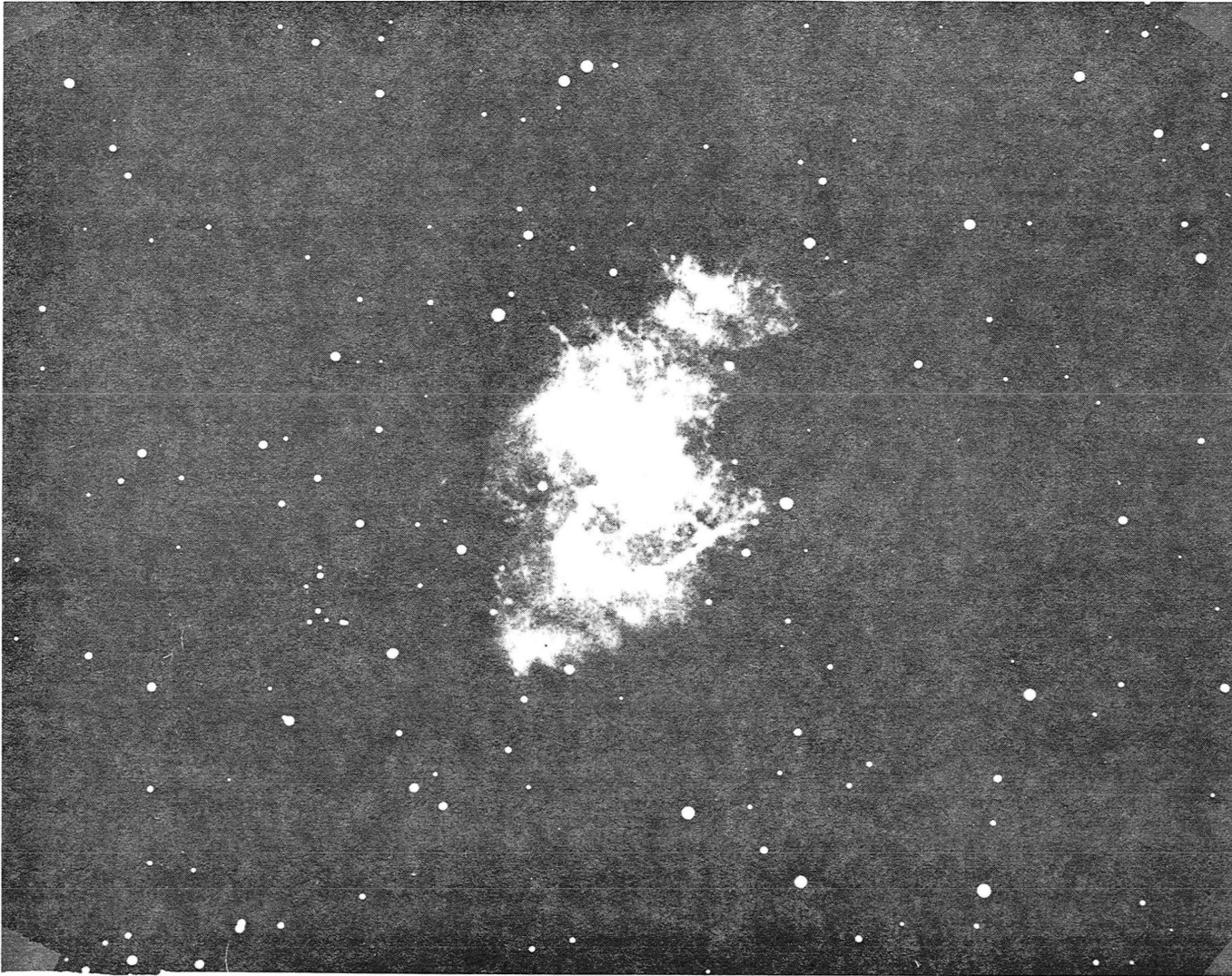


Figure 6. The Crab Nebula (from a color Hale Observatory photo).



Figure 7. HRI picture of the Crab Nebula. Exposure approximately  $5 \times 10^4$  sec.



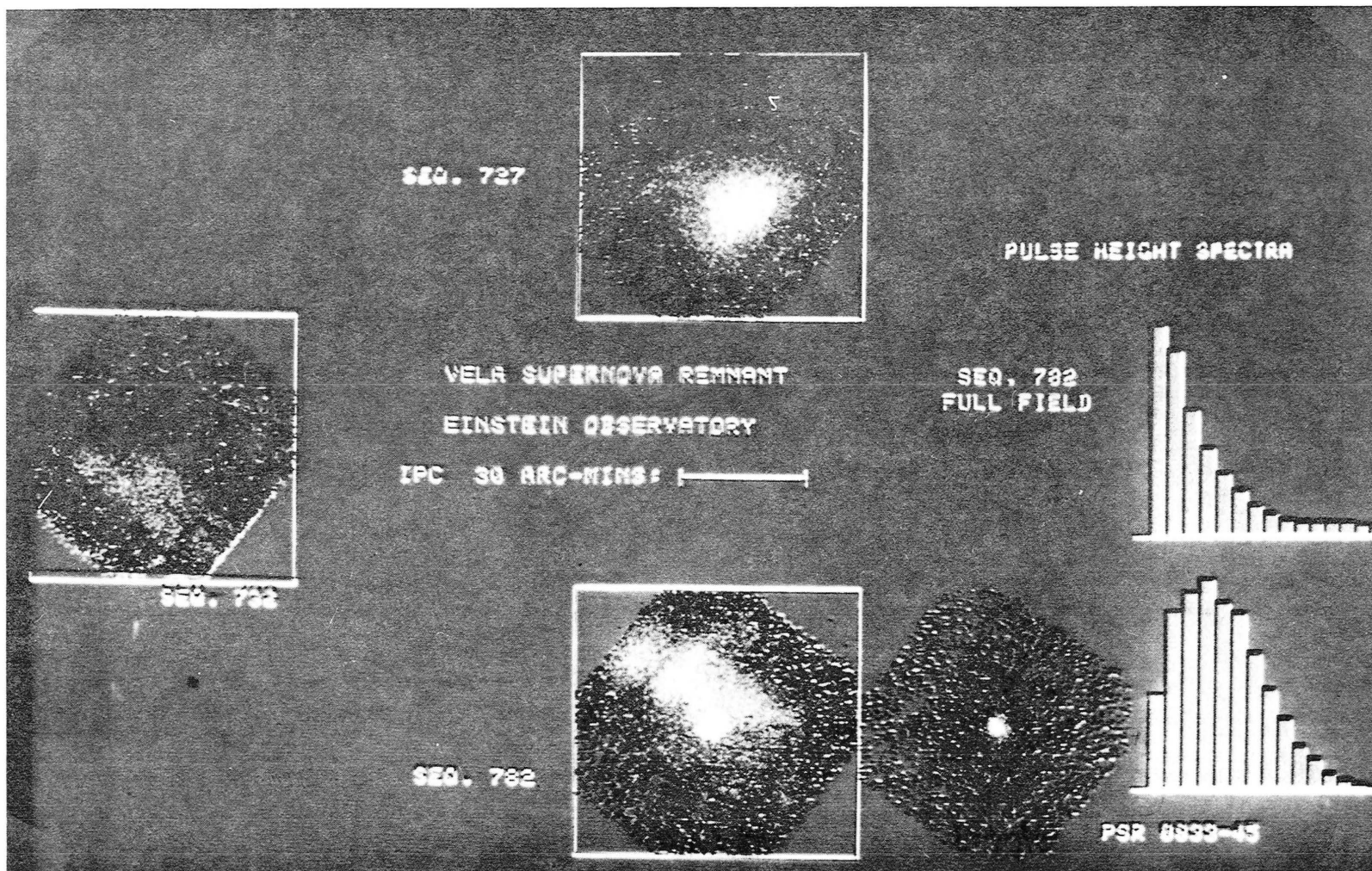


Figure 8. Three IPC fields in the Vela X SNR. The lower right field is shown twice: at left with all energies included and at right with only high energies included.

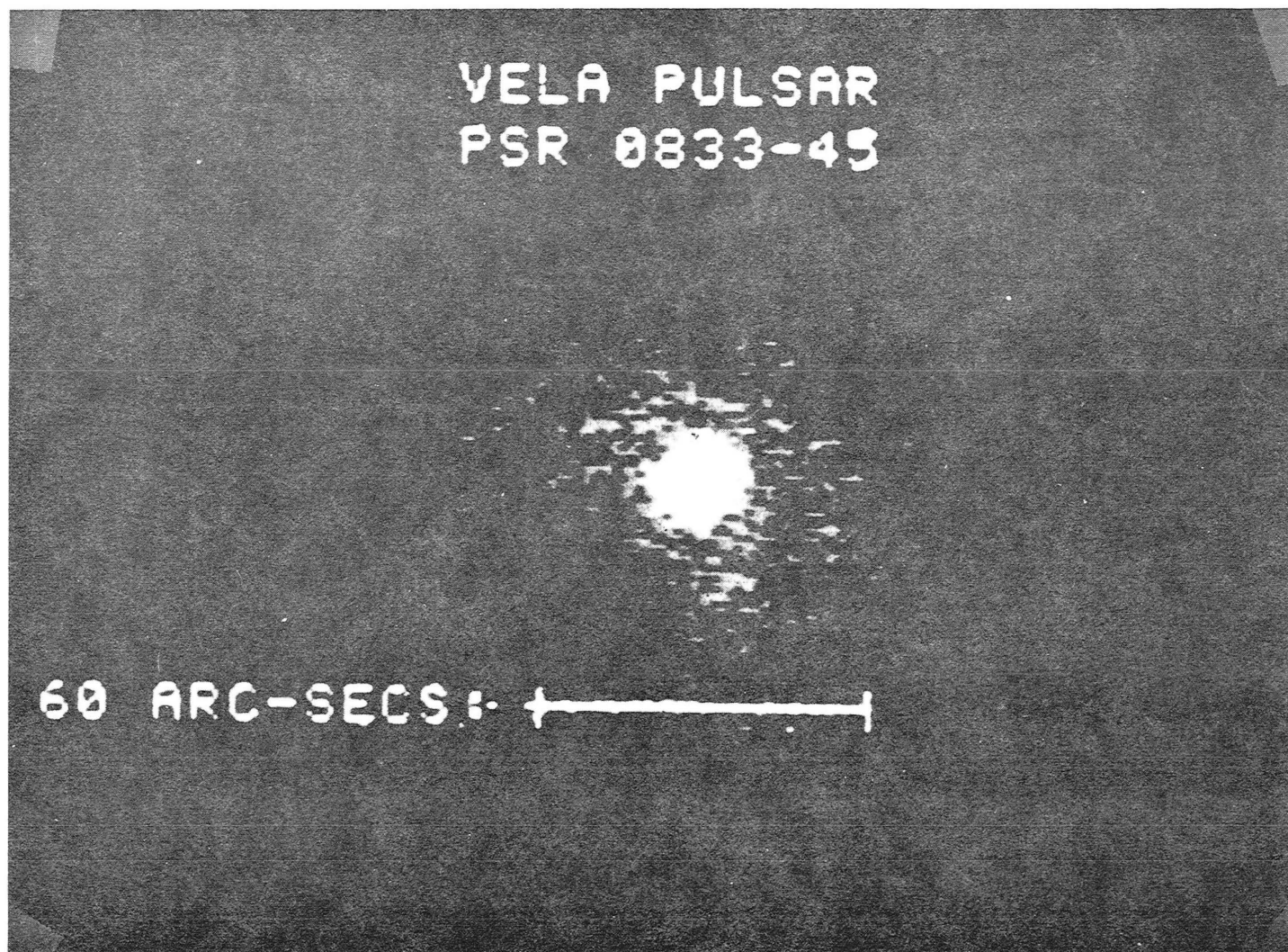


Figure 9. HRI picture of Vela pulsar and surrounding diffuse nebula.  
Exposure approximately  $10^4$  sec.

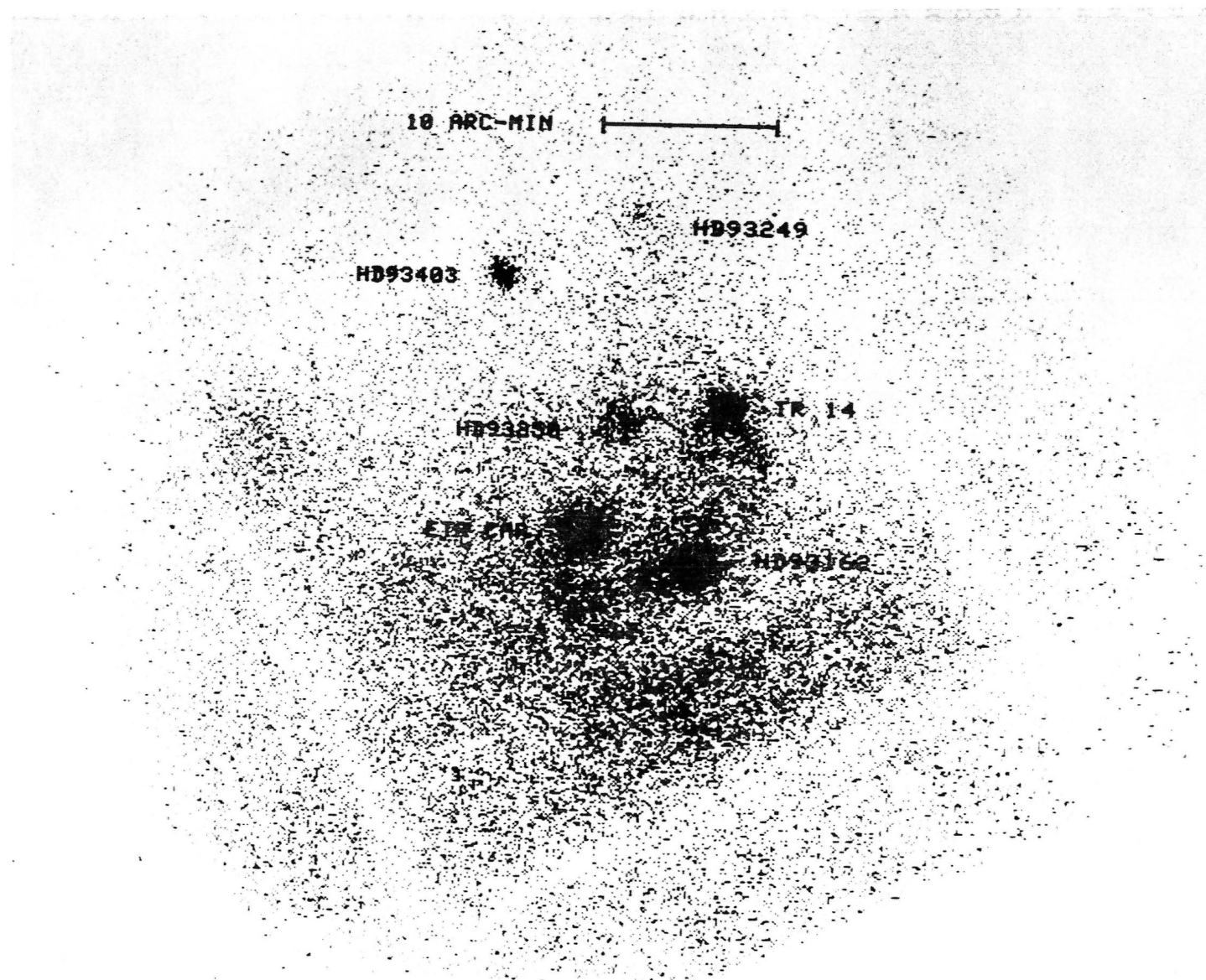


Figure 10. IPC picture of Eta Carinae Nebula. Exposure 8000 sec.



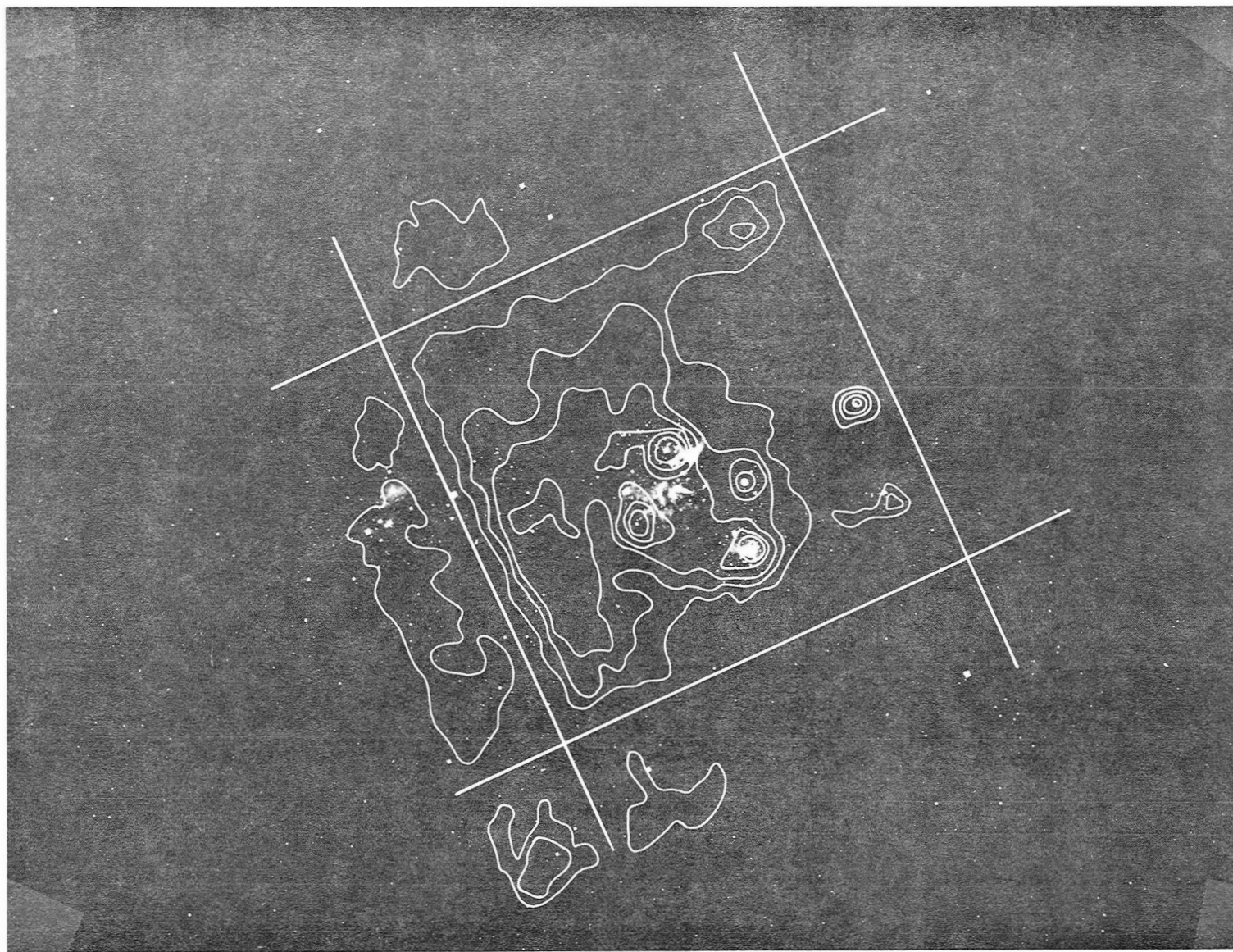


Figure 11. Contours of constant X-ray emission overlaid on optical photograph of Eta Carinae Nebula.

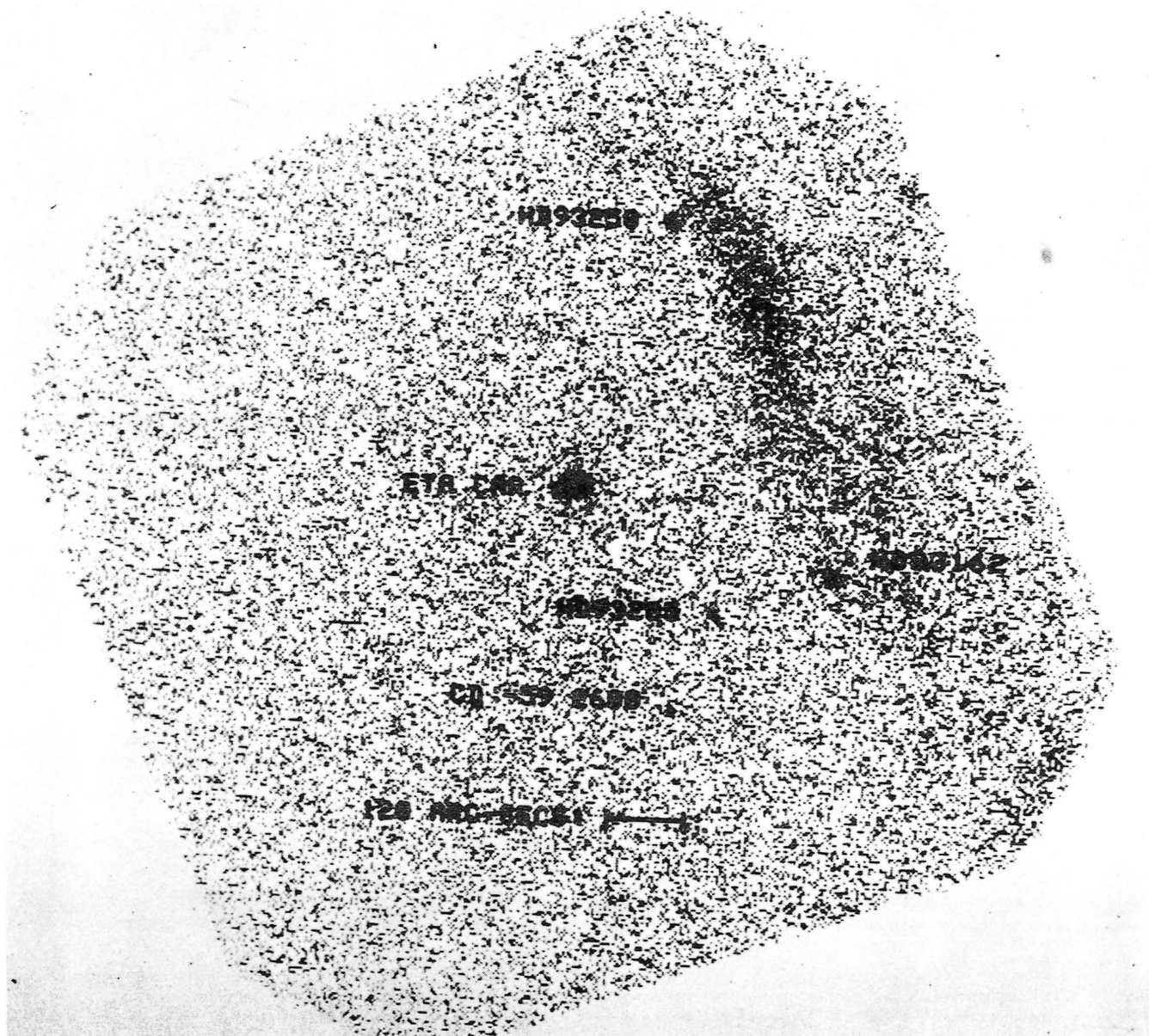


Figure 12. HRI picture of Eta Carinae Nebula. Exposure 13 000 sec.



ETA CARINAE

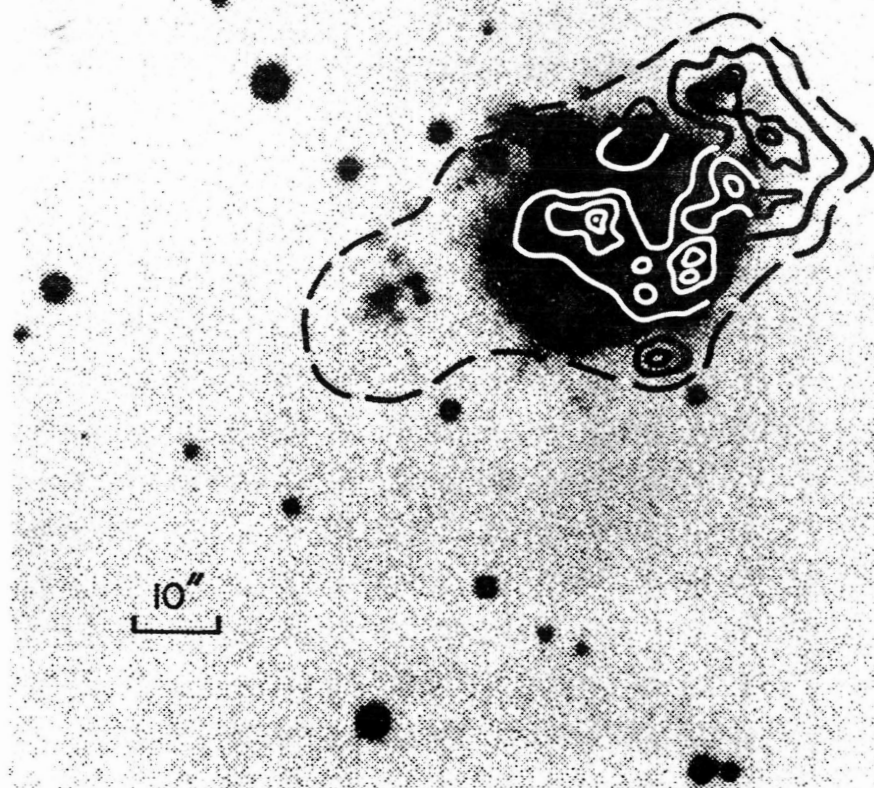


Figure 13. Contours of constant X-ray emission overlaid on an optical photograph of Eta Carinae taken from Walborn (1976).

# EINSTEIN OBSERVATIONS OF ACTIVE GALAXIES AND QUASARS

Ethan J. Schreier  
Harvard/Smithsonian Astrophysical Observatory

## INTRODUCTION

The study of active galaxies in extragalactic X-ray astronomy covers a substantial range of objects between "normal" galaxies, such as our own, and clusters of galaxies. The X-rays from normal galaxies can be considered as the summed emission from individual galactic X-ray sources, as observed in our own galaxy, described as primarily supernova remnants and binary systems containing accreting white dwarfs, neutron stars, or black holes. Clusters of galaxies may contain individual X-ray emitting galaxies, but the emission is dominated by hot intracluster gas. In between these two lies a zoo of X-ray emitting objects including radio galaxies, emission line galaxies, Seyfert galaxies, BL Lac objects and quasars. The nature of these objects, their energy generating mechanisms and their relation to each other is not fully known. However, it is likely that the bulk of the X-ray emission from them all is associated with activity in galactic nuclei. We thus look toward the X-ray observations to help us understand these objects.

The Einstein Observatory can contribute toward this study in two areas, both of which illustrate the power of an imaging observatory. First, we can resolve the comparatively nearby objects and thus obtain direct information on their detailed structure. Second, we can use the greatly increased sensitivity of an imaging instrument to detect many more of each class of object. Since many of these objects, in particular QSO's, are at cosmological distances and thus very faint despite their high intrinsic luminosity, this increase in sensitivity is essential to observing enough objects to study class properties.

This report contains examples of both these areas of study. In the first category, the radio galaxies Centaurus A and Cygnus A will be discussed. Centaurus A is comparatively closeby and has been studied in detail for some time; the Einstein observations have nevertheless revealed new aspects about its structure. Cygnus A is one of the brightest radio sources in the sky; however it is some 60 times farther away and obscured by our own galaxy and thus has been harder to study. In both these sources, a comparison of the radio and imaged X-ray flux is allowing us to measure magnetic fields. The results presented here are from work done personally with assistance from several people at CFA, in particular Rick Feigelson. In the second category, Einstein observations of quasars will be discussed. Here, we not only study details of specific QSO's, but with 1000 times the sensitivity of

previous observations, we have increased the number of known X-ray emitting QSO's from 3 to 22, and have seen QSO's at distances corresponding to an age of 15 billion years. This allows us to show that quasars contribute significantly to the X-ray background. These QSO results are from a group effort headed by Harvey Tananbaum.

## CENTAURUS A

Centaurus A, or NGC 5128, is one of the most unusual and spectacular galaxies in the sky (Fig. 1). At a distance of about 5 Mpc, it is the nearest radio galaxy, providing an excellent laboratory for investigating X-ray emission from active galactic nuclei and extended radio features.

Optically, NGC 5128 appears to be an elliptical galaxy with a dark lane through the central region, most likely a disk at large inclination to the plane of the sky. At radio wavelengths it exhibits two sets of radio lobes, giant ones extending several degrees, and smaller inner lobes several arc min to the northeast and southwest. The nucleus is a compact radio, infrared, X-ray, and gamma ray source. Its hard X-ray emission, with 2-10 keV luminosity of approximately  $1 \times 10^{42}$  erg/sec, is variable on timescales of years to hours. The light travel time thus limits the size of the hard X-ray emitting region to be  $\leq 10^{15}$  cm in size. The X-ray spectrum is strongly cut off at low energies, consistent with the source being at the nucleus.

We have used both the HRI and IPC detectors of the Einstein Observatory in a complementary fashion to study the structure of the X-ray emission in the central regions of Centaurus A. Our data show four distinct spatial components representing a variety of physical conditions and emission mechanisms:

- 1) The previously known point source at the nucleus.
- 2) A diffuse component extending approximately 2 arc min from the nucleus.
- 3) X-ray emission associated with the inner radio lobes.
- 4) A new feature or X-ray jet between the nucleus and the northeast radio lobe.

Figure 2 shows the IPC image, containing about 20 000 counts in a 3 hr exposure. Although the central component is dominant, there are asymmetries associated with the inner radio lobes. These can be displayed by suppressing the central source as shown in Figure 3. A more quantitative display of the data on Figure 4 shows that the excess flux associated with the lobes is significant at the 4-sigma level. The lobes

contain approximately 1000 counts, or 5 percent of the nuclear emission in the IPC spectral band, corresponding to an X-ray luminosity of  $10^{39}$  to  $10^{40}$  ergs/sec. This weak feature is comparable to the entire X-ray emission from a normal galaxy. The most likely model is inverse Compton scattering of highly relativistic electrons with the  $3^\circ$  microwave background. If this model is correct, comparison of the X-ray and radio fluxes allows us to measure the mean magnetic field in the lobes to be a few micro-Gauss. This is an order of magnitude lower than the equipartition field strength. However, inverse Compton scattering of less energetic electrons off starlight photons may contribute substantially to the X-ray flux, allowing greater magnetic fields. The important thing is that we are measuring a magnetic field in intergalactic space.

Figure 5 shows the HRI image of Centaurus A. The inner lobes are not apparent due to their extent and low surface brightness. However, a previously unknown feature one arc min to the northeast of the central point source is clearly seen. The new component lies much closer to the center than the inner radio lobe. The HRI also shows a diffuse component distributed isotropically about the nucleus. A plot of the radial surface brightness distribution is shown in Figure 6. There is a significant excess of counts above background, as compared to a calibration point source. The new northeast component produces the small bump at 1 arc min, and is not responsible for the isotropic, diffuse halo about the nucleus.

Figure 7 shows a contour map of the same data, along with a diagram of recently discovered optical filaments shown on the same scale. The X-ray and optical features are clearly coaligned and appear to be related to each other. Furthermore, they are aligned with the radio lobes. One can interpret the new X-ray feature either as a new lobe, which has not yet cooled and expanded enough to start emitting in the radio, or alternatively, as evidence for a jet from the central energy source. This would be consistent with the need for an energy supply from the central source to power the radio lobes.

The radio lobes require about  $10^{41}$  erg/sec to stay alight. If this energy is provided by a relativistic jet of particles from the galactic nucleus, this jet would have sufficient pressure to shock heat about  $10^6 M_\odot$  of plasma to X-ray temperatures. This would provide  $10^{39}$  to  $10^{40}$  erg/sec, about what we see. (The optical filaments could have been accelerated to their current position from the nucleus by the jet, or could have condensed out of the hotter medium by thermal instability.) Thus, the same energy source could power the inner lobes and account for the close-in X-ray/optical features. The lack of a jet to the southwest is not yet explained, although there have been suggestions of alternating production of lobes in double radio sources.

To review, the Einstein observations clearly show four components in the X-ray emission from Centaurus A. First, there is the point source, whose HRI position lies  $1 \pm 2$  arc sec of the infrared nucleus, and is clearly the highly variable source that dominates the hard X-ray band. It is comparatively weak in the Einstein observations (particularly the HRI) because of the absorption of the soft X-rays by matter surrounding the nucleus of the galaxy. Second, there is a diffuse arc min "halo" about the nucleus, which may be due to Thompson scattering of X-rays from the central source due to electrons in the surrounding gas. Such an electron scattering halo has been predicted. Third, there is X-ray emission from the inner lobes, which is allowing us to measure the magnetic field in the source. Fourth, there is an X-ray jet pointed toward the northeast radio lobe, and associated with unusual optical features. This may be a link between the central source and the radio lobes, and would thus help solve the long standing problem of how radio lobes are powered.

### CYGNUS A

Moving on to Cygnus A, we have another radio galaxy some 10 000 times more luminous than Centaurus A, but 65 times further away. It is one of the brightest radio sources, consisting of two lobes separated by about 2 arc min with a luminosity of approximately  $2 \times 10^{45}$  erg/sec, and a weak compact component centered on a cD galaxy. The galaxy itself has a luminosity of approximately  $10^{45}$  erg/sec in line emission and there is comparable emission in the IR. The galaxy looks superficially like Centaurus A, with an obscuring dust lane. However, it is located at the center of a rich cluster; X-ray emission at a level of a few Uhuru counts/sec, also close to  $10^{45}$  ergs/sec, has been seen.

Cygnus A has been well studied in the radio, being relatively nearby for a very strong source. However, its location in the galactic plane has made optical studies very difficult. The X-ray data has also been subject to various interpretations ranging from hot cluster gas to active galaxy models, although HEAO/A-3 observations reported recently by Fabbiano fairly conclusively established the existence of a small extended source of order 2 arc min.

The Einstein Observatory looked at Cygnus A shortly after launch in November 1978. The trials and tribulations of activation led to both good and bad results. Only a portion of the desired data was obtained, due to ACDS problems. However, the problems with the BOD control of the filter gave us some spectral data. Interesting features on several spatial scales have begun to resolve the remaining observational contradictions.

Figure 8 shows a 16 000 sec HRI image of the 10 arc min field centered on Cygnus A. The HRI has a resolution of several arc seconds;

the arc minute extent of Cygnus A is obvious. The formal centroid of the X-ray emission lies approximately 7 arc sec from the galaxy. This is greater than the estimated aspect error of approximately 2 arc sec, however, it is important to note that the X-ray emission is not radially symmetric. Thus, the formal centroid is not meaningful at the arc second level. It is in fact apparent from Figure 9 that the emission is more extended in the east-west direction. This may be compared with the alignment of the radio lobes which is approximately 20 degrees from the east-west line.

To study the spatial structure further, we performed azimuthal summations at various radii centered on the active galaxy (Fig. 10). Both the observed and background subtracted surface brightness distributions are shown. The 50 percent power point is at a radius of approximately 2 arc min; in fact, only one-third of the total power is seen within the 1 arc min radius which contains the radio lobes. The emission extends out to greater than 9 arc min, where the data becomes too dependent on background subtraction. This, along with the asymmetric distribution within the central arc minute, leads to the obvious working hypothesis that there are two components to the X-ray emission: one tied to the active galaxy and radio source, and the other to emission from the cluster.

Figure 11 shows a rough fit of isothermal sphere models to the data outside about 2 arc min. The core radius would appear to be about 600 to 800 kpc. The measurements allow us to estimate cluster density and mass, which are intriguingly high, but not inconsistent with a very rich cluster. Although these results are preliminary, the X-ray observations again appear to tell us about clusters even where optical data is lacking. Further IPC observations of Cygnus A are scheduled, to obtain spatially resolved spectral data on a larger spatial scale.

The MPC data was used to calibrate the HRI flux. The equivalent of approximately 3 UFU (2-6 keV) was seen, with a canonical spectral fit. The total HRI counting rate of approximately 0.16 cts/sec is consistent with this flux and spectrum.

The central structure of the X-ray source was also examined in some detail. In the central arc minute or so, a formal FWHM of approximately 35 arc sec is seen. An upper limit of approximately 1 percent is obtained for a point source at the active galaxy; this corresponds to a few times  $10^{42}$  erg/sec. If significant intrinsic absorption of a point source is present, as with Cen A, this upper limit becomes about  $1 \times 10^{43}$ . The deviations from radial symmetry are being mapped in more detail. One area of particular interest is of course emission from the radio lobes. We binned the data azimuthally in an annulus from 40 arc sec to 80 arc sec from the central galaxy. Figure 12 shows the result: an enhanced emission located to the east-southeast at the 2.5 sigma level.

This increased emission appears correlated with the E(sf) radio lobe. We then performed the same analysis on the data taken with and without the Beryllium filter which attenuates the lower energy X-rays. The apparent excess in flux is more pronounced with the filter, indicating a harder spectrum which would be characteristic of inverse Compton emission of the microwave background scattered by the relativistic electrons. If we consider the 2.5 sigma detection, the positional coincidence, and the spectral hardness as evidence of X-ray emission from the radio lobe, we can calculate the magnetic field in the lobe based on the inverse Compton model. The resultant field is within a factor of two of that predicted by equipartition. Again, we will for the first time be able to measure and compare magnetic fields in different regions of intergalactic space.

### QSO OBSERVATIONS

Leaving the comparatively nearby radio galaxies, I would like to briefly review the status of the Einstein observations of quasars, objects which are most likely at very large distances and of direct cosmological significance. It is relevant to note that prior to the launch of Einstein there were only three known X-ray emitting quasars, all nearby. With a thousandfold increase in sensitivity, we are carrying out a program of observations of known quasars with a wide variety of radio and optical properties, over a significant range of redshifts. In addition, we are discovering new quasars through optical identification of X-ray sources detected in our sky survey; three such quasars have already been identified in Einstein deep surveys.

The first QSO ever seen in X-rays was 3C273; it is not only among the most luminous quasars, but is comparatively nearby. A very deep exposure of 3C273 was taken to try to resolve any emission from the optical jet. Figure 13 is not 3C273, but for comparison and historical interest is an image of an X-ray test source from the observatory calibration here at MSFC in 1977 and shown at a software review approximately a year ago. The mirror support structure is obvious here as in Figure 14, which shows some 70 000 photons from 3C273 from an 80 000 sec exposure. Pat Henry is currently analyzing this data and so far can limit any contribution from the jet to less than 1 percent of the flux. We may eventually be able to relate the jet of 3C273 with the features just discovered in Cen A and those seen for other sources.

The IPC image obtained for the quasar B2 1225+31 at a redshift of 2.2 is shown in Figure 15. In 6000 sec of observation, a total of 296 counts were observed from a  $3.6 \times 3.6$  arc min region centered on the source. In X-rays, the quasar stands out clearly; in visible light there are at least 200 objects as bright as the 16th magnitude quasar in the same area of sky, requiring detailed spectral observations to pick out the quasar. We have now observed two known quasars even further

away, at a redshift of 3.1 (a redshift 3.1 corresponds to an age of about 15 billion years). Figure 16 is a 10 000 sec exposure for the 20th magnitude quasar 0537-286 which emits more than  $10^{47}$  erg/sec<sup>-1</sup> in the 0.5 to 4.5 keV band. Again we readily detected the quasar. Other objects detected in the field include a 5.3<sup>m</sup> F2 and a 7.2<sup>m</sup> F5 star, as well as 3 or 4 other sources whose optical counterparts are fainter than 15<sup>m</sup> and which are probably extragalactic.

Our observations of two bright quasars at redshifts of 3.1 indicate that we can expect to detect still more distant quasars. In the next few months we will be observing 15 of the most distant known quasars with redshifts from 3 to 3.5. An interesting question is whether still more distant quasars exist; none have yet been observed in the visual. Since the quasars were probably the first objects to condense out of the expanding big bang gas, the time at which they first formed is a most intriguing issue. Either the optical observations to date have been limited by instrumental effects as many have suggested, or the quasars only formed at the epoch given by redshift 3.5. Since our X-ray deep surveys are capable of detecting and locating sources much weaker than these, and hence, possibly much more distant than we have discussed, we should be capable of detecting these more distant quasars if they exist at all.

A second important question about the quasars concerns the nature of the underlying energy mechanism capable of producing luminosities up to  $10^{47}$  ergs/sec<sup>-1</sup>. The X-ray observations may be able to provide insight into this question. Figure 17 shows time variability of 3C273: approximately 10 percent in less than a day. Figure 18 shows our observations of the quasar OX169, which is a weak X-ray source, but nonetheless, easily detected by Einstein. The slide shows the data we obtained for six orbits of HRI observations. The decrease from 6.5 counts/1000 sec to 2.0 counts/1000 sec is not consistent with a constant source. The probability of such an occurrence is less than  $10^{-4}$  for a constant intensity. The observed intensity variation in  $\leq 100$  min corresponds to a nominal decrease in luminosity from 2.0 to  $0.6 \times 10^{44}$  ergs/sec<sup>-1</sup>, although the exact size of the decrease is not known precisely.

Observations of time variability, such as we show for OX169, may be a signature of the ultimate energy source in the quasars. For a process involving conversion of a mass into energy, rapid variations in a powerful emitter require a high conversion efficiency, supporting models involving release of gravitational energy through accretion onto a compact object. If one assumes that the X-ray emission is powered by accretion onto a massive black hole, the observed luminosity and time scale for variability can be used to estimate the mass of the black hole. A minimum central mass is required to produce a given luminosity. On the other hand, the time scale for variability sets a maximum size for the



emitting region. Our observations of OX169 would require a black hole of between 1 and 100 million solar masses based on scattering models with gas temperature  $\geq 10^9$  K. Observations such as these show the importance, and perhaps the unique role, of the X-rays as a probe of the central energy source. The short time scales indicate that the X-rays are produced very close to the central source, and may therefore provide the means for ultimately understanding the quasars and active galaxies in general.

Figure 19 summarizes some of our observations of quasars. We have plotted the observed 0.5 to 4.5 keV X-ray luminosity, as well as a few upper limits, for the individual sources as a function of redshift. The three nearby quasars known prior to the launch of Einstein are shown, as are the Einstein observations for more than 20 quasars now extending to a redshift of 3.1. The luminosities range from  $10^{44}$  erg/sec<sup>-1</sup> to  $10^{47}$  erg/sec<sup>-1</sup> with no obvious dependence of luminosity on redshift. The absence of low luminosity, high redshift quasars is primarily a measure of the instrument sensitivity limit for a several thousand second observation.

Our observations to date clearly do not satisfy the statistical requirements for a complete sample; for example, they are strongly biased towards radio quasars. Thus, we cannot yet formulate an X-ray luminosity function to be studied on its own or to be used in estimating the contribution of the quasars to the diffuse X-ray background. Eventually through the Einstein Observatory surveys and follow-up optical identifications, we should be able to generate an unbiased, complete sample of X-ray emitting quasars.

In the meantime, we can use the optical luminosity function for quasars plus a tentative relationship between the optical and X-ray fluxes in order to estimate the possible contribution of the quasars to the X-ray background.

Figure 20 shows the local optical luminosity function that different observers have obtained. I show this mainly to point out that the Seyfert galaxies merge with quasars near an equivalent X-ray luminosity of  $10^{44}$  ergs/sec<sup>-1</sup> which suggests a possible link between these two types of active galaxies. Using rough estimates of evolution, etc., we have estimated the contribution of quasars to the X-ray background. The rough calculation actually predicts an X-ray background 2.5 times the observed "extragalactic" background at 2 keV. The disagreement suggests that one of several hypotheses used is wrong. This problem will be helped by further data and analysis, but it is already clear that the presence of the diffuse X-ray background (and the gamma ray background as well) can provide significant constraints on the quasar numbers, particularly as we accumulate more data on the individual source luminosities. Going the other way, it is also clear that the QSO's contribute significantly to the X-ray background.

In a related context, there have been suggestions that quasar redshifts are noncosmological or local. A local interpretation of the redshifts would however require many more faint quasars. This in turn would require a large optical to X-ray slope if the X-ray background were not to be exceeded, in contradiction with what we observe, strongly suggesting that QSO's are indeed at great distances.

A wide range of cosmological questions can be approached by means of observations and analyses such as the ones described. Time variability measurements as discussed may give unique insights into the basic energy generating mechanism. Studies of the spatial structure of the nearer active galaxies should also contribute, as will the class property studies which may allow better comparison between the various types of galaxies. The Einstein Observatory is adding a qualitatively new dimension to this extragalactic research.

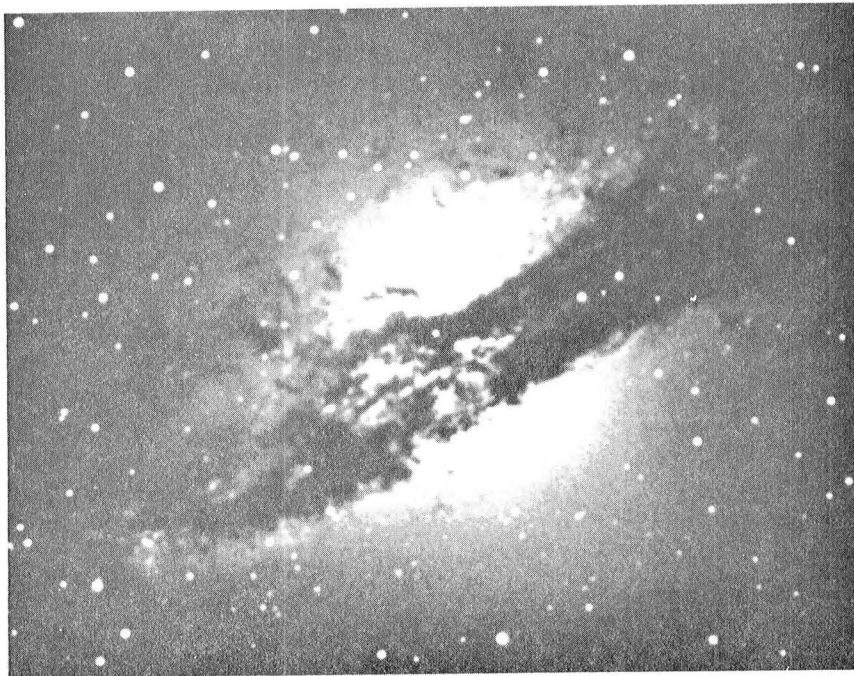


Figure 1

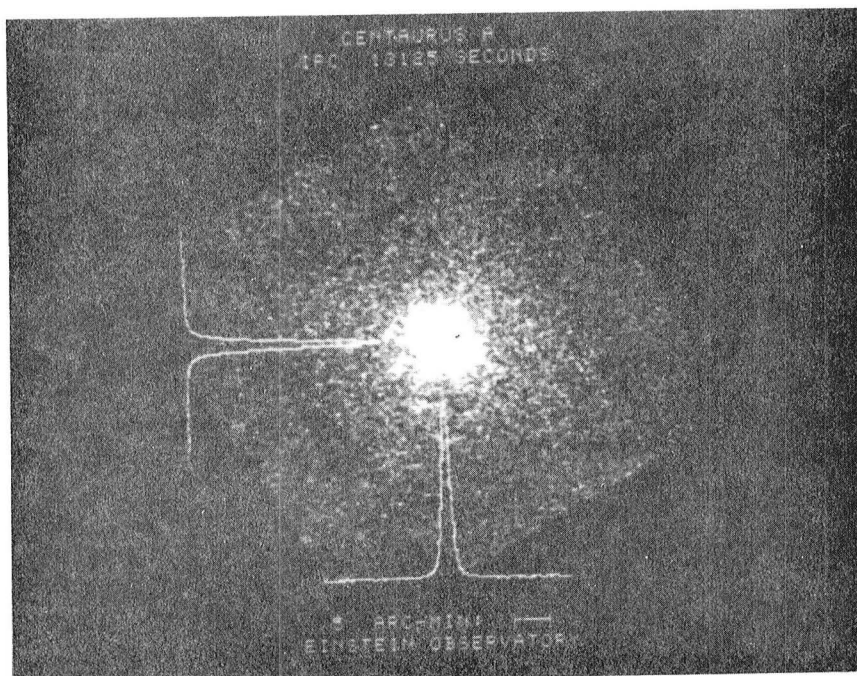


Figure 2

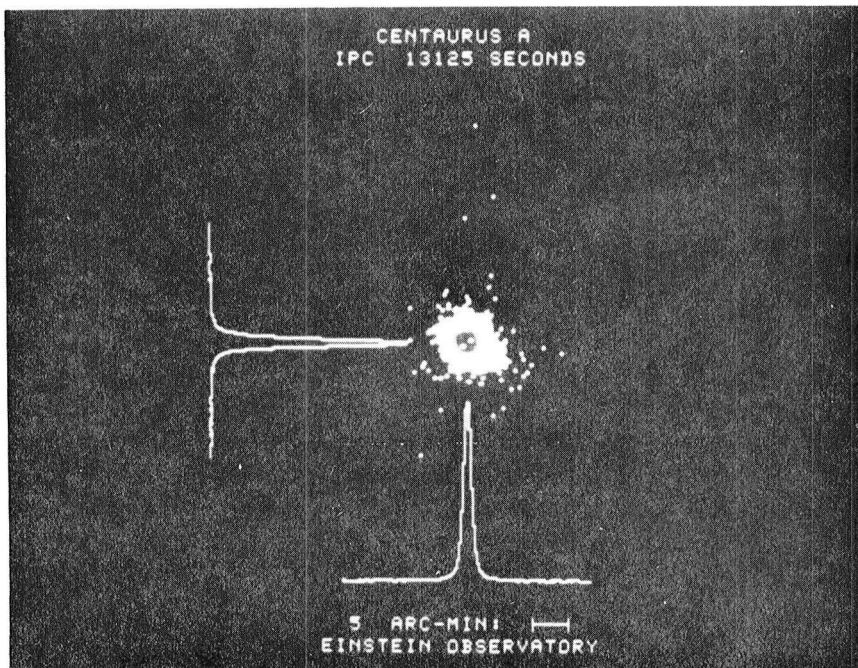


Figure 3

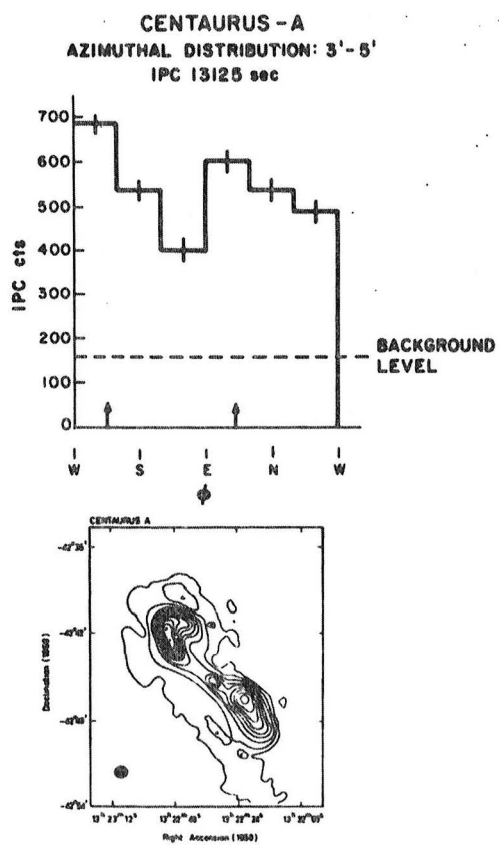


Figure 4

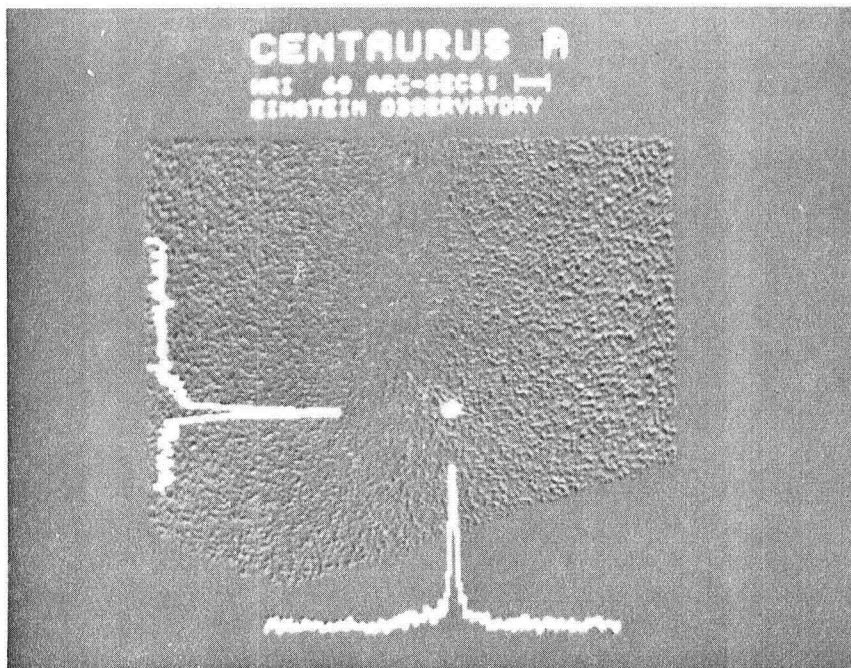


Figure 5

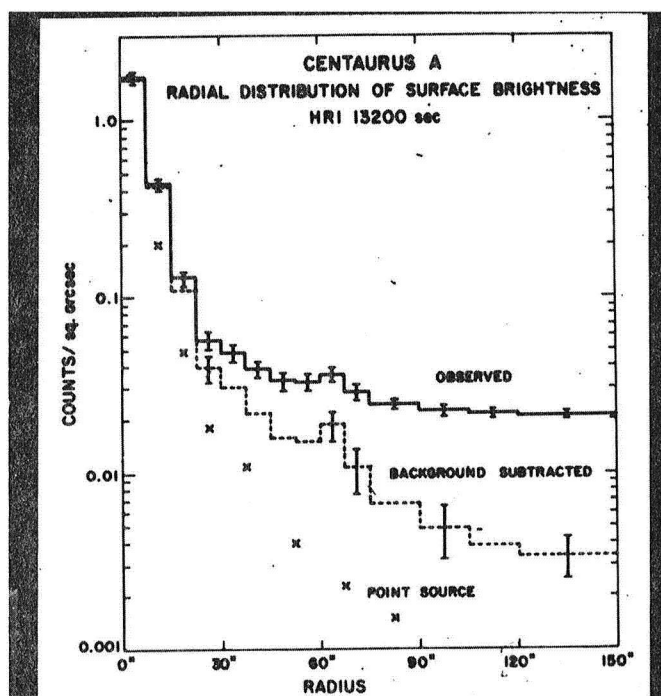


Figure 6

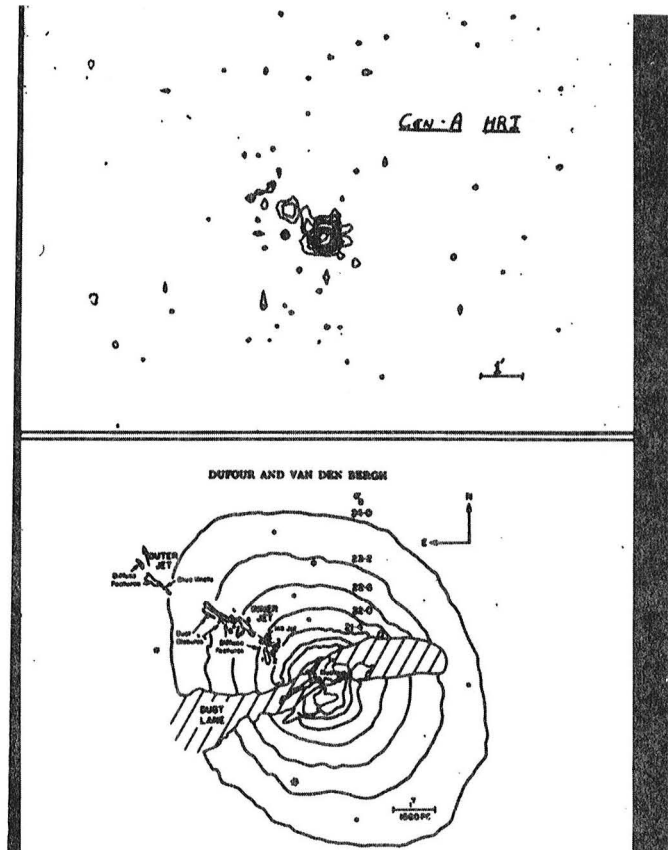


Figure 7

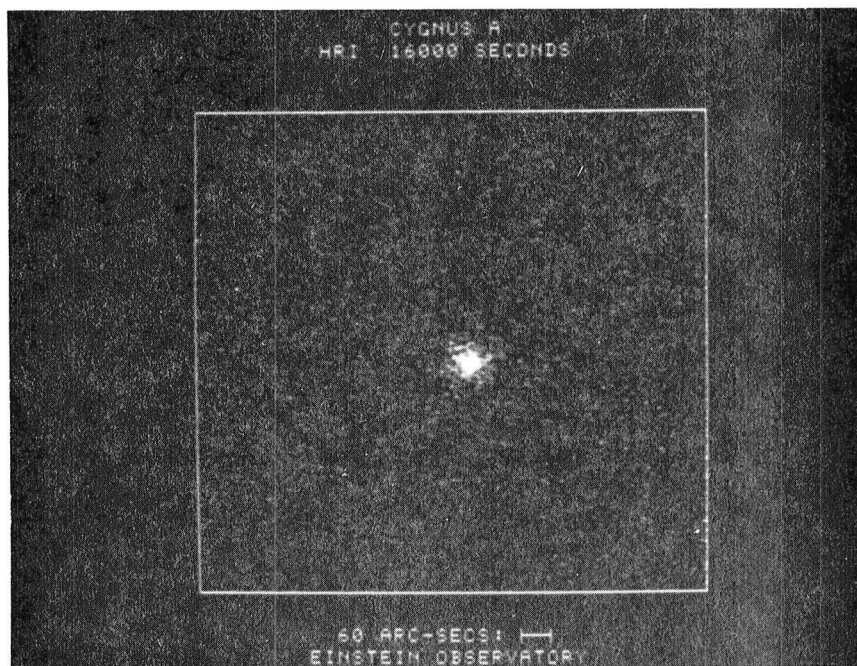


Figure 8

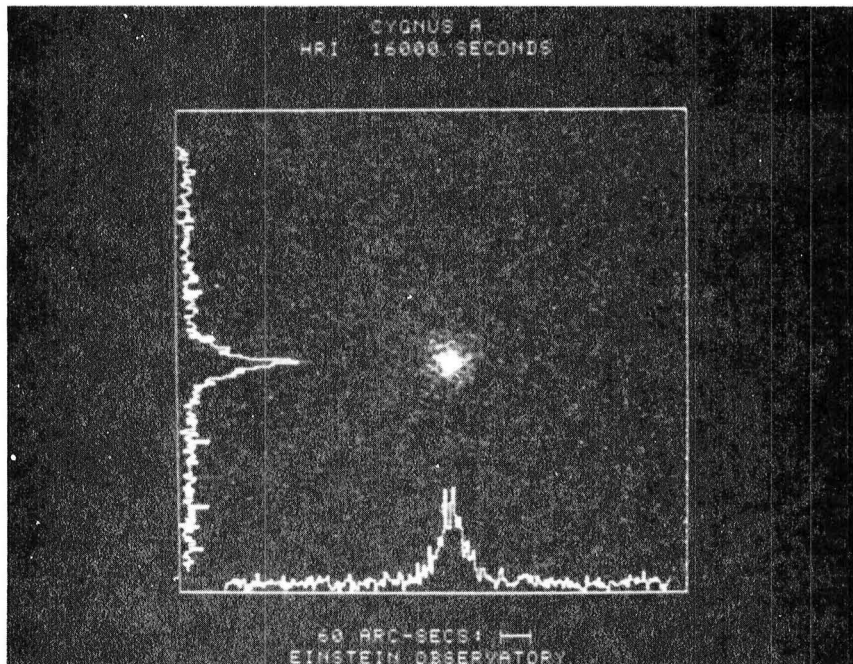


Figure 9

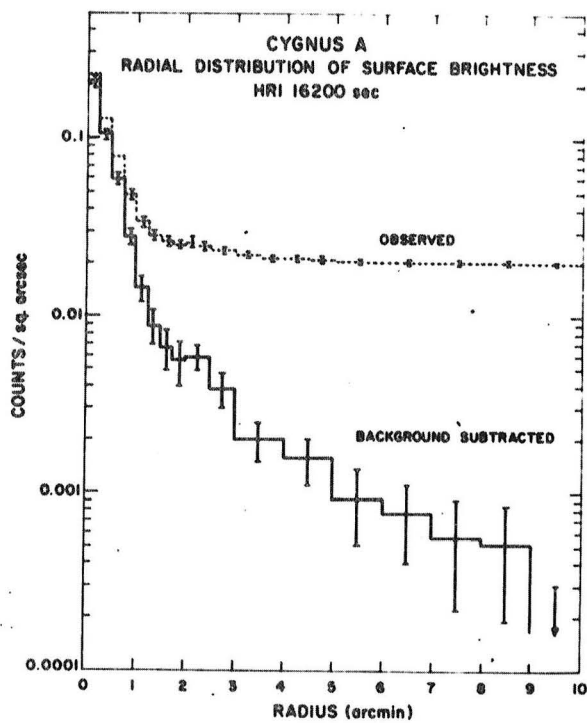


Figure 10

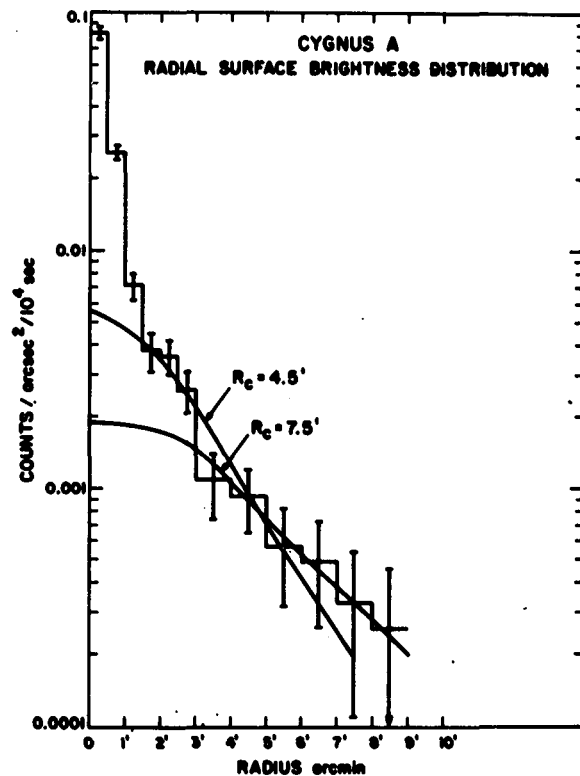


Figure 11

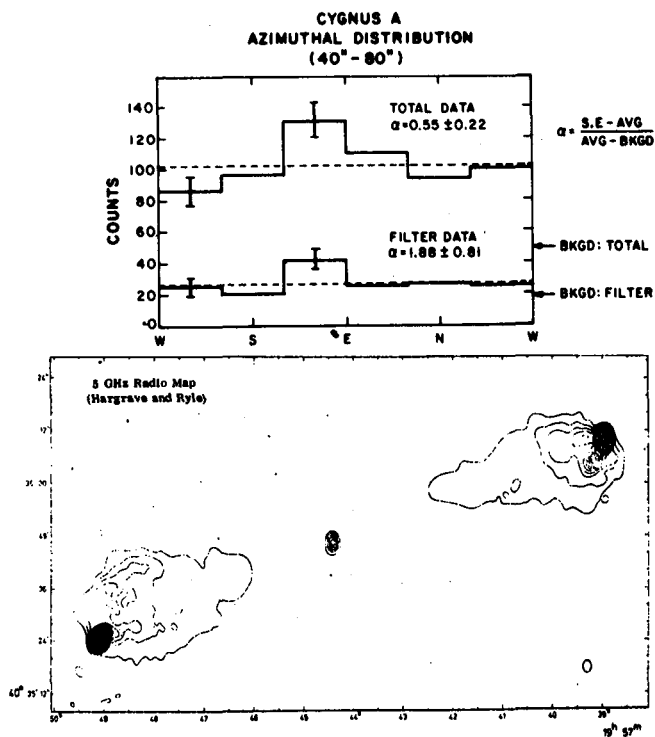


Figure 12



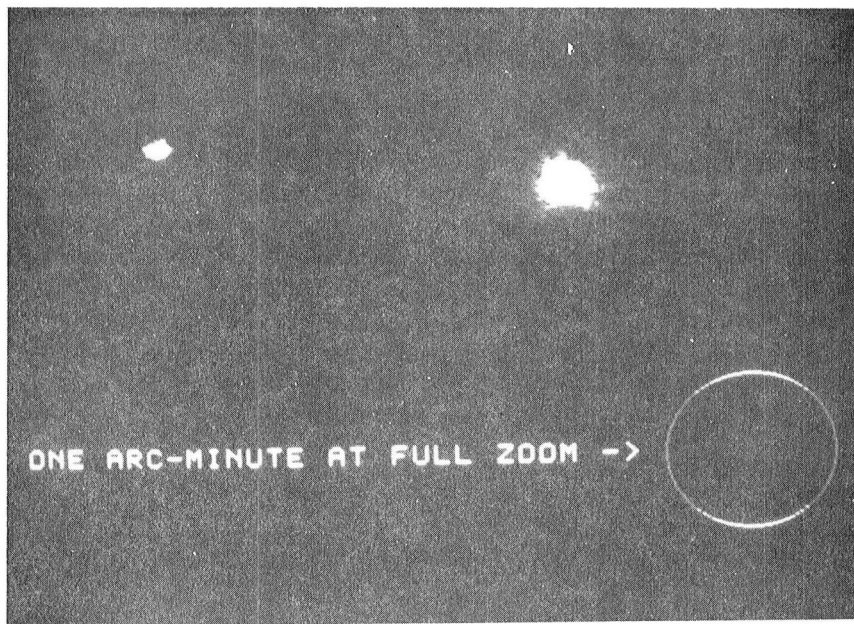


Figure 13

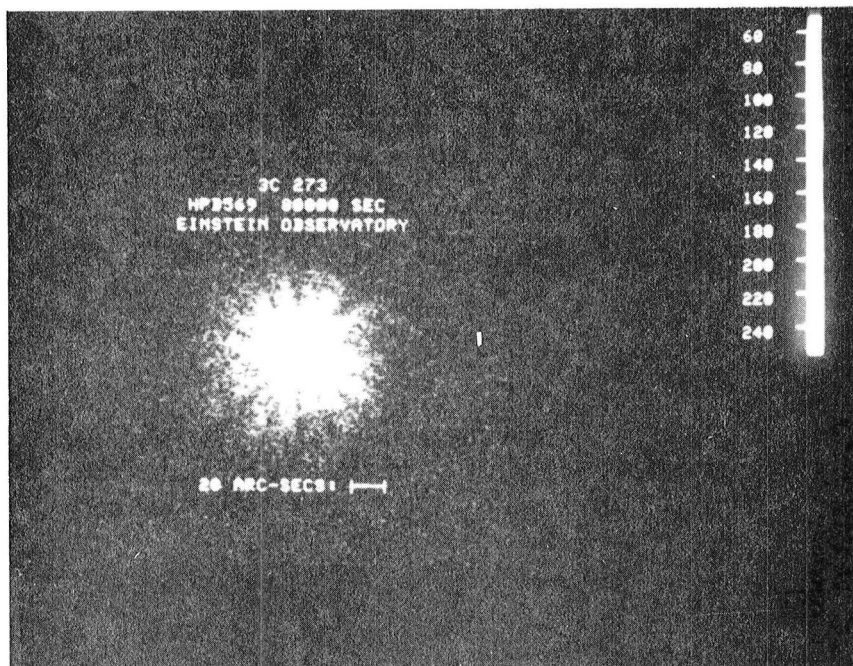


Figure 14

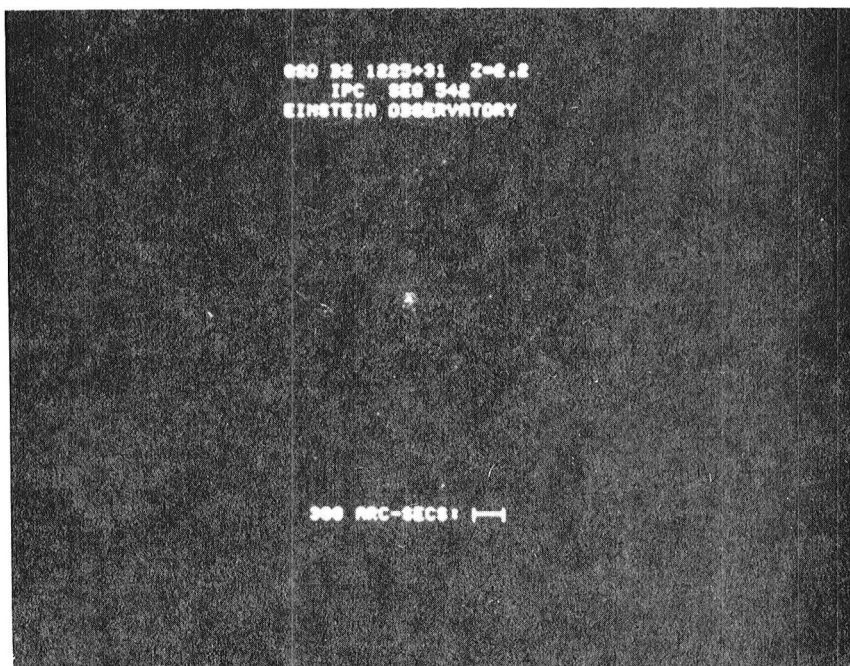


Figure 15

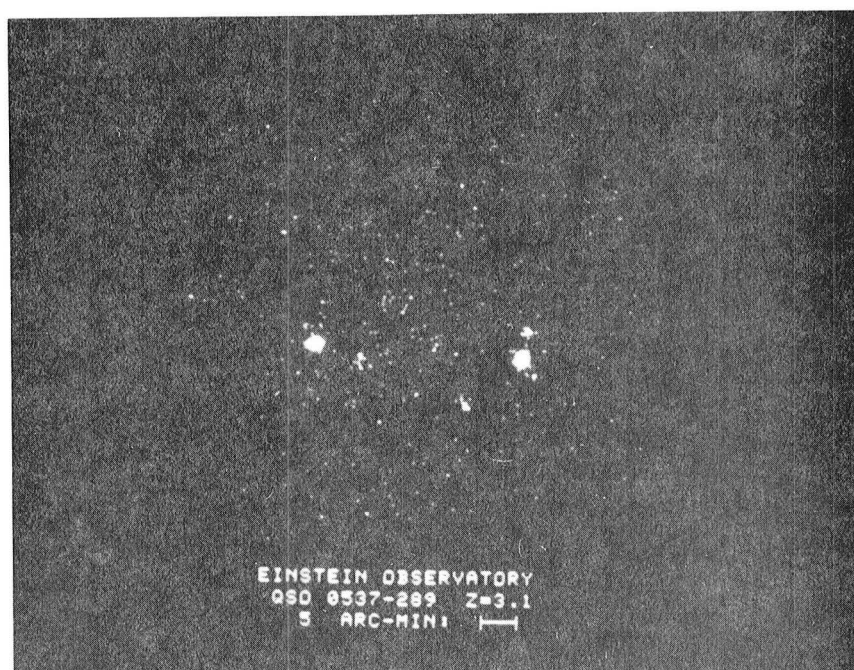


Figure 16

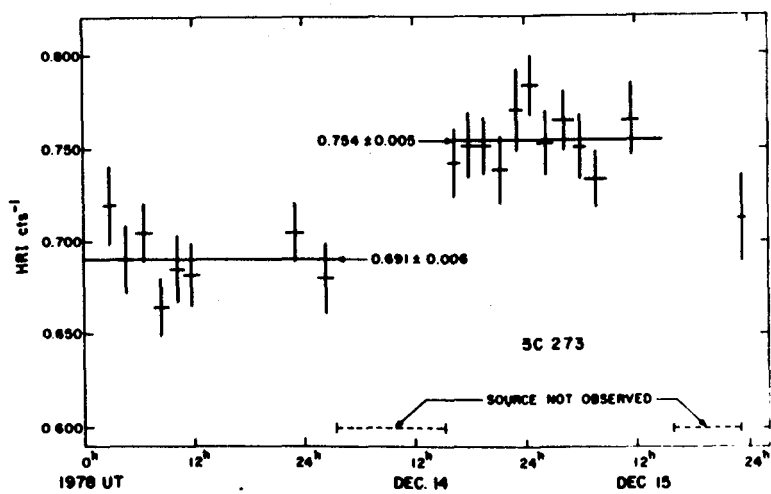


Figure 17

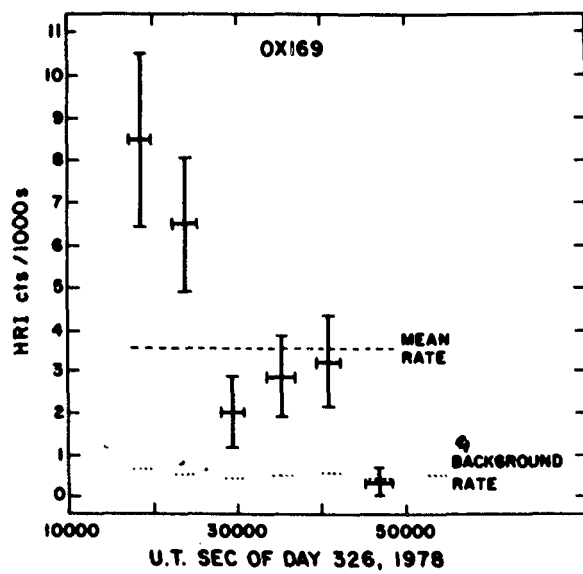


Figure 18

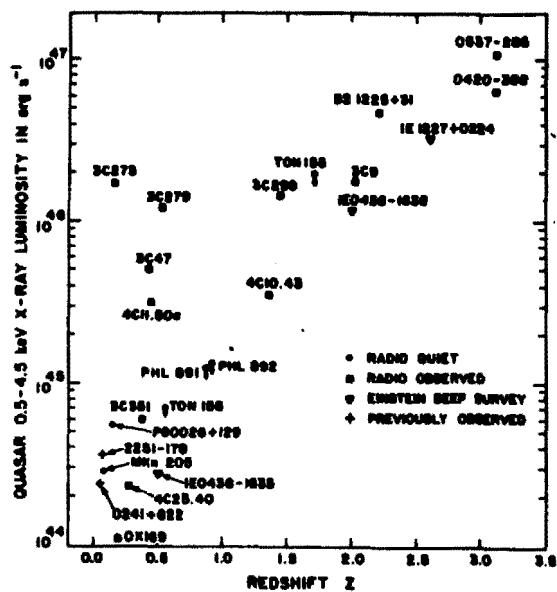


Figure 19

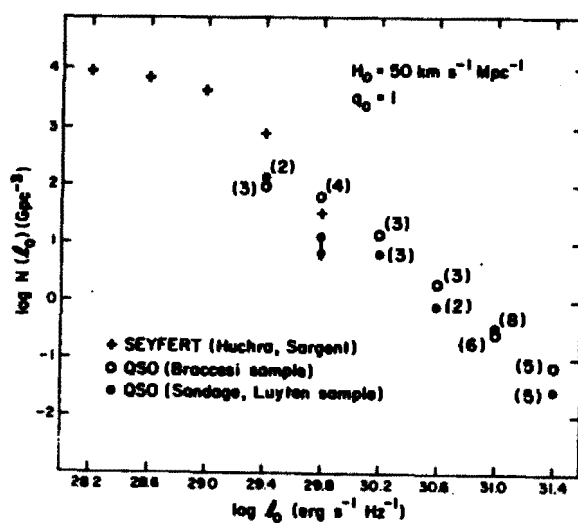


Figure 20

# THE STRUCTURE AND EVOLUTION OF X-RAY CLUSTERS OF GALAXIES

C. Jones

Harvard/Smithsonian Astrophysical Observatory

Rich clusters are the largest, well-studied aggregates of matter in the universe. It is a basic observational fact that the distribution of galaxies on the sky shows a high degree of clumpiness (Fig. 1). A cluster is essentially an enhancement in the density of galaxies projected on the sky. Abell (1958), who has done much of the basic work of systemizing the concept of cluster, includes in his catalog clusters that have at least 50 galaxies in a particular magnitude range and 3 Mpc radius of the cluster center. For richer clusters, there may be more than several hundred galaxies within this radius. Several schemes have been suggested to classify clusters with different morphology. The cluster in Figure 1 is the Coma cluster (138 Mpc) and is a so-called "binary" system dominated by a pair of giant galaxies.

One of the main types of clusters that figures prominently in the realm of X-ray clusters is called a cD cluster. These clusters are dominated by a single giant of cD type galaxy. cD's are the largest galaxies known and have the core of a giant elliptical galaxy and an extended envelope of low surface brightness. Ostriker and his co-workers have suggested that these galaxies are formed by a process in which massive galaxies in a dense cluster core lose energy by dynamical friction as they move towards equipartition with less massive galaxies; consequently, they spiral in towards the center of the cluster's potential well. There, the cD's grow by cannibalizing other galaxies whose envelopes approach nearby. This theory predicts that cD galaxies will be found at or near the cluster center. The Einstein X-ray observations, can be used to determine the cluster center and can even improve on galaxy counts as a means of determining the center. We therefore can compare the X-ray center and the position of the cD galaxy.

Figure 2 gives an example of a cluster that has quite a different central structure from both Coma and cD clusters. This is the Perseus cluster (at a distance of 110 Mpc), in which several bright galaxies are spread out along a line.

Figure 3 shows a result for the Perseus cluster produced by Forman and colleagues from the first X-ray satellite, Uhuru. Indicated are the contours of an extended radio source associated with the cluster, tailed radio sources around galaxies, as well as the error ellipse and extent for the X-ray source. Observations of this type showed for the first time that X-ray emission from clusters originates in a diffuse region (radius  $\sim 15$  arc min) rather than a point-like source. This

ability to distinguish between a point and an extended source was about the limit of the Uhuru, SAS, and HEAO-1 satellites, and then that analysis was only possible for very bright, nearby clusters. However, now the era of imaging allows one to study the detailed structure of clusters.

Let's begin with Einstein imaging observations of the nearby Virgo cluster which is being studied by Forman and colleagues. These observations were made with the Imaging Proportional Counter (IPC) at the focus of the Einstein X-ray Observatory. The observations cover the energy range from approximately 0.5 to 3.0 keV, and have a spatial resolution of about 2 arc min. Figure 4 shows one of the fields in the Virgo cluster. There are five sources in this one square degree field. All but the bottom one are associated with galaxies. From this figure it is apparent that one source is extended. Also there is more emission on the left edge than on the bottom edge. This diffuse emission is associated with the giant elliptical galaxy M87. Fabricant and co-workers are analyzing the imaging observations of M87 and can trace this extended emission out to more than a degree from the galaxy.

Figure 5 shows the contour plot of this field superposed on a Kitt Peak 4-meter photograph. The X-ray emission is clearly associated with the galaxies. Their luminosities range from a few times  $10^{40}$  ergs/sec to a few times  $10^{41}$  ergs/sec for M86. The total emission from our galaxy or Andromeda is a few times  $10^{39}$  ergs/sec. The emission from M86 appears diffuse and extended by as much as 10 arc min. Its isothermal core radius corresponds to 20 kpc.

This is an interesting group of galaxies. M84 contains a 3C radio source. The galaxy NGC 4388 is an ARP object and appears tidally disrupted by its companion. The other spiral (NGC 4438) was observed by W. Liller with the Z-machine at Mt. Hopkins and found to be an emission line galaxy. Based on optical and radio information, one might have concluded that M86 was the least unusual. However, these X-ray observations show that M86 is also worthy of study.

The discovery of diffuse X-ray emission from clusters and the realization, primarily from the discovery of iron emission by Midell and Serlemitsos and their colleagues, that most of the observed emission was due to thermal bremsstrahlung, brought about the question of the origin of the hot gas. Two basic types of models involved either the infall of primordial gas into the cluster from the intergalactic medium (Gunn and Gott 1972) or the injection (or stripping) of evolved gas in galaxies to form the intracluster medium (Yahil and Ostriker 1973, and Cowie and Binney 1977). The iron emission lines indicated that roughly solar abundances of iron were present and provided support for the models in which the X-ray cluster emission is produced by gas which has been processed in stars and then subsequently lost to the intracluster region.

Earlier observations have presented a picture of the Virgo cluster X-ray emission consisting of two components — a cool 2 keV gas contained by the gravitational potential of M87, and a hotter ( $\sim 10$  keV) gas of lower density contained by the gravitational potential of the entire cluster. The hot material must have a low density ( $\sim 10^{-4}$  cm $^{-3}$ ) to account for its low surface brightness. This hot gas could be either primordial, or a result of injection since we have no detailed positional and spectral information which would determine its abundances and thereby its origin.

The Einstein observations have added to this picture and show that cool gas surrounds several of the Virgo galaxies. Embedded in such a system, the gas surrounding M86 originated within M86 itself, rather than from infall of intracluster gas, since the hot intracluster gas could not cool sufficiently rapidly. Second, our preliminary spectral analysis of the emission implies that the gas around M86 is similar to that associated with M87 and has a cool temperature of  $\sim 1$  keV, and that it contains line emission and is therefore evolved. Although most of these galaxies have unusual optical or radio properties which may account for their X-ray emission, another possibility is that all these galaxies like M87 and M86 are gravitationally binding some of the cool gas.

The Virgo cluster phenomenon of gas associated with galaxies is not unique. We have studied several nearby rich clusters of galaxies with the Einstein Observatory IPC. These observations have shown that clusters display a variety of structures in their X-ray surface brightness distributions. We will discuss our observations in terms of the theoretical models for dynamic evolution in clusters. We have selected A85 and A1367 to discuss since they are representative of the types of clusters which have been observed.

Figure 6 shows the IPC observation of A1367. The cluster fills much of the IPC image. We have projected the flux onto each axis to illustrate the broad, extended cluster profile. From this picture it is also apparent that the cluster emission is elongated. At one end of the cluster is the radio galaxy 3C 264 whose X-ray emission is seen above that of the cluster, although its luminosity is only a few percent that of the cluster's.

Figure 7 shows a contour plot of the X-ray emission in A1367 superposed on an enlargement from the Palomar Sky Survey. The bright source at the bottom is 3C 264 whose 0.25 to 3.0 keV luminosity is a few ( $2$ ) times  $10^{42}$  ergs/sec. The strong radio emission in this galaxy suggests unusual activity and, therefore, a higher X-ray luminosity than for other cluster members. Several other galaxies can be associated with regions of enhanced X-ray emission. The two galaxies, NGC 3842 and NGC 3841, have X-ray luminosities of several ( $3.5$  and  $5.5$ ) times  $10^{42}$  ergs/sec. These luminosities are about 100 times greater than the X-ray luminosity of our galaxy or Andromeda, but comparable to the luminosity of M86 in the Virgo cluster.

This contour plot shows that the X-ray emission is highly clumped. Although some of the X-ray fluctuations correspond to bright galaxies, others do not. Given a relation between the mass of a galaxy and the associated X-ray emission, the enhancements which do not correlate with bright galaxy may indicate the presence of previously undetected mass in the cluster.

Figure 8 shows the IPC observation of A85 for which we have again shown the image projected onto each axis. Unlike the broad surface brightness profile for A1367, for A85 the emission is sharply peaked.

Figure 9 shows the contour plot for A85 on the Palomar print. The peaked of the emission coincides with the giant cD galaxy. The X-ray emission of this cluster is concentrated toward the cluster center and does not show the clumping that was so apparent for A1367.

Of the clusters which we have studied with the Einstein observatory, several have shown broad, highly clumped X-ray emission, while for others the emission is smooth, and centrally peaked.

Although time does not permit a detailed discussion of each cluster, we can use the broad versus peaked features of the surface brightness distribution to characterize the cluster. Figure 10 shows the radial distribution of the X-rays for several clusters. The angular dimensions have been converted to linear size with the axis ending at 1 Mpc. We have also normalized the clusters to the same peak central intensities to illustrate their different extents. For these clusters, which all contain cD galaxies, the emission is centrally peaked while for the others, the emission is broader. Contour plots of these extended clusters also show that the emission often is clumped although for a few clusters with extended profiles, the emission is smooth.

These observations can be compared with the models for dynamic evolution in clusters. Through numerical simulations, Peebles, Aarseth and White have shown that a cluster which begins as a large cloud of galaxies will collapse and often subcluster and finally reach equilibrium with an extended halo around a dense core. The broad, highly clumped clusters could be interpreted as clusters in their early evolutionary stages in which the gas escaping the galaxies is bound more by the gravitational potential of the individual galaxies than by the relatively weak potential field of the cluster. We can use the cluster velocity dispersion as a measure of the cluster potential. Clusters with low velocity dispersion would have weak cluster potentials and the potentials of individual galaxies would cause substantial deviation from a smooth surface brightness distribution. The Virgo cluster and the bright galaxy group in A1367 have low velocity dispersions — less than half the value measured for Perseus (Noon 1973, Tifft and Tarenghi 1973).



Both clusters show substantial clumping of the X-ray luminosity around galaxies. Clusters in this early stage would be expected to have a lower density of hot intracluster gas and, therefore, a higher fraction of spirals than in more evolved clusters in which the ram pressure of the gas would strip the galaxies of their interstellar matter (Gunn and Gott 1972, Gisler 1976) thereby transforming spirals into SO's. Bahcall (1978) has determined the percentage of spirals in A1367 to be 40 percent which is considerably higher than the  $\sim 10$  percent spirals she found in Coma and Perseus.

During the second phase of cluster evolution, a high density core or subcluster is formed, thereby enhancing the chances for building a cD galaxy at the cluster center. The clusters in our rather limited sample which show strongly peaked X-ray radiation are all Bautz-Morgan type I clusters. These cD clusters have greater central surface brightnesses than do the less evolved clusters. This increased surface brightness is probably due to the increased gas density at the cluster center as the gas becomes bound by the cluster potential.

In the final stage of cluster evolution, the cluster has reached equilibrium. For this phase, we would expect the X-ray emission to follow the cluster potential as traced by the galaxies. Since the gas distribution is dominated by the cluster potential, it should be smooth. Also, the percentage of spiral galaxies should remain small. Coma and the cD clusters are possible examples of clusters in this final stage. We have found that the gas distribution in the cD clusters is quite smooth. The surface brightness distribution of Coma and other evolved clusters such as A2256 is also smooth, although not as centrally peaked as the cD clusters.

In summary, we have found from the first observations of the structure of clusters with the Einstein Observatory that the nature of the X-ray emission is complex and varies from broad and highly clumped, to smooth and centrally peaked. The clusters whose emission is clumped tend to be rich in spirals and to have X-ray temperatures in the few kilovolt range and low velocity dispersions. The smooth, centrally peaked clusters are spiral poor, and have higher temperatures and larger velocity dispersions. For many of the clusters, the emission is irregular and cannot be described by the simple, spherically symmetric models for a hot isothermal or adiabatic cluster gas. For these clusters, the low density, intracluster gas is strongly influenced by the potential of individual bright galaxies.

The observed X-ray structure combined with optical properties such as the spiral fraction and central density complement the theoretical model for dynamic evolution in clusters.

Many of the X-ray properties of clusters, including their structure and luminosity appear to be strongly influenced by their dynamical evolution. However, since clusters do not all evolve at the same rate due to differences in cluster properties such as richness, we are able to observe clusters at the same epoch but in a variety of evolutionary phases.

We were surprised by the complexity and variety in the surface brightness of nearby clusters. This great variety complicated the search for evolutionary changes with distance. Figure 11 shows the IPC image of 3C 295 which is one of the distant clusters studied by Pat Henry and co-workers. This cluster has a redshift of 0.46 and is one of the several distant clusters observed with Einstein. Optical observations of this cluster showed that although there was a dominant galaxy, and therefore the cluster should be evolved, about half the galaxies were spirals which is larger than would be expected in a centrally condensed cluster. One possible explanation for the high spiral percentage had been that there was no intergalactic medium to strip the spirals of their gas and thus, convert them to SO's. However, the observation of extended X-ray emission from this cluster rules out that possibility. Another possibility which is consistent with the observation is that in this distant cluster with its young galaxies, the rate of gas injection from stars is high. This high rate could slow the stripping process and cause spirals to remain spirals longer.

Thus, to summarize the Einstein observations of clusters it appears, somewhat ironically, that we are learning about the evolution of young galaxies in distant clusters and about the evolution of clusters from our observations of nearby clusters.

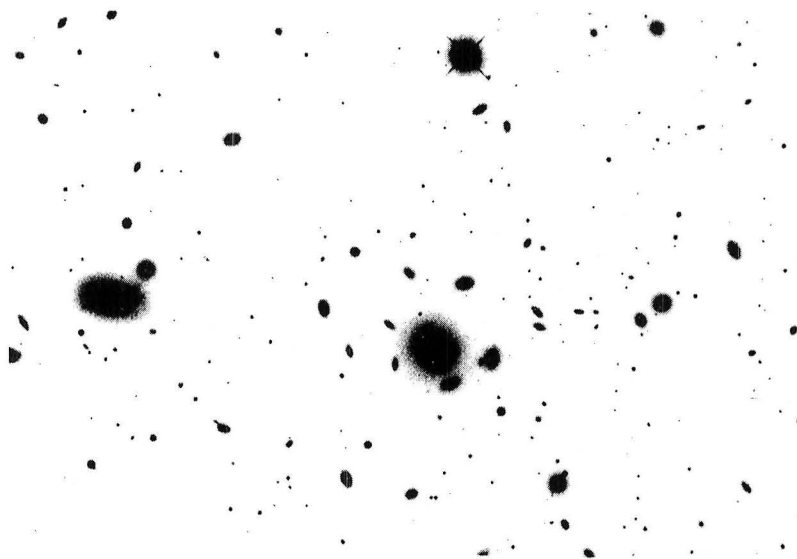


Figure 1

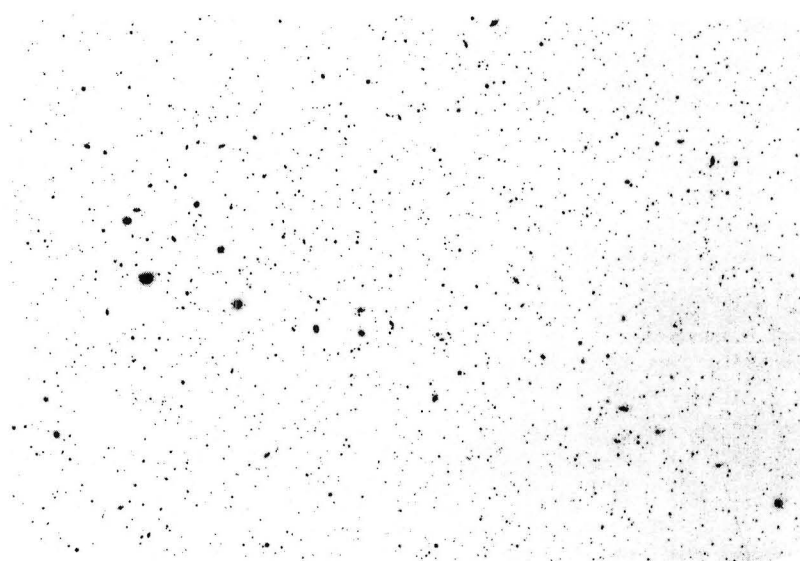


Figure 2

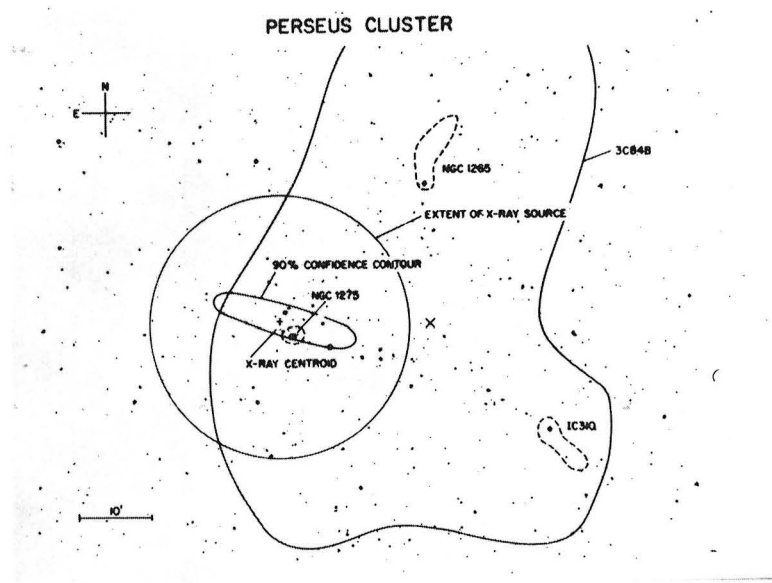


Figure 3

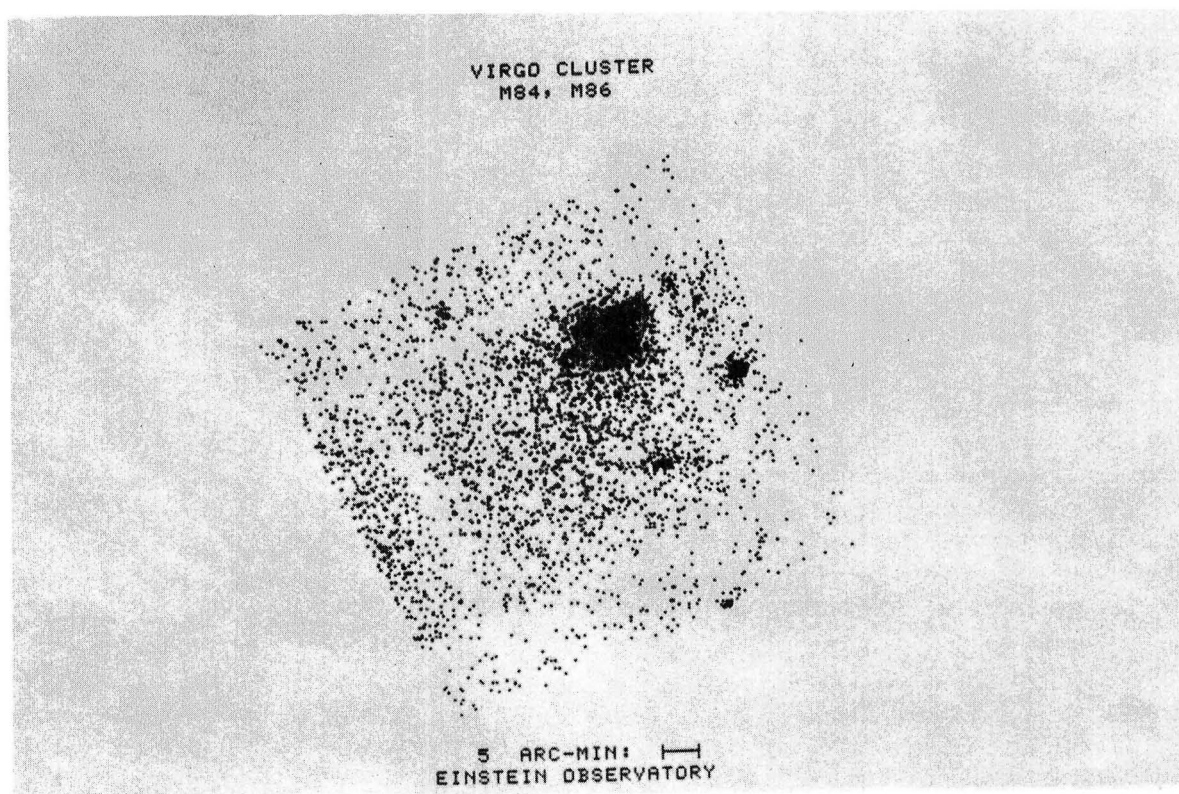


Figure 4



Figure 5

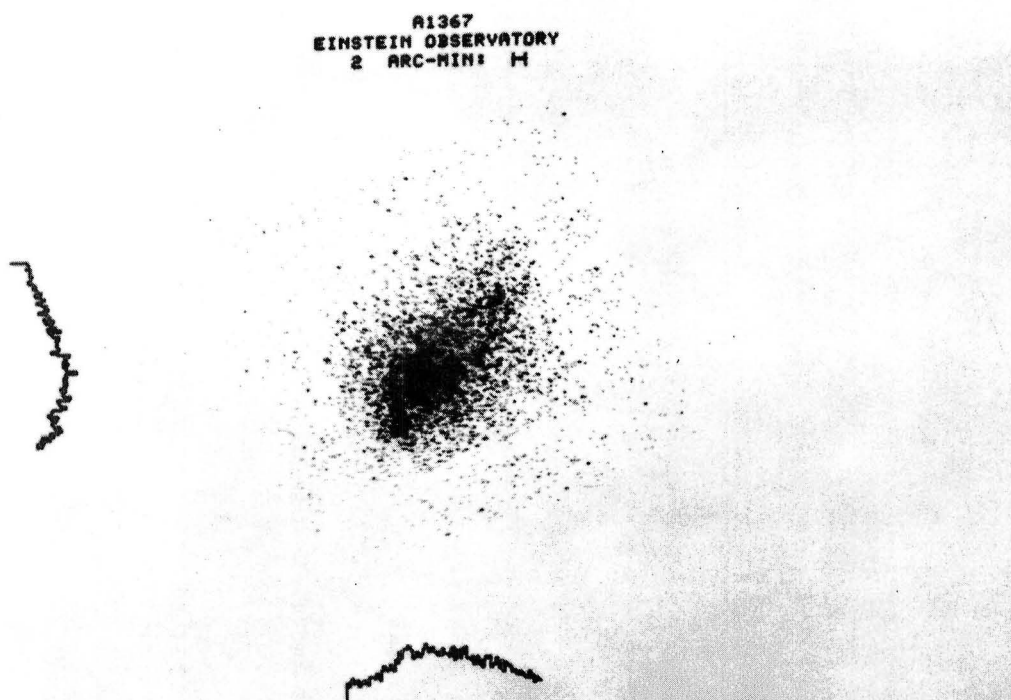


Figure 6

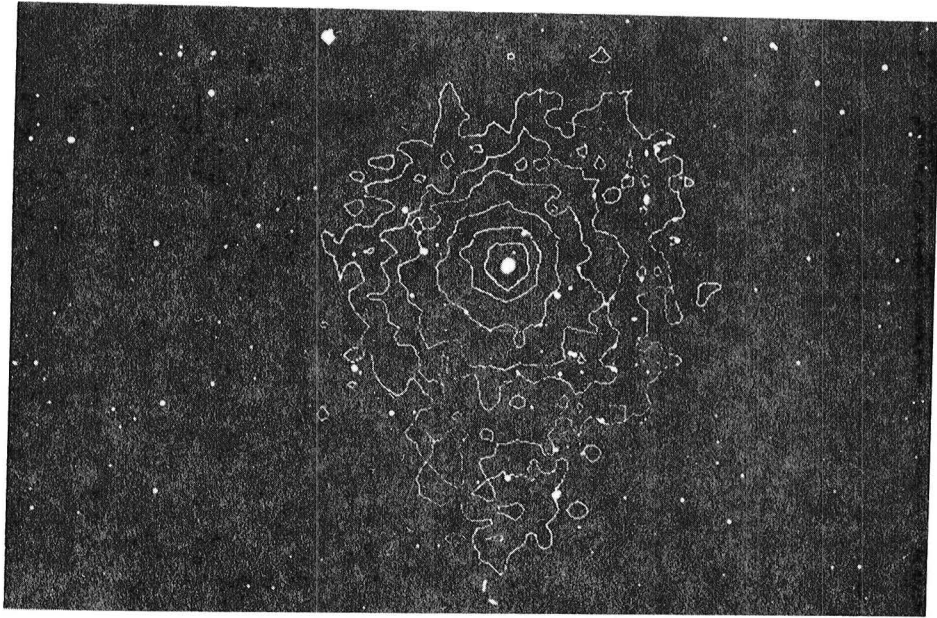


Figure 7

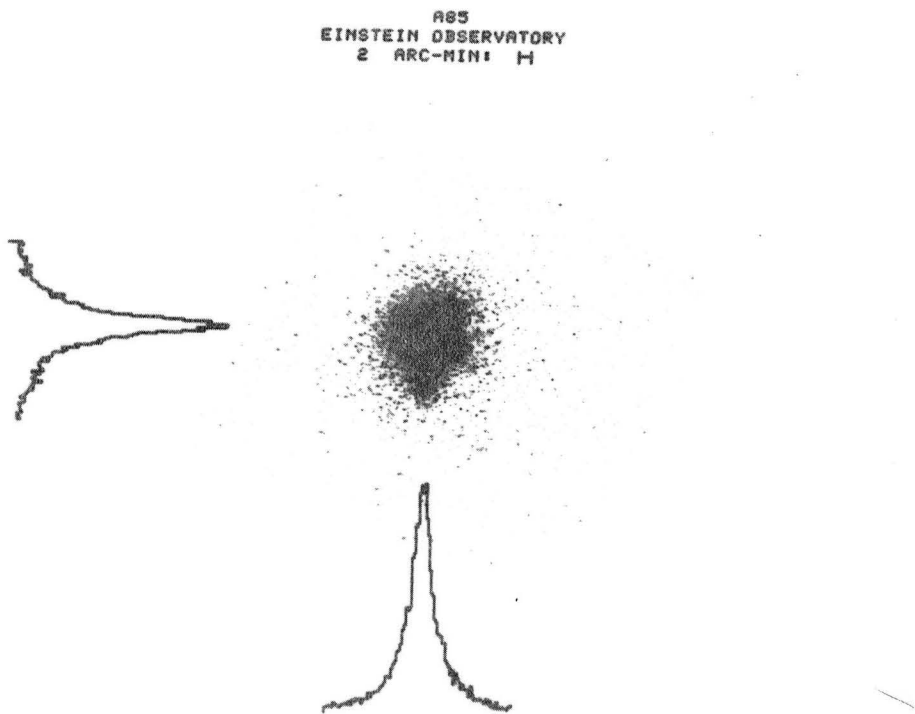


Figure 8

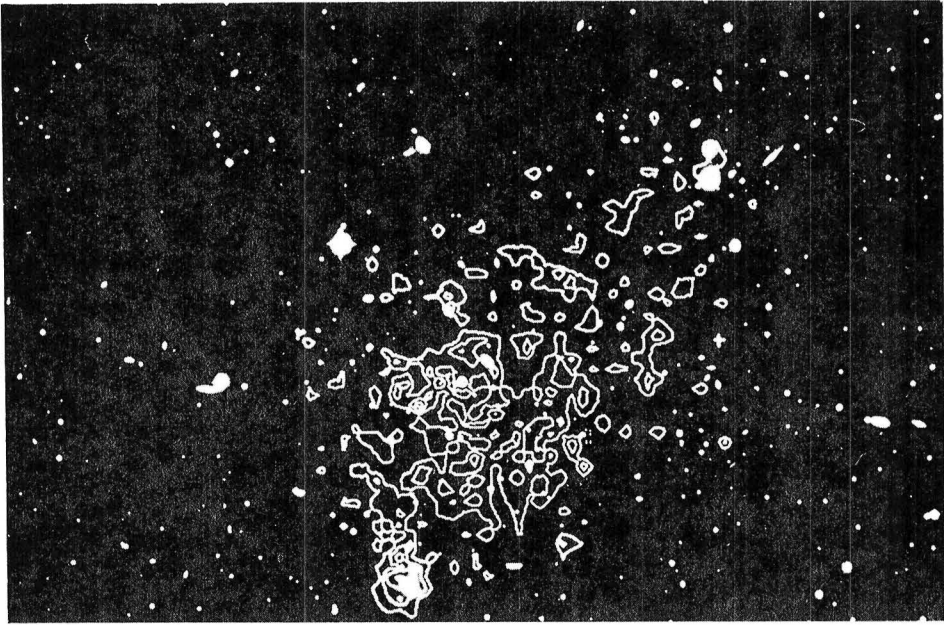


Figure 9

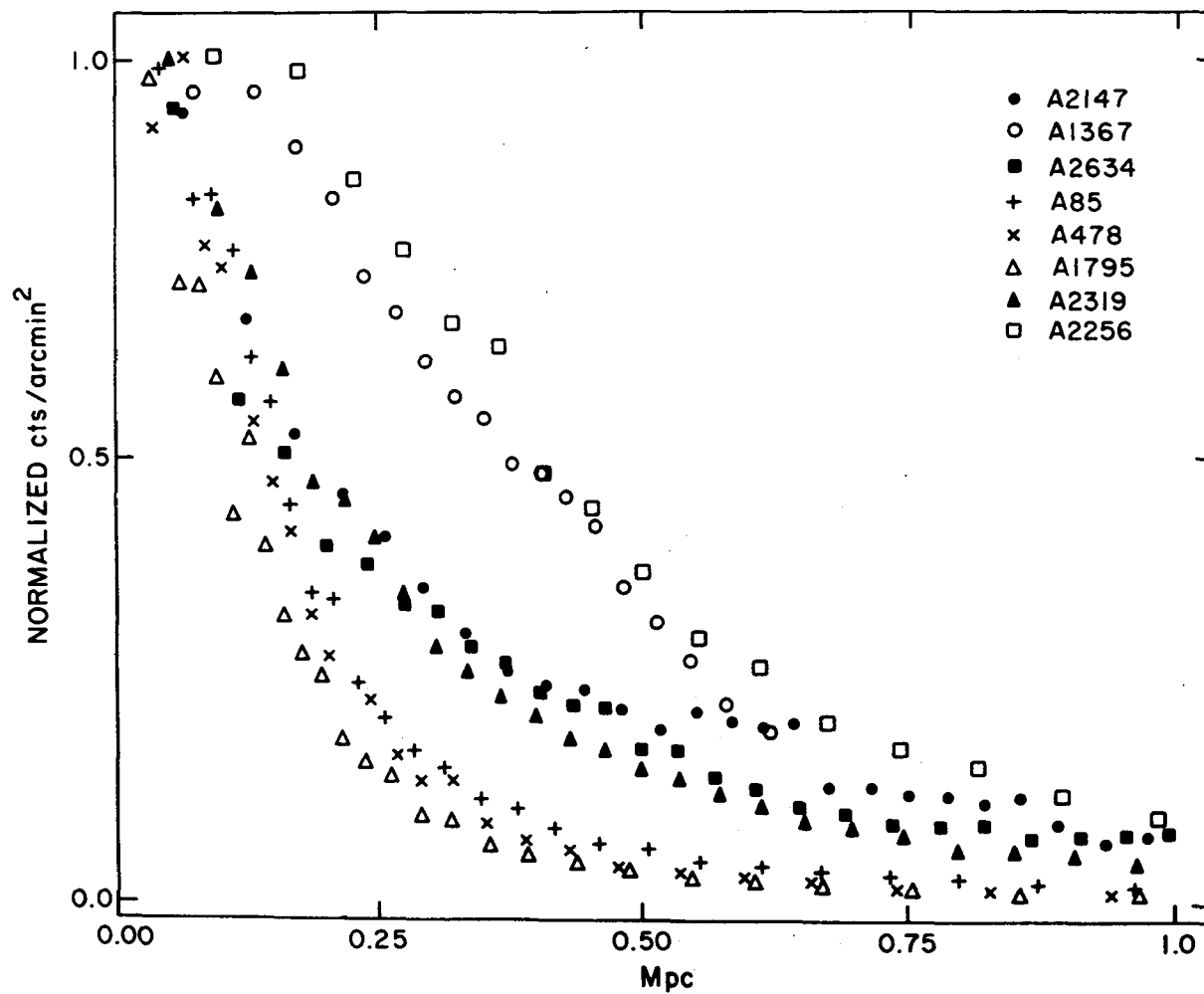


Figure 10



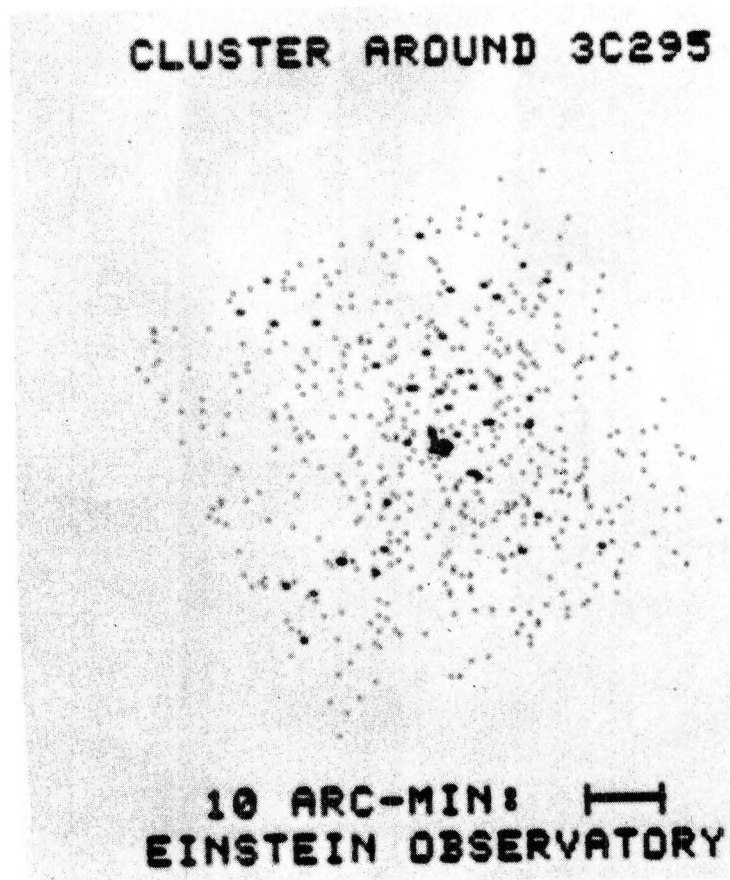


Figure 11

# COLUMBIA/EINSTEIN OBSERVATIONS OF GALACTIC X-RAY SOURCES

Knox S. Long  
Columbia Astrophysics Laboratory

The imaging proportional counter (IPC) has been used to observe a large variety of galactic X-ray sources in the first months of operation of the Einstein satellite. We will now discuss some of those observations, namely, those carried out for Columbia University. The observations to date fall into three broad categories: pre-main-sequence stars in the Orion Nebula, isolated main- and post-main-sequence stars, and supernova remnants.

The Orion Nebula is the newest, large region of active star formation in the Galaxy. Prior to the launch of the Einstein satellite, a relatively weak ( $10^{33}$  erg s $^{-1}$ ) source of X-ray emission had been localized in the Orion Nebula, coincident with the four OB stars which comprise the Trapezium (Bradt and Kelley 1979 and references therein). The first of several planned observations of the Orion region was carried out early this year, and the results are shown in Figure 1. The strongest source in the field is coincident with the Trapezium, but in addition there are many other sources, 22 at a confidence level of  $4\sigma$  or greater. These sources have typical luminosities of  $10^{31}$  ergs s $^{-1}$ . Several of these sources may be identified with relatively bright O or B stars in the field. However, a detailed analysis carried out by Ku and Chanan (1979) revealed that, as a group, the Orion sources are strongly correlated with the positions of bright nebular variables, as cataloged by Kukarkin et al. (1968, 1971, 1974, 1977). Nebular variables are a heterogeneous class of pre-main-sequence stars, which include T Tauri variables with UV Ceti-like flare stars, which exhibit irregular light curves. A large number of nebular variables have been cataloged in the Orion Nebula. A Monte Carlo simulation indicates that  $5 \pm 5$  ( $2\sigma$  error) stars would be expected to fall within the error circles of the X-ray positions, whereas the 22 error circles (excluding the Trapezium) contain a total of 25 bright ( $m_v < 15$ ) nebular variables. The test implies that either the nebular variables are X-ray sources or that they are tracers of X-ray activity, presumably because both are associated with star formation. In fact, we cannot exclude the second possibility, based on the observations to date. However, in the absence of another suitable class of X-ray sources and because X-ray emission from pre-main-sequence stars had been previously predicted (den Boggende et al. 1976; Kuhl 1964; Ulrich 1978; Mullan 1976), we favor the hypothesis that nebular variables are indeed X-ray emitters, a new class of X-ray object. This is a hypothesis that can be resolved by carrying out extended observations with the high resolution imager (HRI).

The first main-sequence star detected at X-ray wavelengths was the Sun. Its X-ray luminosity is highly variable but is typically  $10^{26}$  ergs  $s^{-1}$ . X-ray emission from the Sun arises from the plasma which constitutes the solar corona and is created by the dissipation of mechanical energy in the atmosphere of the Sun. This mechanical energy arises from convection in the outer envelope of the Sun. Model calculations and some observational data [notably the decrease in the strength of He  $\lambda 10830$  emission in early type stars (Zirin 1978)] indicate that convection disappears in stars earlier than spectral type F. Hence it was somewhat surprising to detect X-ray emission from  $\beta$  Cen A, a nearby B1 giant as indicated in Figure 2. The X-ray luminosity of  $\beta$  Cen A is approximately  $8 \times 10^{30}$  ergs  $s^{-1}$ . The fraction of the total energy radiated from the star as X-rays is approximately  $10^{-7}$ , which is similar to the fractional flux radiated at X-ray wavelengths by the Sun. Assuming that convection does indeed disappear in early type stars, the solution to understanding the X-ray emission from these objects presumably is connected to the massive stellar winds associated with O and B stars which have maximum velocities of order  $10^8$  km  $s^{-1}$ . The X-ray luminosity of  $\beta$  Cen A is a small fraction of the energy which is available from such a wind. Since model calculations (Nelson and Hearn 1978) indicate that such winds are unstable, it may not be surprising, in retrospect, that X-rays are emitted. In the data which have been analyzed at Columbia, approximately 30 main- and post-main-sequence stars have been detected, many serendipitously. The detection of X-ray emission from a large number of normal stars makes possible, for the first time, a systematic study of the X-ray emitting properties of normal stars which do, after all, constitute the dominant form of mass in the Galaxy.

Tycho's supernova was first observed in 1572. A type I supernova, its optical emission peaked at magnitude of  $-4.0 \pm 0.3$  (van den Bergh 1970). The remnant was first observed at X-ray wavelengths by Friedman, Byram, and Chubb (1967). This SNR was the first remnant observed as part of an extensive survey of SNR being conducted at Columbia. The image shown in Figure 3 represents the result of that 2500 sec pointing. The important features of the image are the bright shell which can be traced over three-fourths of the circumference and the apparent break in the shell in the southeast. The peak brightness in the shell is approximately 2.5 times that of the center. The total counting rate from the remnant was approximately 20 counts  $s^{-1}$ . The diameter of the remnant is approximately  $8'$  which should be compared to the full width at half maximum of the point response function approximately  $1.5'$ . The edges of the remnant are sharp except possibly in the southeast, consistent with the angular resolution of the IPC. Assuming a distance of 3 kpc (Woltjer 1972), this means that the shock has a width of 1 pc or less. The radius of the remnant in the southeast appears approximately 20 percent greater than elsewhere. Since the remnant has most likely swept up substantially more matter from the interstellar medium (ISM) than was ejected from the star in the SN

explosion, the Sedov solutions to SNR evolution may be applied. In order to explain the difference in expansion rates, the density encountered by the shock in the southeast must have been approximately half that encountered in other directions.

A comparison between the X-ray and radio contours is shown in Figure 4. The two maps are quite similar. (The radio map of Strom and Duin 1973 has somewhat finer resolution.) The X-ray and radio shells have the same radii within the errors and both lie inside the optical filaments. There are differences however. For example, the radio contours peak in the northeast whereas X-ray emission peaks in the northwest. The polarization of radio emission is relatively lower in the northeast than in other parts of the shell (Strom and Duin 1973), which may be due to depolarization in the increased density of that portion of the radio shell. Preliminary analyses of the X-ray spectra of various regions of the remnant indicate that the increased flux in the shell is due to density and line-of-sight effects rather than differences in the temperature of a hot plasma.

A second SNR observed in the early months of operation of the Einstein satellite is W28 (Fig. 5). X-ray emission had not been detected prior to the launch of the Einstein satellite. This remnant which has a diameter of approximately 40' fills a single IPC field, and more observations will be required to understand the details of its structure. The X-ray luminosity of W28 is approximately  $10^{35}$  ergs  $s^{-1}$  if the distance is taken to be 3 kpc (Woltjer 1972). Unlike Tycho's SNR, the X-ray picture of W28 shows no evidence of shell structure. The surface brightness appears relatively featureless and peaks near the center of the remnant, well inside the nonthermal radio shell which was observed by Shaver and Goss (1970). The optical picture obtained by van den Bergh et al. (1973) shows sharp optical filaments and considerable nebulosity. The lack of a distinct X-ray shell, and the X-ray luminosity and the size of W28 indicate that this SNR is at a much more advanced stage of evolution than Tycho's SNR.

An important feature of the map of the Einstein observation of Tycho's SNR is that there appears to be no bright object at the center of the remnant, as might be expected had a hot neutron star formed when the SN occurred approximately 400 years ago. If a neutron star had been created, it would not have moved from the central region of the remnant since pulsars are known to have typical velocities of 200 km  $s^{-1}$  (Helfand and Tademaru 1977), whereas the shock front in Tycho's SNR has expanded with a mean velocity of 9000 km  $s^{-1}$ . As discussed by Helfand, Chanan, and Novick (1979), the X-ray data obtained for Tycho's SNR can be used to place a limit of approximately  $2 \times 10^6$  K for the temperature of a 10 km neutron star radiating as a blackbody. Since all models of SNR which produce neutron stars indicate that the neutron stars will be formed at temperatures of approximately  $10^{10}$  K,

the lack of enhanced emission from the center of Tycho's SNR implies either that no pulsar was formed or that it cooled rapidly. The cooling curves for various neutron star models have been summarized recently by Tsuruta (1979). Figure 6 is abstracted from her paper. The solid curves represent envelopes for neutron star cooling in which the center of the neutron star does not contain pion condensates; the dashed curves represent the envelope for cooling curves which do contain pion condensates. In models with pion condensates, the neutron star cools rapidly at early times because of the additional channels for neutrino cooling provided by the existence of pions. The X-ray observations of Tycho's SNR seem to require pion condensates, if, in fact, a pulsar were formed.

A serious problem arises in studying the generic properties of supernova remnants using a sample of galactic remnants because the distance and the line-of-sight absorption to many SNR is poorly known. One way to circumvent this problem is to survey the properties of SNR in external galaxies. Our nearest neighbor galaxy is the Large Magellanic Cloud, an irregular galaxy with a prominent bar. In the tradition of Henrietta Leavitt, we therefore set out to study the properties of SNR in the LMC as part of a more general survey of that galaxy. A number of SNR had been identified in the LMC prior to the launch of the Einstein satellite, based on the existence of nonthermal radio sources in regions exhibiting filamentary structure in  $H\alpha$  and strong (S II) emission.

To date, observations of 10 of the 14 SNR and SNR candidates listed by Mathewson and Clarke (1973, hereafter MC) have been carried out. An initial analysis of these data has been completed (Long and Helfand 1979). Eight of the 10 SNR were detected, the first SNR ever detected at X-ray wavelengths in an external galaxy. Six of the remnants have 0.5–3.0 keV luminosities exceeding  $10^{36}$  ergs  $s^{-1}$ . Also observed were sources coincident with two additional objects which were a part of a less rigorous list of SNR candidates compiled by Davies, Elliott, and Meaburn (1976; hereafter DEM).

A spectacular example of emission from SNR in the LMC is shown in Figure 7. Both bright sources there are SNR. The remnant in the southeast (lower left), known as N49, is approximately twice as bright as the remnant in the northwest, known as (N49). There is, in fact, an  $H\alpha$  bridge which joins N49 and (N49) and a break in the optical shell in the direction of (N49). As a result, MC suggested that (N49) was not a separate SNR but was perhaps the result of a massive compact object ejected from N49. The detection of (N49) as a separate X-ray source seems to confirm (N49) as a separate SNR. Evans et al. (1979) have recently reported the detection of a giant gamma-ray burst whose position is coincident with N49. Data obtained before and after the gamma-ray burst indicate no change in the X-ray luminosity of N49, but if the gamma-ray burst was located there, it had a peak luminosity of approximately  $5 \times 10^{44}$  ergs  $s^{-1}$  (Mazets et al. 1979). (The constraints

placed on the burst by the Einstein observations of this field are discussed by Helfand and Long (1979).

A plot of the X-ray luminosity of LMC supernova remnants versus their optical diameters is shown in Figure 8. Optical diameters for the plot were obtained from the compilation of MC (1973), where possible, or from the list of DEM (1976) if they were not in the MC survey. The determination of the optical diameters of SNR is somewhat subjective, and for remnants included in both lists, there are considerable differences in the optical diameters derived by MC and DEM.<sup>1</sup> Since the optical counterparts of N157B and N158A are yet to be established, the diameters for these sources were estimated by MC on the basis of a radio surface brightness ( $\Sigma - D$ ) relation for the other SNR in their survey. There appears to be a considerable range in luminosity for SNR of the same general size; however, a general trend is evident for luminosities to decrease as the radius exceeds 30 pc, as it is for similar plots of SNR in our own Galaxy. The Sedov solution for a symmetric blast wave propagating into a uniform density medium allows one to solve for the age of the remnant and the ratio of the energy of the initial explosion to the ambient density  $n_0$  of the ISM, given the radius and temperature of the remnant. Following Gorenstein and Tucker (1976), we have estimated  $n_0$  directly from the X-ray luminosity and temperature, assuming that X-ray emission from the SNR originates in a shell of uniform density  $4 n_0$ . This degree of compression corresponds to conditions behind a strong shock in a gas having a ratio of specific heats equal to 5/3. Ages derived from this analysis range from just over 1000 years to 20 000 years and are reasonably consistent with the observed optical expansion rates. As expected, the calculated explosion energies are not dependent upon remnant size or age; they range from 0.8 to  $3.4 \times 10^{50}$  ergs, with a mean of  $2 \times 10^{50}$  ergs and are similar to energies derived from galactic remnants when the same model is applied (Gorenstein and Tucker 1976). However, the ISM densities derived from the model are highly correlated with observed remnant diameters, as shown in Figure 9, ranging from 0.047 to  $11 \text{ cm}^{-3}$ , which is inconsistent with the simple blast wave model in which  $n_0$  should be independent of the diameter. McKee and Ostriker (1977) have developed a detailed theory of supernova shock waves expanding into a tenuous ISM ( $n_0 > 10^{-2.5} \text{ cm}^{-3}$ ), studded with small clouds ( $n_0 > 10 \text{ cm}^{-3}$ ).

1. Work is now in progress on a more accurate way of determining the optical diameters from HRI observations of the SNR in the LMC. Results obtained since this paper was presented indicate that the optical diameters of MC considerably underestimate the X-ray diameters of the brighter remnants at least.

The clouds have only a small effect on the dynamics of the shock. X-ray emission in this model is dominated by matter which is evaporated from the cool, relatively dense clouds. The importance of the evaporation decreases as a function of time, and hence McKee and Ostriker (1977) predict an apparent density decrease similar to what is observed.

The initial survey of the LMC is now approximately half complete. In addition to the known SNR, approximately 30 other sources have been detected. These sources include the emission nebula 30 Doradus, shown in Figure 10. The emission nebula is the extended source in the center. It has a luminosity of approximately  $10^{36}$  ergs  $s^{-1}$ . This nebula resembles in some aspects the Orion Nebula; both are hydrogen rich regions with active star formation. However, according to Bok (1966), if 30 Doradus were placed at the distance of the Orion Nebula, it would cover almost 25 degrees of the sky and cast permanent shadows on the Earth. One of the challenges presented by the Einstein observations is to understand emission from this region, which is  $10^3$  brighter than the Trapezium. Other sources in this field include LMC X-1, which is distorted because of its position near the edge of the field, and the SNR N157B and N158A, as well as several unidentified sources.

In concluding, let me note that work has only just begun on analyzing the first observations of the LMC, as well as of SNR and normal and pre-main-sequence stars. The surveys themselves are only partially complete. Many more and often deeper observations are planned. However, I think that the implications of the current observations are clear. The horizon of X-ray astronomy has expanded with the Einstein satellite to include not only rare and exotic objects, such as supernova remnants and pulsars, but stars of all types and many other objects as well. In that sense, X-ray astronomy has changed from a separate discipline with its own parochial interests to a field in which X-ray observations serve as a tool to understand sources of general interest to astrophysicists.

We at Columbia wish to join other members of the HEAO-2 Consortium in thanking the many individuals at the NASA George C. Marshall Space Flight Center, the NASA Goddard Space Flight Center, the NASA John F. Kennedy Space Center, the NASA Headquarters, and in private industry without whom the Einstein Observatory would not have become a reality. This work was supported by the National Aeronautics and Space Administration under contract NAS8-30753. This paper is Columbia Astrophysics Laboratory Contribution No. 179.

## REFERENCES

- Bok, B. J., 1966, *Ann. Rev. Astron. Astrophys.*, 4, 95.
- Bradt, H. V., and Kelley, R. L., 1979, *Astrophys. J. (Letters)*, 228, L33.
- Davies, R. D., Elliott, K. H., and Meaburn, J., 1976, *Mem. Roy. Astron. Soc.*, 81, 89 (DEM).
- den Boggende, A. J. F., Mewe, R., Gronenschild, E. H. B. M., Heise, J., and Grindlay, J. E., 1978, *Astron. Astrophys.*, 62, 1.
- Evans, D., Klebesadel, R., Baros, J., Cline, T., Desai, U., Teegarden, B., and Pizzichini, G., 1979, *I.A.U. Circ.*, No. 3356.
- Friedman, H., Byram, E. T., and Chubb, T. A., 1967, *Science*, 156, 374.
- Gorenstein, P., and Tucker, W. H., 1976, *Ann. Rev. Astron. Astrophys.*, 14, 373.
- Helfand, D. J., Chanan, G. A., and Novick, R., 1979, *Nature*, in press.
- Helfand, D. J., and Long, K. S., 1979, preprint.
- Helfand, D. J., and Tademaru, E., 1977, *Astrophys. J.*, 216, 842.
- Ku, W. H.-M., and Chanan, G. A., 1979, *Astrophys. J. (Letters)*, in press.
- Kuhi, L. V., 1964, *Astrophys. J.*, 140, 1409.
- Kukarkin, B. V., et al., 1968, *General Catalogue of Variable Stars* (Moscow: Publishing House of the Academy of Sciences, USSR); Suppls. 1971, 1974, 1977.
- Long, K. S., and Helfand, D. J., 1979, *Astrophys. J. (Letters)*, in press.
- Mathewson, D. S., and Clarke, J. N., 1973, *Astrophys. J.*, 180, 725 (MC).
- Mazets, E. P., Golenetskii, S. V., Il'inskii, V. N., Aptekar', R. L., and Guryan, Yu. A., 1979, *Nature*, in press.
- McKee, C. F., and Ostriker, J. P., 1977, *Astrophys. J.*, 218, 148.
- Mullan, D. J., 1976, *Astrophys. J.*, 207, 289.



## REFERENCES (Concluded)

- Nelson, G. D., and Hearn, A. G., 1978, *Astron. Astrophys.*, 65, 223.
- Strom, R. G., and Duin, R. M., 1973, *Astron. Astrophys.*, 25, 351.
- Shaver, P. A., and Goss, W. M., 1970, *Australian J. Phys. Astrophys. Suppl.*, 14, 77.
- Tsuruta, S., 1979, *Phys. Reports*, in press.
- Ulrich, R. K., 1978, in *Protostars and Planets*, ed., T. Gehrels (Tucson: Univ. of Arizona Press).
- van den Bergh, S., 1970, *Nature*, 225, 503.
- van den Bergh, S., Marscher, A. P., and Terzian, Y., 1973, *Astrophys. J. Suppl.*, 26, 19.
- Woltjer, L., 1972, *Ann. Rev. Astron. Astrophys.*, 10, 129.
- Zirin, H., 1978, *Astrophys. J.*, 208, 414.

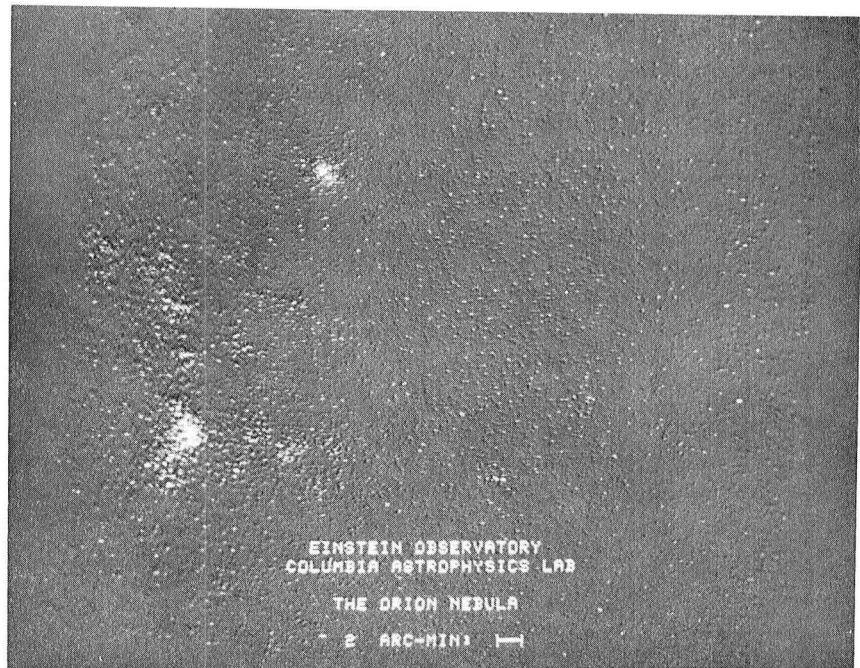


Figure 1. The results of an initial observation of the Orion region with the IPC. The bright source in the southeast is the Trapezium.

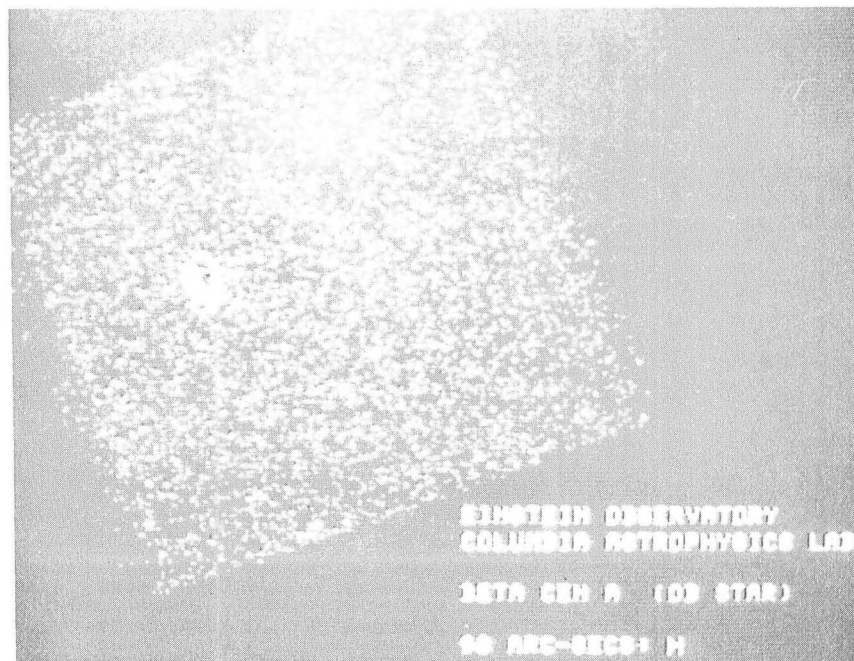


Figure 2. The B supergiant  $\beta$  Cen A as observed in a short observation with the Einstein IPC.



Figure 3. Tycho's supernova remnant.

## TYCHO'S SNR

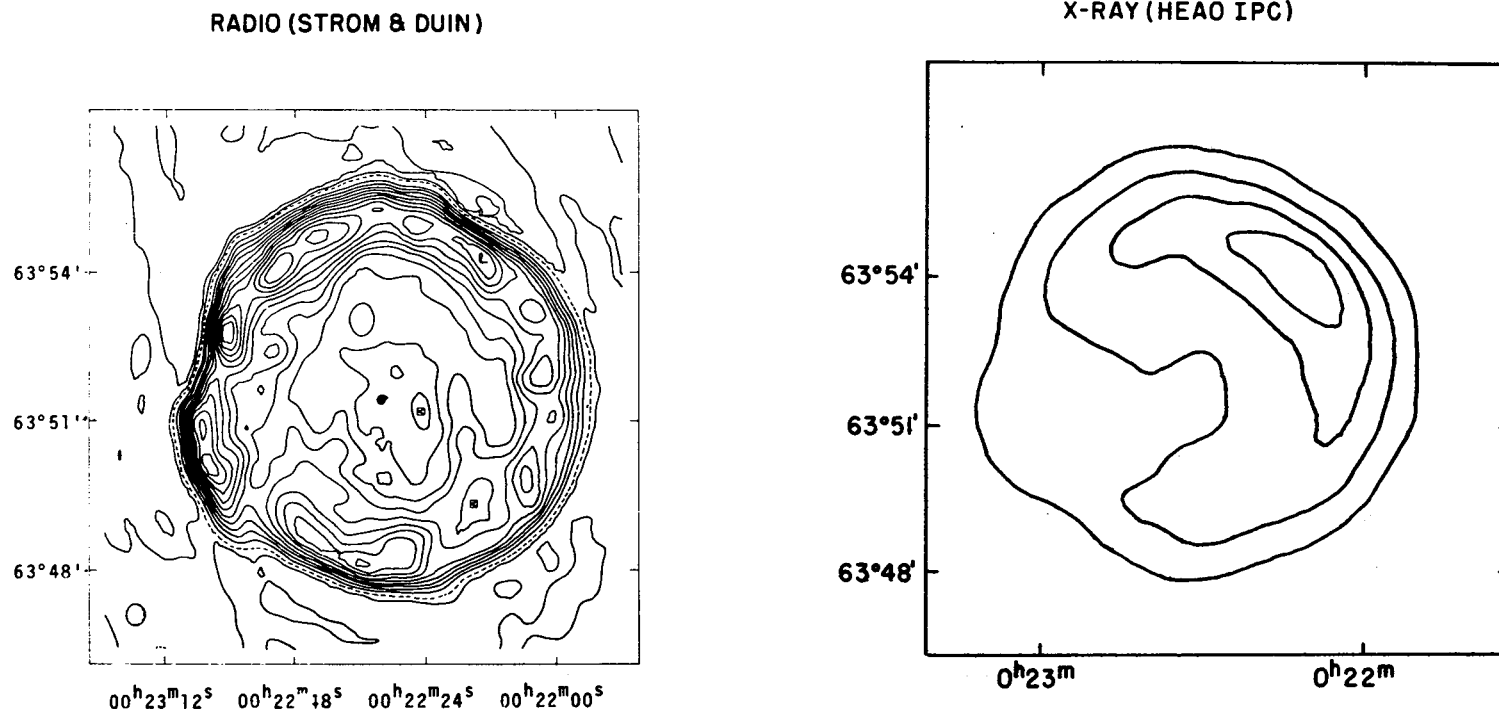


Figure 4. A comparison of radio and X-ray contours of Tycho's SNR. The radio map was taken from Strom and Duin (1973). The contour levels in the X-ray map correspond to approximately 1, 2, 3, and 4 counts  $(1' \times 1')^{-1} \text{ s}^{-1}$ .

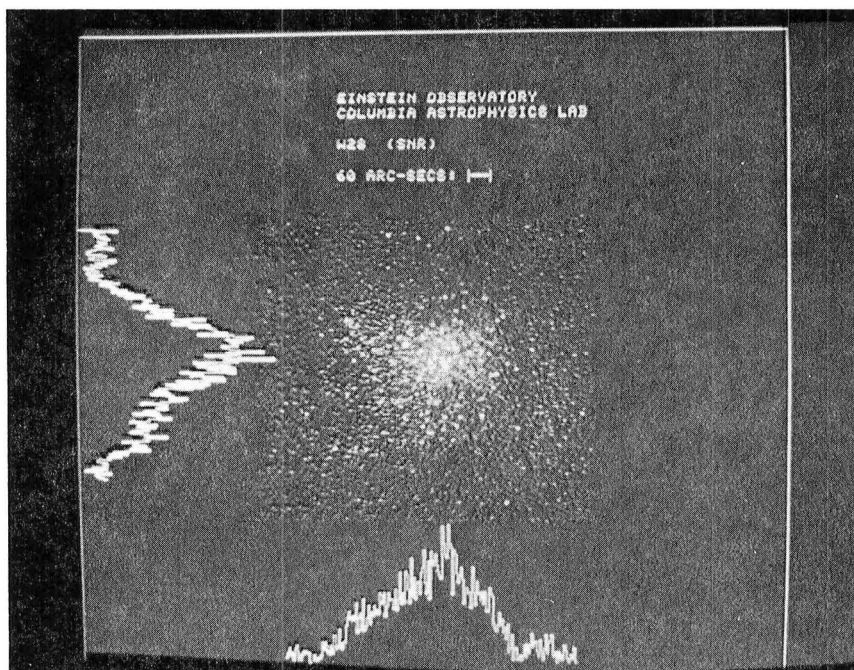


Figure 5. The supernova remnant W28.

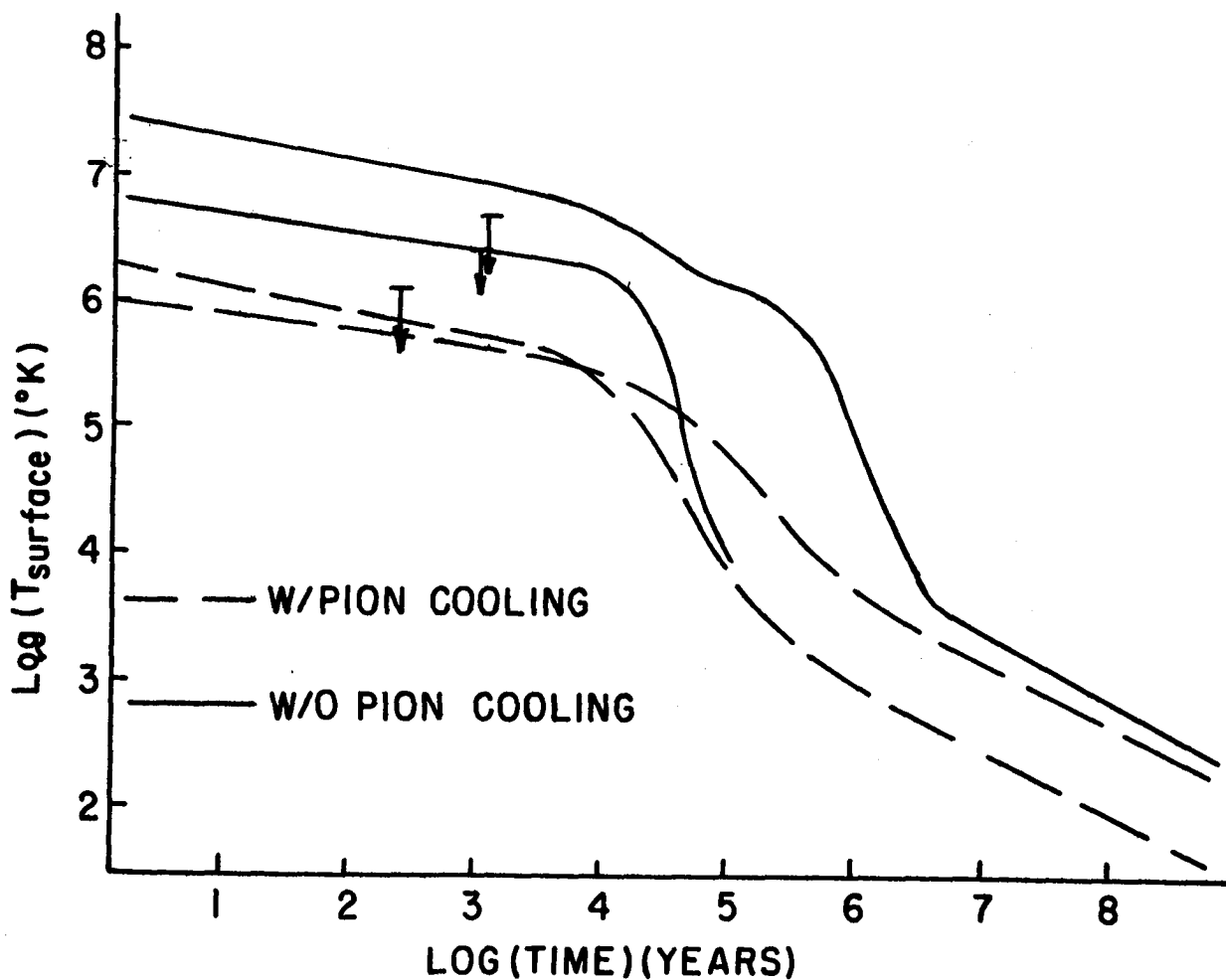


Figure 6. Cooling curves for neutron stars with limits derived from X-ray observations. The cooling curves shown represent the envelopes of various models for neutron star cooling without pion condensates (solid lines) and with pion condensates (dashed lines).



Figure 7. An IPC observation of two supernova remnants in the LMC. The remnant N49 in the southeast is approximately twice as bright as (N49) in the northeast.

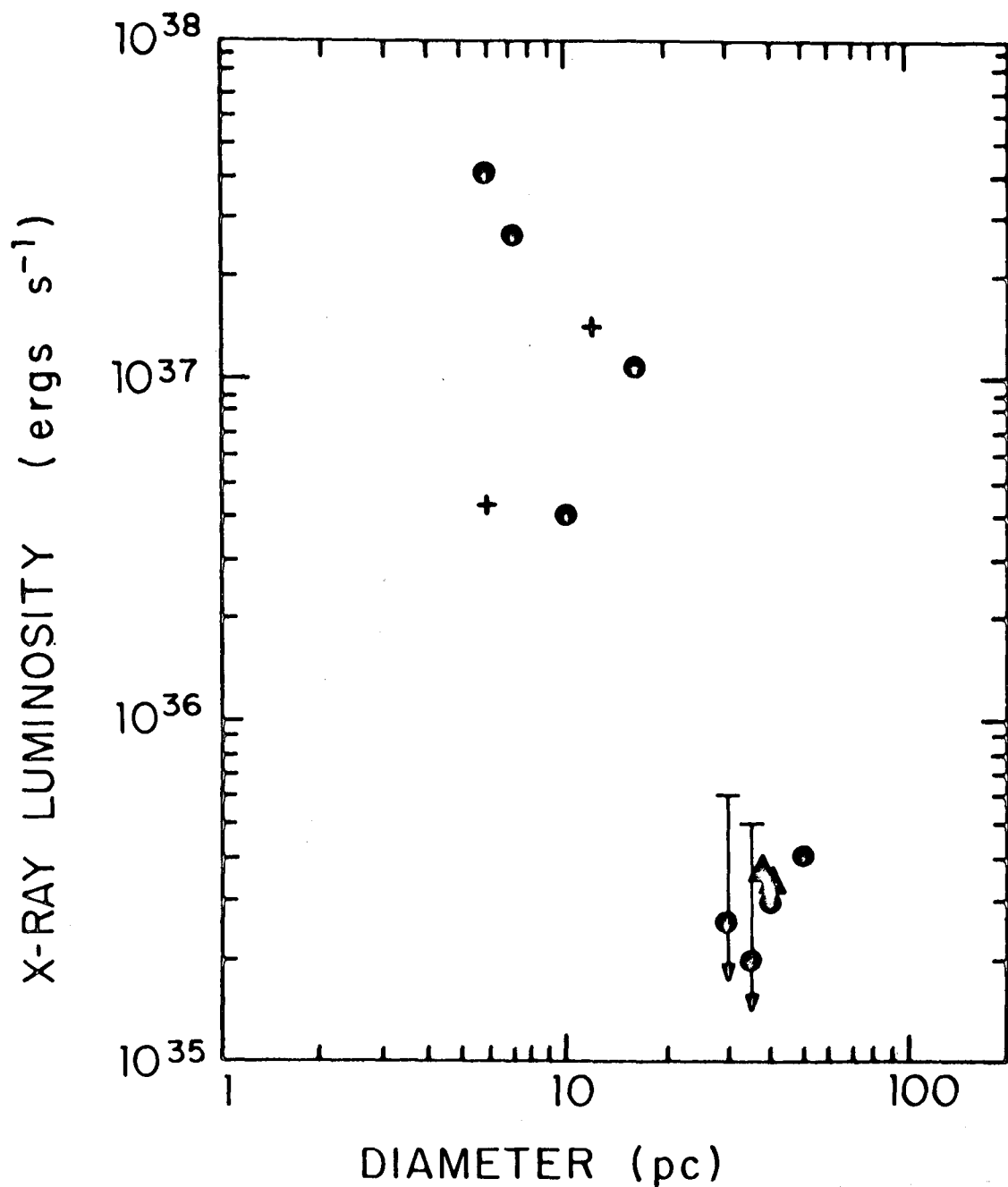


Figure 8. The X-ray luminosity of SNR in the LMC as a function of optical diameter. Diameters for N151B and N158A (+) were determined from a  $\Sigma - D$  relation by MC. The rest of the diameters were determined directly (MC = filled circles; DEM = filled triangles).



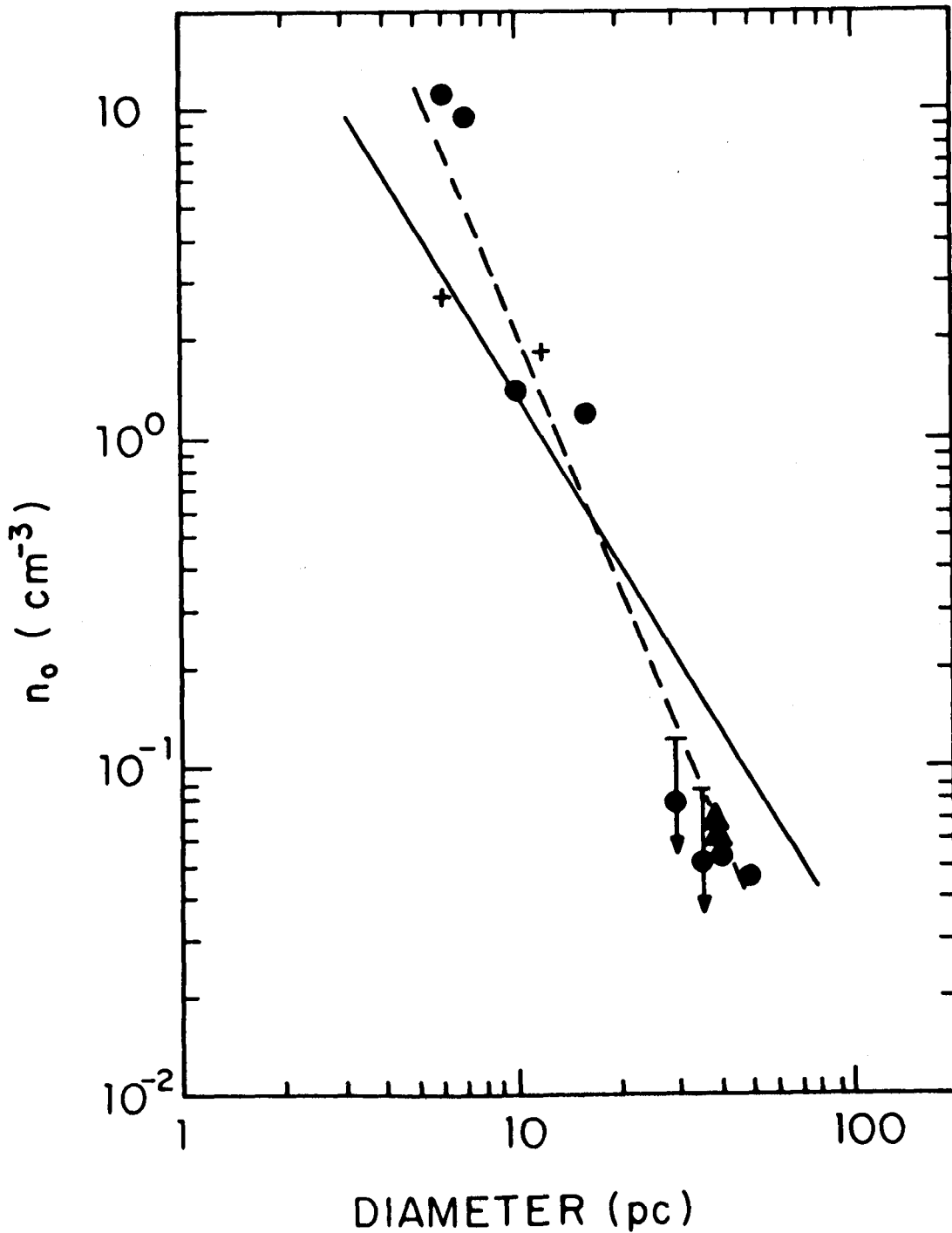


Figure 9. Derived values of  $n_0$  from the Sedov solutions for SNR in the LMC as a function of SNR diameter. The solid line indicates an approximate fit to a law,  $n_0 \propto D^{-5/3}$ , as predicted by McKee and Ostriker (1977). The actual slope is better fit by a somewhat steeper law,  $n_0 \propto D^{-5/2}$  (dashed line). Symbols are as in Figure 8.



Figure 10. An IPC image of the 30 Doradus field.  
Sources are discussed in the text.

## COLUMBIA/EINSTEIN OBSERVATIONS OF EXTRAGALACTIC X-RAY SOURCES

William H.-M. Ku  
Columbia Astrophysics Laboratory

I would like to report on the preliminary results of our analysis of data from the first 3 months of the Columbia Astrophysics Laboratory's (CAL) observations of extragalactic objects with the imaging proportional counter (IPC) on board the Einstein Observatory. CAL has an extensive program of extragalactic astronomy planned with the Einstein Observatory including surveys of normal galaxies, radio galaxies, active galaxies, quasars and BL Lacs, and clusters of galaxies. Early results from each one of these surveys have been received and analyzed at CAL. These observations have already allowed us to look as far out to the edge of the Universe as any observer in history, and they have improved our understanding of how our own Galaxy may have evolved through time.

### NORMAL GALAXIES

X-ray observations of normal galaxies should aid us in the understanding of our own Galaxy. Observations of the galaxies in the Local Group, such as the Large Magellanic Cloud discussed by Dr. Long, allow us to study the population of discrete X-ray sources in detail, as well as to examine diffuse emission associated with large-scale structures. Galaxies just outside the Local Group may also be studied in this way. For example, a 13 000 sec IPC image of M101, a normal spiral Sc galaxy, reveals the presence of three or four discrete sources associated with the beautiful spiral arm structure of the galaxy (Fig. 1). Possible diffuse or unresolved emission is also noticeable in the IPC image. In contrast to other galaxies, no strong emission is associated with the center or the nucleus of the galaxy. The total X-ray emission is comparable to that from our Galaxy, approximately  $3 \times 10^{39}$  erg s<sup>-1</sup>. Shorter observations of the spiral galaxy NGC5866 and the irregular galaxy NGC520 have yielded positive detections of these galaxies as weak extended X-ray sources. The explosive spiral galaxies, NGC1097 and NGC4756, have both been detected as moderately strong X-ray sources, although the latter is source confused with A1631 cluster. NGC1097 is particularly interesting because Arp (1976) has obtained deep optical plates which show the operation of an ejection phenomenon evidenced by the presence of three jets. A bright X-ray source is coincident with the bright optical nucleus and is consistent with a point source. A second source, possibly aligned with a jet, is seen 10' to the northeast. Early results from observations of four other galaxies including three radio bright galaxies have yielded null results.

Table 1(a) summarizes the results from our survey of normal galaxies and radio galaxies. Columns (1) and (2) give the name and

type of object observed. Column (3) gives the distance in megaparsecs or the redshift. Columns (4), (5), and (6) give the monochromatic flux at radio, optical, and X-ray frequencies, respectively. Column (7) gives the integrated 0.5-4.5 keV X-ray luminosity at the source (cosmological parameters of  $q_0 = 0$  and  $H_0 = 50 \text{ km s}^{-1} \text{ Mpc}^{-1}$  are used). From column (8) in Table 1(a), we see that the X-ray emission is in general  $\lesssim 10^{-3}$  of the optical emission. However, radio brightness does not seem to be a strong determinant of X-ray brightness. Ultimately these observations should allow us to understand and correlate the X-ray emission from normal galaxies with their structure, mass, and dynamics as well as with their radiation in other parts of the electromagnetic spectrum.

## ACTIVE GALAXIES

NGC1097 may be the precursor or the remnant of an active galaxy phase through which every galaxy goes. X-ray studies of active galaxies can improve our understanding of the evolution of galaxies. Several types of active galaxies including Seyferts, BL Lacs, and quasars were known to be X-ray emitters before the launch of the Einstein Observatory. We have now confirmed that active galaxies are indeed prodigious sources of X-ray emission. Every Seyfert galaxy (generally a spiral galaxy with a bright nucleus) or N-type galaxy (a radio bright Seyfert) examined thus far has shown itself to be a strong X-ray emitter. The source 3C109 is an extremely distant N-type galaxy. It is a strong radio and optical source. It is notable that the emission from 3C109 recorded by the IPC on March 8 is highly absorbed below 1 keV, unlike that from other active galaxies. Its luminosity,  $1.7 \times 10^{45} \text{ ergs s}^{-1}$ , places it well within the quasar class, thus linking N-galaxies to quasars. X Comae, a type I Seyfert which is believed once to have had a quasar-like appearance (Bond and Sargent 1973), was detected strongly in a 200-s observation of the Coma cluster field on January 6. The compact Zwicky galaxy, VII Zw674, was discovered serendipitously in the 3C351 field. Its optical spectrum is similar to spectra of other normal galaxies, devoid of strong emission lines. Further observations are required to confirm the suggested identification and to understand the nature of this optically "inactive" source. Finally, the N-type galaxy RN73 was also detected as an X-ray source.

These results are summarized in Table 1(b). It can be seen from the summary table that the ratios of the X-ray to optical luminosities of these active galaxies are all several hundred times higher than those for normal galaxies. We note the similarity in their multifrequency spectra (Fig. 2). It should be emphasized, however, that since most of these galaxies vary significantly from observation to observation, simultaneous wide-band coverage of each source is important.

This is essentially what we achieved with the early April observations of the quasar 3C351 in cooperation with O'Dell (Fig. 3). Simultaneous radio observations were not available, but 3C351 is not known to be a radio variable. The 3C351 field shown in Figure 4 is extremely interesting. During our first observation of this source on January 6, the IPC image showed the presence of three strong sources, one centered  $\lesssim 0.5'$  away from 3C351 and two serendipitous sources. One of the two is the compact Zwicky galaxy previously noted. The other is not a catalogued source but has since been identified as the 18th mag Seyfert galaxy. The first observation also detected a weak fourth source,  $3'$  to the northwest of 3C351. This source is now suspected to be the quasar candidate KP1703.5+609, discussed by Sramek and Weedman (1978). 3C351 is additionally interesting because Hinzen and Scott (1978) had proposed that, along with other asymmetrical radio quasars, it may be used to probe the presence of surrounding cluster emission. The 4600 sec of summed IPC data provide marginal evidence for diffuse emission surrounding 3C351. Confirmation of the association of quasars with clusters of galaxies at large redshifts would be an important piece of evidence supporting the cosmological nature of quasar redshifts. We plan to study this region in greater depth.

Five other quasars and BL Lacs have been examined with the IPC, and five have been found to emit X-rays. The object 0237-23 is a high redshift ( $z = 2.26$ ) quasar with multiple absorption redshift systems. At its cosmological distance, it has a measured 0.5-4.5 keV luminosity of more than  $10^{47}$  ergs  $s^{-1}$ . The first 6000 sec of data received thus far have been searched for the existence of intervening clusters of galaxies which may be responsible for the rich absorption line systems. No evidence for such clusters has been found although the deeper pointings that are planned may yet reveal their presence. The field containing Ton 256 and NAB1612 was examined in a short 1300-sec observation. Ton 256 was found to be a strong X-ray quasar and NAB1612 to be a weak X-ray quasar. The BL Lac object A00235+164 was detected as a weak X-ray source in a short pointing. This interesting object is one of the most violently variable of all active galaxies. It had undergone a large upward transition in November 1975 and most recently in February 1979. Unfortunately, we were unable to observe this object during its violent outburst.

Table 1(c) summarizes our results for the quasars and BL Lacs in our survey. The table shows that quasars and BL Lacs, like other active galaxies, emit nearly as much radiation in the X-ray regime as in the optical. All types of active galaxies exhibit similar X-ray to optical luminosities, approximately 0.3. Their multifrequency spectra demonstrate the close connection between optical and X-ray behavior but reveal no obvious relationship with the radio behavior (Fig. 5). Multiband simultaneous observations are required to decide the true relationship between various segments of the total electromagnetic output. Such spectral

observations in addition to detailed time studies can serve to test models of possible energy sources which can generate as much as  $10^8$  times the power of our own Galaxy.

Thus we see that galaxies exhibiting a wide variety of optical and radio behavior also exhibit a diversity of X-ray behavior, with X-ray luminosities ranging from  $10^{39}$  to  $10^{47}$  ergs  $s^{-1}$ . They may, however, all be linked in a common evolutionary scheme as suggested, for example, by X-ray observations of the inactive normal spiral galaxy M101, the explosive "normal" galaxy NGC1097, the N-galaxy 3C109, and quasars and BL Lacs such as 3C351 and 0109+22.

## CLUSTERS OF GALAXIES

Another way in which to study the evolution of galaxies is to examine the behavior of normal and active galaxies, and possibly quasars, in clusters of galaxies. A majority of galaxies are believed to exist in cluster associations, and if quasars are really cosmological, they should be found in distant clusters and may, moreover, be the power source behind some of the cluster emission.

The existence of clusters of galaxies as X-ray sources was well established even before the launch of the Einstein Observatory. The discovery of strong iron line emission established the predominantly thermal nature of their emission. Modulation collimator observations were able to identify X-ray centroids with dominant cD galaxies in BM type I clusters (Schwartz et al. 1979). Careful statistical analysis of a large sample of 40-50 clusters led several authors including Jones and Forman (1978) to propose positive correlations in the X-ray emission with cluster richness or central galaxy density, and with other aspects of cluster morphology and cluster dynamics. However, much uncertainty remains concerning the exact nature of the emission mechanism and the role of cluster gas in the evolution of galaxies and the Universe.

Early results from CAL's cluster survey have already improved our understanding of clusters of galaxies. The Einstein IPC has been used to study the arc-minute morphology of several of the brighter X-ray clusters in several different "colors." One of the first clusters examined by us in detail was the distant, rich cluster A2142. A2142 is one of the most intrinsically luminous of cluster X-ray sources. At a measured redshift of  $z = 0.090$ , the 2-10 keV X-ray luminosity is  $3-6 \times 10^{45}$  ergs  $s^{-1}$ , as measured by Uhuru, Ariel V, and OSO 8. We observed the cluster for 5500 sec on January 30, 1979.

From the IPC image (Figures 6a and 6b), we see that the distribution of X-rays from A2142 is sharply peaked around a central point less than  $20''$  from the optical center of the cluster. This is  $3'$  south of the head-tail radio galaxy mapped by Harris et al. (1977). The distribution

of X-rays is not spherically symmetric but elongated along the northwest-southeast direction with a half peak projected radius of  $1.6' = 0.25$  Mpc. The half peak projected radius in the orthogonal direction is  $1.0'$ . The southeast extension is evident in the 610 MHz map by Harris et al., although several other bright radio sources observed by them are not bright in the X-ray regime. Examination of the X-ray map shows that there is a distinct secondary peak  $5'$  northeast of the main peak. This source, consistent with a point source, contains about 8 percent of the total cluster flux. This secondary peak has no optical counterpart brighter than 16th mag on the Palomar plates. The possibility exists that this is a foreground object, but the high galactic latitude of  $50$  degrees makes this unlikely. The source, however, may be a field galaxy similar to the Seyfert galaxy discovered in the southeast corner of this IPC field. Our search did not reveal evidence for an extended halo, a possible signature of massive gas clouds, that Forman et al. (1978) had suggested. However, the presence of a low luminosity halo beyond the  $10'$ , 1 percent level radius cannot now be ruled out. A more detailed quantitative estimate of the flux contained in this halo will have to await the receipt of the remaining half of the planned observation, and a careful comparison of off-target versus on-target rates.

The importance of discrete source emission is better seen in CAL's observation of A539, a nearby, rich cluster previously detected by Uhuru. The IPC image of this irregular cluster, shown in Figures 7a and 7b, reveals the presence of several discrete components. Source (a) is identified with a 15.1 mag double galaxy in Zwicky's catalog which is close to the optical center of the clusters. Source (b) is identified with another catalogued galaxy. Source (c) is unidentified and does not correspond to any catalogued source. With receipt of the remaining 75 percent of the data, other discrete sources of emission may be identified in this nearby cluster.

In sharp contrast to these two images, early results from our planned detailed survey of the Coma cluster show that the X-ray morphology is dramatically different for this rich nearby cluster. An IPC observation of the center of the Coma cluster shows the X-ray distribution to be remarkably smooth overall and flat in the region between the dominant binary galaxies NGC4874 and NGC4889 (Fig. 8). From this and two other shorter pointings near the edge of Coma, we calculate that diffuse emission accounts for more than 99 percent of the flux from this cluster. Marginal detection of emission from discrete sources associated with galaxies at the edge of the cluster has been obtained. NGC4839, a possible cD galaxy discussed by Bahcall (1977), emits X-rays at the level of  $10^{41}$  ergs  $s^{-1}$ . Mkn 059, an emission-line galaxy member of the cluster, is also found to emit X-rays at this level, a few times  $10^{-4}$  of the total cluster emission. Receipt of the remaining 80 percent of the planned IPC observation should decide exactly how much discrete galactic emission may contribute to the total cluster emission. It will also aid us

in mapping possible halo emission from the cluster. A detailed pointing with the high resolution imager (HRI) will allow us to study the arc-second structure of the central 25' of the cluster.

In addition to the detailed studies of nearby clusters, CAL also plans to survey a large number of randomly selected clusters. A significant number of clusters should also be detected in a number of medium deep survey fields. Table 2 summarizes our results for the first 13 clusters surveyed. Column (1) gives the name of the object. Column (2) gives the Abell (1958) distance class code and the measured redshift. Column (3) gives the Abell richness class code, which is a rough measure of the number of galaxies in the cluster. Columns (4) and (5) give the Bautz-Morgan and Rood-Sastry classifications for cluster morphology. Column (6) gives the raw counts detected per 1000 sec of IPC observation. Column (7) gives the 0.2-3 keV source luminosity, and the last column (8) gives the estimated half peak radial size of each cluster. All clusters richer than class 0 and closer than distance class 5 have been detected as X-ray sources, including A1631, SC1251, A2089, and A2142. A variety of Bautz-Morgan and Rood-Sastry morphology is represented. It can be seen that a wide range of intrinsic cluster luminosities can now be surveyed by Einstein. Furthermore, clusters as distant as distance class 6, such as A348, have a good chance of being detected in short, approximately 1000-sec observations. For some of the nearby clusters, short observations may also permit a determination of the surface brightness distribution. For example, we have been able to map the distribution of A2079 in a 2500-sec observation and compare it with A539 and A2142 (Fig. 9). Thus far, the X-ray core size, which measures the distribution of hot gas, appears to be comparable to the galaxy core size of 0.25 Mpc determined by Bahcall (1977). Further observations and analysis can help us determine whether they differ, and if so, how and for what types of clusters. In addition, X-ray energy or "color" information available from IPC observations can help us decide how the temperature of the hot gas varies as a function of location in the cluster. These observations, carried out to large redshifts, should improve our understanding of how clusters form and how the gas and the galaxies evolve in these clusters.

## COSMOLOGY

The study of individual active galaxies and clusters of galaxies will help us understand their underlying emission mechanism and source of energy, but we have only just begun to tackle the more interesting cosmological questions which their study may help solve. Construction of accurate X-ray luminosity functions for active galaxies and clusters of galaxies from the large number expected to be detected with the Einstein Observatory should permit significant tests of cosmological models. The discovery of quasars as prodigious X-ray sources has already improved our understanding of the diffuse cosmic X-ray background. If all quasars emit X-rays at a level comparable to their optical



emission and if the optical count of quasars is valid to the 21st mag (e.g., Bohuski and Weedman 1979), they may account for a large portion of the observed diffuse cosmic X-ray background, and one need not invoke the suggestion that a large amount of hot gas, sufficient to close the Universe, is present. The open expanding Universe is still favored. Direct measurement of the Big Bang expansion parameters is in principle possible through the study of distant quasars and clusters of galaxies. Unfortunately, quasars are not very good standard candles due to large differences in their intrinsic luminosities. Deep X-ray observations should lead to discovery of clusters more distant than those surveyed by Abell and others. Core radii of distant clusters may be used as standard rules in cosmological tests of the deceleration parameter out to a redshift  $z \sim 1$ . The maximum total X-ray cluster luminosity (approximately  $3 \times 10^{45}$  ergs  $s^{-1}$ ) may serve as a standard candle. Schwartz (1976) has also suggested that counts of X-ray clusters of galaxies may be used to extract cosmological information. It is clear then that the Einstein Observatory has opened a new and important window onto the edge of the Universe, permitting us to view events which occurred near the very beginning of time. These studies should increase our understanding of the Universe.

We express our appreciation to the entire group whose efforts realized the success of the Einstein Observatory. This work was supported by the National Aeronautics and Space Administration under contract NAS8-30753. This paper is Columbia Astrophysics Laboratory Contribution No. 180.

## REFERENCES

- Abell, G. O., 1958, *Astrophys. J. Suppl.*, 3, 211.
- Arp, H., 1979, *Astrophys. J. (Letters)*, 207, L147.
- Bahcall, N. A., 1977, *Ann. Rev. Astron. Astrophys.*, 15, 505.
- Bohuski, T. J., and Weedman, D. W., 1979, *Astrophys. J.*, 231, 653.
- Bond, H. E., and Sargent, W. L., 1973, *Astrophys. J. (Letters)*, 185, L109.
- Forman, W., Jones, C., Murray, S., and Giacconi, R., 1978, *Astrophys. J. (Letters)*, 225, L1.
- Harris, D. E., Bahcall, N. A., and Strom, R. G., 1977, *Astron. Astrophys.*, 60, 27.
- Hinzen, P., and Scott, J. S., 1978, *Astrophys. J. (Letters)*, 224, L47.
- Jones, C., and Forman, W., 1978, *Astrophys. J.*, 224, 1.
- Schwartz, D. A., 1976, *Astrophys. J. (Letters)*, 206, L95.
- Schwartz, J., et al., 1979, preprint submitted to *Astrophys. J.*
- Sramek, R. A., and Weedman, D. W., 1978, *Astrophys. J.*, 221, 468.

TABLE 1. SUMMARY OF COLUMBIA/EINSTEIN OBSERVATIONS OF NORMAL AND ACTIVE X-RAY GALAXIES

Name (1)	Type (2)	Distance		Radio Flux: 1.4 GHz (Jy) (4)	Optical Flux: 548 THz (mJy) (5)	X-Ray Flux: 1 keV (μJy) (6)	X-Ray Luminosity: 0.5-4.5 keV * (ergs s <sup>-1</sup> ) (7)	$L_x/L_o$ (8)
		(Mpc) (3)	<i>z</i>					
(a) Normal Galaxies and Radio Galaxies								
M101	Sc	7.2	...	0.74	2700	0.26	$3 \times 10^{39}$	$4 \times 10^{-5}$
NGC5866	SO	18	...	0.016	76	0.1	$2 \times 10^{40}$	$7 \times 10^{-4}$
NGC520	Ir II	45	...	0.25	36	~0.1	$1 \times 10^{41}$	$1 \times 10^{-3}$
NGC5101	SBO <sub>3</sub>	...	...	...	58	~0.1	...	$5 \times 10^{-4}$
NGC1097	SBb	25	...	0.54	210	0.25	$1 \times 10^{41}$	$7 \times 10^{-4}$
NGC4756	SO	...	...	0.1	18	≤0.1	...	$<2 \times 10^{-3}$
3C296	Rad/DB	142	...	4.32	48	<0.2	$<9 \times 10^{40}$	$<1 \times 10^{-3}$
3C315	Rad	650	...	3.70	0.7	<0.2	$<2 \times 10^{43}$	<0.04
PKS0349-27	Rad	1458	...	~5.0	0.7	<0.2	$<7 \times 10^{43}$	<0.04
(b) Seyferts and N Galaxies								
3C109	N	...	0.306	7.0	1.6	0.8	$1.7 \times 10^{45}$	0.32
X Comae	Sy I	...	0.092	...	1(V)	1.0	$8 \times 10^{43}$	0.37
VII Zw674	Comp	...	...	...	0.6	0.2	...	0.15
RN73	N	...	0.047	...	0.36	0.14	$5 \times 10^{42}$	0.25
(c) Quasars and BL Lacs								
109+22	BL	...	...	0.67	1.3	0.14	...	0.04
A00235+164	BL(V)	...	0.853	2.61	0.5	0.3	$8 \times 10^{45}$	~0.3
0237-23	QSO	...	2.263	7.0	0.80	0.18	$1.4 \times 10^{47}$	0.45
Ton 256	QSO	...	0.131	0.021	2.5	0.97	$3.4 \times 10^{44}$	0.30
NAB1612	QSO	...	0.395	...	0.44	0.15	$3 \times 10^{44}$	0.14
3C351	QSO	...	0.371	3.14	1.68	0.17	$9 \times 10^{44}$	0.13
KP1703.5+60.9	QSO	...	1.98	...	0.36	0.03	$2.5 \times 10^{46}$	0.26

\* At the source,  $H_0 = 50 \text{ km s}^{-1} \text{ Mpc}^{-1}$ ,  $q_0 = 0$ .

TABLE 2. SUMMARY OF COLUMBIA/EINSTEIN OBSERVATIONS OF CLUSTERS OF GALAXIES

Name (1)	Distance		Abell Rich- ness Class (3)	Morpholog- ical Type		$E$ [counts (1000 s) <sup>-1</sup> ] (6)	X-Ray Lum- inosity: <sup>*</sup> 0.2-3 keV (ergs s <sup>-1</sup> ) (7)	X-Ray Size (') (8)
	Abell Class (2)	$z$		Bautz- Morgan (4)	Rood- Sastry (5)			
A348	6	0.274	1	II-III	...	23	$4.7 \times 10^{44}$	<1
A351	5	...	0	...	...	<27	$<7 \times 10^{43}$	...
A358	3	0.052	0	...	C	<100	$<4 \times 10^{43}$	...
A539	2	0.028	1	III	F	870	$2.4 \times 10^{44}$	5
A1631	3	0.034	0	I	...	70	$3 \times 10^{43}$	3
SC1251	3	0.056	0	...	cD	62	$1 \times 10^{43}$	<2
A1656	1	0.023	2	II	B	...	$\sim 6 \times 10^{44}$	12.7
A2079	3	0.059	1	II-III	cD	260	$1 \times 10^{44}$	2.5
A2089	4	0.070	1	II	...	9	$6 \times 10^{42}$	<2
A2142	4	0.090	2	II	...	1750	$1.8 \times 10^{44}$	1.5
A2160	6	0.271	1	III	...	<100	$<1 \times 10^{45}$	...
A2162	1	...	0	II-III	I	100	$1 \times 10^{43}$	10
A2165	6	...	0	...	...	<40	$<2 \times 10^{44}$	...

\* At the source,  $H_0 = 50 \text{ km s}^{-1} \text{ Mpc}^{-1}$ ,  $q_0 = 0$ .

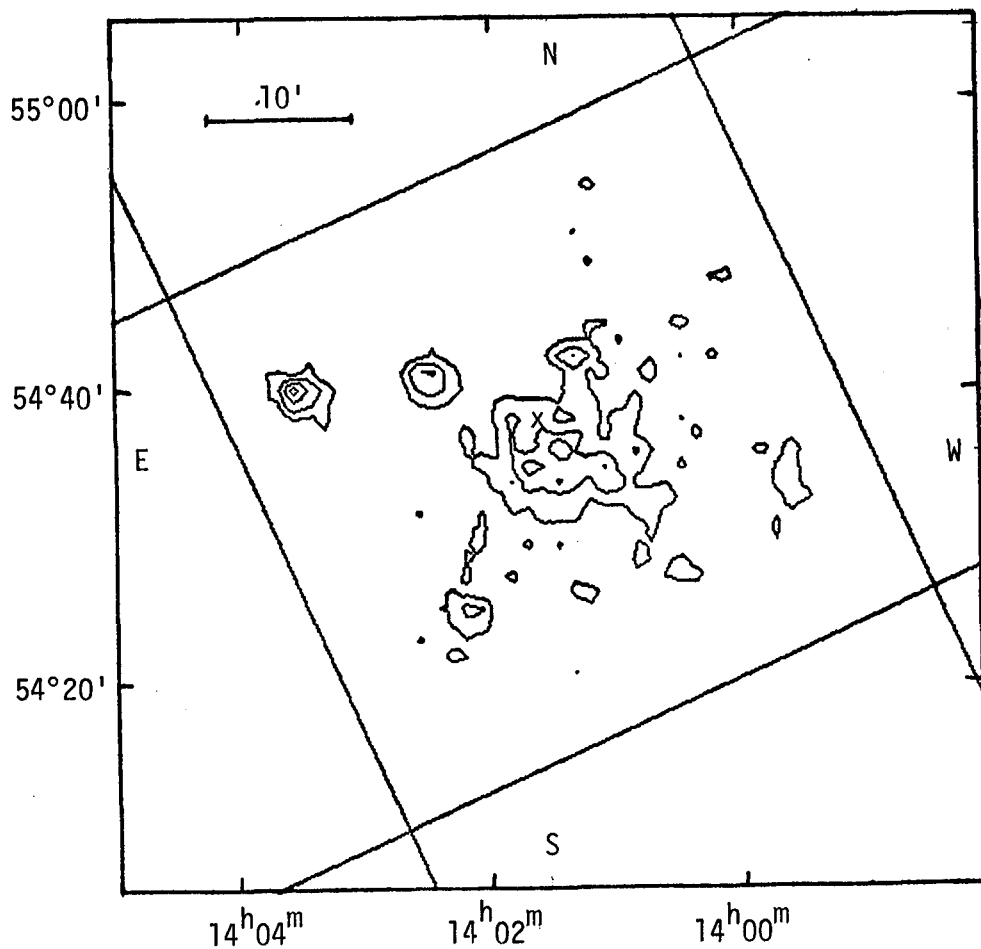


Figure 1. A 13000-sec IPC image of M101. The cross (X) marks the center of NGC5457. The four contour levels are 22, 29, 38, 49 counts per 64"  $\times$  64" cell. The intersecting lines indicate the location of the shadows of the counter support structure.

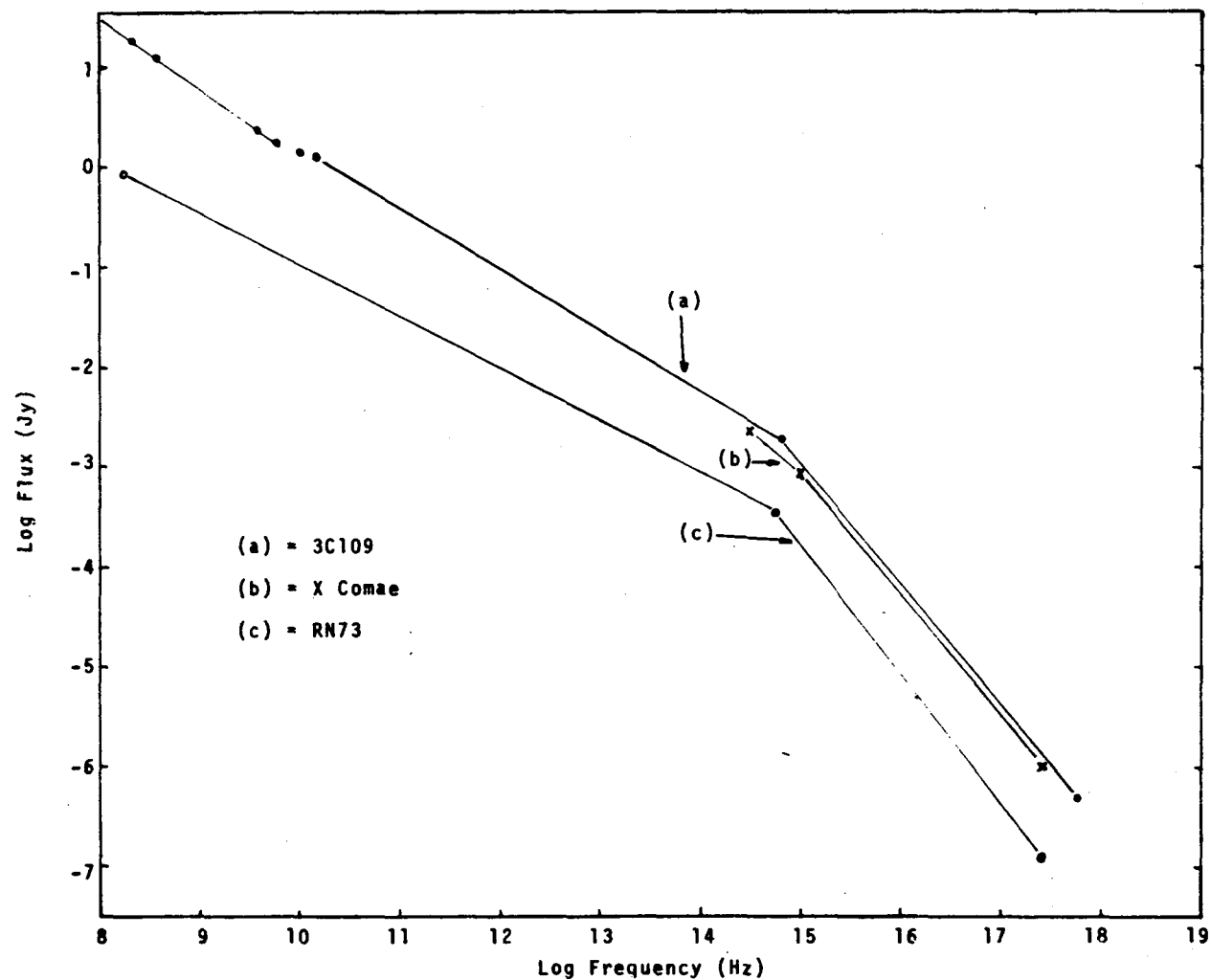


Figure 2. Multifrequency spectra of 3C109, X Comae, and RN73. Lines connecting symbols do not represent real physical relationships but are drawn to lead the eye.

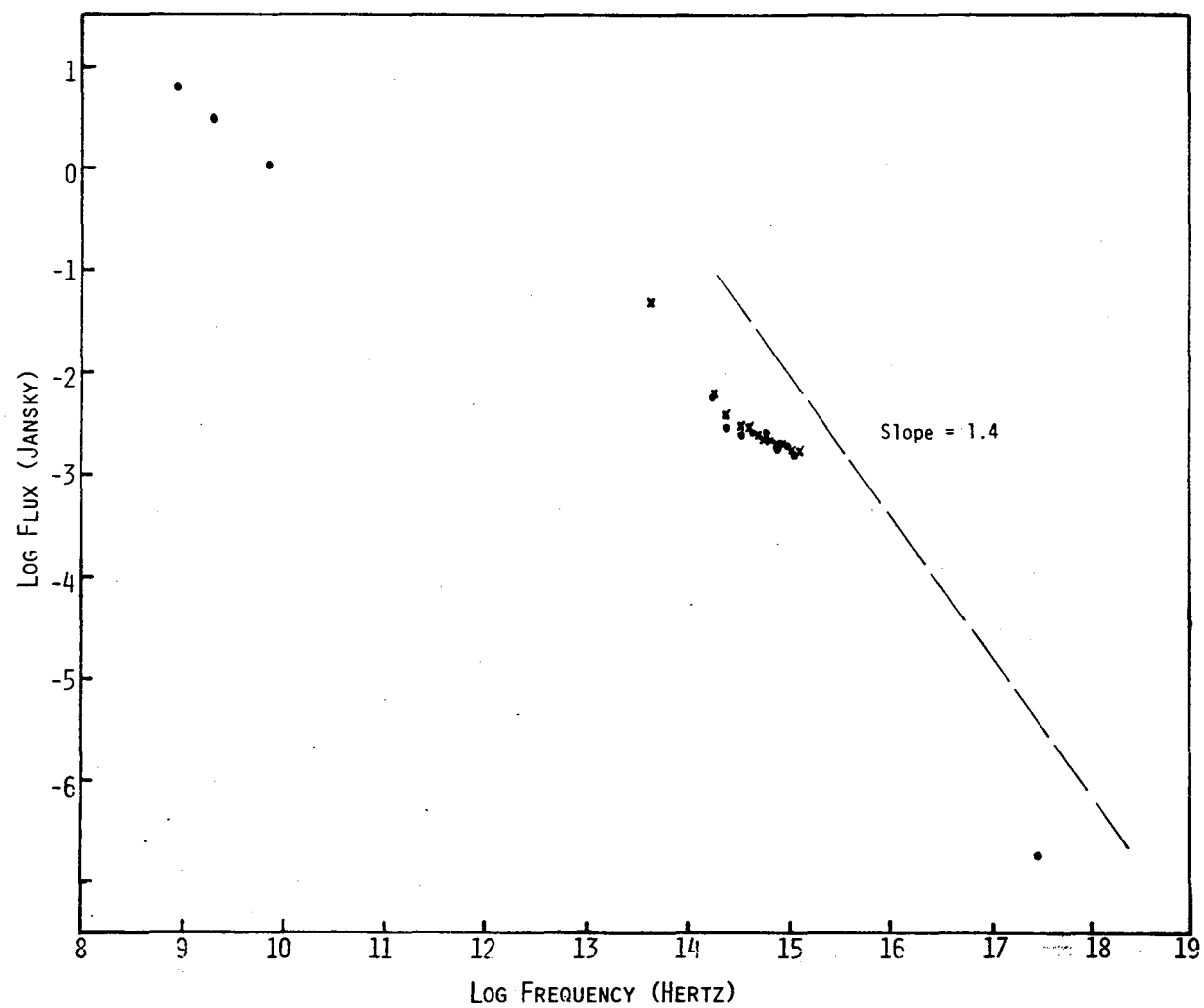
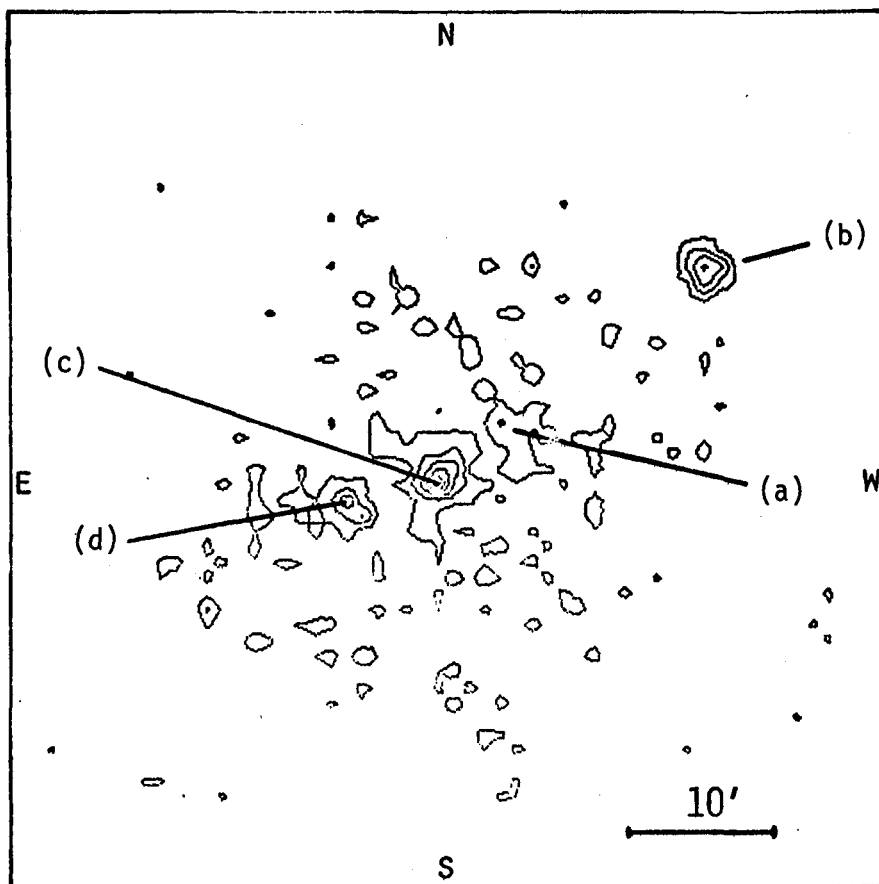


Figure 3. Multifrequency spectra of 3C351. Optical data (filled circles) are from O'Dell (March 1979).



(a) KP1703.5+60.9

(c) 3C351

(b) VII Zw674

(d) Seyfert

Figure 4. A 4820-sec IPC image of the  $1^\circ \times 1^\circ$  field centered on 3C351. Contour levels are 9, 15, 22.7, 32.3, and 43.6 counts per  $64'' \times 64''$  cell.



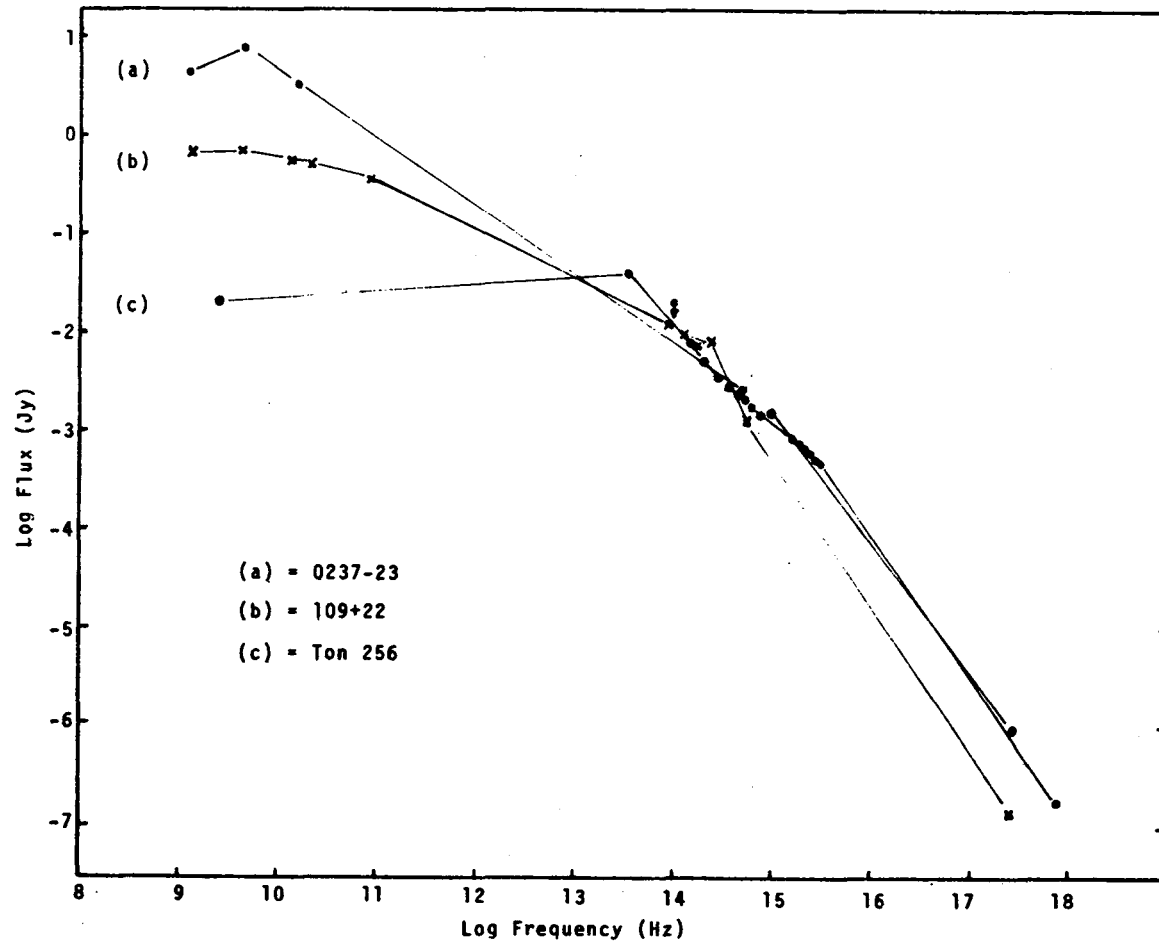


Figure 5. Multifrequency spectra of quasars 0237-23 and Ton 256 and BL Lac object 109+22.

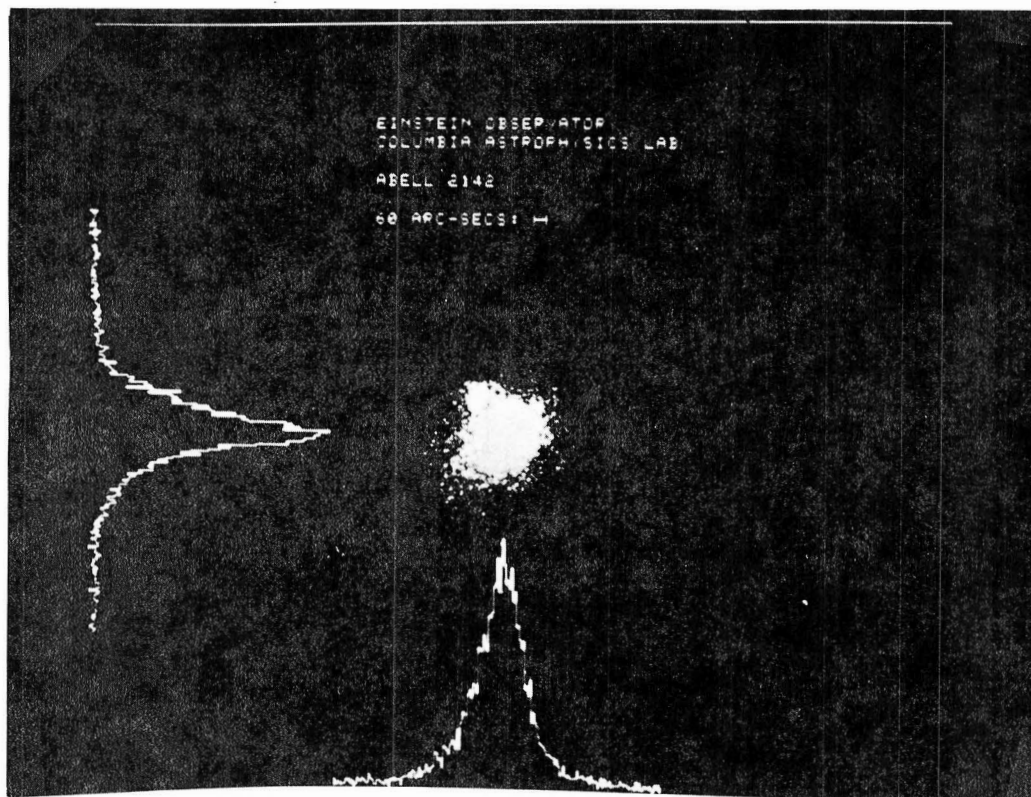
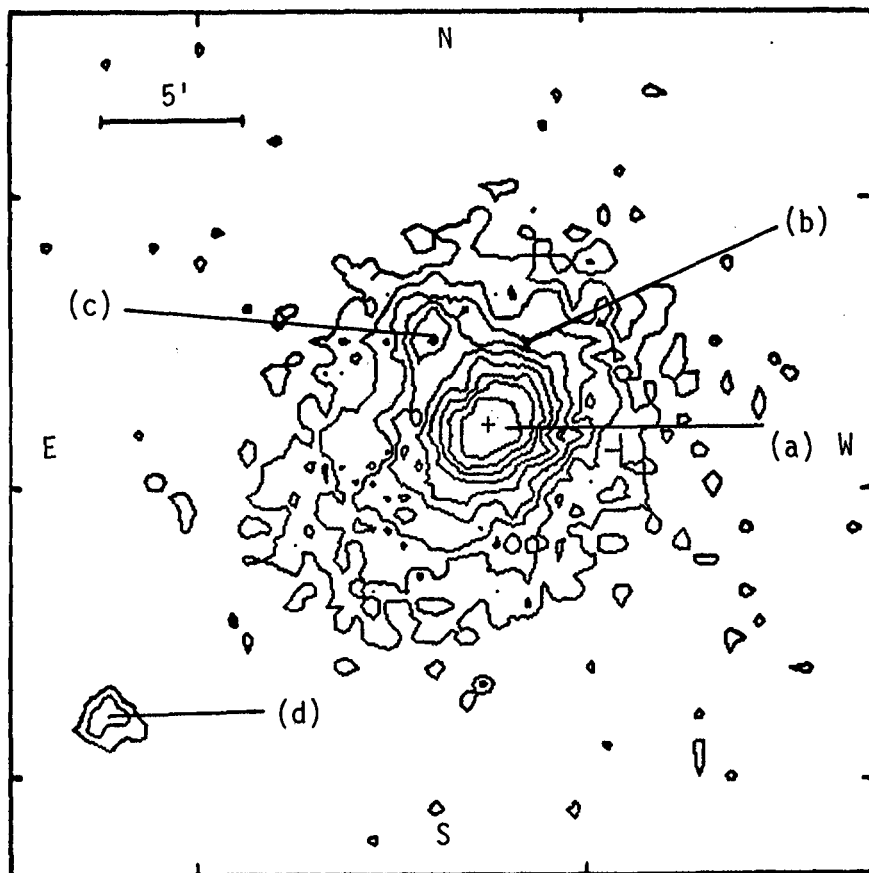


Figure 6a. IPC image of A2142. The line plots show the projected intensity of X-rays from this cluster along NS and EW axes.



(a) Optical center:  $15^{\text{h}}56^{\text{m}}13^{\text{s}}$ ,  $27^{\circ}22'27''$

(b) Radio head-tail galaxy

(c) Seyfert 1E1557+2712,  $z = 0.066$

(d) Unidentified point source:  $15^{\text{h}}56^{\text{m}}25^{\text{s}}$ ,  $27^{\circ}25'40''$

Figure 6b. A 5900-sec IPC image of A2142 cluster.

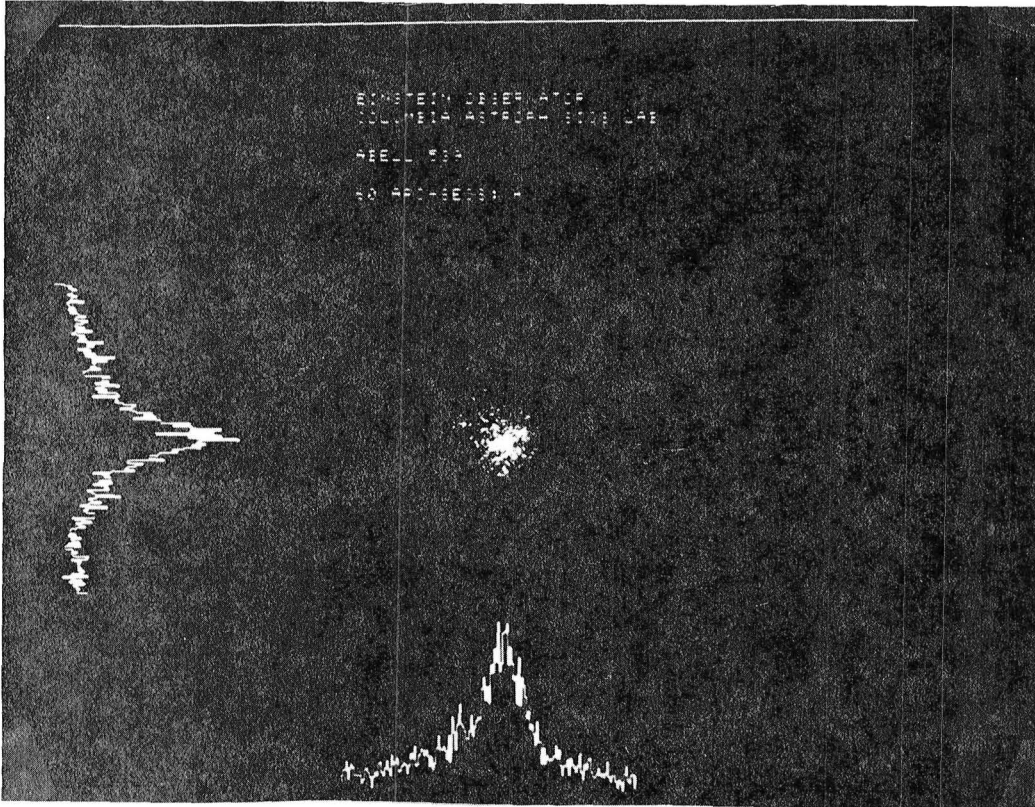
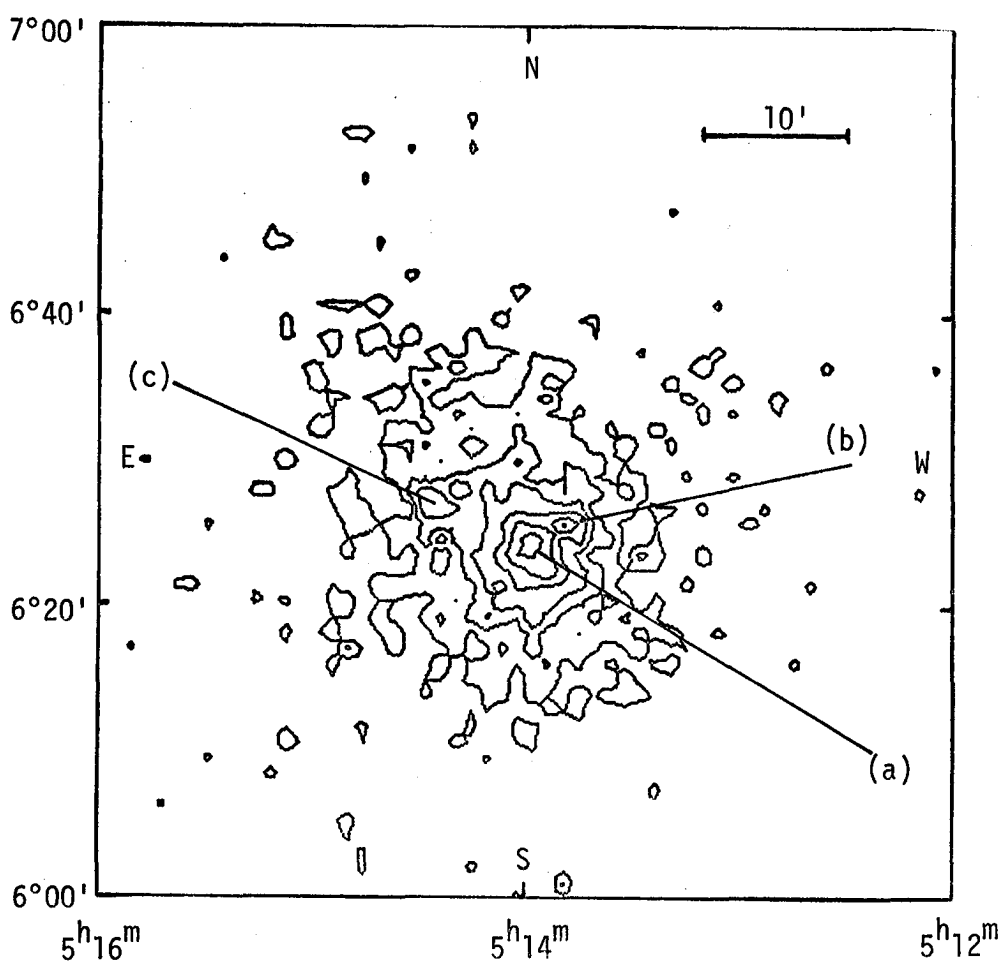


Figure 7a. IPC image of A539. The line plots show the projected intensity of X-rays from this cluster along NE and EW axes.



(a) Pair of galaxies:  $5^{\text{h}}13^{\text{m}}54^{\text{s}}, 6^{\circ}24'10''$

(b) Zwicky galaxy:  $5^{\text{h}}13^{\text{m}}46^{\text{s}}, 6^{\circ}25'45''$

(c) Unidentified:  $5^{\text{h}}14^{\text{m}}23^{\text{s}}, 6^{\circ}27'10''$

Figure 7b. A 5200-sec IPC image of A539 cluster. The six contour levels are 9, 15, 23, 32, 44, and 57 counts per  $64'' \times 64''$  cell.

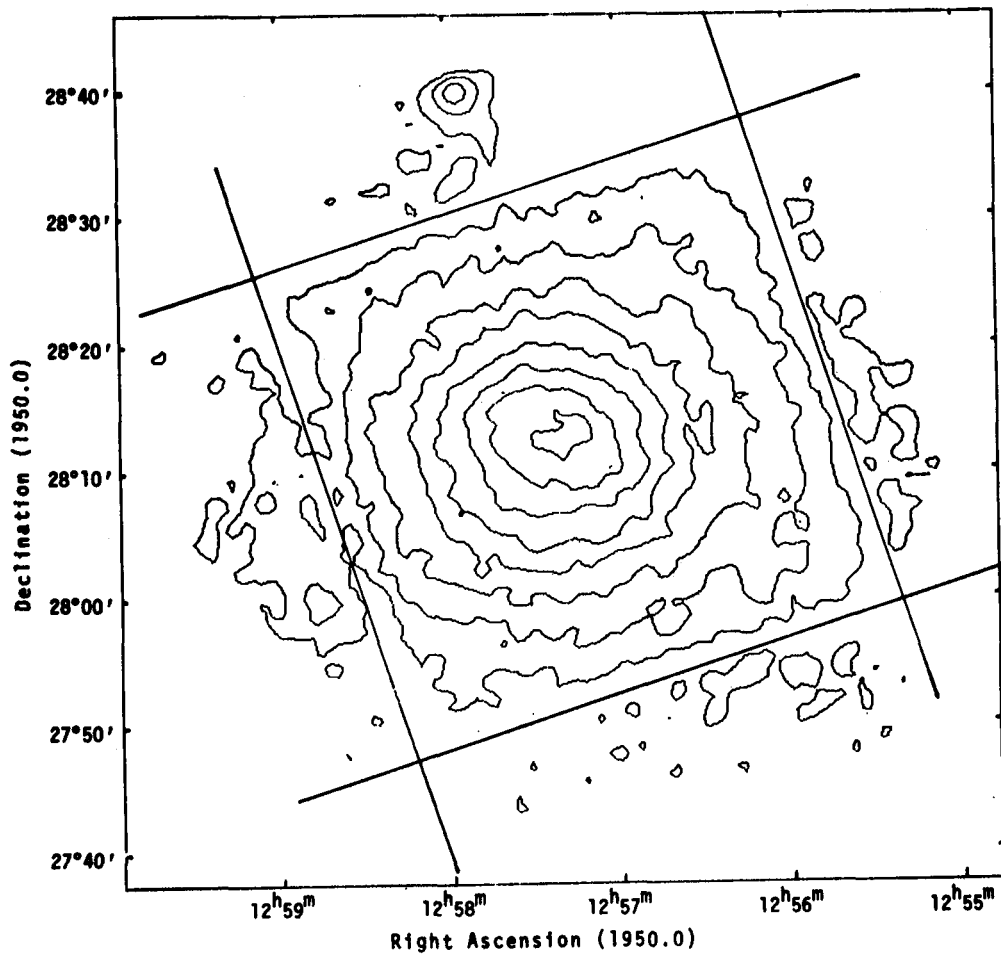


Figure 8. An 8000-sec IPC image of the center of the Coma cluster. The point source near the top of the field is X Comae, A Seyfert galaxy. The intersecting lines indicate the location of the shadows of the support structure.

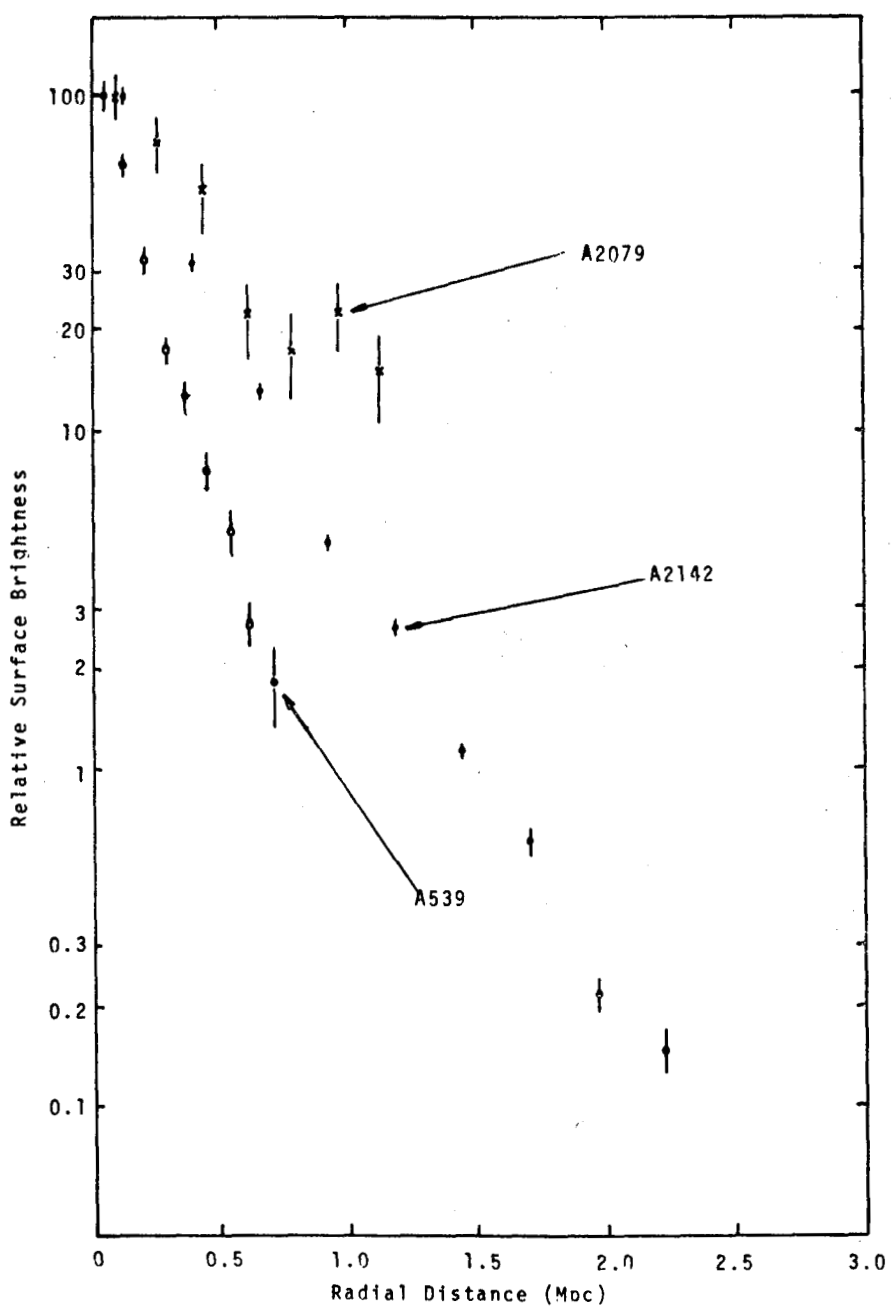


Figure 9. Radial surface brightness distribution of X-rays for A2079, A2142, and A539.

## APPROVAL

HEAO SCIENCE SYMPOSIUM HELD AT MSFC MAY 8 - 9, 1979

Edited by Carroll Dailey and Wendell Johnson

The information in this report has been reviewed for technical content. Review of any information concerning Department of Defense or nuclear energy activities or programs has been made by the MSFC Security Classification Officer. This report, in its entirety, has been determined to be unclassified.



---

F. A. SPEER

Manager, Space Sciences Project Office